

Sheffield Hallam University

A novel technique for tube sinking.

PANWHER, Mohammad Ibrahim.

Available from the Sheffield Hallam University Research Archive (SHURA) at:

<http://shura.shu.ac.uk/20183/>

A Sheffield Hallam University thesis

This thesis is protected by copyright which belongs to the author.

The content must not be changed in any way or sold commercially in any format or medium without the formal permission of the author.

When referring to this work, full bibliographic details including the author, title, awarding institution and date of the thesis must be given.

Please visit <http://shura.shu.ac.uk/20183/> and <http://shura.shu.ac.uk/information.html> for further details about copyright and re-use permissions.

SHEFFIELD CITY
POLYTECHNIC LIBRARY
FOND STREET
SHEFFIELD S1 1WB

00884

100 593 801 6 TELEPEN



Sheffield City Polytechnic Library

REFERENCE ONLY

ProQuest Number: 10700828

All rights reserved

INFORMATION TO ALL USERS

The quality of this reproduction is dependent upon the quality of the copy submitted.

In the unlikely event that the author did not send a complete manuscript and there are missing pages, these will be noted. Also, if material had to be removed, a note will indicate the deletion.



ProQuest 10700828

Published by ProQuest LLC (2017). Copyright of the Dissertation is held by the Author.

All rights reserved.

This work is protected against unauthorized copying under Title 17, United States Code
Microform Edition © ProQuest LLC.

ProQuest LLC.
789 East Eisenhower Parkway
P.O. Box 1346
Ann Arbor, MI 48106 – 1346

A NOVEL TECHNIQUE FOR

TUBE SINKING

by

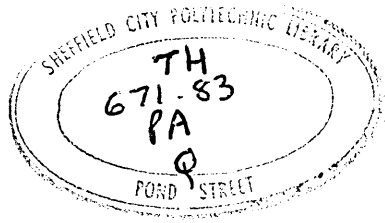
MOHAMMAD IBRAHIM PANWHER B Eng

A Thesis submitted to the COUNCIL FOR NATIONAL ACADEMIC AWARDS
in partial fulfilment for the degree of
DOCTOR OF PHILOSOPHY

Sponsoring Establishment : Department of Mechanical and
Production Engineering
Sheffield City Polytechnic
Sheffield, U.K.

Collaborating Establishment : R. S. Steel Services
Barrow Road
Sheffield 9

May 1986



ACKNOWLEDGEMENTS

The author wishes to express his sincere gratitude to Dr M S J Hashmi, Director of Studies, for his encouragement and helpful supervision during the course of this project. Sincere thanks are also expressed to Dr R Crampton, for his constructive suggestions and comments.

The technical assistance offered by Mr R Teasdale and his staff was much appreciated and in particular the author wishes to thank Messrs R Sidebottom, R Wilkinson and R C Wainwright for their support at various stages of this work.

The author acknowledges the assistance given by the Government of Pakistan for providing financial support towards this research.

The author would also like to express his gratitude to the authorities of the Mehran University for granting leave of absence in order to complete this work.

Finally, the support and encouragement of my wife and family deserve greater acknowledgements than words can express.

DECLARATION

The author declares that no part of this work has been submitted in support of another degree or qualification to this or any other establishment. The author further declares that he has not been a registered candidate or enrolled student for another award of the CNAA or other academic or professional institution during the course of the research programme.

M. I. Panwher

ABSTRACT

A NOVEL TECHNIQUE FOR TUBE SINKING

M. I. PANWHER

A new technique for tube sinking has been developed which should, in a number of ways, help to solve the problems associated with conventional tube sinking processes, eg die wear and the need for a swaged down leading end for easy insertion through the die. The conventional reduction die is altogether replaced by a die-less reduction unit of stepped bore configuration. The deformation is induced by means of hydrodynamic pressure and drag force generated in the unit due to the motion of the tube through the viscous fluid medium (polymer melt). The dimensions of the die-less reduction unit are such that the smallest bore size is dimensionally greater than the nominal diameter of the undeformed tube, thus metal to metal contact and hence wear, should no longer be a problem. As no conventional reduction die is used, the need for a reduced diameter leading end is also eliminated. Experimental results show that greater reduction in tube diameter and the coating thickness were obtained at slower drawing speeds (about 0.1 m/s). The maximum reduction in diameter noted was about 7 per cent.

Analytical models have been developed, assuming with Newtonian and non-Newtonian characteristics of the pressure medium, which enabled prediction of the length of the deformation zone, percentage reduction in diameter and drawing stress. In the non-Newtonian analysis account was taken of the pressure coefficient of viscosity, derived from the available data; the limiting shear stress, which manifests itself as slip in the polymer melt and the strain hardening and the strain rate sensitivity of the tube material.

The percentage reduction in diameter predicted using the Newtonian analyses appear to differ considerably from the experimental results both in trend and magnitude. Non-Newtonian analysis predicted theoretical results which are much closer to the ones observed experimentally.

<u>CONTENTS</u>	<u>Page</u>
ACKNOWLEDGEMENT	(I)
DECLARATION	(II)
ABSTRACT	(III)
INDEX TO FIGURES	(VII)
NOTATION	(XXI)
CHAPTER 1 : INTRODUCTION	1
1.1 The Tube Sinking Process	1
1.2 Background Literature to Die-Less Drawing	3
1.3 Present Project And Its Aim	6
CHAPTER 2 : RHEOLOGY OF POLYMER MELTS	13
2.1 Introduction	13
2.2 The Effect of Temperature On Viscosity	13
2.3 The Effect of Shear Stress And Strain On Viscosity	14
2.3.1 Critical Shear Stress	15
2.3.2 Shark-Skin	17
2.4 The Effect of Pressure on Viscosity	18
2.5 The Effects of The Polymer Flow Characteristics	19
CHAPTER 3 : EXPERIMENTAL EQUIPMENT AND MATERIALS	32
3.1 General Description	32
3.2 Instrumentation of the Experimental Equipment	33
3.2.1 Load Cell	33
3.2.2 Load Indicator	33
3.2.3 Pressure Transducers	34
3.2.4 Temperature Controllers	34
3.2.5 Heater Bands	34
3.2.6 Thermo-Couples	35
3.2.7 U-V Recorder	35

<u>Contents</u>	<u>Page</u>
3.3 Modification To The Experimental Draw-Bench	35
3.4 Design Of The Die-Less Reduction Unit	36
3.5 Determination Of The Stress-Strain Characteristics Of The Tube Materials	38
 CHAPTER 4 : EXPERIMENTAL RESULTS	 54
4.1 Experimental Procedure	54
4.2 Experimental Results	55
4.2.1 Results of Percentage Reduction In Diameter Versus Drawing Speed	57
4.2.2 Results of Drawing Stress Versus Drawing Speed	83
4.2.3 Results of Pressure Measurements	108
4.2.4 Results of Coating Thickness	145
4.3 Determination of The Deformation Profiles	155
4.4 Roundness Tests	158
 CHAPTER 5 : THEORETICAL MODEL BASED ON NEWTONIAN FLUID CHARACTERISTICS	 170
5.1 Introduction	170
5.2 Analysis	170
5.2.1 Linear Deformation Profile	176
5.2.2 Curved Deformation Profile	183
5.2.3 Numerical Solution	190
5.3 Theoretical Results	197
5.3.1 Results Based on Linear Deformation Profile	197
5.3.2 Curved Profile	213
5.3.3 Numerical Solution	243
 CHAPTER 6 : ANALYSIS BASED ON NON-NEWTONIAN FLUID CHARACTERISTICS	 275
6.1 Introduction	275
6.2 Analysis	276

<u>Contents</u>	<u>Page</u>
6.3 Results From The Analysis	246
6.3.1 Percentage Reduction In Diameter	297
6.3.2 Coating Thickness	299
6.3.3 Yielding Position of the Tube	300
6.3.4 Pressure	301
6.3.5 Drawing Stress	301
6.3.6 Deformation Profile	302
6.4 Discussion on the Theoretical And Experimental Results	303
6.4.1 Test Procedure And Experimental Results	303
6.4.2 Discussion On The Analyses And The Theoretical Results	309
6.4.3 Comparison Between The Experimental And Theoretical Results	316
 CHAPTER 7 : CONCLUSIONS AND SUGGESTIONS FOR FUTURE WORK	 353
7.1 Conclusions	353
7.2 Suggestions for Future Work	354
 CHAPTER 8 : REFERENCES	 357
 APPENDIX 1 : Experimental Results Obtained Using Thin Wall Copper Tubes	 A1.1
APPENDIX 2 : Solution Of The Cubic Equation	A2.1
APPENDIX 3 : Listing of the Computer Programme For The Theoretical Models Based On Newtonian Fluid Characteristics	A3.1
3.1 - Assumed Linear Deformation Profile	A3.1
3.2 - Assumed Curved Deformation Profile	A3.2
3.3 - Numerical Solution	A3.3
APPENDIX 4 : Listing of the Computer Programme for the Analysis Based on Non-Newtonian Fluid Characteristics	A4.1
APPENDIX 5 : Paper Published	A5.1

LIST OF FIGURES

<u>Fig No</u>		<u>Page</u>
1	Tube sinking through a conical die	8
2	Typical inlet tube and die	9
3	B.I.S.R.A. nozzle-die unit	9
4	Die employed in tube-sinking tests	10
5	Experimental device for tube-sinking	10
6	Christopherson tube-die assembly	11
7	Stepped bore reduction unit assembly	12
8	Effect of temperature on viscosity of polymers	20
9	Effect of temperature on viscosity of WVG23, KM61, Rigidex and polystyrene	20
10	Flow curves for Alkathene WVG23	21
11	Flow curves for Polypropylene KM61	22
12	Flow curves for Rigidex	23
13	Flow curves for Polystyrene	24
14	Effect of shear rate on viscosity of Alkathene WVG23	25
15	Effect of shear rate on viscosity of Polypropylene KM61	26
16	Effect of shear rate on viscosity of Rigidex	27
17	Effect of shear rate on viscosity of Polystyrene	28
18	A possible mechanism of sharkskin	29
19	Flow curves for 0.92 polyethylene at 130°C after Westover (23)	30
20	Viscosity versus pressure for different shear rates (0.92 polyethylene 130°C)	31
21	Die-less tube sinking drawing bench	40
22	Tube support stand	41
23	Stepped bore reduction unit assembly	42
24	Stepped bore reduction unit	43

<u>Fig No</u>		<u>Page</u>
25	Melt chamber and hopper assembly	44
26	Plate attached with the DRU	45
27(a)	Compression test of the copper-ring under different frictional conditions	46
27(b)	Compression test of the Aluminium-ring under different frictional conditions	46
28	The yield characteristics of the copper tube	47
29	The yield characteristics of the aluminium tube	48
30(a)	Alternate dimple type defect	62
30(b)	Continuous folding type defect	62
31	Effect of gap ratio on percentage reduction in diameter for copper tube with WVG23 at 130°C	63
32	Effect of gap ratio on percentage reduction in diameter for copper tube with KM61 at 220°C	64
33	Effect of gap ratio on percentage reduction in diameter for copper tube with Rigidex at 230°C	65
34	Effect of gap ratio on percentage reduction in diameter for copper tube with polystyrene at 240°C	66
35	Effect of gap ratio on percentage reduction in diameter for aluminium tube with WVG23 at 130°C	67
36	Effect of gap ratio on percentage reduction in diameter for aluminium tube with KM61 at 220°C	68
37	Effect of gap ratio on percentage reduction in diameter for aluminium tube with Rigidex at 230°C	69
38	Effect of gap ratio on percentage reduction in diameter for aluminium tube with polystyrene at 240°C	70
39	Effect of length ratio on percentage reduction in diameter for copper tube with WVG23 at 130°C	71
40	Effect of length ratio on percentage reduction in diameter for copper tube with KM61 at 220°C	72
41	Effect of length ratio on percentage reduction in diameter for copper tube with Rigidex at 230°C	73
42	Effect of length ratio on percentage reduction in diameter for copper tube with polystyrene at 240°C	74
43	Effect of viscosity on percentage reduction in diameter for copper tube with WVG23	75

<u>Fig No</u>		<u>Page</u>
44	Effect of viscosity on percentage reduction in diameter for copper tube with KM61	76
45	Effect of viscosity on percentage reduction in diameter for copper tube with Rigidex	77
46	Effect of viscosity on percentage reduction in diameter for copper tube with polystyrene	78
47	Effect of viscosity on percentage reduction in diameter for aluminium tube with WVG23	79
48	Effect of viscosity on percentage reduction in diameter for aluminium tube with KM61	80
49	Effect of viscosity on percentage reduction in diameter for aluminium tube with Rigidex	81
50	Effect of viscosity on percentage reduction in diameter for aluminium tube with polystyrene	82
51	Effect of gap ratio on drawing stress for copper tube with WVG23 at 130°C	88
52	Effect of gap ratio on drawing stress for copper tube with KM61 at 220°C	89
53	Effect of gap ratio on drawing stress for copper tube with Rigidex at 230°C	90
54	Effect of gap ratio on drawing stress for copper tube with polystyrene at 240°C	91
55	Effect of gap ratio on drawing stress for aluminium tube with WVG23 at 130°C	92
56	Effect of gap ratio on drawing stress for aluminium tube with KM61 at 220°C	93
57	Effect of gap ratio on drawing stress for aluminium tube with Rigidex at 230°C	94
58	Effect of gap ratio on drawing stress for aluminium tube with polystyrene at 240°C	95
59	Effect of length ratio on drawing stress for copper tube with WVG23 at 130°C	96
60	Effect of length ratio on drawing stress for copper tube with KM61 at 220°C	97
61	Effect of length ratio on drawing stress for copper tube with Rigidex at 230°C	98
62	Effect of length ratio on drawing stress for copper tube with polystyrene at 240°C	99

<u>Fig No</u>		<u>Page</u>
63	Effect of viscosity on drawing stress for copper tube with WVG23	100
64	Effect of viscosity on drawing stress for copper tube with KM61	101
65	Effect of viscosity on drawing stress for copper tube with Rigidex	102
66	Effect of viscosity on drawing stress for copper tube with polystyrene	103
67	Effect of viscosity on drawing stress for aluminium tube with WVG23	104
68	Effect of viscosity on drawing stress for aluminium tube with KM61	105
69	Effect of viscosity on drawing stress for aluminium tube with Rigidex	106
70	Effect of viscosity on drawing stress for aluminium tube with polystyrene	107
71	Pressure versus speed for copper tube with WVG23 at 130°C	113
72	Pressure versus speed for copper tube with WVG23 at 180°C	114
73	Pressure versus speed for copper tube with KM61 at 200°C	115
74	Pressure versus speed for copper tube with KM61 at 220°C	116
75	Pressure versus speed for copper tube with Rigidex at 230°C	117
76	Pressure versus speed for copper tube with Rigidex at 240°C	118
77	Pressure versus speed for copper tube with polystyrene at 230°C	119
78	Pressure versus speed for copper tube with polystyrene at 240°C	120
79	Pressure versus speed for aluminium tube with WVG23 at 130°C	121
80	Pressure versus speed for aluminium tube with WVG23 at 180°C	122

<u>Fig No</u>		<u>Page</u>
81	Pressure versus speed for aluminium tube with KM61 at 200°C	123
82	Pressure versus speed for aluminium tube with KM61 at 220°C	124
83	Pressure versus speed for aluminium tube with Rigidex at 230°C	125
84	Pressure versus speed for aluminium tube with Rigidex at 240°C	126
85	Pressure versus speed for aluminium tube with polystyrene at 230°C	127
86	Pressure versus speed for aluminium tube with polystyrene at 240°C	128
87	Pressure distributions for copper tube with WVG23 at 130°C	129
88	Pressure distributions for copper tube with WVG23 at 180°C	130
89	Pressure distributions for copper tube with KM61 at 200°C	131
90	Pressure distributions for copper tube with KM61 at 220°C	132
91	Pressure distributions for copper tube with Rigidex at 230°C	133
92	Pressure distributions for copper tube with Rigidex at 240°C	134
93	Pressure distributions for copper tube with polystyrene at 230°C	135
94	Pressure distributions for copper tube with polystyrene at 240°C	136
95	Pressure distributions for aluminium tube with WVG23 at 130°C	137
96	Pressure distributions for aluminium tube with WVG23 at 180°C	138
97	Pressure distributions for aluminium tube with KM61 at 200°C	139
98	Pressure distributions for aluminium tube with KM61 at 220°C	140

<u>Fig No</u>		<u>Page</u>
99	Pressure distributions for aluminium tube with Rigidex at 230°C	141
100	Pressure distributions for aluminium tube with Rigidex at 240°C	142
101	Pressure distributions for aluminium tube with polystyrene at 230°C	143
102	Pressure distributions for aluminium tube with polystyrene at 240°C	144
103	Coating thickness on copper tube with WVG23	147
104	Coating thickness on copper tube with KM61	148
105	Coating thickness on copper tube with Rigidex	149
106	Coating thickness on copper tube with polystyrene	150
107	Coating thickness on aluminium tube with WVG23	151
108	Coating thickness on aluminium tube with KM61	152
109	Coating thickness on aluminium tube with Rigidex	153
110	Coating thickness on aluminium tube with polystyrene	154
111	Deformation profiles for copper tube with WVG23 at 130°C	156
112	Deformation profiles for aluminium tube with WVG23 at 130°C	157
113	Roundness test on received copper tube	160
114	Roundness test on copper tube drawn at 0.1 m/s with WVG23, 130°C 6.13% reduction in diameter	160
115	Roundness test on copper tube drawn at 0.5 m/s with WVG23, 130°C 2.66% reduction in diameter	161
116	Roundness test on copper tube drawn at 0.1 m/s with KM61, 200°C 5.64% reduction in diameter	161
117	Roundness test on copper tube drawn at 0.5 m/s with KM61, 200°C 4.26% reduction in diameter	162
118	Roundness test on copper tube drawn at 0.1 m/s with Rigidex, 230°C 4.06% reduction in diameter	162
119	Roundness test on copper tube drawn at 0.5 m/s with Rigidex, 230°C 2.00% reduction in diameter	163
120	Roundness test on copper tube drawn at 0.1 m/s with polystyrene, 240°C 6.73% reduction in diameter	163

<u>Fig No</u>		<u>Page</u>
121	Roundness test on copper tube drawn at 0.5 m/s with polystyrene, 240°C 3.03% reduction in diameter	164
122	Roundness test on received aluminium tube	164
123	Roundness test on aluminium tube drawn at 0.1 m/s with WVG23, 130°C 5.4% reduction in diameter	165
124	Roundness test on aluminium tube drawn at 0.5 m/s with WVG23, 130°C 1.8% reduction in diameter	165
125	Roundness test on aluminium tube drawn at 0.1 m/s with KM61, 200°C 4.5% reduction in diameter	166
126	Roundness test on aluminium tube drawn at 0.5 m/s with KM61, 200°C 1.6% reduction in diameter	166
127	Roundness test on aluminium tube drawn at 0.1 m/s with Rigidex, 230°C 3.4% reduction in diameter	167
128	Roundness test on aluminium tube drawn at 0.5 m/s with Rigidex, 230°C 2.2% reduction in diameter	167
129	Roundness test on aluminium tube drawn at 0.1 m/s with polystyrene, 230°C 6.0% reduction in diameter	168
130	Roundness test on aluminium tube drawn at 0.5 m/s with polystyrene, 230°C 2.0% reduction in diameter	168
131(a)	Geometrical configuration of the stepped bore reduction unit and the tube	169
131(b)	Stresses acting on a small element of the tube	169
132(a)	Showing theoretically assumed deformation made within the DRU	174
132(b)	Linear deformation profile	174
132(c)	Stresses acting on a small element of the tube	175
133(a)	Showing theoretically assumed deformation mode within the DRU	182
133(b)	Curved deformation profile	182
134(a)	Geometry used in the analysis	188
134(b)	Stresses acting on a small element of the tube	189
135(a)	Theoretical effect of gap ratio on percentage reduction in diameter for copper tube	201
135(b)	Theoretical effect of gap ratio on yielding position of the copper tube	202

<u>Fig No</u>		<u>Page</u>
136	Theoretical effect of length ratio on percentage reduction in diameter for copper tube	203
137(a)	Theoretical effect of viscosity on percentage reduction in diameter for copper tube	204
137(b)	Theoretical effect of viscosity on yielding position of the copper tube	205
138	Theoretical effect of tube wall-thickness on percentage reduction in diameter for copper tube	206
139	Theoretical effect of tube wall-thickness on percentage reduction in diameter for aluminium tube	207
140	Theoretical effect of initial yield stress on percentage reduction in diameter for copper tube	208
141	Theoretical effect of initial yield stress on percentage reduction in diameter for aluminium tube	209
142	Theoretical effect of strain hardening constant on percentage reduction in diameter for aluminium tube	210
143	Theoretical effect of strain hardening index on percentage reduction in diameter for aluminium tube	211
144	Theoretical effect of tube diameter on percentage reduction in diameter for copper tube	212
145(a)	Theoretical effect of gap ratio on percentage reduction in diameter for aluminium tube	217
145(b)	Theoretical effect of gap ratio on yielding position of aluminium tube	218
146(a)	Theoretical effect of gap ratio on percentage reduction in diameter for copper tube	219
146(b)	Theoretical effect of gap ratio on yielding position of copper tube	220
147	Theoretical effect of gap ratio on percentage reduction in diameter for aluminium tube	221
148(a)	Theoretical effect of length ratio on percentage reduction in diameter for aluminium tube	222
148(b)	Theoretical effect of length ratio on yielding position of aluminium tube	223
149(a)	Theoretical effect of length ratio on percentage reduction in diameter for copper tube	224

<u>Fig No</u>		<u>Page</u>
149(b)	Theoretical effect of length ratio on yielding position of copper tube	225
150(a)	Theoretical effect of viscosity on percentage reduction in diameter for aluminium tube	226
150(b)	Theoretical effect of viscosity on yielding position of aluminium tube	227
151(a)	Theoretical effect of viscosity on percentage reduction in diameter for copper tube	228
151(b)	Theoretical effect of viscosity on yielding position of copper tube	229
152	Theoretical effect of tube wall-thickness on percentage reduction in diameter for aluminium tube	230
153(a)	Theoretical effect of initial yield stress on percentage reduction in diameter for aluminium tube	231
153(b)	Theoretical effect of initial yield stress on yielding position of aluminium tube	232
154(a)	Theoretical effect of initial yield stress on percentage reduction in diameter for copper tube	233
154(b)	Theoretical effect of initial yield stress on yielding position of copper tube	234
155	Theoretical effect of strain hardening constant on percentage reduction in diameter for aluminium tube	235
156	Theoretical effect of strain hardening index on percentage reduction in diameter for aluminium tube	236
157	Theoretical effect of gap ratio on coating thickness for aluminium tube	237
158	Theoretical effect of length ratio on coating thickness for aluminium tube	238
159	Theoretical effect of viscosity on coating thickness for aluminium tube	239
160	Theoretical effect of initial yield stress on coating thickness for aluminium tube	240
161	Theoretical effect of strain hardening constant on coating thickness for aluminium tube	241
162	Theoretical effect of strain hardening index on coating thickness for aluminium tube	242

<u>Fig No</u>		<u>Page</u>
163(a)	Theoretical effect of gap ratio on percentage reduction in diameter for copper tube	248
163(b)	Theoretical effect of gap ratio on yielding position of copper tube	249
164(a)	Theoretical effect of gap ratio on percentage reduction in diameter for aluminium tube	250
164(b)	Theoretical effect of gap ratio on yielding position of the aluminium tube	251
165	Theoretical effect of length ratio on percentage reduction in diameter for copper tube	252
166(a)	Theoretical effect of viscosity on percentage reduction in diameter for copper tube	253
166(b)	Theoretical effect of viscosity on yielding position of copper tube	254
167(a)	Theoretical effect of viscosity on percentage reduction in diameter for aluminium tube	255
167(b)	Theoretical effect of viscosity on yielding position of aluminium tube	256
168(a)	Theoretical effect of initial yield stress on percentage reduction in diameter for copper tube	257
168(b)	Theoretical effect of initial yield stress on yielding position of copper tube	258
169(a)	Theoretical effect of initial yield stress on percentage reduction in diameter for aluminium tube	259
169(b)	Theoretical effect of initial yield stress on yielding position of aluminium tube	260
170	Theoretical effect of strain hardening constant on percentage reduction in diameter for copper tube	261
171	Theoretical effect of strain hardening index on percentage reduction in diameter for copper tube	262
172(a)	Theoretical effect of tube wall-thickness on percentage reduction in diameter for copper tube	263
172(b)	Theoretical effect of tube wall-thickness on yielding position of copper tube	264
173(a)	Theoretical effect of tube diameter on percentage reduction in diameter for copper tube	265

<u>Fig No</u>		<u>Page</u>
173(b)	Theoretical effect of tube diameter on yielding position of copper tube	266
174	Theoretical effect of strain rate sensitivity index on percentage reduction in diameter for copper tube	267
175	Theoretical effect of strain rate sensitivity constant on percentage reduction in diameter for copper tube	268
176	Theoretical effect of gap ratio on coating thickness for copper tube	269
177	Theoretical effect of length ratio on coating thickness for copper tube	270
178	Theoretical effect of viscosity on coating thickness for copper tube	271
179	Theoretical effect of initial yield stress on coating thickness for copper tube	272
180	Theoretical effect of tube wall-thickness on coating thickness for copper tube	273
181	Theoretical deformation profiles for copper tube	274
182	Theoretical effect of gap ratio on percentage reduction in diameter	320
183	Theoretical effect of gap ratio on percentage reduction in diameter	321
184	Theoretical effect of length ratio on percentage reduction in diameter	322
185	Theoretical effect of initial viscosity on percentage reduction in diameter	323
186	Theoretical effect of initial yield stress on percentage reduction in diameter	324
187	Theoretical effect of strain hardening constant on percentage reduction in diameter	325
188	Theoretical effect of strain hardening index on percentage reduction in diameter	326
189	Theoretical effect of tube wall-thickness on percentage reduction in diameter	327
190	Theoretical effect of tube diameter on percentage reduction in diameter	328

<u>Fig No</u>		<u>Page</u>
191	Theoretical effect of shear stress constant on percentage reduction in diameter	329
192	Theoretical effect of gap ratio on coating thickness	330
193	Theoretical effect of length ratio on coating thickness	331
194	Theoretical effect of initial yield stress on coating thickness	332
195	Theoretical effect of tube wall-thickness on coating thickness	333
196	Theoretical effect of tube diameter on coating thickness	334
197	Theoretical effect of gap ratio on yielding position of tube	335
198	Theoretical effect of length ratio on yielding position of tube	336
199	Theoretical effect of initial yield stress on yielding position of tube	337
200	Theoretical effect of gap ratio on pressure distributions	338
201	Theoretical effect of initial yield stress on pressure distributions	339
202	Theoretical effect of tube wall-thickness on pressure distributions	340
203	Theoretical effect of tube diameter on pressure distributions	341
204	Theoretical effect of gap ratio on drawing stress	342
205	Theoretical effect of length ratio on drawing stress	343
206	Theoretical effect of tube diameter on drawing stress	344
207	Theoretical effect of strain hardening index on drawing stress	345
208	Theoretical deformation profiles	346
209	Comparison between experimental and theoretical percentage reduction in diameter for copper tube	347

<u>Fig No</u>		<u>Page</u>
210	Comparison between experimental and theoretical drawing stress for copper tube	348
211	Comparison between experimental and theoretical pressure distributions for copper tube	349
212	Comparison between experimental and theoretical pressure distributions for copper tube	350
213	Comparison between experimental and theoretical deformation profiles for copper tube	351
214	Comparison between experimental and theoretical deformation profiles for copper tube	352
A1(a)	Alternate dimple type defects	A1.2
A1(b)	Continuous folding type defects	A1.2

LIST OF PLATES

<u>Plate No</u>		<u>Page</u>
1	General view of the draw bench	49
2	Load indicator, Pressure transducers, Thermo-couples	50
3	Temperature controllers, U-V recorder	51
4	Positioning of the heater bands	52
5	Load cell	53

NOTATION

- P'_1 Pressure gradient in the first section of the unit prior to the deformation of tube.
- P'_2 Pressure gradient in the second part of the unit prior to the deformation of tube.
- τ_1 Shear stress in the melt in the first part of unit.
- τ_2 Shear stress in the melt in the second part of unit.
- K Non-Newtonian factor.
- τ_{c1} Shear stress on the tube in the first section of the unit prior to deformation
- τ_{c2} Shear stress on the tube in the second section of the unit prior to deformation.
- τ_{ca} Critical shear stress.
- μ_0 Initial viscosity of polymer melt.
- a Viscosity constant.
- b Pressure coefficient of viscosity.
- V Velocity of tube prior to deformation.
- Q_1 Flow of polymer in the first section of the unit.
- Q_2 Flow of polymer in the second section of the unit.
- U_1 Velocity of polymer in the first section of the unit.
- U_2 Velocity of polymer in the second section of the unit.
- P_m Maximum pressure if no deformation occurs.
- h_1 Radial gap in the first section of the unit prior to deformation of tube.
- h_2 Radial gap in the second section of the unit prior to deformation of tube.
- L_1 Length of the first section of the unit.] (See Fig 131a)
- L_2 Length of the second section of the unit.
- V_s Tube speed at commencement of slip.
- $\dot{\gamma}$ Apparent shear rate in the first section of the unit.
- X_1 Yielding position of tube.
- σ_x Axial stress in the tube.

σ_{xi} Axial stress in the tube at commencement of plastic deformation.
 σ_{θ} Hoop stress in the tube.
 P_1 Radial pressure in the melt at commencement of plastic deformation.
 t Constant wall thickness of the tube.
 r_1 Initial tube radius.
 r_2 Final tube radius.
 r_i Radius of the tube within the deformation zone.
 h_i Radial gap in the deformation zone.
 α Semi-angle of the effective die.
 Δx Step size in the deformation zone.
 B Slope of the deformation line within Δx .
 τ_{ci} Shear stress on the tube in the deformation zone.
 σ_{xi} Axial stress in the deformation zone.
 P_i Pressure in the melt in the deformation zone.
 $\sigma_{\theta i}$ Hoop stress in the tube within the deformation zone.
 Q_i Flow of polymer in the deformation zone.
 V_i Velocity of tube in the deformation zone.
 Y_0 Initial yield stress in the tube.
 K_0 Strain hardening constant.
 n Strain hardening index.
 ϵ Natural strain
 Y_i Yield stress in the deformation zone.
 V_d Velocity of tube at the end of deformation zone.
 S_i Dynamic/static stress ratio.
 h_3 Polymer coating thickness.

SUBSCRIPTS

- 1 First section of the unit
- 2 Second section of the unit
- i Deformation zone
- r Denotes radial direction
- x Denotes axial direction

$$1 \text{ inch} = 25.4 \text{ mm}$$

$$1 \text{ foot} = 12 \text{ inches}$$

$$1 \text{ bar} = 10^5 \text{ N/m}^2$$

$$1 \text{ psi} = 6897.11 \text{ N/m}^2$$

CHAPTER 1 : INTRODUCTION

1.1 The Tube Sinking Process

The tube sinking (or Hollow-Sinking) is a well known and common process for reducing the diameter of the tube without any significant change in the wall thickness. In this process, a tube is pulled through a tungsten-carbide reduction die and the material deforms plastically whilst passing through the die. In this case the die acts primarily to reduce the tube diameter to a specific size with an acceptable surface finish. The process is illustrated schematically in Fig(1). Its main functions are:

- (i) to reduce the tube diameter,
- (ii) to modify the mechanical properties of the material,
- (iii) to obtain a closer tolerance on the outside diameter, and
- (iv) to improve the degree of surface finish.

Compared with tube drawing, in which a mandrel (or Plug) is inserted in the die to govern the final thickness of the drawn tube, the hollow-sinking method generally gives a heavier draft.^{1,2}

A standard design of industrial die profile usually lies between 20 and 40 degrees, and possible reduction in area at each die varies from about 10 to 40 per cent. In industrial tube sinking practice, lubrication is used to reduce the drawing load and die wear and hence improve the machine life and surface finish of the product, but still there is high friction due to metal contact.

There is no unified opinion on the nature and the mechanism of surface friction.³ It is, however, obvious that the surface friction, developing between the tool and the product under conditions of plastic deformation at high pressures and temperatures, possesses a nature and mechanism of action rather different from the friction occurring in other processes.

Let us briefly examine the difference between dry, boundary and fluid friction from the standpoint of their action on the surface of the product being worked. In dry friction, there should be no foreign interlayer between the rubbing surfaces moving relative to one another. Kragel et al³ have expressed the opinion that surface friction is only possible with a positive gradient of mechanical properties as the depth increases; in other words, if there is a soft layer on the surface of the material. Hence the classification of friction into dry and boundary types is a mere convention. Boundary friction pre-supposes the presence of a lubricant film between the friction surfaces. Generally two types of lubrication are used in the tube sinking process. These are (i) liquid lubrication and (ii) solid lubrication. Both the liquid and solid lubricants are employed in metal working processes involving generation of pressure at the interfaces. The mechanism of the action of these lubricants under boundary lubrication conditions is to form a film on the friction surface. Liquid lubricants must possess surface active properties, ie the molecules of the lubricant must be capable of absorption on the surface atoms of metals.

The strength of a boundary film of lubricant is sometimes inadequate, because of the high stresses (specific pressures) and temperatures during drawing, to fully separate the rubbing surfaces. An essential condition for the existence of the qualitatively different hydrodynamic friction is the pressure of the layer of lubricant, which is capable of keeping the friction bodies apart. Fluid conditions during drawing can be produced by delivery of the lubricant to the deformation zone under a certain pressure. Such a method was proposed by Milliken.⁴ In this method, oil at high pressure was fed into a special device.

1.2 Background Literature To Die-less Drawing

In 1955, Christopherson and Naylor⁵ presented a paper which showed a method of reducing friction in wire drawing by hydrodynamic lubrication. It had been assumed that friction in conventional wire drawing was of a boundary nature and that a change of mode to hydrodynamic lubrication should greatly reduce friction (see Fig 2). Wistreich⁶ conducted experimental work on forced lubrication based on a pressure tube system. Soap powder was used as the lubricant in a short nozzle which was attached to the entry side of the die. The experimental results showed that the speed, temperature and the tube gap had a direct effect on the property of the film thickness produced. He also showed that when the soap powder was replaced by oil, an increase rather than the decrease of film thickness was observed. (The schematic diagram of the BISRA unit is shown in figure 3), but all these experiments were carried out on wire drawing.

In 1961 the first tests were conducted on tube sinking under conditions of hydrodynamic lubrication.⁷ On the basis of the experience of wire drawing under hydrodynamic conditions, the equipment shown in Fig(4) was employed. In contrast to similar devices for wire drawing, there was no seal between the nozzle and the die, because the lubricant pressure in tube sinking was much lower. Soda-soap powder was used as the lubricant. The tubes were drawn on chain type draw benches at a drawing speed of 0.17 - 0.58 m/s.

It was necessary, however, to provide a leader (or swaging) to the full size tube in order to induce effective lubrication at the starting condition. Nevertheless some die wear was still present.

A further development⁷ in tube sinking under conditions of hydrodynamic lubrication was a device consisting of a system of dies, which acted as a nozzle (see Fig 5).

This device consists of working and delivery dies, contained in a special casing. The delivery dies perform the function of a nozzle, ie serve to feed the lubricant into the deformation zone under pressure. In this process deformation was taking place before the die, and the die itself was working as a seal. The arrangement of the unit was in such a way that a die (seal) just smaller than the nominal tube diameter was placed before the main die and the gap between the delivery dies was filled with lubricant. As the volume of the lubricant increased in the gap, the pressure increased to a point that hydrodynamic lubrication was achieved.

Although a different way of true lubrication was introduced, nevertheless, the important problems in the tube sinking processes remained unsolved. For the majority of lubrication purposes, soda-soap powder and oil are selected for their flexible properties, but very recently, attention has been drawn to the use of high viscous materials as lubricant agents at areas where particularly high loads are applied. Non-Newtonian lubricants have been previously investigated for Journal Bearings⁸ and it has been found advantageous to bearings subjected to oscillatory loads which induces fatigue loading.

A programme of research has been undertaken at the Sheffield City Polytechnic with a view to introducing alternative lubricating systems in wire drawing which would have very different characteristics from those currently in use. It has been shown that a pressure tube based on the work of reference⁵ improved some of the operating characteristics when polymer melt was used as a lubricant.

The use of a polymer melt as a lubricant in wire drawing was suggested by Symmons and Thompson⁹ to investigate the adherence of the polymer coat onto the drawn wire. Although hydrodynamic lubrication of wire was claimed to be achieved successfully, the adhesion between the wire and the polymer was reported to be unsatisfactory.

Stevens¹⁰ conducted a limited experimental work in wire drawing and polymer melt lubrication investigating the coating properties of the polymer. Practical results showed a decrease in the coating thickness with increasing speed which gave some correlation with his Newtonian solution.

Crampton¹¹ carried out an in depth study of the wire drawing process based on the similar unit adopted by Stevens¹⁰ again using polymer melt as a lubricant. The apparatus consisted of a pressure tube connected to the forward end of a conventional die. The polymer melt was dragged into the tube by the motion of the wire, generating high pressures which resulted in hydrodynamic lubrication and coating of wire during the drawing process. A section view of the unit is shown in Fig(6). On the basis of experimental evidence it was apparent that the deformation of the wire commenced in the tube itself before reaching the reduction die, which effectively acted only as a seal. Under these conditions the die geometry becomes of secondary importance and deformation actually takes place as if an effective die of continuously changing die angle is being used.

Furthermore, experimental work carried out by Hashmi et al¹²⁻¹⁴ showed that effective reduction of the wire should be possible using a polymer melt in conjunction with a stepped bore tubular unit only, the least diameter of the stepped bore reduction unit being greater than the nominal wire diameter.

1.3 Present Project And Its Aim

A new technique of tube sinking, using a stepped bore unit, is developed based on the works reported in references (9-14) in relation to wire drawing. This new technique would be useful in a number of ways in solving the problems associated with the conventional tube sinking process, eg die wear and the need for a swaged down leading end for easy insertion through the reduction die. The results of the initial research on tube sinking led to the suggestion that under special conditions, it may be possible to eliminate the conventional die from the tube reduction unit and yet generate enough pressure within the die-less reduction unit (DRU) to deform the tube. The smallest bore size of such a device is dimensionally greater than the nominal tube diameter, thus metal to metal contact and hence wear, would no longer be a problem.

As no conventional reduction die is used, the need for a reduced diameter leading end is also eliminated (shown in Fig 7). The polymer melt, in addition to acting as a pressure medium, is found to form a coating on the drawn tube. This coating is thought to be useful in protecting the tube against corrosion.

Exploratory experimental work has been carried out to investigate the performance of this new system. Initial research on the new system showed certain limitations as follows:

- (i) In the case of thin wall tube being drawn at slower speeds and using polymer melt at lower temperatures, buckling (folding) was apparent. This buckling disappears at higher drawing speeds, producing smaller reductions in diameter (results are shown in Appendix 1).
- (ii) In the case of thicker wall tube, reduction in diameter may only be obtained at very slow speeds. This could be the effect of the phenomenon referred to as the slip

condition, where at a certain speed, the value of the shear stress acting on the tube reaches a maximum and remains constant, irrespective of the increase in speed. These rheological effects and their consequences are discussed in detail in Chapter 2.

- (iii) At higher drawing speeds the performance of the unit, in terms of the obtainable reduction in diameter and coating thickness, decreased.

Since the design and manufacturing of the stepped bore reduction unit proved simpler, extensive experimental and theoretical work was carried out for this unit.

The objectives of the present work are:

- (a) To investigate the performance of the unit in detail.
- (b) To provide a mathematical model of the process account of the detailed rheological and metallurgical properties of the pressure medium and the tube.
- (c) To examine the correlation between the experimental and theoretical results.
- (d) To investigate other means of improving the process in order to make it more acceptable to industry.

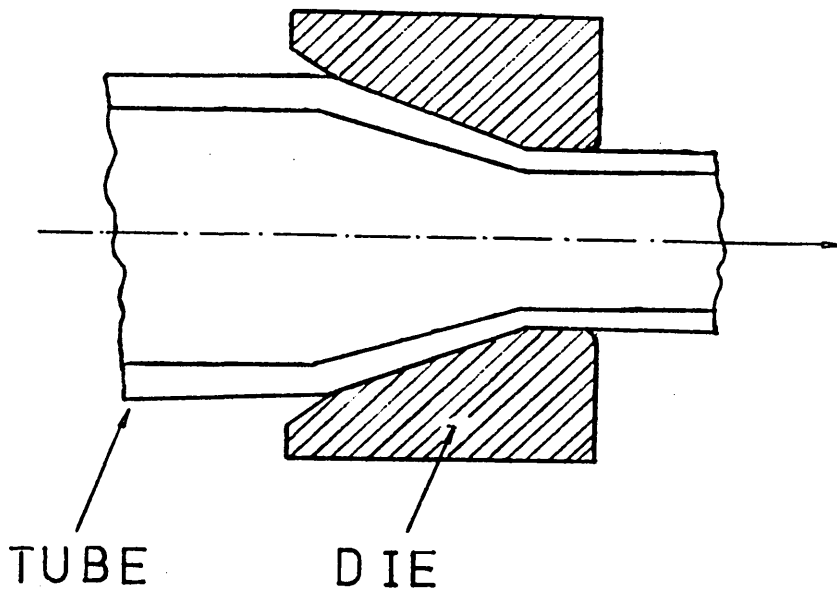


FIG 1 - TUBE-SINKING THROUGH A CONICAL DIE

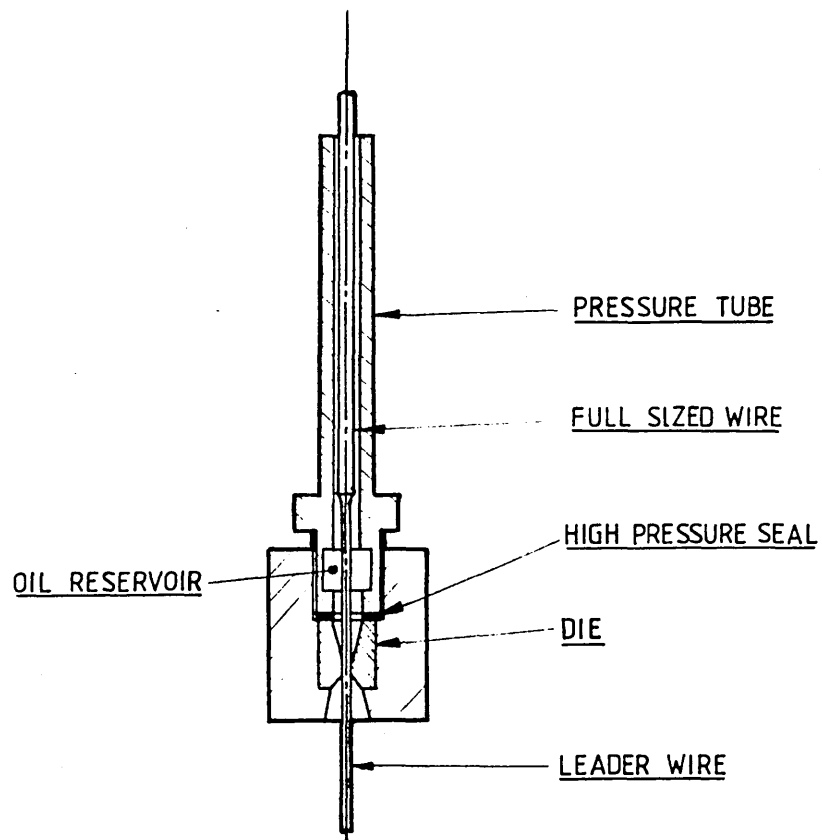


FIG 2 - TYPICAL INLET TUBE AND DIE

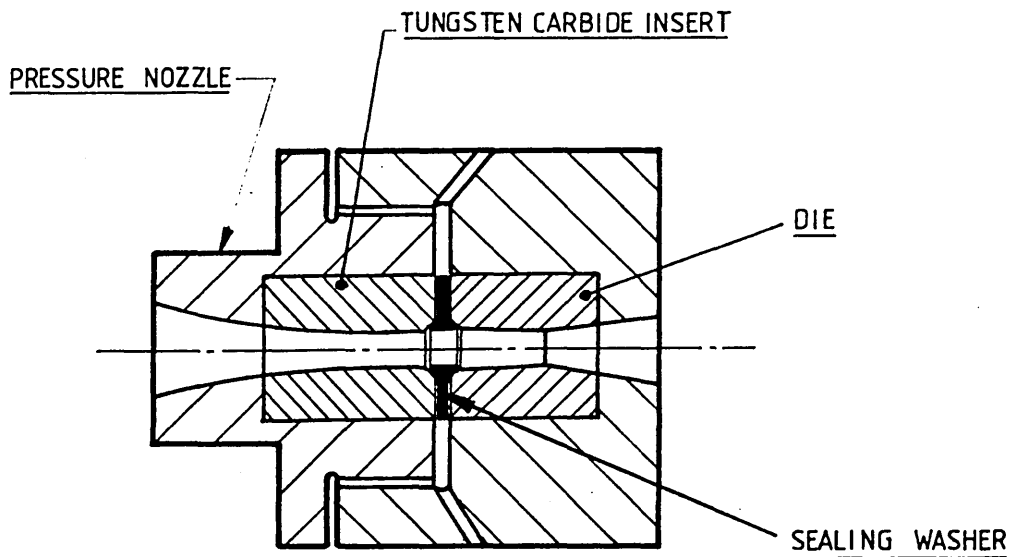


FIG 3 - B.I.S.R.A. NOZZLE-DIE UNIT

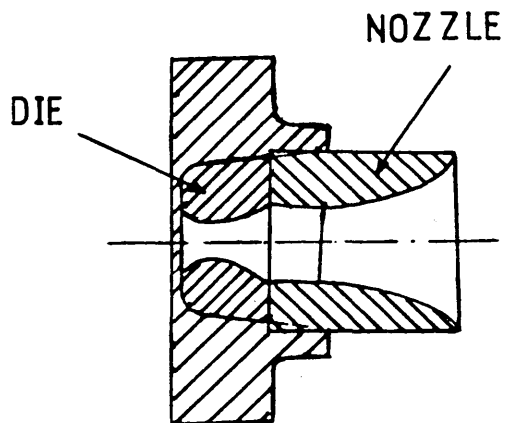


FIG 4 - DIE EMPLOYED IN TUBE-SINKING TESTS

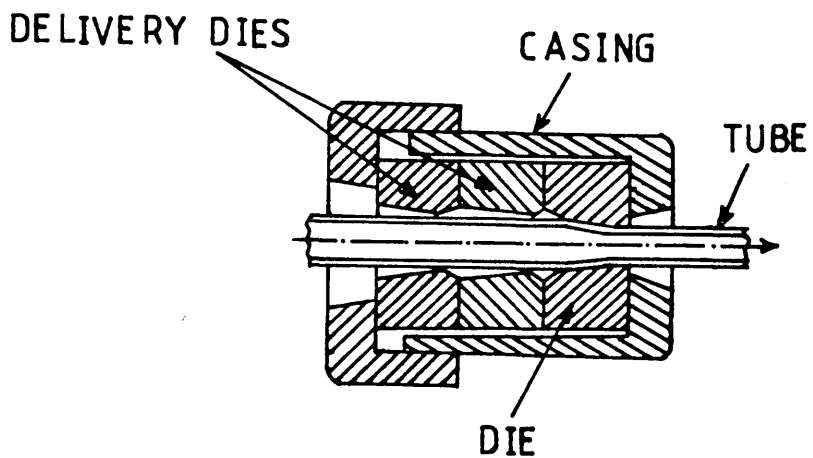


FIG 5 - EXPERIMENTAL DEVICE FOR TUBE-SINKING

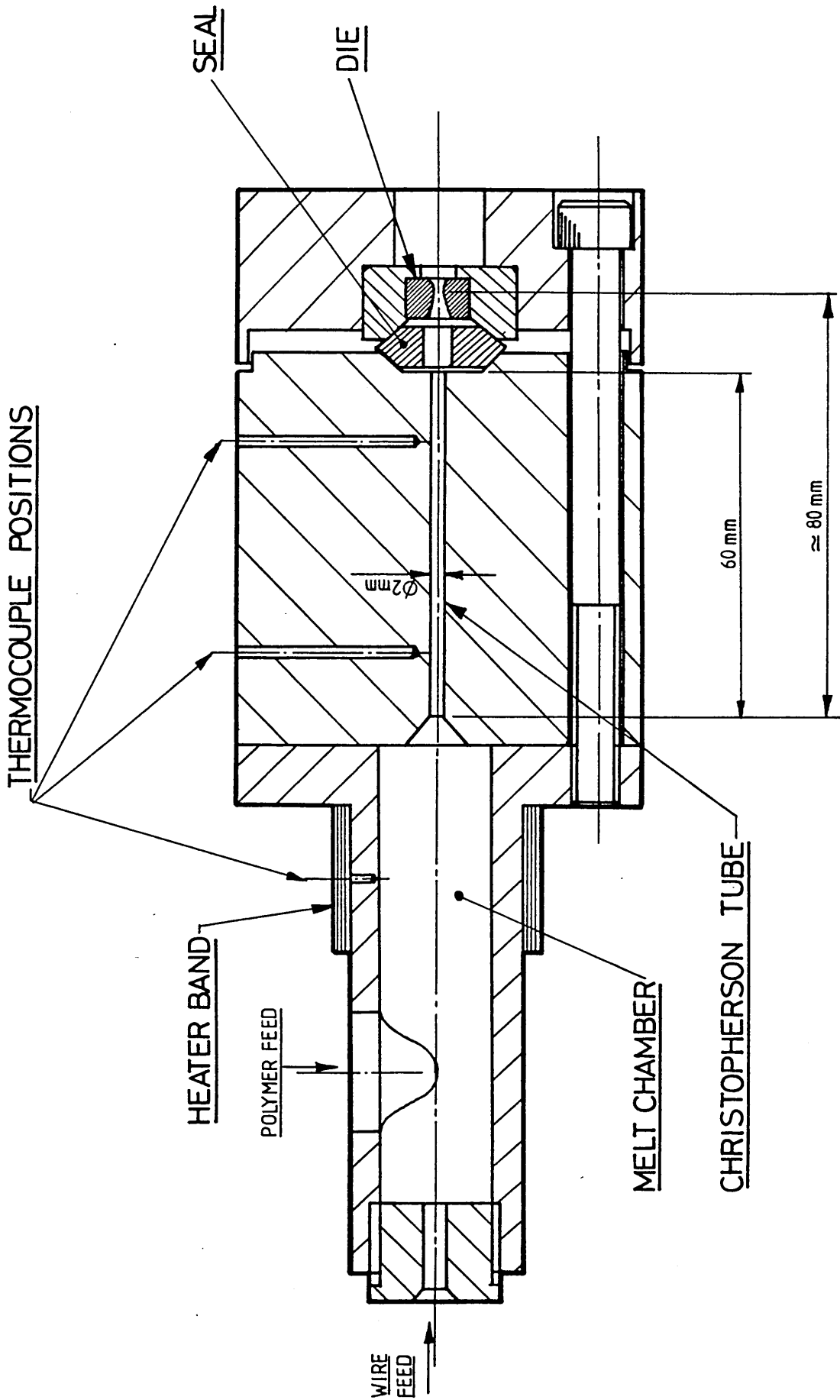


FIG 6 - CHRISTOPHERSON TUBE-DIE ASSEMBLY

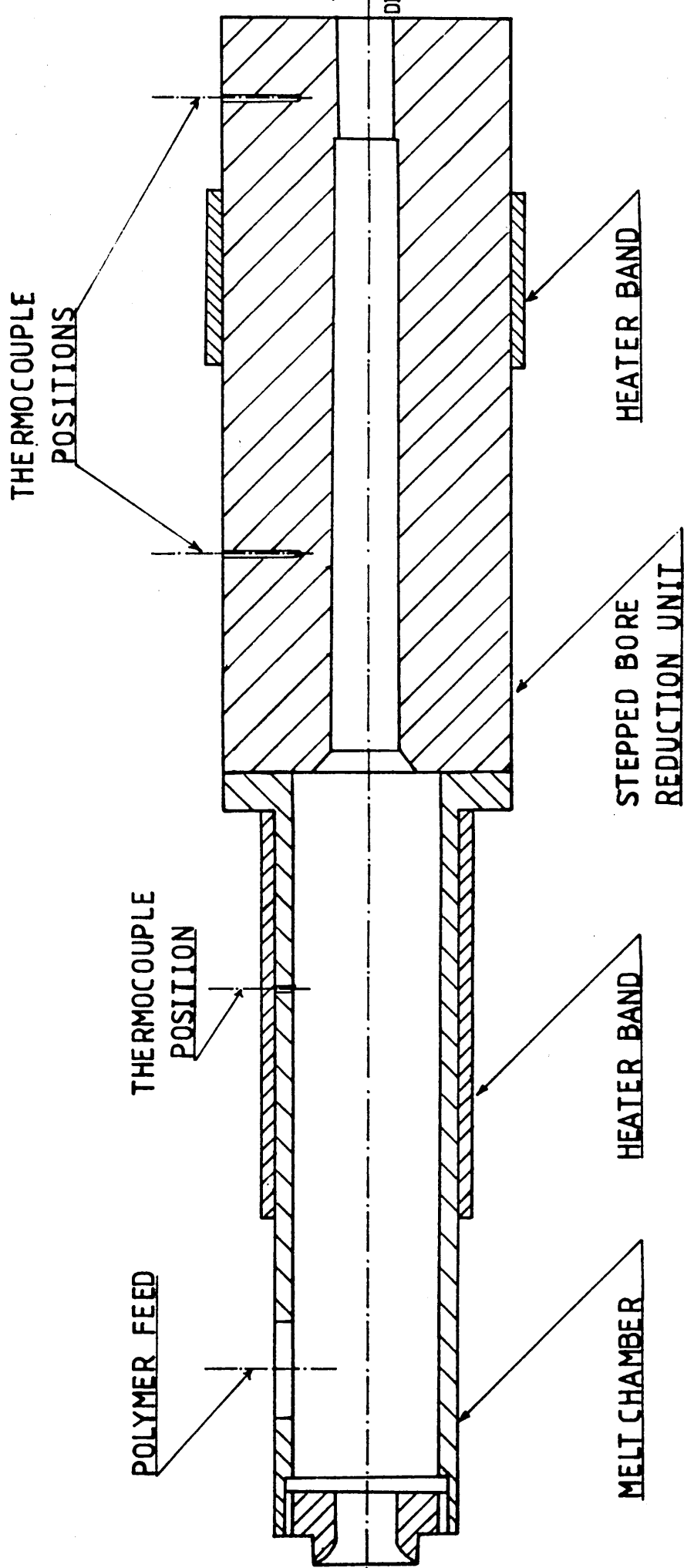


FIG 7 - STEPPED BORE REDUCTION UNIT ASSEMBLY

CHAPTER 2 : RHEOLOGY OF POLYMER MELTS

2.1 Introduction

Rheology can be defined as the science of the flow and deformation of materials. In this work, however, the meaning of rheology will be restricted to polymer melts. Polymers generally consist of very long molecular chains, the bonding between the molecules is cross-linking which is referred to as thermo-setting polymers. The forces of attraction between the molecules is the Van der Waals forces and polymers with this type of bonding are commonly called thermo-plastic polymers. A useful image of the structure is a mass of randomly distributed long strands of sticky wool. When the polymers are heated the inter-molecular forces are weakened so that they become soft and flexible and eventually, at high temperatures, it is a viscous melt. If the stress applied together with a temperature increase is high enough to overcome the Van der Waals forces, a relative molecular motion takes place causing the polymer to flow. The type of flow will depend on the mobility of the molecular chains and the forces holding them together. In thermoplastic polymers long molecules take up a non-random configuration under the stress which would be partially recovered when the stress is removed. The thermosetting polymers show distinct brittle behaviour. The flow characteristics of polymer melts are very different to those of conventional lubricants such as oil. In this chapter, discussions are made of flow characteristics of the polymer melts, which are influenced by many factors in relation to the present work.

2.2 The Effect of Temperature on Viscosity

An increase in the temperature of a molten polymer decreases viscosity by varying extents, dependent upon the type of polymer. Figure (8) shows typical changes in viscosity against the reciprocal

of absolute temperature at zero shear rates. The slope of each line is a measure of the activation energy for each polymer. A temperature increase in polymers with higher activation energies has more deterioration effect on viscosity compared to those of lower activation energies. Polyethylene, which is the most non-polar of the materials shown, has a very low activation energy because the forces between the chains are very weak. Dienes²⁸ suggested that as the temperature increases, the molecular arrangements within the polymer changed more towards a random configuration, making it easier for the polymer to flow at higher temperatures.

Polymers used for the experimental tests in the present study were of low density polyethylene (Alkathene WVG23) of 0.913 specific density, polypropylene (KM61) with specific density of 0.908, Rigidex and polystyrene with specific densities of 0.490 and 1.04 respectively. Figure (9) shows the variation of viscosity with temperature for the four polymers at zero shear rate. These graphs do not represent the complete behaviour since viscosity measurements are affected by pressure, shear rate, temperature etc. and it is necessary to include these effects on viscosity of polymer melts.

2.3 The Effect of Shear Stress and Strain on Viscosity

An outstanding characteristic of polymer melts is their non-Newtonian behaviour whereby the apparent* viscosity decreases as the rate of shear increases. Figures 10 to 13 show the effect of shear rate on viscosity where the influence of temperature may be noticed. These curves were produced by extruding polymer melts (Alkathene WVG23, polypropylene KM61, Rigidex (HDP) and Polystyrene) through an extrusion rheometer at different temperatures. A non-linear relationship is seen to exist between shear stress and

* Conventional way to describe variable nature of viscosity

shear rate. The viscosity of the polymer may be calculated at any known shear rate by measuring the slope of the curve. Newtonian fluid under shear stress condition exhibit linear relationship with shear rate where the slope of the line represents the viscosity of the fluids. Figures 14 to 17 show another way of representing the effect of shear rate on viscosity, where the viscosity may be read off directly from known shear rate values. (For a Newtonian fluid this curve would be a horizontal straight line).

2.3.1 Critical Shear Stress

At low rates of shear, polymer melts flow through capillaries to produce smooth strands. At higher rates of shear, several kinds of flow instabilities can develop in which the surface of the extruded strand becomes rough or non-uniform in cross-section, and the rate of flow is no longer steady but pulsates (20 - 24). The flow irregularities were shown to take the form of spiral, ripple, bamboo, zigzag or helix for different types of polymers. Non-uniformity of the flow for polypropylene KM61 and polystyrene were observed while being extruded at 200°C and 230°C at shear rate of 2.20×10^5 and $1.53 \times 10^5 \text{ s}^{-1}$ respectively as shown in figures 11 and 13. This phenomenon was not observed for Alkathene WVG23 and Rigidex.

The terms melt fracture, elastic turbulence and distortion have been used to describe this effect, however, this phenomenon has been investigated by a number of workers (15 - 19) and there is general agreement on the following points:

- (i) Critical shear stress is independent of die length and diameter.
- (ii) Critical shear stress has values in the region of 0.1 - 1.0 MN/m² for most polymers.

- (iii) Critical shear stress does not vary widely with temperature.
- (iv) A discontinuity in the viscosity - shear stress curves occurred.
- (v) The flow defect always took place when non-Newtonian fluids were involved.
- (vi) The flow defect is often associated with the die inlet.

Several theories have been proposed to account for this defect. Nason²³ noted that in extruding, the product became rough and wavy at higher pressure, and attributed it to a critical Reynolds number. Dillon and Spencer²⁴ concluded that the irregularity was due to buckling of the material on emerging from the orifice. This was due to a larger amount of strain recovery in the outer layers. Severs²⁵ observed this defect for a variety of polymers, and noted that, for a given polymer and a given orifice, the critical shear stress was the same for different temperatures. Tordella²⁶, after a detailed examination of the extruded polymer, concluded that the phenomenon was due to a fracture of the melt before the entrance of the tube. He believed that shearing occurred at the edge of the melt on entering the tube, and in the case of spiral flow, it made its way circumferentially around the piece as it emerged. Melt fracture generally is the result of tensile stresses rather than shear stress. Tensile stresses result when the size of the flow channel goes from a larger to a smaller cross section (Nielsen¹⁷). Westover³⁴ carried out a study of polymer slip on an ultra high molecular weight linear polyethylene incorporating hydrostatic pressure. Two interesting observations were made:

- (i) Flow rate above the critical shear stress increased rather than decreasing as for most of the polymers.

- (ii) The critical shear stress occurred at lower shear rate as the hydrostatic pressure upon the melt increased.

Westover concluded that the basic concepts of maximum shear stress, apparent shear rate and viscosity are invalid after slip occurs and that the non-Newtonian equation becomes inapplicable.

2.3.2 Shark-Skin

Shark-skin is another flow defect which occurs at shear stresses below the critical value and Figure (11) clearly shows these differences for polypropylene polymers. Although this defect is also a visual imperfection of the extrudate it is usually differentiated from melt fracture because the defects are perpendicular to the flow direction rather than helical or irregular. A schematic representation of the shark-skin mechanism is shown in Fig 18 (after Brydson). The shark-skin effect has usually been distinguished from melt fracture for the following reasons:

- (i) Shark skin has a perpendicular distortion, whereas melt fracture gives helical pattern.
- (ii) Shark-skin can occur at lower extrusion rates than those for melt fracture.
- (iii) Shark-skin appears to be unaffected by the geometry of the die (15, 19).

This defect is a function of the linear output rate rather than the shear rate or die dimensions. The most probable mechanism of shark skin relates to the velocity of skin layers of the melt inside and outside the die (22, 27). Inside the die the skin layers are almost stationary whereas when the extrudate emerges from the die there must be a rapid acceleration of the skin layers to bring the skin velocity up to that of the rest of the extrudate. This sets up tensile stresses in the melt which can be sufficient to cause surface defects.

2.4 The Effect of Pressure on Viscosity

Several theories suggest that the viscosity of a liquid polymer is determined by its free volume (29-34). The free volume of a liquid polymer is defined in various ways, but a common definition is the difference between the actual volume and a volume in which such close packing of the molecules occurs that no motion can take place. The greater the free volume the easier it is for flow to take place. Free volume increases with temperature because of thermal expansion. However, the most direct influence on free volume should be of the pressure. An increase in hydrostatic pressure decreases free volume and increases the viscosity of a liquid. Viscosity, by definition, is the internal resistance to shearing stress due to inter-molecular forces of attraction. It was thought that when molecular attraction is encouraged, the apparent viscosity of the polymer, which is one of the most important properties of these materials, may be increased. However, the effect of hydrostatic pressure on the apparent viscosity and other flow properties of polymer melts is not as well understood as the effects of temperature and shear rate. Westover³⁴ has described a double piston apparatus for measuring viscosity as a function of pressure of up to 25000 psi. He found the viscosity of polystyrene to increase by a factor of over a hundred times and the viscosity of polyethylene to increase by a factor of five at a constant rate of shear as the pressure was increased. Maxwell and Jung³⁵ found that the viscosity of polystyrene increased by a factor of 135 when the pressure was increased from zero to 18000 psi at 196°C. The viscosity of polyethylene increased by 14 times in the same pressure range at 149°C. Cogswell³⁶ suggested that the effect of an increase in pressure may be likened to that due to a drop in temperature. He observed that

for low density polyethylene, an increase in pressure of 100 MN/m^2 had the same effect on viscosity as that due to a drop in temperature of 53°C within the melt range.

It had been noted that at very high pressure (above 150 MN/m^2) the melt tended to recrystallise and in consequence, the melt acted like a solid plug.³⁵ For this reason, pressure-viscosity measurements are often conducted at relatively high temperatures.

Most of the experimental work carried out by Westover³⁷ was on a branched 0.92 density polyethylene with pressure varying from 14 MN/m^2 to 170 MN/m^2 . Since the work carried out by Westover was found to be the most comprehensive, these have been used to determine the pressure coefficient of viscosity in the present work. Figure(19) shows the effect of pressure on shear stress - shear rate curves and Figure(20) shows how the shear rate affects the influence of pressure on viscosity.

2.5 The Effects of the Polymer Flow Characteristics.

In the present work polymer melt is subjected to very high shear rates and pressures, much greater than those capable of being investigated in any extrusion rheometer. Crampton¹¹ concluded that the decrease in coating thickness was due to the presence of a critical shear stress at low shear rates. However, it is also believed that, the poor performance of the units at higher drawing speeds is related to a combination of factors such as shear rate, melt flow instability, partial crystallization, compressibility etc. The high pressures generated are believed to have the effect of increasing the melt viscosity in the unit. Temperature was maintained at a steady value when the tests were conducted, minimising the effects inherent with changing temperature. However, more investigation is needed to understand these effects fully.

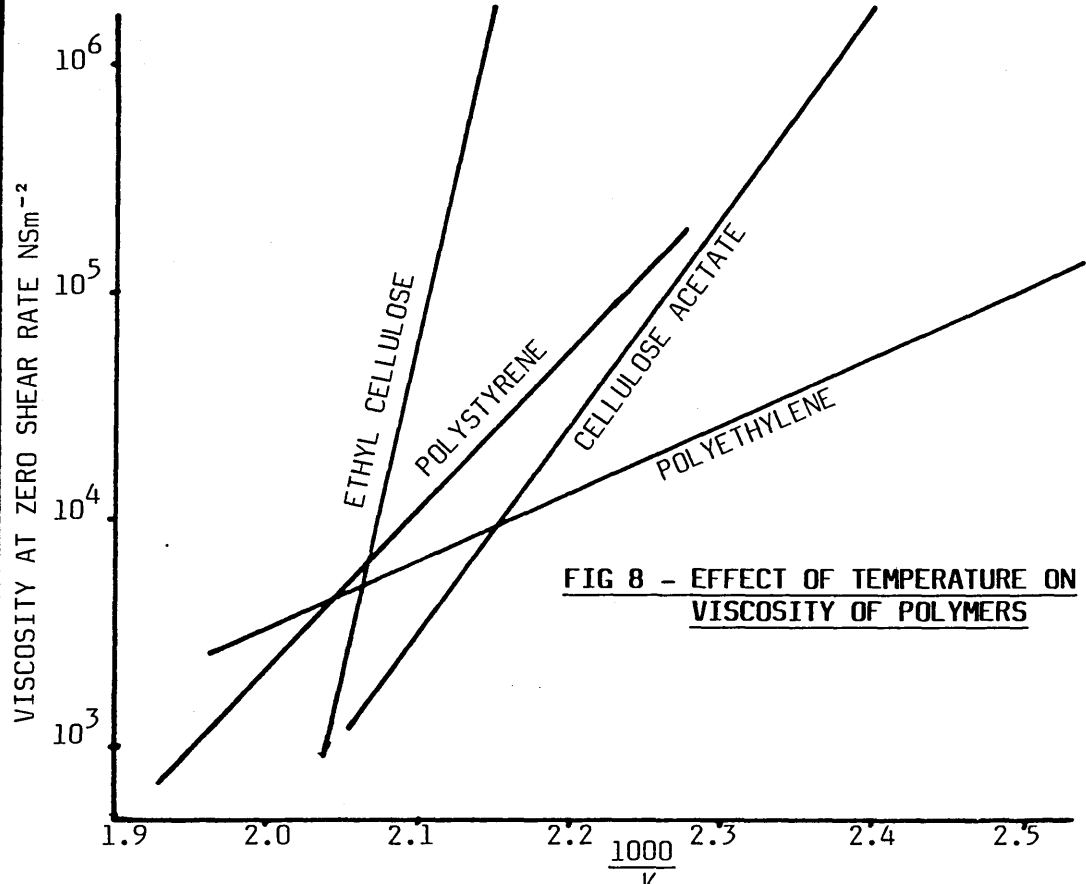
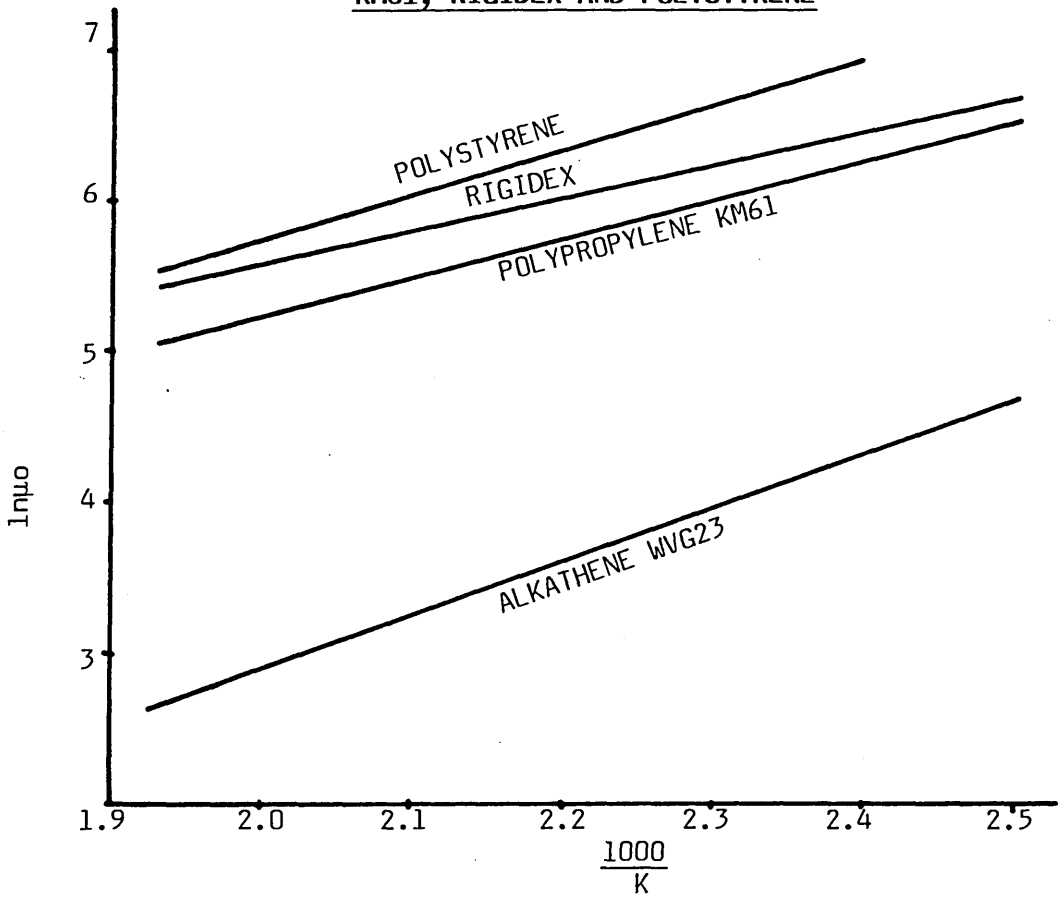


FIG 9 - EFFECT OF TEMPERATURE ON VISCOSITY OF WVG23, KM61, RIGIDEX AND POLYSTYRENE



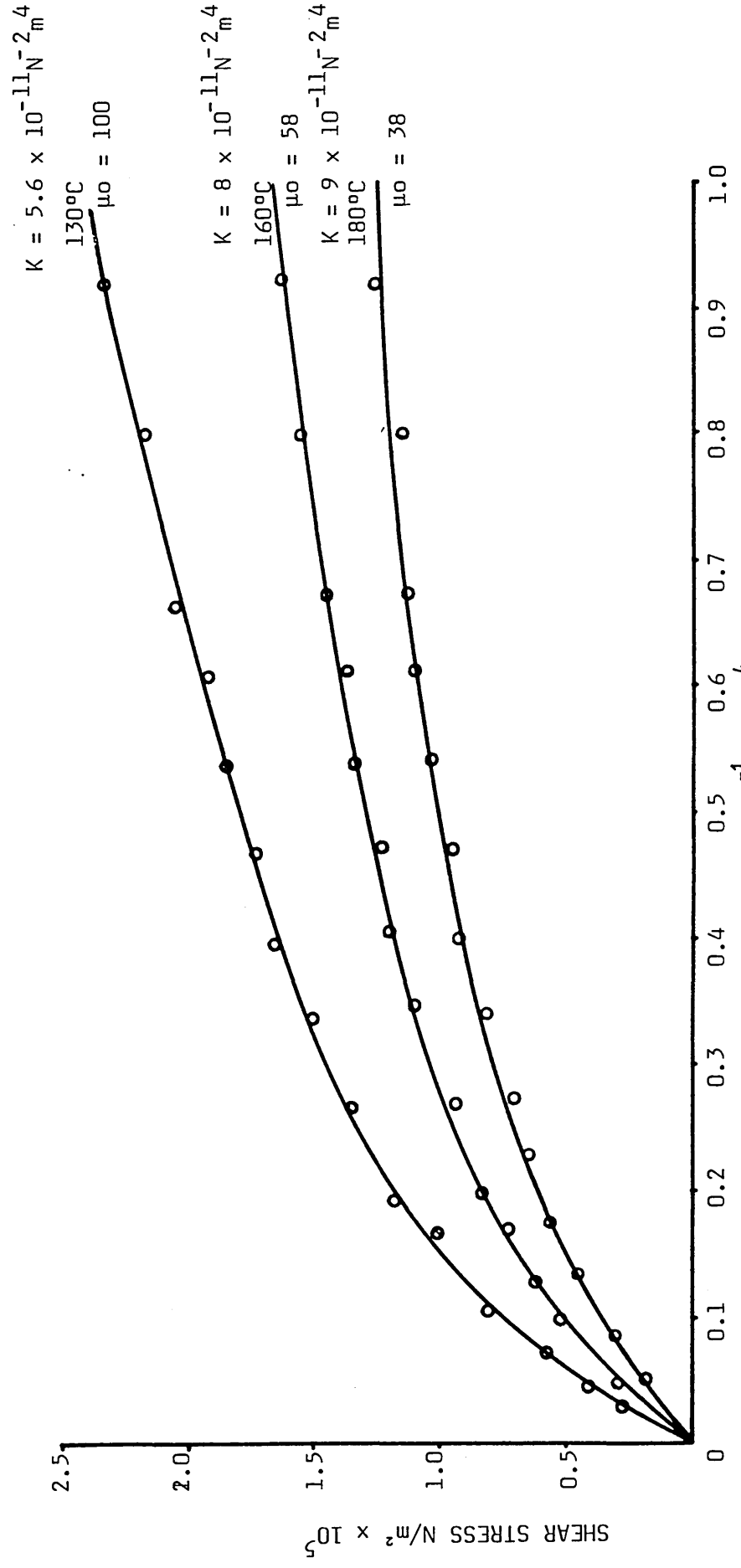


FIG 10 - FLOW CURVES FOR ALKATHENE WVG23

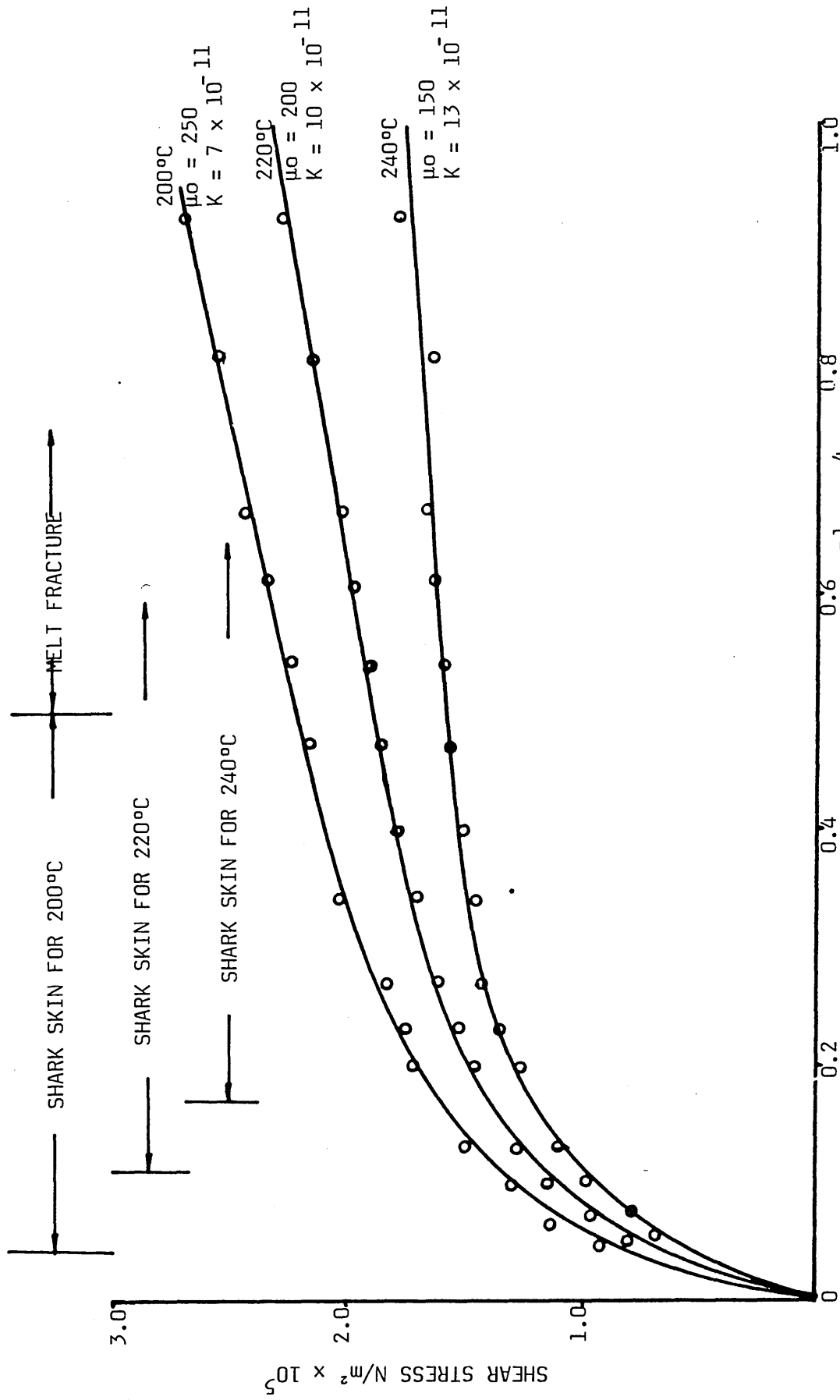


FIG 11 - FLOW CURVES FOR POLYPROPYLENE KM61

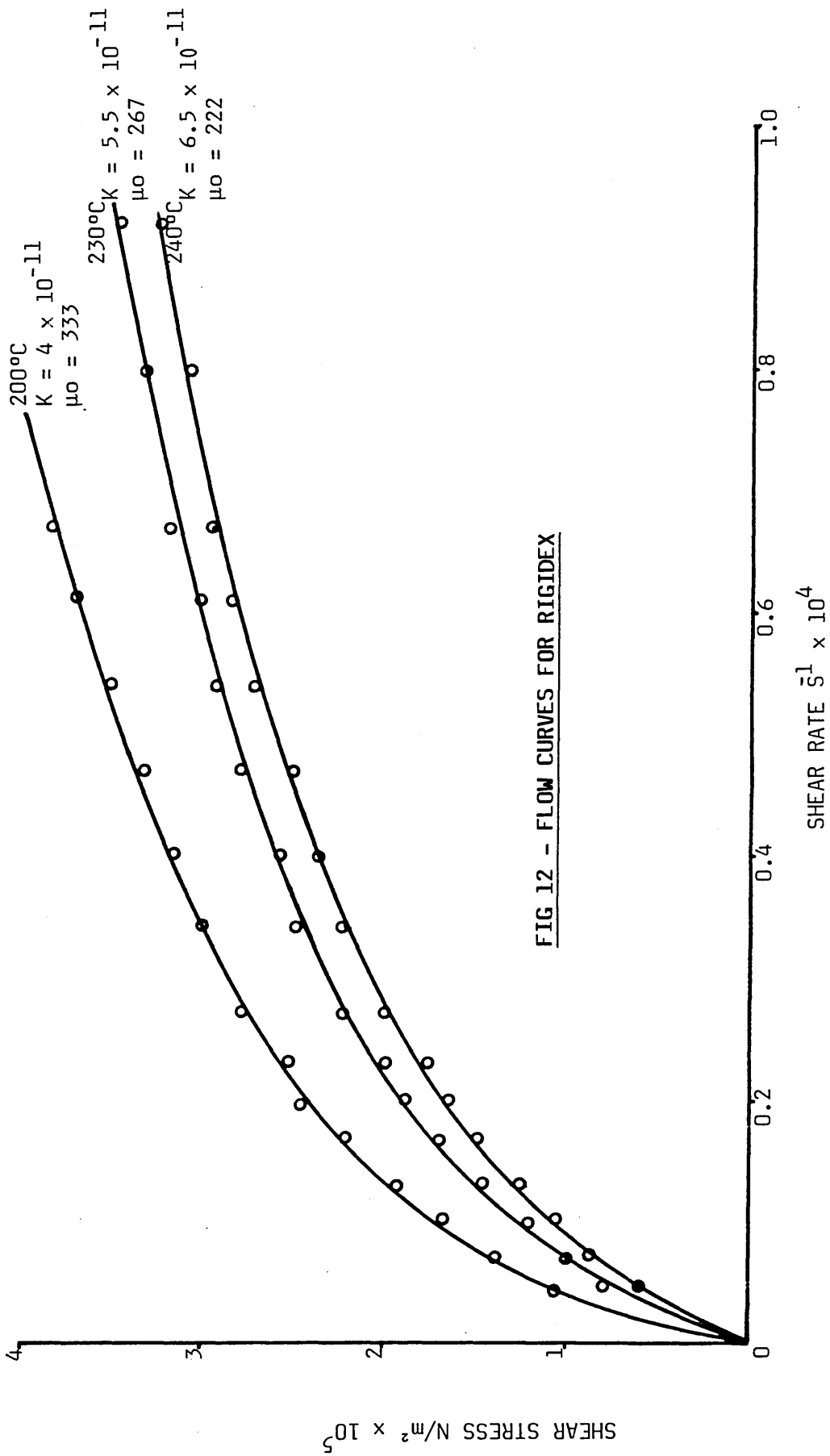


FIG 12 - FLOW CURVES FOR RIGIDEX

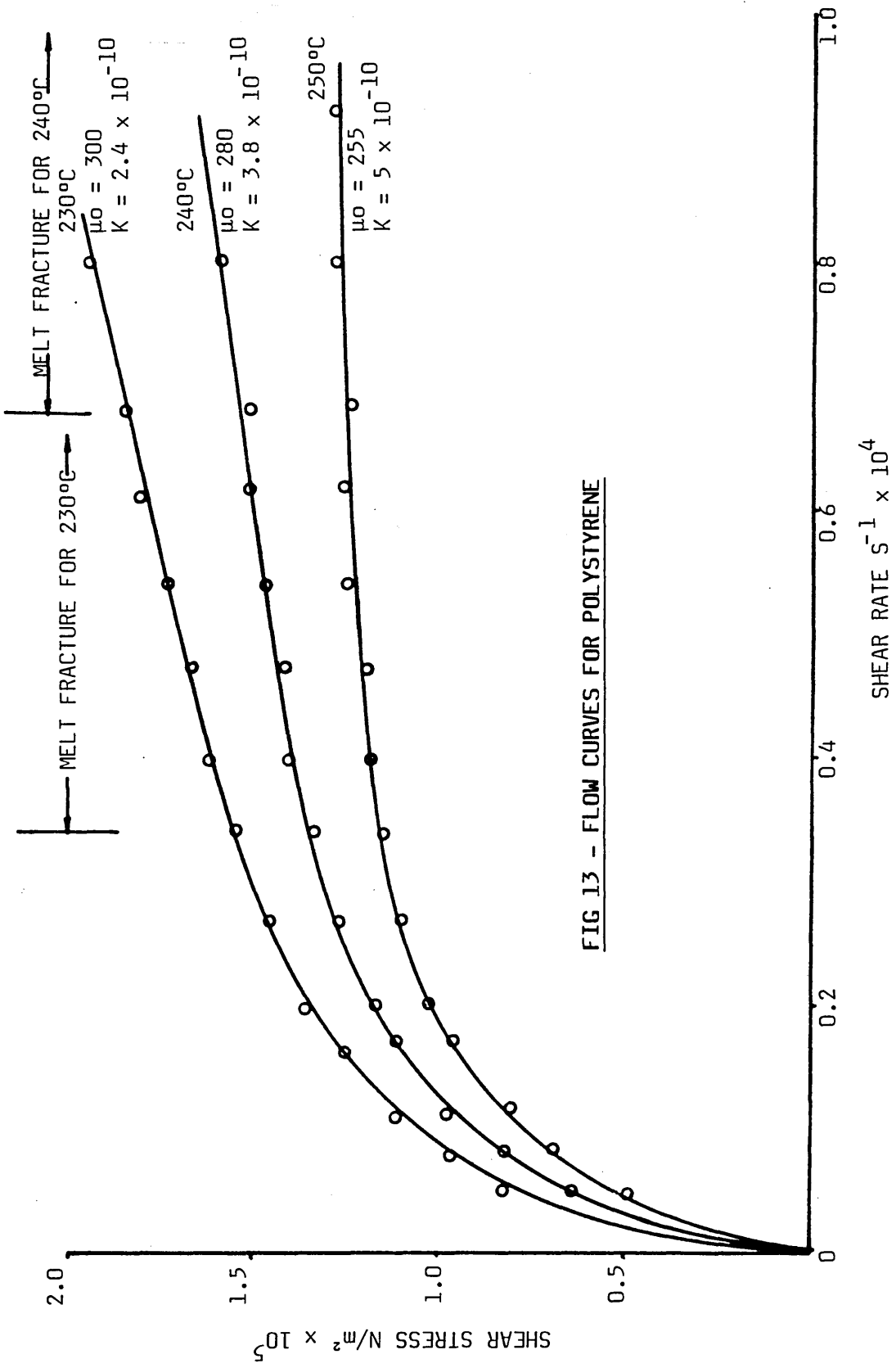


FIG 13 - FLOW CURVES FOR POLYSTYRENE

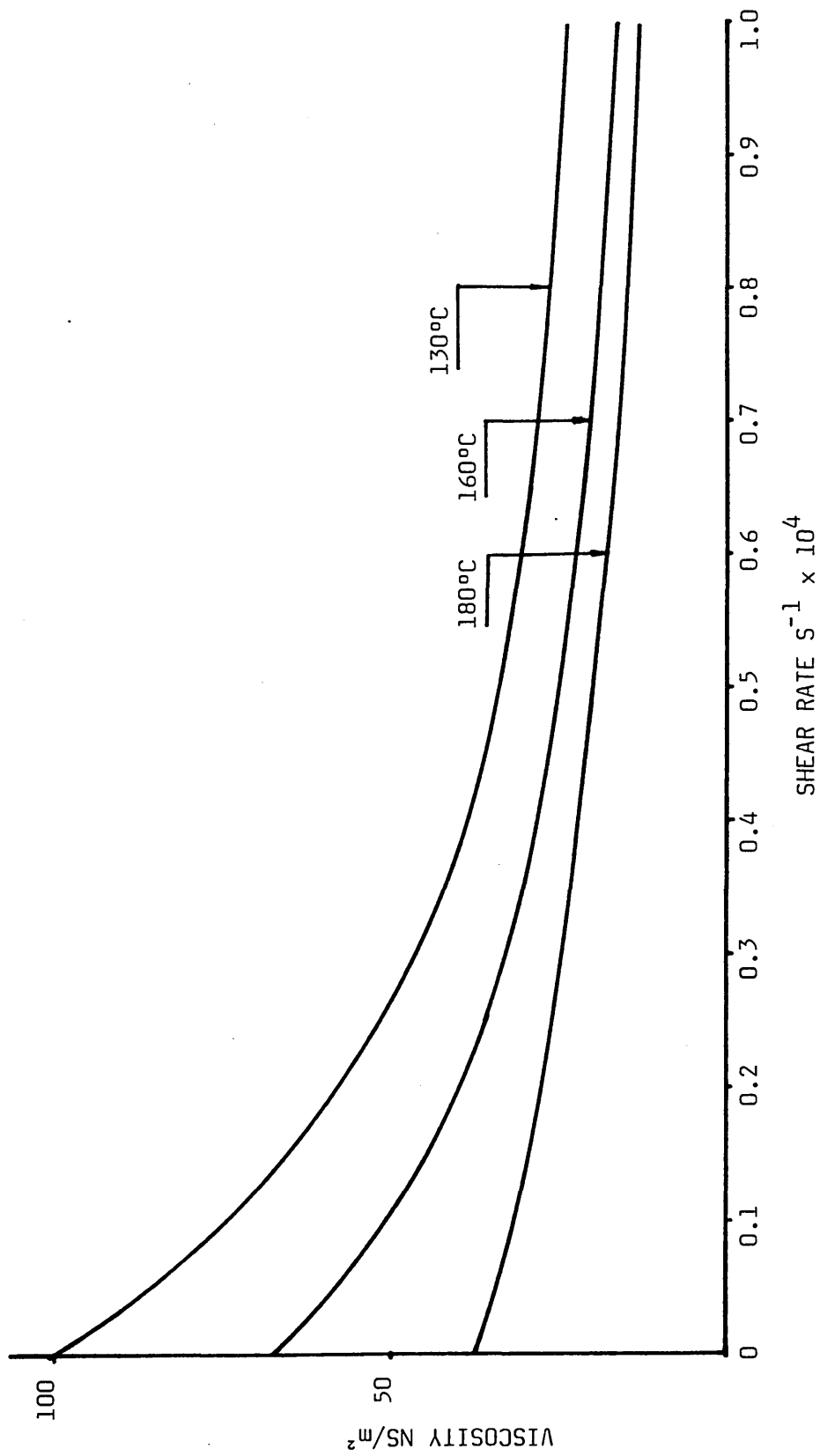


FIG 14 - EFFECT OF SHEAR RATE ON VISCOSITY OF ALKATHENE WVG23

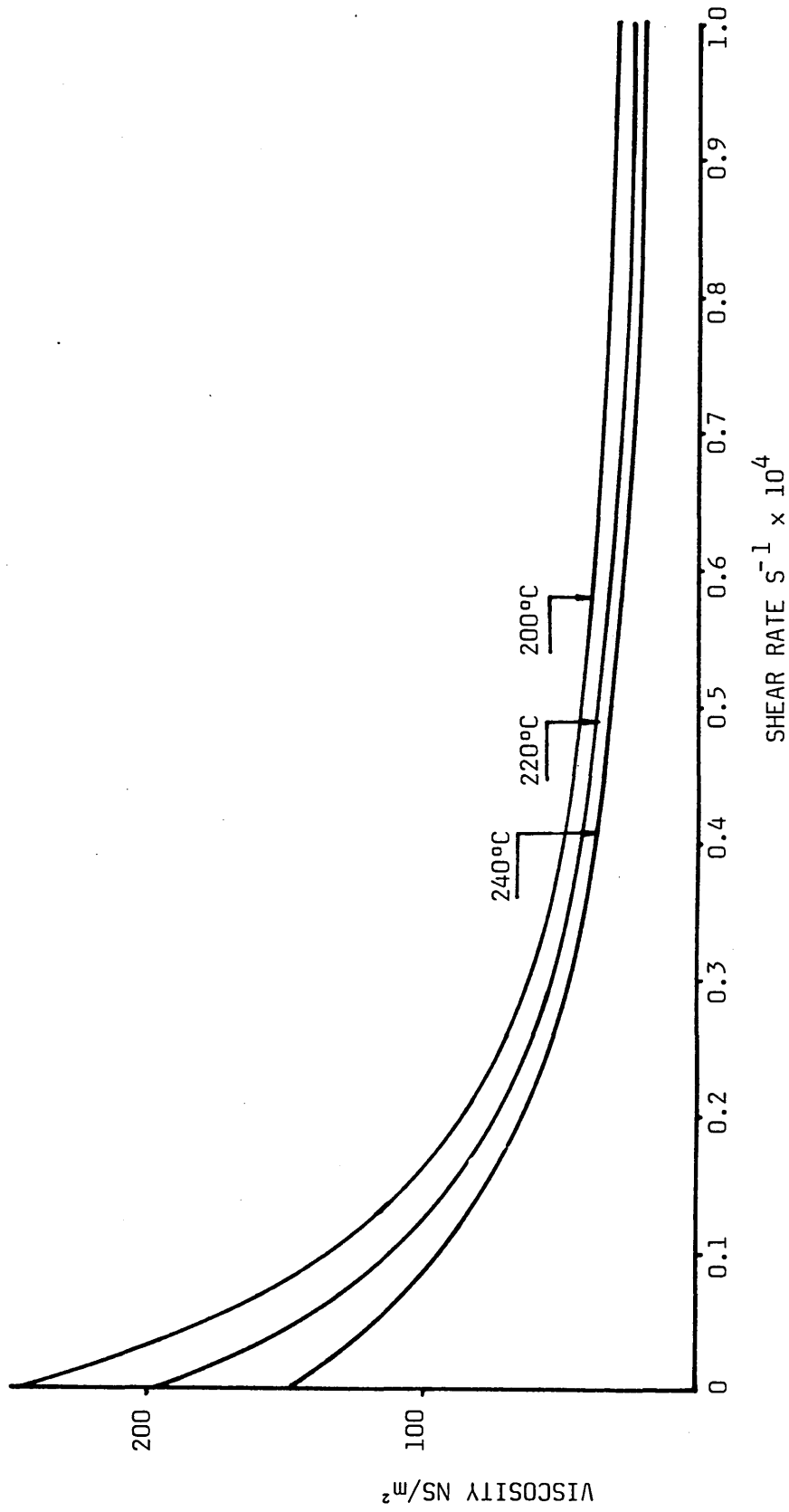
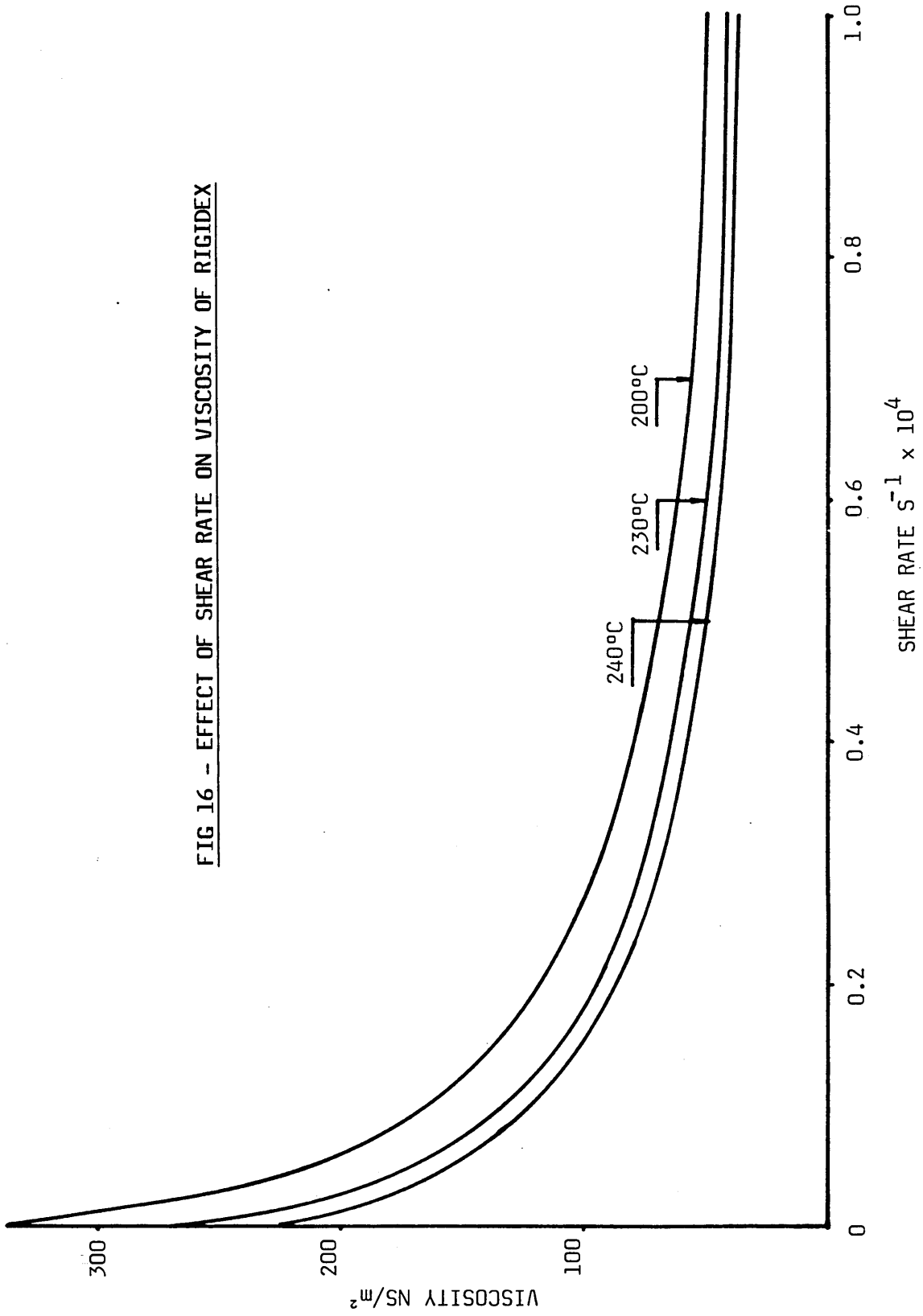
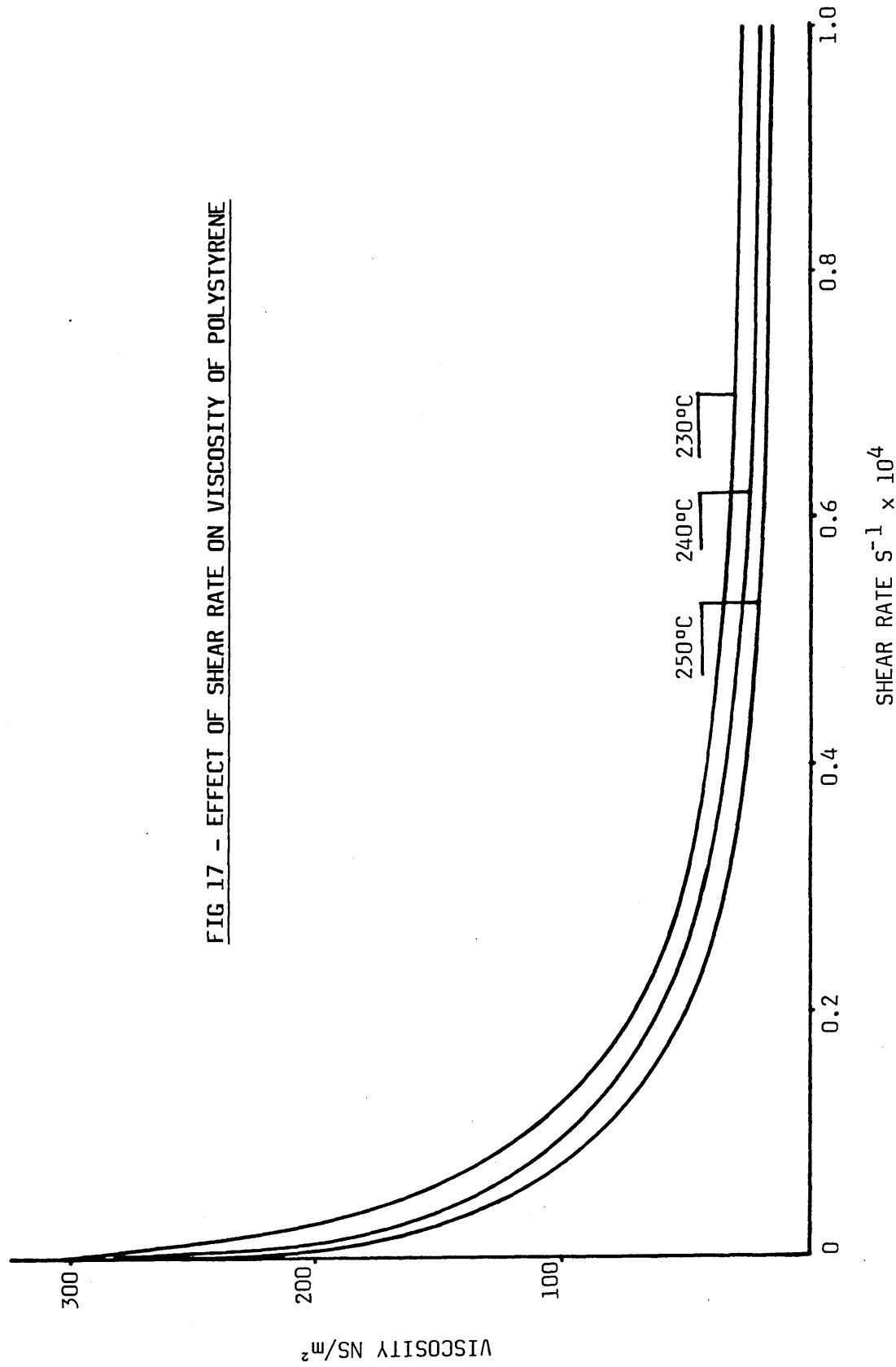


FIG 15 - EFFECT OF SHEAR RATE ON VISCOSITY OF POLYPROPYLENE KM61

FIG 16 - EFFECT OF SHEAR RATE ON VISCOSITY OF RIGIDEX





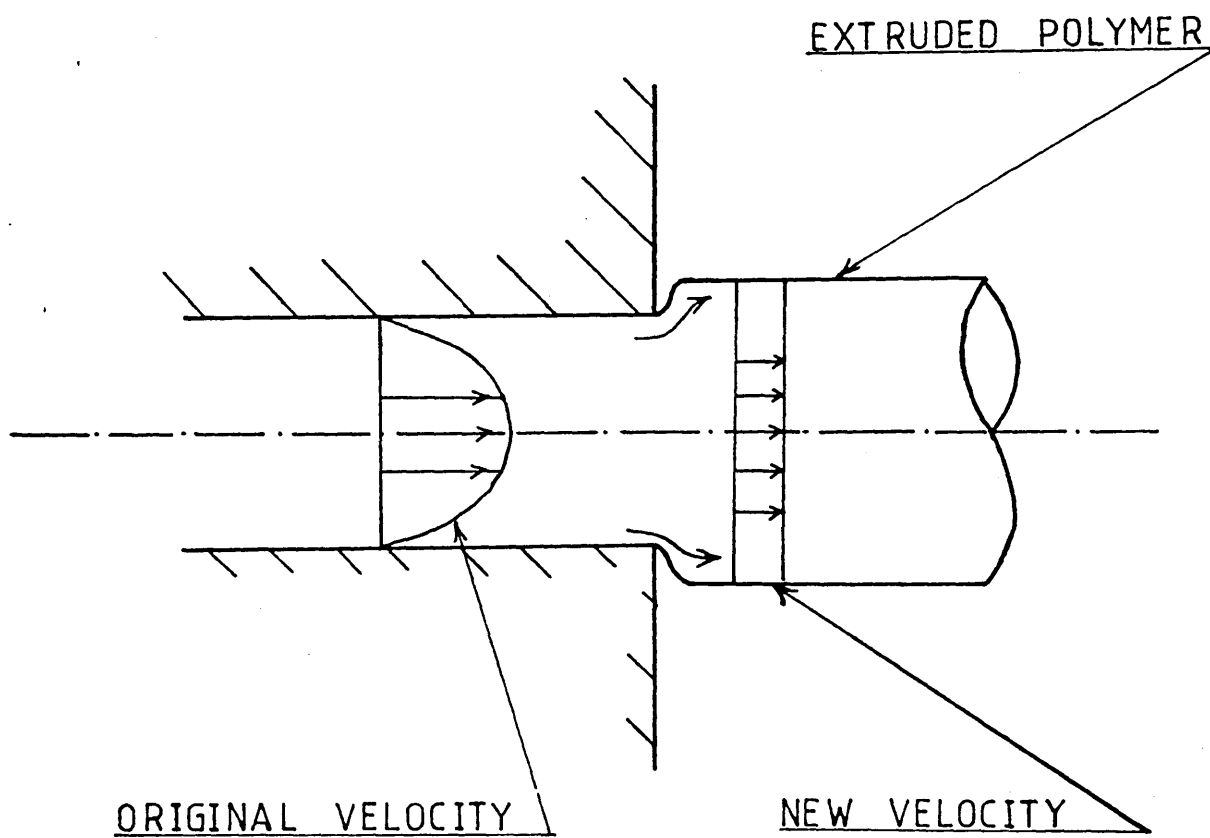


FIG 18 - A POSSIBLE MECHANISM OF SHARKSKIN

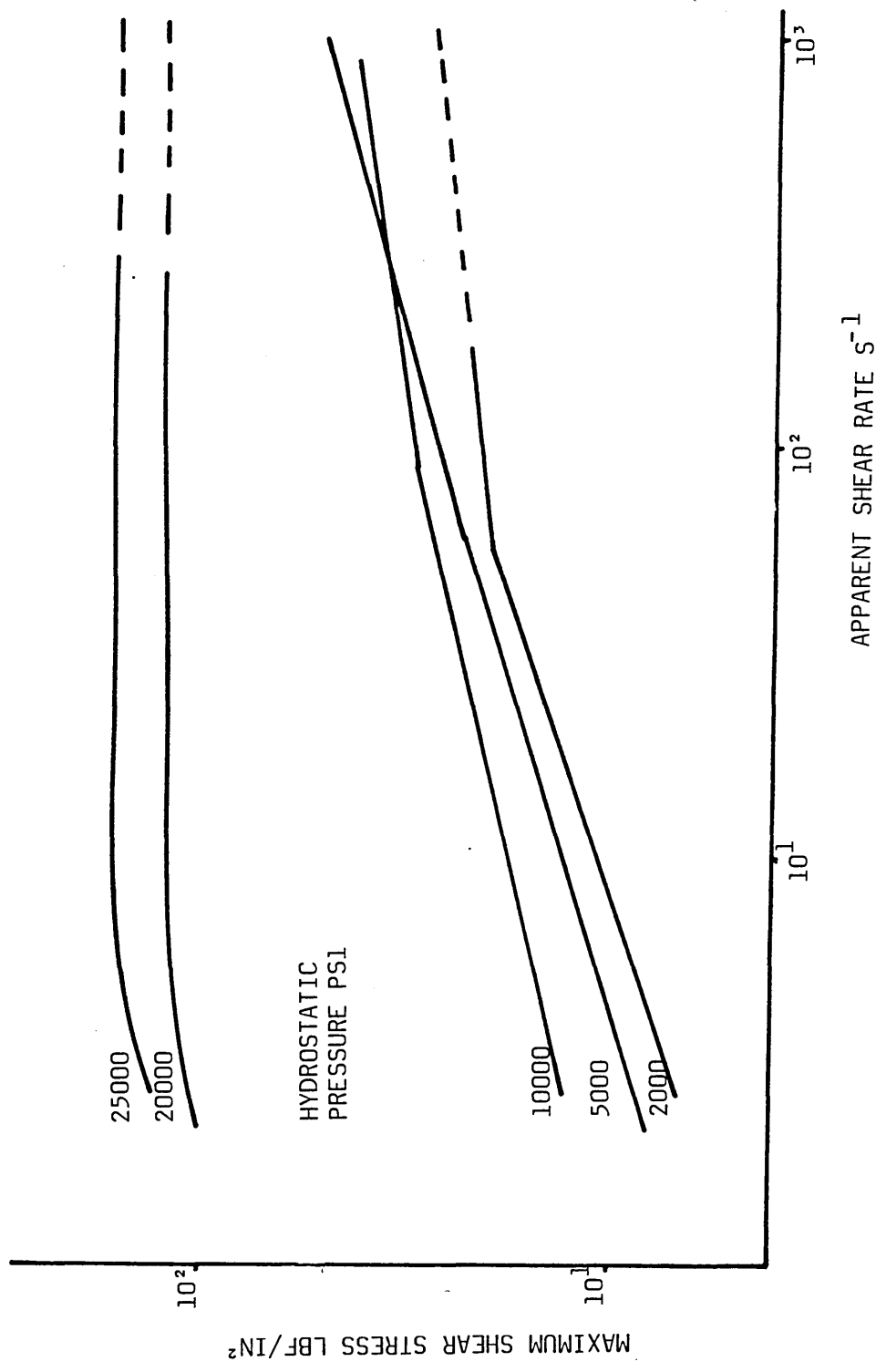


FIG 19 - FLOW CURVES FOR 0.92 POLYETHYLENE AT 130°C
AFTER WESTOVER (23)

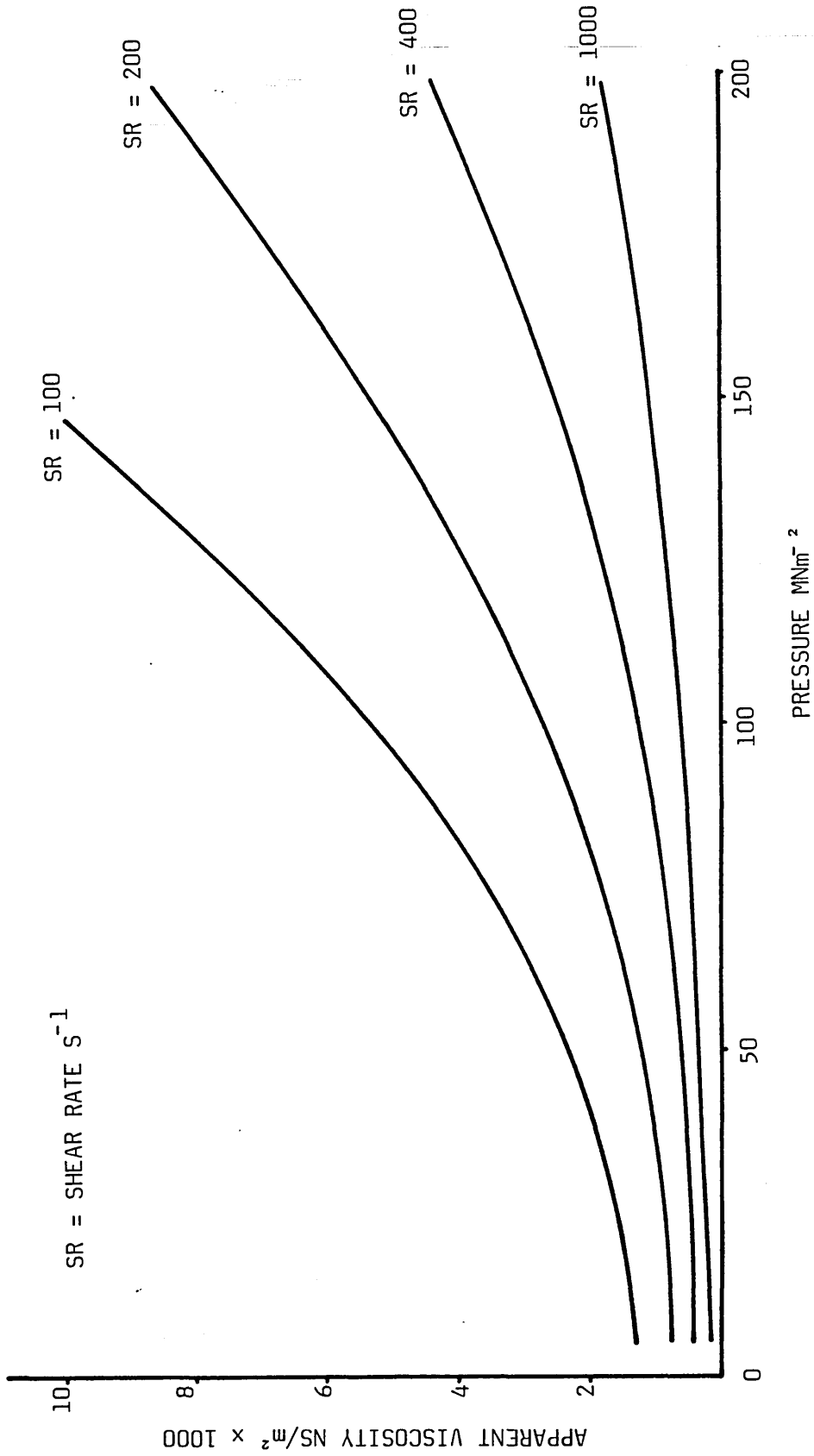


FIG 20 - VISCOSITY VERSUS PRESSURE FOR DIFFERENT SHEAR RATES (0.92 POLYETHYLENE 130°C)

CHAPTER 3 : EXPERIMENTAL EQUIPMENT AND MATERIALS

3.1 General Description

Drawing tests were carried out on a chain-type draw bench made by Marshall Richards. The schematic diagram and general view of the draw bench are shown in Fig(21) and Plate 1 respectively. The total length of the draw bench is approximately 12 feet, and the maximum length of the tube which may be drawn is 8 feet. The machine is driven by means of a high capacity electric motor made by Crofts (11 kW/415 v/3 phase/50 cycles) with integral speed reduction gear unit made by Ronald Power Transmission (GM6T ratio 47.08). The output speed of the unit being variable between 0.1 to 0.5 meter per second.

The experimental rig consists of a dog clamp welded to a trolley which can move freely between rail guides. The die-less reduction unit (DRU) is bolted to a plate which rests against a load cell block during drawing. The plate in turn is hinged onto the machine. The drawing load is then read from a load indicator which is connected to the strain gauge load cell. The melting chamber and the DRU are held together with four socket cap screws. At the other end of the drawing bench an emergency ramp is bolted to the mainframe which disengages the dog clamp from the chain; thus stopping the drawing process.

The polymer was heated by means of an electric heater band and the temperature was controlled thermostatically within $\pm 4^{\circ}\text{C}$ of the pre-set temperature using a temperature regulator. The temperature was monitored continuously by means of thermocouples. Three piezo-electric quartz pressure transducers (Kistler type 6203) were mounted on the die-less reduction unit, which enabled the pressure variation along the unit to be measured. The output from the

transducers was fed into a u-v recorder via charge amplifiers. The tube was supported by stands of adjustable height with freely rotating rollers, so that a horizontal feed to the unit could be achieved. The schematic diagram is shown in Fig(22) and also plate 4 shows the supporting arrangement for tube.

The drawing speed was controlled by means of the variable speed motor which facilitated drawing at speeds ranging from 0.1 to 0.5 meter per second.

3.2 Instrumentation of the Experimental Equipment

A number of equipments and devices were used to monitor, record and control various parameters during the tests on die-less tube sinking. These include load cell, load indicator, pressure transducers, temperature controllers, heater bands, thermo-couples and u-v recorder. Details of each are given below.

3.2.1 Load Cell

Basically the load cell consists of a steel billet to which are bonded four resistance strain gauges. When a load is applied to the load cell the change in the dimension causes the bonded strain gauges to change their lengths and hence the resistance. This change in resistance is directly proportional to the load applied. The maximum load capacity of the load cell is 40 kN. The load cell is shown in plate 5.

3.2.2 Load Indicator

The Elliott load indicator (type BCF/2) is an electronic instrument designed to provide an accurate indication of load. (The load indicator is shown in plate 2). Operating in conjunction with the resistance strain gauge load cell located at the sensing point, the installation forms a closed loop circuit incorporating a self-balancing load to reference error signal system. The load is

indicated by means of a mechanical pointer and a circular graduated scale. The pointer movement is linear and proportional to the changes in the load applied to the load cell. The maximum load capacity of the indicator is 40 kN.

3.2.3 Pressure Transducers

High pressure piezo-electric quartz transducers (Kistler type 6203) were used for these experiments to measure the pressure in the die-less reduction unit. The maximum pressure that these transducers could measure is 5000 bar and the working temperature at which these pressure transducers may be used is up to 240°C. The schematic diagram of the arrangement for pressure measurement is shown in Fig(23) and also in plate 2.

3.2.4 Temperature controllers

An electronic ON-OFF temperature controller relay (type K) was used for these experiments to control the preset temperature. This temperature controller is mounted in a 48 x 48 DIN standard case. The unit is designed to be used with nickel-chrome/nickel-aluminium type K thermo-couples to monitor temperature. A relay changeover contact within the unit operates at a predetermined temperature previously set by a potentiometer knob mounted on the face of the unit. A graduated scale marked 0-400°C indicates the set temperature. Included on the unit are two LEDs, indicating supply and relay status. The unit is failsafe, protected against thermo-couple breaks, ie if the thermo-couple goes open circuit, the relay will automatically return to the off condition. The temperature controllers are shown in plate 3.

3.2.5 Heater bands

Watlow heater bands were used for these tests. The dimensional details are given below;

Heater Bands for DRU and Hopper

Type	I.D (mm)	Width (mm)	Volts	Watts
A	63.85	60.65	240	250

Heater Bands for Melt Chamber

Type	I.D (mm)	Width (mm)	Volts	Watts
A	38.31	76.62	240	350

The heater bands are shown in plate 5.

3.2.6 Thermo-Couples

Incorel sheathed mineral insulated, 1.5mm O.D. thermo-couples were used for these experiments to monitor the temperature continuously. Their operating temperature range is -200 to +1100°C and the response time is 0.3 sec. These thermo-couples are shown in plate 2.

3.2.7 U-V Recorder

The output from the pressure transducers was fed into an ultra-violet (u-v) recorder via charge amplifiers. These u-v recorders are made by Southern Instruments (type M.1300) and the charge amplifiers are supplied by Fylde Electronic Laboratories (type FE-128-CA). Plate 3 shows the arrangements for the u-v recorder and charge amplifiers.

3.3 Modification to the Experimental Draw-Bench

Initial exploratory drawing tests were carried out using an existing draw-bench with a fixed speed electric motor which was found to be unsuitable for the speed range and load requirements of this work. Therefore, a higher capacity electric motor (11 kW/ 415 V/3 phase/50 cycles) with integral variable speed reduction gear unit was commissioned (GM6T ratio 47.08). The output speed being variable between 0.1 to 0.5 meter per second.

3.4 Design of the Die-Less Reduction Unit

The principal aim of the present investigation has been to investigate the feasibility of using a stepped bore die-less reduction unit for sinking tubes; thus avoiding metal to metal contact and hence die wear and the need for the swaged down leading end.

Experimental work carried out by Hashmi et al¹⁴ showed that under special geometrical configuration effective reduction of a wire should be possible using a polymer melt in conjunction with a stepped bore die-less tubular unit. Thus, cylindrical die-less reduction units geometrically similar to those used for wire drawing were designed and constructed. The combined melt chamber and the stepped bore reduction unit was made according to the following specifications which were finalised after some initial tests.

1. The Unit

The stepped bore reduction unit was made from mild steel. Initially a solid piece of mild steel of about 200mm long and 75mm diameter was machined down to the required external dimensions. Then a centrally located hole was drilled through the cylinder. However, in order to produce a hole with good quality finish and accuracy reamers were used for final machining. The stepped bore was obtained by counter drilling the initially drilled hole through part of its length.

The die-less reduction unit was bolted to a plate with four socket cap screws. The dimensions of the plate and screw holes are shown in Figs(26)and(24)respectively. The dimensions of the unit are as follows:

Total length = 190mm
Inlet length, L_1 = 160mm
Outlet length, L_2 = 30mm
Inlet diameter = 13.62mm
Outlet diameter = 13.54mm

(See also Fig 24)

Three pressure transducers were mounted on the die-less reduction unit to measure the pressures generated in the unit. Two thermo-couples were used to maintain the temperature of the unit. The dimensions and the positions of holes for the pressure transducers and thermo-couples are shown in Fig(24)

2. Melt Chamber

The melt chamber was also made from mild steel bar which was machined down to the size on a lathe machine and then bored out to form the cavity. An outlet hole was also machined for attaching the hopper.

The melt chamber and the die-less reduction unit were held together with four socket cap screws. The dimensions of the screw holes are shown in Fig(24). The dimensional details of the melt chamber are shown in Fig(25).

The heater bands were used for heating the polymer and the unit. Each heater band was about 38.31mm inside diameter and 76.62mm width, they covered about 153.24mm distance from the hopper side of the melt chamber. The positioning of the heater bands are shown in plate 4 . The hopper for feeding the polymer was made from mild steel bar material. The dimensional details of the hopper are shown in Fig(25).

3.5 Determination of the Stress-Strain Characteristics of the Tube Materials.

The stress-strain characteristics of the tube materials were determined using a Mayes testing machine. Small ring shaped samples with $\frac{h}{t} \approx 1$ were cut from the tube and subjected to uniaxial compression. The contact surfaces between the specimen and the compression plates were lubricated using graphite in order to minimise the frictional effects and to obtain homogenous deformation. Typical original and deformed shapes of the specimens are shown in the photographs in Figs 27(a) and (b) for copper and aluminium respectively. Readings of load and compression were taken at close intervals throughout the tests. These readings were converted to true stress and natural strain values, knowing the initial height and diameter of the specimen and assuming constant volume. No visible barrelling effect was apparent and was ignored.

$$\text{True stress } \sigma = \frac{L}{A}$$
$$\text{Natural strain } \epsilon = \ln\left(\frac{h_0}{h}\right)$$

where,

L = Load

A = Current area

h₀ = Original height

h = Current height

The compression tests for copper and aluminium produced the curves as shown in Figs (28) and (29) respectively. The stress-strain characteristics were assumed to take the form;

$$Y = Y_0 + K_0 \epsilon^n$$

where,

Y₀ = initial yield stress N/m²

K₀ = strain hardening constant N/m²

n = strain hardening index

ϵ = natural strain

Using the experimental results, the above parameters were evaluated, by curve fitting, for each tube material, these being;

for copper tube,

$$\gamma = (50 \times 10^6) + (700 \times 10^6) \epsilon^{0.18} \text{ N/m}^2$$

for aluminium tube,

$$\gamma = (40 \times 10^6) + (640 \times 10^6) \epsilon^{0.26} \text{ N/m}^2$$

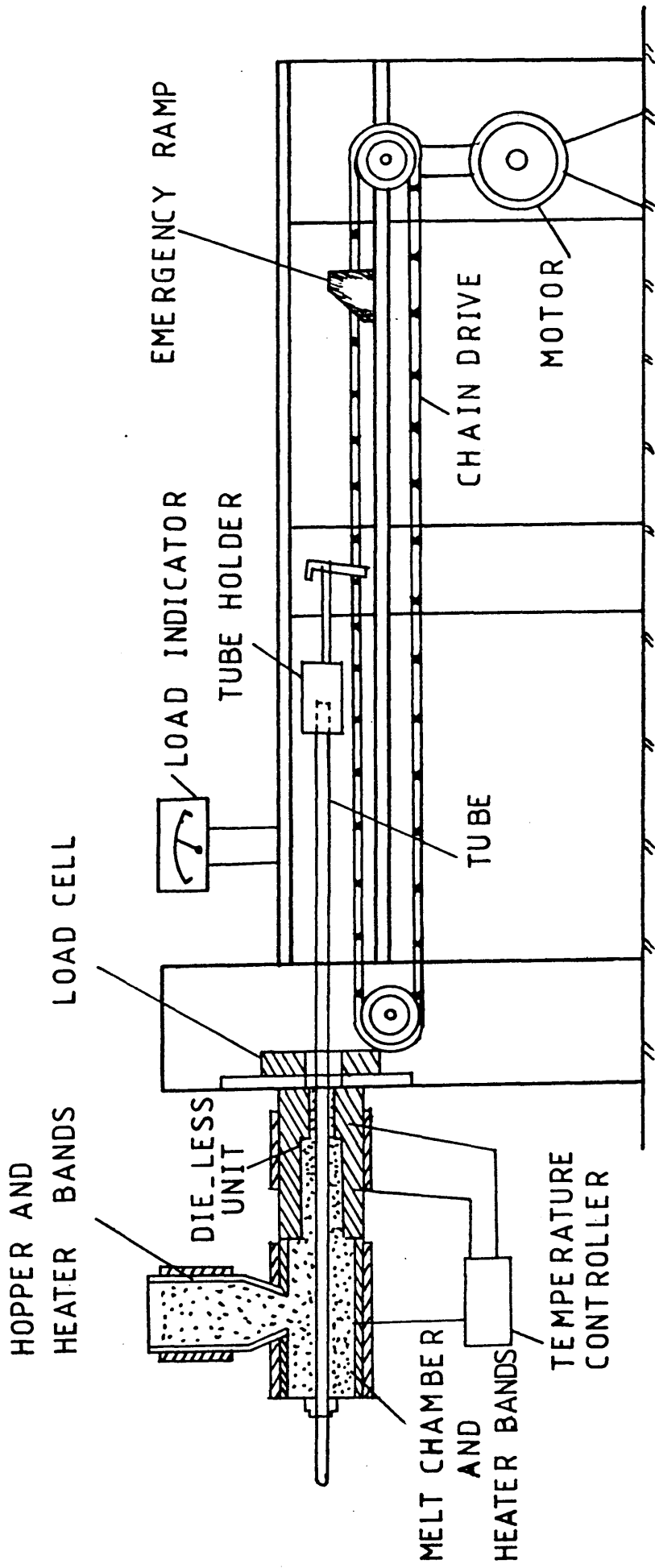
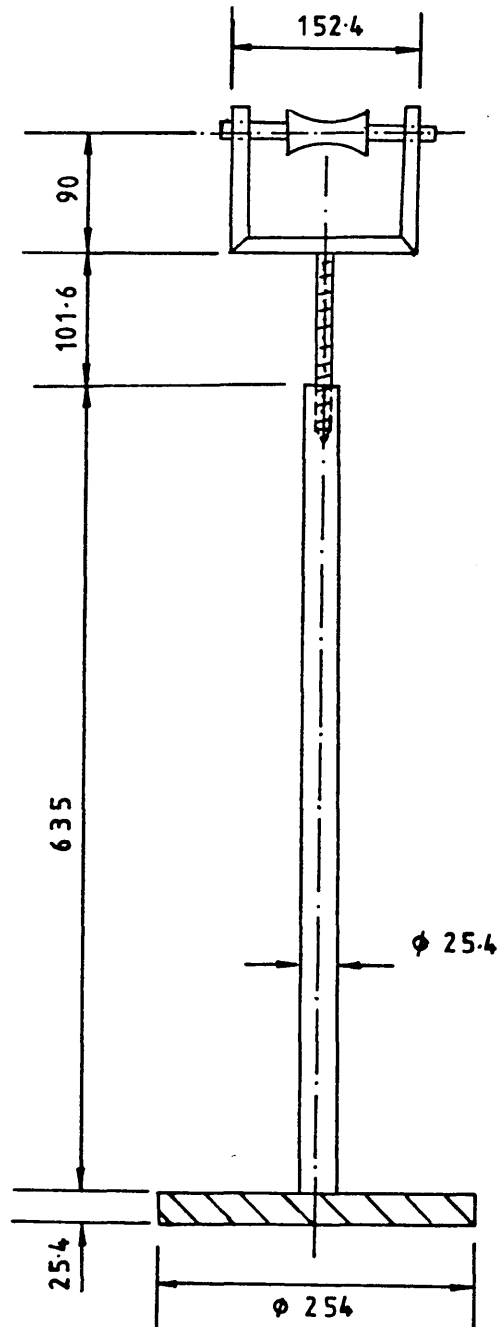


FIG 21 - DIE-LESS TUBE SINKING DRAWING BENCH



DIMENSIONS IN mm

FIG 22 - TUBE SUPPORT STAND

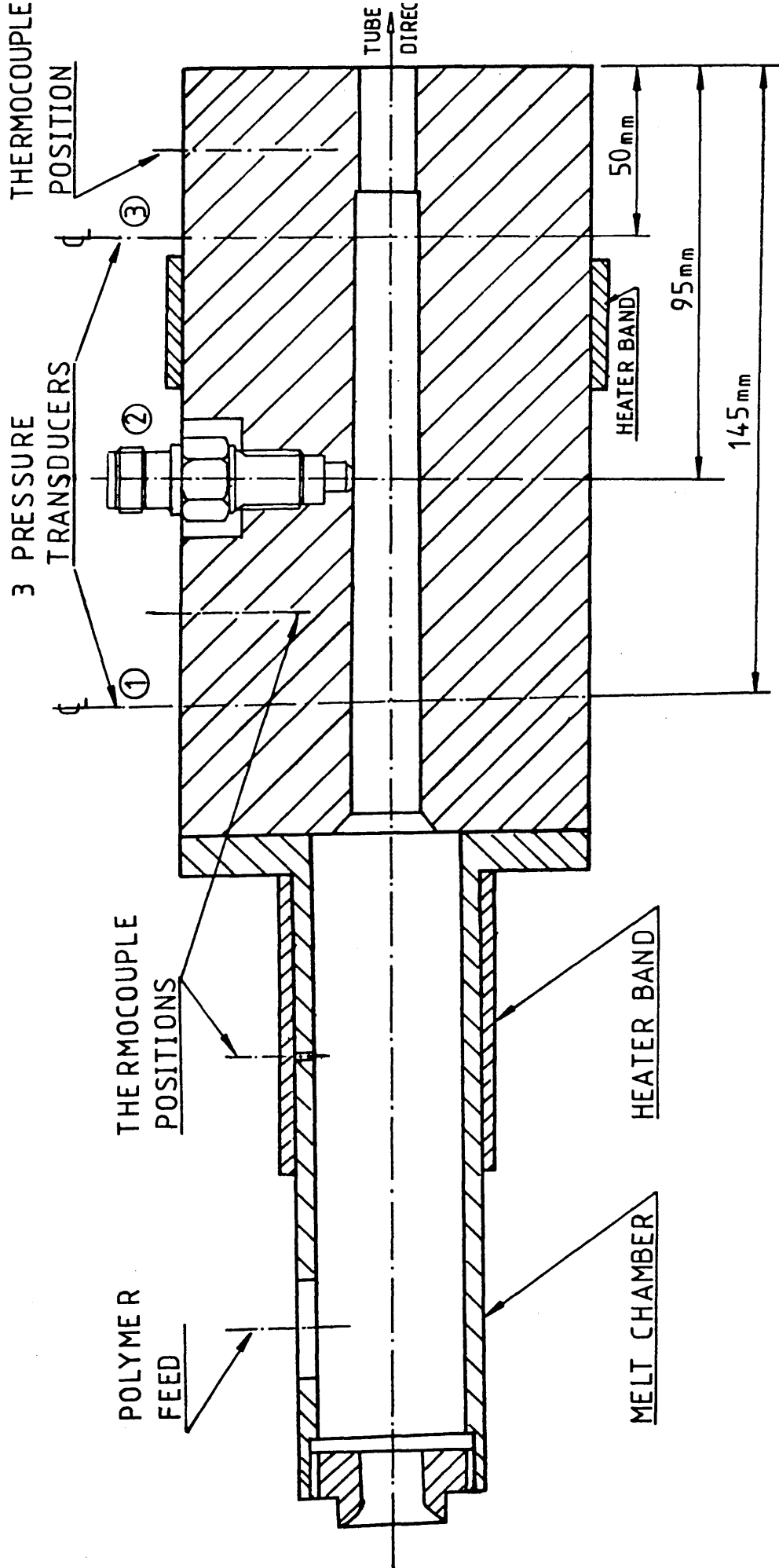


FIG 23 - STEPPED BORE REDUCTION UNIT ASSEMBLY

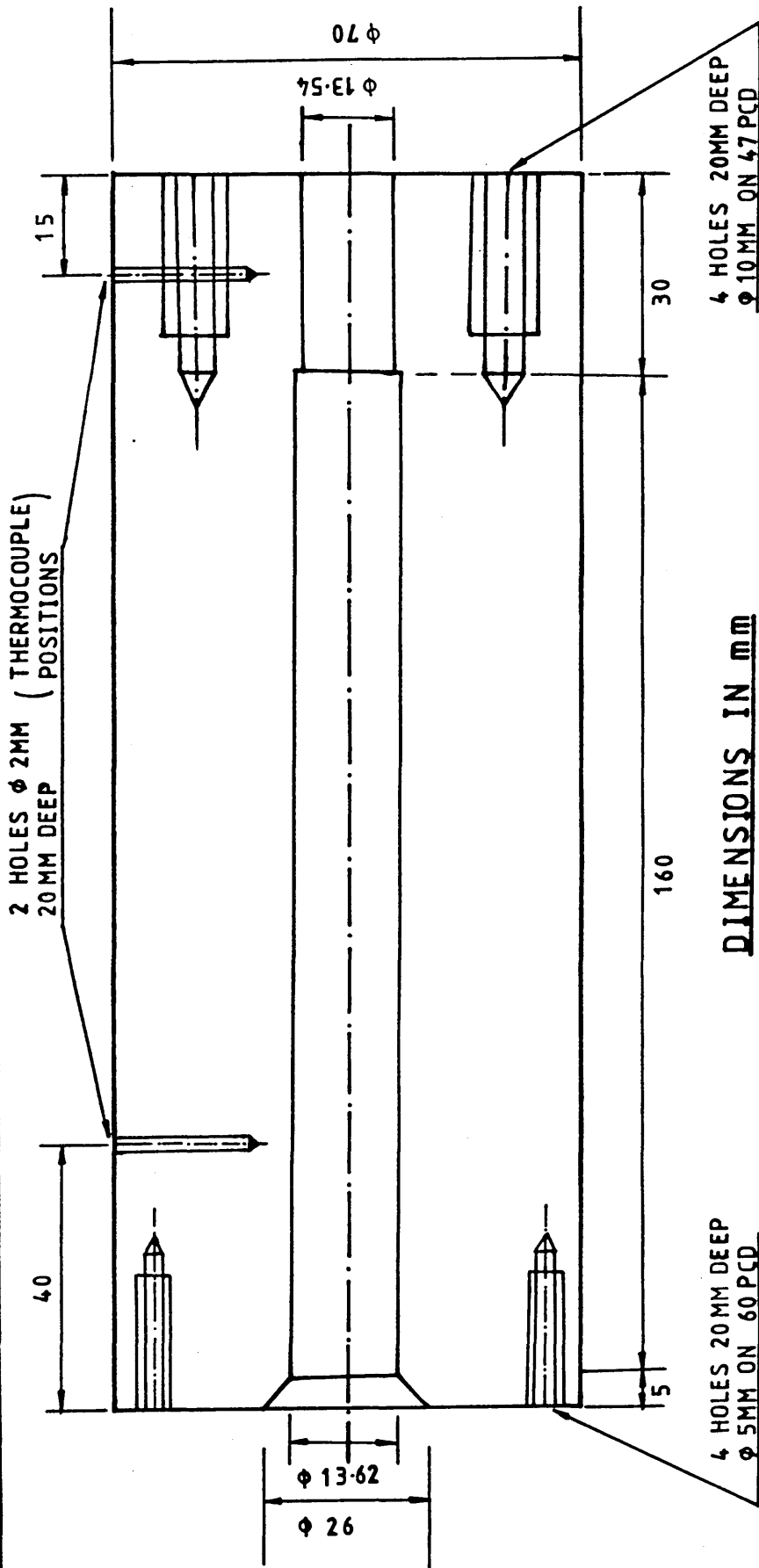


FIG 24 - STEPPED BORE REDUCTION UNIT

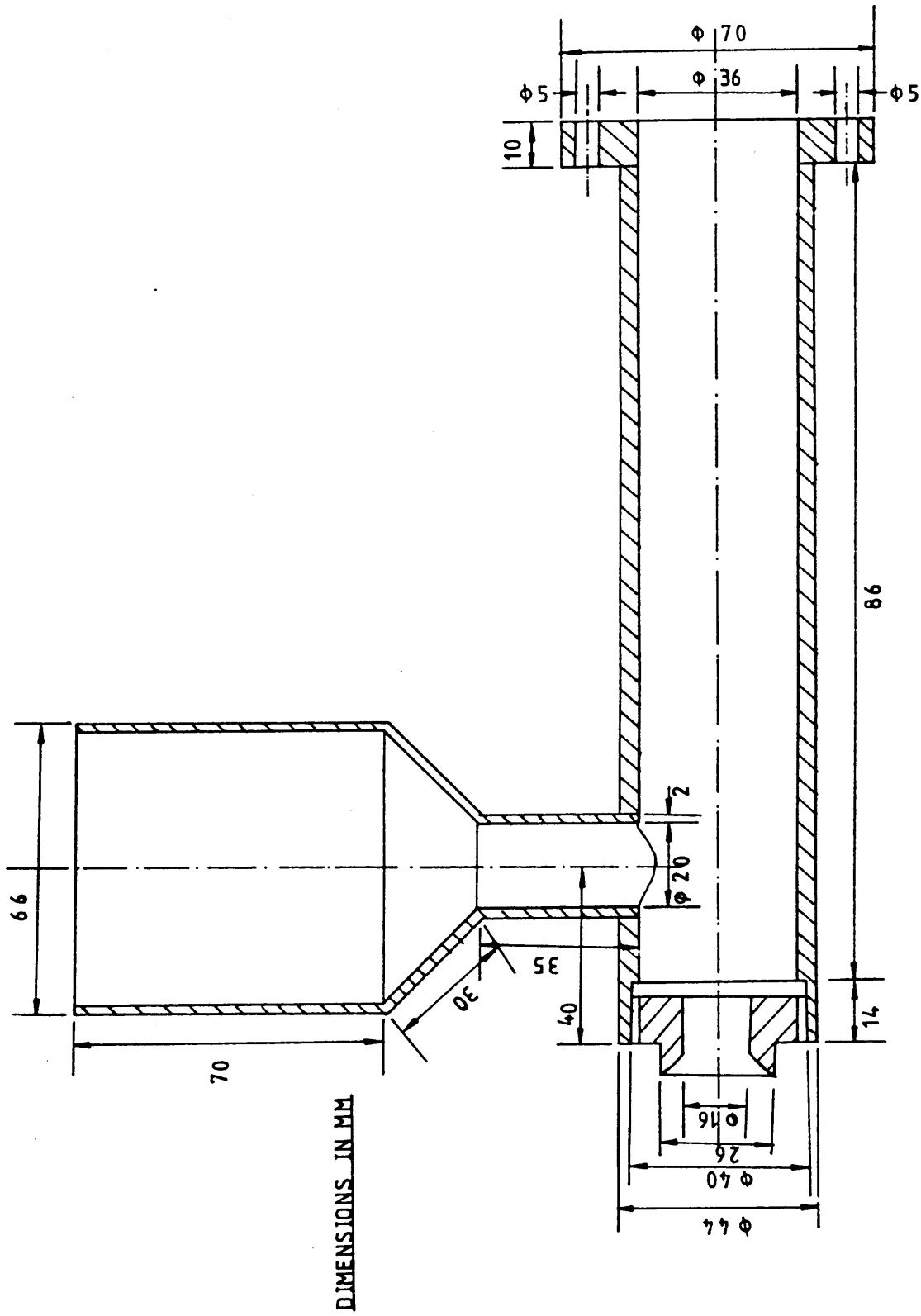


FIG. 25 - MELT CHAMBER AND HOPPER ASSEMBLY

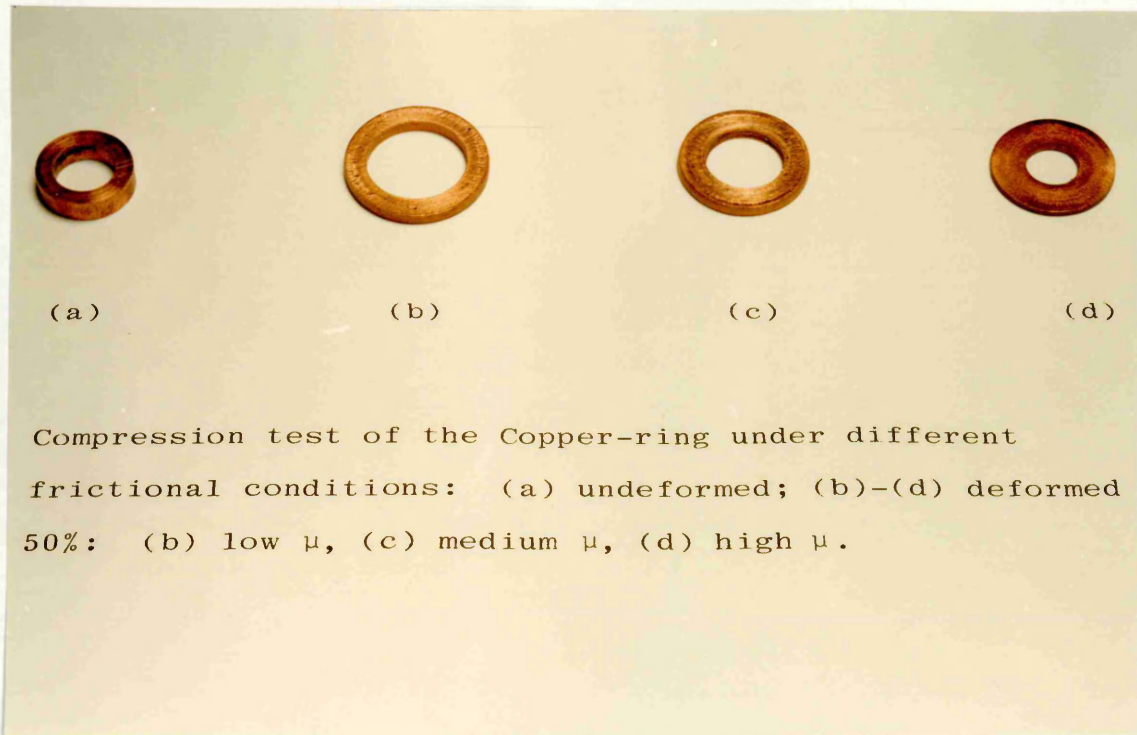


FIG 27(a)

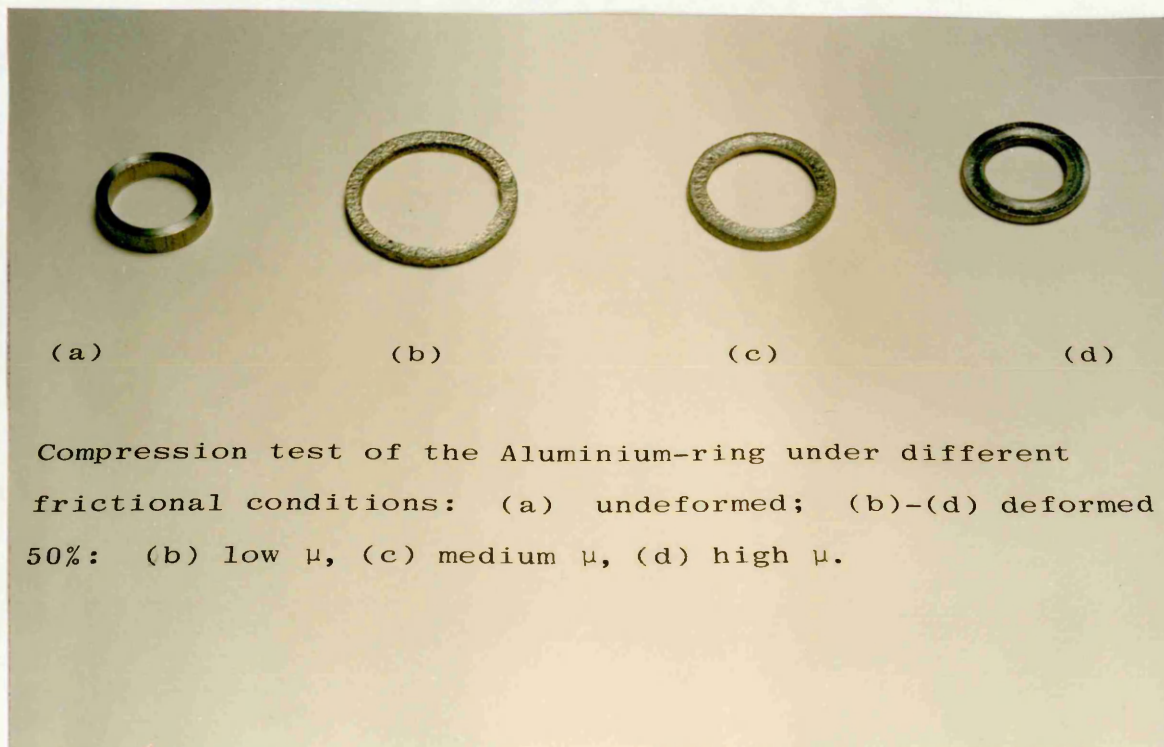


FIG 27(b)

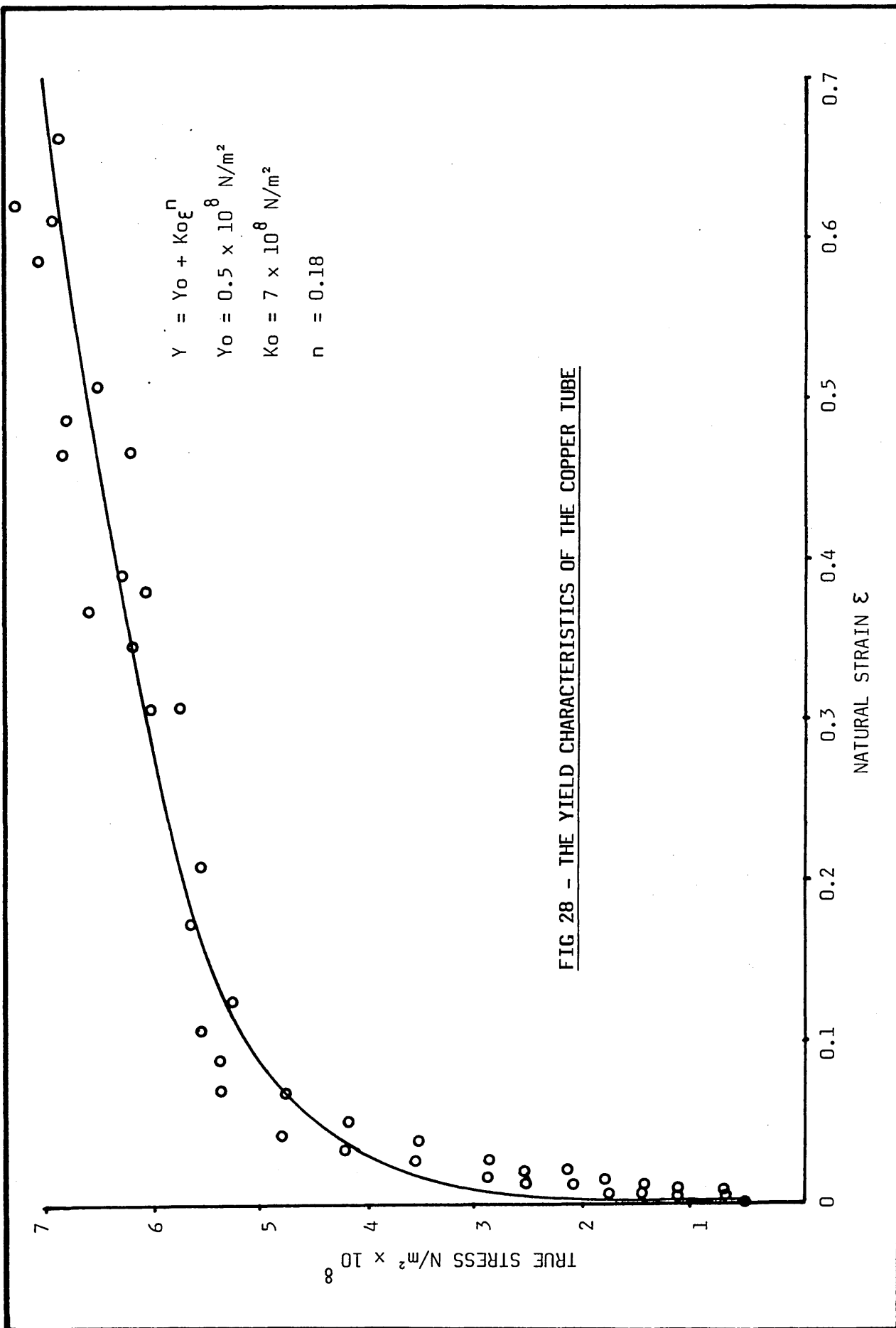


FIG 28 - THE YIELD CHARACTERISTICS OF THE COPPER TUBE

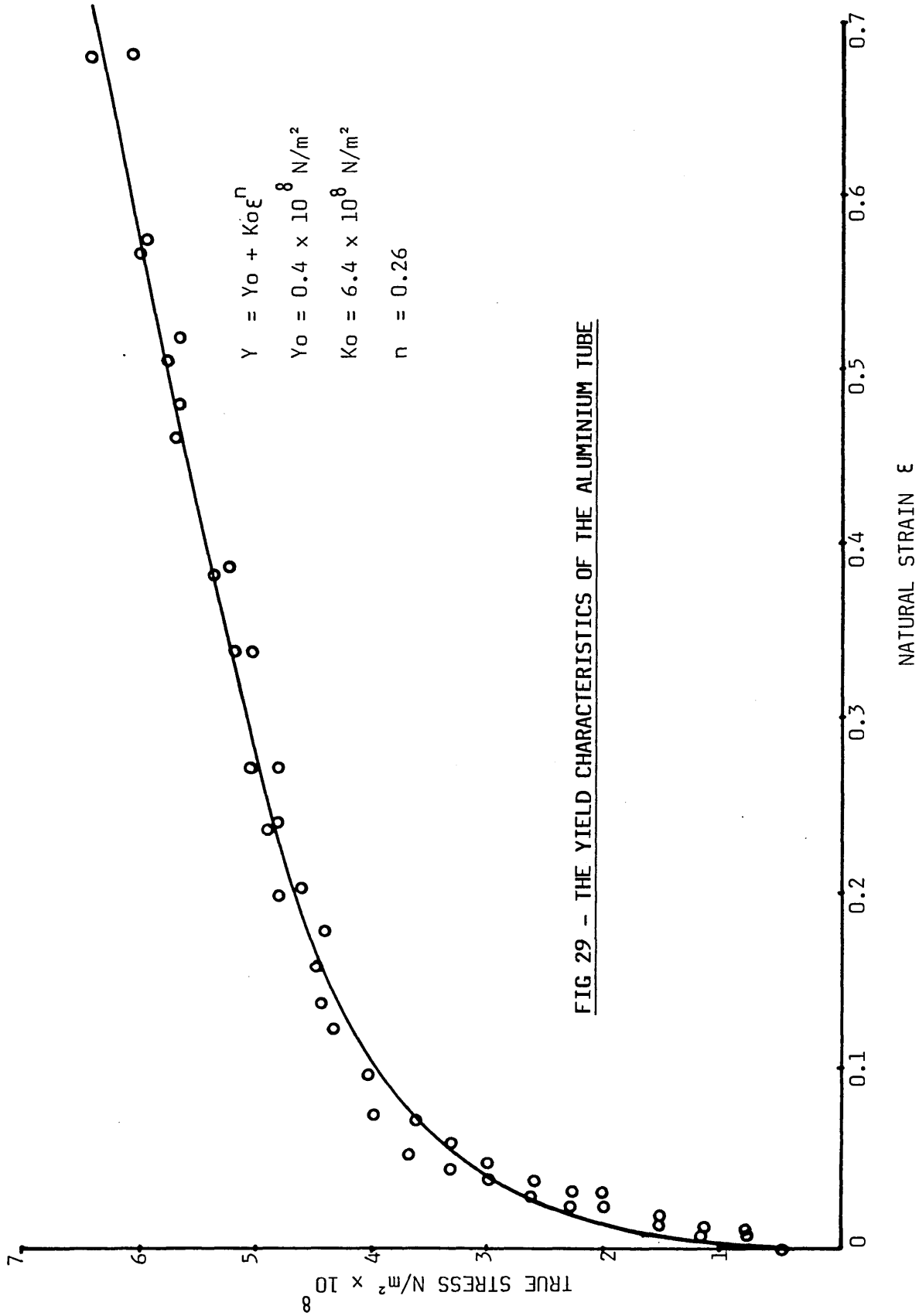


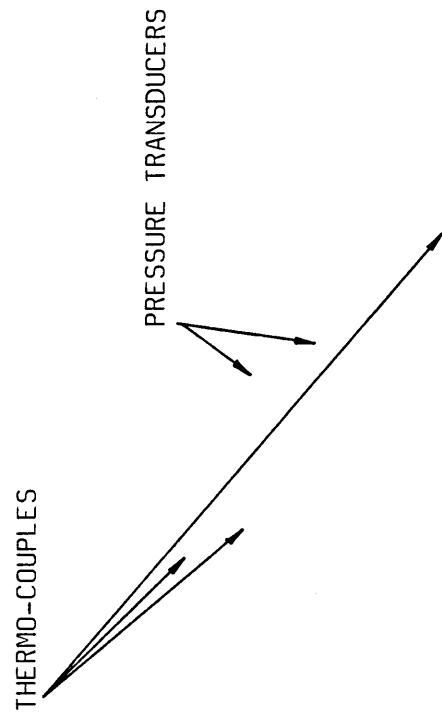
FIG. 29 - THE YIELD CHARACTERISTICS OF THE ALUMINIUM TUBE

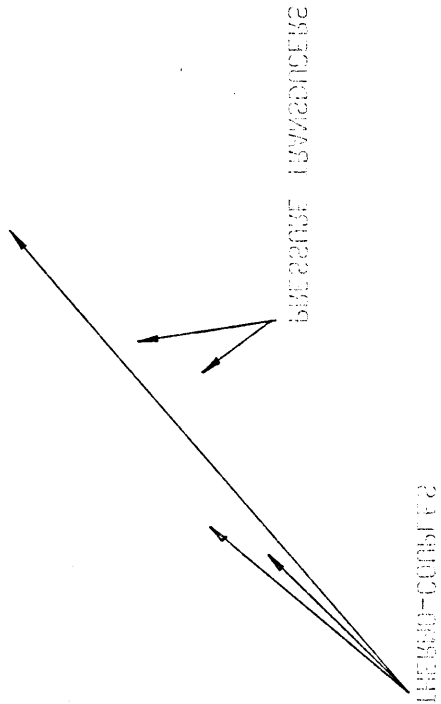
GENERAL VIEW OF THE DRAW BENCH

CEMENT ALKALI LINE DATA SHEET

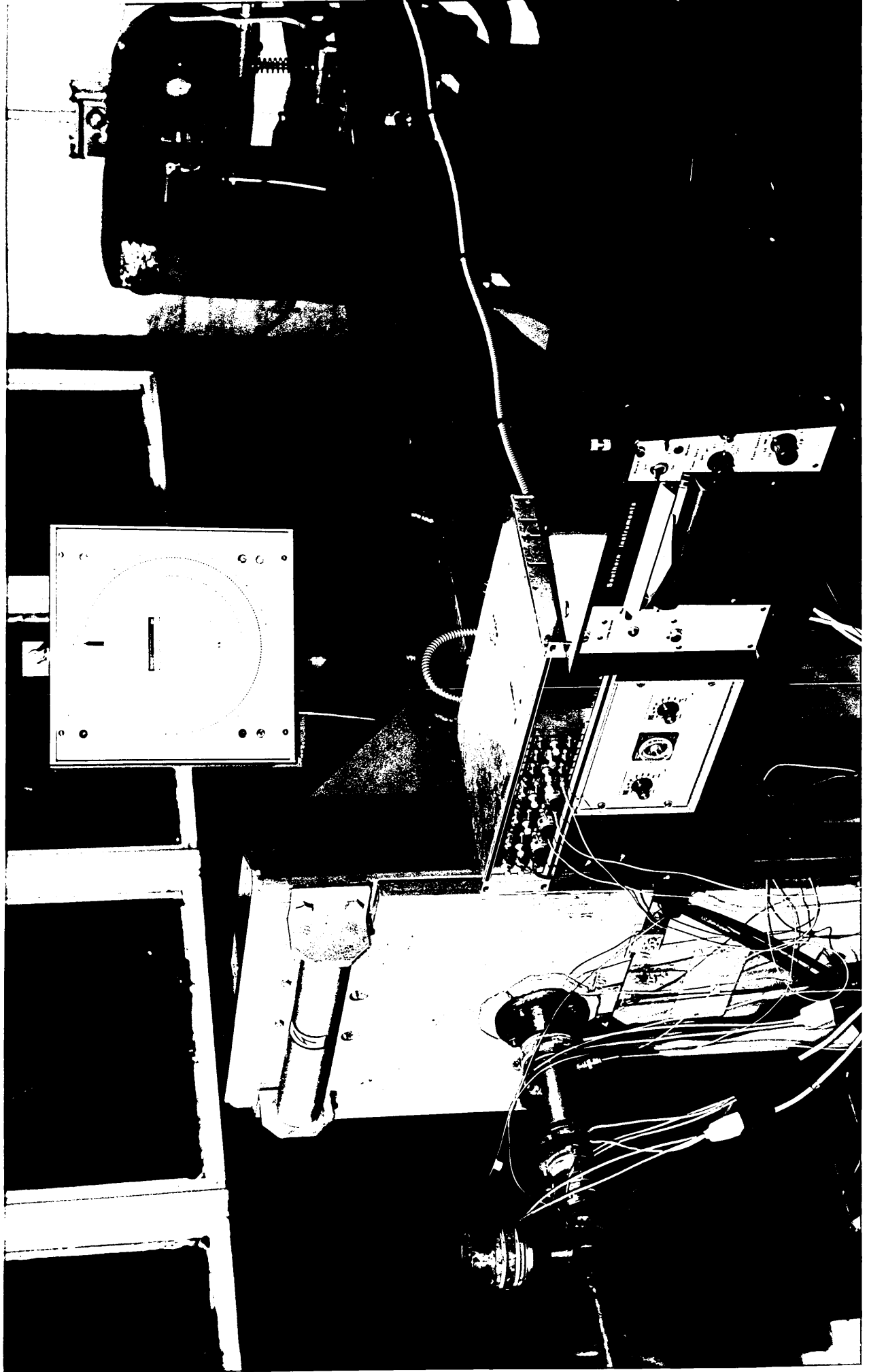


LOAD INDICATOR





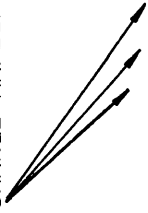
1000-10000



U-V RECORDER



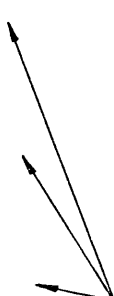
CHARGE AMPLIFIERS



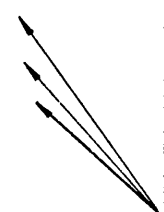
TEMPERATURE CONTROLLERS



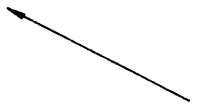
REVERSE LOBE COMPONENTS

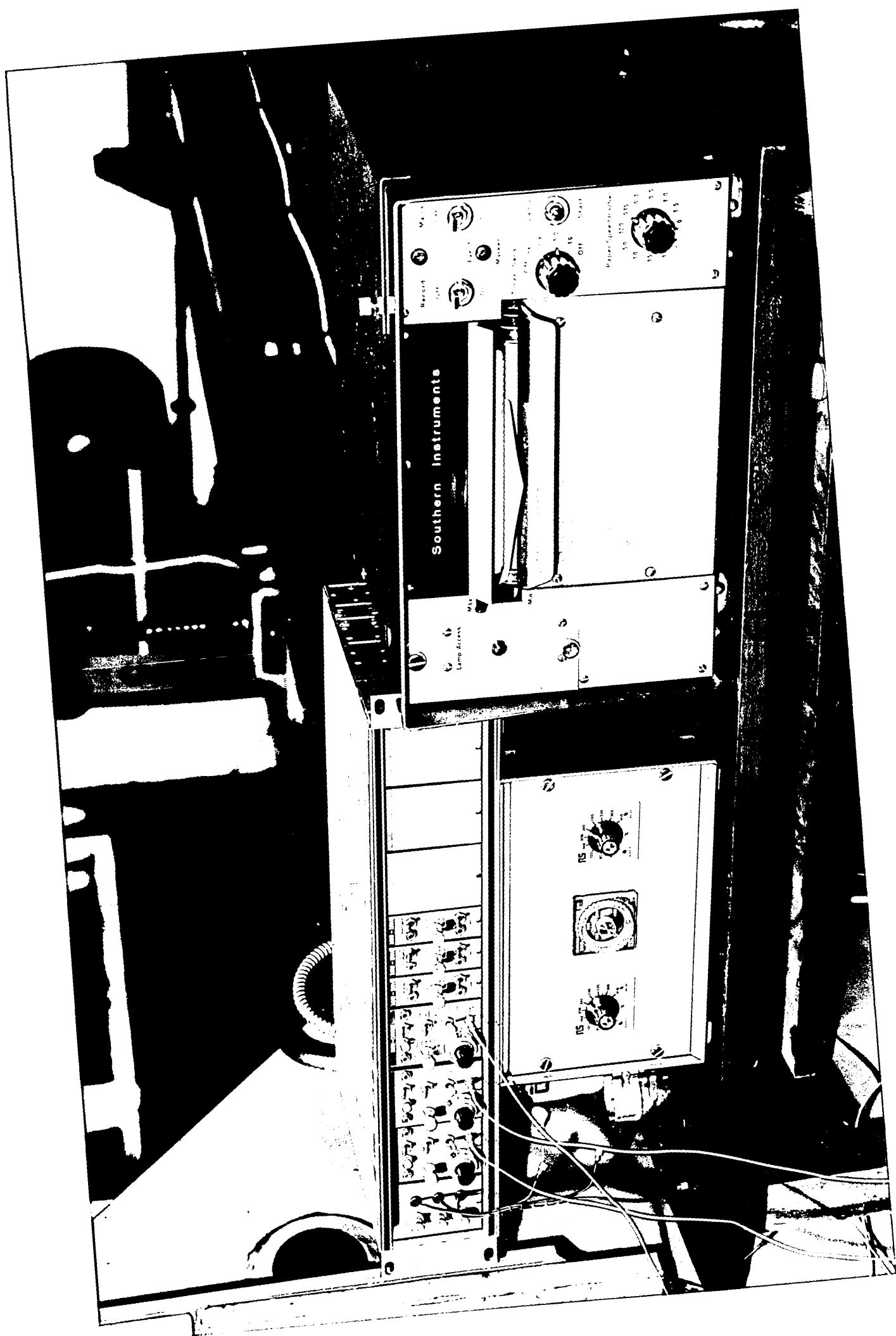


CHANCE VIBRATIONS

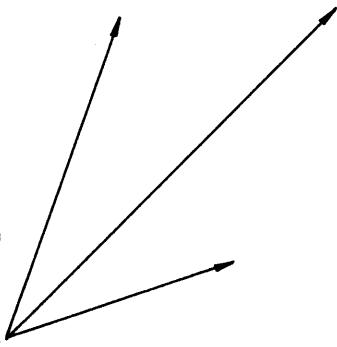


R-A RECORDER

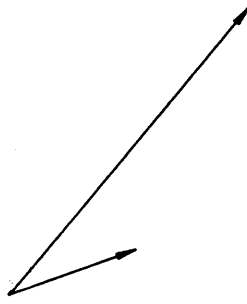


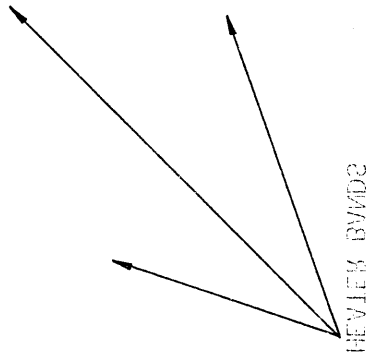
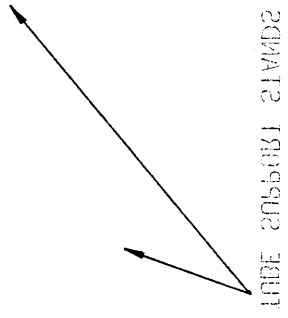


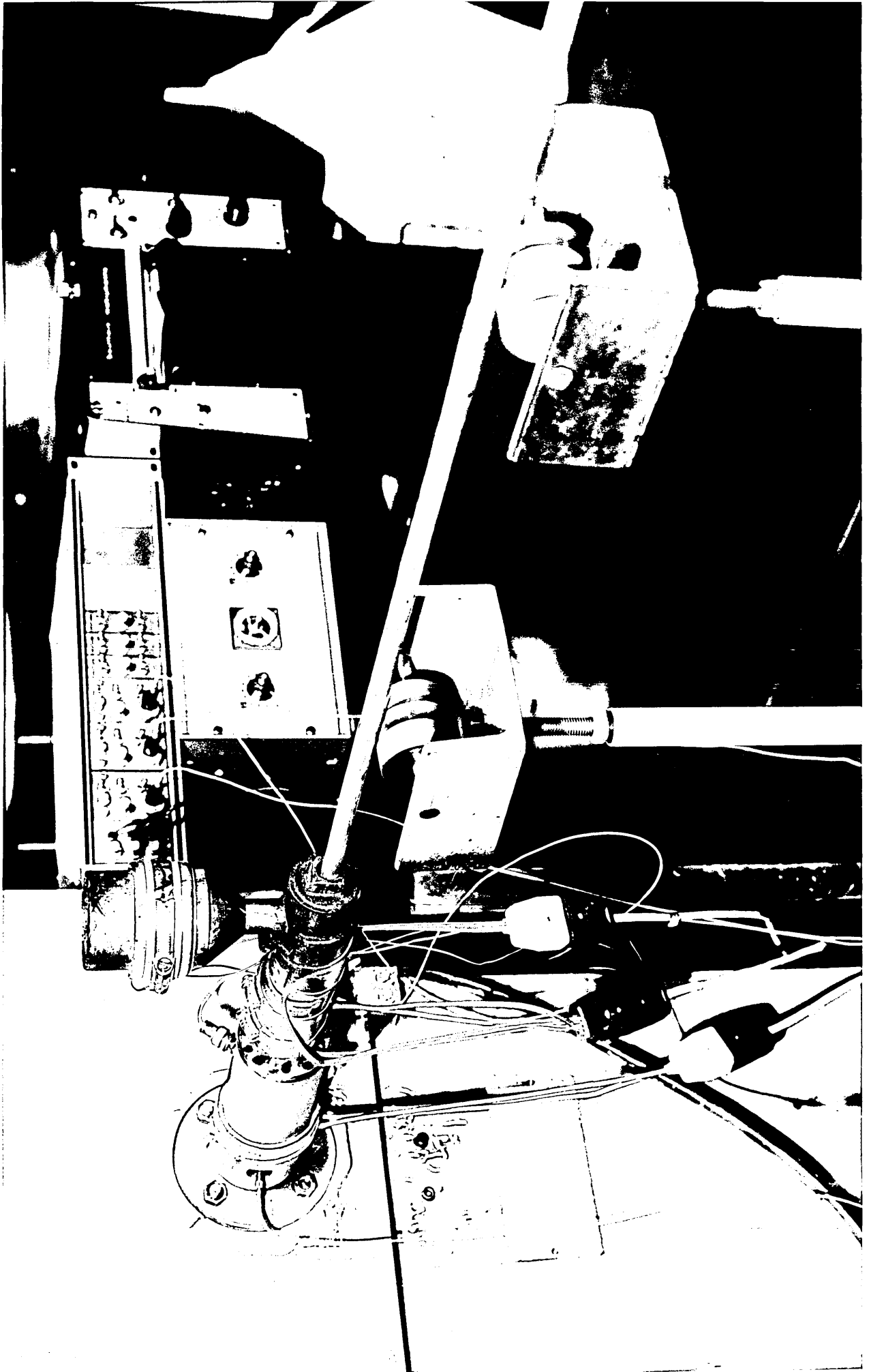
HEATER BANDS



TUBE SUPPORT STANDS







LOAD CELL

—

LOAD CELL



CHAPTER 4 : EXPERIMENTAL RESULTS

4.1 Experimental Procedure

Before starting any test the heater bands were first switched on and were controlled thermostatically to maintain the temperature at the pre-set level. The hopper and melt chamber were filled with polymer (usually in granulated form) and the other instruments were also switched on. The unit was left for two hours to reach the steady state temperature level. The tube was supported by adjustable stands and freely rotating rollers were used to guide the tube so that a horizontal feed to the unit was achieved. Then the tube was pushed through the melt chamber and the die-less reduction unit and was then clamped into the dog jaws.

The electric motor was started and set running at the desired speed (the motor speed was adjusted by turning the speed regulator knob). Charge amplifiers for the pressure transducers were switched to long time positions which gave a steady and uniform reading through the run. The dog was engaged with the chain which disengaged when it reached the emergency ramp. During the drawing procedure the drawing load was noted from the load indicator. The electric motor, the u-v recorder and the charge amplifiers were switched back to their original positions. Test number was recorded on the data sheet and also on the u-v paper for subsequent collection and analysis. The speed of the electric motor was then increased in suitable steps and the procedure was repeated for each speed increment. At the end of each run, the tube was marked by a label, recording the number of each run. Tubes of approximately five feet length were drawn each time.

When analysing the experimental results pressure recordings on the u-v paper were measured and noted on the data sheet for each test.

Three lengths of approximately one foot (from the end of the tube) each were then sawn off from the tube. The polymer coating was peeled off and the thickness of the coat was measured. The diameter of the uncoated tube was then measured to determine the amount of reduction.

4.2 Experimental Results

The initial experimental work was carried out with copper tubes of 15mm O.D., 0.7mm wall-thickness and 13.52mm O.D., 2.5mm wall thickness. When 15mm O.D. copper tubes were drawn through the die-less reduction unit at lower temperatures, two different types of defects were observed on the products. The types of defects are shown in the photographs in Figs 30(a) and (b) and discussed in Appendix 1. Subsequent tests with 13.52mm O.D. and 2.5mm wall thickness copper tubes and 15.92mm O.D. and 1.64mm wall-thickness aluminium tubes produced products without any such defects. The diameter of the tube was found to be fairly constant over the entire drawn length and there was no sign of any ovality or out of circularity in the cross-section except for aluminium tubes drawn with KM61 polymer at lower temperature and low speed.

Four different types of polymers were used as the pressure medium for these tests. These are polyethylene (Alkathene WVG23) and high density polyethylene (Rigidex) polymers produced by ICI, and polypropylene (KM61) and polystyrene produced by Shell.

Roundness tests of the cross-section of the tubes were also conducted to determine and compare the quality of the tubes drawn using the die-less reduction unit and those drawn with the conventional reduction die.

Experimental results obtained using the die-less reduction unit are presented in graphical forms in this section. Dimensional details

of the die-less reduction unit used for the tests are shown in the schematic diagram below and are as follows:

DRU for Copper Tube

$$L_1 = 160\text{mm}$$

$$L_2 = 30\text{mm}$$

$$L_1/L_2 = 5.33$$

$$h_1 = 0.5\text{mm}$$

$$h_2 = 0.01\text{mm}$$

$$h_1/h_2 = 50$$

DRU for Aluminium Tube

$$L_1 = 150\text{mm}$$

$$L_2 = 30\text{mm}$$

$$L_1/L_2 = 5$$

$$h_1 = 1.035\text{mm}$$

$$h_2 = 0.035\text{mm}$$

$$h_1/h_2 = 29.57$$

The length and gap ratios of the die-less reduction unit for both tubes were later changed as follows:

New Length and Gap Ratios for

Copper Tube

$$L_1 = 160\text{mm}, h_1 = 0.5\text{mm}$$

$$L_2 = 60\text{mm}, h_2 = 0.01\text{mm}$$

$$L_1/L_2 = 2.66, h_1/h_2 = 50$$

$$L_1 = 130\text{mm}, h_1 = 0.5\text{mm}$$

$$L_2 = 30\text{mm}, h_2 = 0.01\text{mm}$$

$$L_1/L_2 = 4.33, h_1/h_2 = 50$$

New Gap Ratio for

Aluminium Tube

$$L_1 = 150\text{mm}, h_1 = 0.53\text{mm}$$

$$L_2 = 30\text{mm}, h_2 = 0.02\text{mm}$$

$$L_1/L_2 = 5, h_1/h_2 = 26.50$$

$$L_1 = 160\text{mm}, h_1 = 0.4\text{mm}$$

$$L_2 = 30\text{mm}, h_2 = 0.01$$

$$L_1/L_2 = 5.33, h_1/h_2 = 40$$

$$\left. \begin{array}{l} h_1 = 0.25 \\ h_2 = 0.01 \\ h_1/h_2 = 25 \end{array} \right\} L_1/L_2 = 5.33$$

$$\left. \begin{array}{l} h_1 = 0.2 \\ h_2 = 0.04 \\ h_1/h_2 = 5 \end{array} \right\} L_1/L_2 = 5.33$$

The results obtained using units of these length and gap ratios are also presented in this section.

4.2.1 Results of Percentage Reduction in Diameter versus Drawing Speed

Fig 31 shows the performance of the die-less reduction unit with different gap ratio on percentage reduction in diameter for the copper tube using WVG23 polymer at 130°C. At higher gap ratio, the reduction in the tube obtained is higher with the lower drawing speeds and decreases as the drawing speed is increased. The amount of reduction in the copper tube was found to be the same for gap ratios of 40, 25 and 5 at higher drawing speeds.

The effect of gap ratios on the percentage reduction in diameter for copper tube using KM61 polymer at 220°C is shown in Fig 32. This polymer produced higher deformation in the tube at higher drawing speeds compared to those obtained using WVG23 polymer. Further increase in the speed caused the deformation of the tube to reduce at higher gap ratio. At higher drawing speeds, the general trends were found to be the same for the smaller gap ratios as shown in Fig 31.

When Rigidex polymer used as a pressure medium the percentage reduction in diameter was found to be minimum for different gap ratios (see Fig 33). At a lower drawing speed (0.1 m/s) the percentage reduction in diameter was found to be approximately 4% at higher gap ratio. As the drawing speed was increased the performance of the die-less reduction unit was decreased for all the gap ratios.

Fig 34 shows the percentage reduction in diameter measured for different gap ratios using polystyrene polymer at 240°C. When copper tube was drawn at lower drawing speeds through a die-less reduction unit at higher gap ratio, there was a marked difference between the results obtained by using polystyrene polymer and those obtained using the other three polymers. This polymer produced about 7% reduction in diameter at a low drawing speed. The amount of reduction in the tube was found to be the same at the drawing speed of 0.5 m/s for all gap ratios.

Figs 35 to 38 show the effect of the gap ratio on the percentage reduction in diameter for aluminium tube using four different polymers at different temperatures. The general trends were found to be the same as shown in Figs 31 to 34.

Fig 39 shows the effect of the length ratio on the percentage reduction in diameter for copper tube using WVG23 polymer at 130°C and using units of a constant gap ratio. The trend of the results were found to be such that the maximum percentage reduction in diameter is obtained at lower drawing speeds and as the drawing speed was increased the decreased reduction in diameter was obtained. In Fig 39(a) results are shown for different length ratios obtained by varying the length of the second part of the unit whilst keeping the length of the first part (L_1) constant. It is evident that the reduction in the tube diameter is not significantly affected by the length ratio obtained in this manner. However, as shown in Fig 39(b) there was marked difference in the reduction of the tube diameter when the length of the entry part of the unit (L_1) was changed in order to vary the length ratio. At the drawing speed of 0.1 m/s the reduction in diameter differs by about 2% (see Fig 39(b)).

Fig 40 shows the effect of the length ratio on percentage reduction in diameter for copper tube when KM61 polymer was used at melt temperature of 220°C. It is evident that the reduction in diameter is significantly influenced by the length ratio irrespective of whether the length ratio is varied by changing L_1 or L_2 .

Fig 41 shows the effect of length ratios on the percentage reduction in diameter when Rigidex polymer was used at melt temperature of 230°C with constant gap ratio. This polymer produced smaller deformation in the tube compared to those obtained using WVG23 and KM61 polymers.

Fig 42 shows plots of percentage reduction in diameter against drawing speeds when polystyrene polymer was used as the pressure medium at 240°C. The trend is similar to those observed in the previous figures, ie smaller percentage reduction in diameter was obtained with greater drawing speeds.

Fig 43 shows the effect of viscosity on percentage reduction in diameter for copper tube using WVG23 polymer at 130°C, 160°C and 180°C with constant gap and length ratios. At all speeds larger reductions in diameter were obtained at the lowest temperature of 130°C.

Fig 44 gives the percentage reduction in diameter when copper tube was drawn through a die-less reduction unit with KM61 polymer at 200°C, 220°C and 240°C. This polymer produced comparatively higher deformation in the tube at higher drawing speeds compared to those obtained using WVG23 polymer (see Fig 43). At the temperature of 200°C, the flow of polymer started at the speed of about 0.2 m/s and below this speed, the tube was reduced randomly. After the commencement of flow of the polymer melt, an increase in the percentage reduction in diameter was observed which eventually

reached a maximum (5.5%) at about 0.3 m/s. Further increase in the drawing speed caused reduced deformation of the tube. At other temperatures the percentage reduction in diameter was found to decrease with increasing drawing speeds.

Fig 45 shows the effect of viscosity on percentage reduction in diameter for copper tube using Rigidex polymer at 200°C, 230°C and 240°C. When copper tube was drawn at a temperature of 200°C it was noted that there was no coating on the tube at any speed, and the tube was reduced randomly. A maximum amount of reduction was found at the melt temperature of 230°C and at the drawing speed of 0.1 m/s.

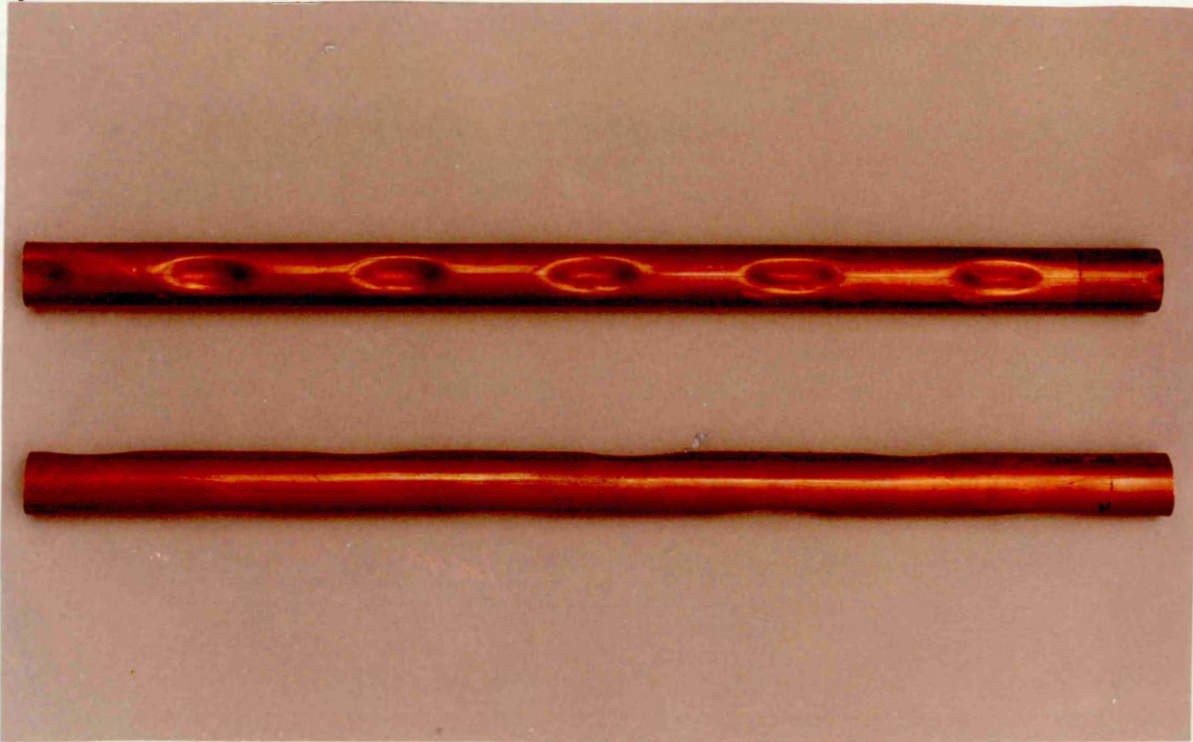
Fig 46 shows the percentage reduction in diameter for the copper tube using polystyrene polymer at 230°C and 240°C and there appears to be very little effect on the reduction over the whole range of drawing speed.

Fig 47 shows the effect of viscosity on the percentage reduction in diameter for aluminium tube using WVG23 at melt temperature of 130°C, 160°C and 180°C. With the polymer temperature at 130°C, the maximum reduction in diameter obtained was about 5.5% at 0.1 m/s. The reduction in diameter decreased at higher drawing speeds. At higher polymer temperature (180°C), the maximum reduction in diameter was noted 2.6% at 0.1 m/s. As the drawing speed was increased, the reduction in diameter fell down to about 1%.

Fig 48 gives the percentage reduction in diameter measured for aluminium with KM61 polymer at 220°C and 240°C. When the tube was drawn through a die-less reduction unit using KM61 polymer at 200°C, the tube was found to be squeezed and folded along the entire length of the drawn tube at all speeds. The maximum reduction in diameter (about 4.5%) was observed at the melt temperature of 220°C and at 0.1 m/s.

Figs 49 and 50 show the effect of viscosity on the percentage reduction in diameter for aluminium tube using Rigidex and Polystyrene polymers at 230°C and 240°C. When Rigidex polymer was used as the pressure medium at 230°C, the maximum percentage reduction in diameter obtained was about 3.6% at 0.1 m/s. The reduction in diameter decreased at higher drawing speeds. Using Rigidex polymer the reduction in diameter falls down to about 2.3% and using polystyrene polymer the reduction in diameter falls down to about 2% corresponding to drawing speeds ranging from 0.1 to 0.5 m/s as shown in Figs 49 and 50 respectively.

(a)



(b)

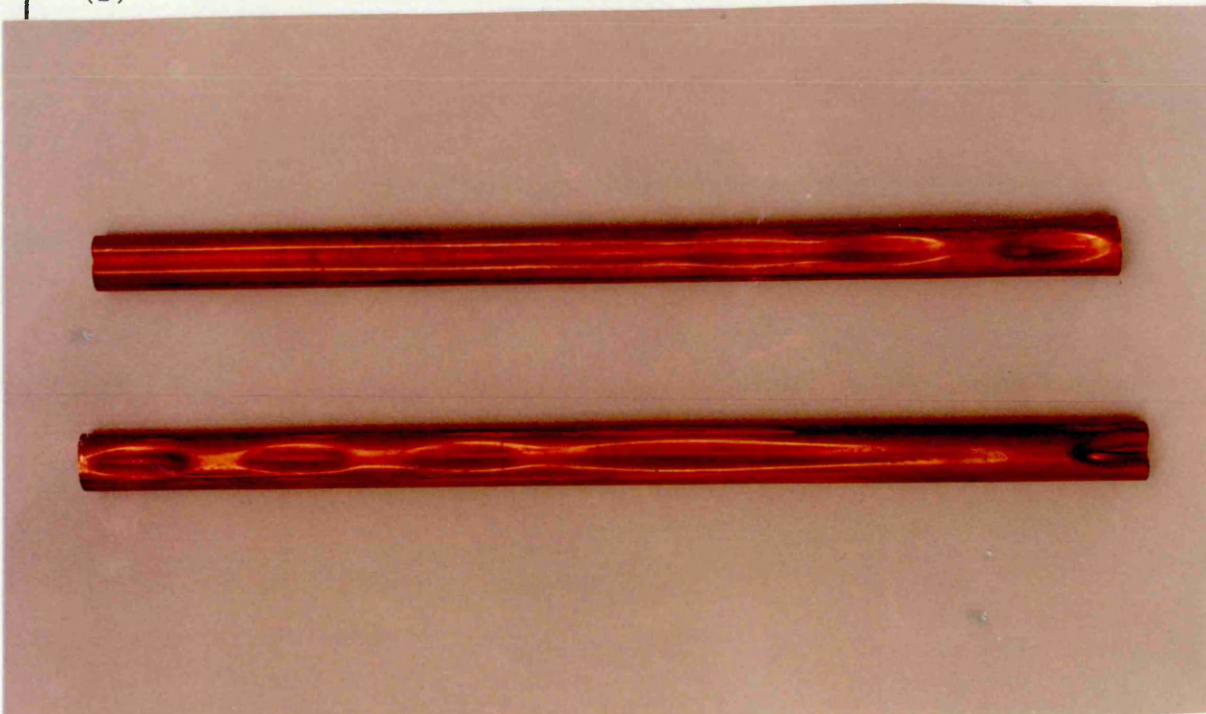


FIG 30 (a) - ALTERNATE DIMPLE TYPE AND
(b) - CONTINUOUS FOLDING TYPE DEFECTS

$\frac{h_1}{h_2} = 100$ - No deformation

$\frac{L_1}{L_2} = 5.33$

(x) $\frac{h_1}{h_2} = 50$

(o) $\frac{h_1}{h_2} = 40$

(●) $\frac{h_1}{h_2} = 25$

(●) $\frac{h_1}{h_2} = 5$

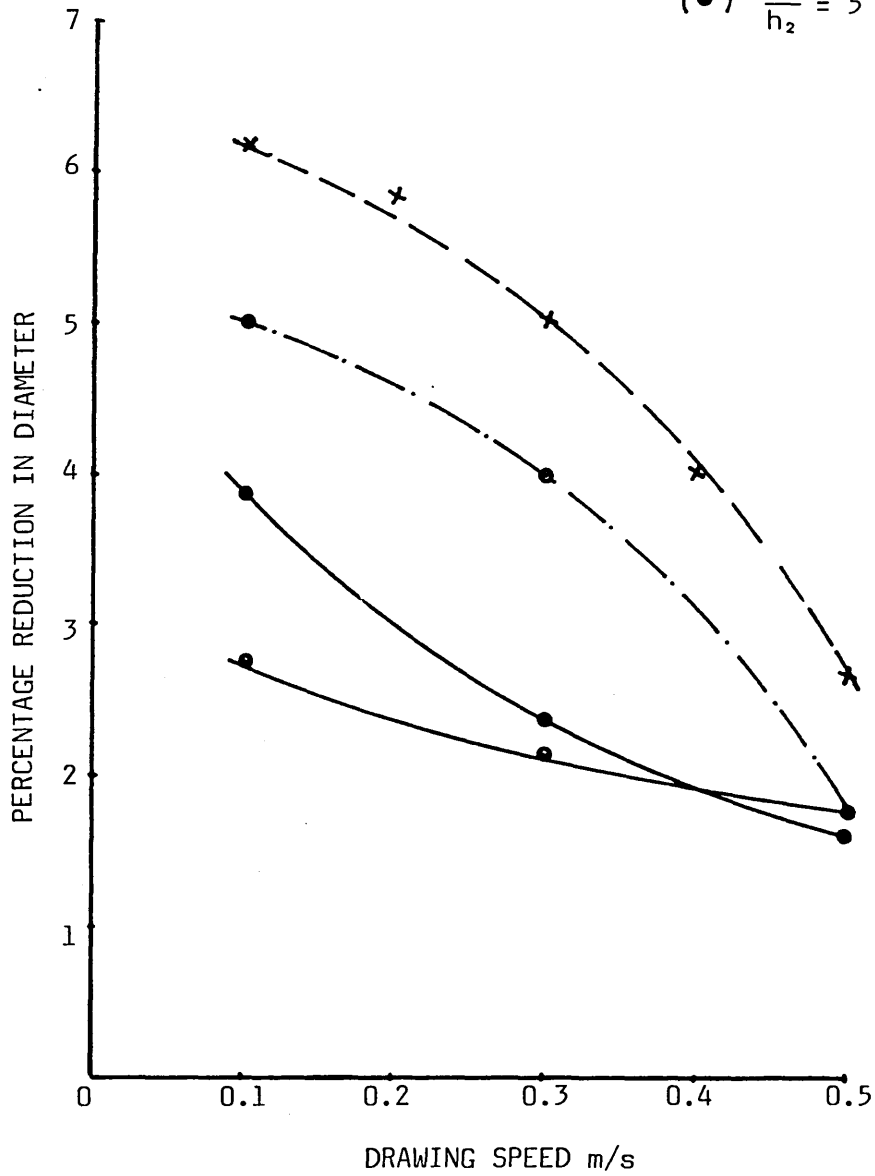


FIG 31 - EFFECT OF GAP RATIO ON PERCENTAGE REDUCTION IN DIAMETER FOR COPPER TUBE WITH WVG23 AT 130°C

$$\frac{L_1}{L_2} = 5.33$$

$$(\times) \frac{h_1}{h_2} = 50$$

$$(\circ) \frac{h_1}{h_2} = 40$$

$$(\bullet) \frac{h_1}{h_2} = 25$$

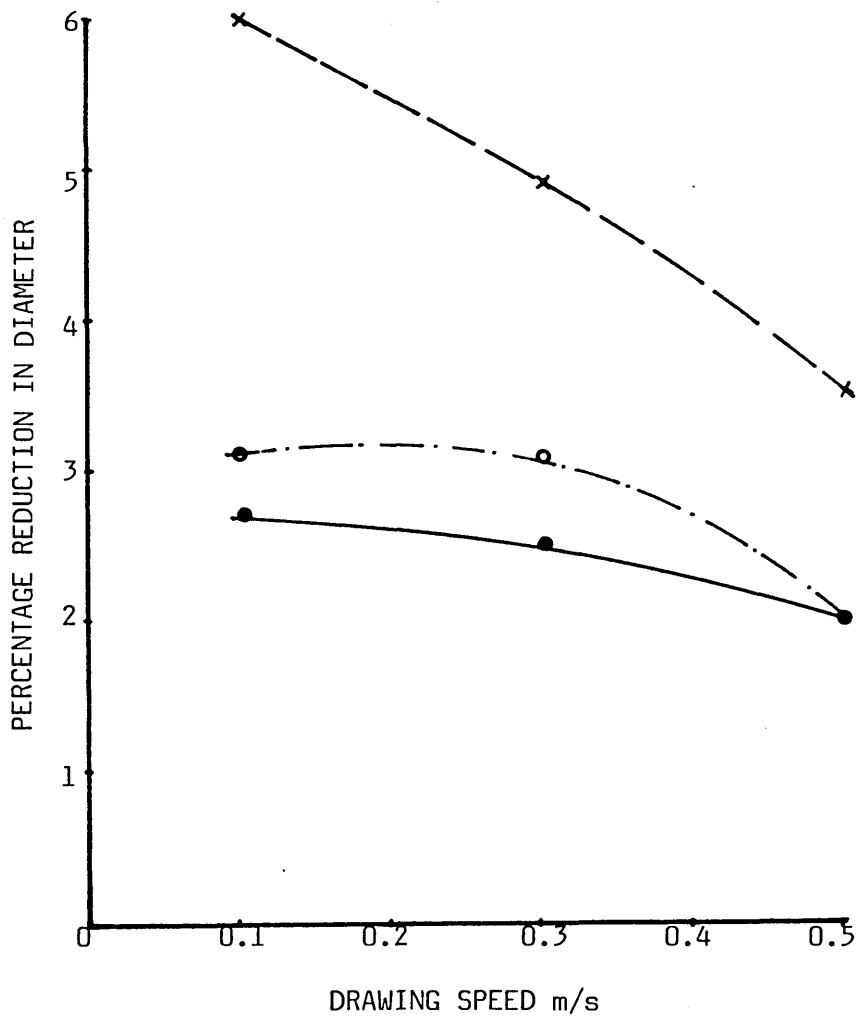


FIG 32 - EFFECT OF GAP RATIO ON PERCENTAGE REDUCTION IN DIAMETER FOR COPPER TUBE WITH KM61 AT 220°C

$$\frac{L_1}{L_2} = 5.33$$

$$(x) \frac{h_1}{h_2} = 50$$

$$(\circ) \frac{h_1}{h_2} = 40$$

$$(\bullet) \frac{h_1}{h_2} = 25$$

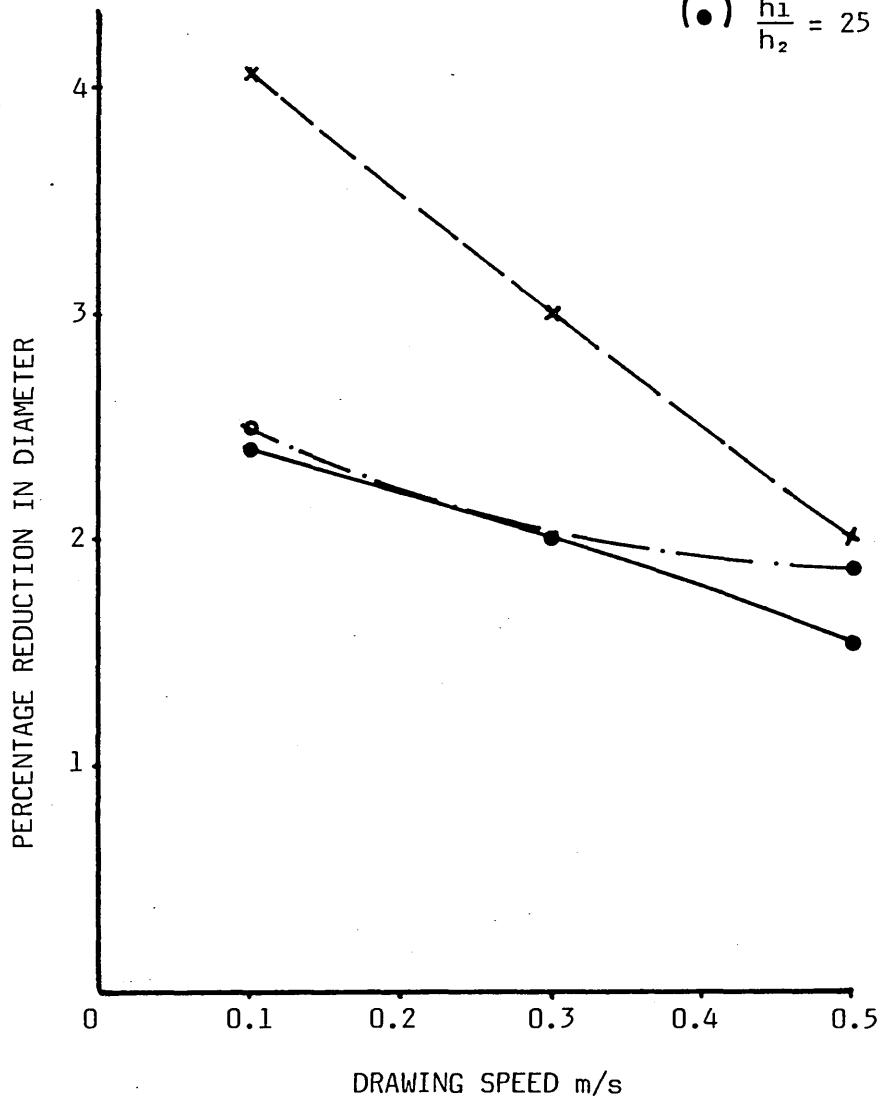


FIG 33 - EFFECT OF GAP RATIO ON PERCENTAGE REDUCTION IN DIAMETER FOR COPPER TUBE WITH RIGIDEX AT 230°C

$$\frac{L_1}{L_2} = 5.33$$

$$(x) \frac{h_1}{h_2} = 50$$

$$(\circ) \frac{h_1}{h_2} = 40$$

$$(\bullet) \frac{h_1}{h_2} = 25$$

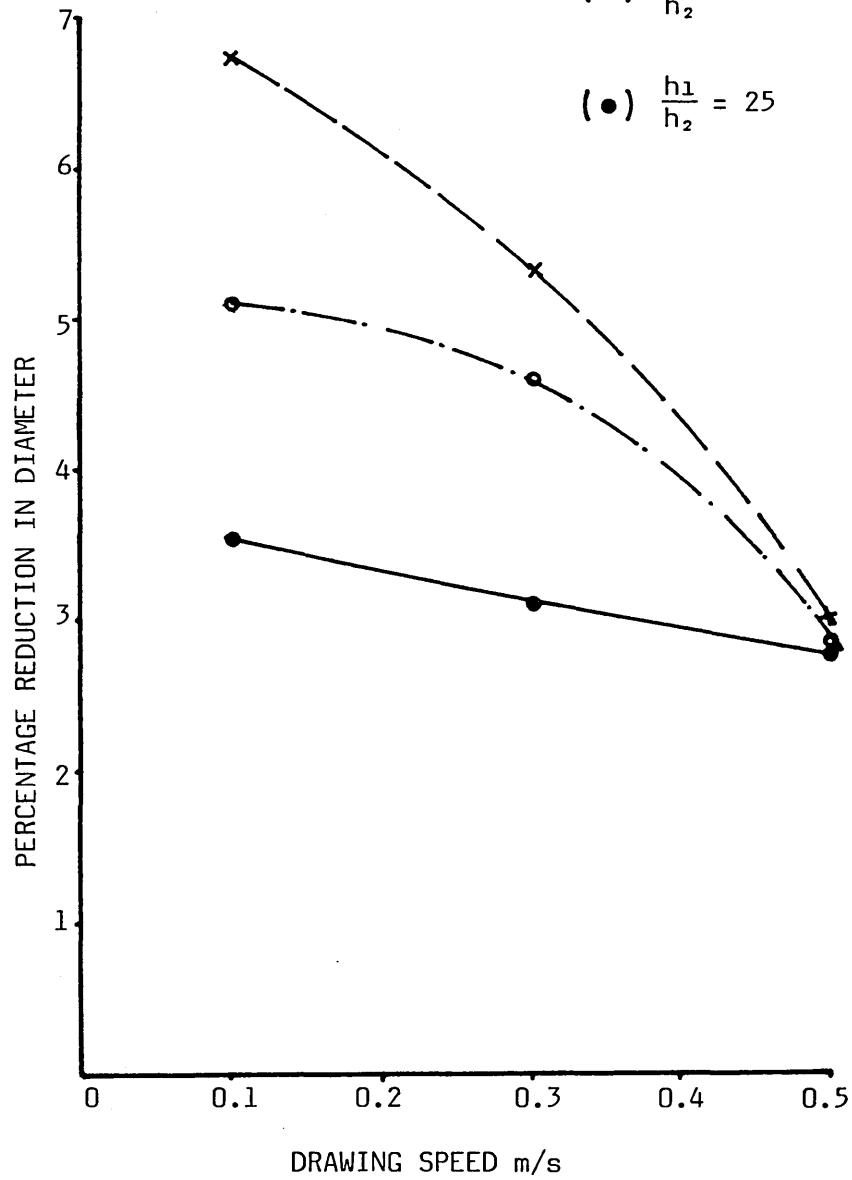


FIG 34 - EFFECT OF GAP RATIO ON PERCENTAGE REDUCTION IN DIAMETER FOR COPPER TUBE WITH POLYSTYRENE AT 240°C

$$\frac{L_1}{L_2} = 5$$

$$(\times) \frac{h_1}{h_2} = 29.57$$

$$(\circ) \frac{h_1}{h_2} = 26.5$$

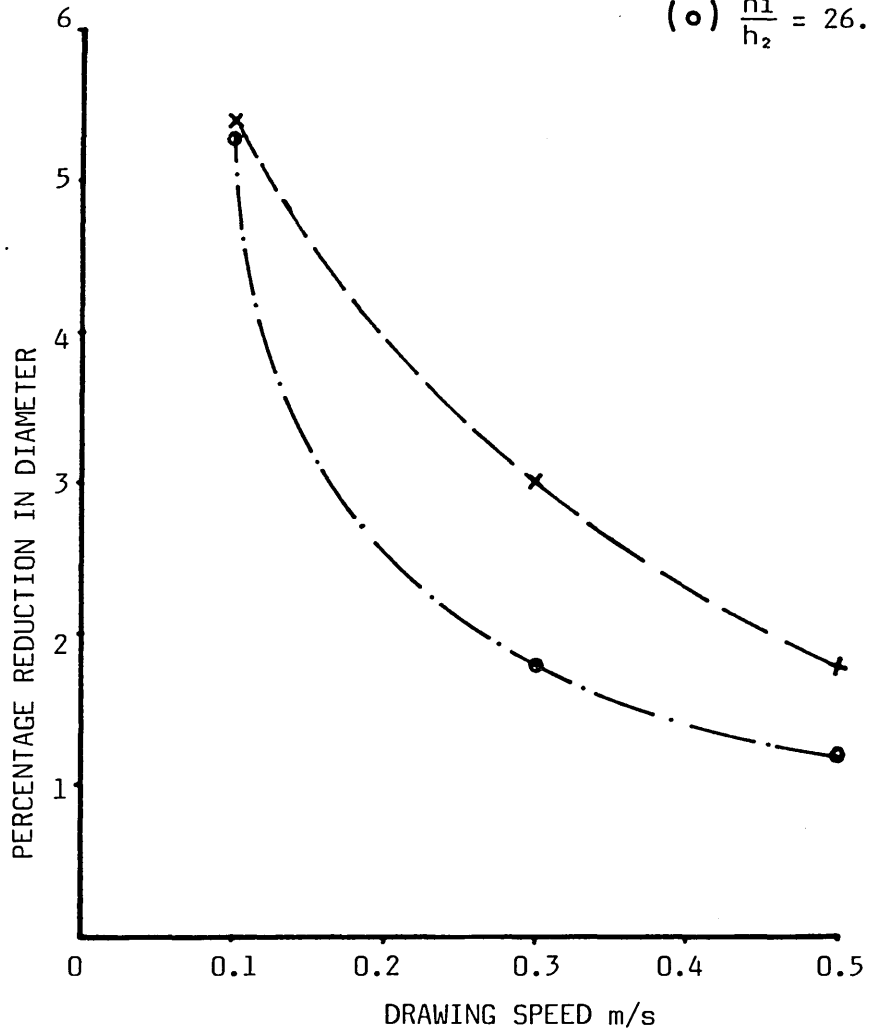


FIG 35 - EFFECT OF GAP RATIO ON PERCENTAGE REDUCTION IN DIAMETER FOR ALUMINIUM TUBE WITH WVG23 AT 130°C

$$\frac{L_1}{L_2} = 5$$

$$(\times) \frac{h_1}{h_2} = 29.57$$

$$(\circ) \frac{h_1}{h_2} = 26.5$$

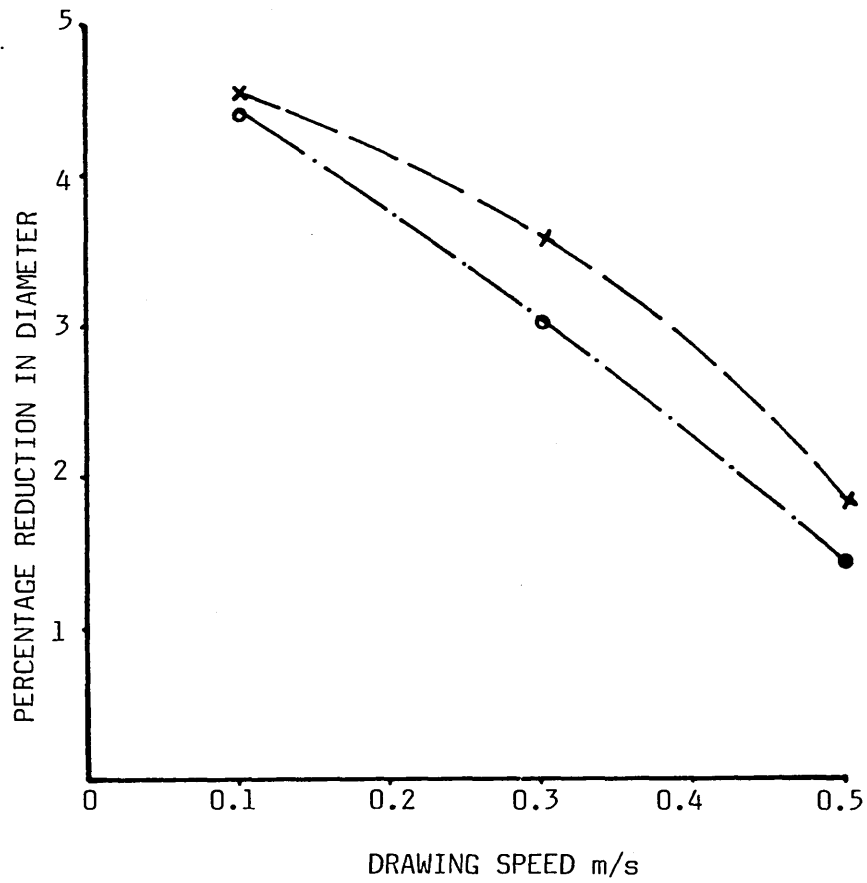


FIG 36 - EFFECT OF GAP RATIO ON PERCENTAGE REDUCTION IN DIAMETER FOR ALUMINIUM TUBE WITH KM61 AT 220°C

$$\frac{L_1}{L_2} = 5$$

$$(x) \frac{h_1}{h_2} = 29.57$$

$$(o) \frac{h_1}{h_2} = 26.5$$

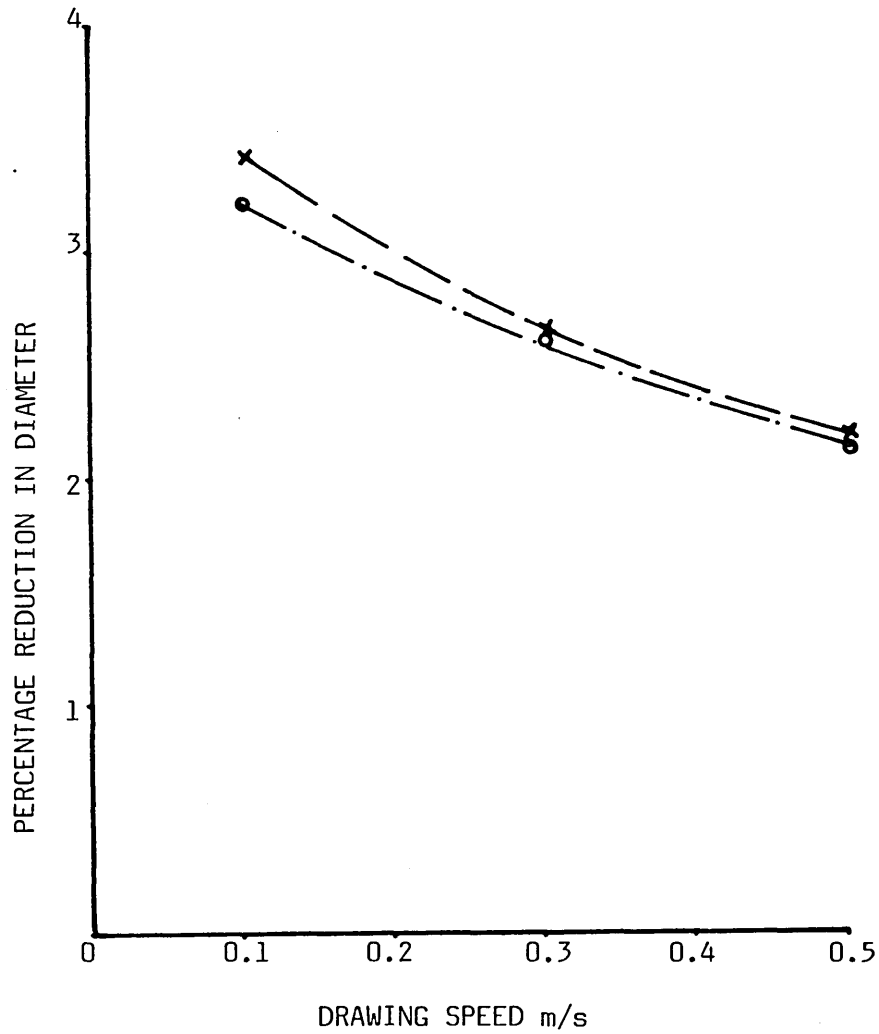


FIG 37 - EFFECT OF GAP RATIO ON PERCENTAGE REDUCTION IN DIAMETER FOR ALUMINIUM TUBE WITH RIGIDEX AT 230°C

$$\frac{L_1}{L_2} = 5$$

$$(x) \frac{h_1}{h_2} = 29.57$$

$$(o) \frac{h_1}{h_2} = 26.5$$

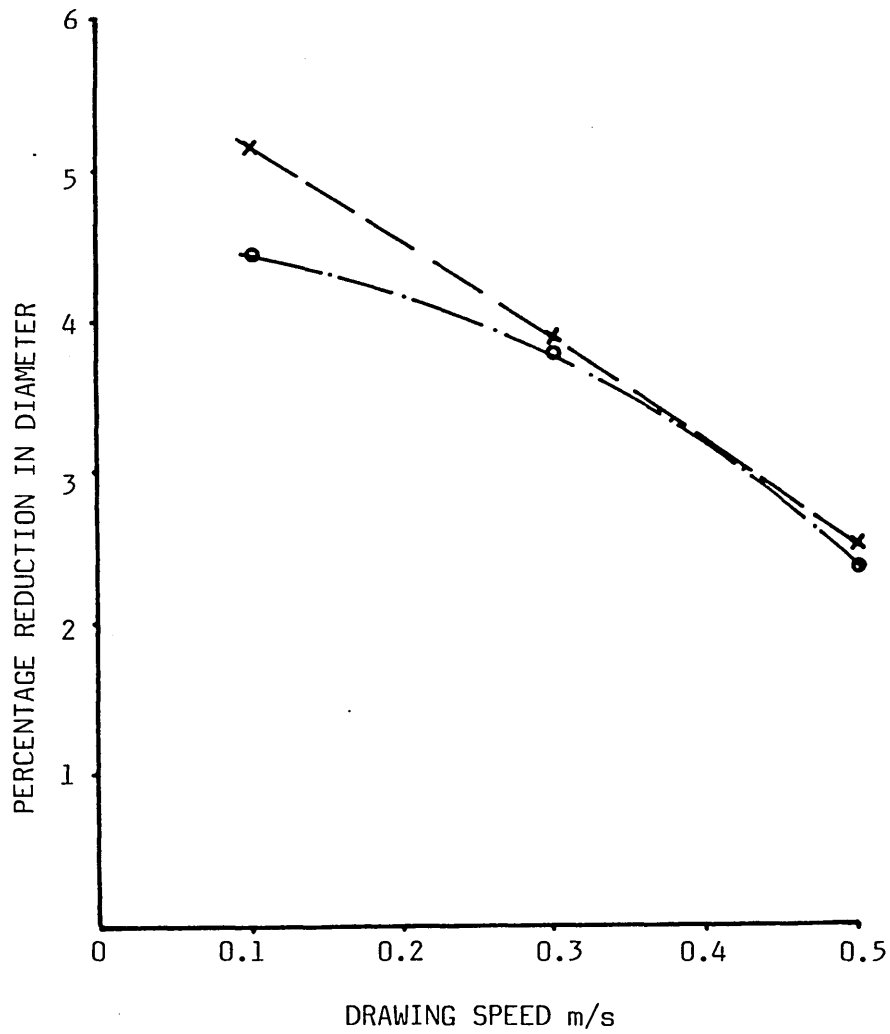


FIG 38 - EFFECT OF GAP RATIO ON PERCENTAGE REDUCTION IN DIAMETER FOR ALUMINIUM TUBE WITH POLYSTYRENE AT 240°C

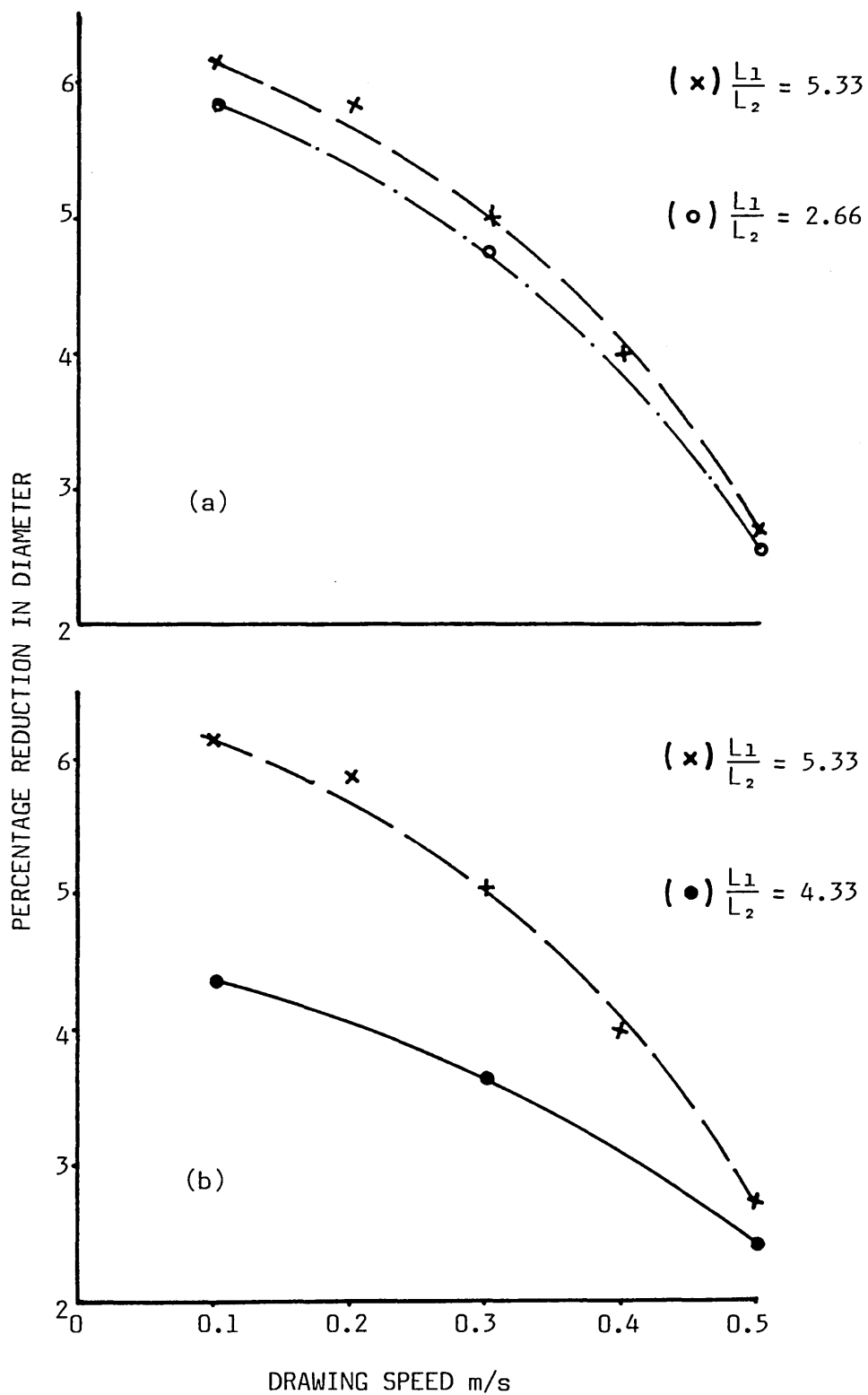


FIG 39 - EFFECT OF LENGTH RATIO ON PERCENTAGE REDUCTION IN DIAMETER FOR COPPER TUBE WITH WVG23 AT 130°C
(a) $L_1 = \text{Const}$ (b) $L_2 = \text{Const}$ ($h_1/h_2 = 50$)

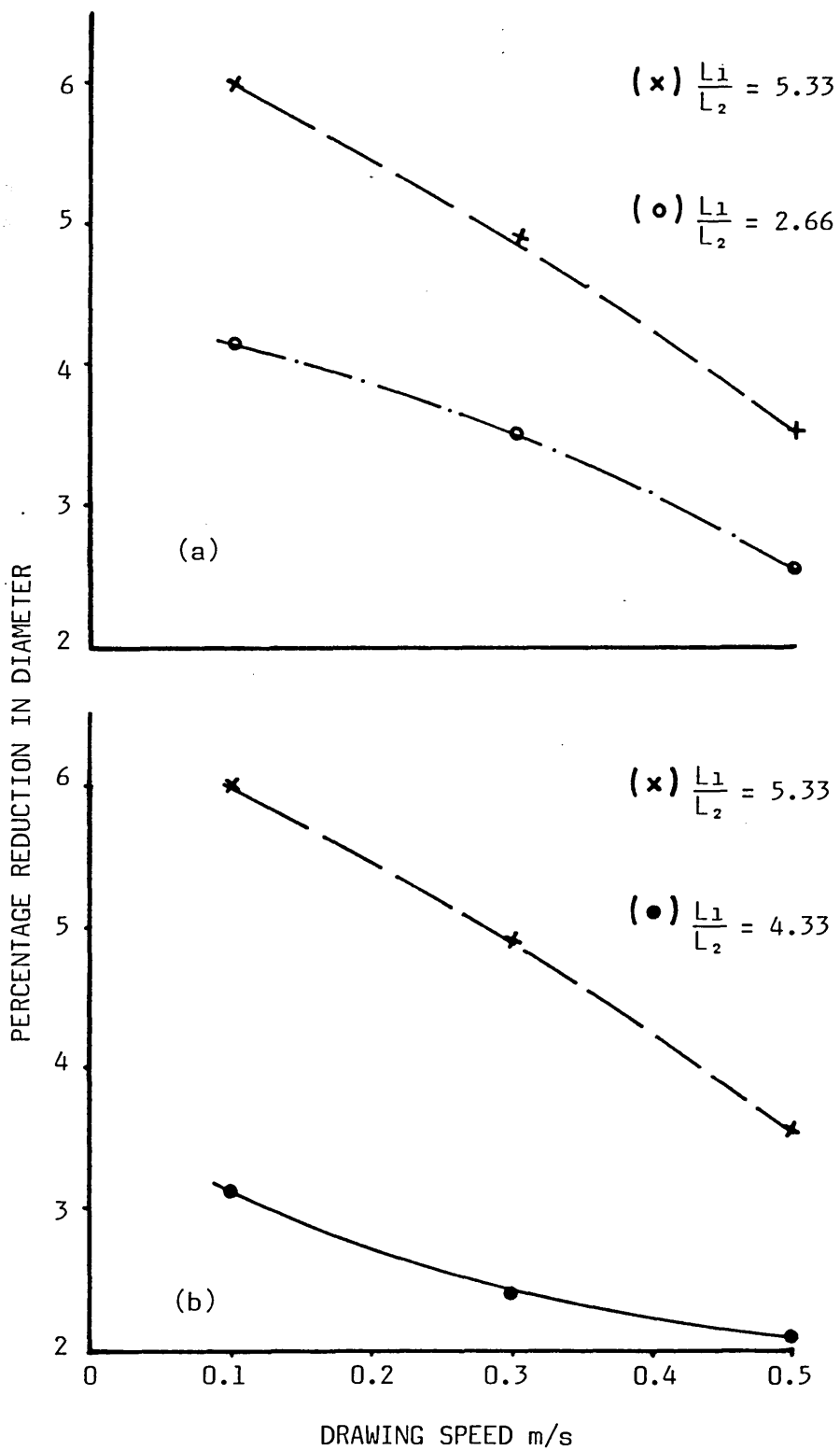


FIG 40 - EFFECT OF LENGTH RATIO ON PERCENTAGE REDUCTION IN DIAMETER FOR COPPER TUBE WITH KM61 AT 220°C
(a) $L_1 = \text{Const}$ (b) $L_2 = \text{Const}$ ($h_1/h_2 = 50$)

$$\frac{h_1}{h_2} = 50$$

$$(x) \frac{L_1}{L_2} = 5.33$$

$$(\bullet) \frac{L_1}{L_2} = 4.33$$

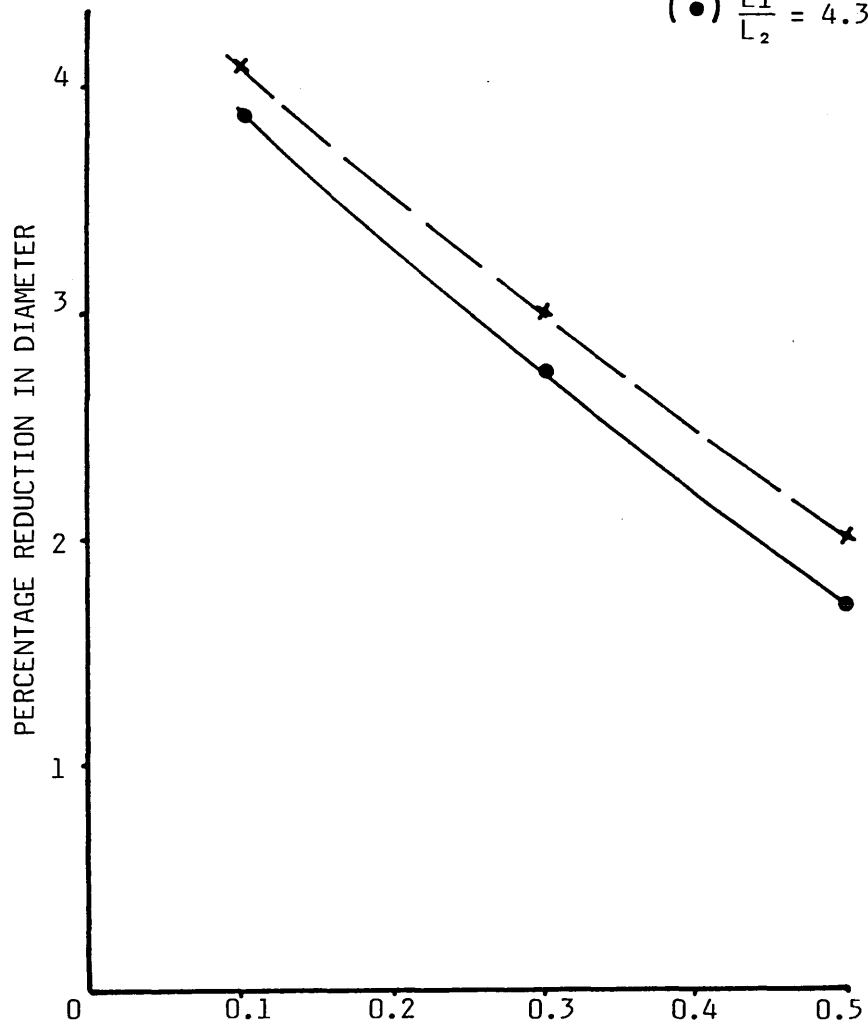


FIG 41 - EFFECT OF LENGTH RATIO ON PERCENTAGE REDUCTION
IN DIAMETER FOR COPPER TUBE WITH RIGIDEX AT 230°C

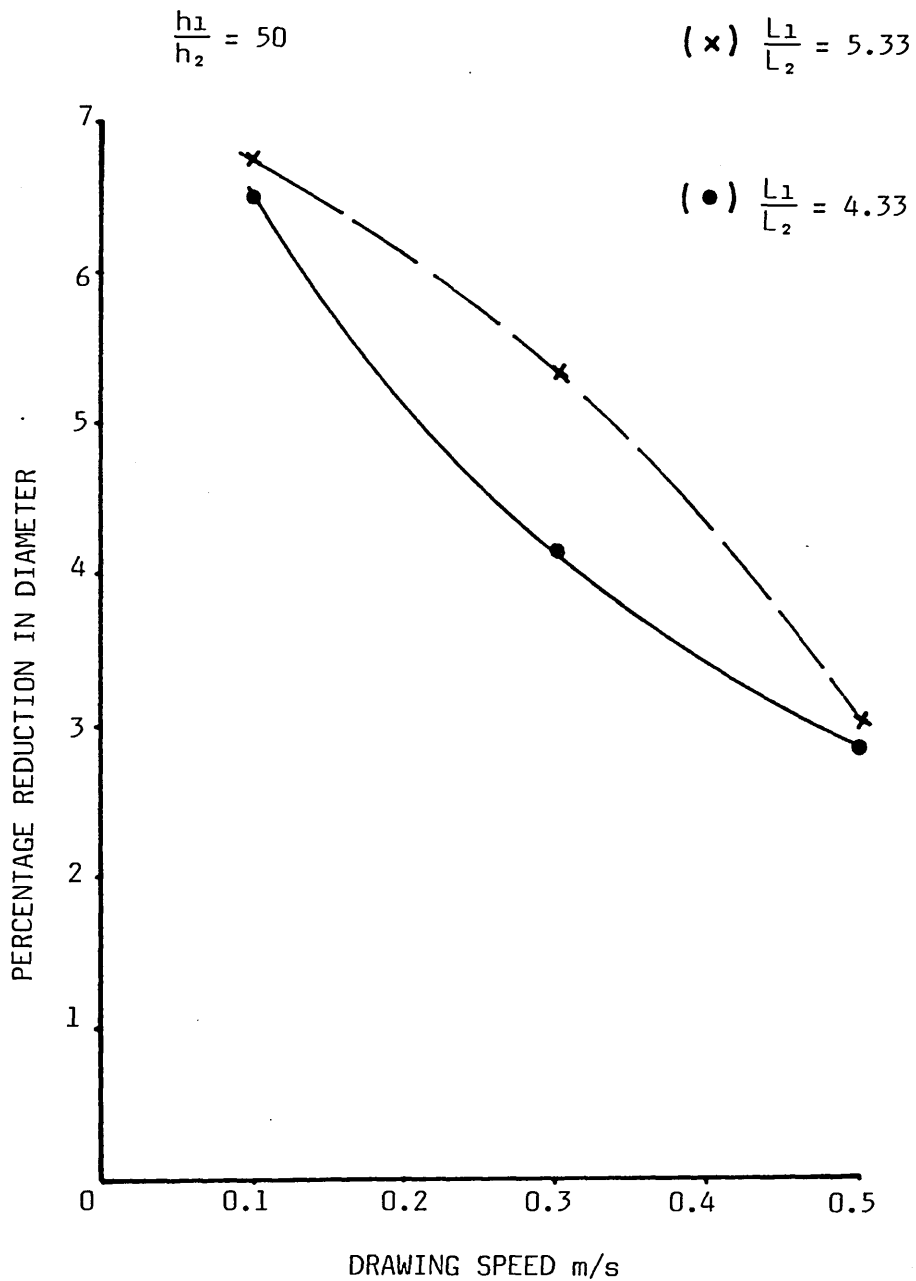


FIG 42 - EFFECT OF LENGTH RATIO ON PERCENTAGE REDUCTION
IN DIAMETER FOR COPPER TUBE WITH POLYSTYRENE AT 240°C

$$\frac{h_1}{h_2} = 50$$

(x) 130°C ($\mu_0 = 100\text{N}\cdot\text{s}/\text{m}^2$)

(o) 160°C ($\mu_0 = 58$)

(•) 180°C ($\mu_0 = 38$)

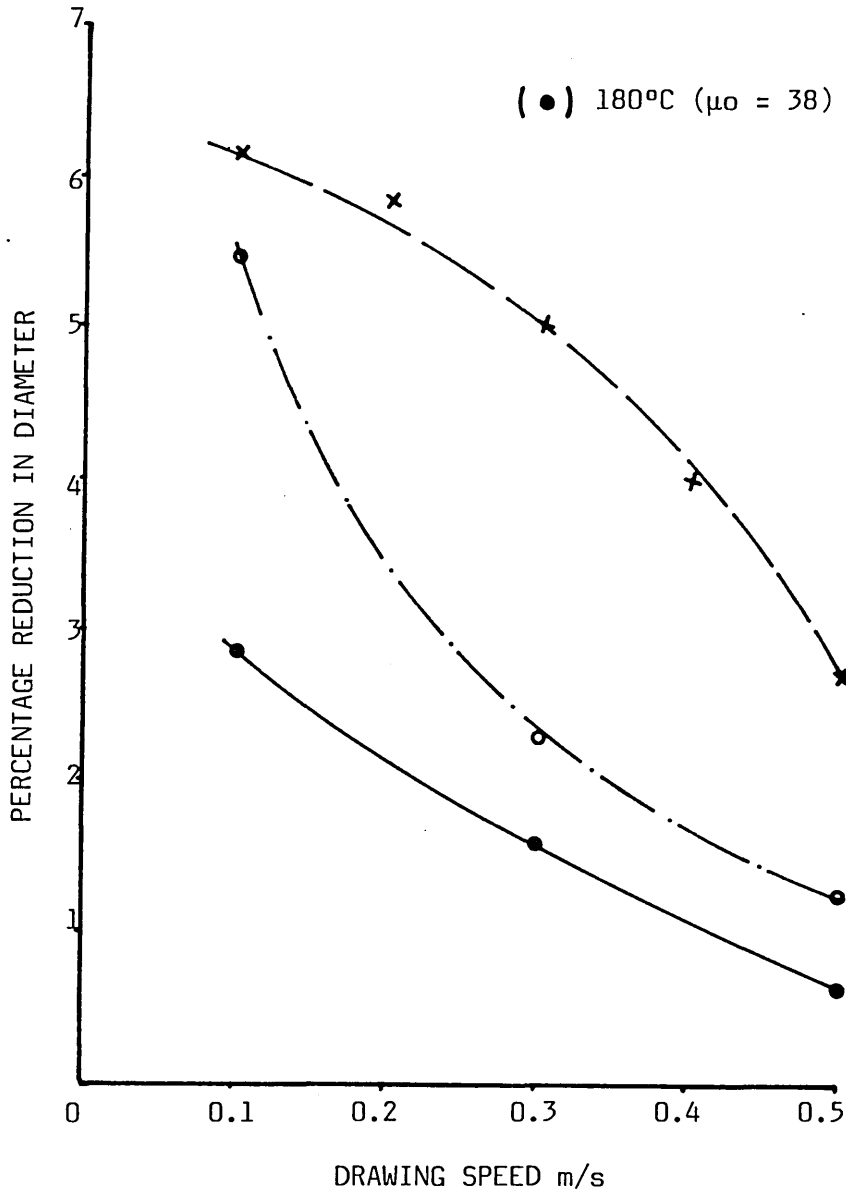


FIG 43 - EFFECT OF VISCOSITY ON PERCENTAGE REDUCTION
IN DIAMETER FOR COPPER TUBE WITH WVG23

$$\frac{h_1}{h_2} = 50$$

(x) 200°C ($\mu_0 = 250 \text{ Ns/m}^2$)

(o) 220°C ($\mu_0 = 200$)

(●) 240°C ($\mu_0 = 150$)

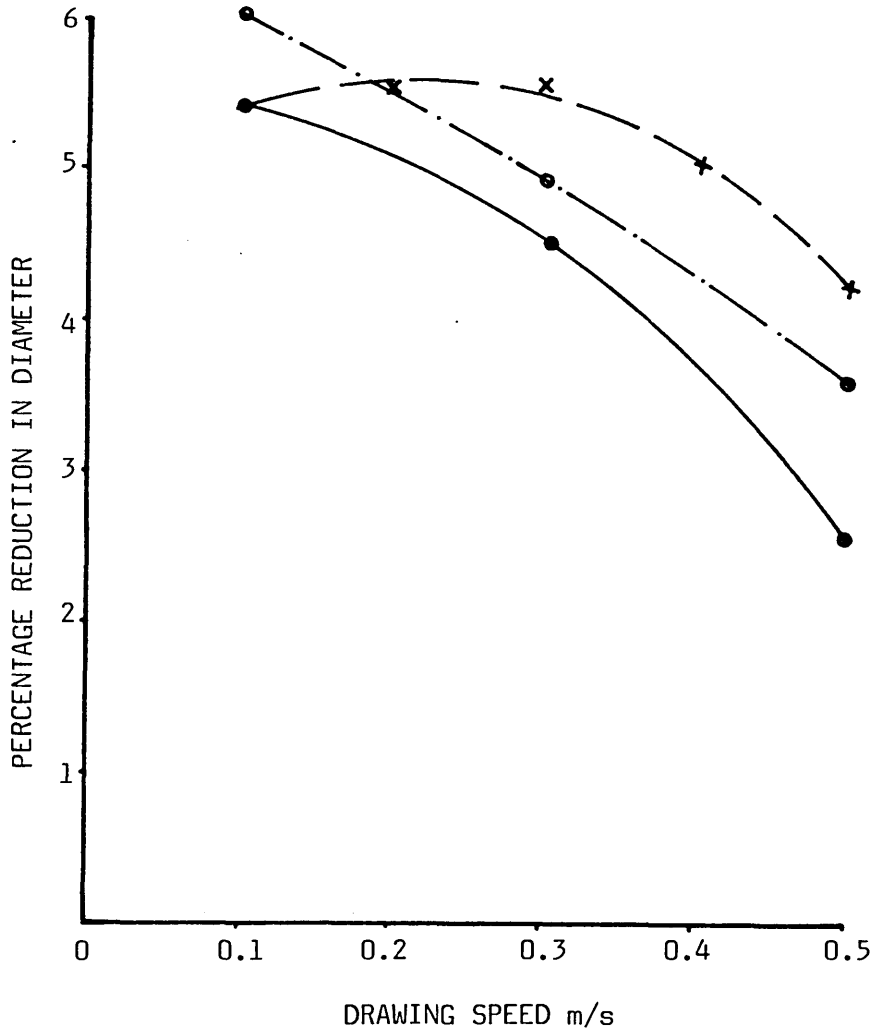


FIG 44 - EFFECT OF VISCOSITY ON PERCENTAGE REDUCTION
IN DIAMETER FOR COPPER TUB WITH KM61

$$\frac{h_1}{h_2} = 50$$

(x) 200°C ($\mu_0 = 333 \text{ N s/m}^2$)

(o) 230°C ($\mu_0 = 267$)

(•) 240°C ($\mu_0 = 222$)

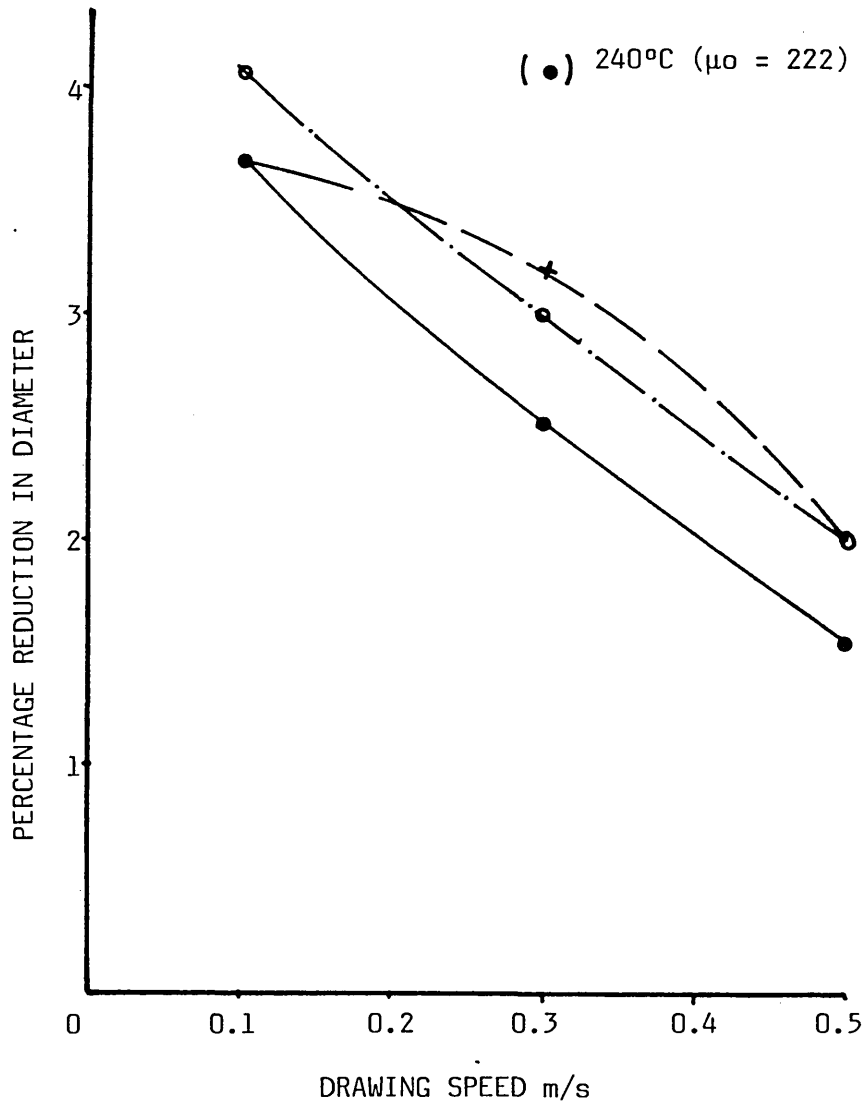


FIG 45 - EFFECT OF VISCOSITY ON PERCENTAGE REDUCTION
IN DIAMETER FOR COPPER TUBE WITH RIGIDEX

$$\frac{h_1}{h_2} = 50$$

(x) 230°C ($\mu_0 = 300 \text{ N s/m}^2$)

(o) 240°C ($\mu_0 = 280$)

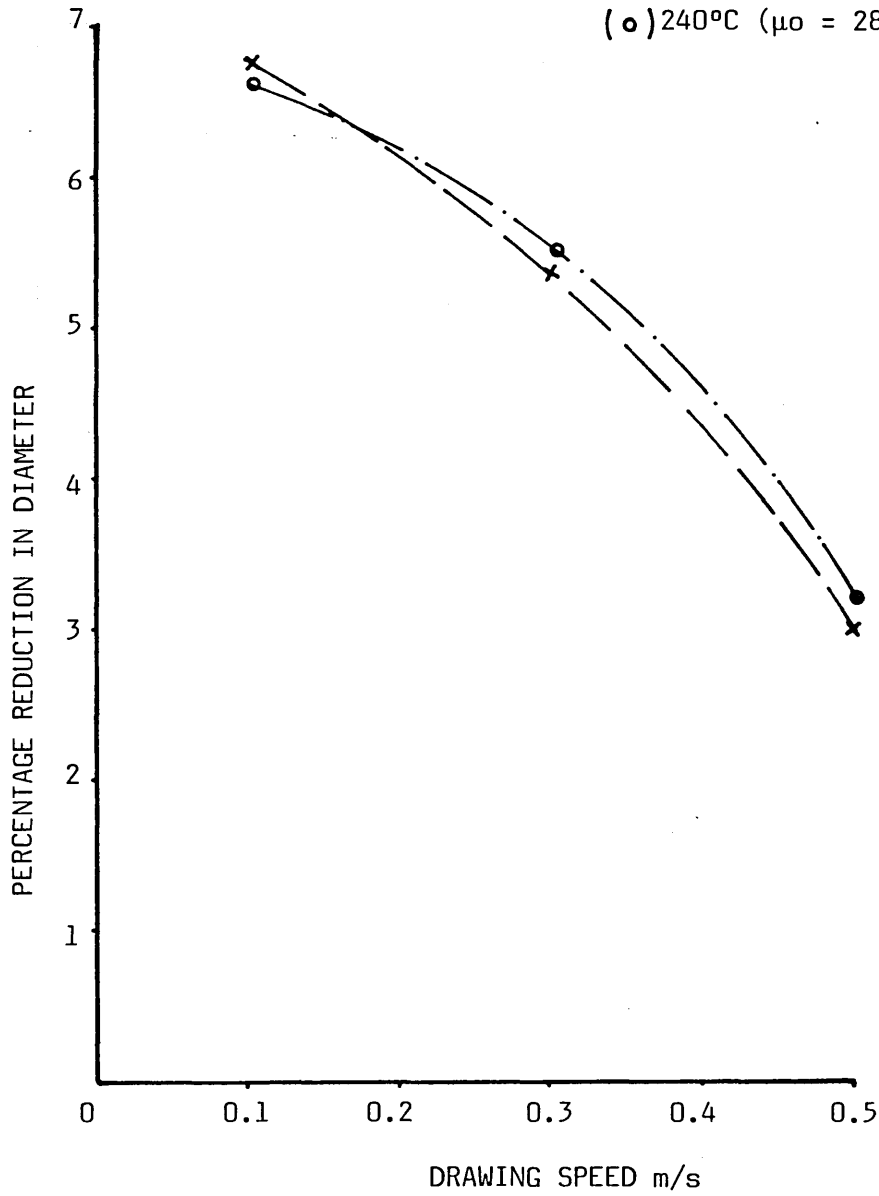


FIG 46 - EFFECT OF VISCOSITY ON PERCENTAGE REDUCTION
IN DIAMETER FOR COPPER TUBE WITH POLYSTYRENE

$$\frac{h_1}{h_2} = 29.57$$

(x) 130°C ($\mu_0 = 100 \text{ N s/m}^2$)

(o) 160°C ($\mu_0 = 58$)

(●) 180°C ($\mu_0 = 38$)

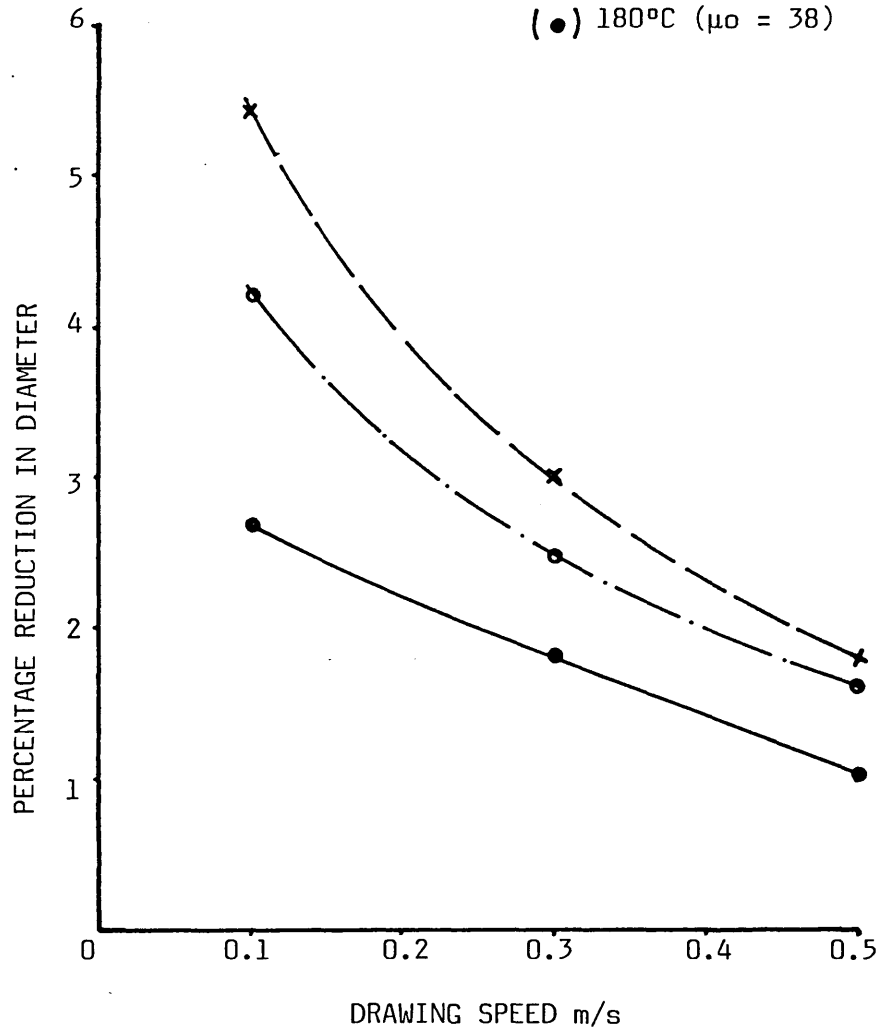


FIG 47 - EFFECT OF VISCOSITY ON PERCENTAGE REDUCTION IN DIAMETER FOR ALUMINIUM TUBE WITH WVG23

$$\frac{h_1}{h_2} = 29.57$$

(x) 220°C ($\mu_0 = 200 \text{ N s/m}^2$)

(o) 240°C ($\mu_0 = 150$)

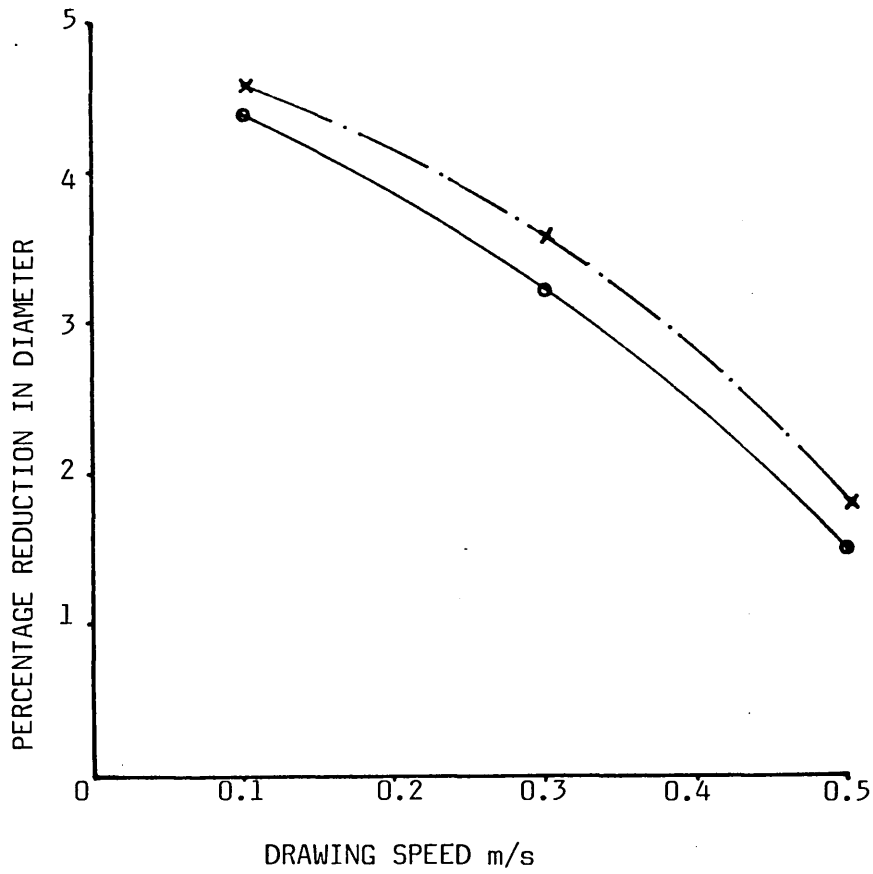


FIG 48 - EFFECT OF VISCOSITY ON PERCENTAGE REDUCTION
IN DIAMETER FOR ALUMINIUM TUBE WITH KM61

$$\frac{h_1}{h_2} = 29.57$$

(x) 230°C ($\mu_0 = 267 \text{ Ns/m}^2$)

(o) 240°C ($\mu_0 = 222$)

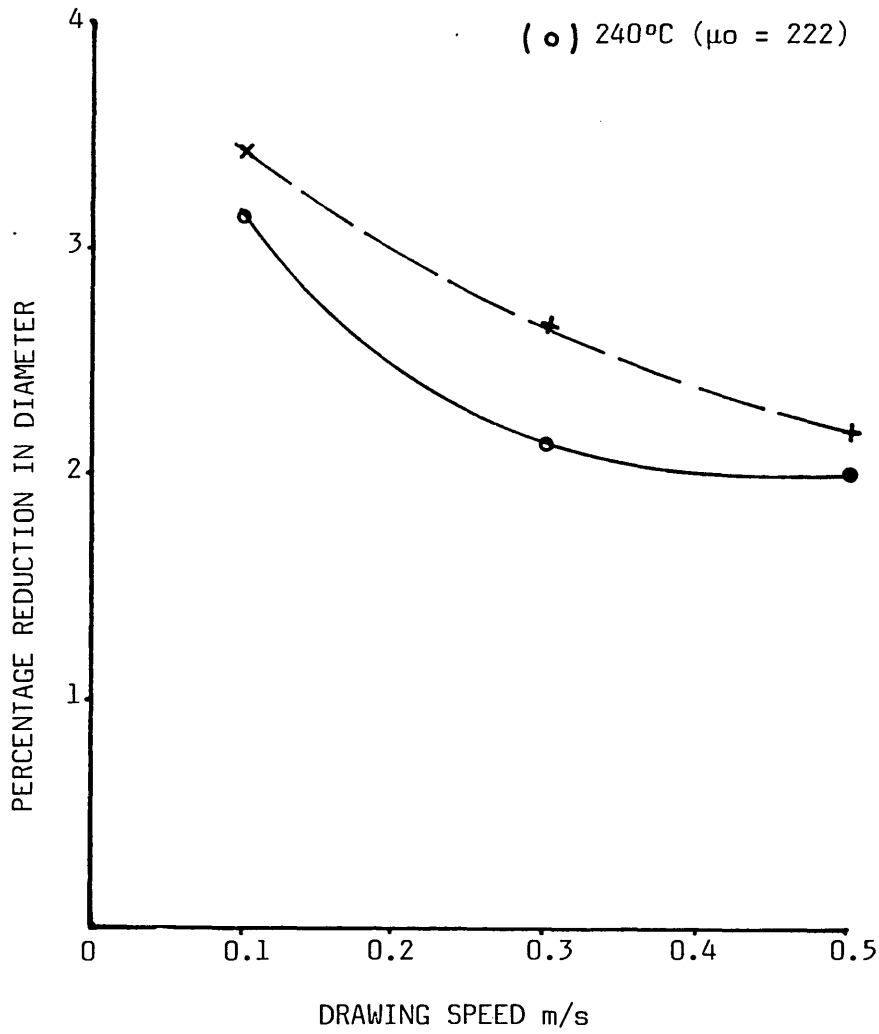


FIG 49 - EFFECT OF VISCOSITY ON PERCENTAGE REDUCTION IN DIAMETER FOR ALUMINIUM TUBE WITH RIGIDEX

$$\frac{h_1}{h_2} = 29.57$$

(x) 230°C ($\mu_0 = 300 \text{ N s/m}^2$)

(o) 240°C ($\mu_0 = 280$)

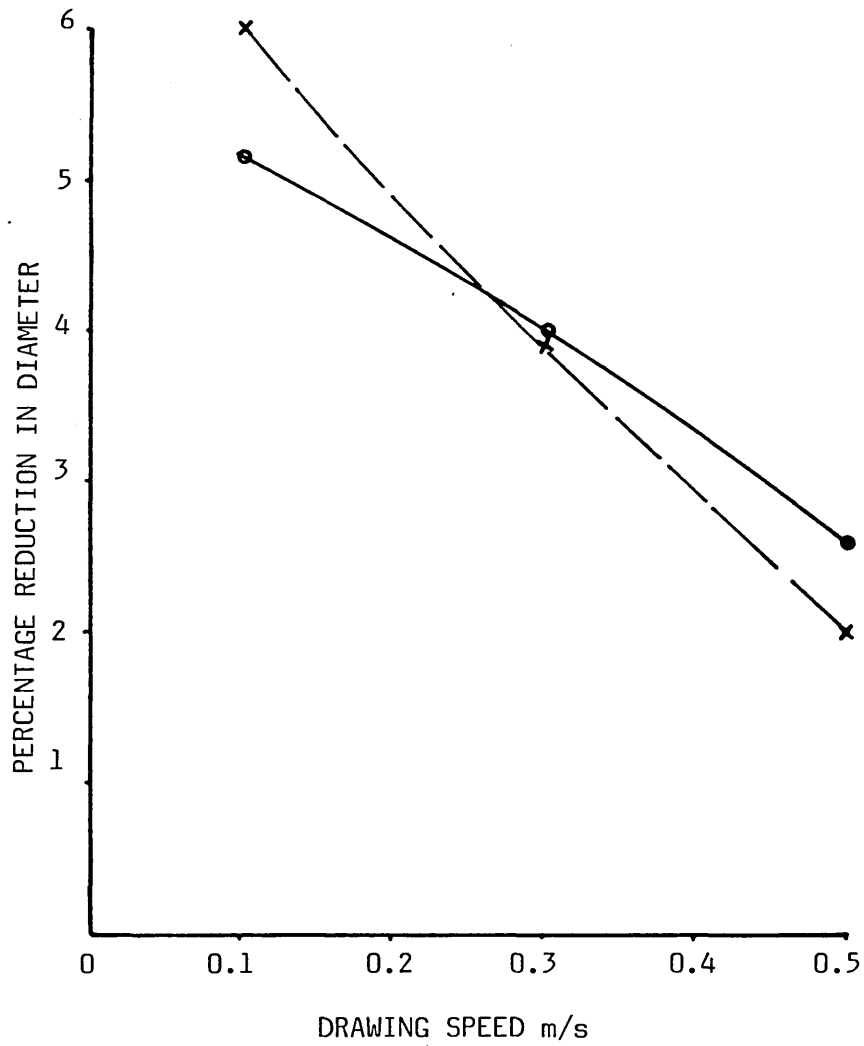


FIG 50 - EFFECT OF VISCOSITY ON PERCENTAGE REDUCTION IN DIAMETER FOR ALUMINIUM TUBE WITH POLYSTYRENE

4.2.2 Results of Drawing Stress versus Drawing Speed

The die-less reduction unit was bolted to the hinged die plate which rests against a load cell during drawing. The drawing load was then noted from the load indicator as shown in plate 2. The results are presented in this section in terms of the drawing stress.

Fig 51 shows the plots of drawing stress versus drawing speed for copper tube corresponding to four different gap ratios using WVG23 polymer at the melt temperature of 130°C. This figure shows that the drawing stress was maximum when the reduction in diameter was maximum, ie at drawing speed of about 0.1 m/s. The maximum drawing stress (about 40 MN/m²) was noted for the gap ratio of 50. Drawing stresses for all the gap ratios decreased as the drawing speed was increased. At speeds in excess of 0.4 m/s approximately same drawing stresses were noted (about 13 MN/m²) for the gap ratios of 41, 25 and 5.

Fig 52 shows the effect of the gap ratio on drawing stress for copper tube when KM61 polymer was used at the melt temperature of 220°C. In the case of the gap ratio of 50, this polymer produced higher drawing stress (about 60 MN/m²) at lower drawing speed. As the drawing speed was increased, the drawing stress fell to about 30 MN/m². Approximately same drawing stresses were noted for gap ratios of 40 and 25 at all drawing speeds.

Figs 53 and 54 show the variations in the drawing stress with drawing speed for copper tube when Rigidex and Polystyrene polymers were used at melt temperatures of 230°C and 240°C respectively. When Rigidex polymer was used as the pressure medium at 230°C, the maximum drawing stress measured was about 36 MN/m² at 0.1 m/s. In the case of polystyrene the drawing stress was noted to be about 46 MN/m² at the same speed and same gap ratio.

Fig 55 shows the effect of gap ratio on drawing stress for aluminium tube versus speed using WVG23 polymer at 130°C. This figure shows that at the drawing speed of about 0.1 m/s, the maximum drawing stress was noted to be about 24 MN/m² for the gap ratio of 29.57.

The maximum drawing stresses were noted when KM61 polymer was used as the pressure medium for aluminium tube at a melt temperature of 220°C as shown in Fig 56. A maximum drawing stress of about 40 MN/m² was obtained at 0.1 m/s for 29.57 gap ratio.

Fig 57 shows the effect of gap ratio on the drawing stress for aluminium tube versus speed using Rigidex at 230°C. At higher gap ratio (29.57), higher drawing stresses were noted. For the gap ratio of 26.5 approximately constant drawing stresses were measured at speeds in excess of 0.4 m/s.

Fig 58 shows the effect of gap ratio on the drawing stress for aluminium tube against drawing speed using polystyrene polymer at 240°C. This figure shows that the maximum drawing stress was noted at 0.1 m/s. Approximately constant drawing stresses were noted at speeds in excess of 0.4 m/s for both gap ratios.

The effect of length ratio on the drawing stress for copper tube when WVG23 polymer was used at 130°C can be seen in Fig 59. These results show similar trends as shown in Fig 51, higher drawing speeds producing lower drawing stresses. Changing the length of the second part of the die-less reduction unit (L_2), it was noted that the effect on the drawing stress was comparatively less than when the length L_1 was changed.

Fig 60 shows the effect of length ratio on drawing stress for copper tube versus drawing speed using KM61 polymer at 220°C with constant gap ratio. Keeping L_1 constant as shown in Fig 60(a), the

maximum drawing stress was noted at drawing speed of 0.1 m/s. The drawing stress was found to be the same in the case of both gap ratios ($L_1/L_2 = 5.33$ and $L_1/L_2 = 2.66$) at higher drawing speed, ie 0.5 m/s.

The effect of length ratio on drawing stress for copper tube using Rigidex polymer at 230°C with constant gap ratio is demonstrated in Fig 61. This figure shows that at lower drawing speeds, the drawing stress was found to be of the same order as shown in Fig 59 corresponding to a length ratio of 4.33.

Fig 62 shows the effect of length ratio on drawing stress for copper tube when polystyrene polymer was used as the pressure medium at a melt temperature of 240°C. The general trends were found to be same as those in Figs 59 to 61.

Fig 63 shows the variations in the drawing stress with speed for copper tube with WVG23 polymer at three different temperatures (130°C, 160°C and 180°C). This figure shows that the minimum drawing stress was noted at lower viscosity. At the temperature of 130°C, generally higher drawing stresses were noted and a maximum was observed at about 0.1 m/s.

Effect of viscosity on drawing stress for copper tube versus speed is shown in Fig 64. When KM61 polymer was used as the pressure medium at three different temperatures (200°C, 230°C and 240°C) comparatively greater drawing stresses were noted when this polymer was used instead of WVG23 polymer (see Fig 63). At lower drawing speed (0.1 m/s), the drawing stress reached about 80 MN/m² at 200°C and as the drawing speed was increased the drawing stress was reduced by about 50% at the same melt temperature. At higher melt temperatures the viscosity of the polymer melt decreased and reduced drawing stresses were noted.

Fig 65 shows the effect of viscosity on drawing stress for copper tube when Rigidex polymer was used at temperatures of 200°C, 230°C and 240°C. Drawing stresses were found to be lower when compared with those obtained using WVG23 and KM61 polymers as shown in Figs 63 and 64 respectively. The drawing stress was found to be the same at temperatures of 200°C and 230°C at higher drawing speed, ie 0.5 m/s.

Fig 66 shows the effect of viscosity on drawing stress for copper tube when polystyrene polymer was used at two different temperatures (230°C and 240°C). At the temperature of 230°C, generally higher drawing stresses were measured and a maximum value was observed at about 0.1 m/s.

The effect of viscosity on drawing stress for aluminium tube versus speed with WVG23 polymer at melt temperatures of 130°C, 160°C and 180°C is demonstrated in Fig 67. This figure shows that maximum drawing stress was noted for the melt temperature of 130°C at about 0.1 m/s. At the melt temperature of 160°C the maximum drawing stress obtained was about 20 MN/m² at 0.1 m/s, as the drawing speed was increased, the drawing stress was reduced by about 50% at 0.5 m/s.

Fig 68 shows the effect of viscosity on drawing stress for aluminium tube when KM61 polymer was used as the pressure medium at three different temperatures (200°C, 220°C and 240°C). The general trends were found to be the same as those for copper tubes (see Fig 64). For the melt temperature of 200°C, the maximum drawing stress occurred at the drawing speed of about 0.1 m/s after which it decreased with increased drawing speed. For the melt temperatures of 220°C and 240°C, approximately same drawing stresses were noted for both melt temperatures at drawing speed of about 0.5 m/s.

Fig 69 shows the effect of viscosity on drawing stress for aluminium tube versus speed with Rigidex polymer at melt temperatures of 230°C and 240°C. This figure shows that the drawing stress was maximum, when the reduction in diameter was maximum, ie at drawing speed of 0.1 m/s. The maximum drawing stress of about 26 MN/m² was noted at the melt temperature of 230°C.

Fig 70 shows the variations in the drawing stress with speed for aluminium tube when polystyrene polymer was used at two different temperatures (230°C and 240°C). Approximately constant drawing stresses were noted at speeds in excess of 0.3 m/s for melt temperature of 240°C. At the temperature of 230°C, generally higher drawing stresses were noted and a maximum value was observed at about 0.1 m/s.

$$\frac{L_1}{L_2} = 5.33$$

$$(\times) \frac{h_1}{h_2} = 50$$

$$(\circ) \frac{h_1}{h_2} = 40$$

$$(\bullet) \frac{h_1}{h_2} = 25$$

$$(\circ) \frac{h_1}{h_2} = 5$$

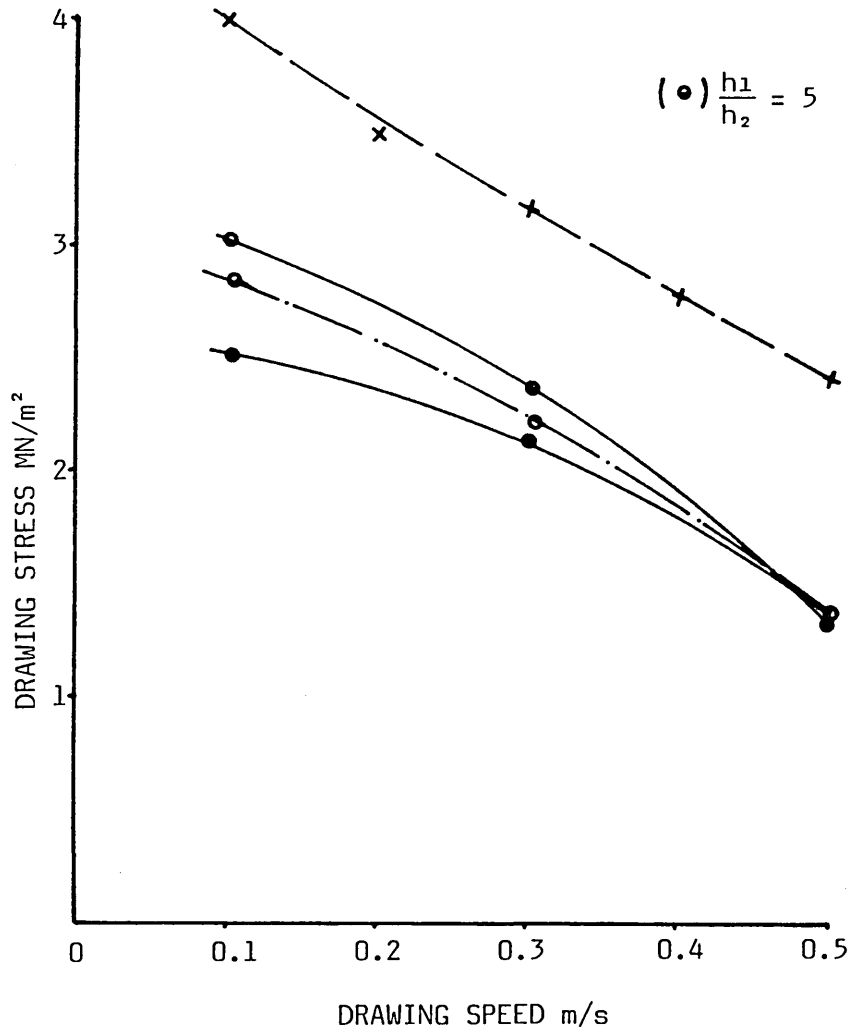


FIG 51 - EFFECT OF GAP RATIO ON DRAWING STRESS
FOR COPPER TUBE WITH WVG23 AT 130°C

$$\frac{L_1}{L_2} = 5.33$$

$$(\times) \frac{h_1}{h_2} = 50$$

$$(\circ) \frac{h_1}{h_2} = 40$$

$$(\bullet) \frac{h_1}{h_2} = 25$$

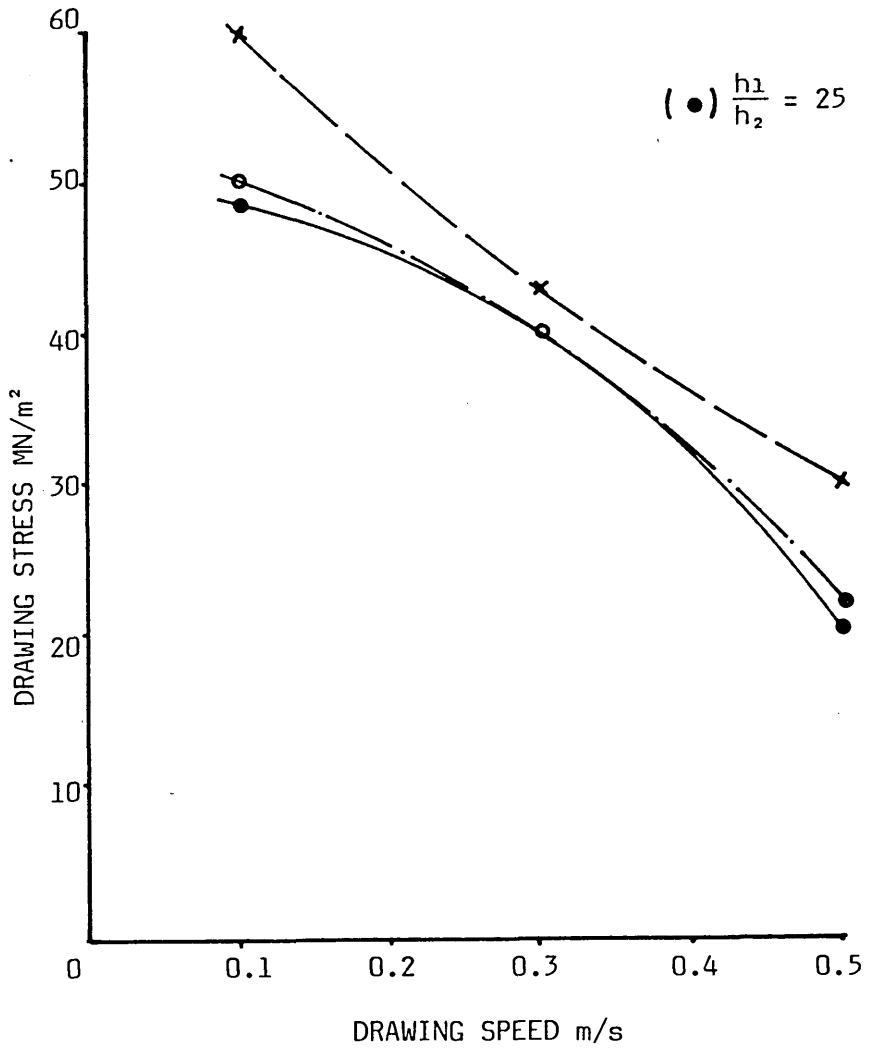


FIG 52 - EFFECT OF GAP RATIO ON DRAWING STRESS FOR
COPPER TUBE WITH KM61 AT 220°C

$$\frac{L_1}{L_2} = 5.33$$

$$(\times) \frac{h_1}{h_2} = 50$$

$$(\circ) \frac{h_1}{h_2} = 40$$

$$(\bullet) \frac{h_1}{h_2} = 25$$

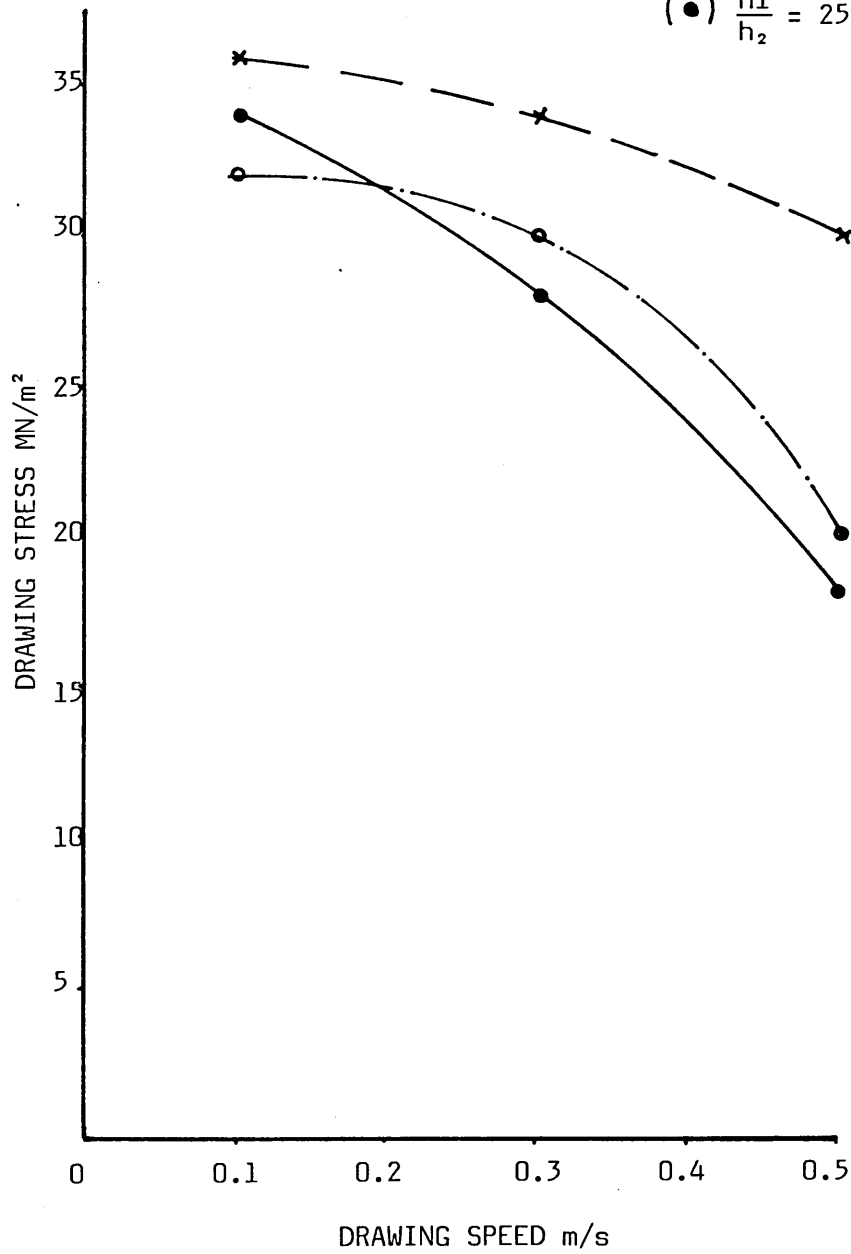


FIG 53 - EFFECT OF GAP RATIO ON DRAWING STRESS FOR COPPER TUBE WITH RIGIDEX AT 230°C

$$\frac{L_1}{L_2} = 5.33$$

$$(\times) \frac{h_1}{h_2} = 50$$

$$(\circ) \frac{h_1}{h_2} = 40$$

$$(\bullet) \frac{h_1}{h_2} = 25$$

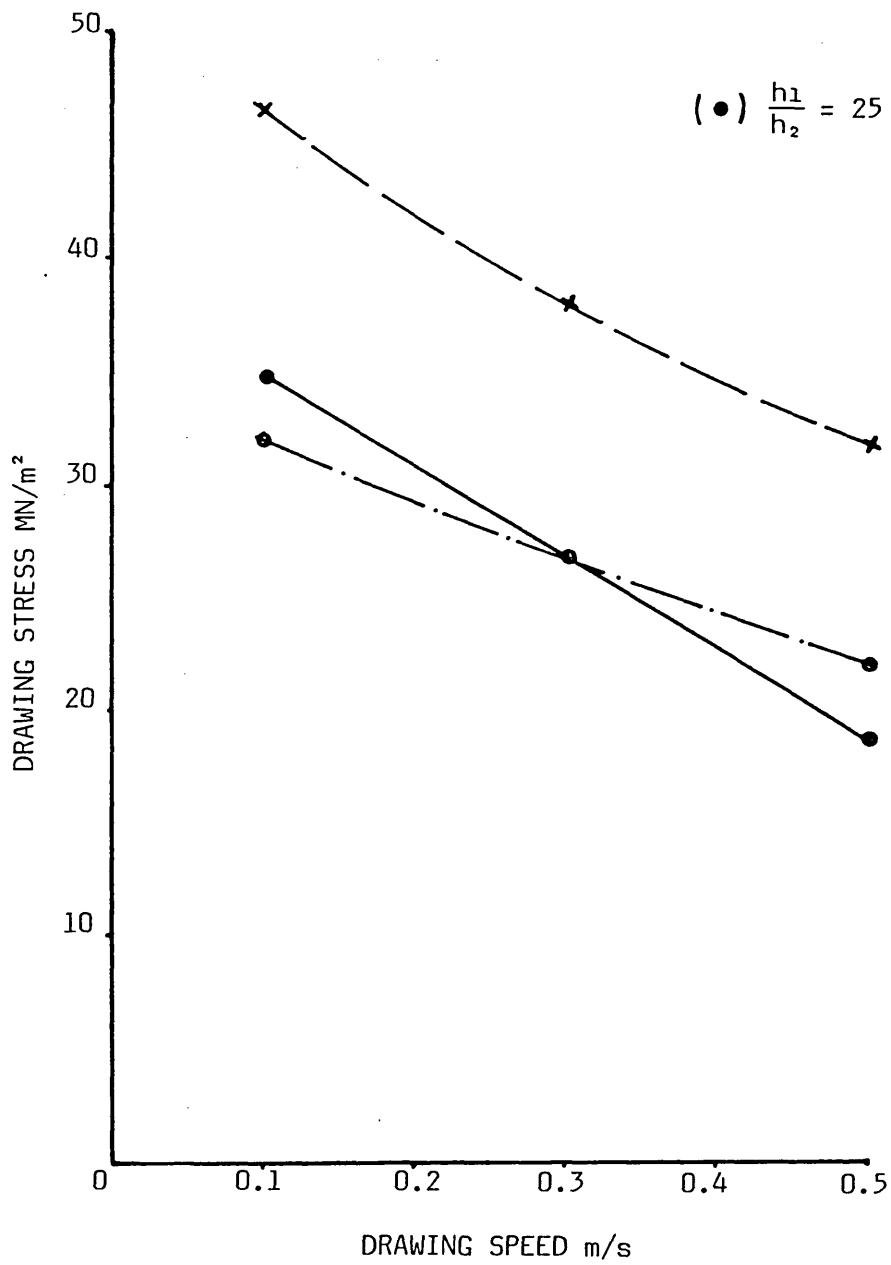


FIG 54 - EFFECT OF GAP RATIO ON DRAWING STRESS FOR
COPPER TUBE WITH POLYSTYRENE AT 240°C

$$\frac{L_1}{L_2} = 5$$

$$(x) \frac{h_1}{h_2} = 29.57$$

$$(o) \frac{h_1}{h_2} = 26.5$$

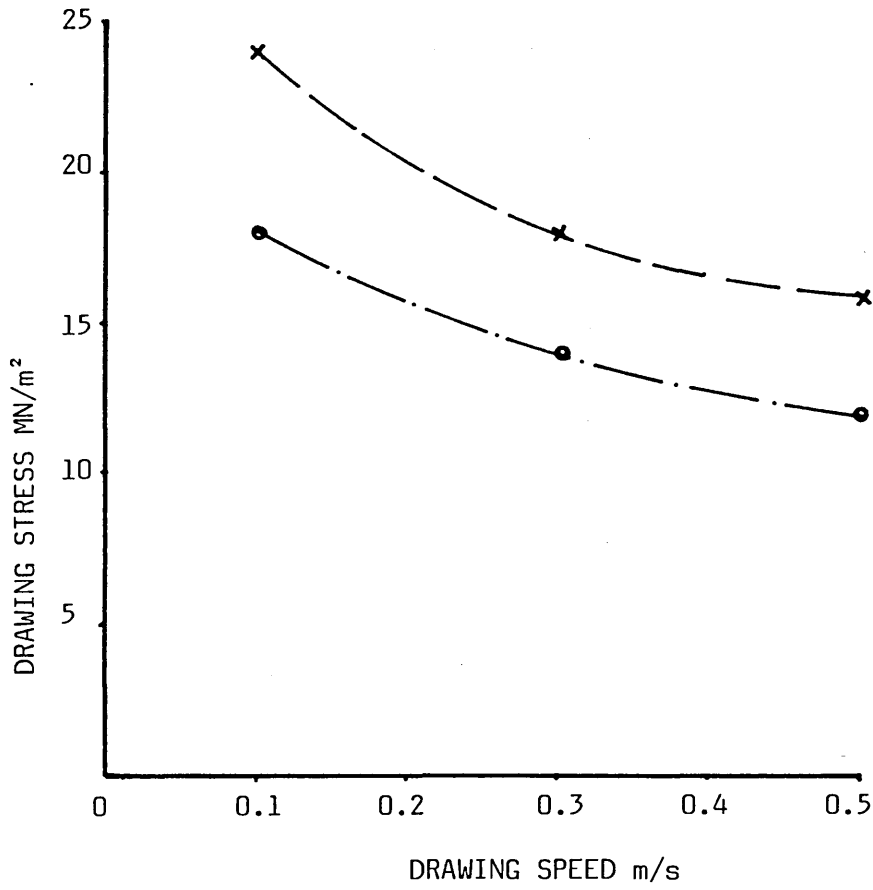


FIG 55 - EFFECT OF GAP RATIO ON DRAWING STRESS FOR ALUMINIUM TUBE WITH WVG23 AT 130°C

$$\frac{L_1}{L_2} = 5$$

$$(\times) \frac{h_1}{h_2} = 29.57$$

$$(\circ) \frac{h_1}{h_2} = 26.5$$

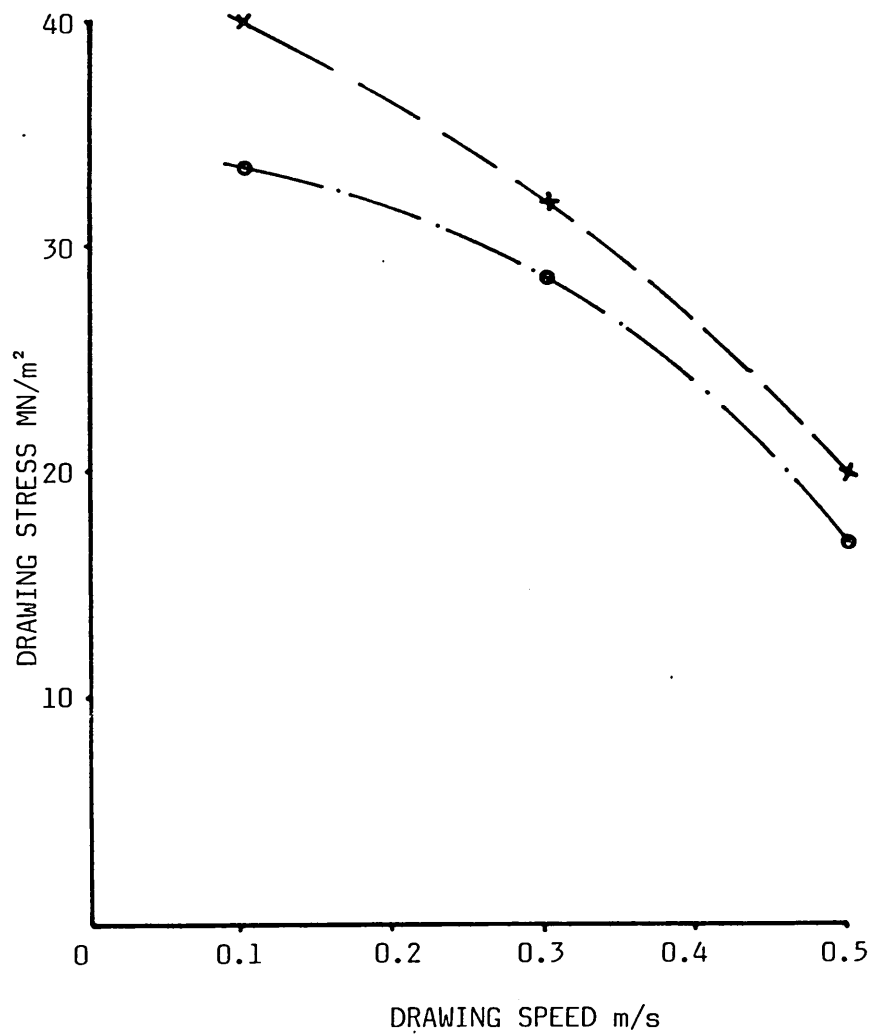


FIG 56 - EFFECT OF GAP RATIO ON DRAWING STRESS FOR ALUMINIUM TUBE WITH KM61 AT 220°C

$$\frac{L_1}{L_2} = 5$$

$$(\times) \frac{h_1}{h_2} = 29.57$$

$$(\circ) \frac{h_1}{h_2} = 26.5$$

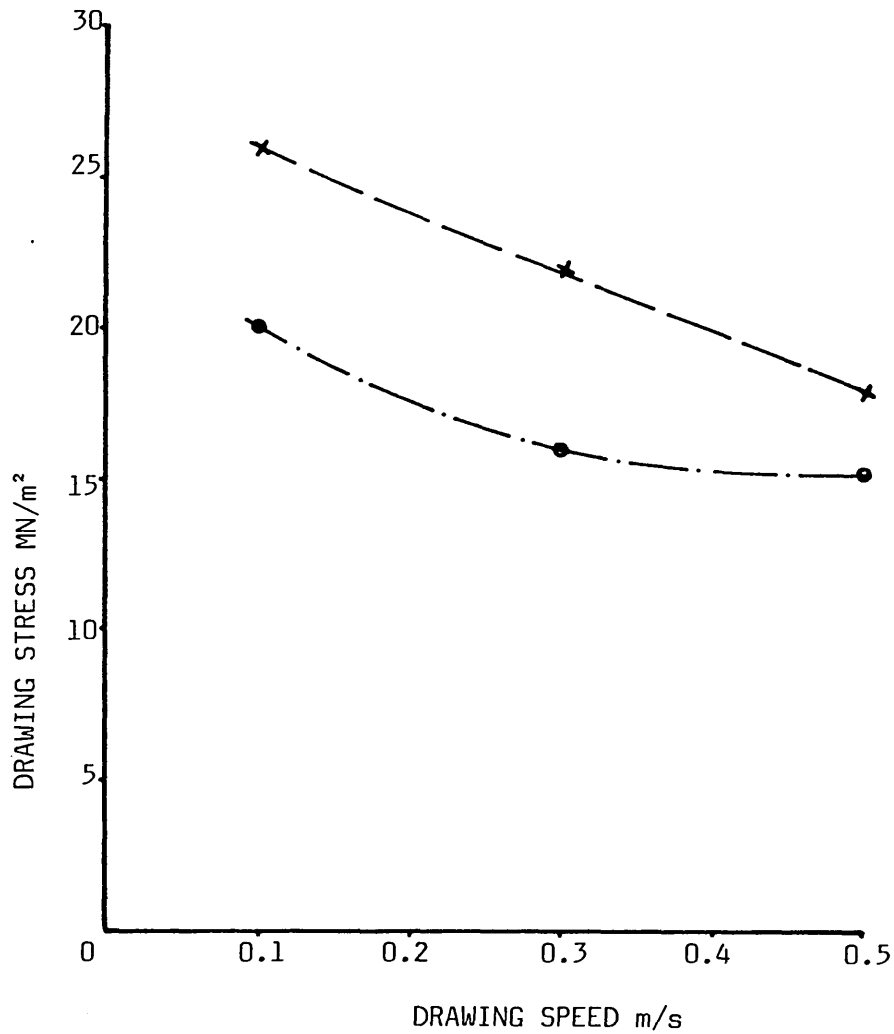


FIG 57 - EFFECT OF GAP RATIO ON DRAWING STRESS FOR ALUMINIUM TUBE WITH RIGIDEX AT 230°C

$$\frac{L_1}{L_2} = 5$$

$$(\times) \frac{h_1}{h_2} = 29.57$$

$$(\circ) \frac{h_1}{h_2} = 26.5$$

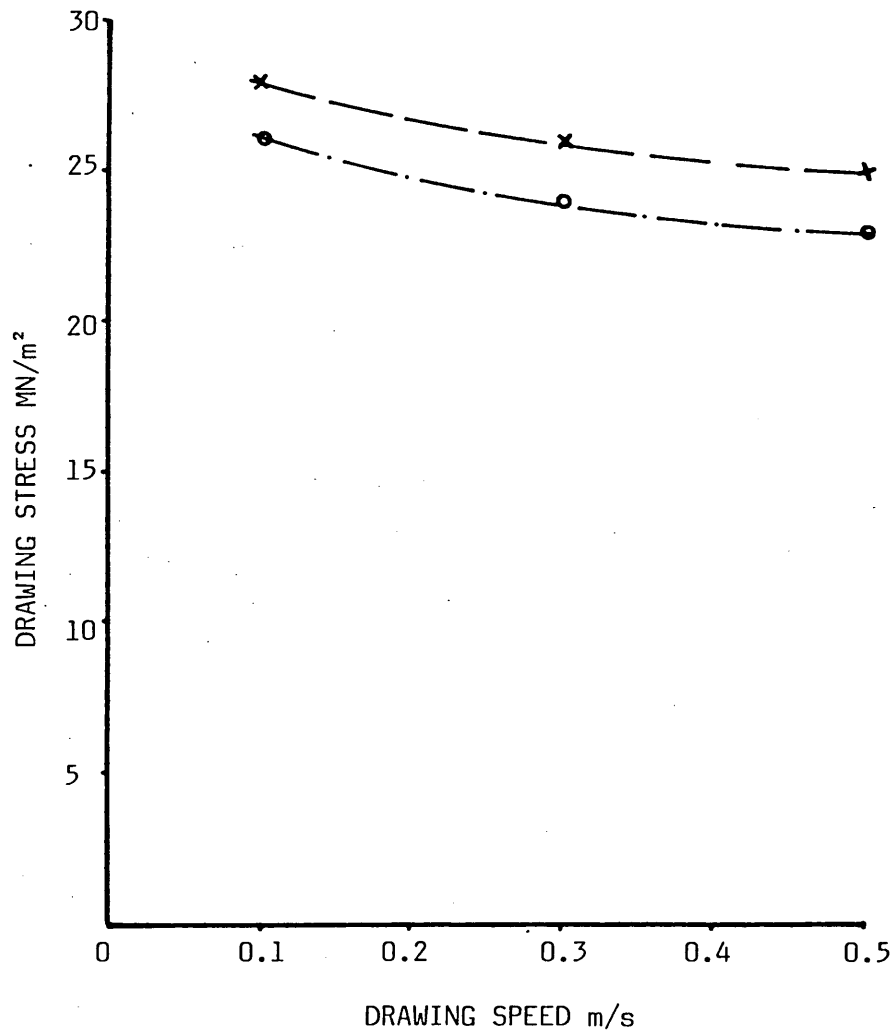


FIG 58 - EFFECT OF GAP RATIO ON DRAWING STRESS FOR ALUMINIUM TUBE WITH POLYSTYRENE AT 240°C

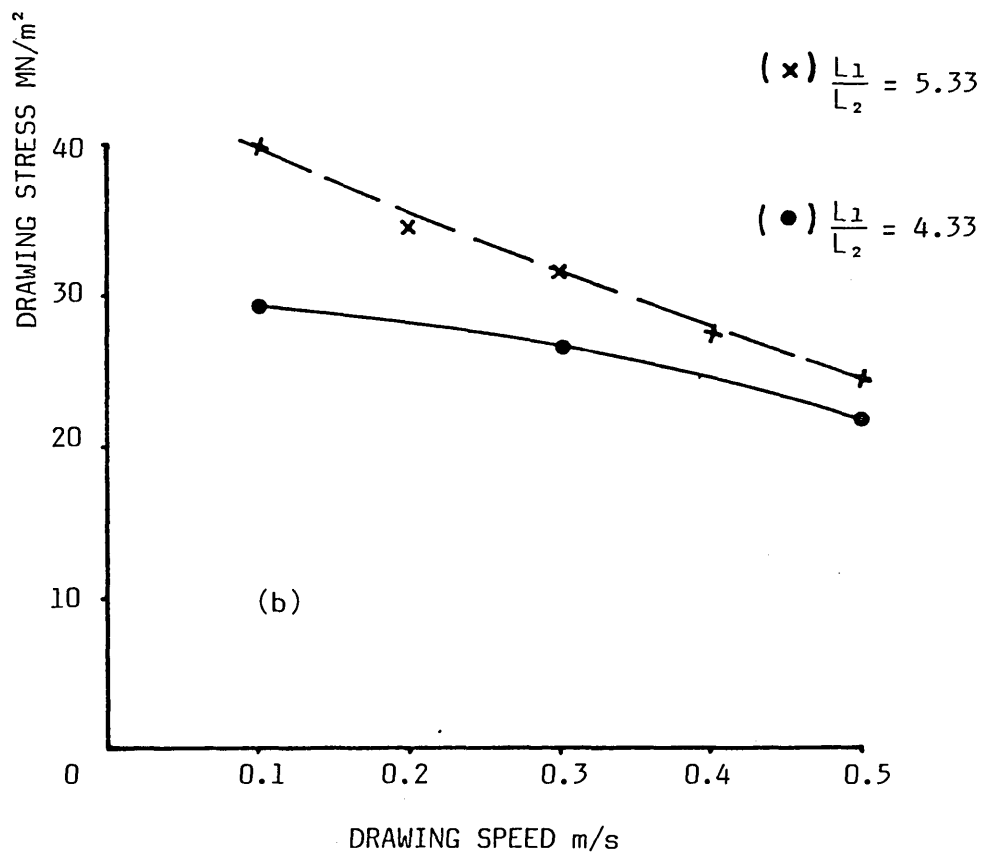
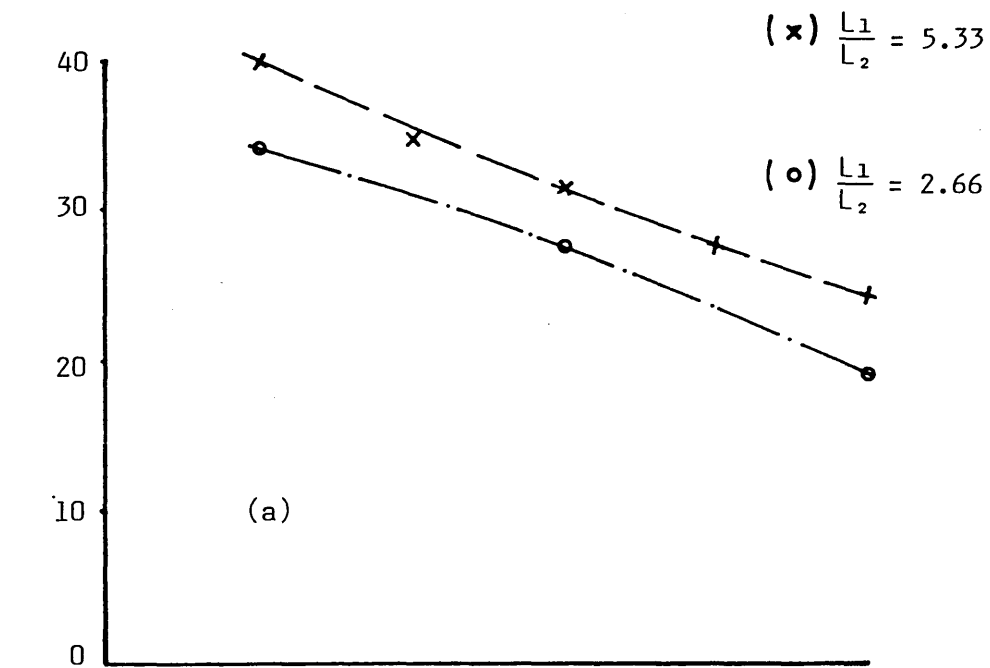
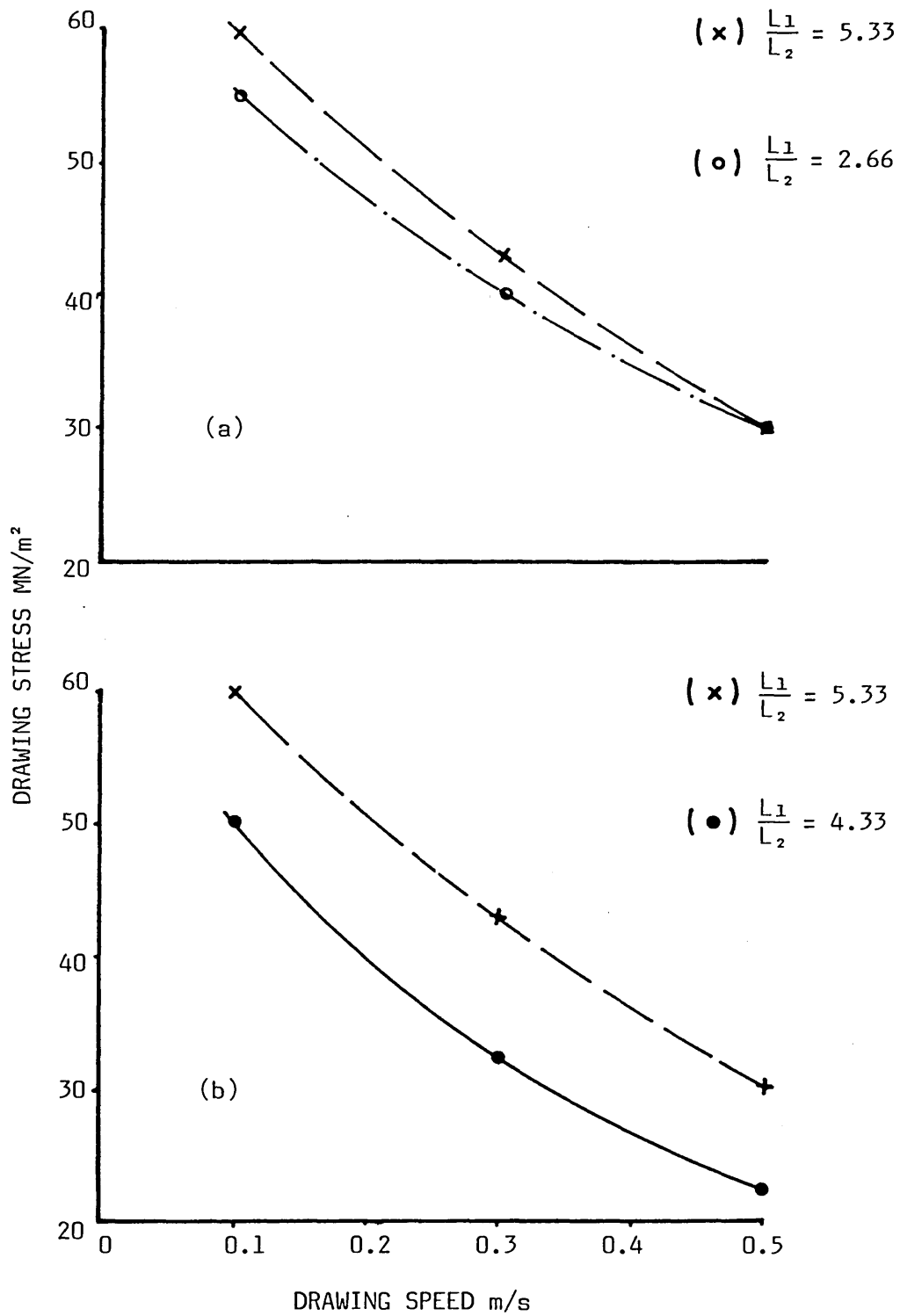


FIG 59 - EFFECT OF LENGTH RATIO ON DRAWING STRESS FOR
 COPPER TUBE WITH WVG23 AT 130°C
 (a) $L_1 = \text{Const}$ (b) $L_2 = \text{Const}$ ($h_1/h_2 = 50$)



**FIG 60 - EFFECT OF LENGTH RATIO ON DRAWING STRESS FOR
COPPER TUBE WITH KM61 AT 220°C**
(a) $L_1 = \text{Const}$ (b) $L_2 = \text{Const}$ ($h_1/h_2 = 50$)

$$\frac{h_1}{h_2} = 50$$

$$(\times) \frac{L_1}{L_2} = 5.33$$

$$(\bullet) \frac{L_1}{L_2} = 4.33$$

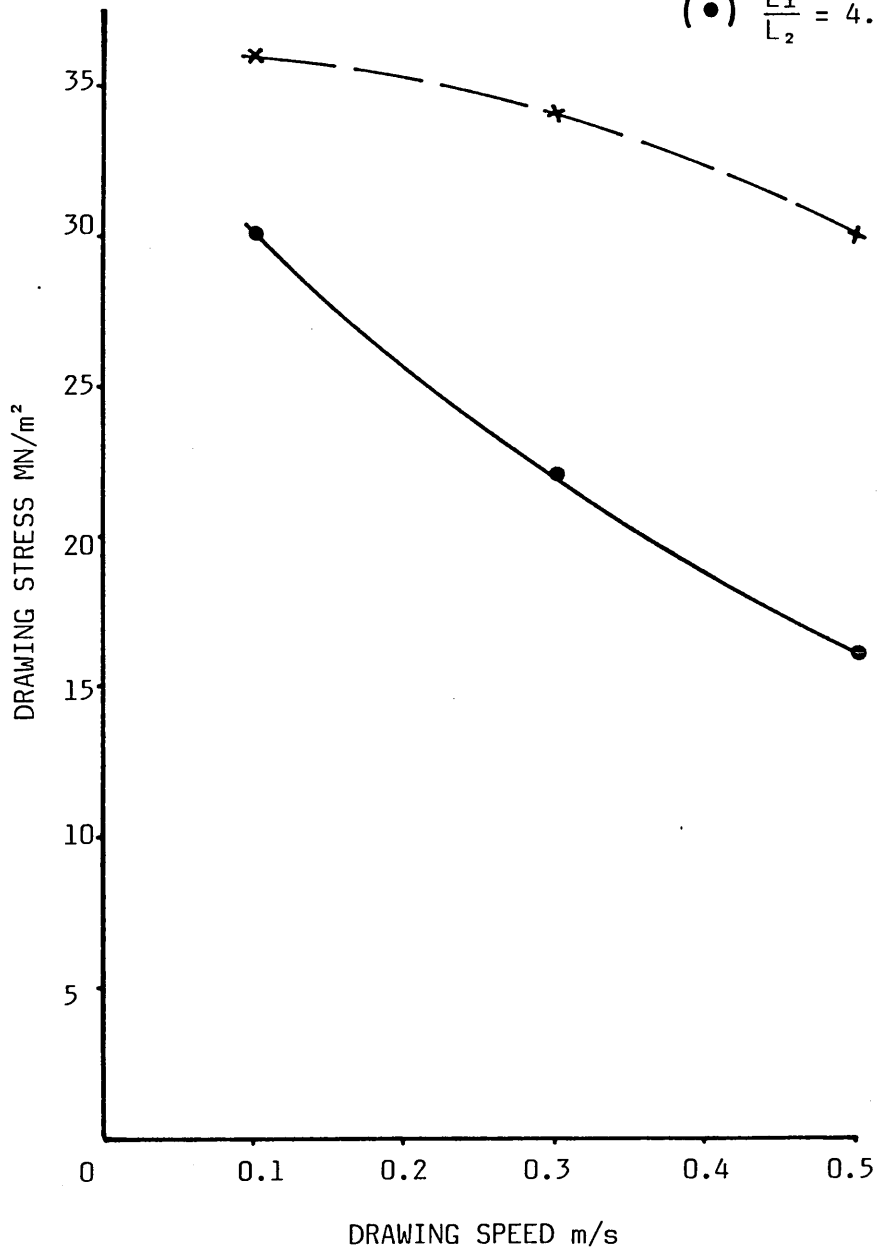


**FIG 61 - EFFECT OF LENGTH RATIO ON DRAWING STRESS
FOR COPPER TUBE WITH RIGIDEX AT 230°C**

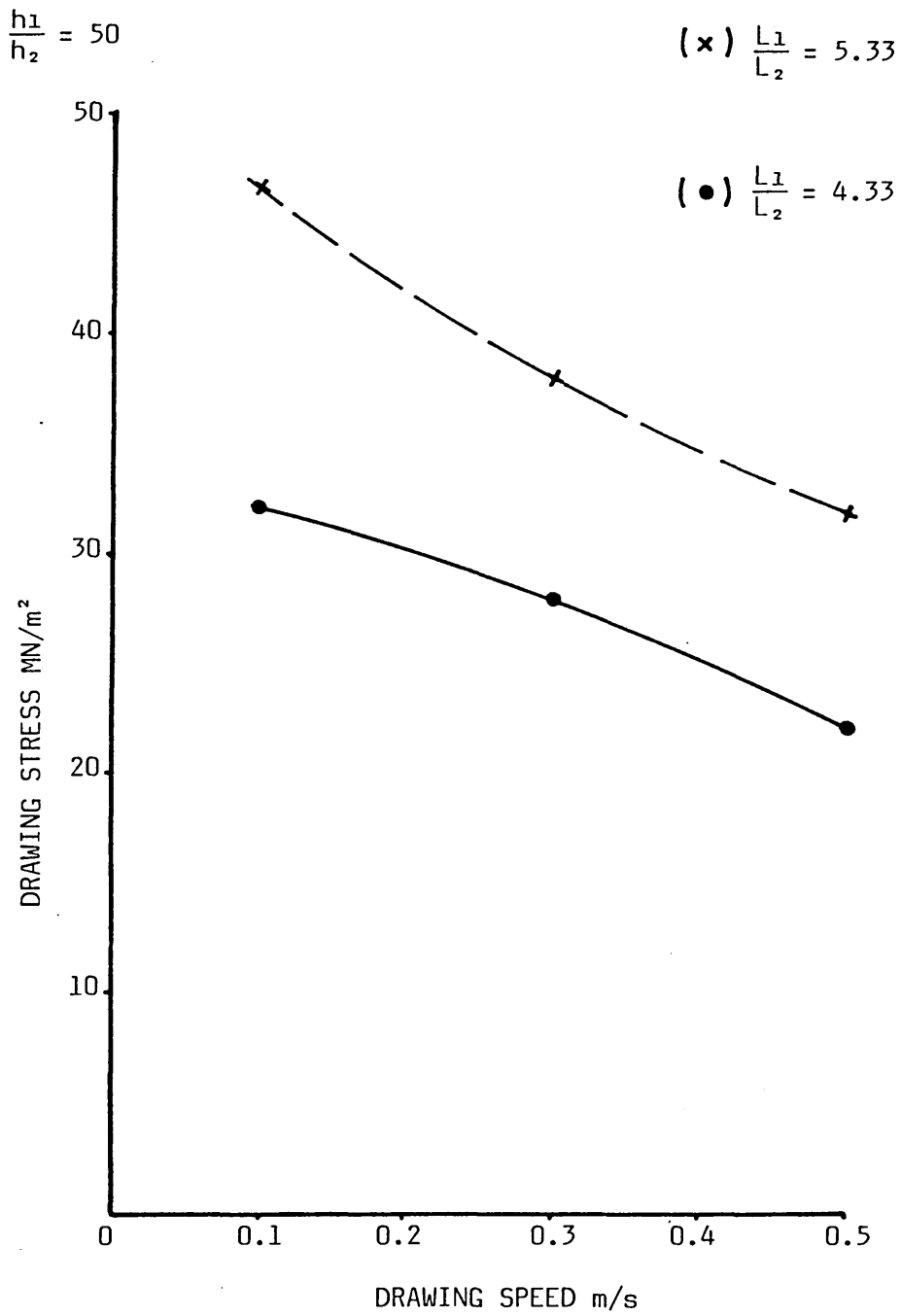


FIG 62 - EFFECT OF LENGTH RATIO ON DRAWING STRESS FOR COPPER TUBE WITH POLYSTYRENE AT 240°C

$$\frac{h_1}{h_2} = 50$$

(x) 130°C ($\mu_0 = 100 \text{ N s/m}^2$)

(o) 160°C ($\mu_0 = 58$)

(●) 180°C ($\mu_0 = 38$)

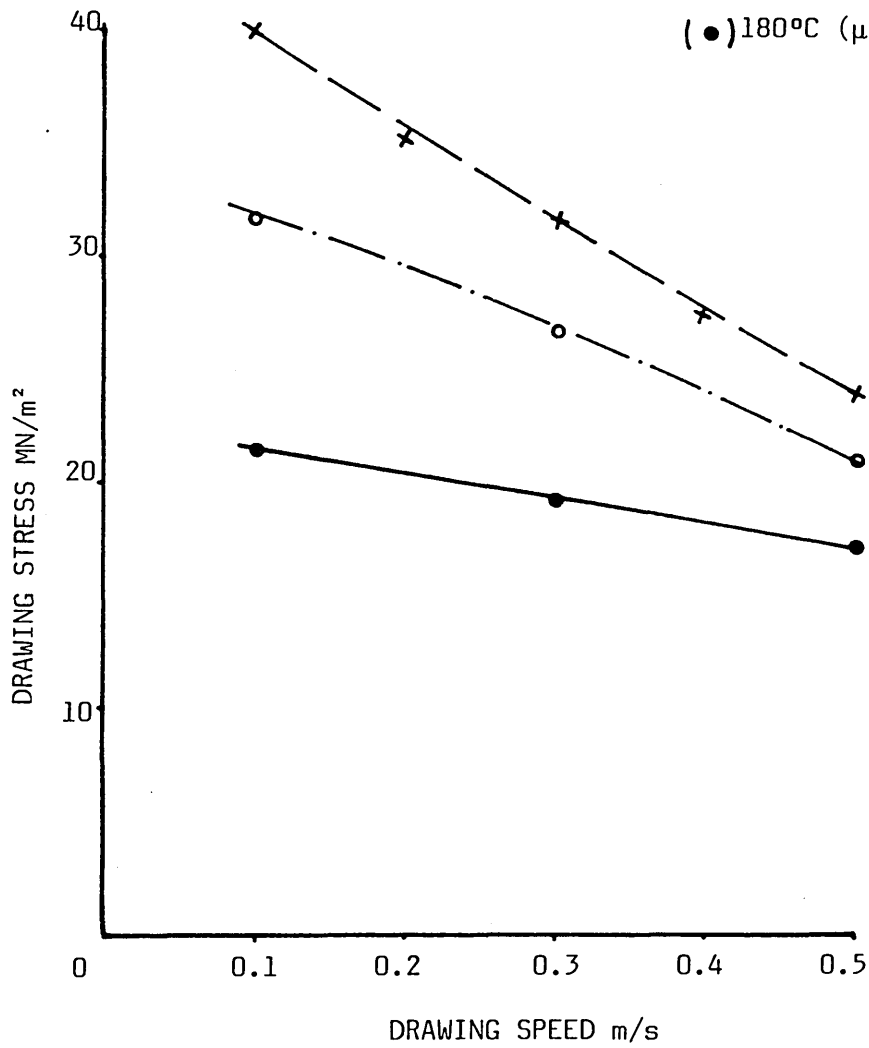


FIG 63 - EFFECT OF VISCOSITY ON DRAWING STRESS
FOR COPPER TUBE WITH WVG23

$$\frac{h_1}{h_2} = 50$$

(x) 200°C ($\mu_0 = 250 \text{ Ns/m}^2$)

(o) 220°C ($\mu_0 = 200$)

(●) 240°C ($\mu_0 = 150$)

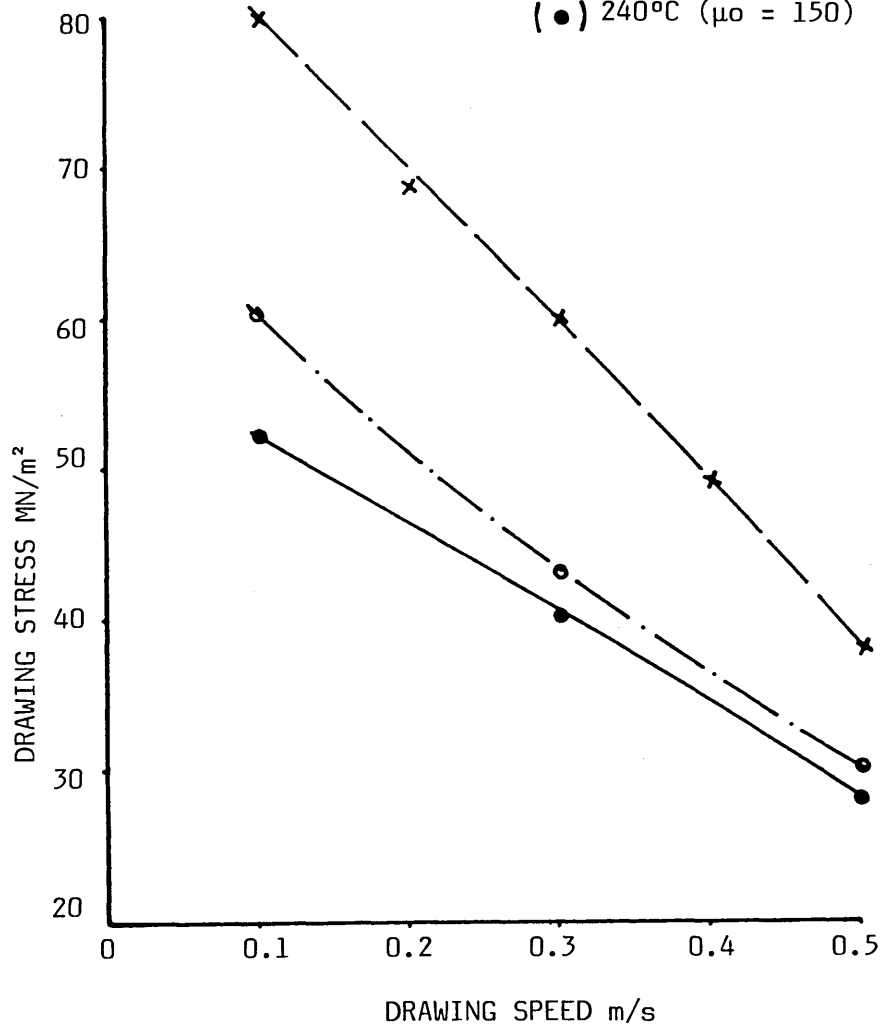


FIG 64 - EFFECT OF VISCOSITY ON DRAWING STRESS
FOR COPPER TUBE WITH KM61

$$\frac{h_1}{h_2} = 50$$

(x) 200°C ($\mu_0 = 333 \text{ Ns/m}^2$)

(o) 230°C ($\mu_0 = 267$)

(•) 240°C ($\mu_0 = 222$)

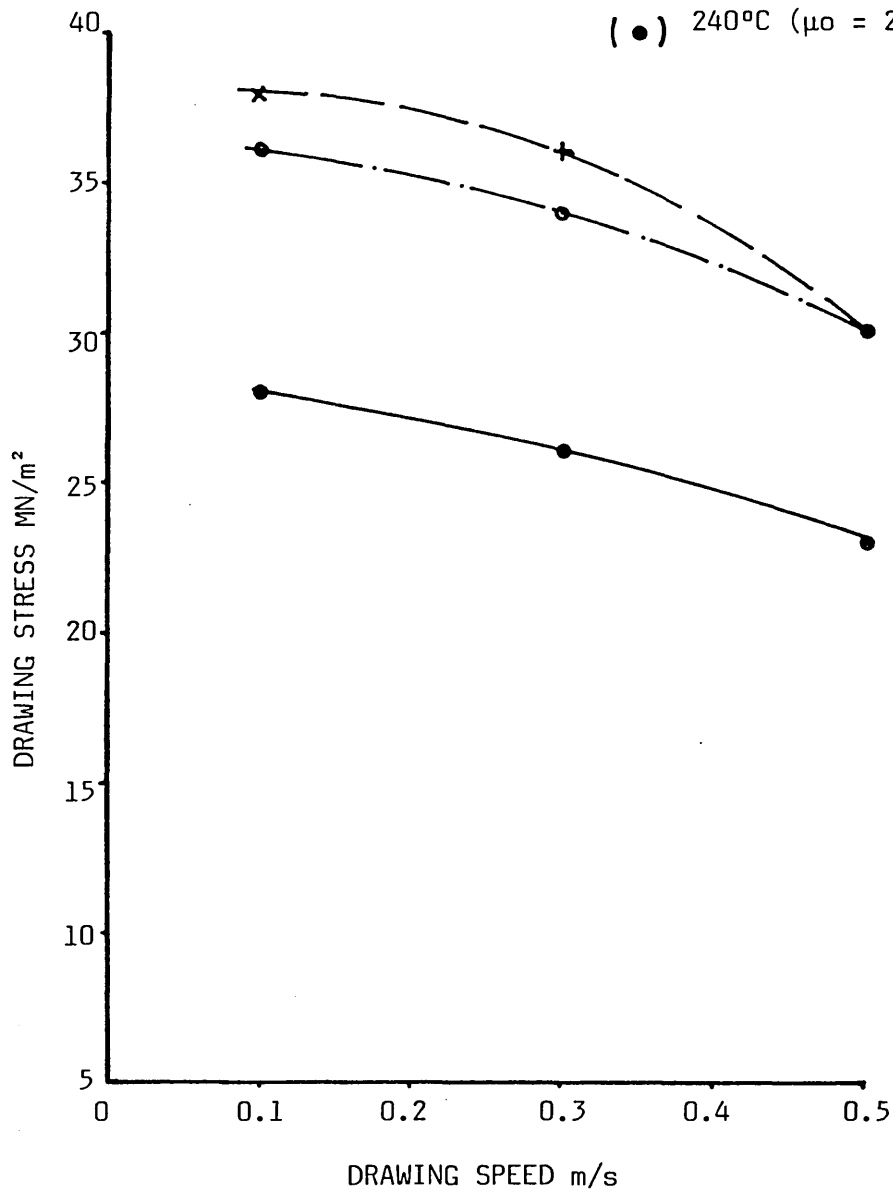


FIG 65 - EFFECT OF VISCOSITY ON DRAWING STRESS FOR
COPPER TUBE WITH RIGIDEX

$$\frac{h_1}{h_2} = 50$$

(x) 230°C ($\mu_0 = 300 \text{ N s/m}^2$)

(o) 240°C ($\mu_0 = 280$)

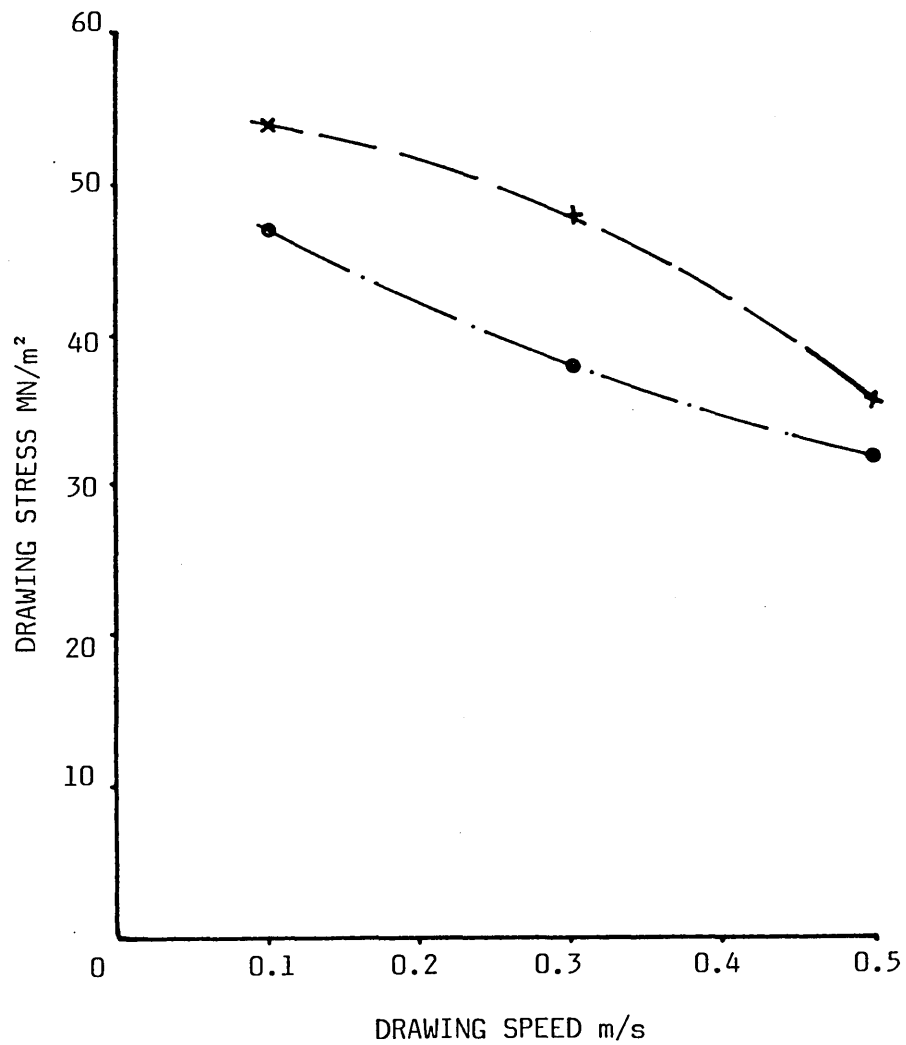


FIG 66 - EFFECT OF VISCOSITY ON DRAWING STRESS
FOR COPPER TUBE WITH POLYSTYRENE

$$\frac{h_1}{h_2} = 29.57$$

(x) 130°C ($\mu_0 = 100 \text{ N s/m}^2$)

(o) 160°C ($\mu_0 = 58$)

(•) 180°C ($\mu_0 = 38$)

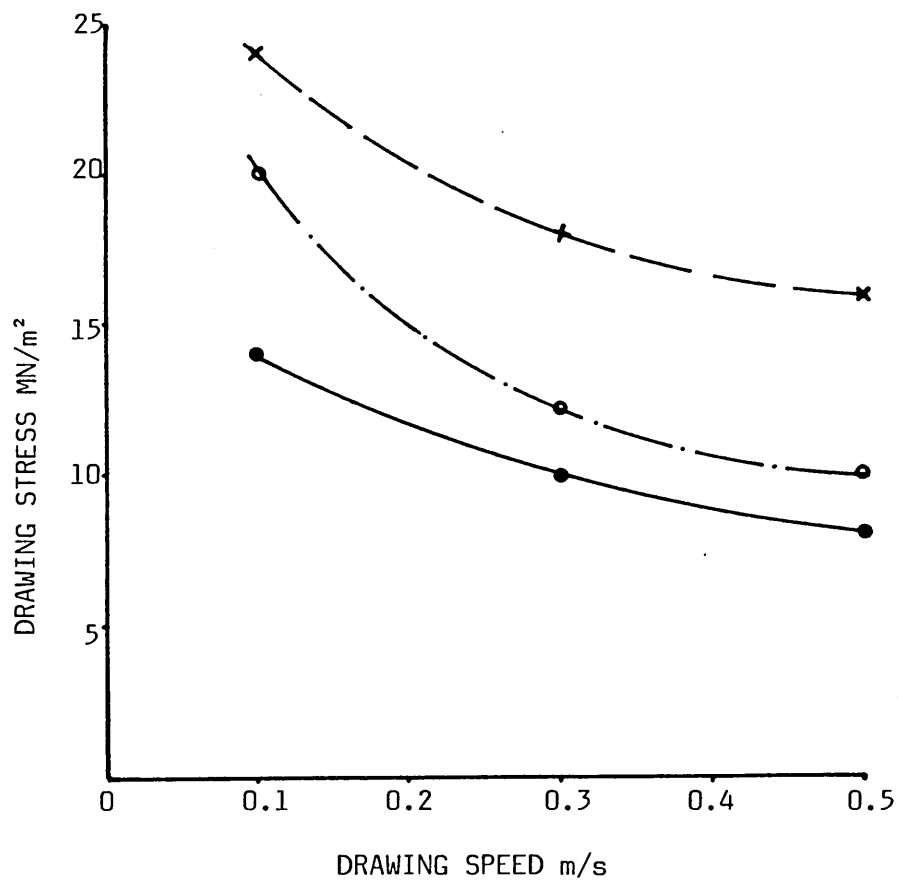


**FIG 67 - EFFECT OF VISCOSITY ON DRAWING STRESS
FOR ALUMINIUM TUBE WITH WVG23**

$$\frac{h_1}{h_2} = 29.57$$

(x) 200°C ($\mu_0 = 250 \text{ Ns/m}^2$)

(o) 220°C ($\mu_0 = 200$)

(•) 240°C ($\mu_0 = 150$)

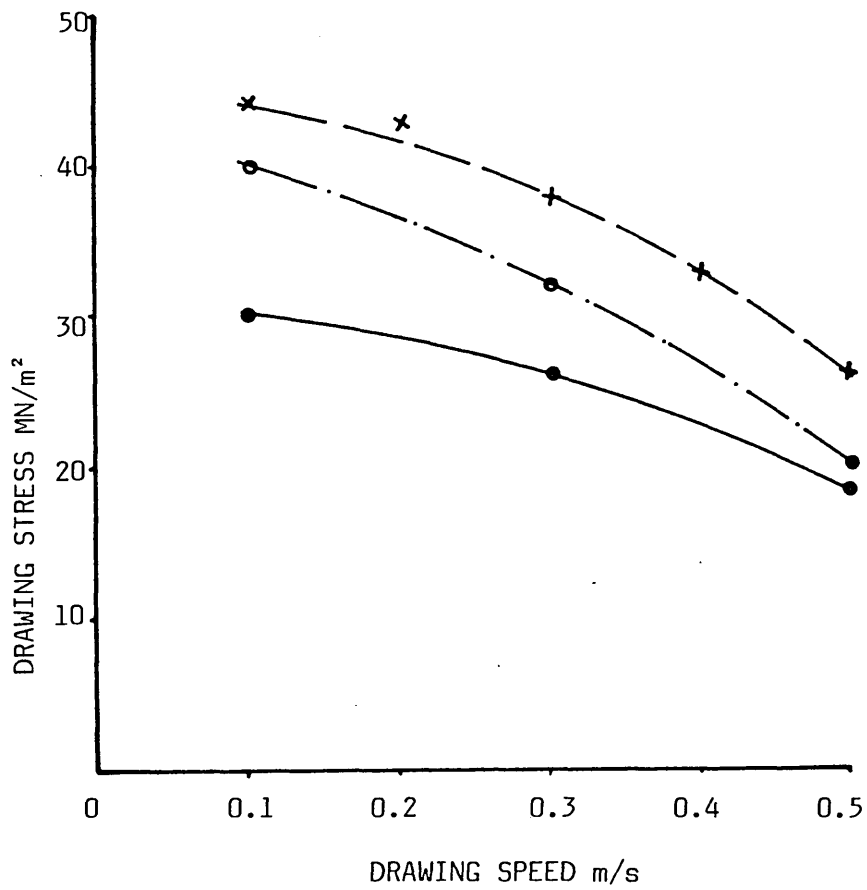


FIG 68 - EFFECT OF VISCOSITY ON DRAWING STRESS
FOR ALUMINIUM TUBE WITH KM61

$$\frac{h_1}{h_2} = 29.57$$

(x) 230°C ($\mu_0 = 267 \text{ N s/m}^2$)

(o) 240°C ($\mu_0 = 222$)

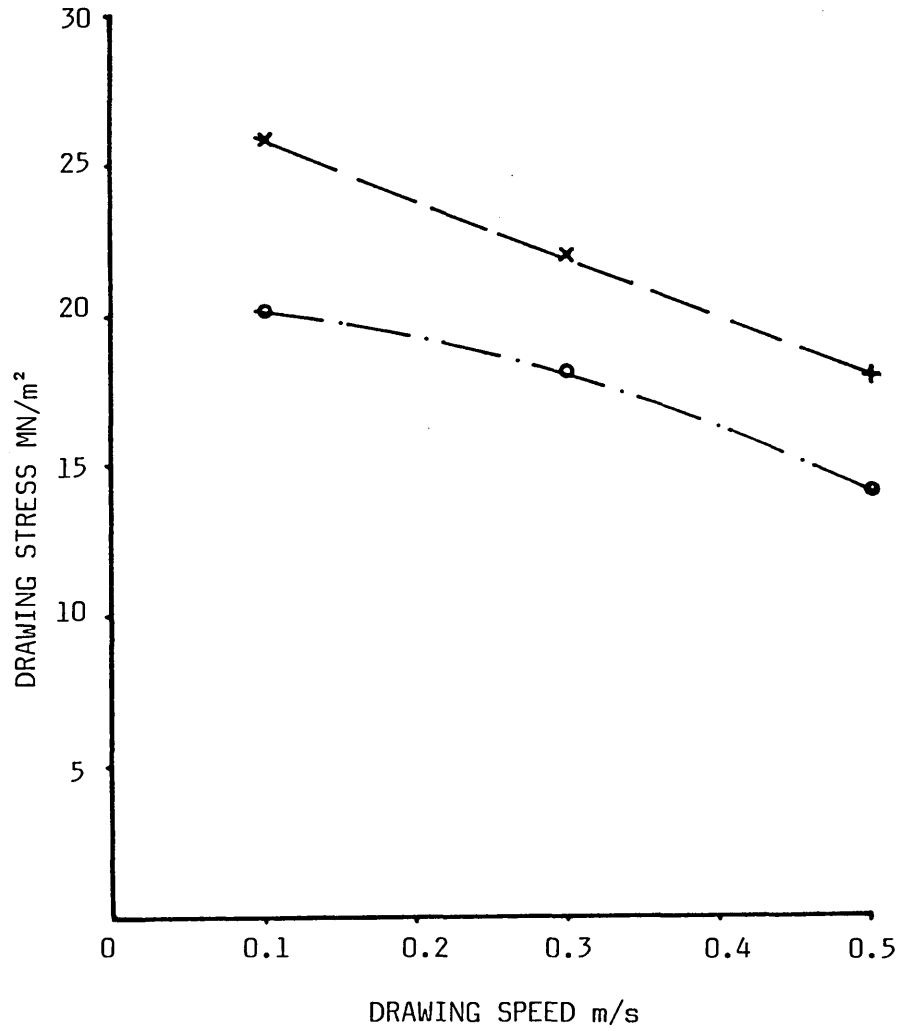


FIG 69 - EFFECT OF VISCOSITY ON DRAWING STRESS
FOR ALUMINIUM TUBE WITH RIGIDEX

$$\frac{h_1}{h_2} = 29.57$$

(x) 230°C ($\mu_0 = 300 \text{ N s/m}^2$)

(o) 240°C ($\mu_0 = 280$)

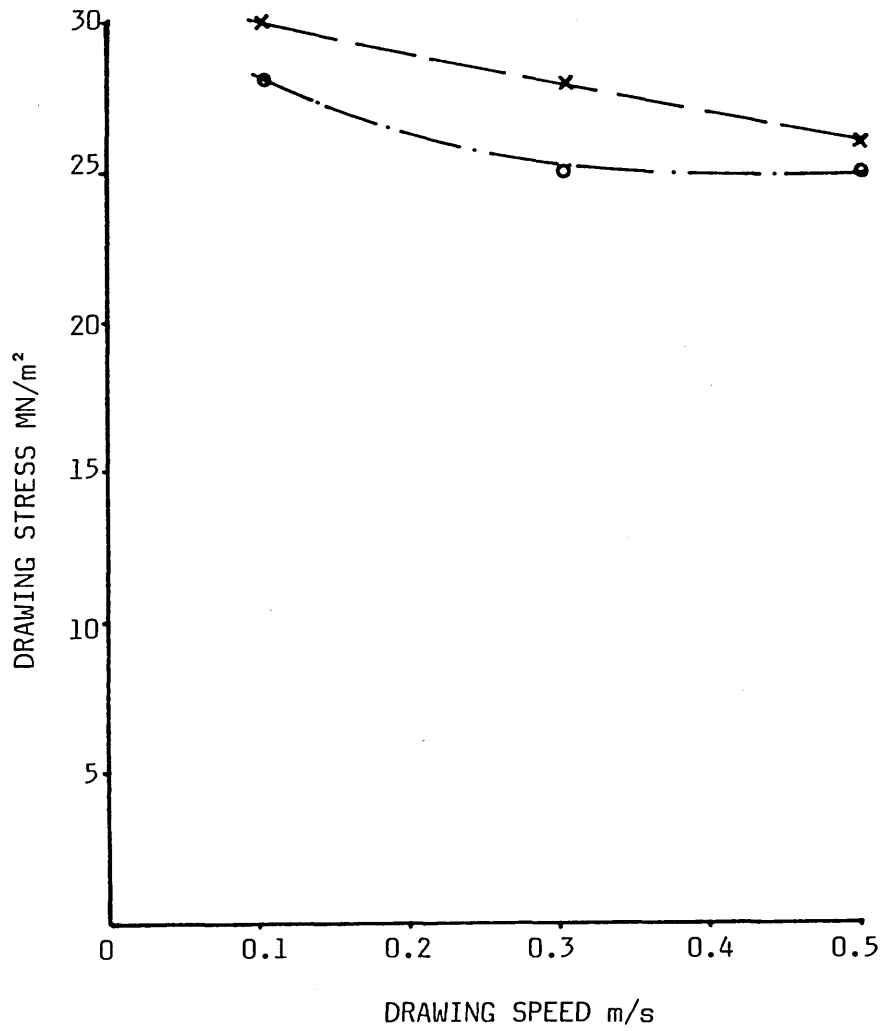


FIG 70 - EFFECT OF VISCOSITY ON DRAWING STRESS
FOR ALUMINIUM TUBE WITH POLYSTYRENE

4.2.3 Results of Pressure Measurements

The pressures generated in the die-less reduction unit were measured by means of pressure transducers mounted on the unit. The results are presented in two sections, (i) the pressure variations versus speed and (ii) the pressure distribution in the die-less reduction unit. Numbers alongside the curves on each figure refer to the locations of the pressure transducers as shown in Fig 23.

(i) Results of Pressure versus Speed

Fig 71 shows the pressures measured for copper tube versus speed with WVG23 polymer at melt temperature of 130°C. The maximum pressures were measured at a speed of 0.3 m/s for all the positions, after which pressures decreased as the drawing speed was increased. At lower drawing speeds reduced pressures were noted.

Fig 72 shows the pressure variations versus speed for copper tube with WVG23 polymer at 180°C. For drawing speeds in excess of about 0.2 m/s the pressure readings were found to be approximately constant for positions 1 and 2 whilst at position 3 the measured pressure was observed to vary significantly with the drawing speed. The maximum pressures for positions 1 and 2 were noted at drawing speed of about 0.1 m/s and for position 3 the maximum pressure was observed at 0.3 m/s.

Fig 73 gives the pressures generated for copper tube with KM61 polymer at melt temperature of 200°C. Higher pressures were recorded with this polymer compared to those in Fig 71 especially at lower drawing speeds. Pressures at position 3 remained reasonably constant with the drawing speed but the pressure at positions 1 and 2 fell sharply with speed.

Fig 74 shows the pressure variations for copper tube versus drawing speed with KM61 polymer at the melt temperature of 220°C. Trends

of the results at this temperature were significantly different compared to those in Fig 73. At lower drawing speeds, pressures decreased as the drawing speed was decreased. The magnitudes of the pressures generated at higher drawing speeds increased significantly at positions 1 and 2. Pressures at position 3 remained reasonably constant at all drawing speeds. This trend may be explained by the fact that at 200°C KM61 is just about melting and at higher speeds there is more chance of slip occurring and hence reduction in pressure.

Fig 75 gives the measured pressures for copper tube with Rigidex polymer at temperature of 230°C. When this polymer was used as the pressure medium the general trends were found to be the same as those in Fig 74. Pressures measured at all points increased as the drawing speed was increased. Higher pressures were recorded at drawing speed of 0.5 m/s.

Fig 76 is showing the variations of pressure versus speed for copper tube with Rigidex polymer at 240°C. The measured pressures at positions 1, 2 and 3 remained fairly constant with speed.

Fig 77 shows the pressure variations for copper tube versus speed with polystyrene polymer at the melt temperature of 230°C. At lower drawing speeds, the maximum pressures were recorded for all positions which remained fairly constant for speeds of up to 0.3 m/s. At higher drawing speeds generally lower pressures were recorded. When polystyrene polymer was used as the pressure medium pressures recorded were generally greater than those observed when the other three polymers were used (see Figs 71, 72 and 75).

Fig 78 shows the pressure variations versus speed for copper tube using polystyrene polymer at the temperature of 240°C. For drawing speeds in excess of about 0.3 m/s the pressure readings were found

to be approximately constant at positions 2 and 3 but at position 1 pressure was found to increase slightly as the drawing speed was increased. The maximum pressures were recorded at all points at 0.1 m/s.

Fig 79 gives the measured pressure for aluminium tube with WVG23 polymer at temperature of 130°C. The general trends were found to change compared to those in Fig 71. At lower drawing speeds approximately constant pressures were recorded at positions 1 and 2 but at position 3 pressure was found to reduce up to 0.3 m/s after which pressures measured at all positions increased as the drawing speed was increased and reached a maximum at about 0.5 m/s.

Fig 80 shows the pressure variations versus speed for aluminium tubes using WVG23 polymer at 180°C. When this polymer was used as the pressure medium the results were found to be slightly different from those in Fig 72. Higher pressures were recorded at higher drawing speeds for all positions. The magnitudes of the generated pressures at lower drawing speeds were similar to those shown in Fig 71.

Fig 81 is showing the variations of pressure with speed for aluminium tube with KM61 polymer at temperature of 200°C. At lower drawing speeds the maximum pressures were noted at all positions. The magnitude of pressure at all positions decreased as the speed was increased.

Fig 82 shows the pressure variations versus speed for aluminium tube using KM61 polymer at 220°C. The pressure curve at position 3 was found to be similar to that in Fig 81.

Fig 83 shows the pressure variations with speed for aluminium tube when Rigidex polymer was used as the pressure medium at a temperature of 230°C. The general trends of the results were found to be

similar to those in Fig 75. At higher drawing speeds the pressures at all positions increased gradually to higher magnitudes. The maximum pressures were recorded at 0.5 m/s.

Fig 84 shows the pressure variations with speed for aluminium tube with Rigidex polymer at the melt temperature of 240°C. At higher drawing speeds, the pressure readings at positions 2 and 3 were found to be about the same as those in Fig 83. The magnitudes of the pressures generated at lower drawing speeds were similar to those shown in Fig 83. The maximum pressures reached at 0.5 m/s.

Fig 85 gives the measured pressures for aluminium tube with polystyrene polymer at temperature of 230°C. Higher pressures were recorded with this polymer compared to those in Fig 84 especially at lower drawing speeds. Pressures at position 3 remained fairly constant with the drawing speed but the pressures at positions 1 and 2 decreased gradually. The maximum pressures were recorded at drawing of 0.1 m/s.

Fig 86 shows the pressure variations versus speed for aluminium tube with polystyrene polymer at 240°C. The general trends of the results were found to be similar to those shown in Fig 85.

(ii) Results of Pressure Distribution

Figs 87 to 94 show the pressure distributions when copper tube was drawn using WVG23, KM61, Rigidex and polystyrene polymers at different melt temperatures but same gap ratio of 50. In all cases the measured pressure was found to be the maximum at the step at all drawing speeds. The maximum pressure was found to vary between 140-160 MN/m². The pressure distribution appears to be linear in most cases except in Fig 91 when the tube was drawn at 0.5 m/s using Rigidex at 230°C.

Figs 95 to 102 show the pressure distributions for the aluminium tube drawn using WVG23, KM61, Rigidex and polystyrene polymers at different melt temperatures and speeds. The maximum pressure readings were obtained at the step in all cases and the magnitudes of the maximum pressure were found to be between 40-70 MN/m².

$$\frac{h_1}{h_2} = 50$$

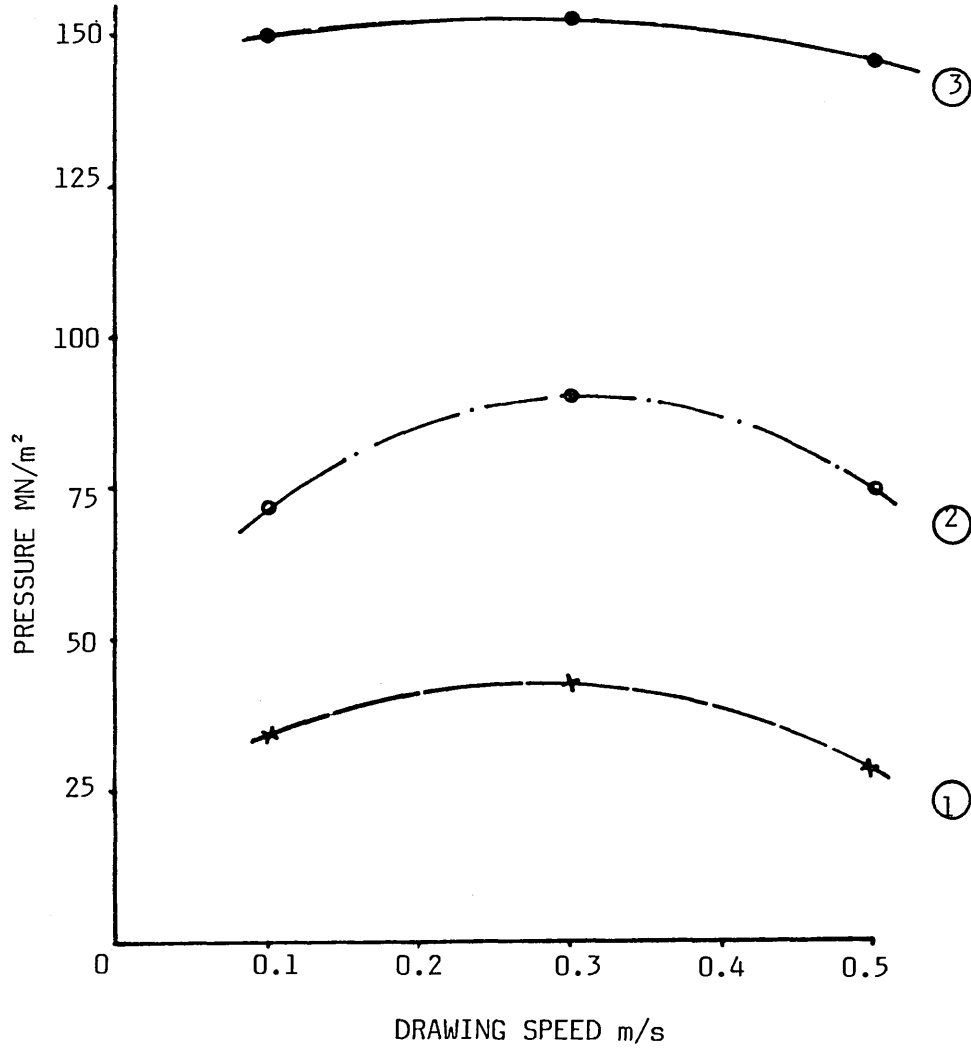
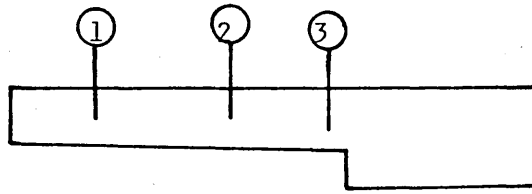


**FIG 71 - PRESSURE VERSUS SPEED FOR COPPER TUBE
WITH WVG23 AT 130°C**

$$\frac{h_1}{h_2} = 50$$

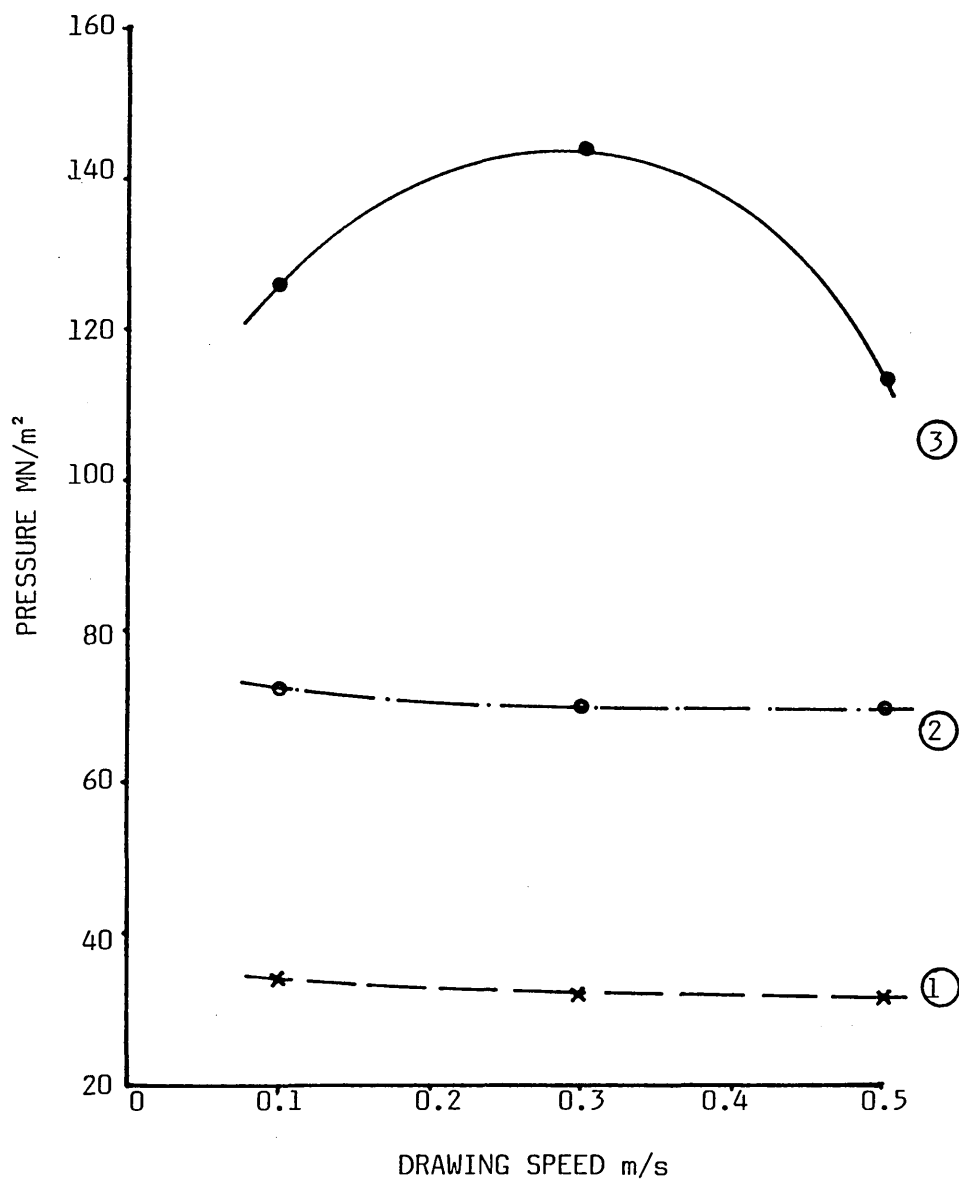


FIG 72 - PRESSURE VERSUS SPEED FOR COPPER TUBE
WITH WVG23 AT 180°C

$$\frac{h_1}{h_2} = 50$$

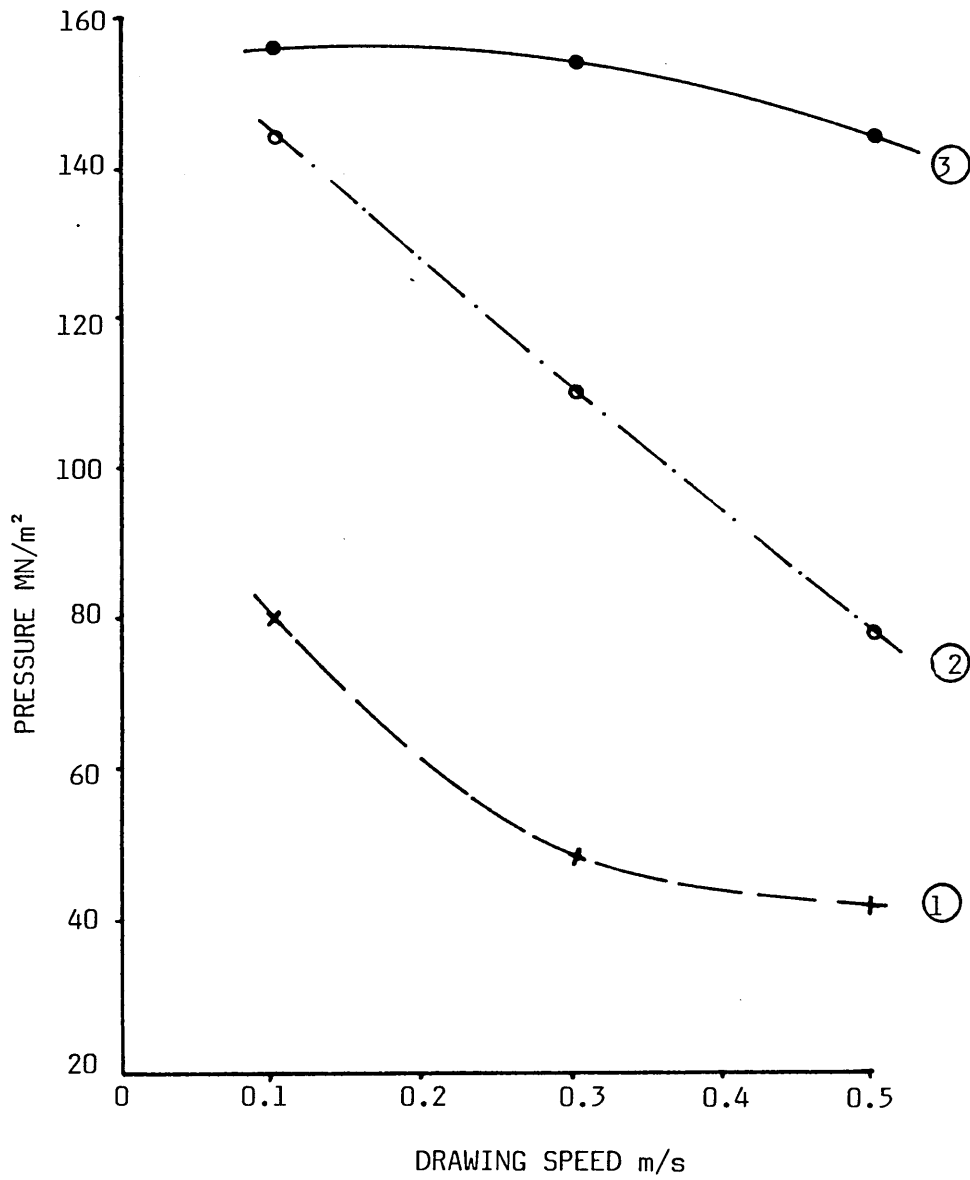


FIG 73 - PRESSURE VERSUS SPEED FOR COPPER TUBE
WITH KM61 AT 200°C

$$\frac{h_1}{h_2} = 50$$

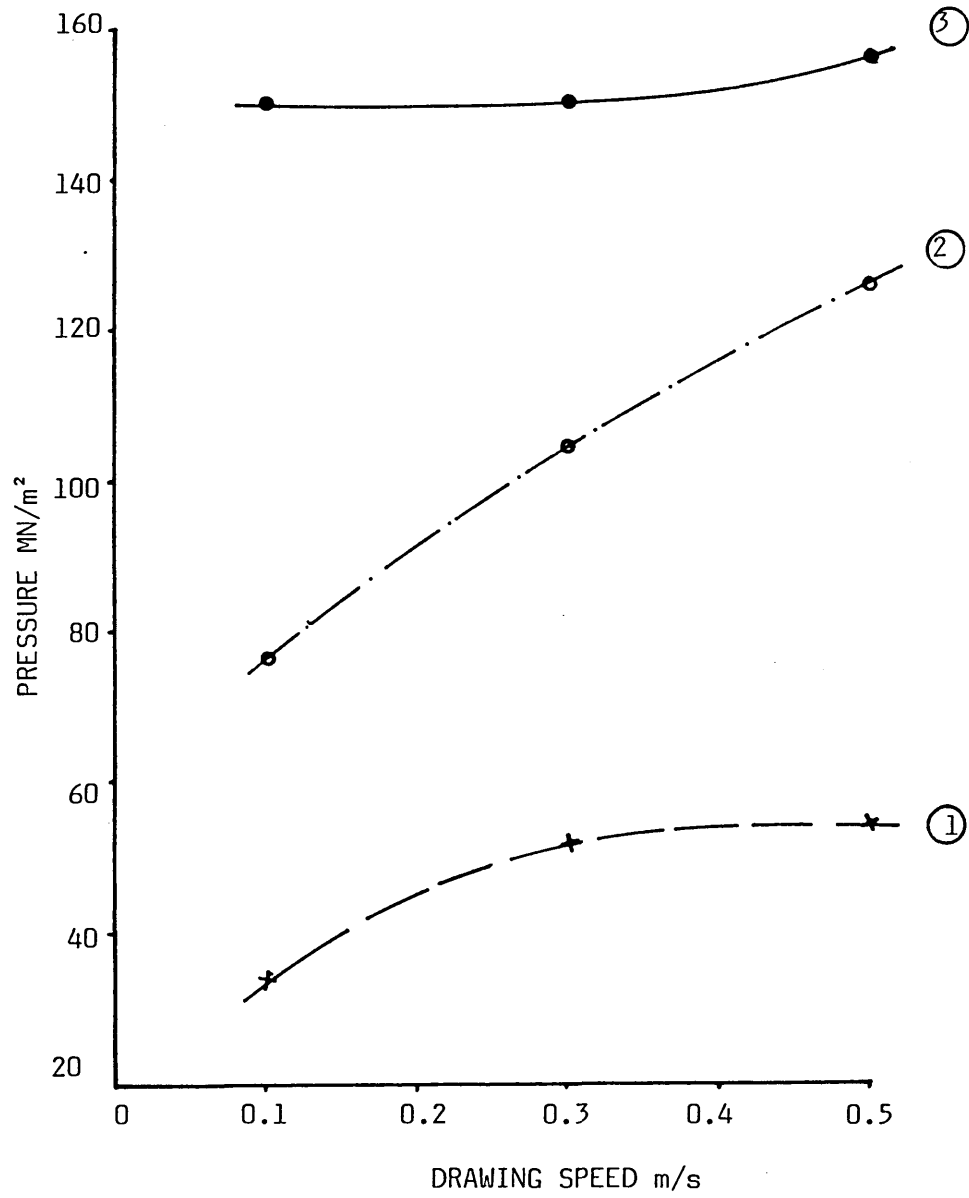


FIG 74 - PRESSURE VERSUS SPEED FOR COPPER TUBE
WITH KM61 AT 220°C

$$\frac{h_1}{h_2} = 50$$

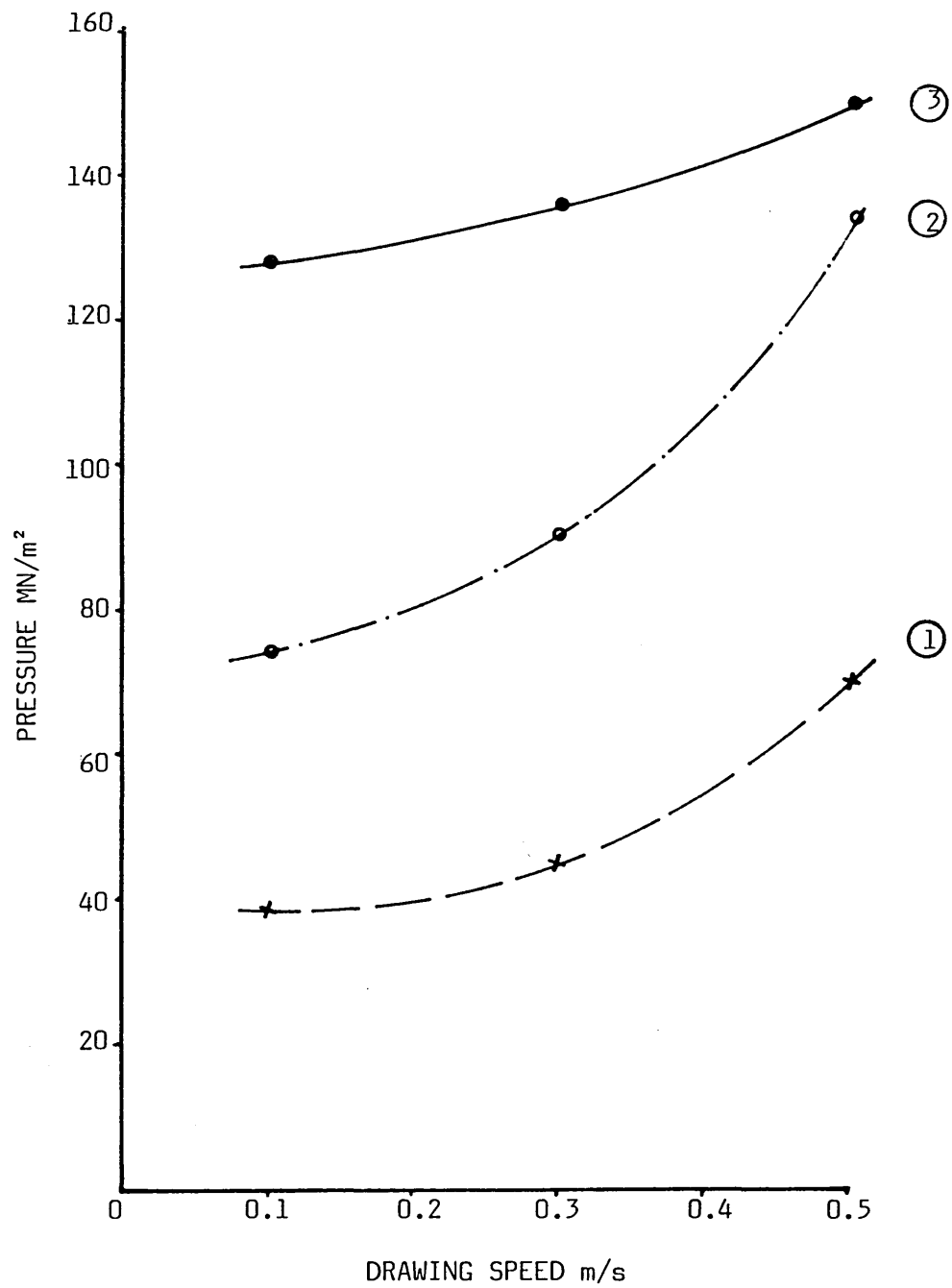


FIG 75 - PRESSURE VERSUS SPEED FOR COPPER TUBE
WITH RIGIDEX AT 230°C

$$\frac{h_1}{h_2} = 50$$

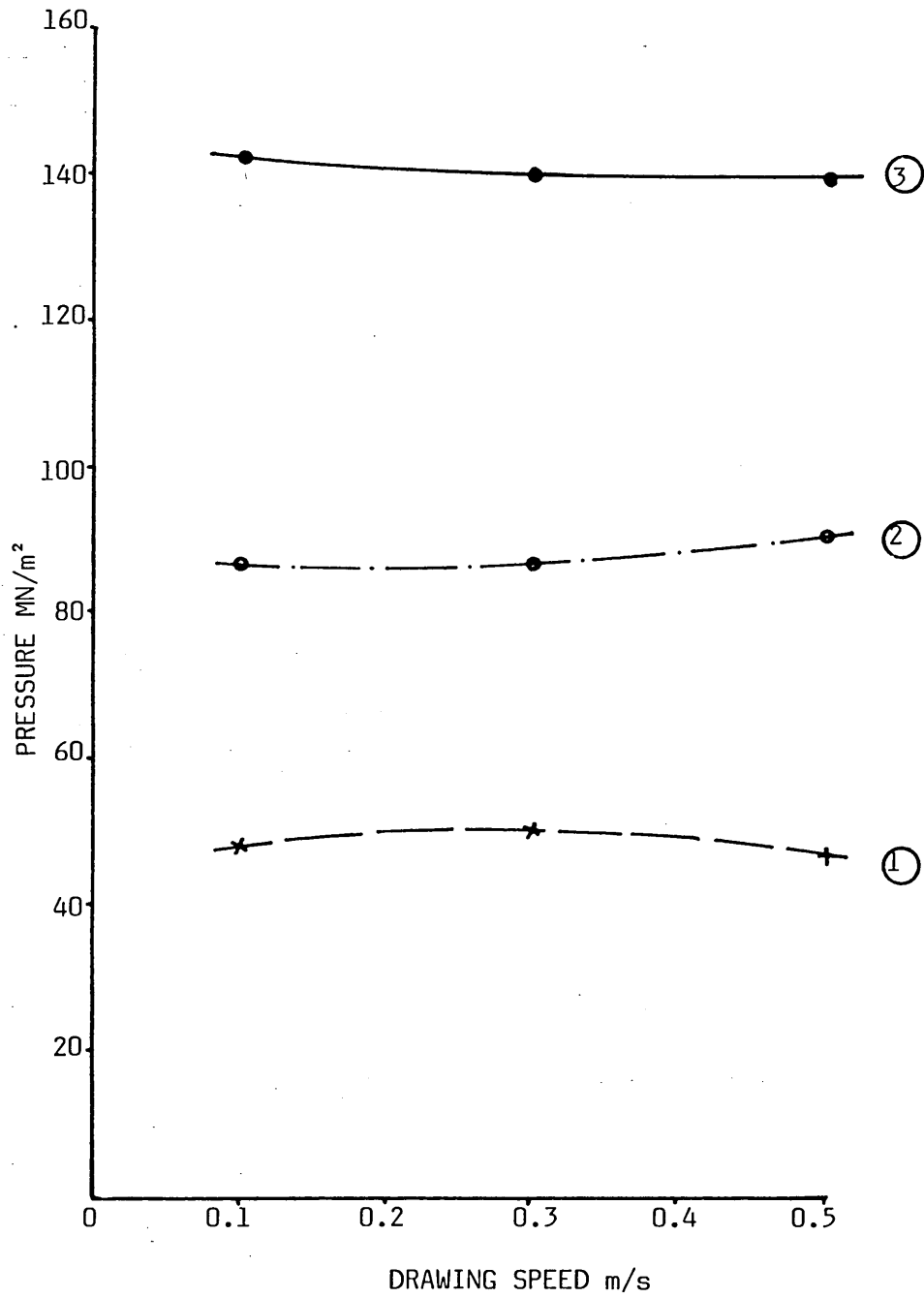


FIG 76 - PRESSURE VERSUS SPEED FOR COPPER TUBE
WITH RIGIDEX AT 240°C

$$\frac{h_1}{h_2} = 50$$

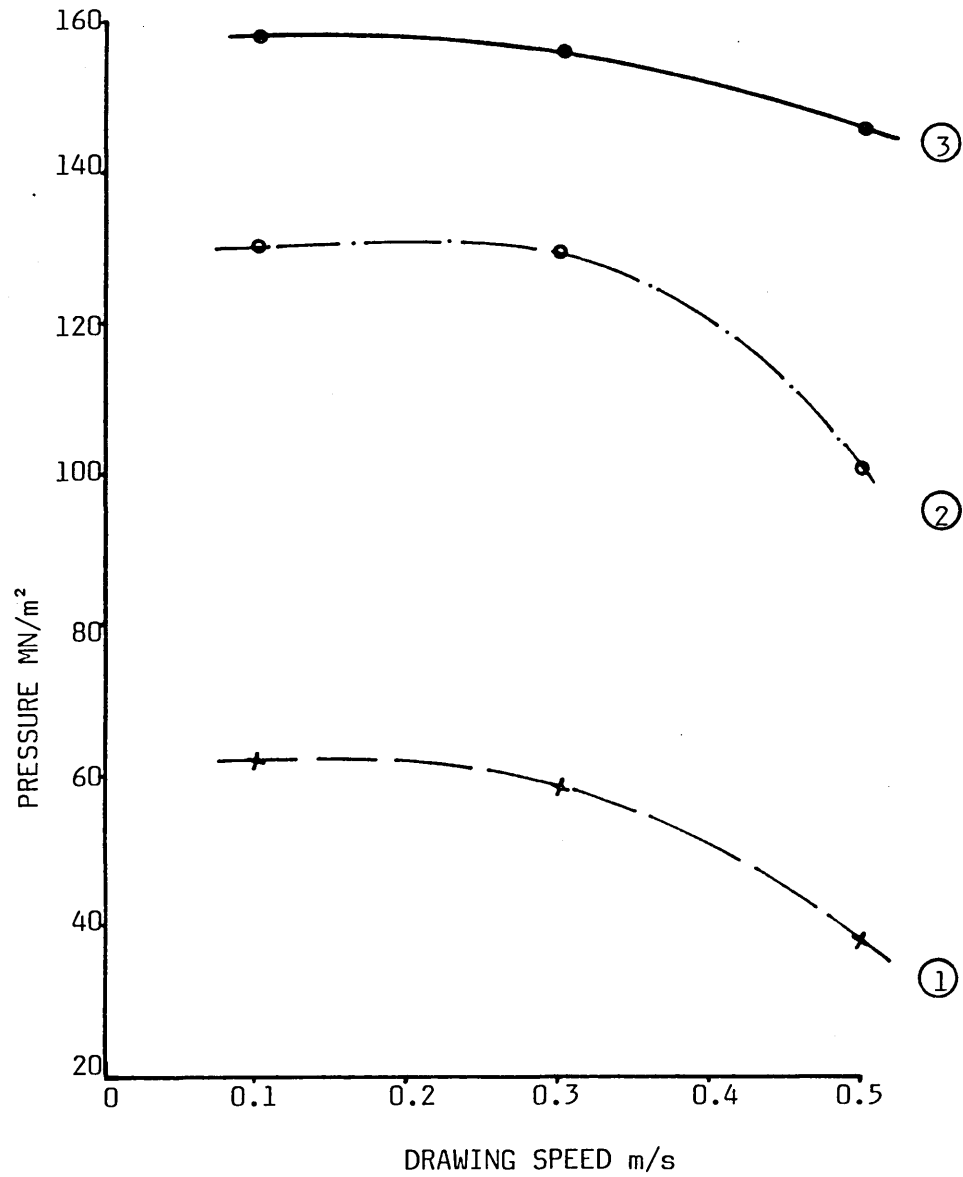


FIG 77 - PRESSURE VERSUS SPEED FOR COPPER TUBE
WITH POLYSTYRENE AT 230°C

$$\frac{h_1}{h_2} = 50$$

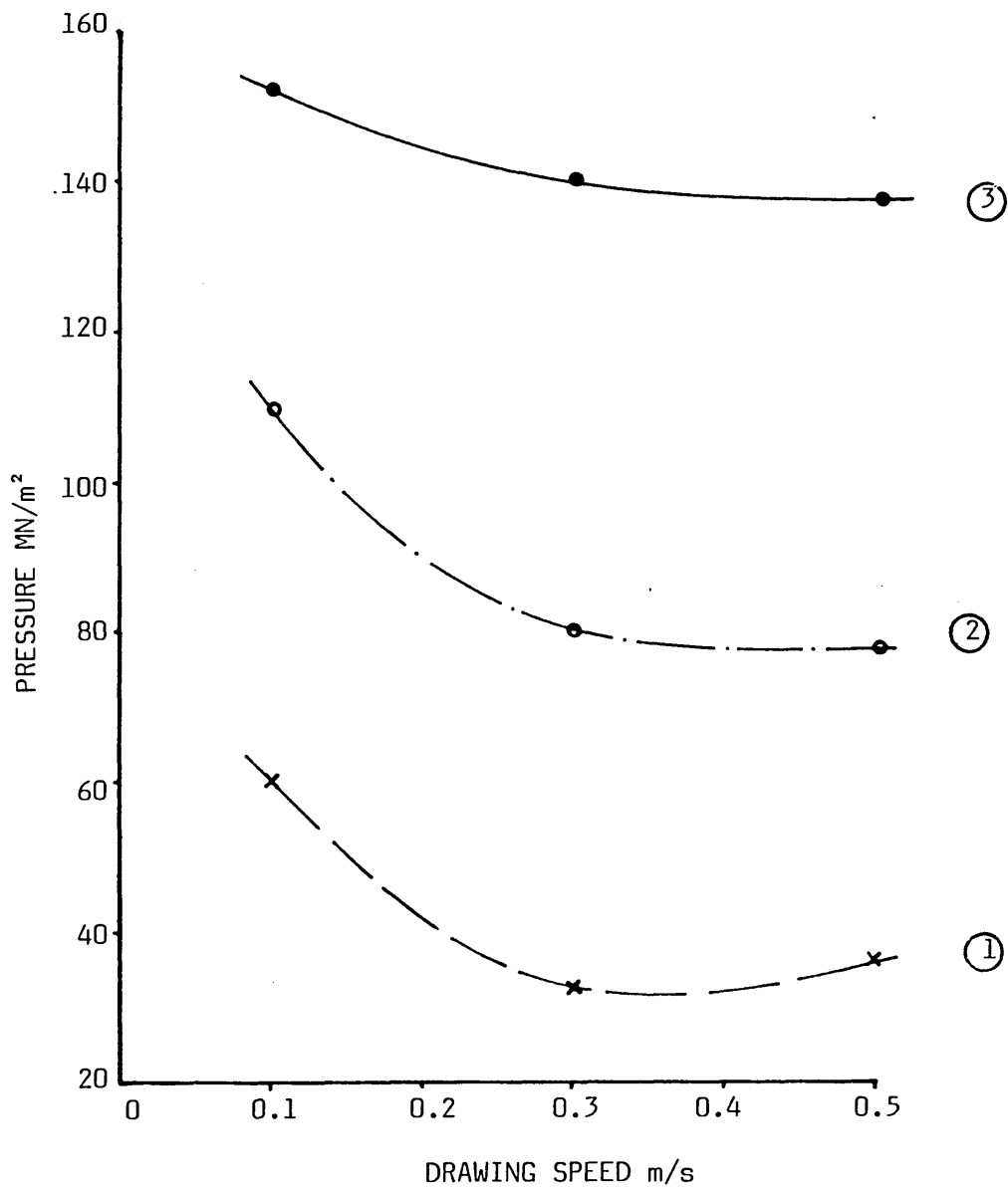


FIG 78 - PRESSURE VERSUS SPEED FOR COPPER TUBE
WITH POLYSTYRENE AT 240°C

$$\frac{h_1}{h_2} = 29.57$$

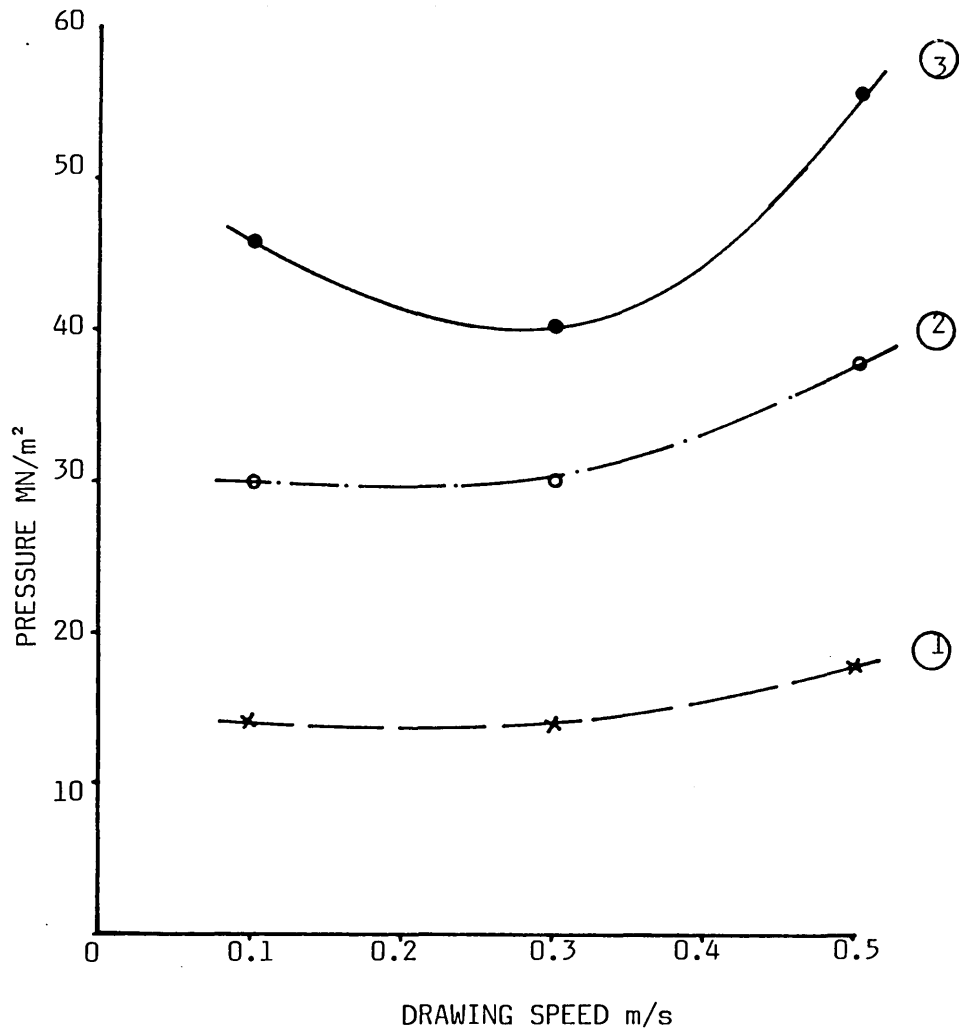


FIG 79 - PRESSURE VERSUS SPEED FOR ALUMINIUM TUBE
WITH WVG23 AT 130°C

$$\frac{h_1}{h_2} = 29.57$$

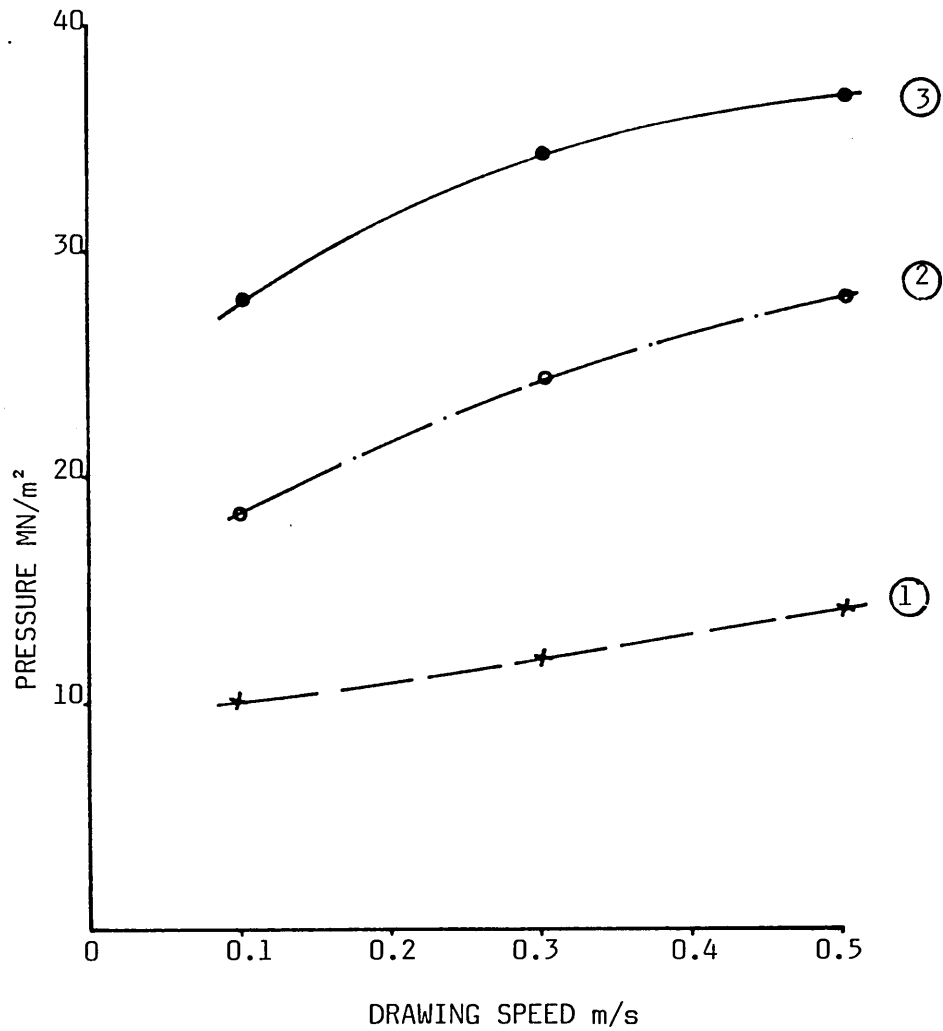


FIG 80 - PRESSURE VERSUS SPEED FOR ALUMINIUM TUBE WITH WVG23 AT 180°C

$$\frac{h_1}{h_2} = 29.57$$

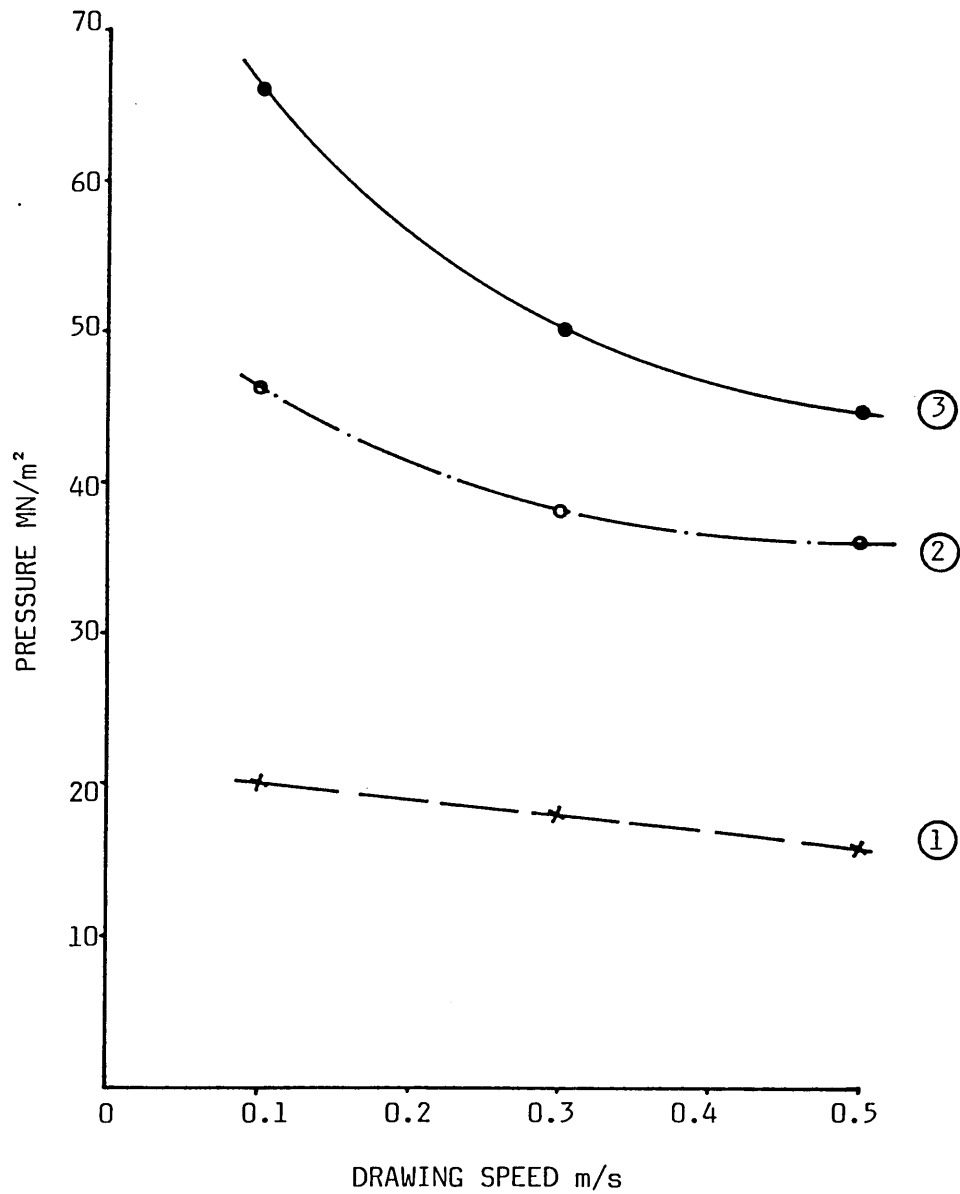


FIG 81 - PRESSURE VERSUS SPEED FOR ALUMINIUM TUBE WITH KM61 AT 200°C

$$\frac{h_1}{h_2} = 29.57$$

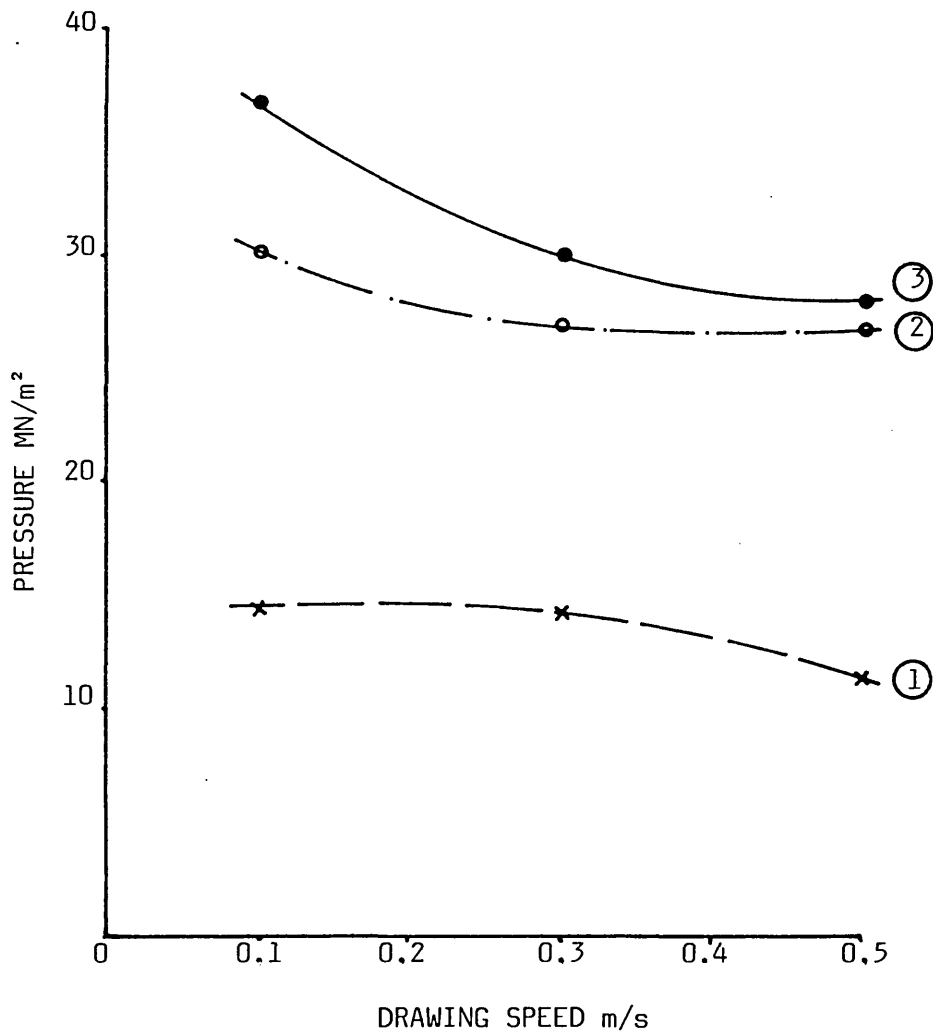
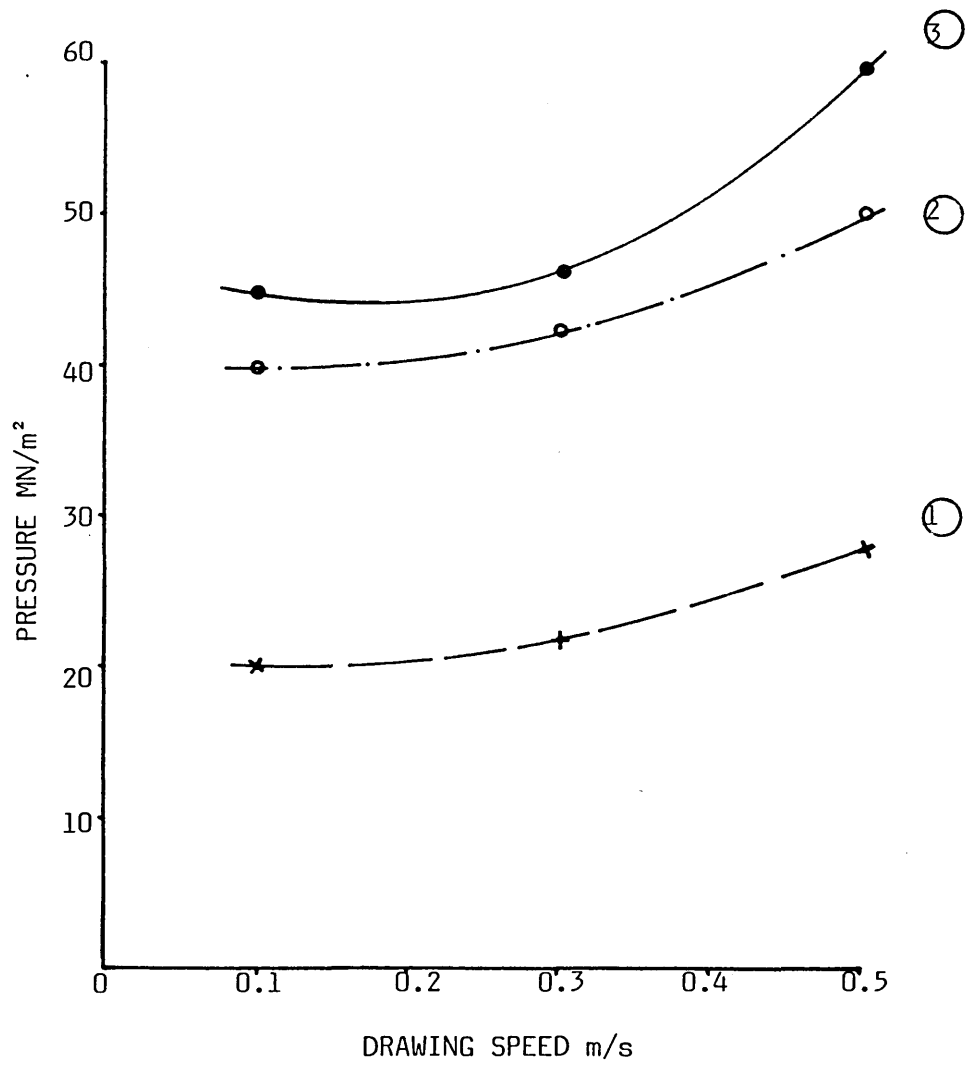


FIG 82 - PRESSURE VERSUS SPEED FOR ALUMINIUM
TUBE WITH KM61 AT 220°C

$$\frac{h_1}{h_2} = 29.57$$



**FIG 83 - PRESSURE VERSUS SPEED FOR ALUMINIUM
TUBE WITH RIGIDEX AT 230°C**

$$\frac{h_1}{h_2} = 29.57$$

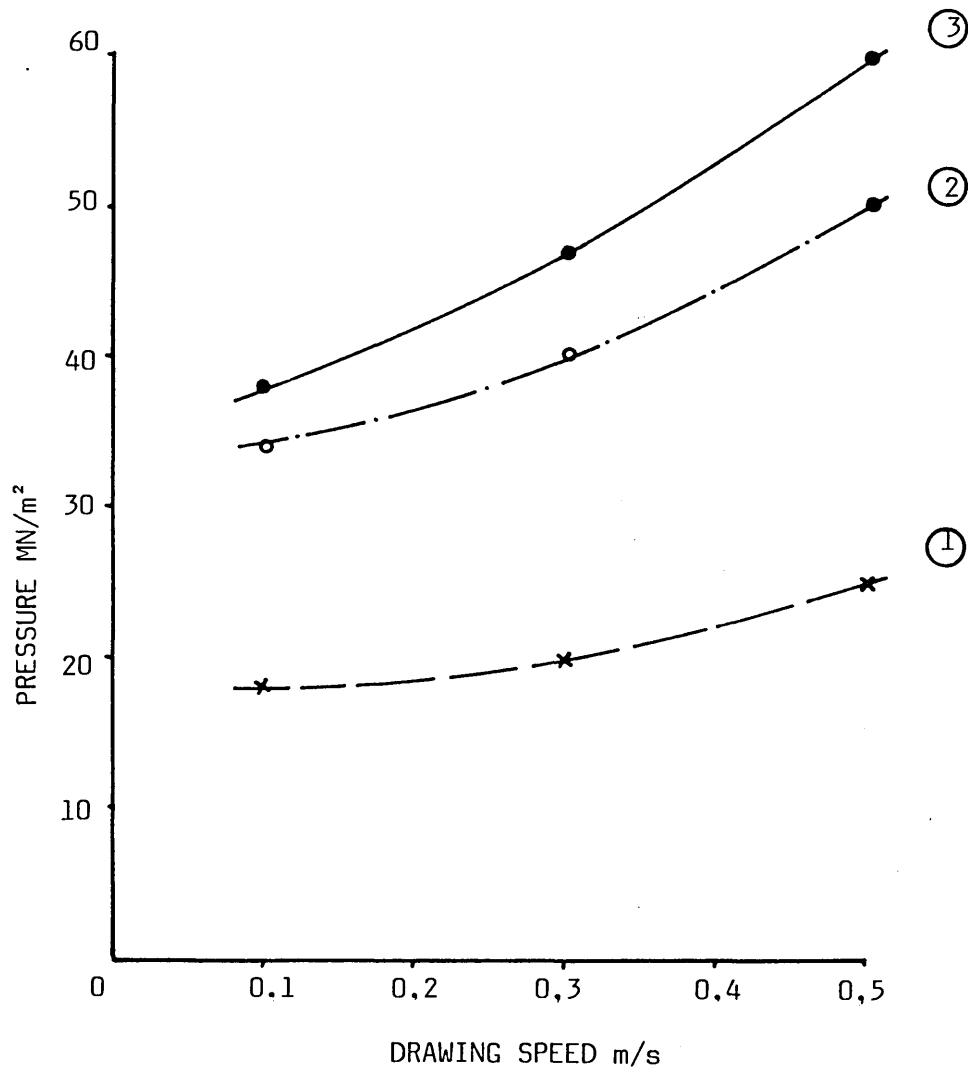


**FIG 84 - PRESSURE VERSUS SPEED FOR ALUMINIUM
TUBE WITH RIGIDEX AT 240°C**

$$\frac{h_1}{h_2} = 29.57$$

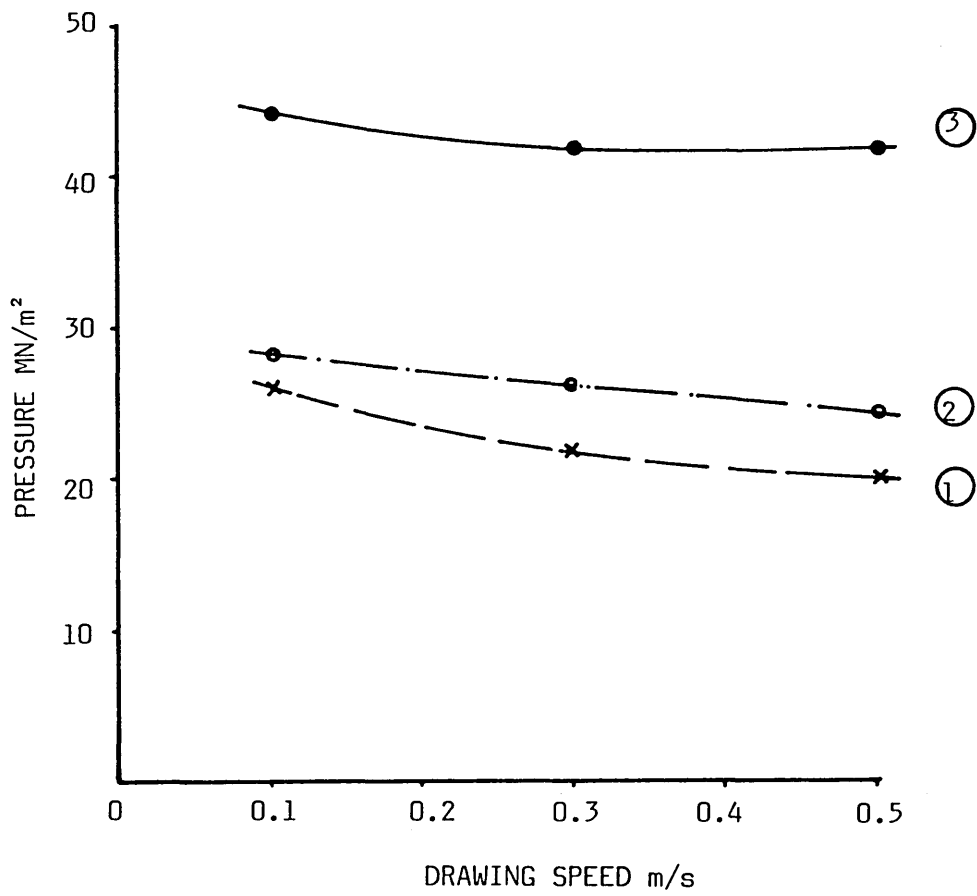


**FIG 85 - PRESSURE VERSUS SPEED FOR ALUMINIUM
TUBE WITH POLYSTYRENE AT 230°C**

$$\frac{h_1}{h_2} = 29.57$$

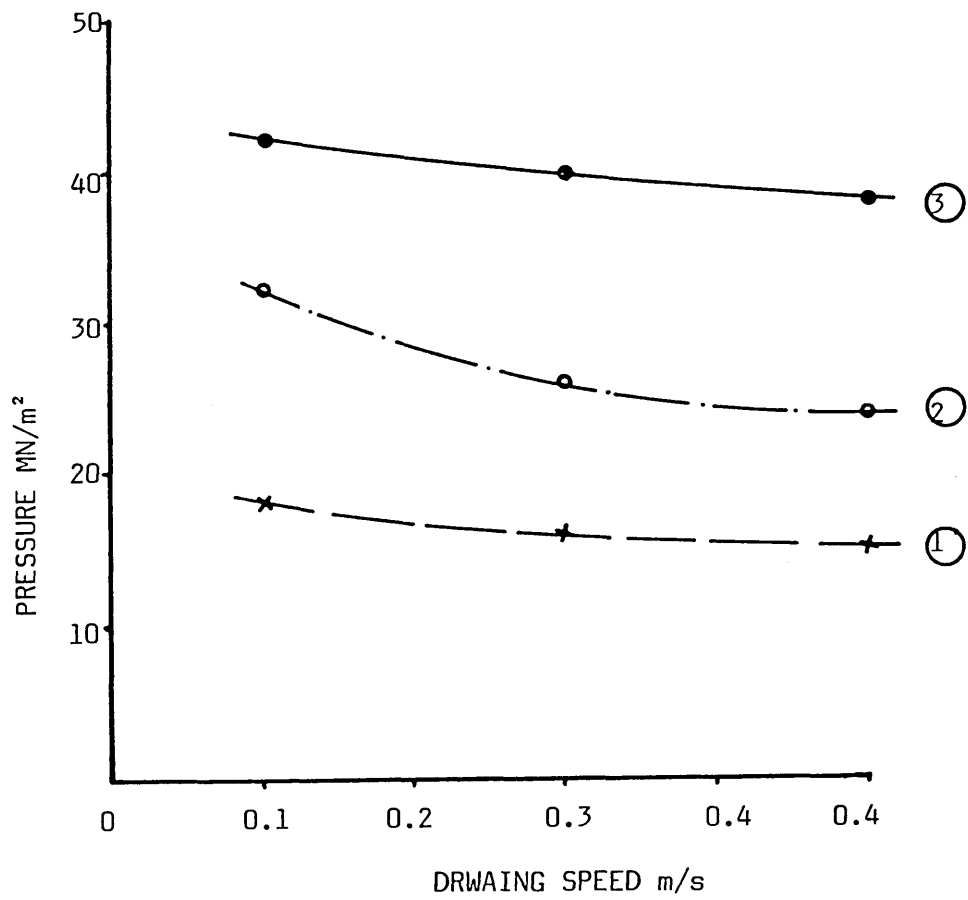


FIG 86 - PRESSURE VERSUS SPEED FOR ALUMINIUM
TUBE WITH POLYSTYRENE AT 240°C

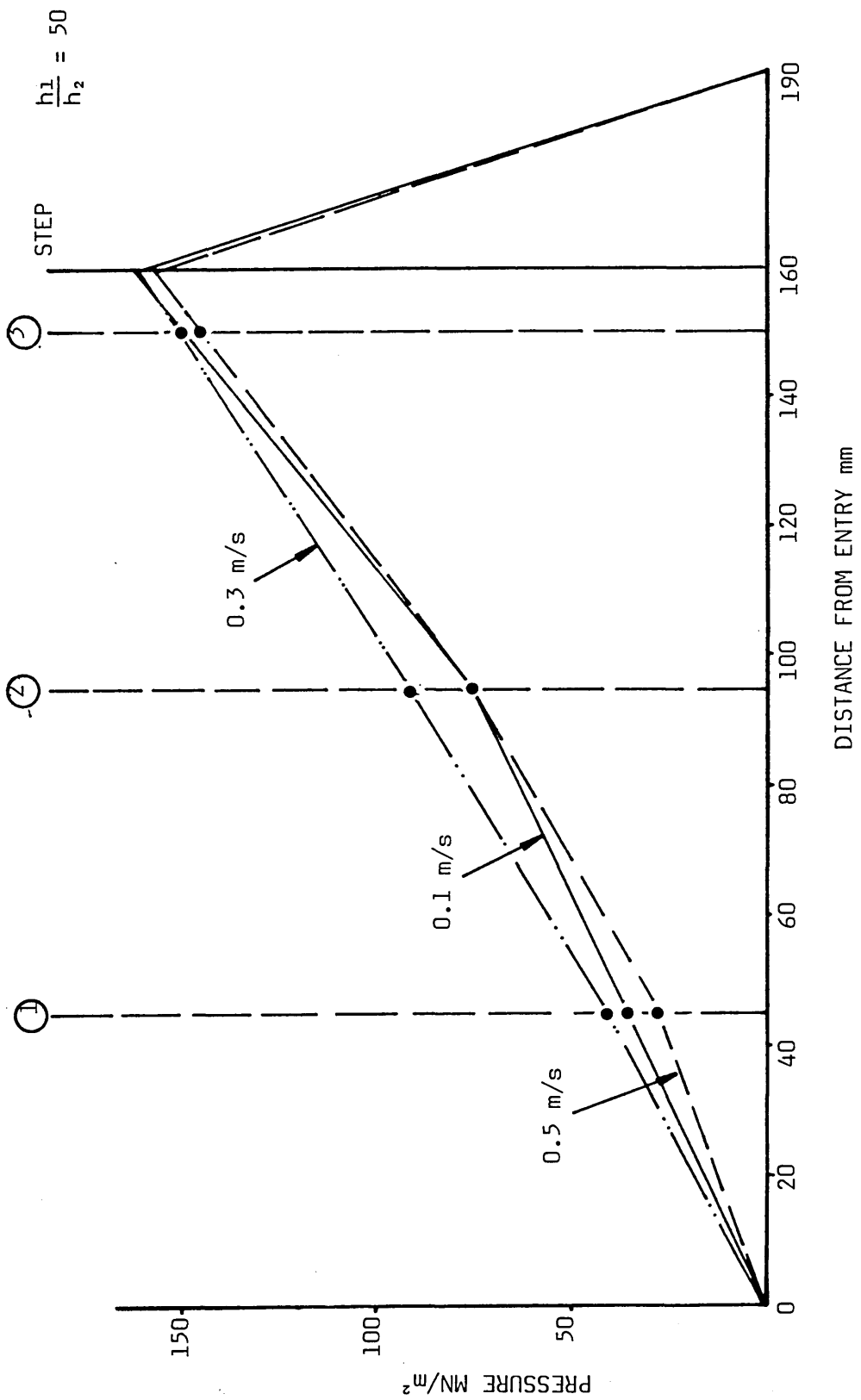


FIG 87 - PRESSURE DISTRIBUTIONS FOR COPPER TUBE WITH WVG23 AT 130°C

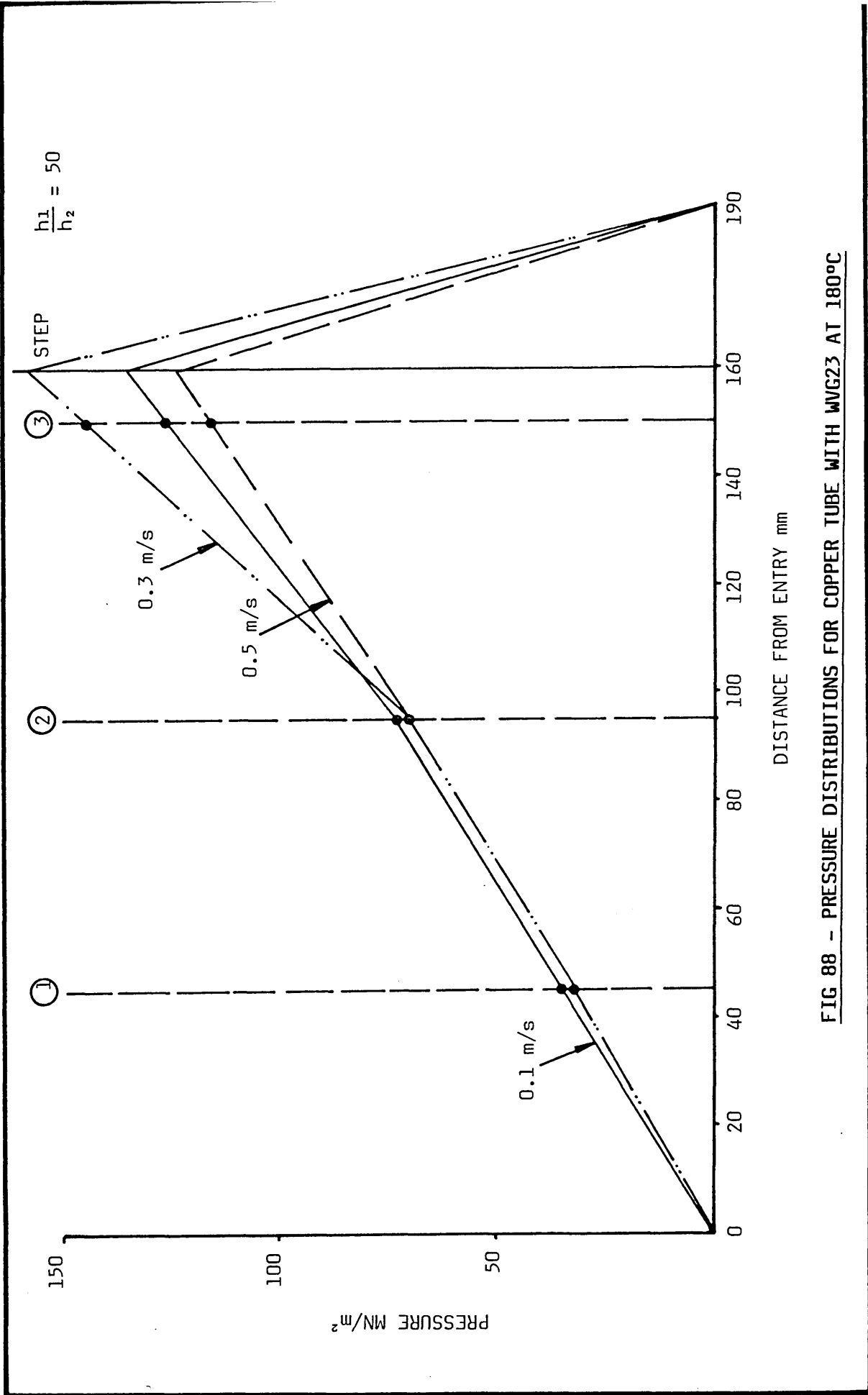


FIG 88 - PRESSURE DISTRIBUTIONS FOR COPPER TUBE WITH WVG23 AT 180°C

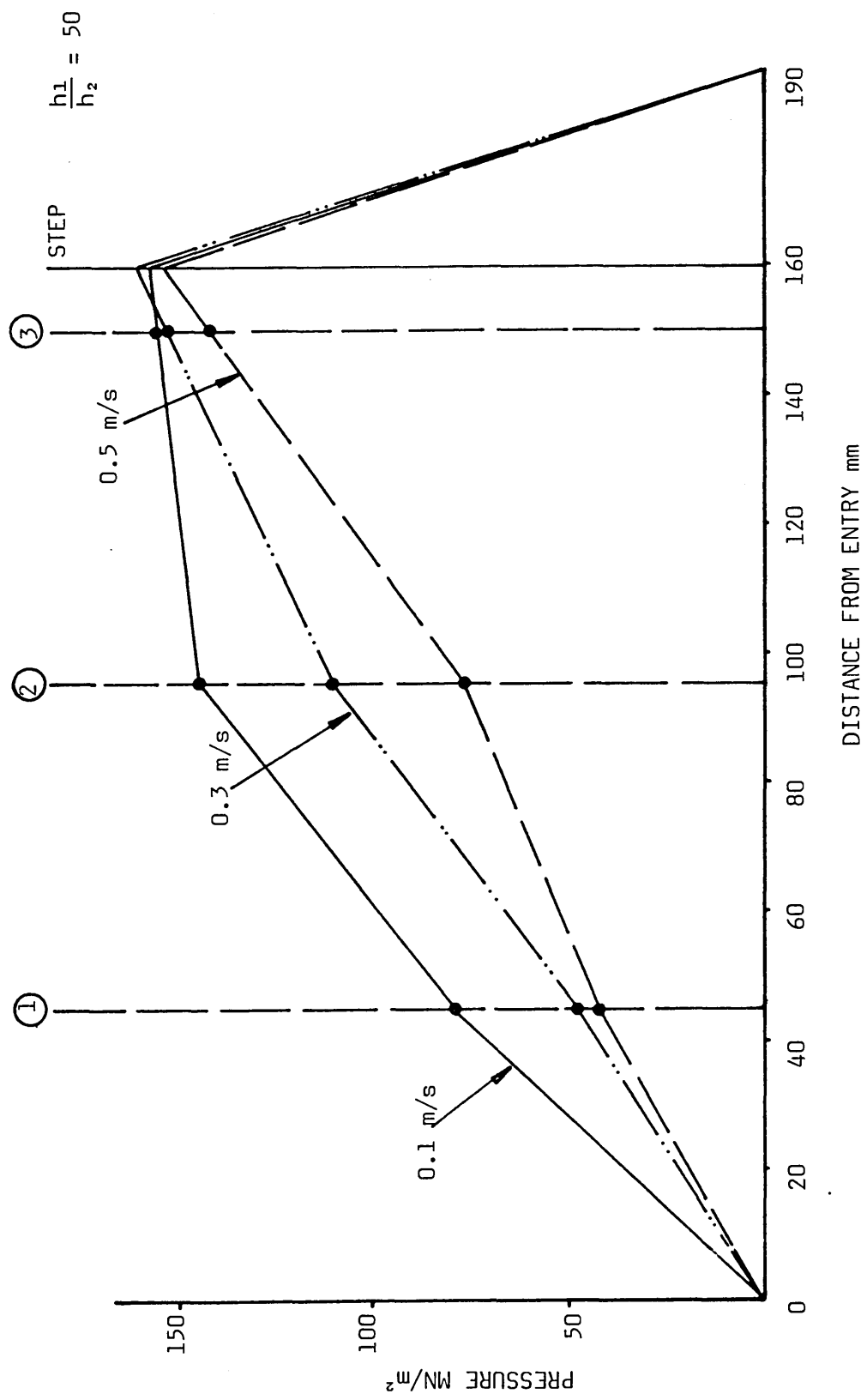


FIG 89 - PRESSURE DISTRIBUTIONS FOR COPPER TUBE WITH KM61 AT 200°C

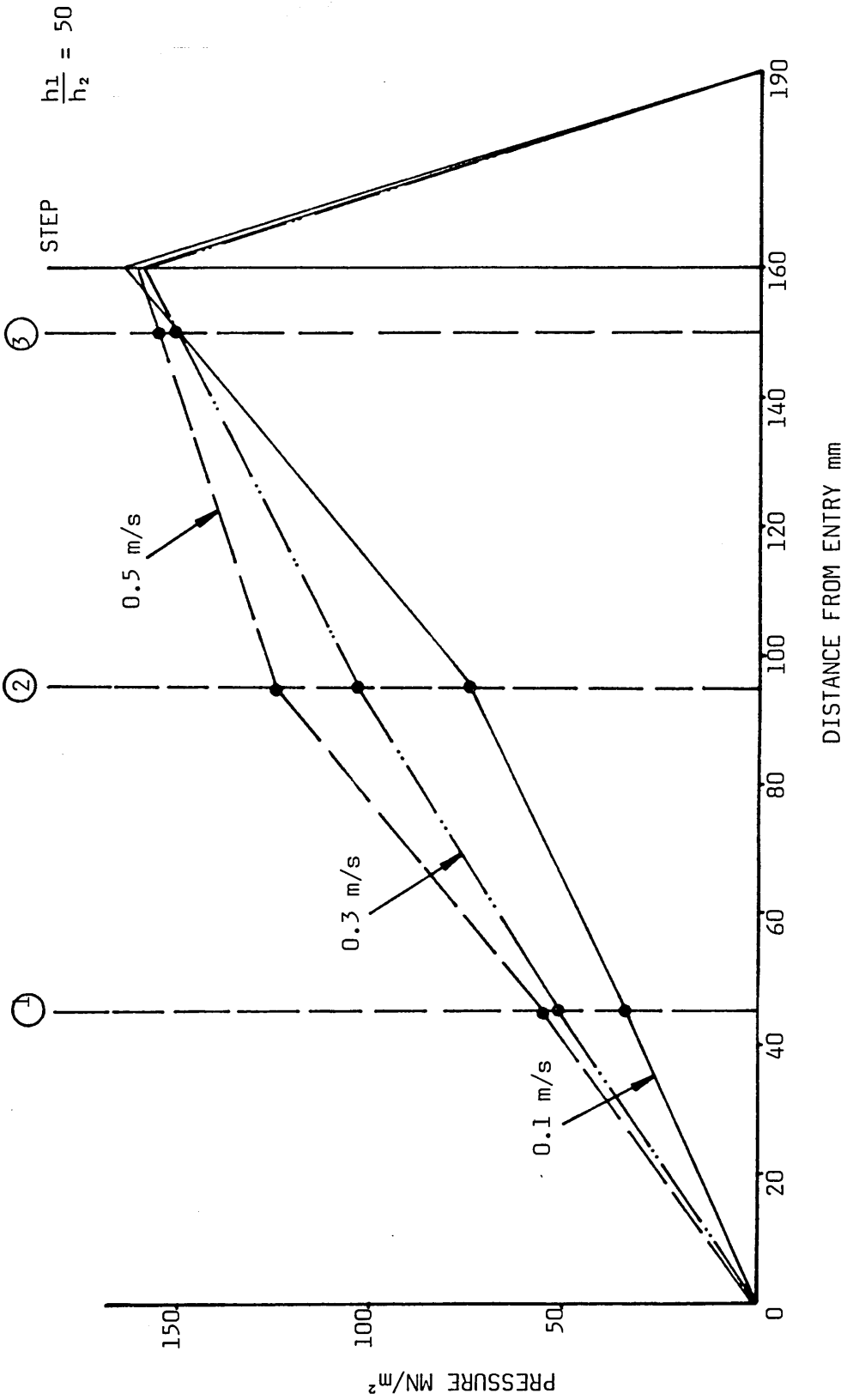


FIG 90 - PRESSURE DISTRIBUTIONS FOR COPPER TUBE WITH KM61 AT 220°C

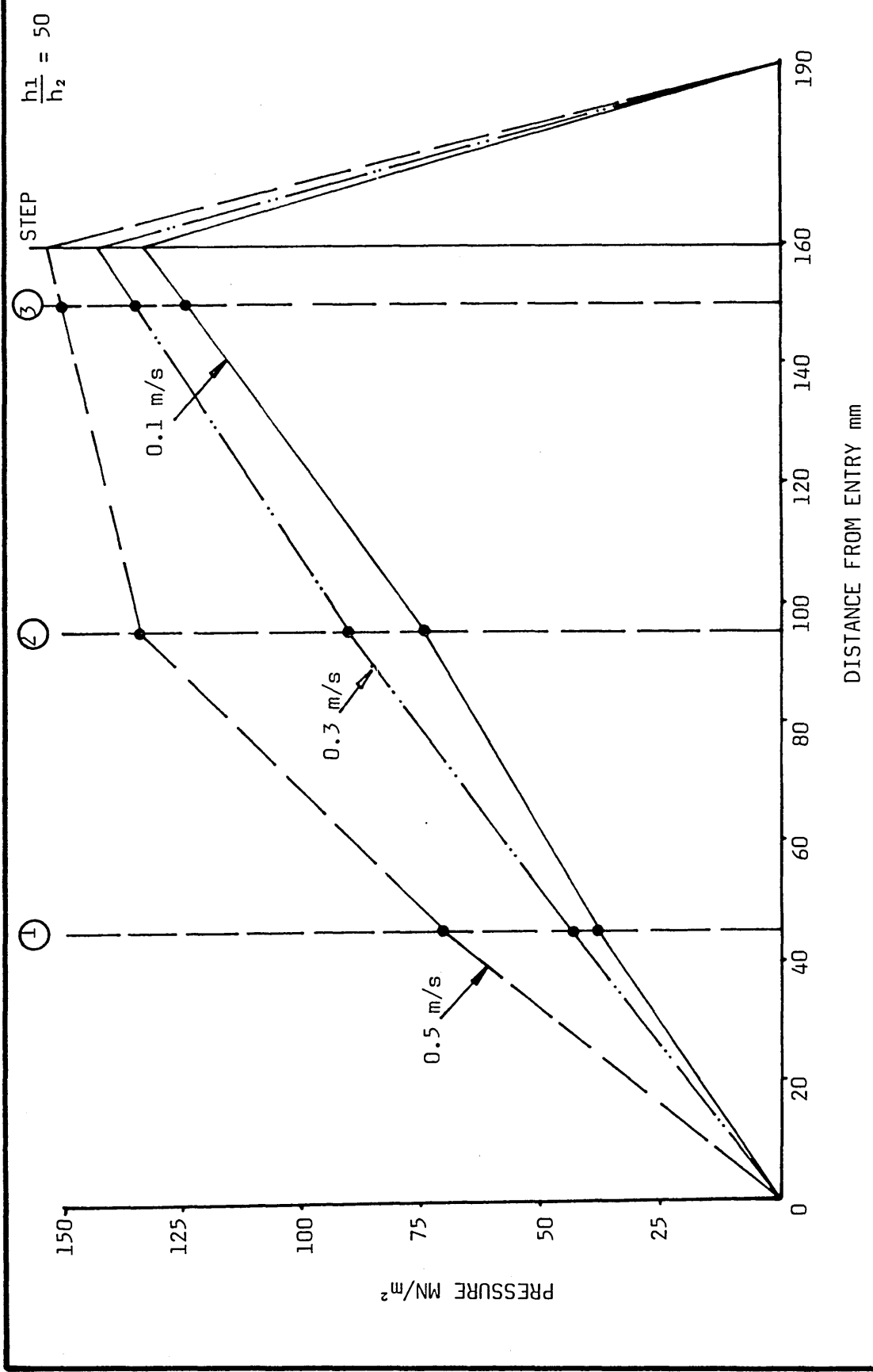


FIG 91 - PRESSURE DISTRIBUTIONS FOR COPPER TUBE WITH RIGIDEX AT 230°C

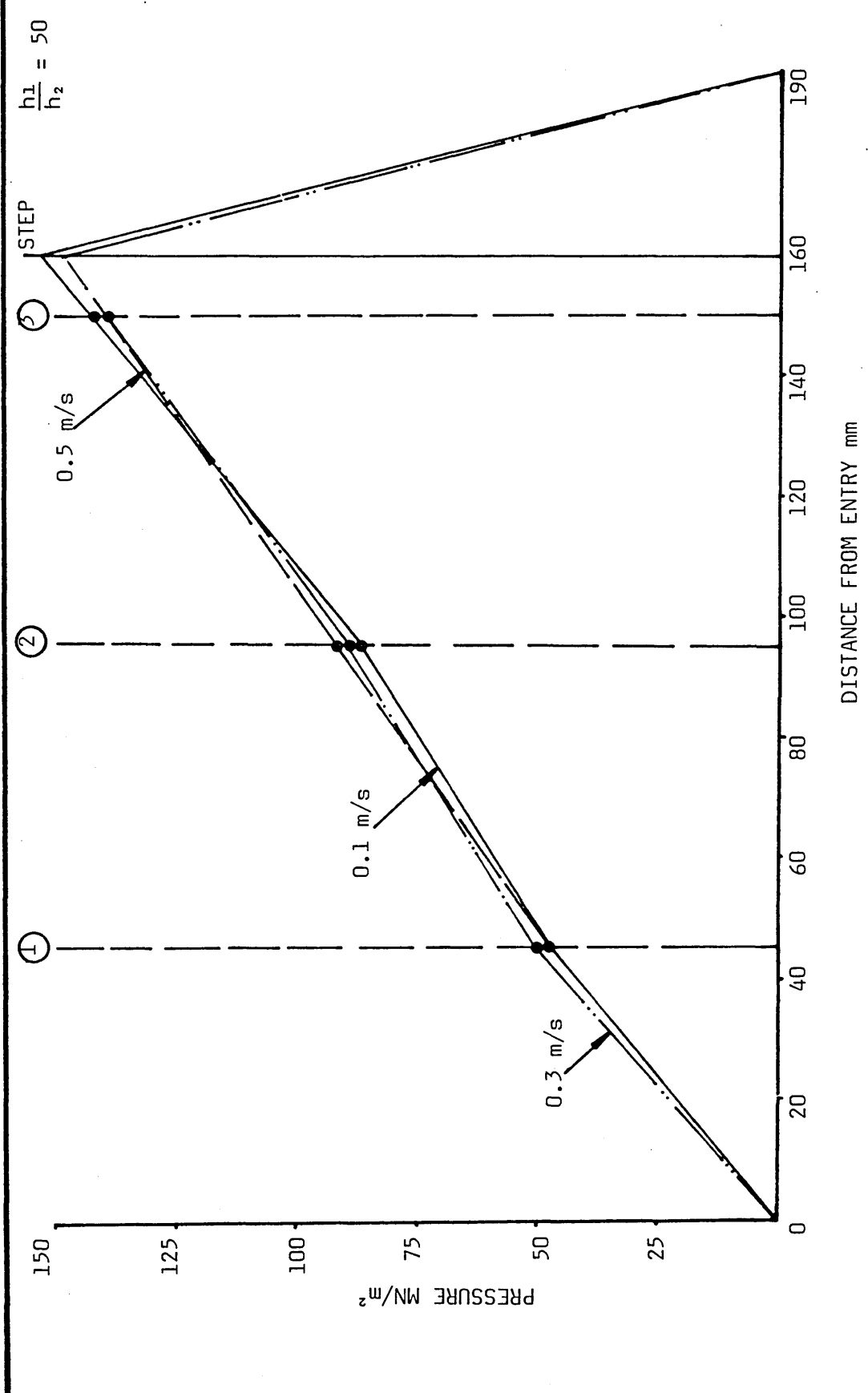


FIG 92 - PRESSURE DISTRIBUTIONS FOR COPPER TUBE WITH RIGIDEX AT 240°C

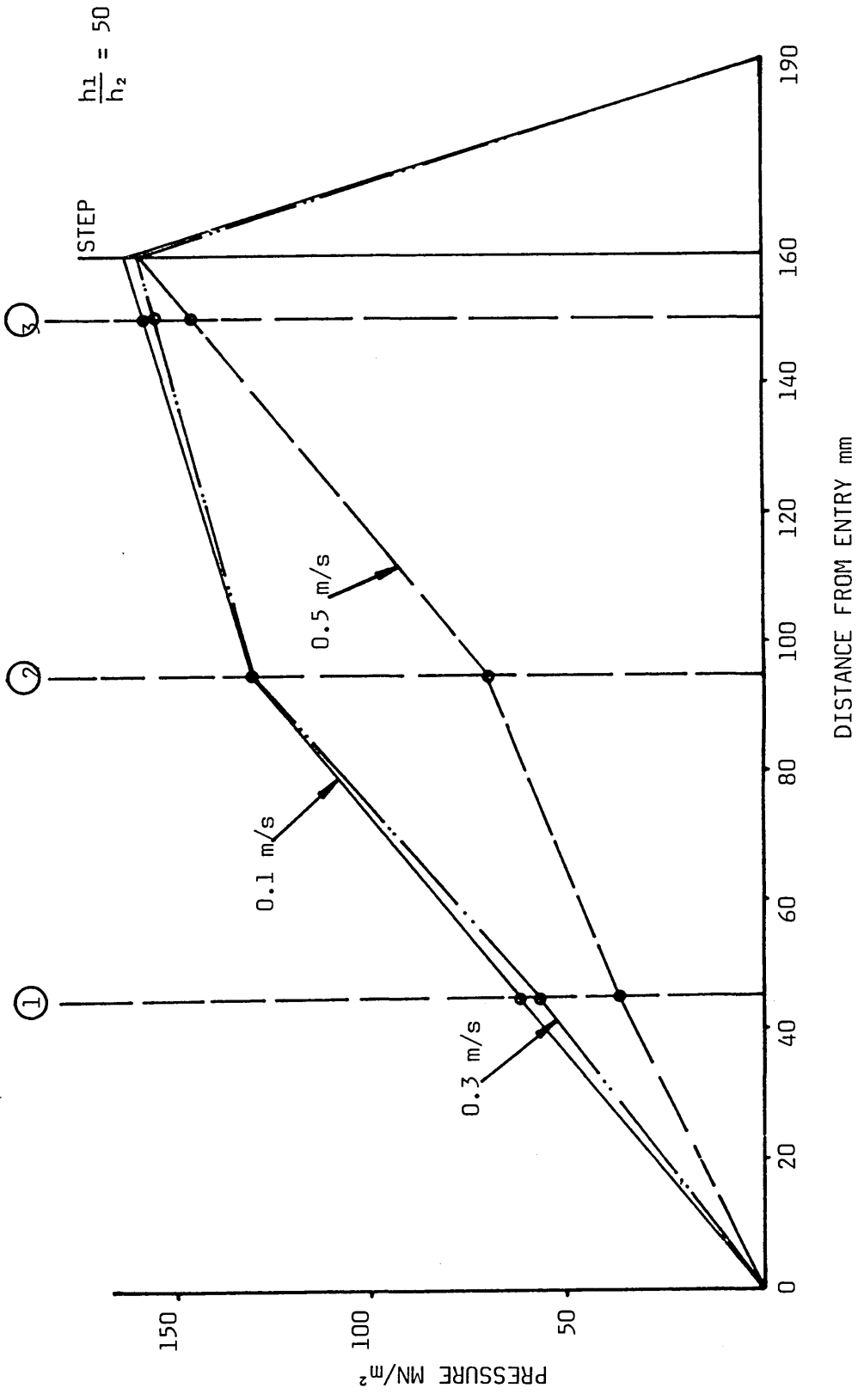


FIG 93 - PRESSURE DISTRIBUTIONS FOR COPPER TUBE WITH POLYSTYRENE AT 230°C

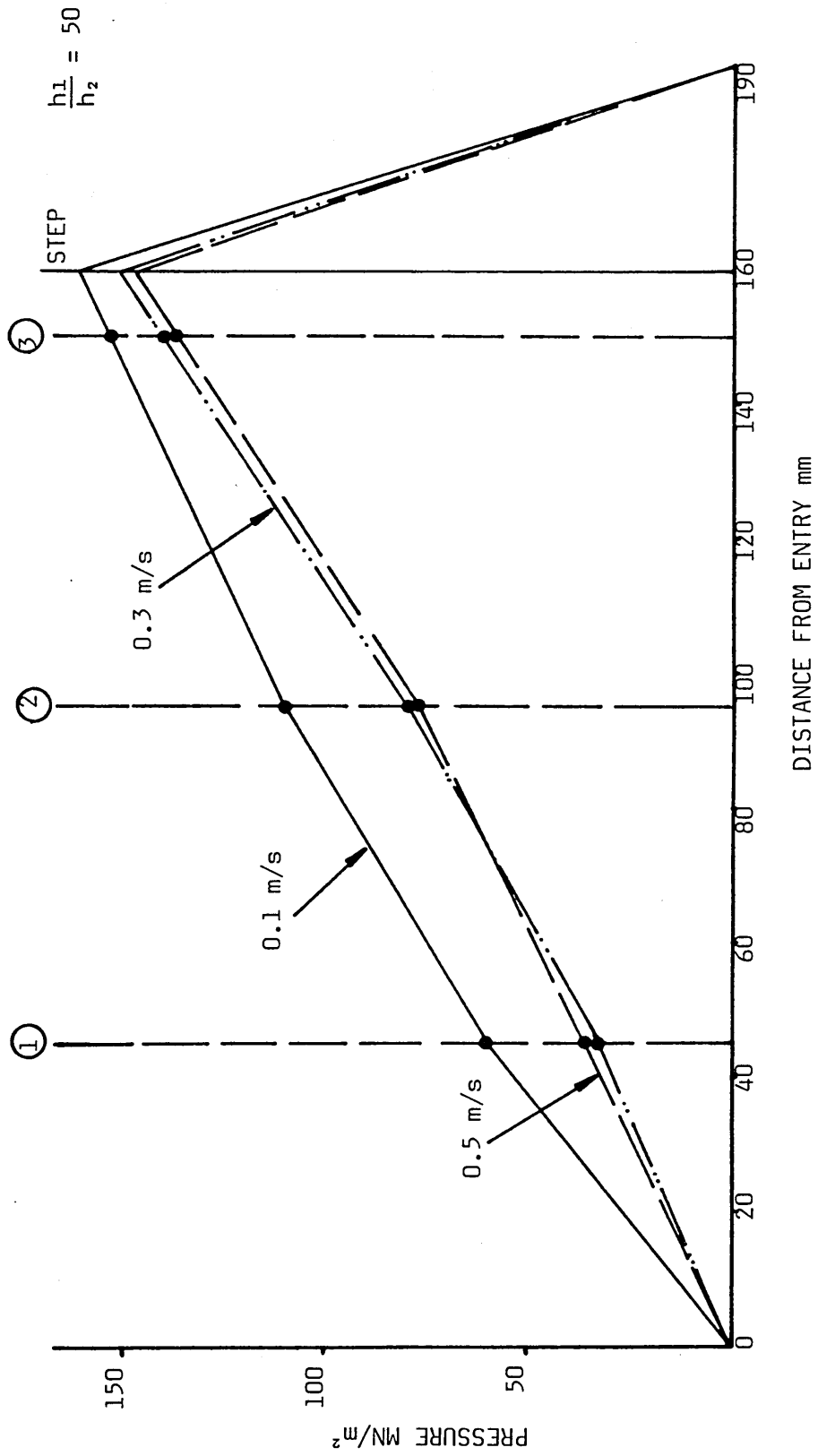


FIG 94 - PRESSURE DISTRIBUTIONS FOR COPPER TUBE WITH POLYSTYRENE AT 240°C

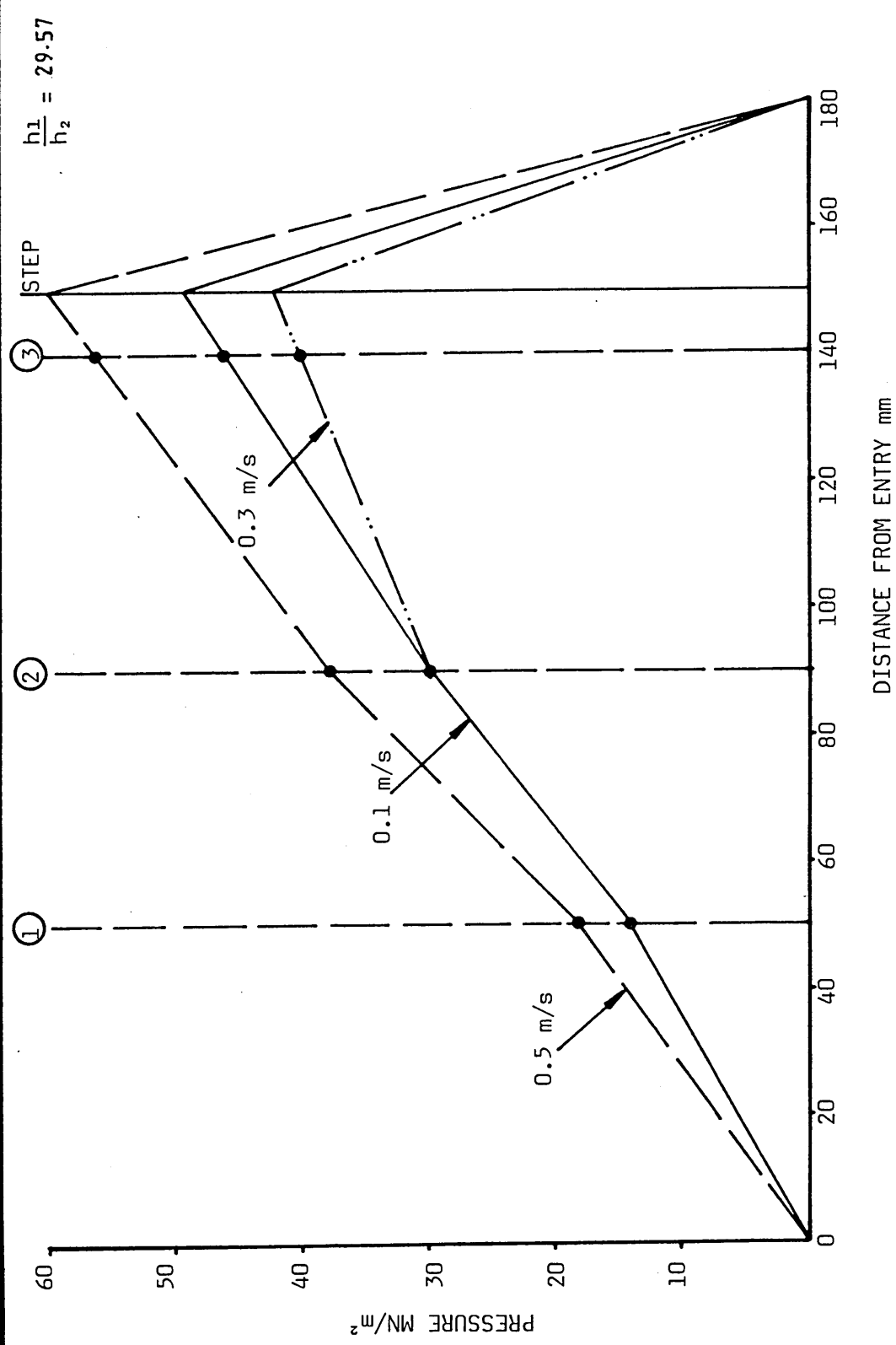


FIG 95 - PRESSURE DISTRIBUTIONS FOR ALUMINIUM TUBE WITH WVG23 AT 130°C

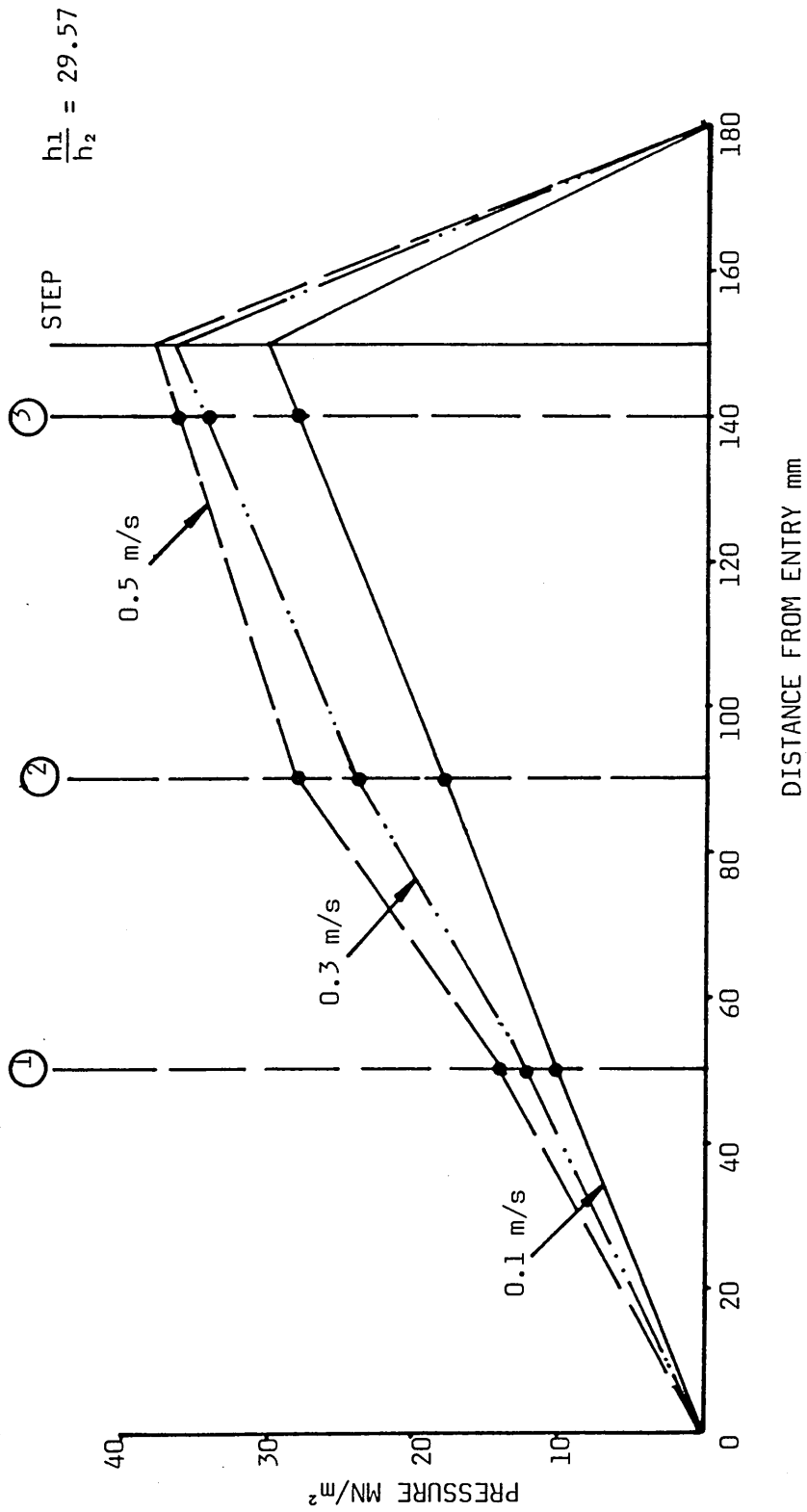


FIG 96 - PRESSURE DISTRIBUTIONS FOR ALUMINIUM TUBE WITH WVG23 AT 180°C

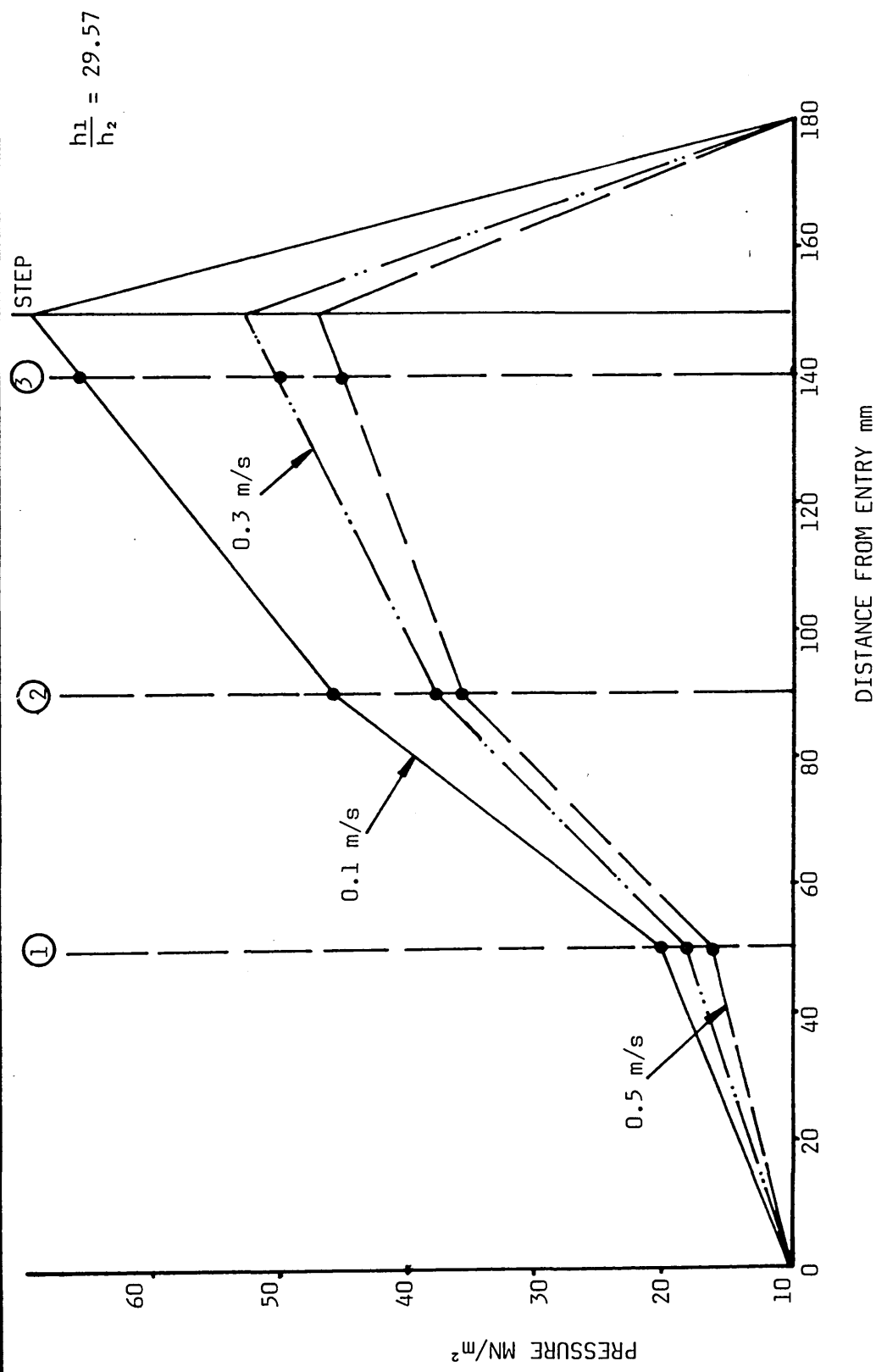


FIG 97 - PRESSURE DISTRIBUTIONS FOR ALUMINIUM TUBE WITH KM61 AT 200°C

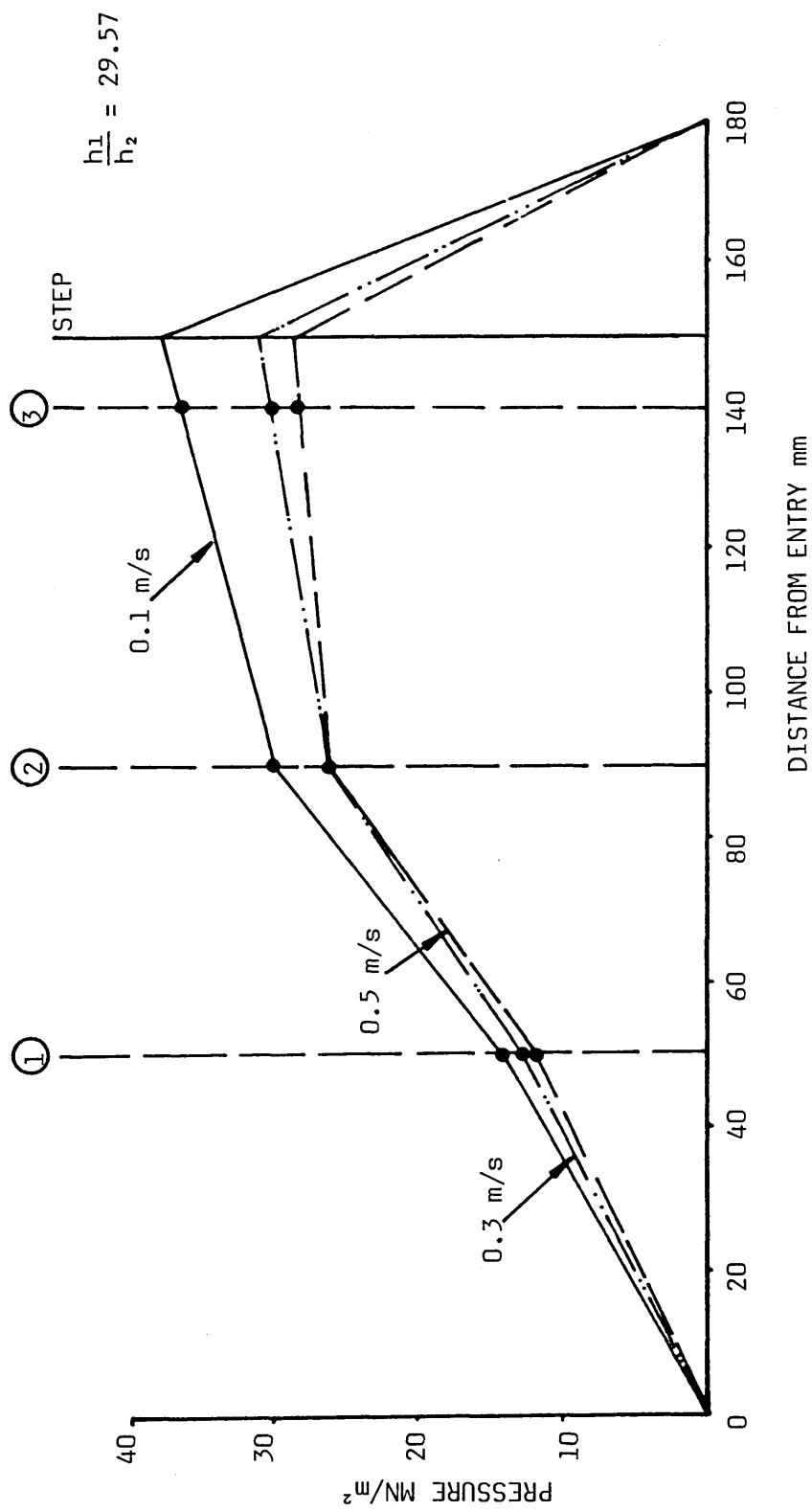


FIG 98 - PRESSURE DISTRIBUTIONS FOR ALUMINIUM TUBE WITH KM61 AT 220 °C

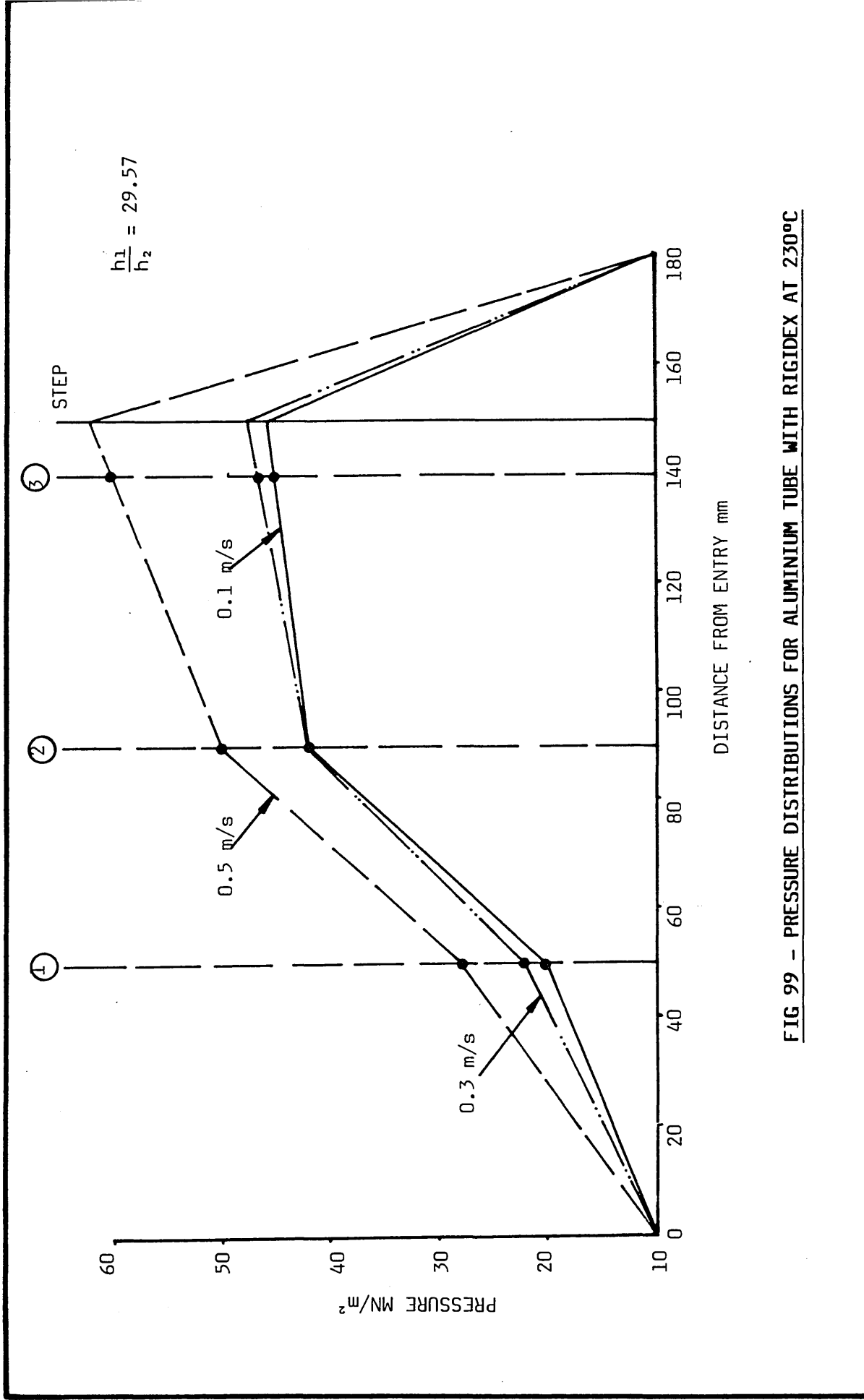


FIG 99 - PRESSURE DISTRIBUTIONS FOR ALUMINIUM TUBE WITH RIGIDEX AT 230°C

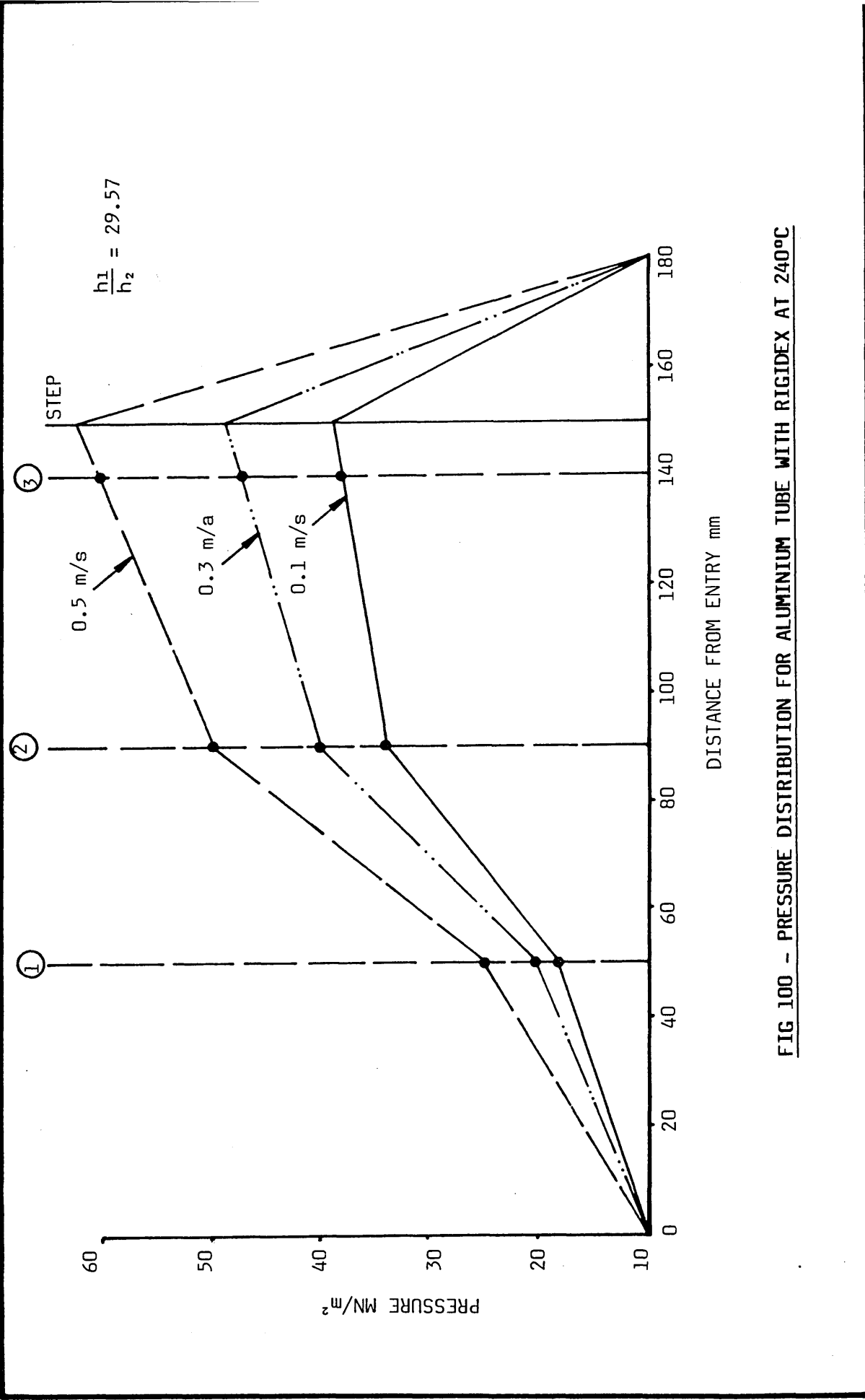


FIG 100 - PRESSURE DISTRIBUTION FOR ALUMINIUM TUBE WITH RIGIDEX AT 240°C

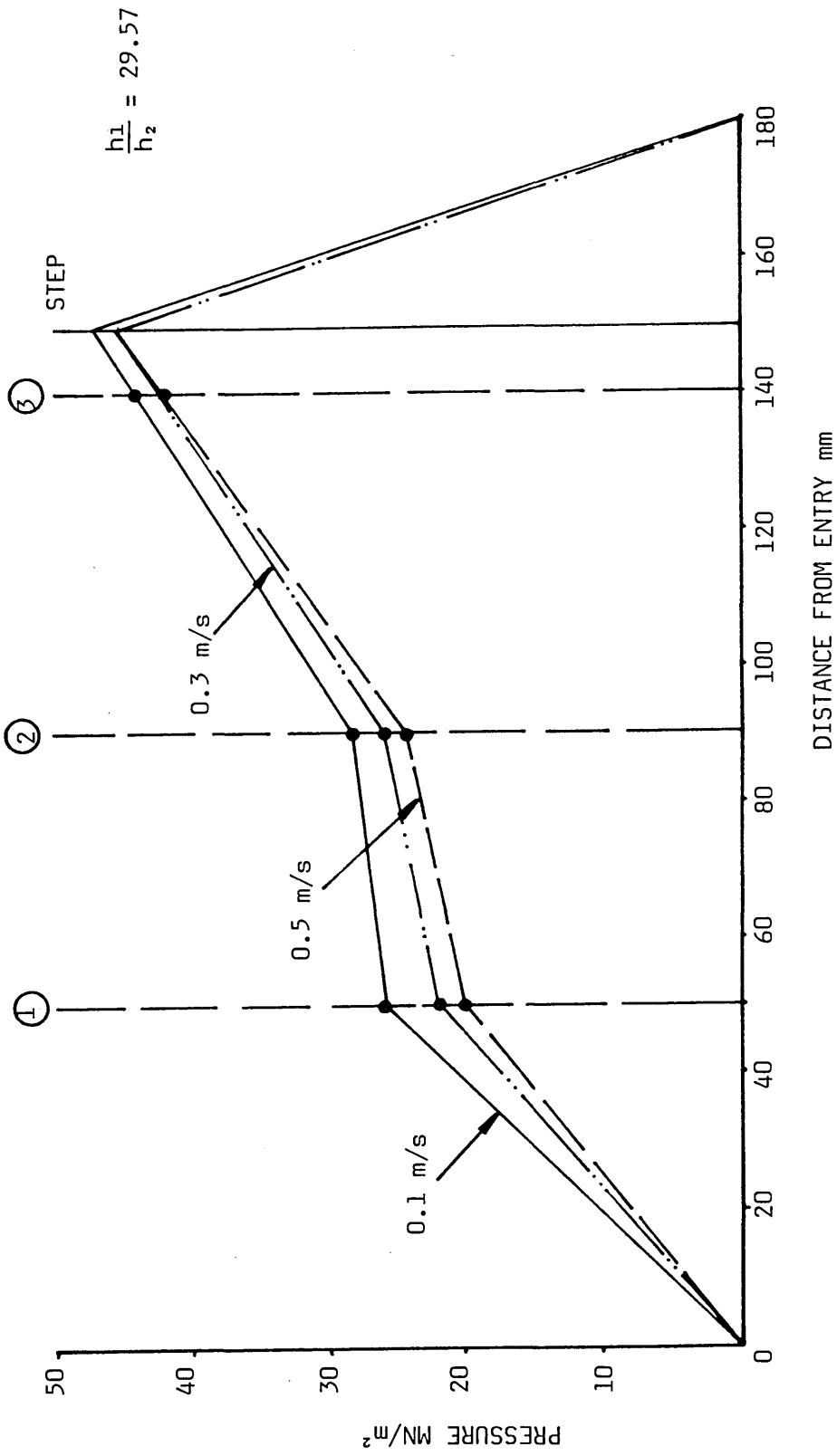


FIG 101 - PRESSURE DISTRIBUTIONS FOR ALUMINIUM TUBE WITH POLYSTYRENE AT 230°C

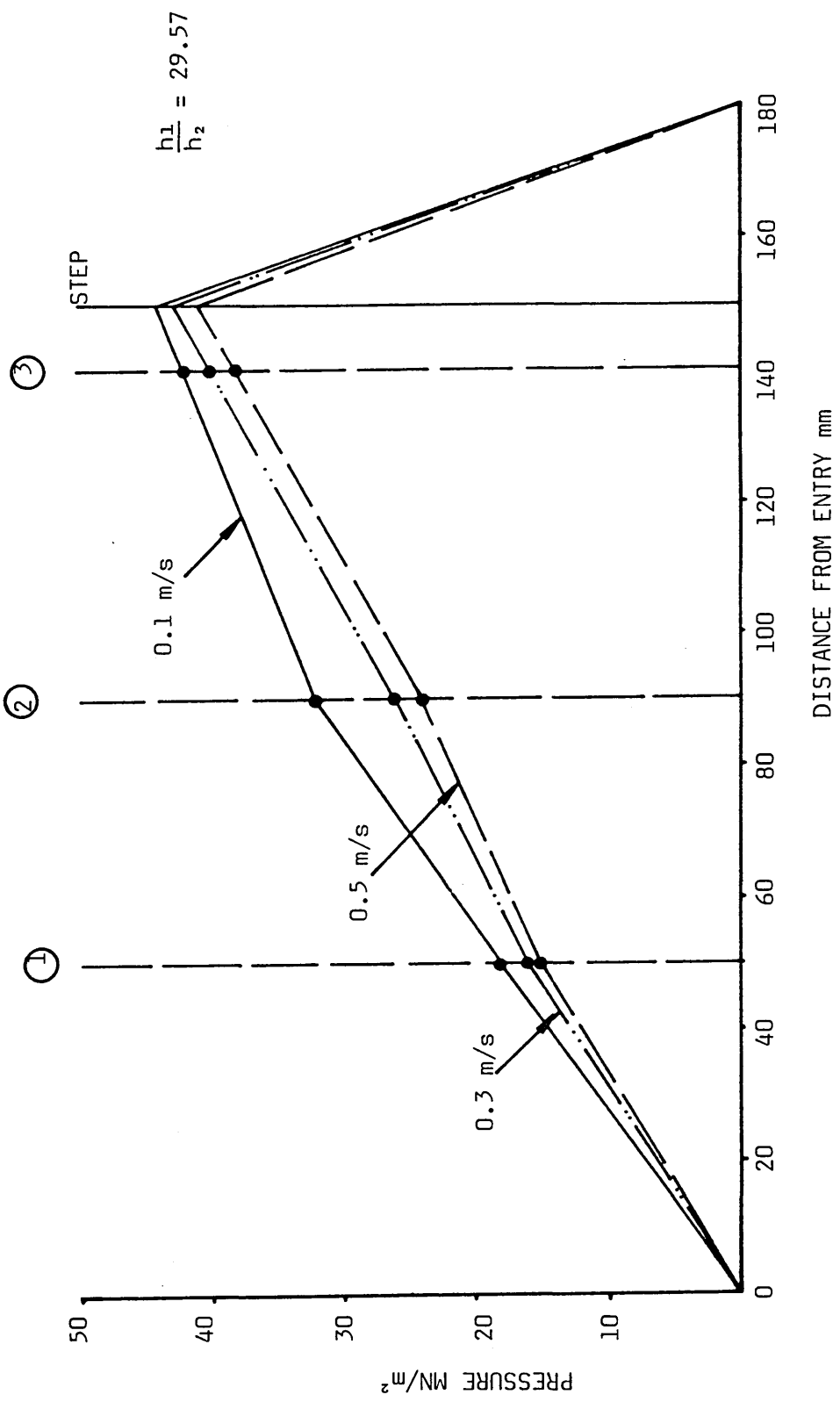


FIG 102 - PRESSURE DISTRIBUTIONS FOR ALUMINIUM TUBE WITH POLYSTYRENE AT 240°C

4.2.4 Results of Coating Thickness

Results of the coating thickness exhibited similar trends to those of the percentage reduction in diameter.

Fig (103) shows the coating thickness produced on the copper tube with WVG23 polymer at varying temperatures and speeds. At the polymer temperature of 130°C the maximum reduction in diameter and coating thickness were obtained at 0.1 m/s, as the drawing speed was increased coating thickness decreased. The thickness of polymer coatings at lower temperatures was found to be greater than those at higher temperatures. At higher drawing speed (0.5 m/s), polymer at temperature of 130°C, the coating thickness was found to be twice that at the polymer temperature of 180°C. It was also found that the coating thickness at higher temperatures and speeds were generally uniform and smooth. At very low drawing speeds and temperatures shark-skin was observed (shark-skin is fully discussed in Chapter 2).

Fig (104) gives the coating thickness obtained with KM61 polymer at 200°C, 220°C and 240°C for copper tube. At the melt temperature of 200°C, flow of this polymer commenced at about 0.2 m/s and below speed thin coating thickness was obtained. Shark-skin was observed on the polymer immediately after the flow occurred and up to drawing speed of about 0.5 m/s. At melt temperatures of 220°C and 240°C, the coating thickness was found to be approximately same at lower drawing speeds.

Fig (105) shows the coating thickness produced on the copper tube drawn with Rigidex polymer at 230°C and 240°C. The results of this polymer show the same general trends as those in figure (103) (WVG23 at 130°C). The thickness of polymer coatings at lower temperature were found to be greater than those at higher temperature.

Fig (106) shows the coating thickness produced on the copper tube with Polystyrene polymer at temperatures of 230°C and 240°C. When this polymer was used as the pressure medium, maximum deformation and coating thickness were obtained at lower drawing speeds. At melt temperatures of 230°C and 240°C approximately same level of coating thickness was found at lower drawing speeds.

Figs (107) to (110) show coating thickness obtained when aluminium tubes were drawn using WVG23, KM61, Rigidex and Polystyrene polymers at different melt temperatures. The general trends of the results were found to be similar to those for the copper tubes when WVG23 polymer was used. When KM61 polymer was used the coating thickness on the aluminium tube showed a different trend than those on the copper tube as shown in Fig (104).

$$\frac{h_1}{h_2} = 50$$

(x) 130°C

(o) 160°C

(•) 180°C

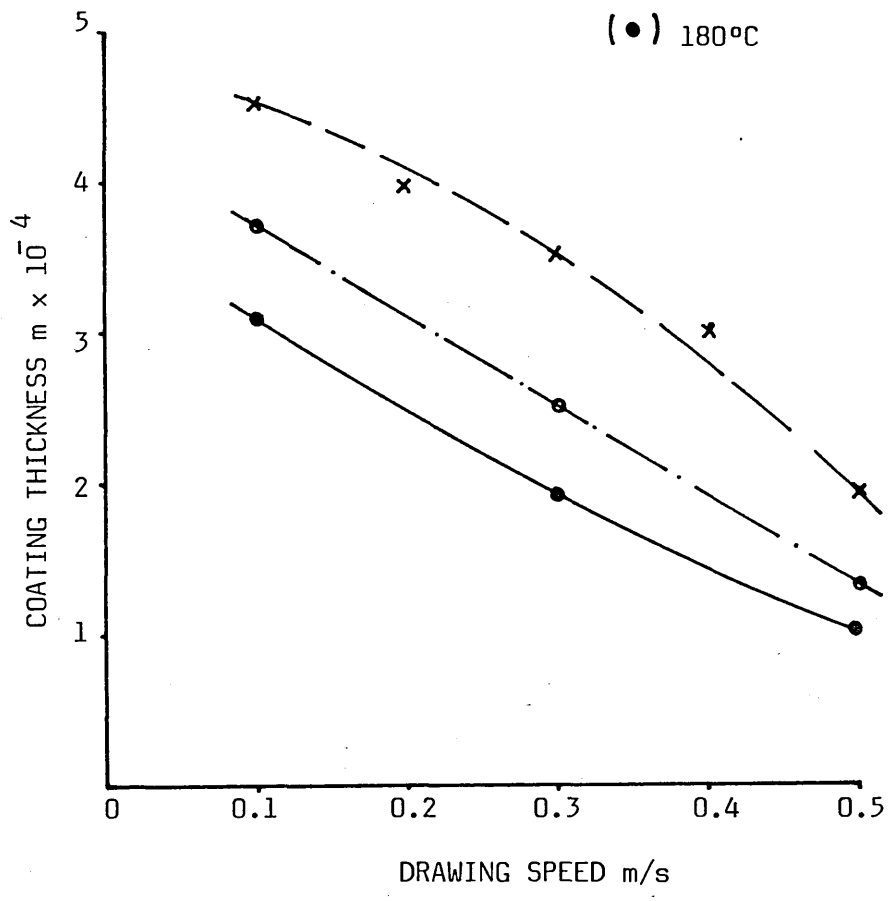


FIG 103 - COATING THICKNESS ON COPPER TUBE WITH WVG23

$$\frac{h_1}{h_2} = 50$$

(x) 200°C

(o) 220°C

(•) 240°C

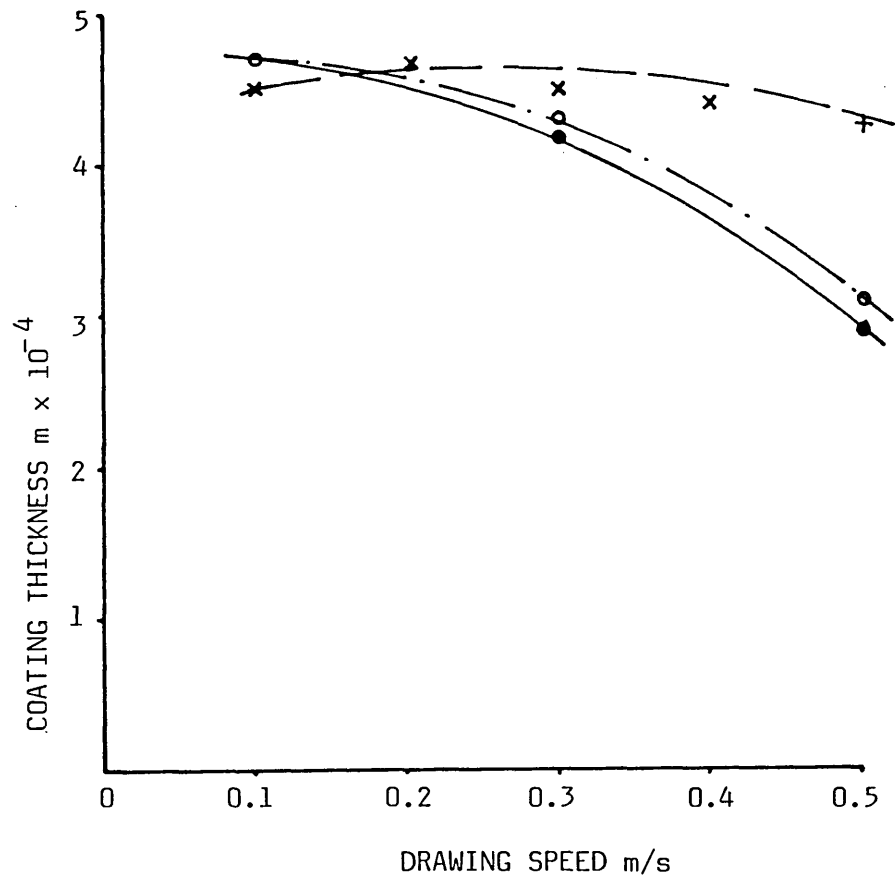


FIG 104 - COATING THICKNESS ON COPPER TUBE WITH KM61

$$\frac{h_1}{h_2} = 50$$

(x) 230°C

(o) 240°C

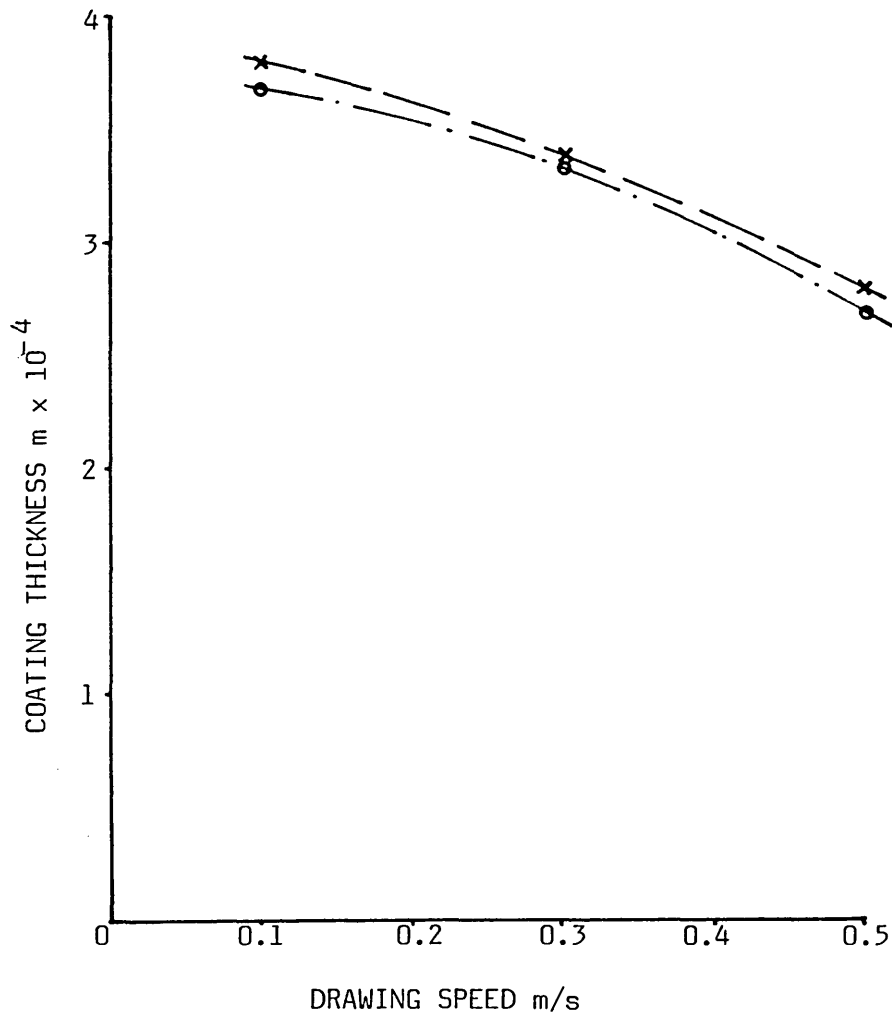


FIG 105 - COATING THICKNESS ON COPPER TUBE WITH RIGIDEX

$$\frac{h_1}{h_2} = 50$$

(x) 230°C

(o) 240°C

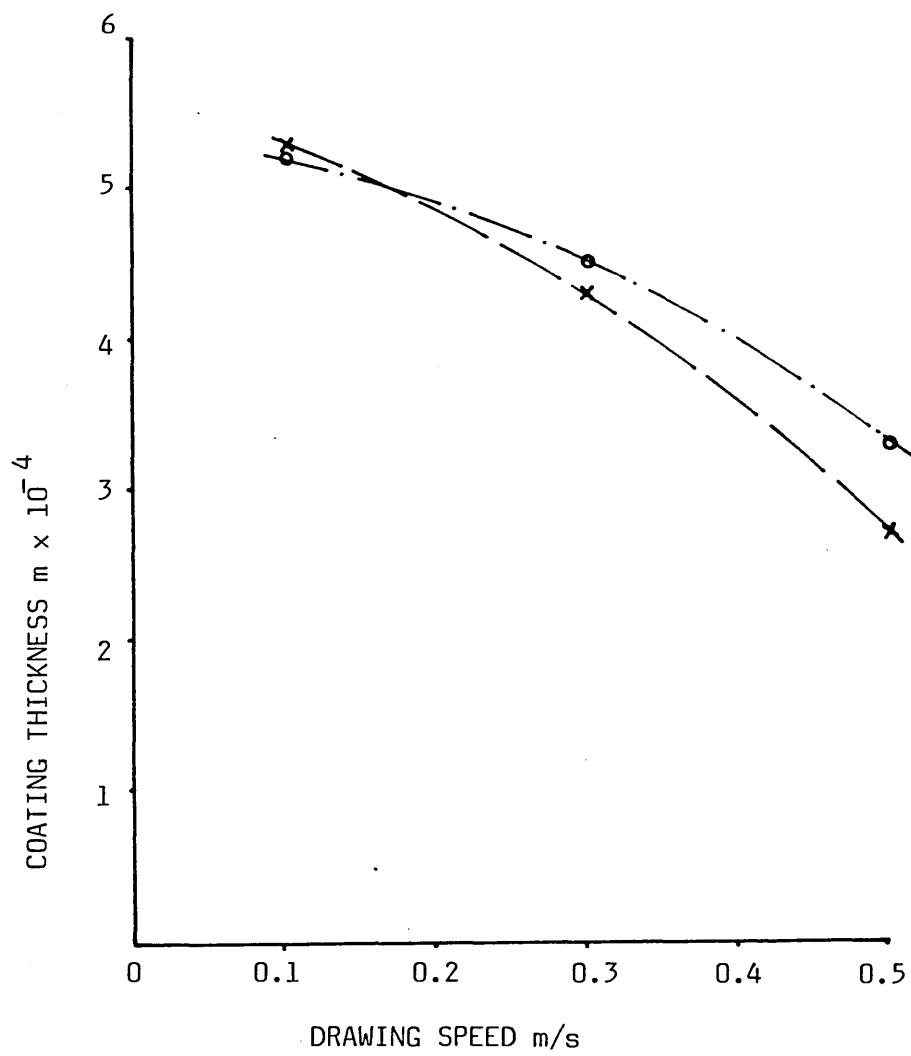


FIG 106 - COATING THICKNESS ON COPPER TUBE WITH POLYSTYRENE

$$\frac{h_1}{h_2} = 29.57$$

(x) 130°C

(o) 160°C

(•) 180°C

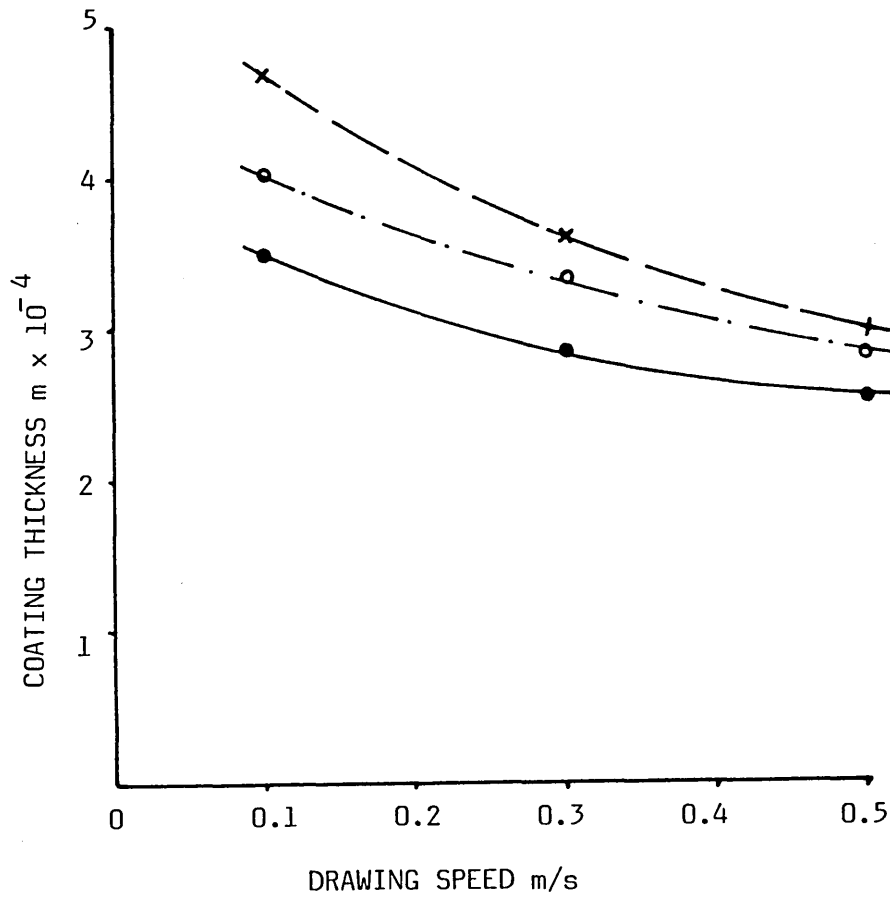


FIG 107 - COATING THICKNESS ON ALUMINIUM TUBE WITH WVG23

$$\frac{h_1}{h_2} = 29.57$$

(x) 200°C

(o) 220°C

(•) 240°C

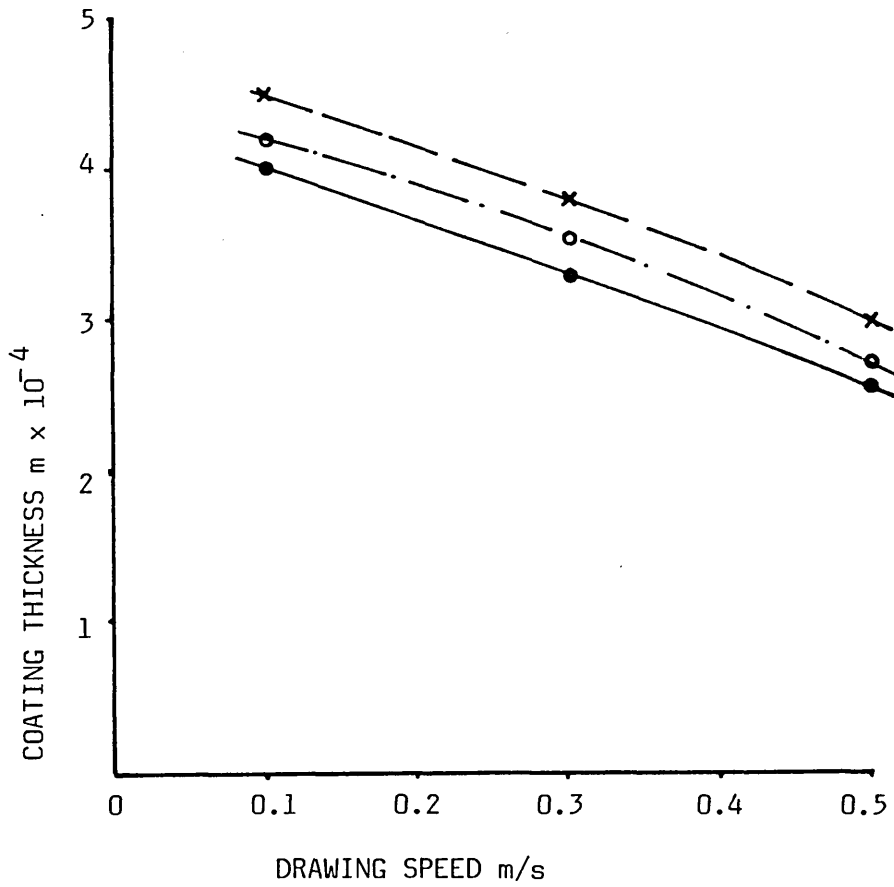


FIG 108 - COATING THICKNESS ON ALUMINIUM TUBE WITH KM61

$$\frac{h_1}{h_2} = 29.57$$

(x) 230°C

(o) 240°C

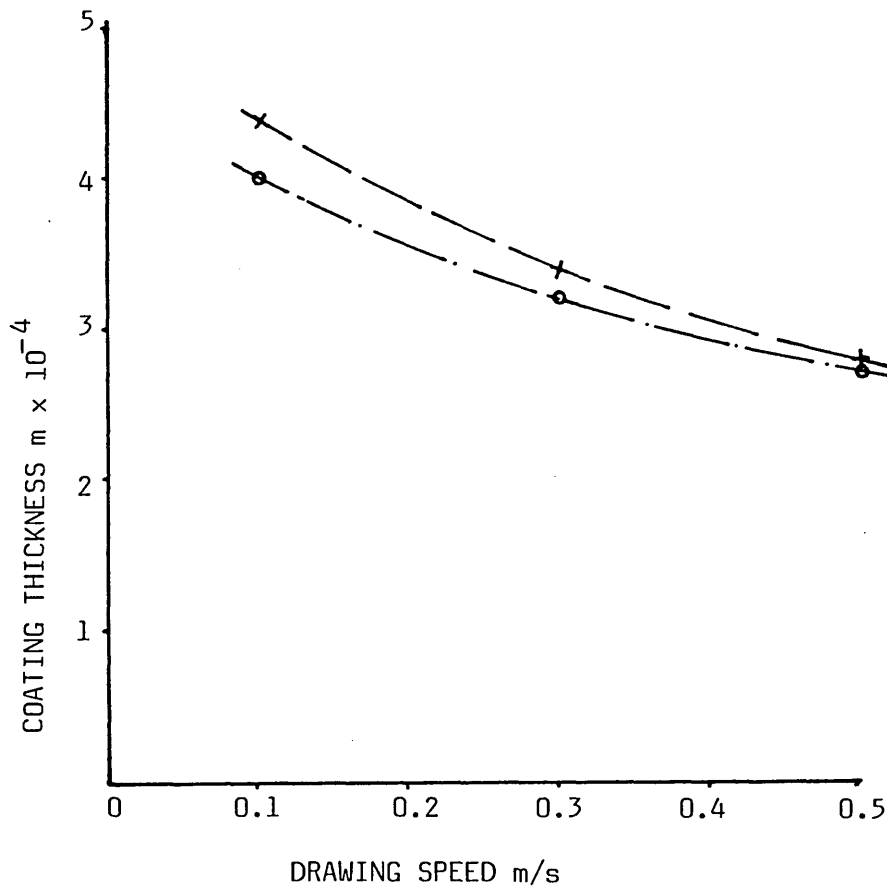


FIG 109 - COATING THICKNESS ON ALUMINIUM TUBE WITH RIGIDEX

$$\frac{h_1}{h_2} = 29.57$$

(x) 230°C

(o) 240°C

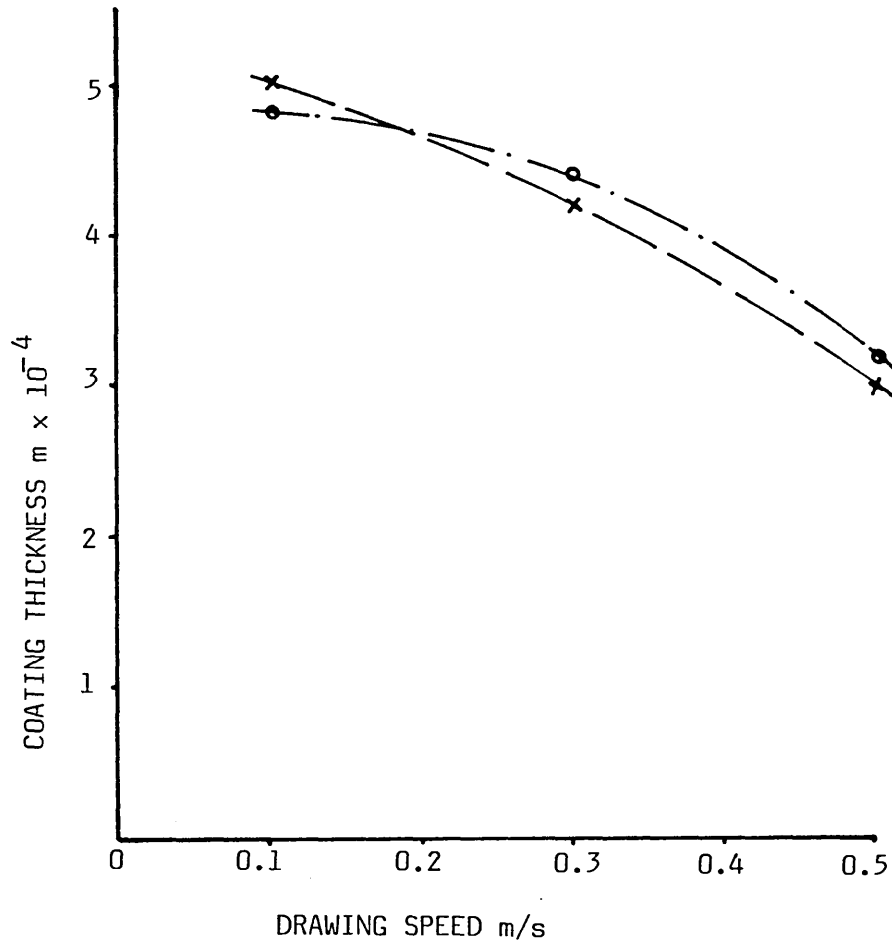


FIG 110 - COATING THICKNESS ON ALUMINIUM TUBE WITH POLYSTYRENE

4.3 Determination of the Deformation Profiles

While the tube was being drawn the process was stopped suddenly by disengaging the tube from the dog jaws. The tube was then marked at the inlet point of the melt chamber and pulled out to cut off a length equal to the melt chamber length for examining the deformation profile. The diameter of the tube was measured at 5mm intervals from the inlet position using a point micrometer. This procedure was repeated for copper and aluminium tubes at different drawing speeds, using WVG23 at temperature of 130°C. Results are shown in Figs (111) and (112) respectively, which clearly exhibit the shapes of the effective die profiles formed in the unit.

Fig (111) shows three deformation profiles for copper tube drawn at three different speeds. The yielding position of the tube was measured at about 122mm in the unit at drawing speed of 0.1 m/s. The position of the deformations, at drawing speeds of 0.3 m/s and 0.5 m/s, was found to be at 140mm from the entry of the die-less reduction unit.

Three deformation profiles at three different drawing speeds for aluminium tube are shown in Fig (112). The yielding positions in the unit were found to take place at 104mm, 118mm and 125mm from the entry side of the die-less reduction unit at drawing speeds of 0.1 m/s, 0.3 m/s and 0.5 m/s respectively.

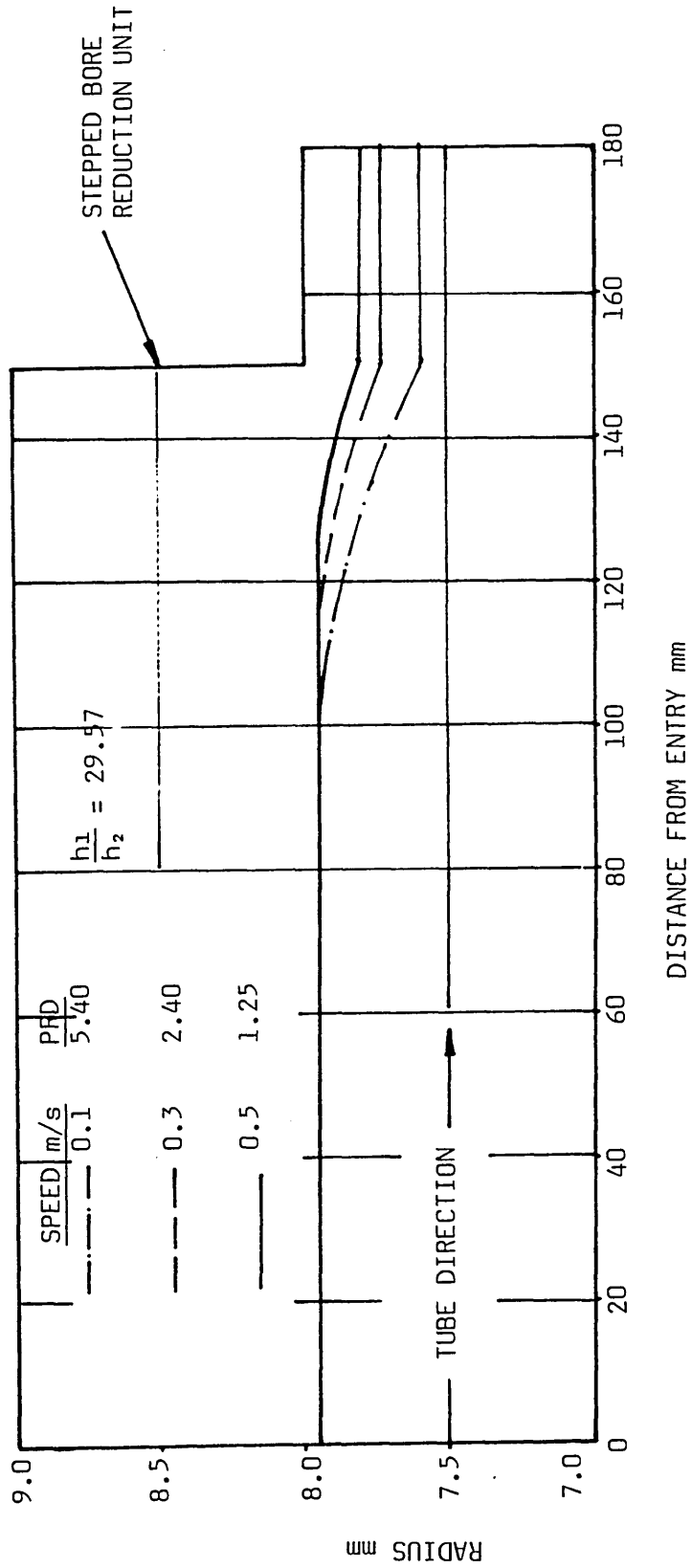


FIG 112 - DEFORMATION PROFILES FOR ALUMINIUM TUBE WITH WVG23 AT 130°C

4.4 Roundness Tests

Roundness tests were carried out using a Tylor Hobson roundness tester (type Talyrond with reference computer). In order to establish the uniformity of roundness along the length of the drawn tube, measurements were taken over the length of a number of specimens drawn at different speeds. Roundness of the as received tubes (reduced by the conventional methods) were also measured and compared with those of the tubes reduced using the die-less reduction unit.

Fig (113) shows the results of roundness tests on as received copper tube. The error of about 0.025mm may be noted from the reference circle. When this tube was drawn through a die-less reduction unit using a WVG23 polymer at 130°C and at the speed of 0.1 m/s, the drawn tube was found to demonstrate similar degree of roundness over the entire length, the error was found to be about 0.03mm as shown in Fig (114).

Figs (115) to (117) show the results of roundness tests on copper tubes, when WVG23 and KM61 polymers were used as the pressure mediums at temperatures of 130°C and 200°C respectively. The level of out of roundness was found to be approximately same whether WVG23 polymer was used at drawing speed of 0.5 m/s or KM61 polymer was used at the drawing speeds of 0.1 m/s and 0.5 m/s.

Figs (118) to (121) show the results of roundness tests on copper tubes when Rigidex and Polystyrene polymers at different temperatures were used. These figures show out of roundness errors varying between 0.02mm and 0.06mm on tubes drawn at 0.1 m/s.

Figs (122) to (126) show the results of roundness on aluminium tubes. The as received tubes showed out of roundness error of about 0.008mm (see Fig 122). When the tube was drawn using WVG23

polymer at the melt temperature of 130°C, roundness measurements on the drawn tube showed larger error of about 0.11mm for the drawing speed of 0.1 m/s (as shown in Fig 123), but at higher drawing speed error was reduced to about 0.02mm, see Fig (124). When KM61 polymer was used as the pressure medium at 200°C the tube was squeezed formed at the drawing speed of 0.1 m/s. At higher drawing speed, roundness test produced slightly different traces, the results are shown in Figs (125) and (126) respectively.

Roundness tests carried out on aluminium tubes drawn using Rigidex and Polystyrene polymers at melt temperature of 230°C produced different results at different drawing speeds. The Rigidex polymer showed about 0.12mm error for the drawing speed of 0.1 m/s, but at higher drawing speed the error was found to be about 0.035mm, as shown in Figs (127) and (128) respectively. When polystyrene polymer was used as the pressure medium for the drawing speeds of 0.1 to 0.5 m/s, the results of roundness tests on aluminium tubes with Polystyrene polymer were found to be similar to those in Figs (120) and (114) respectively, these results are shown in Figs (129) and (130).

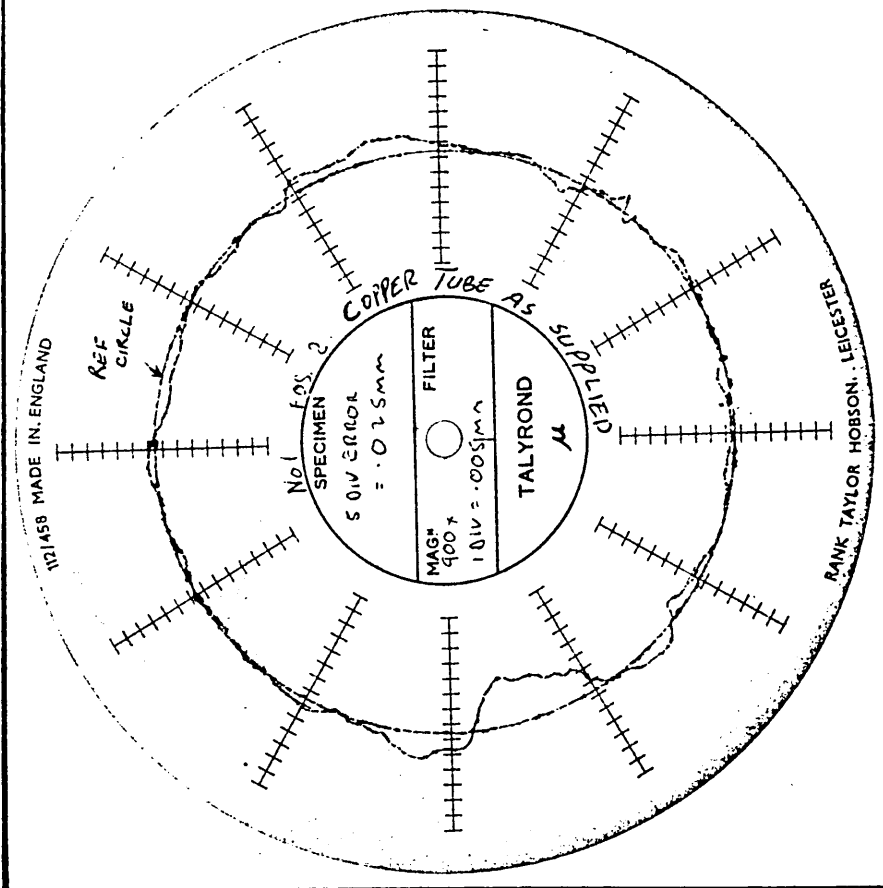


FIG 113 - ROUNDNESS TEST ON RECEIVED COPPER TUBE

1 DIV = 0.005 mm

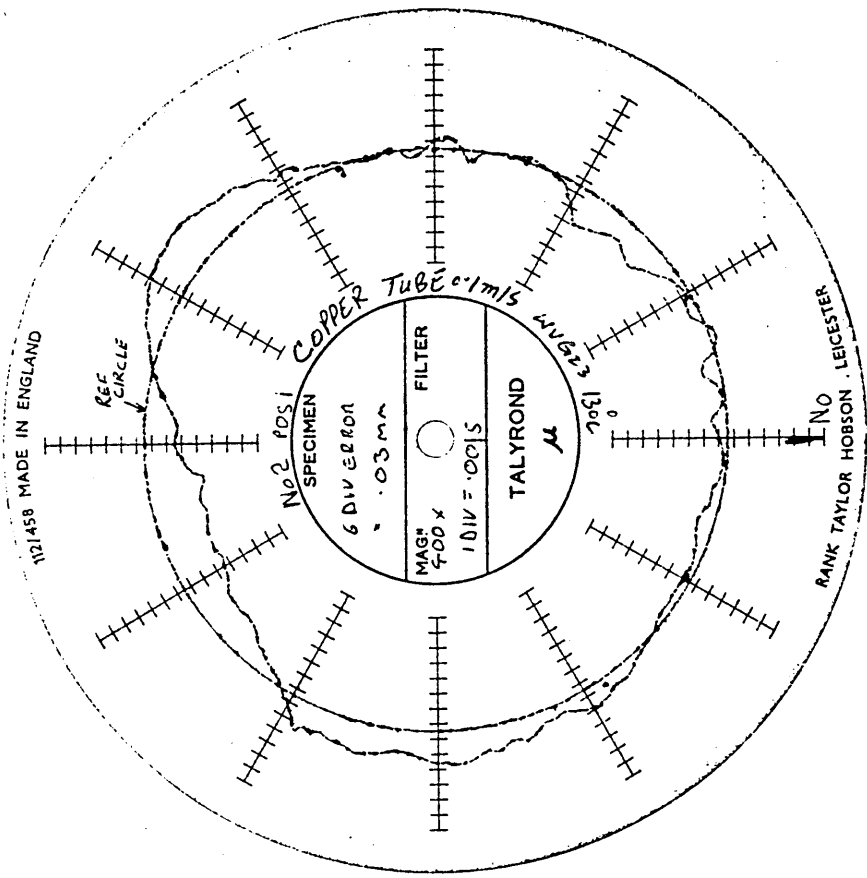


FIG 114 - ROUNDNESS TEST ON COPPER TUBE DRAWN
AT 0.1 m/s WITH WVG23, 130°C
6.13% REDUCTION IN DIAMETER

1 DIV = 0.005 mm

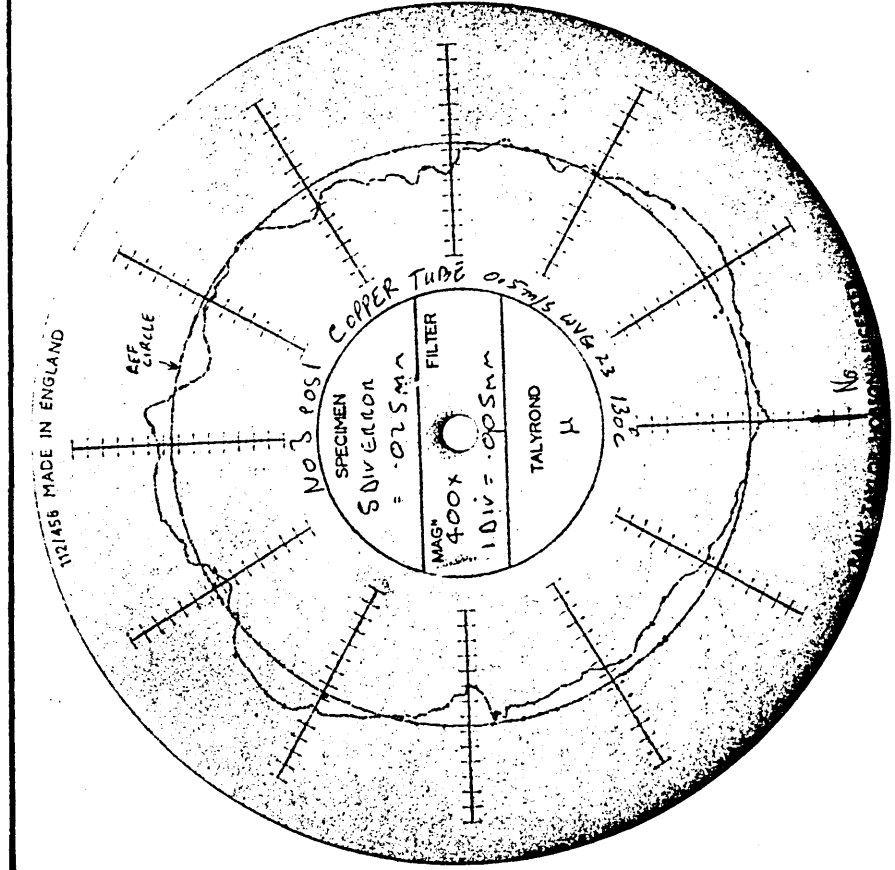


FIG 115 - ROUNDNESS TEST ON COPPER TUBE DRAWN AT
0.5 m/s WITH WVG23, 130°C
2.66% REDUCTION IN DIAMETER

1 DIV = 0.005 mm

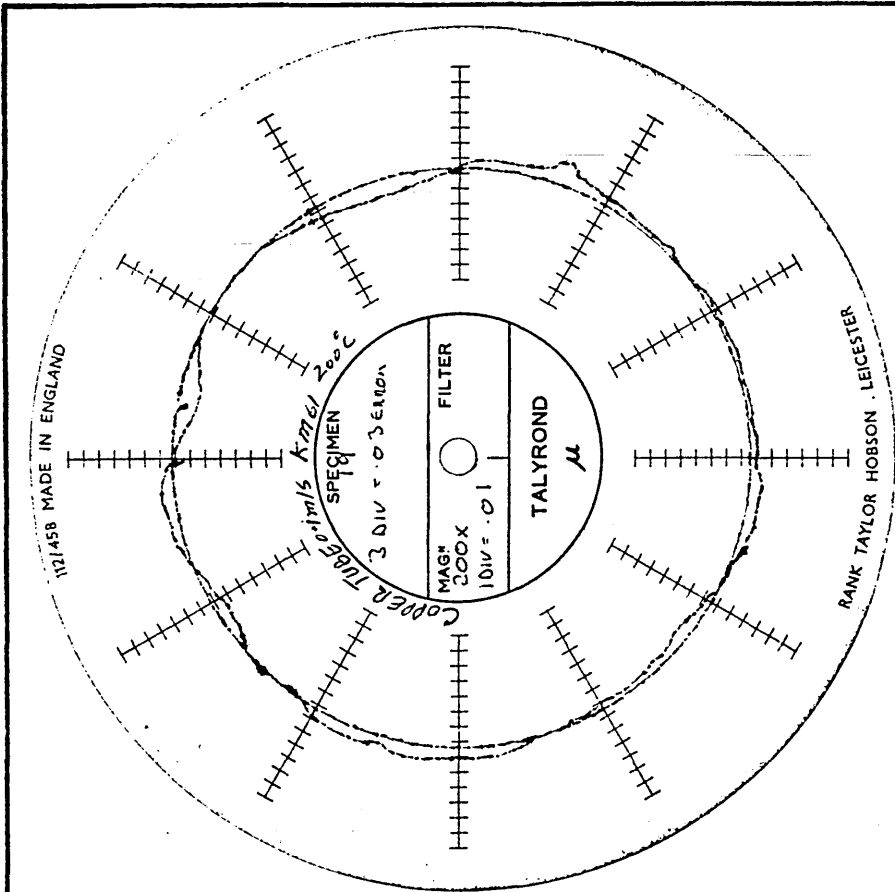


FIG 116 - ROUNDNESS TEST ON COPPER TUBE DRAWN AT
0.1 m/s WITH KM61, 200°C
5.64% REDUCTION IN DIAMETER

1 DIV = 0.01 mm

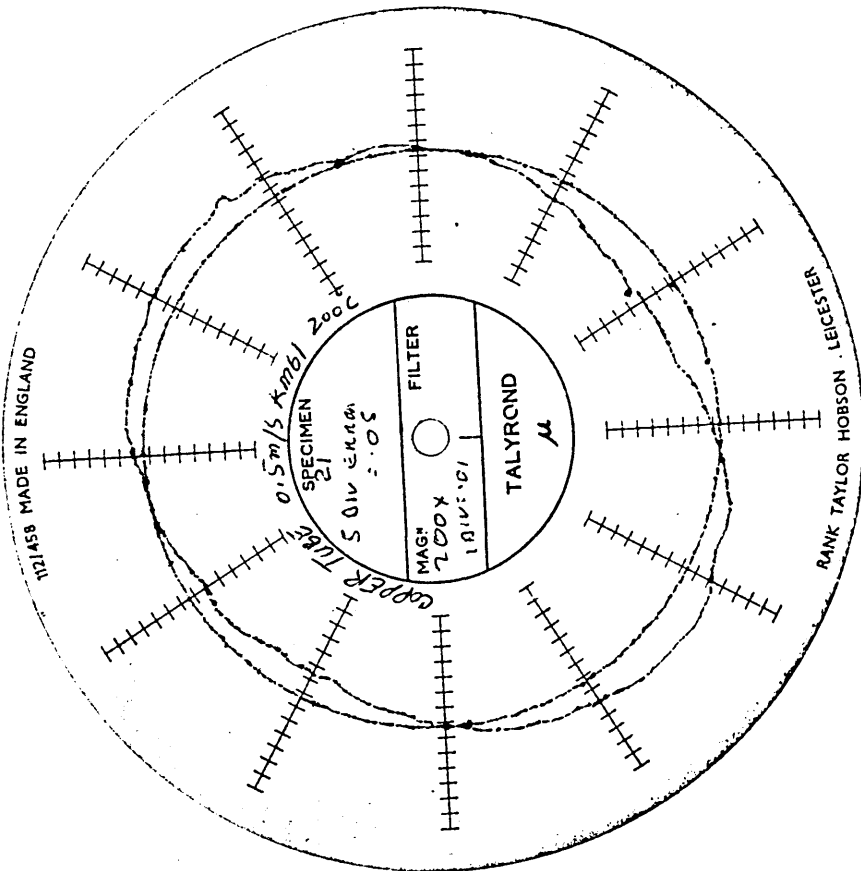


FIG 117 - ROUNDNESS TEST ON COPPER TUBE DRAWN
 AT 0.5 m/s WITH KM61, 200°C
 4.26% REDUCTION IN DIAMETER

1 DIV = 0.01 mm

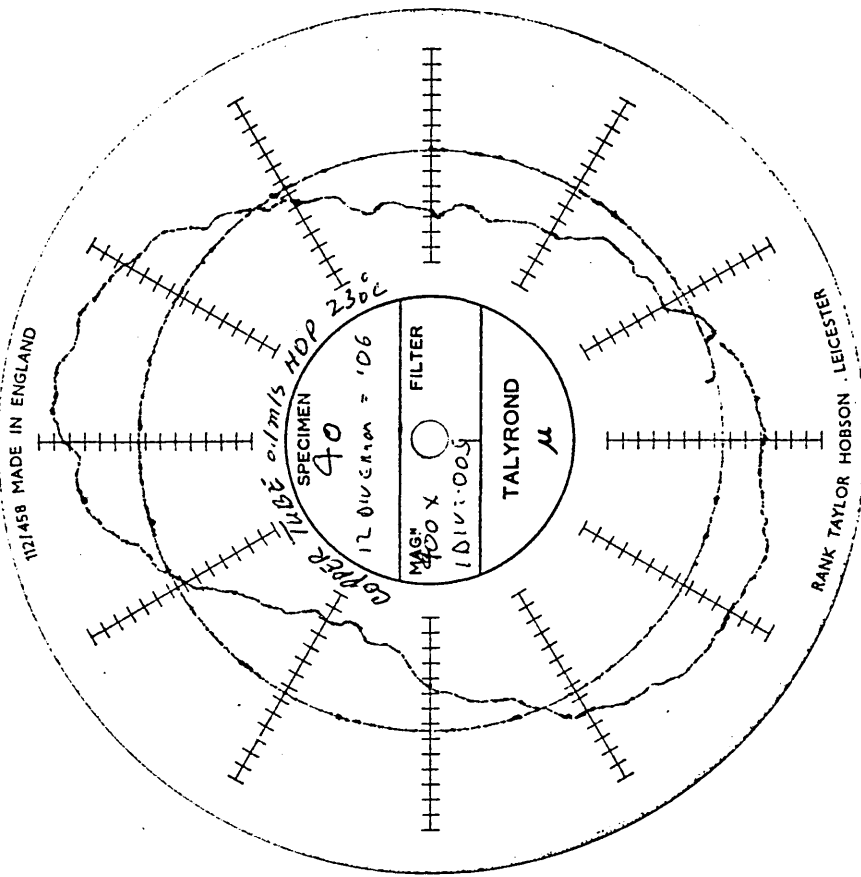


FIG 118 - ROUNDNESS TEST ON COPPER TUBE DRAWN
 AT 0.1 m/s WITH RIGIDEX, 230°C
 4.06% REDUCTION IN DIAMETER

1 DIV = 0.005 mm

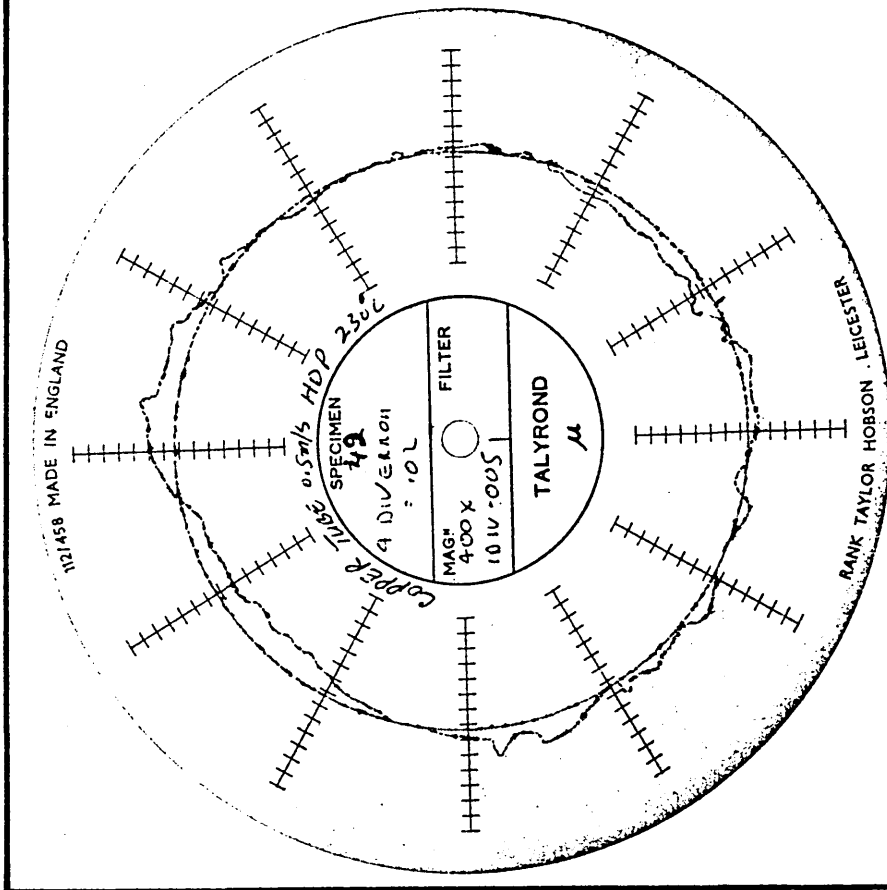


FIG 119 - ROUNDNESS TEST ON COPPER TUBE DRAWN
 AT 0.5 m/s WITH RIGIDEX, 230°C
 2.00% REDUCTION IN DIAMETER

1 DIV = 0.005 mm

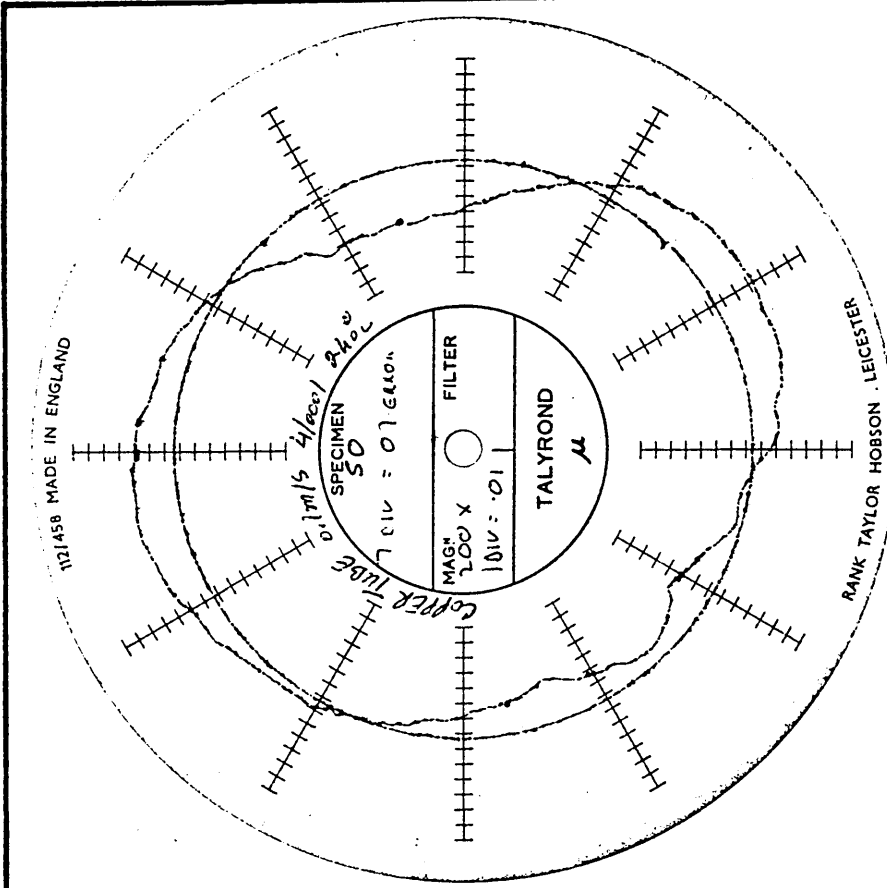


FIG 120 - ROUNDNESS TEST ON COPPER TUBE DRAWN
 AT 0.1 m/s WITH POLYSTYRENE, 240°C
 6.73% REDUCTION IN DIAMETER

1 DIV = 0.01 mm

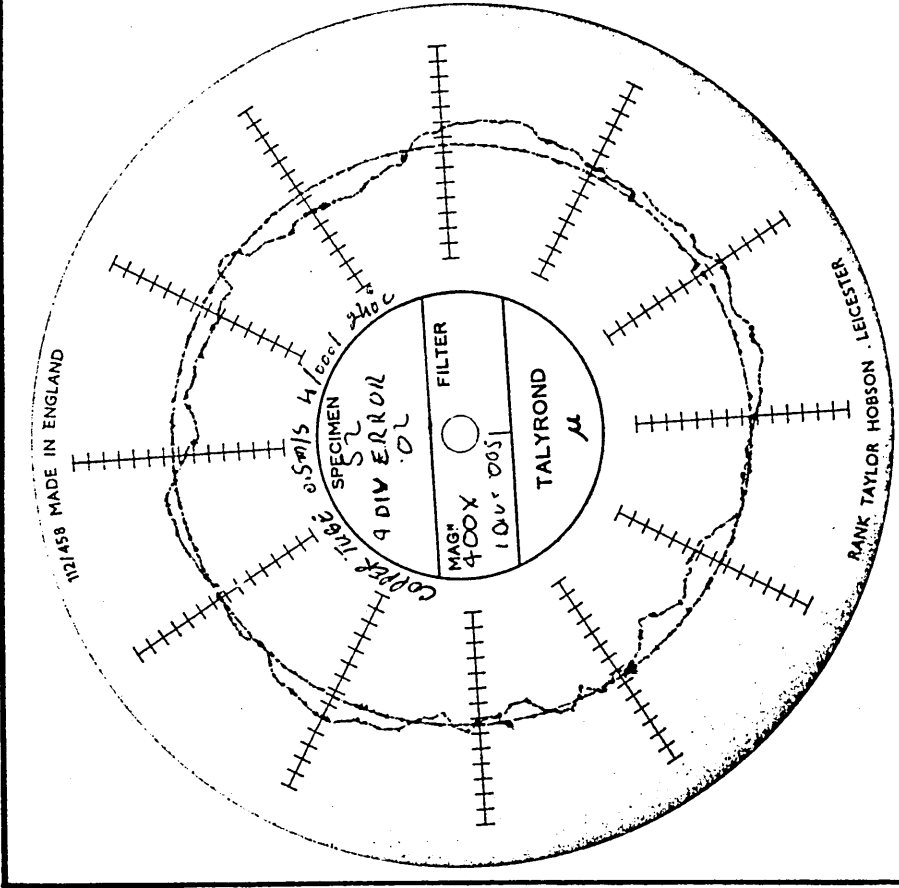


FIG 121 - ROUNDNESS TEST ON COPPER TUBE DRAWN AT 0.5 m/s WITH POLYSTYRENE, 240°C 3.03% REDUCTION IN DIAMETER

1 DIV = 0.005 mm

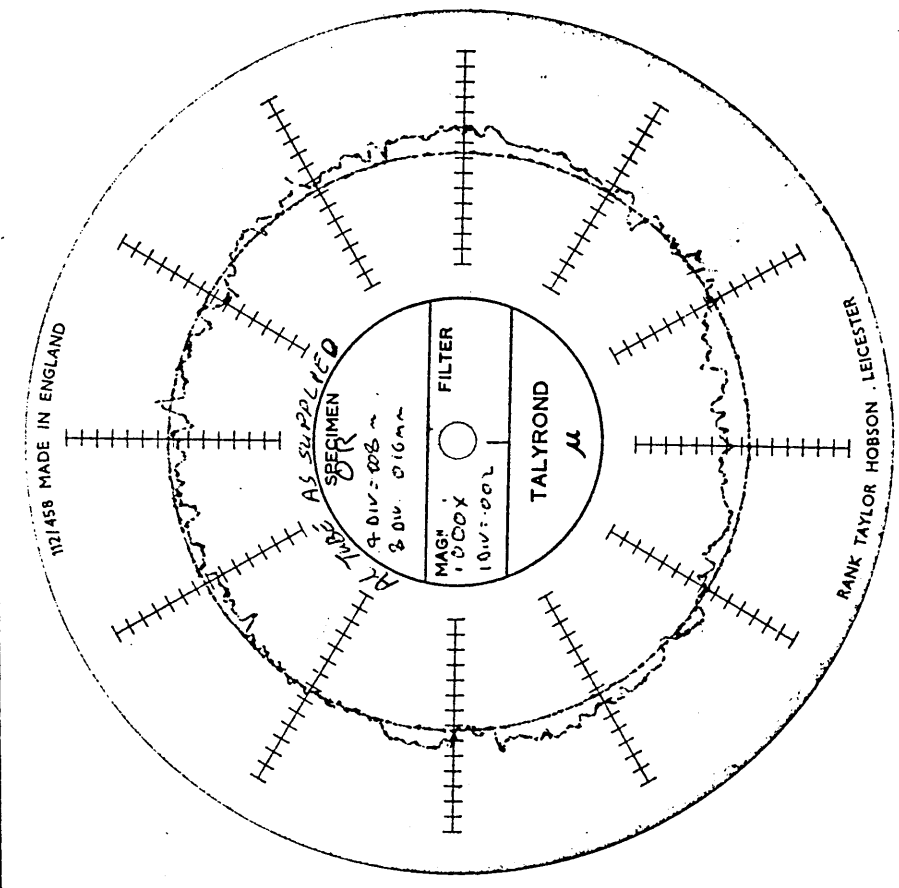


FIG 122 - ROUNDNESS TEST ON RECEIVED ALUMINIUM TUBE

1 DIV = 0.002 mm

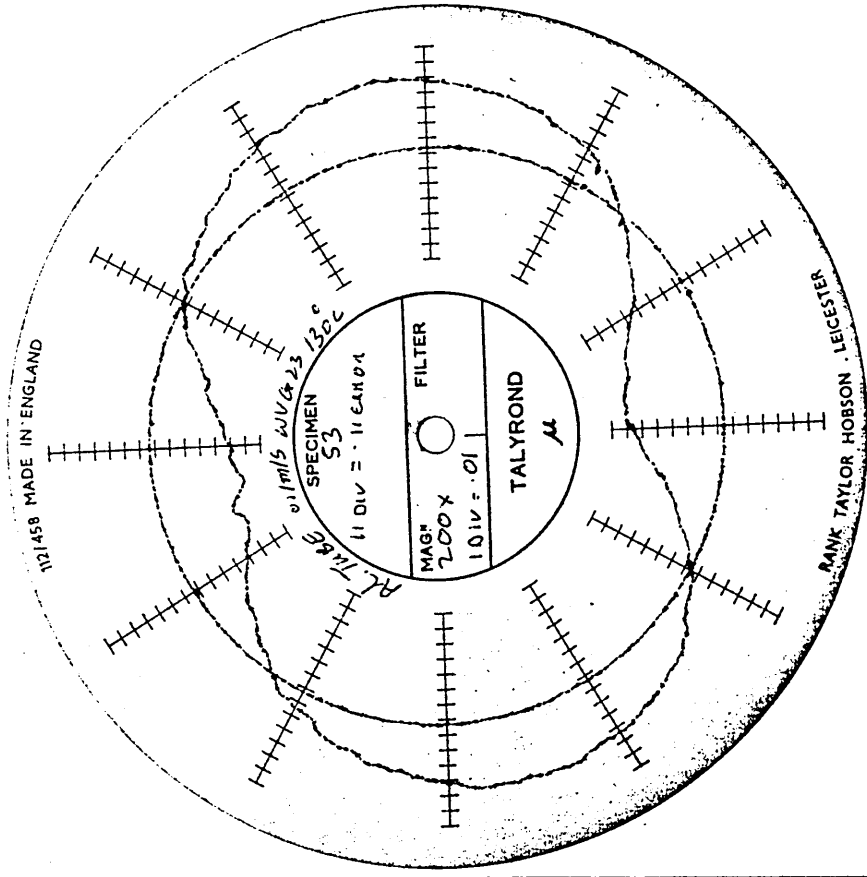


FIG 123 - ROUNDNESS TEST ON ALUMINIUM TUBE DRAWN
AT 0.1 m/s WITH WVG23, 130°C
5.4% REDUCTION IN DIAMETER

1 DIV = 0.01 mm

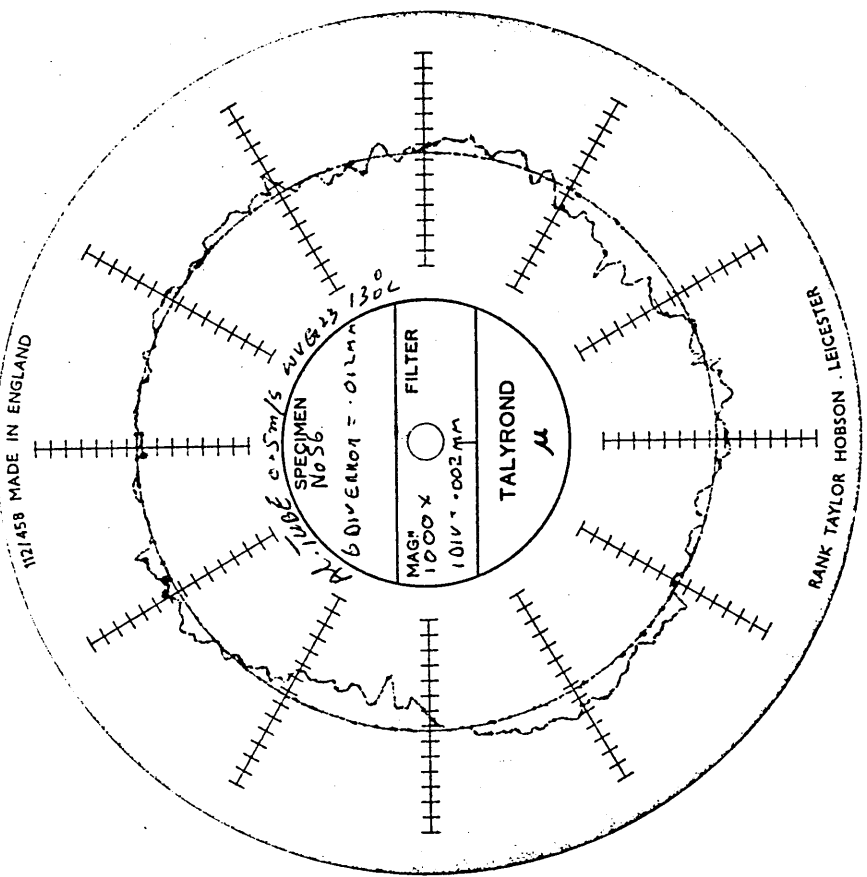
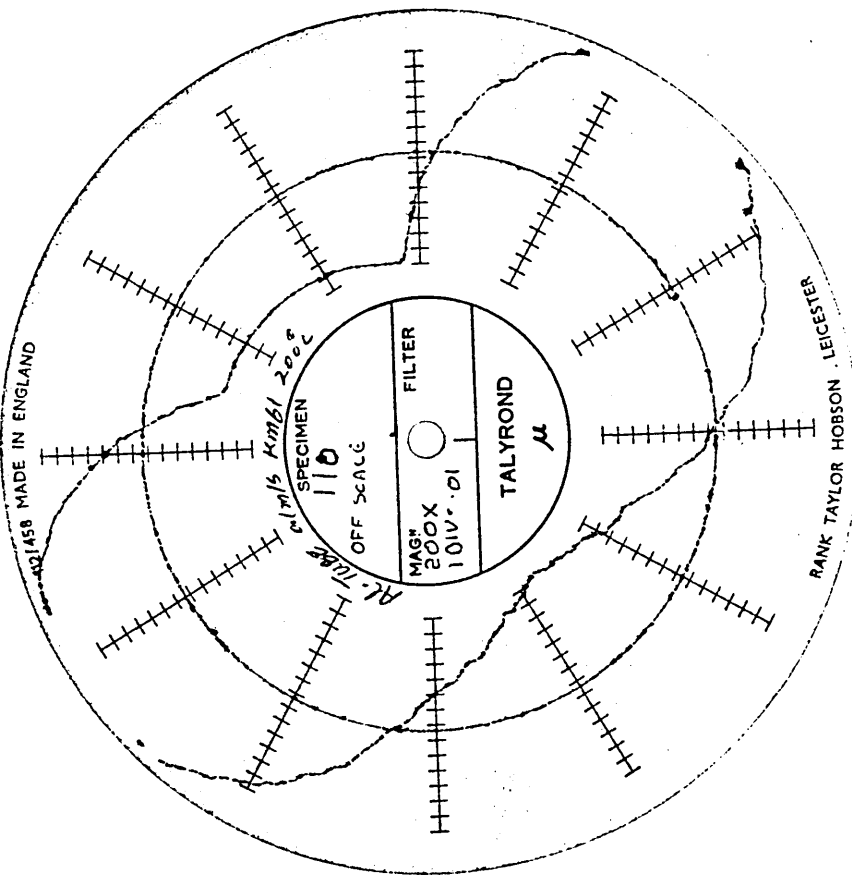


FIG 124 - ROUNDNESS TEST ON ALUMINIUM TUBE DRAWN
AT 0.5 m/s WITH WVG23, 130°C
1.8% REDUCTION IN DIAMETER

1 DIV = 0.002 mm



**FIG 125 - ROUNDNESS TEST ON ALUMINIUM TUBE DRAWN
AT 0.1 m/s WITH KM61, 200°C
4.5% REDUCTION IN DIAMETER**

1 DIV = 0.01 mm

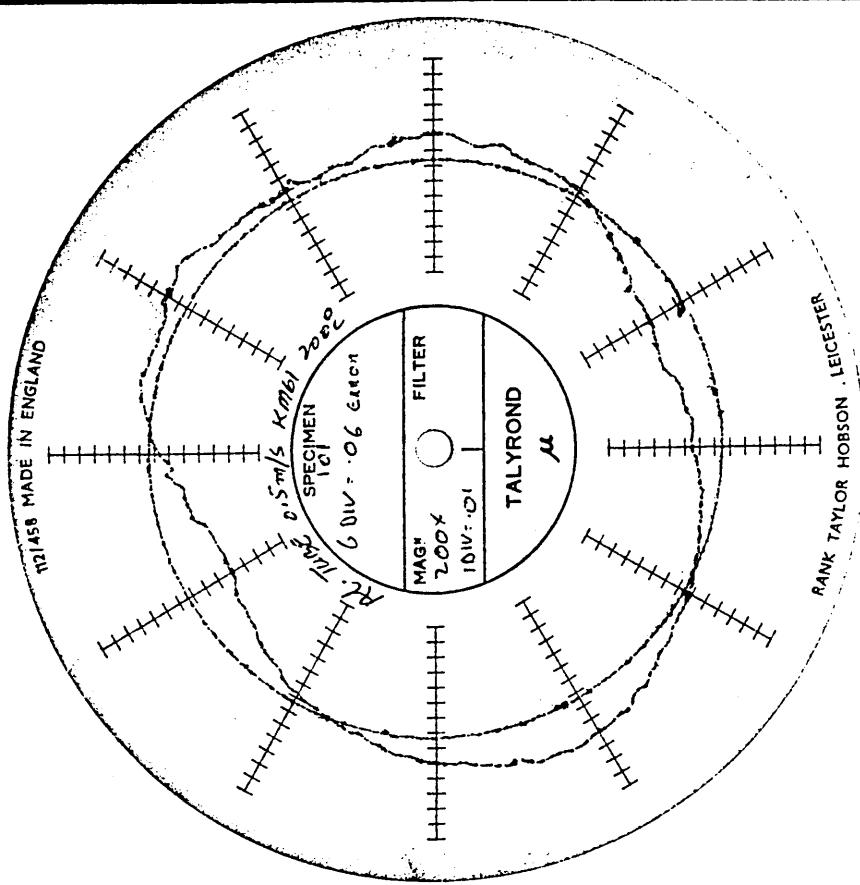


**FIG 126 - ROUNDNESS TEST ON ALUMINIUM TUBE DRAWN
AT 0.5 m/s WITH KM61, 200°C
1.6% REDUCTION IN DIAMETER**

1 DIV = 0.01 mm

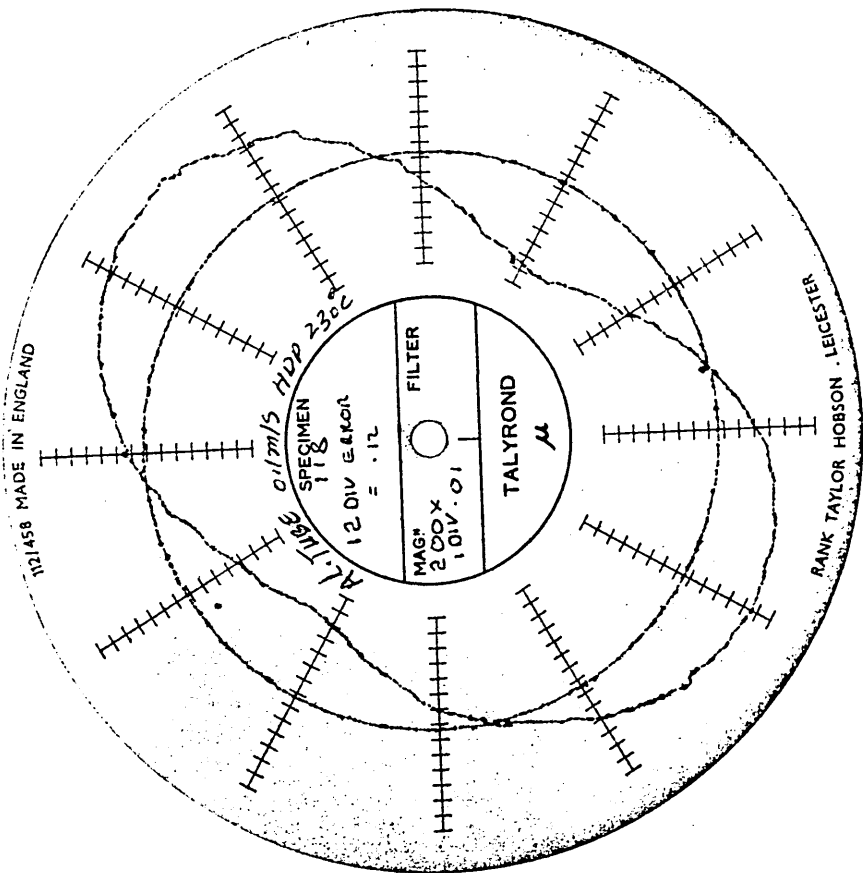


**FIG 127 - ROUNDNESS TEST ON ALUMINIUM TUBE DRAWN
AT 0.1 m/s WITH RIGIDEX, 230°C
3.4% REDUCTION IN DIAMETER**

1 DIV = 0.01 mm

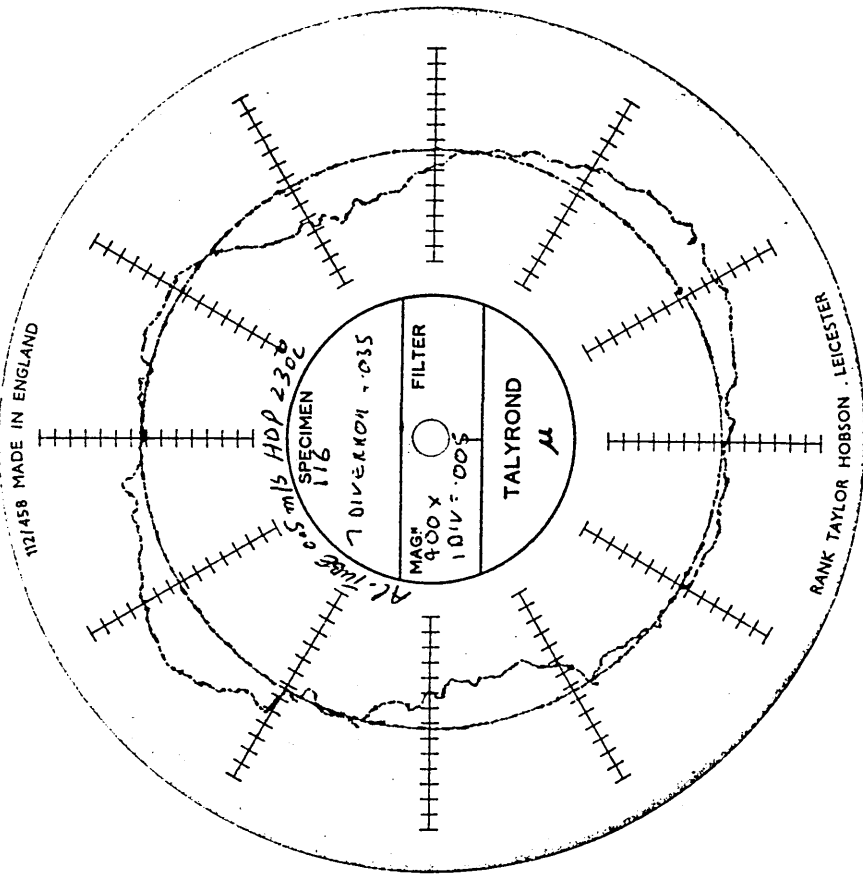


**FIG 128 - ROUNDNESS TEST ON ALUMINIUM TUBE DRAWN
AT 0.5 m/s WITH RIGIDEX, 230°C
2.2% REDUCTION IN DIAMETER**

1 DIV = 0.005 mm

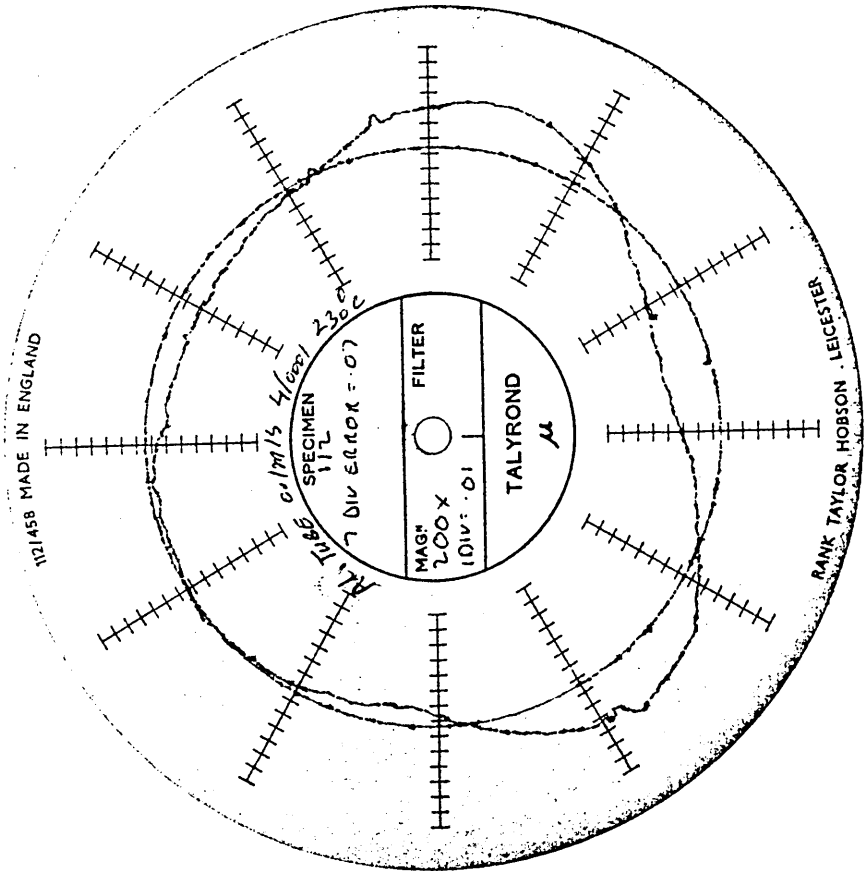


FIG 129 - ROUNDNESS TEST ON ALUMINIUM TUBE DRAWN
 AT 0.1 m/s WITH POLYSTYRENE, 230°C
 6.0% REDUCTION IN DIAMETER

1 DIV = 0.01 mm

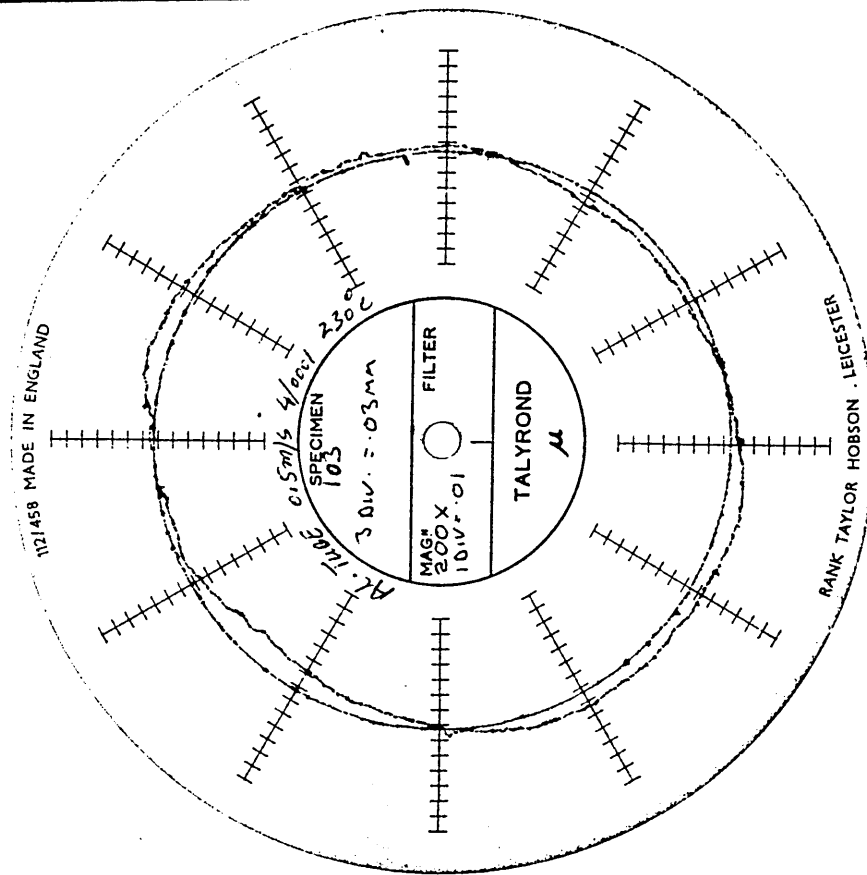
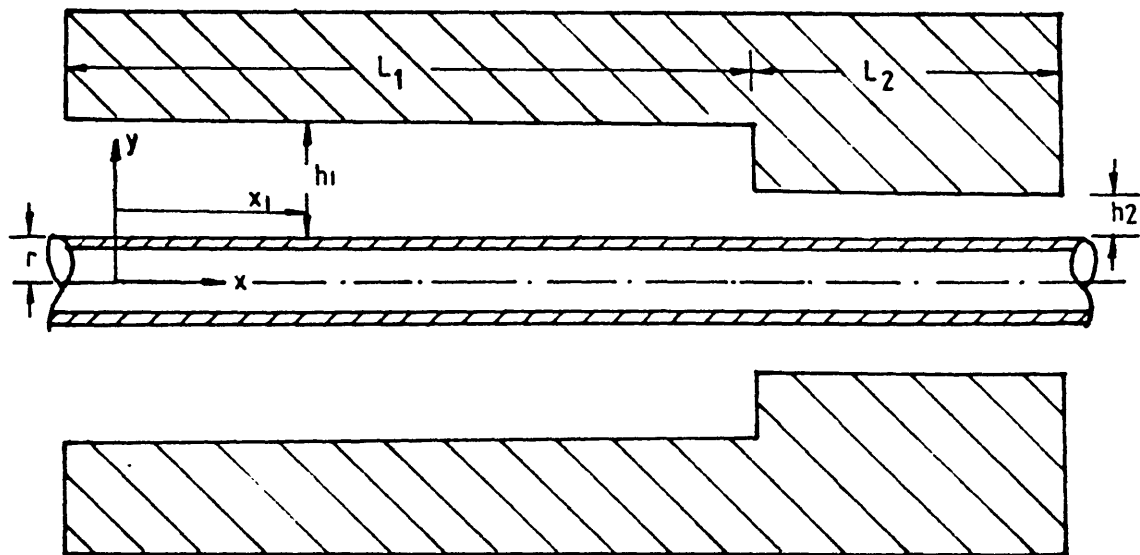
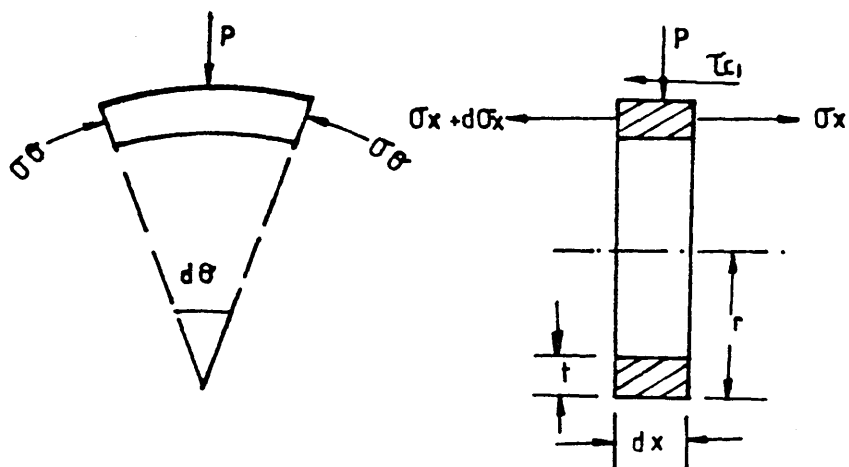


FIG 130 - ROUNDNESS TEST ON ALUMINIUM TUBE DRAWN
 AT 0.5 m/s WITH POLYSTYRENE, 230°C
 2.0% REDUCTION IN DIAMETER

1 DIV = 0.01 mm



(a)



(b)

FIG 131(a) - GEOMETRICAL CONFIGURATION OF THE STEPPED BORE REDUCTION UNIT AND THE TUBE

(b) - STRESSES ACTING ON A SMALL ELEMENT OF THE TUBE

5.1 Introduction

In order to enhance the understanding of the mechanics of the process of die-less tube sinking it is important to develop a suitable mathematical model. As a first step, such a model has been developed based on the assumption that the pressure medium demonstrates ideal Newtonian characteristics. The model presented in this chapter shows clearly as to the mechanics of generating plasto-hydrodynamic pressure which in turn gives rise to very high hoop stress and also the drag force. Combination of these hoop stress and drag force (axial stress) is clearly seen to induce plastic yielding and indeed permanent deformation.

The analysis is done in three different modes, (a) assuming a straight deformation profile, (b) assuming a curved deformation profile and finally (c) applying finite-difference numerical technique in which the deformation profile is determined theoretically and does not require to be prescribed.

5.2 Analysis

The geometrical configuration of the die-less reduction unit and the tube during drawing is shown in Fig 131, the die-less reduction unit (DRU) being filled with the pressure medium. The present analysis requires the following assumptions to be made:

- (a) The fluid pressure medium possesses Newtonian characteristics.
- (b) The flow of the fluid pressure medium is laminar and axial.
- (c) The thickness of the fluid layer is small compared to the base size of the DRU.

(d) The pressure in the fluid medium is uniform in the thickness direction at any point along the length of the DRU.

(i) Analysis under no deformation condition

As the thickness of the pressure medium layer contained in the DRU is small compared with the dimensions of the DRU, the analysis of flow is carried out in rectangular rather than in cylindrical co-ordinates.

In the first part of the unit, the relationship between the pressure and shear stress gradient between the outer surface of the tube and the inner surface of the DRU may be expressed as,

$$\left(\frac{\partial P}{\partial x}\right)_1 = \left(\frac{\partial \tau}{\partial y}\right)_1 \quad (5.1)$$

The relationship between the shear stress and the rate of shear for the Newtonian fluid is given by;

$$\tau_1 = \mu \left(\frac{\partial u}{\partial y}\right)_1 \quad (5.2)$$

where μ is the viscosity and u is the fluid velocity at a distance y from the surface of the tube.

Integrating equation (5.1) w.r.t. y and noting that $\left(\frac{\partial P}{\partial x}\right)_1$ is invariant with y , we have,

$$\tau_1 = P'_1 y + \tau_{c1} \quad (5.3)$$

where $P' = \left(\frac{\partial P}{\partial x}\right)_1$ and τ_{c1} is the shear stress on the tube surface at $y = 0$.

Integrating the equation obtained after combining equations (5.2) and (5.3)

$$\mu u_1 = \frac{1}{2} P'_1 y^2 + \tau_{c1} y + \text{constant} \quad (5.4)$$

Applying the boundary condition that at $y = 0$ (at the surface of the tube) $u_1 = v_1$ in equation (5.4) and rearranging we get,

$$U_1 = \frac{P'_1 y^2}{2\mu} + \frac{\tau_{c1} y}{\mu} + v_1 \quad (5.5)$$

Applying the boundary condition that at $y = h_1$ (at the surface of the unit) $u_1 = 0$ in equation (5.5) and rearranging we have,

$$\tau_{c1} = -\frac{1}{2}P'_1 h_1 - \frac{v_1 \mu}{h_1} \quad (5.6)$$

The flow of the pressure medium in the axial direction within the gap before the step may be given by,

$$Q_1 = \int_0^{h_1} U_1 dy$$

which upon substituting for U_1 from equation (5.5) and integrating, becomes

$$Q_1 = \frac{P'_1 h_1^3}{6\mu} + \frac{\tau_{c1} h_1^2}{2\mu} + v_1 h_1$$

and substituting for τ_{c1} from equation (5.6) into the above equation we get

$$Q_1 = -\frac{h_1^3}{12\mu} \left(\frac{\partial P}{\partial x} \right)_1 + \frac{v_1 h_1}{2} \quad (5.7)$$

The continuity of fluid flow dictates that

$$\left(\frac{\partial Q}{\partial x} \right) + \left(\frac{\partial Q}{\partial y} \right) + \left(\frac{\partial Q}{\partial z} \right) = 0$$

but

$$\frac{\partial Q}{\partial y} = \frac{\partial Q}{\partial z} = 0$$

hence

$$\frac{\partial Q}{\partial x} = 0$$

Therefore, for given h_1, h_2, μ and v_1

$\frac{\partial P}{\partial x}$ in equation (5.7) must be constant.

Let the pressure at the step be P_m which is the maximum pressure under no deformation condition. Thus $\left(\frac{\partial P}{\partial x}\right)_1 = \frac{P_m}{L_1}$. The expression for Q_2 in the second part of the unit can be derived in the same manner as above. Hence

$$Q_2 = \frac{1}{12\mu} \left(\frac{\partial P}{\partial x}\right)_2 h_2^3 + \frac{v_2 h_2}{2} \quad (5.8)$$

and following the above reasoning $\left(\frac{\partial P}{\partial x}\right)_2 = -\frac{P_m}{L_2}$. For continuity of flow we have, $Q_1 = Q_2$. Equating the expression for Q_1 and Q_2 and noting that $\left(\frac{\partial P}{\partial x}\right)_1 = \frac{P_m}{L_1}$, $\left(\frac{\partial P}{\partial x}\right)_2 = -\frac{P_m}{L_2}$, and $v_1 = v_2$

we have after simplification,

$$P_m = 6\mu v (h_1 - h_2) / \left(\frac{h_1^3}{L_1} + \frac{h_2^3}{L_2} \right) \quad (5.9)$$

Criterion for Plastic Deformation

Considering the axial force equilibrium of an element of the tube, within the die-less reduction unit before any deformation commences (see Fig131(b)) we have,

$$d\sigma_x \times 2\pi r t - 2\pi r \cdot dx \cdot \tau_{c1} = 0$$

so that

$$d\sigma_x = \frac{\tau_{c1} dx}{t}$$

integration of the above equation gives,

$$\sigma_x = \frac{\tau_{c1} x}{t} + C$$

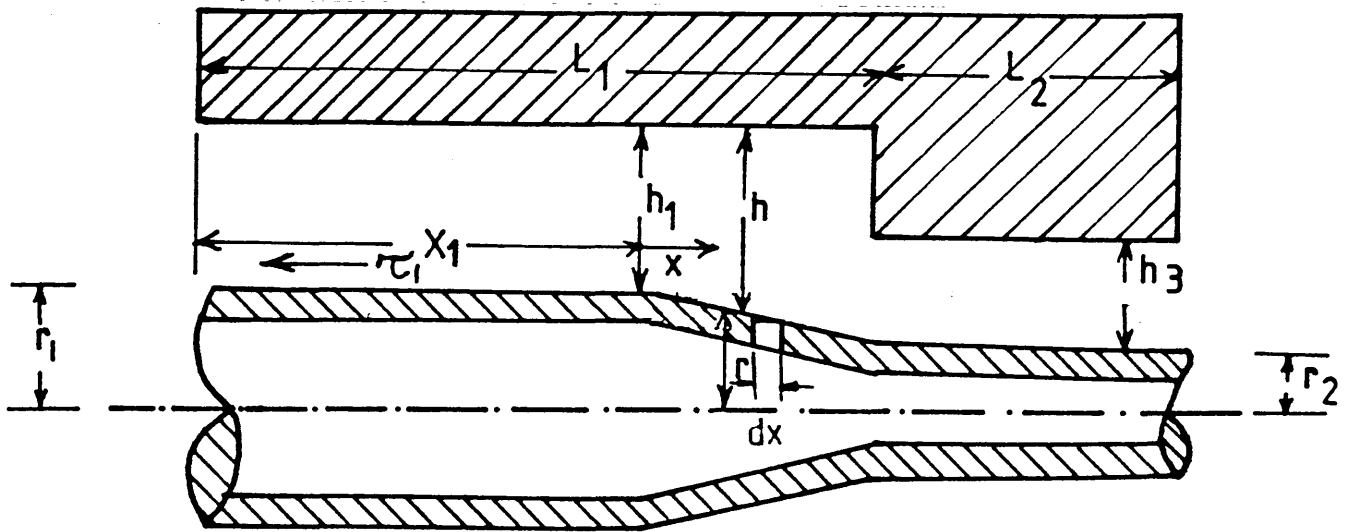
$$\text{at } x = 0, \sigma_x = 0, \text{ hence } C = 0 \text{ and } \sigma_x = \frac{\tau_{c1} x}{t} \quad (5.10)$$

The radial force equilibrium gives

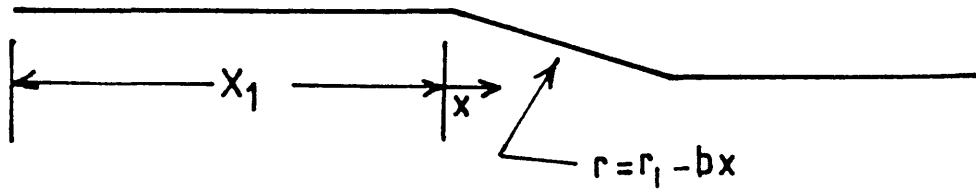
$$P \cdot r \cdot d\theta \times dx = 2 \sigma_{\theta} \cdot t \cdot dx \cdot \sin \frac{d\theta}{2}$$

which for small angle, $d\theta$, becomes

$$\sigma_{\theta} = \frac{P r}{t}$$



(a)



(b)

FIG 132(a) - SHOWING THEORETICALLY ASSUMED DEFORMATION MODE WITHIN THE DRU

(b) - LINEAR DEFORMATION PROFILE

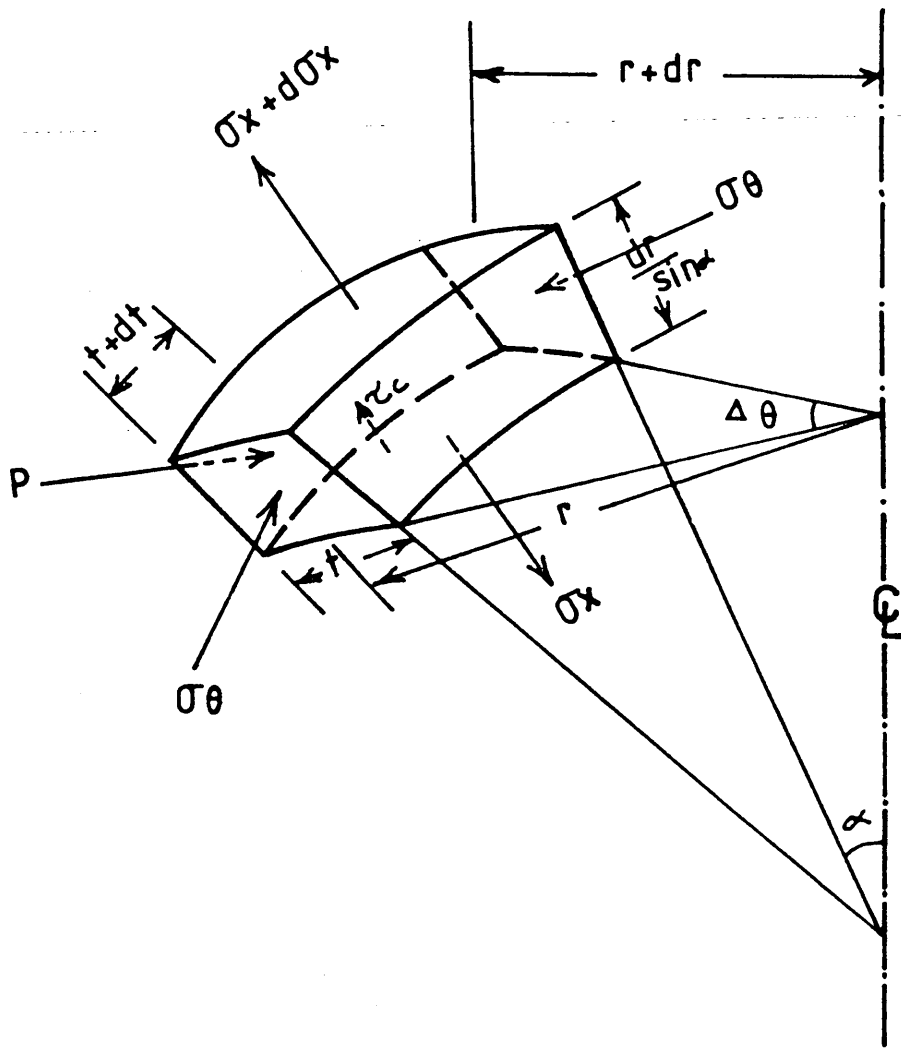


FIG 132(c) - STRESSES ACTING ON A SMALL ELEMENT OF THE TUBE

Where σ_θ is the hoop stress and p is the pressure and

$$\sigma_x + p = \sigma_\theta$$

For plastic deformation to commence the yield criterion according to Tresca gives

$$\sigma_1 - \sigma_3 = \sigma_0$$

where σ_0 is the initial yield stress of the tube material.

$$\text{But } \sigma_1 = \sigma_x \text{ and } \sigma_3 = -\sigma_\theta, \text{ so that } \sigma_x + \sigma_\theta = \sigma_0 \quad (5.11)$$

Let x_1 be the distance from the entry to the unit where plastic deformation commences, so that

$$\sigma_x = \frac{\tau c_1 x_1}{t} \text{ and } \sigma_\theta = \frac{Pr}{t} = \frac{Pm x_1 r_1}{L_1 t}, \text{ since } P = \frac{Pm x_1}{L_1}$$

Equation (5.11) thus becomes

$$\frac{\tau c_1 x_1}{t_1} + \frac{Pm x_1 r_1}{L_1 t} = \sigma_0$$

so that

$$x_1 = \sigma_0 / \left(\frac{\tau c_1}{t} + \frac{Pm r_1}{L_1 t} \right) \quad (5.12)$$

Once yielding occurs, plastic deformation will continue as long as the yield criterion

$$\sigma_x + \sigma_\theta = \sigma = \sigma_0 + k\sigma \epsilon^n$$

is satisfied for a strain hardening material of the tube.

(ii) Analyses after Deformation Commences

5.2.1 Linear Deformation Profile

Let the deformation within the DRU take place in a linear profile as shown in Fig 132(b).

The continuity equation for the flow of the pressure medium leads to

$$\frac{\partial}{\partial x} Qx = 0$$

and from equation (5.7) we get

$$\frac{\partial}{\partial x} \left\{ -\frac{1}{12\mu} \left(\frac{\partial P}{\partial x} \right) h^3 + \frac{vh}{2} \right\} = 0$$

or

$$\frac{\partial}{\partial x} (h^3 \frac{\partial P}{\partial x}) = \frac{\partial}{\partial x} (6\mu v h) \quad (5.1A)$$

where h is the gap thickness at any point within the deformation zone and is given by $h = h_1 + bx$.

Now, for a given velocity v and viscosity μ of the pressure medium equation (5.1A) becomes

$$\frac{\partial}{\partial x} (h^3 \frac{\partial P}{\partial x}) = 6\mu v \frac{\partial h}{\partial x} = 6\mu v b$$

$$\text{since } \frac{\partial h}{\partial x} = b$$

Integration of the above equation gives

$$h^3 (\frac{\partial P}{\partial x}) = 6\mu v b x + C_2 \quad (5.2A)$$

where C_2 is the constant of integration. Noting that $h=h_1+bx$

and applying the boundary condition that

$$\frac{\partial P}{\partial x} = \frac{P_m}{L_1} \text{ at } x = 0,$$

the constant C_2 is given by

$$C_2 = h_1^3 \frac{P_m}{L_1}$$

Substituting for h and C_2 equation (5.2A) becomes

$$\frac{\partial P}{\partial x} = 6\mu v \frac{bx}{(h_1 + bx)^3} + \frac{P_m}{L_1} \frac{h_1^3}{(h_1 + bx)^3} \quad (5.3A)$$

Integrating equation (5.3A) we obtain

$$P = 6\mu v \left\{ -\frac{1}{b(h_1 + bx)} + \frac{h_1}{2b(h_1 + bx)^2} \right\} - \left(\frac{P_m}{L_1} \right) \frac{h_1^3}{2b(h_1 + bx)^2} + C_3 \quad (5.4A)$$

Applying the boundary conditions that at a point x_1 from

the entry, where plastic deformation starts, $x = 0$

and the pressure is given by

$$\frac{P}{x_1} = \frac{P_m}{L_1}, \text{ or } P = \left(\frac{P_m x_1}{L_1} \right)$$

Thus,

$$\frac{P_m x_1}{L_1} = 6\mu v \left\{ -\frac{1}{bh_1} + \frac{h_1}{2bh_1^2} \right\} - \left(\frac{P_m}{L_1} \right) \frac{h_1^3}{2bh_1^2} + C_3$$

so that,

$$C_3 = \frac{P_m x_1}{L_1} + \frac{3\mu v}{bh_1} + \frac{P_m h_1}{L_1 2b}$$

substituting for C_3 in equation (5.4A) we get

$$P = \frac{6\mu v}{b} \left\{ \frac{h_1}{2(h_1 + bx)^2} - \frac{1}{(h_1 + bx)} + \frac{1}{2h_1} \right\} - \frac{Pm}{L_1} \left\{ \frac{h_1^3}{2b(h_1 + bx)^2} - \frac{h}{2b} - x_1 \right. \quad (5.5A)$$

Equation (5.5) gives the pressure distribution along the length $(L_1 - x_1)$ within the DRU and up to the step. The expression for the shear stress on the surface of the deformed tube may be given by equation (5.6) by simply replacing τ_c for τ_{c1} , h for h_1 and $\frac{\partial P}{\partial x}$ from equation (5.3A). Thus,

$$\tau_c = -\frac{1}{2}(h_1 + bx) \left\{ 6\mu v \frac{bx}{(h_1 + bx)^3} + \frac{Pm}{L_1} \frac{h_1^3}{(h_1 + bx)^3} \right\} - \frac{\mu v}{(h_1 + bx)} \quad (5.6A)$$

Referring to Figure 132(c) let P be the hydrodynamic pressure normal to the element, σ_x the tensile stress and σ_θ the hoop stress. Also let t be the wall thickness at radius r , τ_c the shear stress and α the semi-angle of the effective deformation profile. Let us consider the stresses acting on a small element of the wall, bounded by meridian planes inclined at angle $\Delta\theta$ and resolve the forces perpendicular to the element.

For equilibrium condition, the sum of these component forces normal to the surface must be zero.

Thus,

$$P(r\Delta\theta \frac{dr}{\sin \alpha}) - \sigma_\theta \left(t \frac{dr}{\sin \alpha} \right) \Delta\theta \cos \alpha = 0$$

which upon simplification becomes $Pr = \sigma_\theta t \cos \alpha$

or

$$P = \sigma_\theta \frac{t}{r} \cos \alpha \quad \left(\text{where } \cos \alpha = \frac{1}{\sqrt{1 + b^2}} \right) \quad (5.7A)$$

Hence P is very small in comparison to σ_θ where $\frac{t}{r}$ is small. The stresses in this deformation process are therefore such that $\sigma_\theta \gg P \gg \sigma_x$.

Hoop stress in the deformation zone can be obtained by substituting P from equation (5.5A) into equation (5.7A).

Thus,

$$\sigma_{\theta} = \frac{r(1+b^2)^{\frac{1}{2}}}{t} \left[\frac{6\mu v}{b} \left\{ \frac{h_1}{2(h_1+bx)^2} - \frac{1}{(h_1+bx)} + \frac{1}{2h_1} \right\} - \frac{Pm}{L_1} \left(\frac{h_1^3}{2b(h_1+bx)^2} - \frac{h_1}{2b} - x_1 \right) \right] \quad (5.8A)$$

Resolving forces parallel to the effective deformation profile, we obtain

$$(\sigma_x + d\sigma_x)(r+dr)\Delta\theta(t+dt) - \sigma_x t r \Delta\theta + \sigma_{\theta} \left(t \frac{dr}{\sin \alpha} \right) \Delta\theta \sin \alpha + \tau_c \left(r \Delta\theta \frac{dr}{\sin \alpha} \right) = 0$$

which after simplification and neglecting second-order smaller quantities becomes

$$\frac{d}{dr}(\sigma_x r) + \sigma_{\theta} + \tau_c \frac{r}{t \sin \alpha} = 0 \quad (5.9A)$$

where τ_c is the shear stress of the pressure medium on the tube surface, t is the constant wall thickness, α is the constant angle such that $\sin \alpha = \frac{b}{\sqrt{1+b^2}}$.

Equation (5.9A) may thus be written as

$$r \frac{d\sigma_x}{dr} + \sigma_x + \sigma_{\theta} + \tau_c \frac{r}{t \sin \alpha} = 0 \quad (5.10A)$$

According to Tresca yield criterion, $\sigma_1 - \sigma_3 = y$ (5.11A)

but $\sigma_1 = \sigma_x$ and $\sigma_3 = -\sigma_{\theta}$

Therefore, equation (5.11A) becomes

$$\sigma_x + \sigma_{\theta} = y \quad (5.12A)$$

Substituting for $\sigma_x + \sigma_{\theta}$ in equation (5.10A) we obtain

$$r \frac{d\sigma_x}{dr} + y + \tau_c \frac{r}{t \sin \alpha} = 0$$

or

$$d\sigma_x = -y \frac{dr}{r} - \tau_c \frac{dr}{t \sin \alpha} \quad (5.13A)$$

Let the material property be represented by

$$y = y_0 + k\epsilon^n \quad (5.14A)$$

where, y is the flow stress of the material, k_0 is the strain hardening constant, $\epsilon = \ln \frac{r_1}{r}$ and y_0 is the initial yield stress of the material.

Substituting the value of y from equation (5.14A) into (5.13A) we obtain

$$d\sigma_x = -y_0 \frac{dr}{r} - k_0 \left(\ln \frac{r_1}{r} \right)^n \frac{dr}{r} - \frac{\tau_c}{t \sin \alpha} dr$$

Integration of the above equation gives,

$$\sigma_x = -y_0 \ln r + \frac{k_0}{n+1} \left(\ln \frac{r_1}{r} \right)^{n+1} - \frac{\tau_c r}{t \sin \alpha} + c_4 \quad (5.15A)$$

where c_4 is the constant of integration.

Applying the boundary conditions that when $r = r_1$ and $x = 0$, $\sigma_x = \sigma_{x_1}$, the axial stress at yielding point. Putting these values in equation (5.15A) gives

$$c_4 = \sigma_{x_1} + y_0 \ln r_1 + \frac{\tau_c r_1}{t \sin \alpha}$$

Substituting for c_4 in equation (5.15A)

we obtain,

$$\sigma_x = y_0 \ln \frac{r_1}{r} + \frac{k_0}{n+1} \left(\ln \frac{r_1}{r} \right)^{n+1} + \frac{\tau_c}{t \sin \alpha} (r_1 - r) + \sigma_{x_1}$$

By substituting the expression for σ_{x_1} from equation (5.10), x_1 from (5.12) and τ_c from (5.6A), the axial stress in the deformation zone can thus be expressed as

$$\begin{aligned} \sigma_x = & y_0 \ln \frac{r_1}{r} + \frac{k_0}{n+1} \left(\ln \frac{r_1}{r} \right)^{n+1} - \frac{\sqrt{(1+b^2)} (r_1 - r)}{bt} \left(3\mu v \frac{bx}{(h_1 + bx)^2} \right. \\ & \left. + \frac{P_m}{2L_1} \frac{h_1^3}{(h_1 + bx)^2} + \frac{\mu v}{h_1 + bx} \right) - \frac{y_0}{\left(\frac{\tau_c L_1}{t} + \frac{P_m r_1}{t L_1} \right)} \left(\frac{h_1}{2t} \frac{P_m}{L_1} + \frac{\mu v}{t h_1} \right) \end{aligned} \quad (5.16A)$$

where, $r = r_1 - bx$, τ_c is given by equation (5.10) and P_m by equation (5.9).

Once plastic yielding commences further permanent deformation will continue to take place in the unit as long as the yield criterion $\sigma_x + \sigma_\theta = y$ is satisfied at any point within the unit, distance x from the point x_1 . Substituting the expression of y from equation (5.14A) we get

$$\sigma_x + \sigma_\theta = y_0 + k_0 \left(\ln \frac{r_1}{r} \right)^n$$

which after substitution for σ_x , σ_θ and P , and assuming that the deformation stops at the step where $x = (L_1 - x_1)$ and $r = r_1 - b(L_1 - x_1)$ may be written as

$$\begin{aligned} & y_0 \ln \frac{r_1}{r} + \frac{k_0}{n+1} \left(\ln \frac{r_1}{r} \right)^{n+1} - \frac{(r_1 - r)(1 + b^2)^{\frac{1}{2}}}{bt} \left(3\mu v \frac{bx}{(h_1 + bx)^2} \right. \\ & + \frac{Pm h_1^3}{2L_1 (h_1 + bx)^2} + \frac{\mu v}{h_1 + bx} - \frac{y_0}{\left(\frac{\tau c_1}{t} + \frac{Pmr_1}{tL_1} \right)} \left(\frac{h_1}{2t} \frac{Pm}{L_1} + \frac{\mu v}{th_1} + \frac{r(1 + b^2)^{\frac{1}{2}}}{t} \right. \\ & \left. \left[6\mu v \left\{ -\frac{1}{b(h_1 + bx)} + \frac{h_1}{2b(h_1 + bx)^2} \right\} - \frac{Pm}{L_1} \frac{h_1^3}{2b(h_1 + bx)^2} \right] \right. \\ & \left. + \frac{Pm}{L_1} \left(\frac{y_0}{\left(\frac{\tau c_1}{t} + \frac{Pmr_1}{tL_1} \right)} + \frac{h_1}{2b} \right) + \frac{3\mu v}{bh_1} \right] - y_0 - k_0 \left(\ln \frac{r_1}{r} \right)^n = 0 \quad (5.17A) \end{aligned}$$

In equation (5.17A) only the parameter 'b' is unknown.

For a given drawing speed the value of 'b' may be determined using iteration process to satisfy equation (5.17A).

Once the value of 'b' is established the deformation profile is obtained and the reduction in diameter at any point for $x_1 \leq x \leq L_1$ is given by $\Delta D = D_1 - 2bx$

and the total percentage reduction in diameter is given by

$$PRD = 100 \times \{2b(L_1 - x_1)\}/D_1 \quad (5.18A)$$

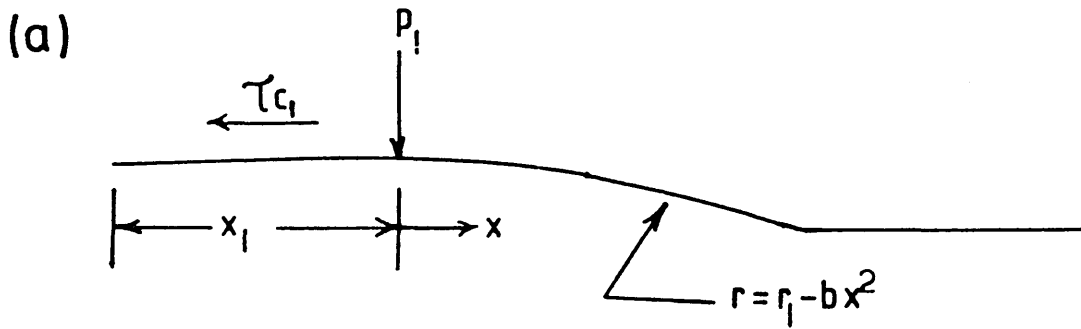
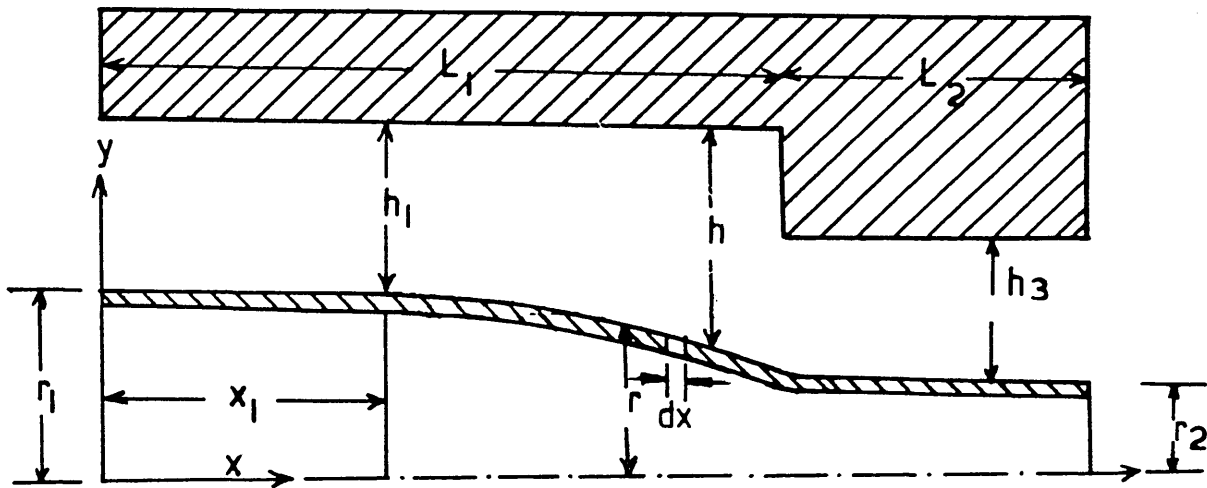
where D_1 is the undeformed diameter of the tube. The

drawing stress ' σ_d ' at the exit end of the DRU is then

$$\text{given by } \sigma_d = \sigma_{x_s} + \sigma_{x_2} \quad (5.19A)$$

where σ_{x_s} is the axial stress at the step and σ_{x_2} is

$$\text{given by } \sigma_{x_2} = \frac{\tau c_2 L_2}{t}$$



(b)

FIG 133(a) - SHOWING THEORETICALLY ASSUMED DEFORMATION MODE WITHIN THE DRU

(b) - CURVED DEFORMATION PROFILE

The shear stress in the small bore section of the unit may be expressed as

$$\tau_{c2} = \frac{h_3 P_s}{2L_2} - \frac{\mu v}{h_3}$$

and

$$h_3 = h_2 + b(L_1 - x_1) \quad (5.20A)$$

where h_3 is the final gap.

5.2.2

Curved Deformation Profile

Let the deformation within the DRU take place in a curved profile as shown in Fig 133(b).

Once again, the continuity equation for the flow can be written as,

$$\frac{\partial}{\partial x} Q_x + \frac{\partial}{\partial y} Q_y + \frac{\partial}{\partial z} Q_z = 0$$

since

$$\frac{\partial}{\partial y} Q = \frac{\partial}{\partial z} Q_z = 0$$

therefore

$$\frac{\partial}{\partial x} Q_x = 0$$

and from equation (5.7) we get

$$\frac{\partial}{\partial x} \left\{ -\frac{1}{12\mu} \left(\frac{\partial P}{\partial x} \right) h^3 + \frac{vh}{2} \right\} = 0 \quad (5.1B)$$

$$\text{where } h = h_1 + bx^2$$

Now, for a given velocity v and polymer viscosity μ , equation (5.1B) becomes

$$\frac{\partial}{\partial x} \left(h^3 \frac{\partial P}{\partial x} \right) = 6\mu v \frac{\partial h}{\partial x}$$

but

$$\frac{\partial h}{\partial x} = 2bx$$

hence

$$\frac{\partial}{\partial x} \left(h^3 \frac{\partial P}{\partial x} \right) = 12\mu v bx$$

which upon integration becomes

$$h^3 \left(\frac{\partial P}{\partial x} \right) = 6\mu v bx^2 + c_1 \quad (5.2B)$$

where c_1 is the constant of integration. Noting that $h = h_1 + bx^2$ and applying the boundary condition that $\frac{\partial P}{\partial x} = \frac{P_m}{L_1}$ at $x = 0$ the constant c_1 is given by

$$c_1 = h_1^3 \frac{P_m}{L_1}$$

where P_m is the maximum pressure at the end of L_1 , under no deformation condition. Substituting for h and c_1 equation (5.2B) becomes

$$\frac{\partial P}{\partial x} = 6\mu v \frac{bx^2}{(h_1 + bx^2)^3} + \frac{P_m}{L_1} \frac{h_1^3}{(h_1 + bx^2)^3} \quad (5.3B)$$

Equation (5.3B) may be integrated by substituting $a^2 = \frac{h_1}{b}$, so that the expression for the pressure becomes

$$P = 6\mu v \left\{ \frac{1}{8a^3b^2} \tan^{-1} \frac{x}{a} + \frac{x^3 - a^2x}{8a^2b^2(a^2 + x^2)^2} \right\} + \frac{P_m}{L_1} \frac{h_1^3}{b^3} \left\{ \frac{3}{8a^5} \tan^{-1} \frac{x}{a} + \frac{5a^2x + 3x^3}{8a^4(a^2 + x^2)^2} \right\} + c_2 \quad (5.4B)$$

Applying the boundary condition that at a point x_1 from the entry, where the plastic deformation starts, $x = 0$ and the pressure is given by

$$P = \left(\frac{P_m x_1}{L_1} \right)$$

so that $\frac{P_m x_1}{L_1} = c_2$

Substituting for c_2 equation (5.4B) becomes

$$P = 6\mu v \left\{ \frac{1}{8a^3b^2} \tan^{-1} \frac{x}{a} + \frac{x^3 - a^2x}{8a^2b^2(a^2 + x^2)^2} \right\} + \frac{P_m}{L_1} \left\{ x_1 + \frac{3}{8} a \tan^{-1} \frac{x}{a} + \frac{5a^4 + 3a^2x^3}{8(a^2 + x^2)^2} \right\} \quad (5.5B)$$

Equation (5.5B) gives the pressure distribution along the length $(L_1 - x_1)$ within the DRU and up to the step. The expression for the shear stress on the surface of the deformed tube may be given by equation (5.6), simply by replacing τ_c for τ_{c1} , h for h_1 and $\frac{\partial P}{\partial x}$ from equation (5.3B). Thus,

$$\tau_c = -\frac{h}{2} \left\{ 6\mu v \frac{bx^2}{(h_1 + bx^2)^3} + \frac{P_m}{L_1} \frac{h_1^3}{(h_1 + bx^2)^3} \right\} - \frac{\mu v}{h}$$

but

$$\frac{h_1}{b} = a^2 \text{ and } h = h_1 + bx^2 = b(a^2 + x^2)$$

By putting these values into the above equations and after simplification we have,

$$\tau_c = -\frac{\mu v(a^2 + 4x^2)}{b(a^2 + x^2)^2} - \frac{Pmh_1}{2L_1} \frac{a^4}{(a^2 + x^2)^2} \quad (5.6B)$$

Once again, referring to Fig 132(c) and resolving forces perpendicular to the element, we obtain

$$\sigma_\theta = \frac{Pr}{t \cos\alpha} \quad (5.7B)$$

where, σ_θ is the hoop stress and $\cos\alpha = \sqrt{1 - 4b(r_1 - r)}$

Hoop stress in the deformation zone can be obtained by substituting P from equation (5.5B) into equation (5.7B).

$$\begin{aligned} \text{Thus, } \sigma_\theta = & \frac{r}{t\sqrt{1 - 4b(r_1 - r)}} \left[6\mu v \left\{ \frac{1}{8a^3b^2} \tan^{-1} \frac{x}{a} + \frac{x^3 - a^2x}{8a^2b^2(a^2 + x^2)^2} \right\} \right. \\ & \left. + \frac{Pm}{L_1} \left\{ x_1 + \frac{3}{8} a \tan^{-1} \frac{x}{a} + \frac{5a^4 + 3a^2x^3}{8(a^2 + x^2)^2} \right\} \right] \quad (5.8B) \end{aligned}$$

Resolving forces parallel to the effective deformation profile, simplifying and neglecting second-order smaller quantities, we get

$$\frac{d}{dr} (\sigma_x r) + \sigma_\theta + \tau_c \frac{r}{t \sin\alpha} = 0 \quad (5.9B)$$

where τ_c is the shear stress of the pressure medium on the tube surface, t is the constant wall thickness, α is the constant angle over the small length and $\sin\alpha = -2b\sqrt{\frac{r_1 - r}{b}}$

Differentiating equation (5.9B) we get,

$$r \frac{d\sigma_x}{dr} + \sigma_x + \sigma_\theta + \tau_c \frac{r}{t \sin\alpha} = 0 \quad (5.10B)$$

According Tresca yield criterion $\sigma_1 - \sigma_3 = y$ (5.11B)

but $\sigma_1 = \sigma_x$ and $\sigma_3 = -\sigma_\theta$

Therefore, equation (5.11B) becomes

$$\sigma_x + \sigma_\theta = y \quad (5.12B)$$

Substituting for $(\sigma_x + \sigma_\theta)$ in equation (5.10B) we obtain

$$d\sigma_x = -y \frac{dr}{r} - \tau_c \frac{dr}{t \sin\chi} \quad (5.13B)$$

Again the material property is represented by

$$y = y_0 + ko\epsilon^n \quad (5.14B)$$

By substituting the value of y from equation (5.14B) into (5.13B) we obtain,

$$d\sigma_x = -y_0 \frac{dr}{r} - ko \left(\ln \frac{r_1}{r}\right)^n \frac{dr}{r} - \tau_c \frac{dr}{t \sin\chi}$$

Integration of the above equation gives,

$$\sigma_x = -y_0 \ln r + \frac{ko}{n+1} \left(\ln \frac{r_1}{r}\right)^{n+1} - \frac{\tau_c r}{t \sin\chi} + c_3 \quad (5.17B)$$

where c_3 is the constant of integration.

Applying the boundary conditions (as before in Section 5.1.1) we get

$$c_3 = \sigma_{x_1} + y_0 \ln r_1 + \frac{\tau_c r_1}{t \sin\chi}$$

By substituting for c_3 in equation (5.17B) we obtain

$$\sigma_x = y_0 \ln \frac{r_1}{r} + \frac{ko}{n+1} \left(\ln \frac{r_1}{r}\right)^{n+1} + \frac{\tau_c}{t \sin\chi} (r_1 - r) + \sigma_{x_1}$$

After substituting for τ_c and σ_{x_1} into the above equation, the axial stress in the deformation zone is given by

$$\sigma_x = y_0 \ln \frac{r_1}{r} + \frac{ko}{n+1} \left(\ln \frac{r_1}{r}\right)^{n+1} - \frac{\sqrt{b}\sqrt{(r_1 - r)}}{bt} \left\{ -\frac{\mu v (a^2 + 4x^2)}{b(a^2 + x^2)^2} - \frac{Pmh_1}{2L_1} \frac{a^4}{(a^2 + x^2)^2} \right\} + \frac{y_0}{\left(\frac{\tau_c}{t} + \frac{Pm r_1}{tL_1}\right)} \left(-\frac{h_1}{2t} \frac{Pm}{L_1} - \frac{\mu v}{th_1} \right) \quad (5.18B)$$

The yield criterion which governs the deformation is given by

$$\sigma_x + \sigma_\theta = y_0 + ko \left(\ln \frac{r_1}{r}\right)^n$$

Substituting for σ_x and σ_θ and assuming that the deformation stops at the step where $x = (L_1 - x_1)$ and $r = r_1 - b(L_1 - x_1)^2$, the above equation may be written as

$$\begin{aligned}
& y_0 \ln \frac{r_1}{r} + \frac{k_0}{n+1} \left(\ln \frac{r_1}{r} \right)^{n+1} - \frac{\sqrt{b} \sqrt{(r_1 - r)}}{bt} \left\{ - \frac{\mu v (a^2 + 4x^2)}{b(a^2 + x^2)^2} - \frac{Pm h_1}{2L_1} \right. \\
& \left. + \frac{a^4}{(a^2 + x^2)^2} \right\} + \frac{y_0}{\left(\frac{\tau c_1}{t} + \frac{Pm r_1}{t L_1} \right)} x \left(- \frac{h_1}{2t} \frac{Pm}{L_1} - \frac{\mu v}{t h_1} \right) + \frac{r}{t \sqrt{1 - 4b(r_1 - r)}} \\
& \left[6\mu v \left\{ \frac{1}{8a^3 b^2} \tan^{-1} \frac{x}{a} + \frac{x^3 - a^2 x}{8a^2 b^2 (a^2 + b^2)} \right\} + \frac{Pm}{L_1} \left\{ x_1 + \frac{3}{8} a \tan^{-1} \frac{x}{a} \right. \right. \\
& \left. \left. + \frac{5a^4 + 3a^2 x^3}{8(a^2 + x^2)^2} \right\} \right] - y_0 - k_0 \left(\ln \frac{r_1}{r} \right)^n = 0 \quad (5.19B)
\end{aligned}$$

In the above equation only the parameter 'b' is unknown which may be evaluated using iteration process. Once the value of 'b' is established the deformation profile is obtained and reduction in diameter at any point for $x_1 \leq x \leq L_1$ is given by

$$\Delta D = D_1 - 2bx^2$$

and the total percentage reduction in diameter is given by

$$PRD = 100 \{2b(L_1 - x_1)^2\}/D_1 \quad (5.20B)$$

The drawing stress ' σ_d ' at the exit end of the DRU is then given by

$$\sigma_d = \sigma_{x_1} + \sigma_{x_2} \quad (5.21B)$$

where σ_{x_1} is the axial stress at the step and σ_{x_2} is given by

$$\sigma_{x_2} = \frac{\tau c_2 L_2}{t}$$

The shear stress in the small bore section of the unit may be expressed as

$$\tau c_2 = \frac{h_3 P}{2L_2} - \frac{\mu v}{h_3}$$

$$\text{and } h_3 = h_2 + b(L_1 - x_1)^2 \quad (5.22B)$$

where h_3 is the final gap.

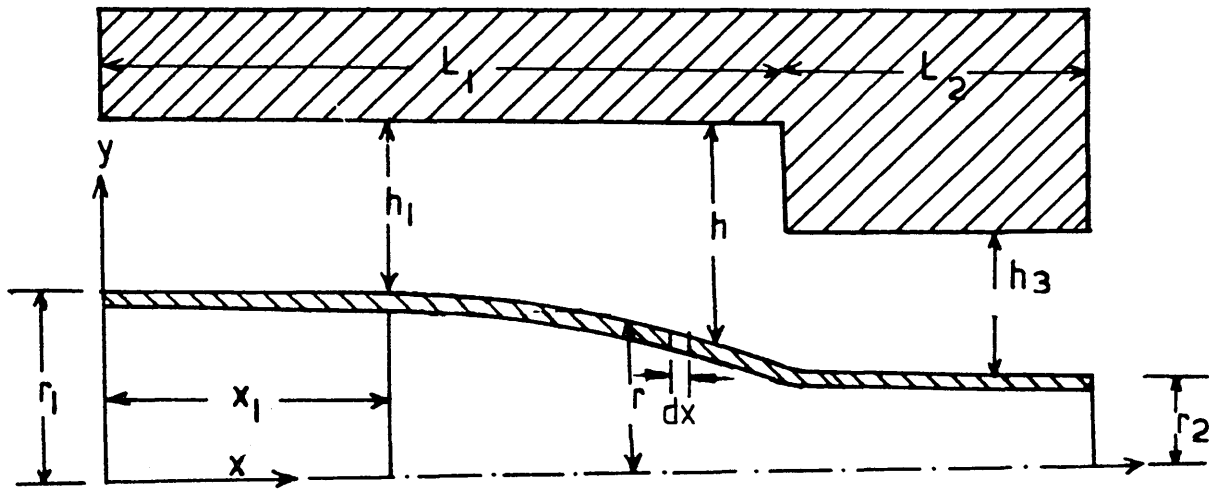


FIG 134(a) - GEOMETRY USED IN THE ANALYSIS

5.2.3

Numerical Solution

Consider the zone of the stepped bore reduction unit where deformation of the tube takes place. Let us assume that between any two points distance 'dx' apart on the deforming tube, the deformation takes place linearly at an angle χ .

Considering a small section of the deforming tube, (shown in Fig134(b)), the equilibrium of forces acting normal to the surface we have

$$P(r d\theta \frac{dr}{\sin\chi}) - \sigma_{\theta}(t \frac{dr}{\sin\chi}) d\theta \cos\chi = 0$$

which after simplification gives

$$P = \sigma_{\theta} \frac{t}{r} \cos\chi \quad (5.1C)$$

Equilibrium of forces in the x-direction gives

$$(\sigma_x + d\sigma_x)(r + dr)\Delta\theta(t + dt) - \sigma_x r \Delta\theta + \sigma_{\theta}(t \frac{dr}{\sin\chi})\Delta\theta \sin\chi + \tau_c(r\Delta\theta \frac{dr}{\sin\chi}) = 0$$

which after simplification, neglecting second-order smaller quantities and dividing by dr becomes

$$\frac{d}{dr}(\sigma_x r t) + \sigma_{\theta} t + \tau_c \frac{r}{\sin\chi} = 0$$

Let the wall-thickness of the tube remain unaltered during the deformation, so that the above equation becomes;

$$\frac{d}{dr}(\sigma_x r) \sigma_{\theta} + \tau_c \frac{r}{t \sin\chi} = 0$$

so that,

$$r \frac{d\sigma_x}{dr} + \sigma_x + \sigma_{\theta} + \tau_c \frac{r}{t \sin\chi} = 0 \quad (5.2C)$$

Substituting for $(\sigma_x + \sigma_\theta)$ in equation (5.2C) we get

$$r \frac{d\sigma_x}{dr} + \sigma_x + \tau_c \frac{r}{t \sin \alpha} = 0$$

or

$$d\sigma_x = -\sigma_x \frac{dr}{r} - \tau_c \frac{dr}{t \sin \alpha} \quad (5.3C)$$

$$\left(\text{where } \sin \alpha = \frac{dr}{\sqrt{dr^2 + dx^2}} \right)$$

This is the governing equation which enables prediction of the axial stress in the tube within the deformation zone.

Let

$$\frac{dr}{dx} = \tan \alpha = B$$

which in finite difference form can be expressed as,

$$\frac{r_{i-1} - r_i}{\Delta x} = \frac{r_{i-1} - r_i}{x_i - x_{i-1}} = \tan \alpha = B$$

so that

$$r_i = r_{i-1} - B\Delta x \quad (5.4C)$$

The variation of gap in between the outer surface of the tube and the inner surface of the DRU in the deformation zone can similarly be written as,

$$dh = dr = Bdx$$

which in finite difference form becomes

$$h_i = h_{i-1} + \Delta x B \quad (5.5C)$$

where B is the slope of the deformation line along distance 'dx'.

The variation of speed of the tube in the deformation zone may be determined from the continuity of flow of metal through the small element (as shown in Fig 134(b)).

Thus

$$(r + dr)\Delta\theta(t + dt)(v + dv) = r\Delta\theta tv$$

which after simplification and neglecting second order smaller quantities becomes

$$\frac{dr}{r} + \frac{dv}{v} + \frac{dr}{r} \frac{dv}{v} = 0$$

hence,

$$\frac{dv}{v} = - \frac{dr}{r + dr}$$

Rewriting the above equation in finite difference form and rearranging we have

$$v_i = \frac{v_{i-1}}{1 - \frac{(r_{i-1} - r_i)}{r_{i-1}}} \quad (5.6C)$$

The pressure gradient and the pressure in the deformation zone with reference to equation (5.7) are given by;

$$P'_i = \frac{12\mu}{h_i^3} \left(\frac{v_i h_i}{2} - Q_1 \right) \quad (5.7C)$$

We know that pressure gradient is

$$\frac{dP}{dx} = P'$$

Rewriting the pressure gradient in finite difference form gives;

$$\frac{P_i - P_{i-1}}{\Delta x} = P'_i$$

$$\text{or } P_i = P'_i \Delta x + P_{i-1} \quad (5.8C)$$

Also the shear stress in the deformation zone may be expressed as;

$$\tau_{ci} = - \frac{1}{2} P'_i h_i - \frac{v_i \mu}{h_i} \quad (5.9C)$$

Rewriting equation (5.3C) in finite difference form and rearranging we have

$$\sigma_{xi} = \frac{(r_{i-1} - r_i)}{r_i} y_i + \frac{\tau_{ci}}{t} \sqrt{(r_{i-1} - r_i)^2 + (x_i - x_{i-1})^2} + \sigma_{xi-1} \quad (5.10C)$$

The hoop stress in the deformation zone is given by equation (5.1C), which after rewriting in finite difference form leads to;

$$\sigma_{\theta i} = \frac{P_{iri} \sqrt{(x_i - x_{i-1})^2 + (r_{i-1} - r_i)^2}}{t(x_i - x_{i-1})} \quad (5.11C)$$

where σ_{θ} is the hoop stress in the deformations zone. The stress-strain relationship of the tube material has been shown in Figs 28 and 29 to take the form,

$$y = y_0 + k_0 \epsilon^n$$

$$\text{where } \epsilon = \ln \left(\frac{r_1}{r} \right)$$

therefore

$$y = y_0 + k_0 \left(\ln \frac{r_1}{r} \right)^n$$

The above equation in finite difference notation becomes;

$$y_i = y_0 + k_0 \left(\ln \frac{r_1}{r_i} \right)^n \quad (5.12C)$$

The strain rate sensitivity of the tube material may also be taken into account in the analysis. The mean strain rate of the material over a small distance 'dx' may be expressed as;

$$\bar{\epsilon} = \left(-2 \frac{dr}{r} \right) \frac{1}{dt}$$

or

$$\bar{\epsilon}_{mi} = \frac{1}{x_i - x_{i-1}} \int_{r_{i-1}}^{r_i} \bar{\epsilon} dx$$

where

$$x = x_{i-1} \quad \text{at } r = r_{i-1}$$

and

$$x = x_i \quad \text{at } r = r_i$$

By substituting $\bar{\epsilon}$ in above equation gives;

$$\bar{\epsilon}_{mi} = \frac{1}{\Delta x} \int_{r_{i-1}}^{r_i} -2 \frac{dr}{r} \frac{dx}{dt}$$

where $x_i - x_{i-1} = \Delta x$

but $\frac{dx}{dt} = v_i$

Therefore,

$$\bar{\epsilon}_{mi} = \frac{-2v_i}{\Delta x} \int_{r_{i-1}}^{r_i} \frac{dr}{r}$$

Integration gives;

$$\bar{\epsilon}_{mi} = \frac{2v_i}{\Delta x} \ln\left(\frac{r_i}{r_{i-1}}\right) \quad (5.13C)$$

A flow rule of the form;

$$s = \frac{y_d}{y_s} = 1 + \left(\frac{\bar{\epsilon}_m}{N}\right)^{\frac{1}{T}}$$

where y_d = dynamic yield stress of the material

and y_s = static yield stress of the material

has been proposed by Hashmi⁴³ and Ting⁴⁴.

In finite difference notation the above equation takes the form

$$s_i = 1 + \left(\frac{\bar{\epsilon}_{mi}}{N}\right)^{\frac{1}{T}}$$

where T and N are material constants.

Combining the above equation with equation (5.12C) gives,

$$y_i = s_i \left(y_0 + k_0 \left(\ln \frac{r_1}{r_i} \right)^n \right) \quad (5.14C)$$

Equation (5.14C) represents the yield stress of the tube, incorporating the strain hardening and strain rate sensitivity of the material. Substituting for y_i into equation (5.10C) we have

$$\sigma_{xi} = \frac{(r_{i-1} - r_i)}{r_i} s_i \left(y_0 + k_0 \left(\ln \frac{r_1}{r_i} \right)^n \right) + \frac{\tau_{ci}}{t} \sqrt{(r_{i-1} - r_i)^2 + \sqrt{(x_i - x_{i-1})^2 + \sigma_{xi-1}^2}} \quad (5.15C)$$

At any point within the deformation zone, the Tresca yield criterion gives,

$$\sigma_x + \sigma_\theta = y \text{ (as before)}$$

Representing this equation in finite difference notation we obtain;

$$\sigma_{xi} + \sigma_{\theta i} = y_i \quad (5.16C)$$

Solution Procedure

At any point 'i' in the deformation zone, r_i and h_i may be calculated from equation (5.4C) and (5.5C) respectively for an arbitrary value of 'B' and a step size of Δx . r_i may be substituted into equation (5.6C) which gives v_i . Also by substituting v_i and h_i into equation (5.7C) where the value of Q_1 is given by equation (5.7), gives \dot{P}_i , and hence from equation (5.8C), P_i may be calculated.

Similarly τ_{ci} can be calculated by substituting the values of \dot{P}_i , v_i and h_i into equation (5.9C). $\sigma_{\theta i}$ can be calculated from equation (5.11C) by substituting for P_i and r_i . Then τ_{ci} , r_i and s_i may be substituted into equation (5.15C) to evaluate σ_{xi} . Equation (5.14C) gives y_i upon substitution for s_i and r_i . Other variables in the above equations are known physical parameters.

Having calculated σ_{xi} , $\sigma_{\theta i}$ and y_i values of 'B' may be iterated until equation (5.16C) is satisfied at any point in the deformation zone. This procedure may be repeated in suitable steps of ' Δx ' from the position of yielding of the tube inside the stepped bore reduction unit where $i = 1$ at $x = x_1$ and upto the step. This procedure may be repeated at each speed increment. Therefore, at the step,

when equation (5.16C) is satisfied the drawing speed, final tube diameter, drawing stress and the final gap are given by;

drawing speed, $v_d = v_i$

final tube diameter, $D_2 = D_i$ or $2r_2 = 2r_i$

drawing stress, $\sigma_D = \sigma_{x1} + \sigma_{x2}$ (5.17C)

where

$$\sigma_{x2} = \frac{\tau_{c2} \times L_2}{t}$$

and

$$\tau_{c2} = \frac{h_3 P_i}{2L_2} - \frac{\mu v_i}{h_3}$$

final gap $h_3 = h_i - h_1 + h_2$ (5.18C)

respectively.

5.3 Theoretical Results

Theoretical results were calculated on the basis of equations derived in the theoretical analysis section. The data below are the known parameters which were used to solve the equations and were varied to show their effect on the performance of the unit.

- (i) Dimensions of the die-less reduction unit;
 - Total length of the die-less reduction unit (DRU) = 190mm
 - Position of step from inlet, $L_1 = 160\text{mm}$
 - Position of step from outlet, $L_2 = 30\text{mm}$
 - Inlet gap, $h_1 = 0.5\text{mm}$, Outlet gap, $h_2 = 0.01\text{mm}$
- (ii) Data for copper tube;
 - Original diameter, $D_1 = 13.52\text{mm}$
 - Wall-thickness, $t = 2.5\text{mm}$
 - Initial yield stress of the tube material, $Y_0 = 50 \text{ MN/m}^2$
 - Strain hardening constant, $K_0 = 700 \text{ MN/m}^2$
 - Strain hardening index, $n = 0.18$
 - Strain rate sensitivity index, $T = 3.8$
 - Strain rate sensitivity constant, $N = 55 \times 10^3$
- (iii) Data for aluminium tube;
 - Original diameter, $D_1 = 15.93\text{mm}$
 - Wall-thickness, $t = 1.63\text{mm}$
 - Initial yield stress of the tube material, $Y_0 = 40 \text{ MN/m}^2$
 - Strain hardening constant, $K_0 = 640 \text{ MN/m}^2$
 - Strain hardening index, $n = 0.26$

Results from the analyses were obtained in tabulated forms but are represented in this section in graphical form for convenience.

5.3.1 Results Based on Linear Deformation Profile

The theoretical percentage reduction in diameter was calculated using equation (5.18B).

Figs (135a) and (b) show the variations in percentage reduction in diameter and yielding position of the copper tube for different gap ratios of the die-less unit. This figure suggests that for a higher value of h_1/h_2 , plastic deformation commences further away from the step and greater percentage reduction in diameter should be obtained for a given drawing speed.

The effect of length ratio on percentage reduction in diameter for copper tube is demonstrated in Fig (136). This figure suggests that for higher values of L_1/L_2 , greater percentage reduction in diameter should be obtained at higher pulling speeds.

The effect of viscosity of the pressure medium on percentage reduction in diameter and on yielding position of the copper tubes is shown in Figs (137a) and (b). It is evident from this figure that higher viscosity should initiate deformation further away from the step of the unit and cause greater percentage reduction in diameter. With a viscosity value of 130 Ns/m^2 , the reduction in diameter of about 11 per cent should be obtained for the drawing speed of 1 m/s. However, if the viscosity is reduced to 100 Ns/m^2 , a reduction in diameter of about 8 per cent is predicted for the same drawing speed.

In order that the effect of the wall-thickness of the copper tube on the extent of permanent deformation may be studied, reduction in diameter with drawing speed was calculated for three different wall-thicknesses and the results are shown in Fig (138). This figure shows that for smaller wall-thickness, greater reduction in diameter is predicted for a given drawing speed and pressure medium. For a tube of wall-thickness 1.5mm, the reduction in diameter of about 15 per cent is predicted at a drawing speed of 1 m/s, but only 5 per cent reduction in diameter may be obtained

for a tube of wall-thickness of 3.5mm at the same drawing speed of 1 m/s.

Fig (139) shows the effect of changes in the wall-thickness on the deformation for aluminium tube with drawing speed. The trends of these results are similar to those in Fig (138). This figure indicates that for a smaller wall-thickness, greater reduction in diameter should be obtained at higher pulling speeds. For a tube wall-thickness of 1.5mm, the reduction in diameter of about 11 per cent should be obtained at a drawing speed of 0.5 m/s, but the reduction in diameter becomes about 9 per cent for a tube of wall-thickness of 3.0mm at the same drawing speed, ie 0.5 m/s.

Figs (140) and (141) show the effect of the initial yield stress, Y_0 , on percentage reduction in diameter for copper and aluminium tubes respectively. The theoretical results were calculated with different values of Y_0 varying from 10 to 80 MN/m². These figures show that for lower values of Y_0 , relatively greater permanent deformation could be obtained at a given drawing speed, but percentage reduction in diameter decreases for higher values of initial yield stress.

The effect of the strain hardening constant, K_0 , on percentage reduction in diameter for aluminium tube is demonstrated in Fig (142). This figure suggests that lower values of K_0 cause greater percentage reduction in diameter of the tube at higher drawing speed.

Fig (143) shows the effect of the strain hardening index, n , on percentage reduction in diameter for aluminium tube. This figure indicates that with the strain hardening index, $n = 0.9$, the reduction in diameter of about 23 per cent should be obtained for the drawing speed of 0.5 m/s and that for lower value of 'n'

smaller reduction in diameter is predicted at the same drawing speed of 0.5 m/s.

Fig (144) shows the effect of changing the diameter on the percentage reduction in diameter for copper tube. This figure suggests that for higher values of D_1 relatively greater permanent deformation could be obtained at higher drawing speeds, but the percentage reduction in diameter decreases with decreasing values of D_1 . The diameter of the tube was varied from 14.5 to 12mm and it is evident that at the drawing speed of 1 m/s, permanent reduction in diameter of about 8.5 per cent may take place in a tube of 14.5mm diameter and about 7 per cent in a tube of 12mm diameter.

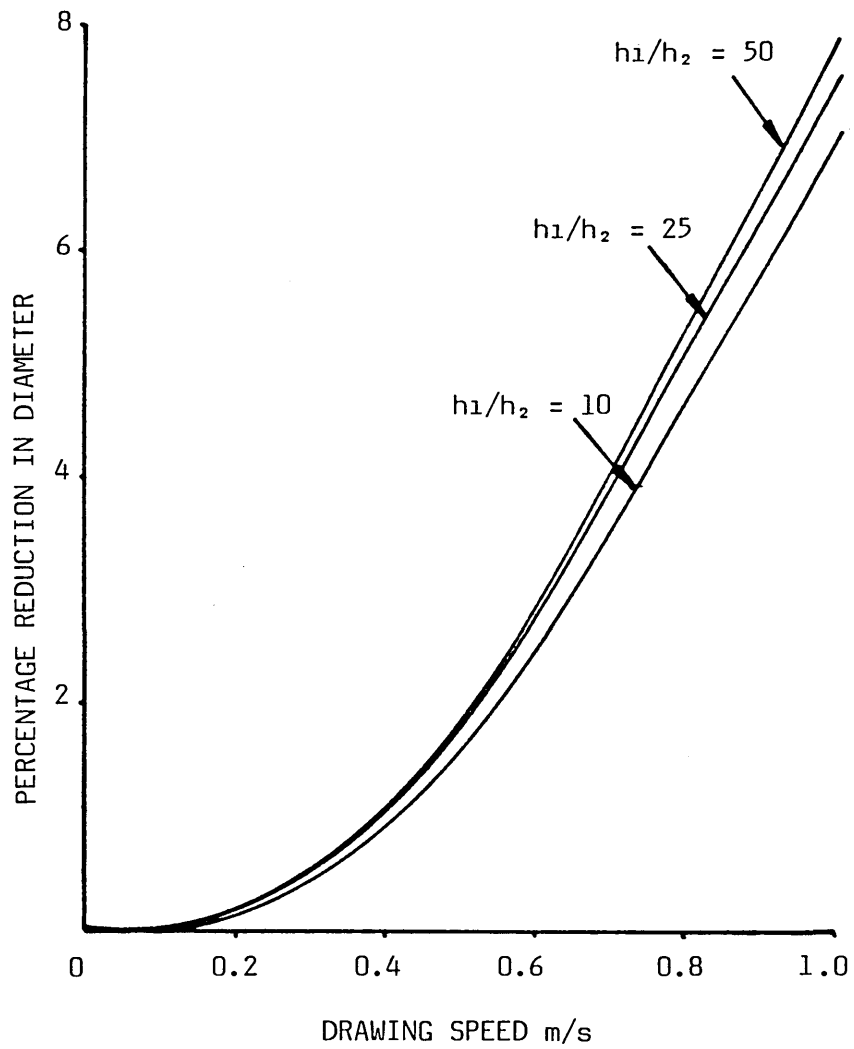


FIG 135(a) - THEORETICAL EFFECT OF GAP RATIO ON PERCENTAGE REDUCTION IN DIAMETER FOR COPPER TUBE

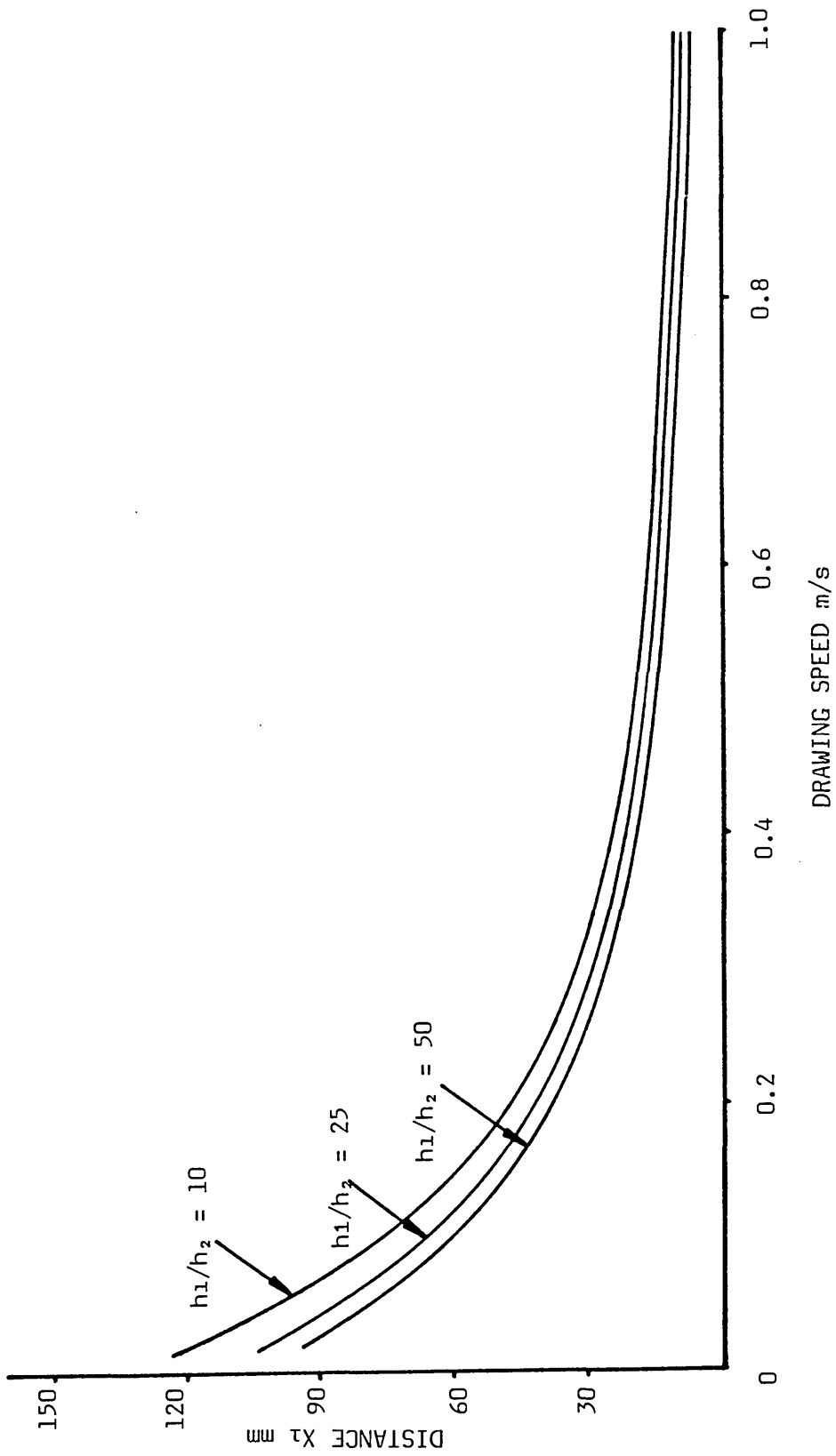


FIG 135(b) - THEORETICAL EFFECT OF GAP RATIO ON YIELDING POSITION OF THE COPPER TUBE

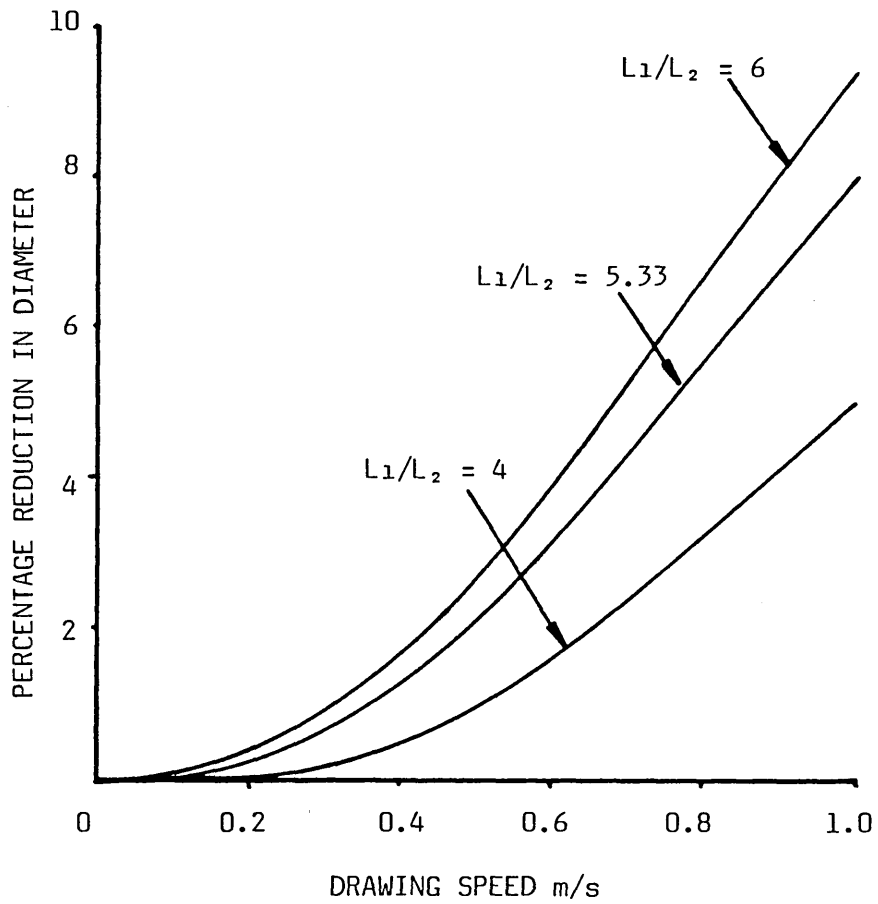


FIG 136 - THEORETICAL EFFECT OF LENGTH RATIO ON PERCENTAGE REDUCTION IN DIAMETER FOR COPPER TUBE

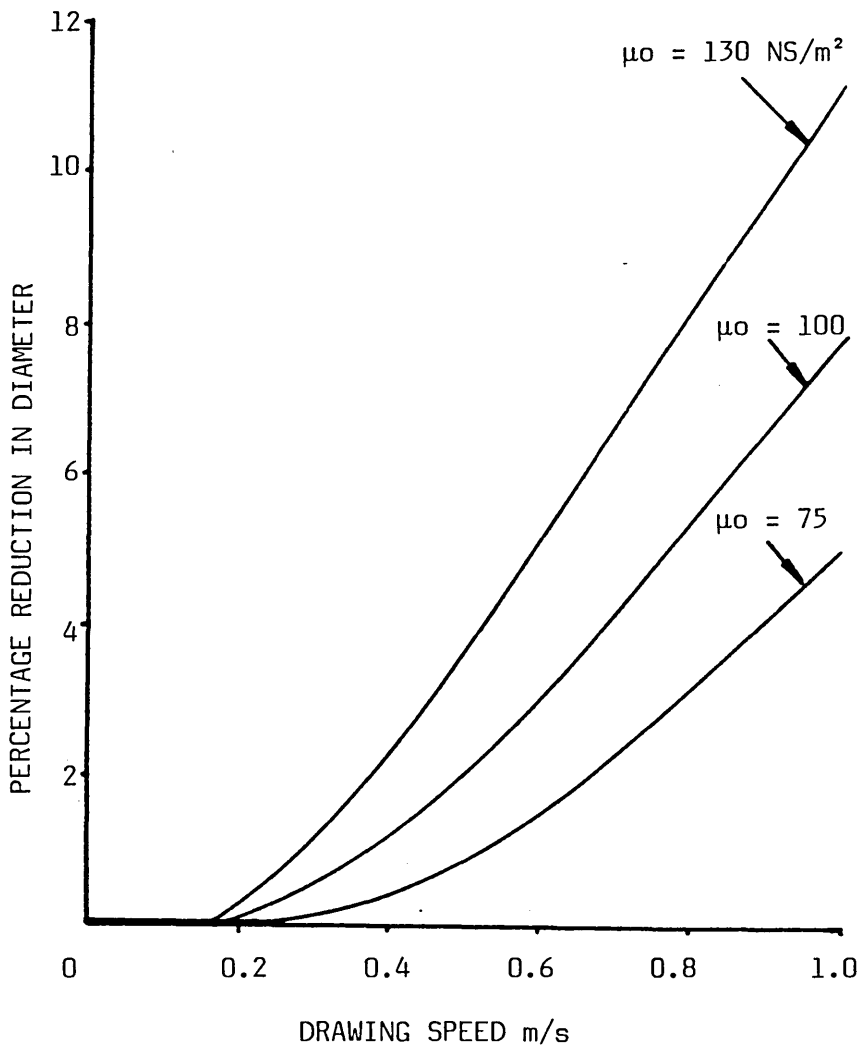


FIG 137(a) - THEORETICAL EFFECT OF VISCOSITY ON PERCENTAGE REDUCTION IN DIAMETER FOR COPPER TUBE

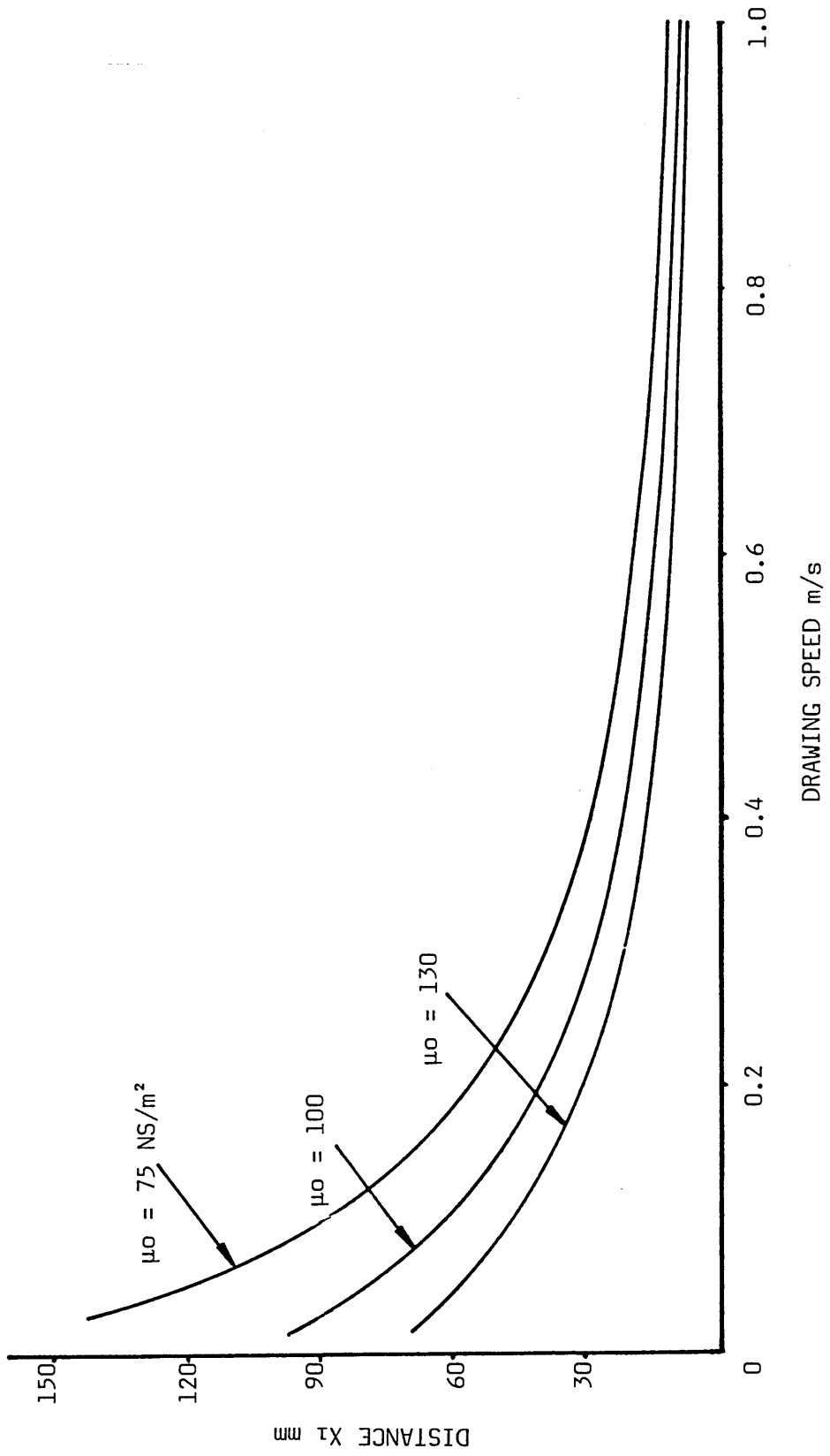


FIG 137(b) - THEORETICAL EFFECT OF VISCOSITY ON YIELDING POSITION OF THE COPPER TUBE

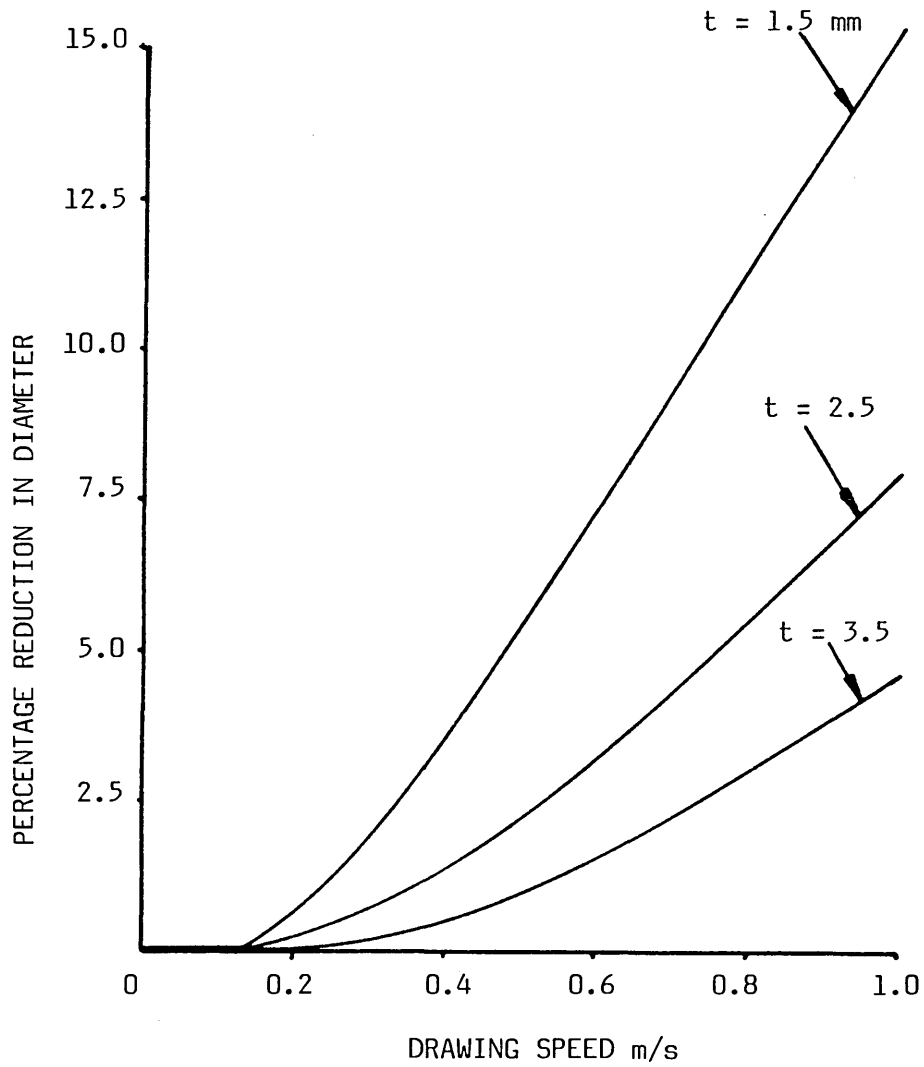


FIG 138 - THEORETICAL EFFECT OF TUBE WALL-THICKNESS ON PERCENTAGE REDUCTION IN DIAMETER FOR COPPER TUBE

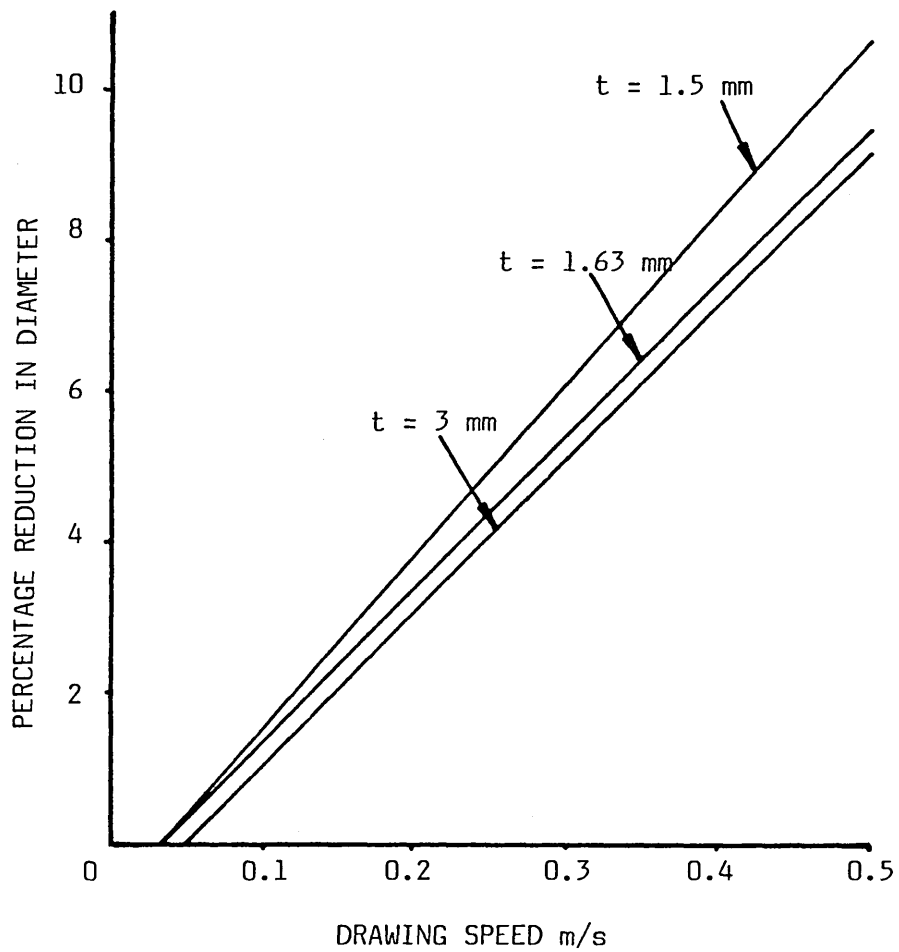


FIG 139 - THEORETICAL EFFECT OF TUBE WALL-THICKNESS ON PERCENTAGE REDUCTION IN DIAMETER FOR ALUMINIUM TUBE

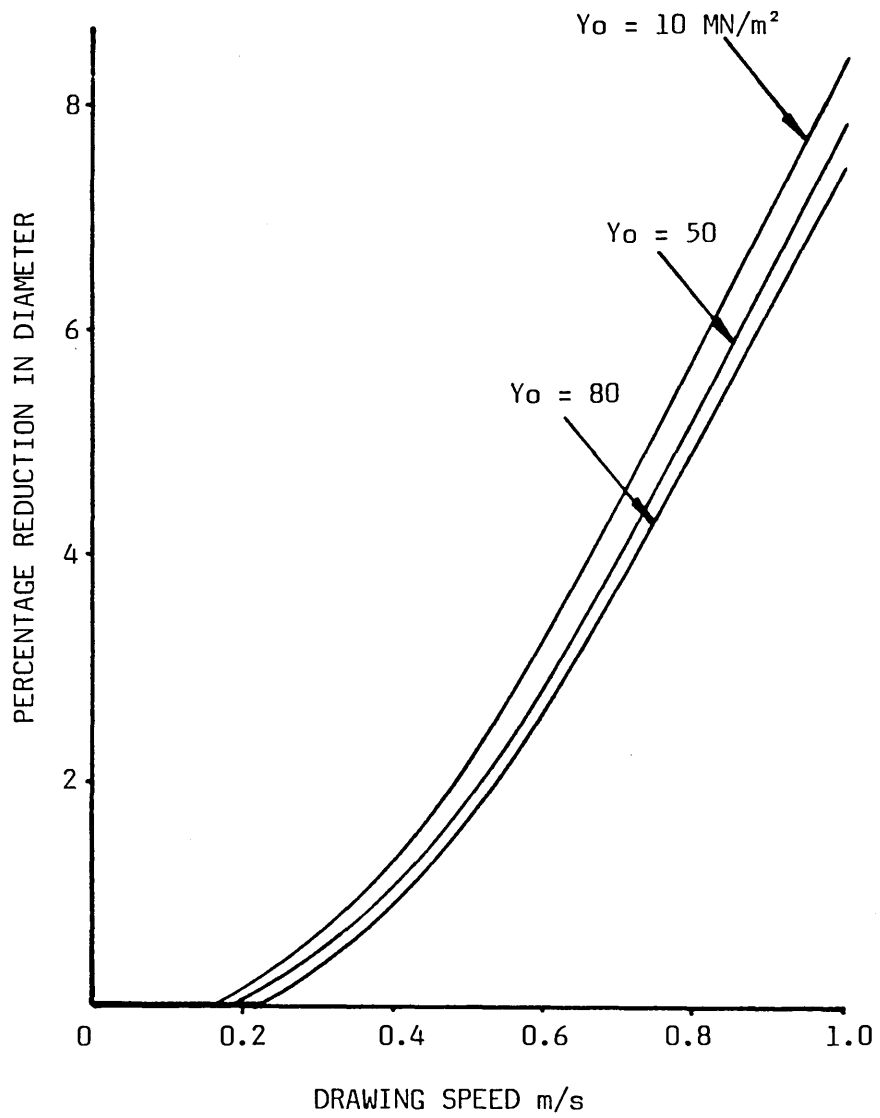


FIG 140 - THEORETICAL EFFECT OF INITIAL YIELD STRESS ON
PERCENTAGE REDUCTION IN DIAMETER FOR COPPER TUBE

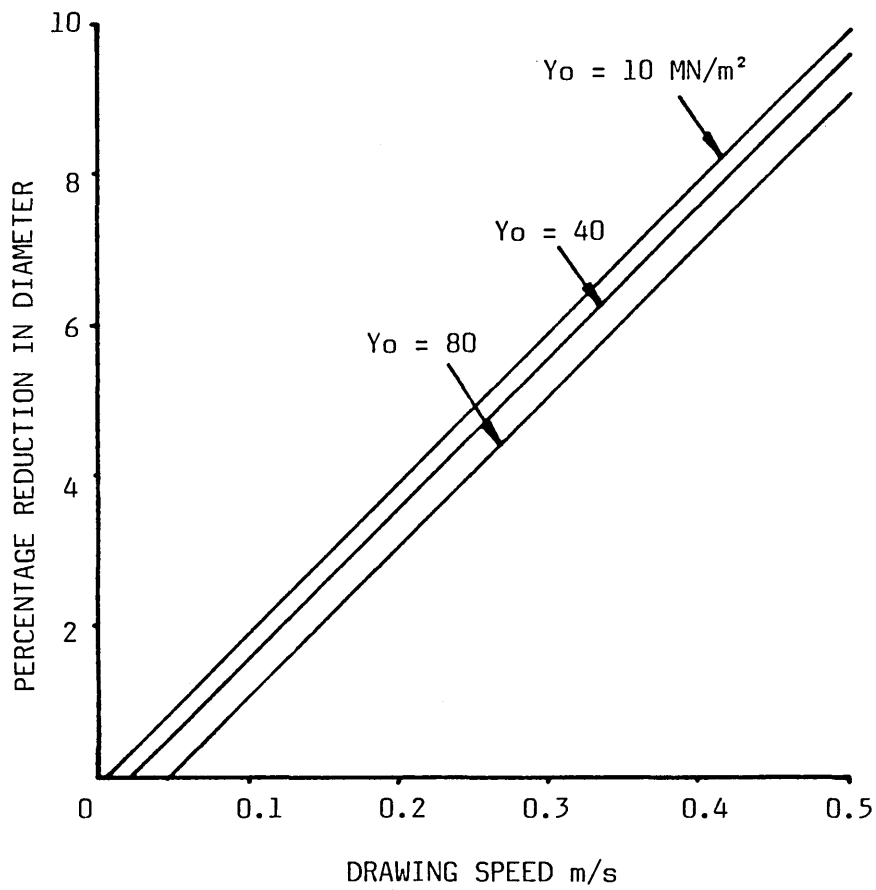


FIG 141 - THEORETICAL EFFECT OF INITIAL YIELD STRESS ON PERCENTAGE REDUCTION IN DIAMETER FOR ALUMINIUM TUBE

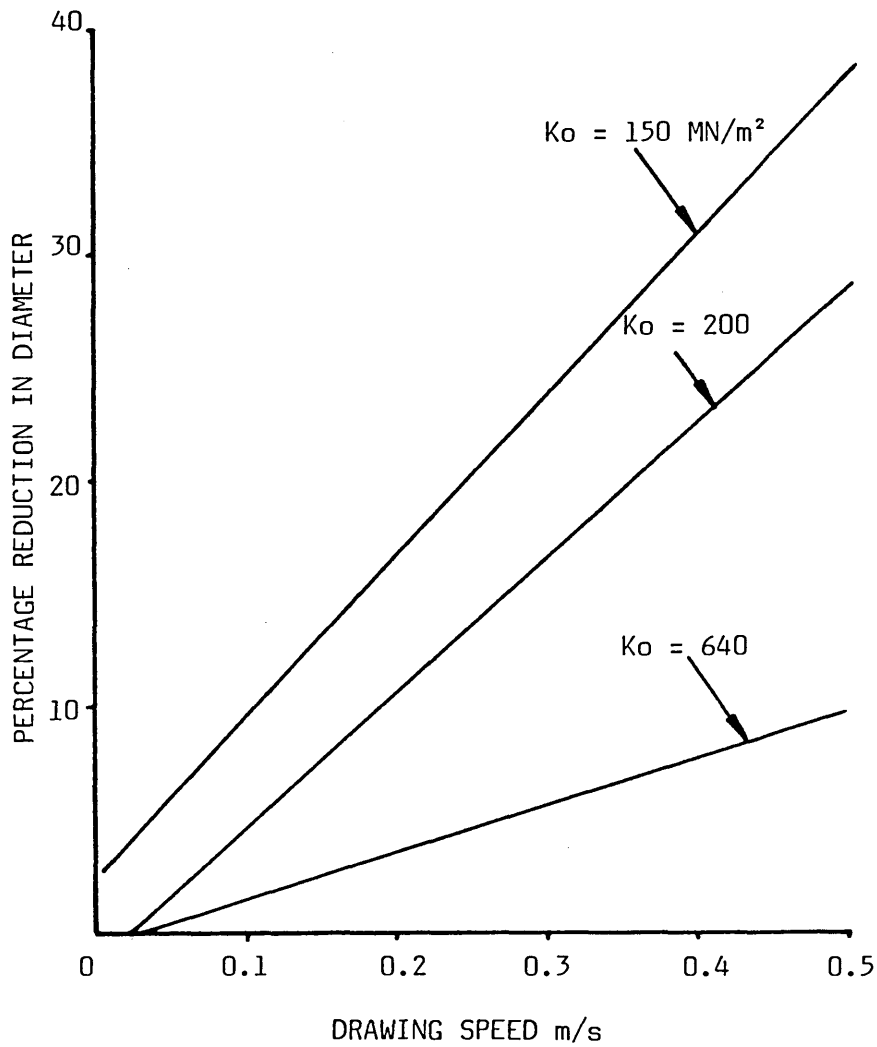


FIG 142 - THEORETICAL EFFECT OF STRAIN HARDENING CONSTANT ON PERCENTAGE REDUCTION IN DIAMETER FOR ALUMINIUM TUBE

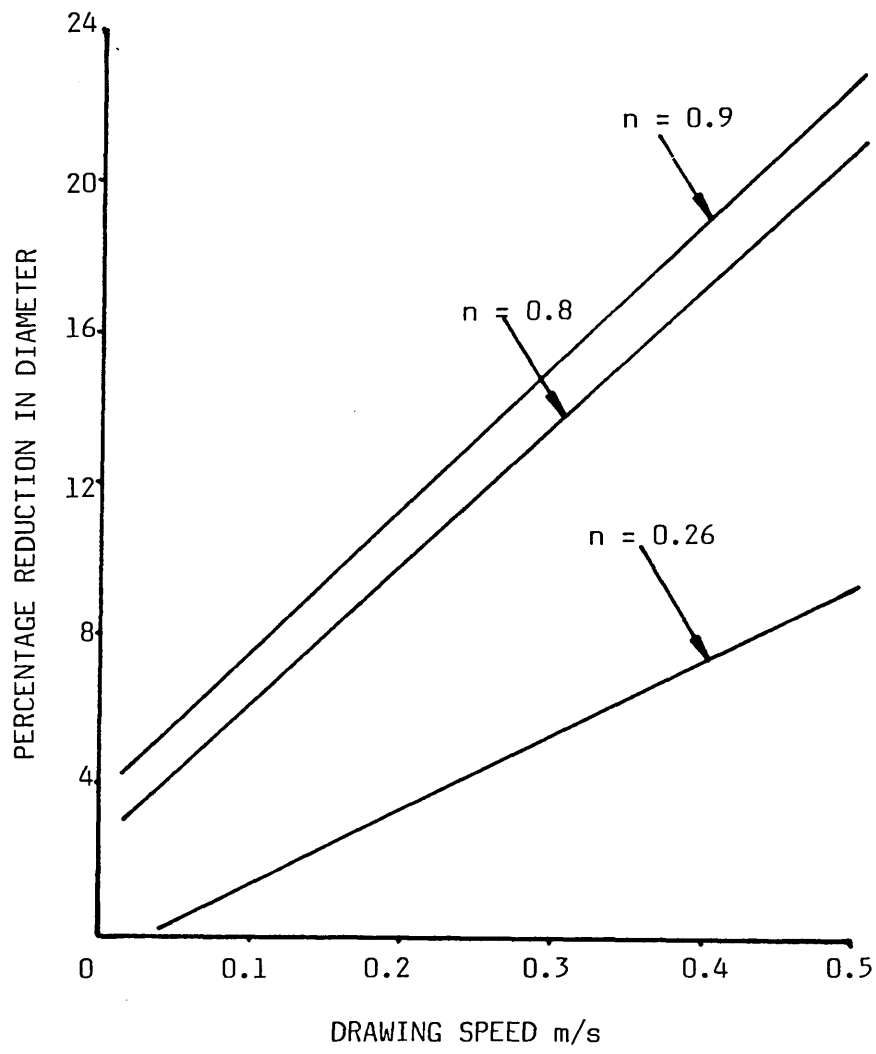


FIG 143 - THEORETICAL EFFECT OF STRAIN HARDENING INDEX ON PERCENTAGE REDUCTION IN DIAMETER FOR ALUMINIUM TUBE

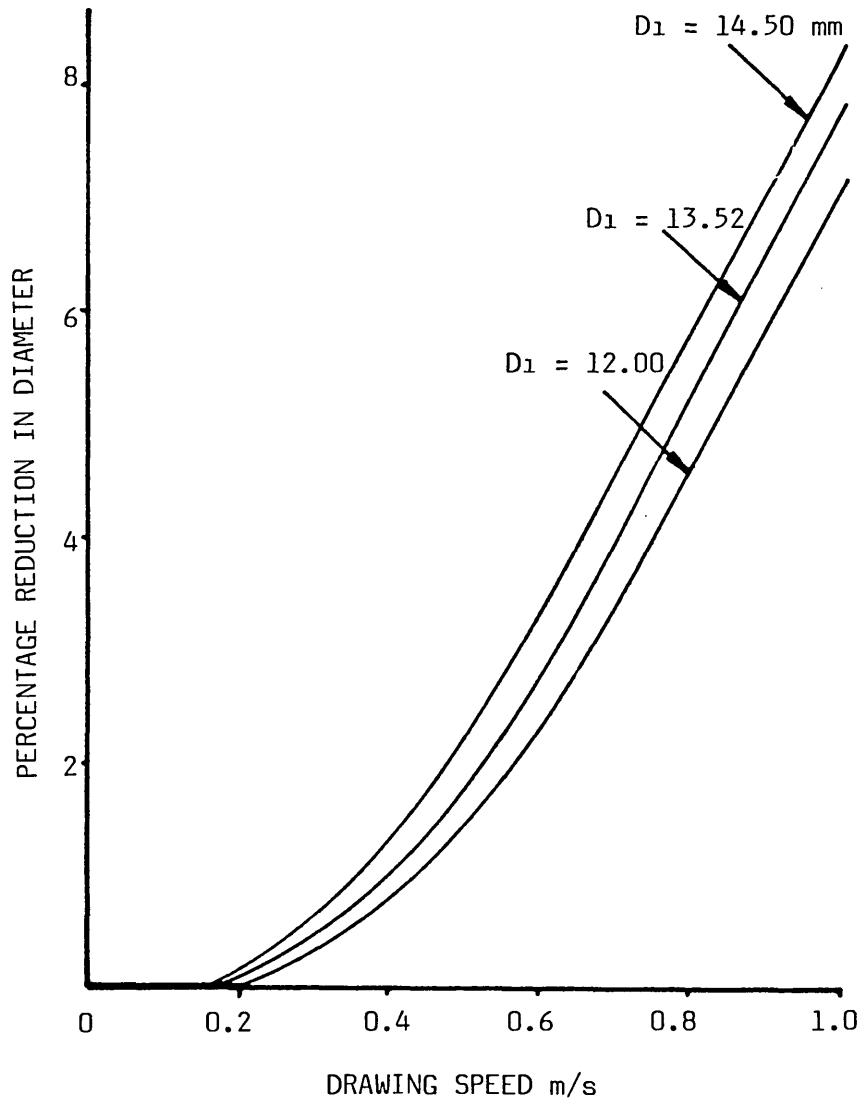


FIG 144 - THEORETICAL EFFECT OF TUBE DIAMETER ON PERCENTAGE REDUCTION IN DIAMETER FOR COPPER TUBE

5.3.2 Curved Profile

The results calculated using the equations derived on the assumption of curved deformation profile have been found to be very similar in trends as well as magnitudes to those calculated on the assumption of straight line deformation profile.

The theoretical percentage reduction in diameter was calculated using equation (5.20B) and Figs (145a) and (b) show the effect of gap ratio on the percentage reduction in diameter and yielding position of the aluminium tubes respectively. This figure suggests that for a higher value of h_1/h_2 plastic deformation commences further away from the step for a given drawing speed and greater percentage reduction in diameter should be obtained. At higher drawing speeds, the deformation of the tube increased. A maximum reduction in diameter was predicted (about 13%) for the gap ratio of 50 at 0.5 m/s. As the gap ratio decreased, the reduction in diameter for lower gap ratio (2.5) fell to about 3% at the same drawing speed (0.5 m/s).

Figs (146a) and (b) show the effect of gap ratio on the percentage reduction in diameter and yielding position of copper tubes respectively. The general trends were found to be similar to those shown in Fig (145).

The effect of gap ratio of the die-less reduction unit (keeping h_2 constant) on the percentage reduction in diameter for aluminium tube is shown in Fig (147). Again the general trend is similar to that observed in the previous figure.

Figs (148a) and (b) show the variations in percentage reduction in diameter and yielding position of aluminium tubes with drawing speed for different values of L_1/L_2 . The general trends of the results were found to be the same as those in Fig (145). This

figure suggests that for higher values of L_1/L_2 plastic deformation takes place further away from the step of the die-less reduction unit for a given drawing speed and greater percentage reduction in diameter should be obtained at higher drawing speeds. The maximum reduction in diameter predicted was about 17% for the length ratio of 6 at 0.5 m/s.

Figs (149a) and (b) show the variations in percentage reduction in diameter and yielding position respectively of copper tubes with the drawing speed for different length ratios. The trends of the predicted results were found to be similar to those in Fig (148).

The effect of viscosity of the liquid polymer on the variations in percentage reduction in diameters and yielding positions of aluminium and copper tubes are shown in Figs (150a-b) and (151a-b) respectively. It is evident from these figures that higher viscosity should initiate deformation further away from the step of the unit and should cause greater percentage reduction in diameter. With a viscosity of 150 Ns/m^2 , the reduction in diameter of about 26 per cent should be obtained for aluminium tube at drawing speed of 0.5 m/s as shown in Fig (150a).

The effects of changes in the wall-thickness on the deformation for aluminium tube is demonstrated in Fig (152) which shows the variations in percentage reduction in diameter with drawing speed. The wall-thickness of the tube was varied from 1.00 to 2.63mm. For a drawing speed of 0.5 m/s it is evident that permanent reduction in diameter of about 30 per cent should be obtained in a tube of 1.00mm wall-thickness, but only 5 per cent reduction in diameter may take place for higher value of tube wall-thickness (2.63mm) at the same drawing speed of 0.5 m/s.

Figs (153a-b) and (154a-b) show the effect of initial yield stress, Y_0 , of the tube materials on percentage reduction in diameters and yielding positions x_1 . Calculations were carried out with different values of Y_0 varying from 10 to 80 MN/m². Both figures show that for lower values of Y_0 relatively greater permanent deformation could be obtained near to the entry side of the unit at higher drawing speed, but percentage reduction in diameter decreases at higher values of Y_0 and deformation takes place further away from the entry side of the unit.

Fig (155) shows the effect of strain hardening constant, K_0 , of the tube material on the percentage reduction in diameter with drawing speed for aluminium tube. This figure suggests that lower values of K_0 , cause greater percentage reduction in diameter with a strain hardening factor value of 500 MN/m², the percentage reduction in diameter predicted was about 20 per cent for the drawing speed of 0.5 m/s.

Theoretical effect of strain hardening index, n , on the percentage reduction in diameter for aluminium tubes is shown in Fig (156). This figure indicates that with a strain hardening index ' n ' value of 0.5, the reduction diameter of about 22 per cent should be obtained for the drawing speed of 0.5 m/s, this figure also suggests that for lower value of ' n ', only 5 per cent reduction in diameter may take place at the same drawing speed, ie 0.5 m/s.

The coating thickness was calculated by using equation (5.22B). Results of the coating thickness exhibits similar trends to those of the percentage reduction in diameter. Fig (157) shows the effect of the gap ratio on coating thickness for aluminium tubes. This figure shows that for higher value of gap ratio relatively greater coating thickness could be obtained at higher drawing speeds.

Fig (158) shows the effect of length ratio on coating thickness for aluminium tubes. To introduce different length ratio, L_2 was kept constant. This result shows that as the length ratio was increased, the coating thickness also increased.

The effect of viscosity on coating thickness for aluminium tubes is shown in Fig (159). This figure shows that for greater values of viscosity relatively greater coating thickness could be obtained at higher drawing speeds.

Fig (160) shows the effect of initial yield stress on coating thickness for aluminium tubes which indicates that maximum coating thickness should be obtained at lower values of Y_0 . Coating thickness reduced gradually as the values of Y_0 increased.

Fig (161) shows the effect of strain hardening constant on the coating thickness for aluminium tubes. The trends of the results predicted are similar to those of the percentage reduction in diameter (see Fig 155). This figure suggests that lower values of K_0 , cause greater coating thickness at higher drawing speed and increasing the strain hardening factor causes coating thickness to decrease.

Fig (162) shows the effect of the strain hardening index on the coating thickness for aluminium tubes. This figure also shows that for greater value of 'n' relatively greater coating thickness should be obtained at higher drawing speeds.

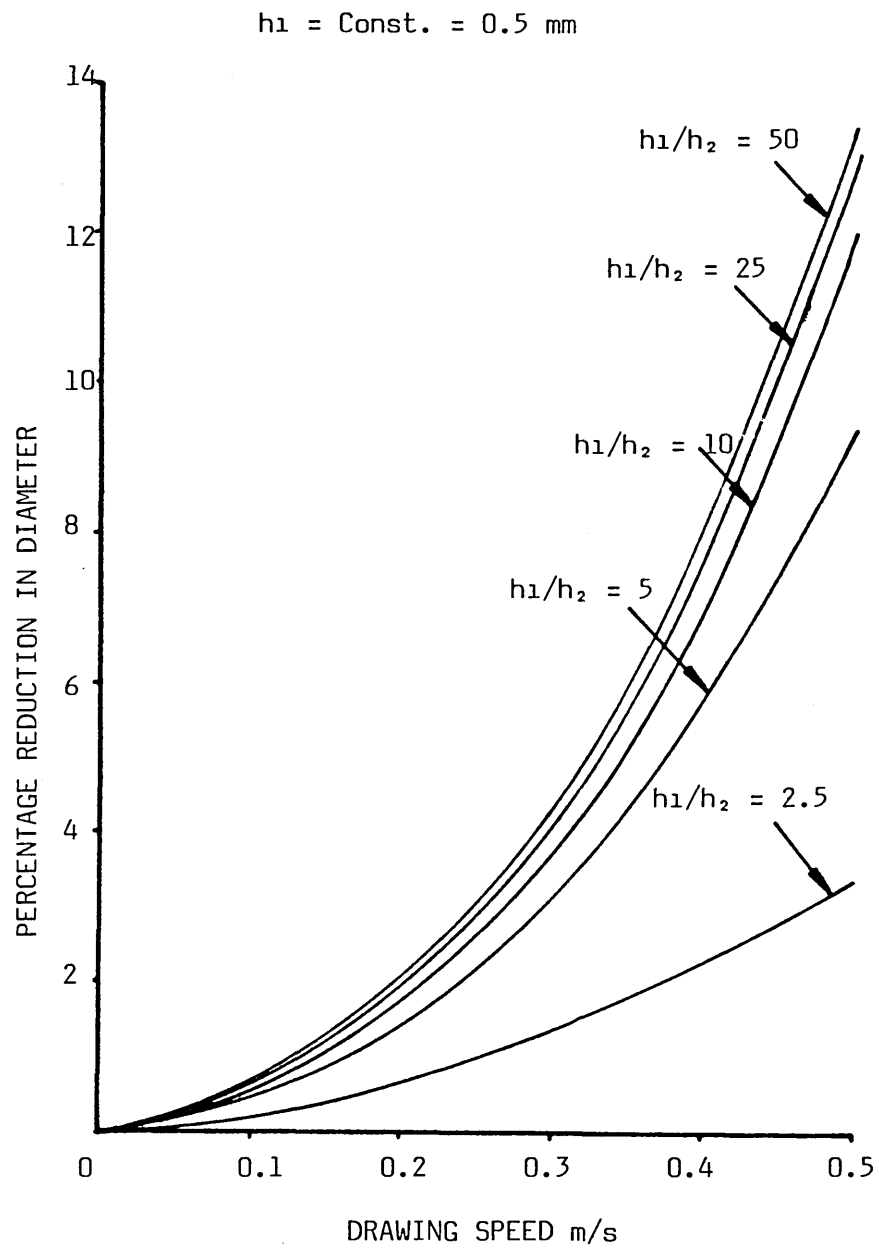


FIG 145(a) - THEORETICAL EFFECT OF GAP RATIO ON PERCENTAGE REDUCTION IN DIAMETER FOR ALUMINIUM TUBE

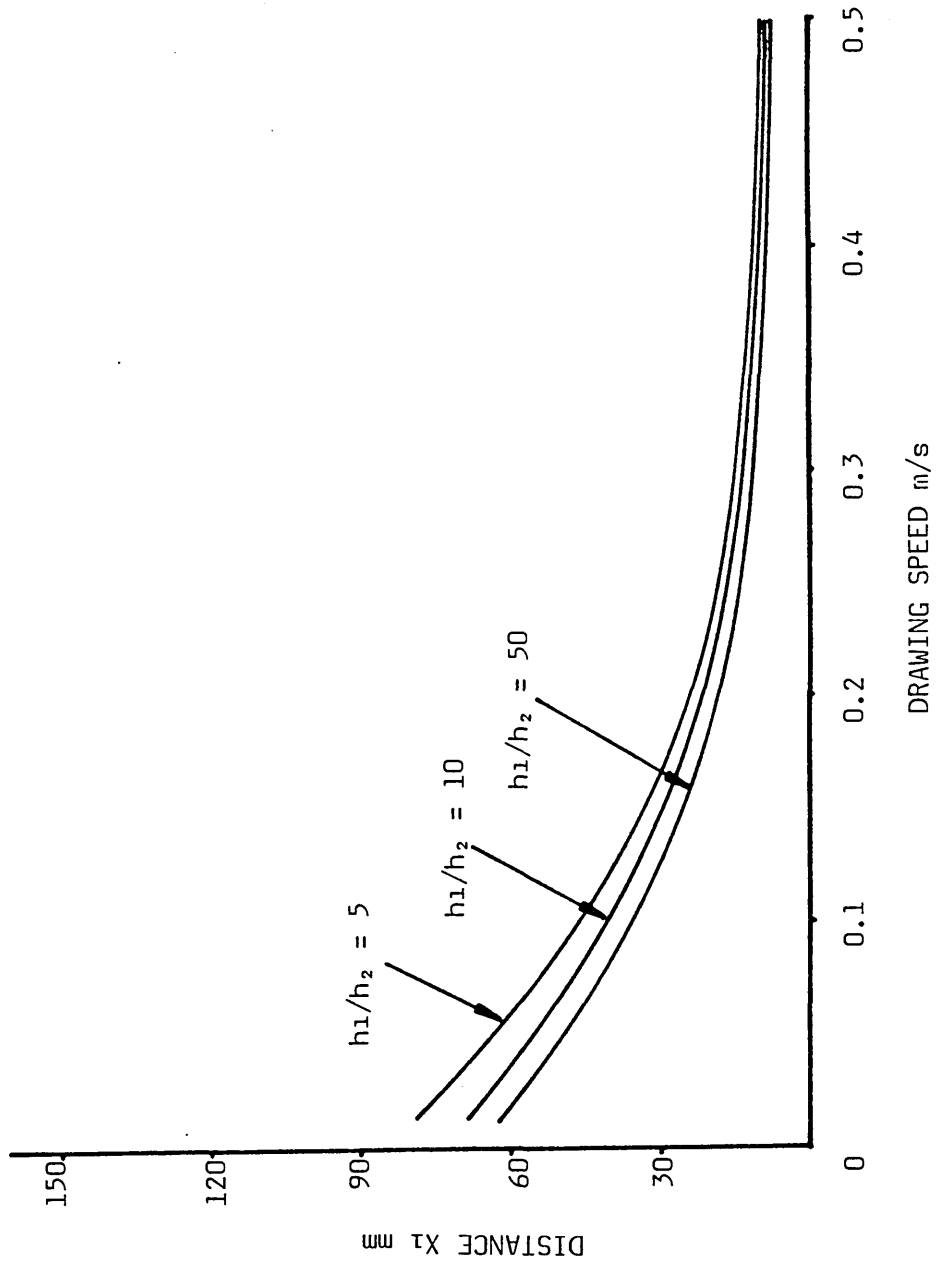


FIG 145(b) - THEORETICAL EFFECT OF GAP RATIO ON YIELDING POSITION OF ALUMINIUM TUBE

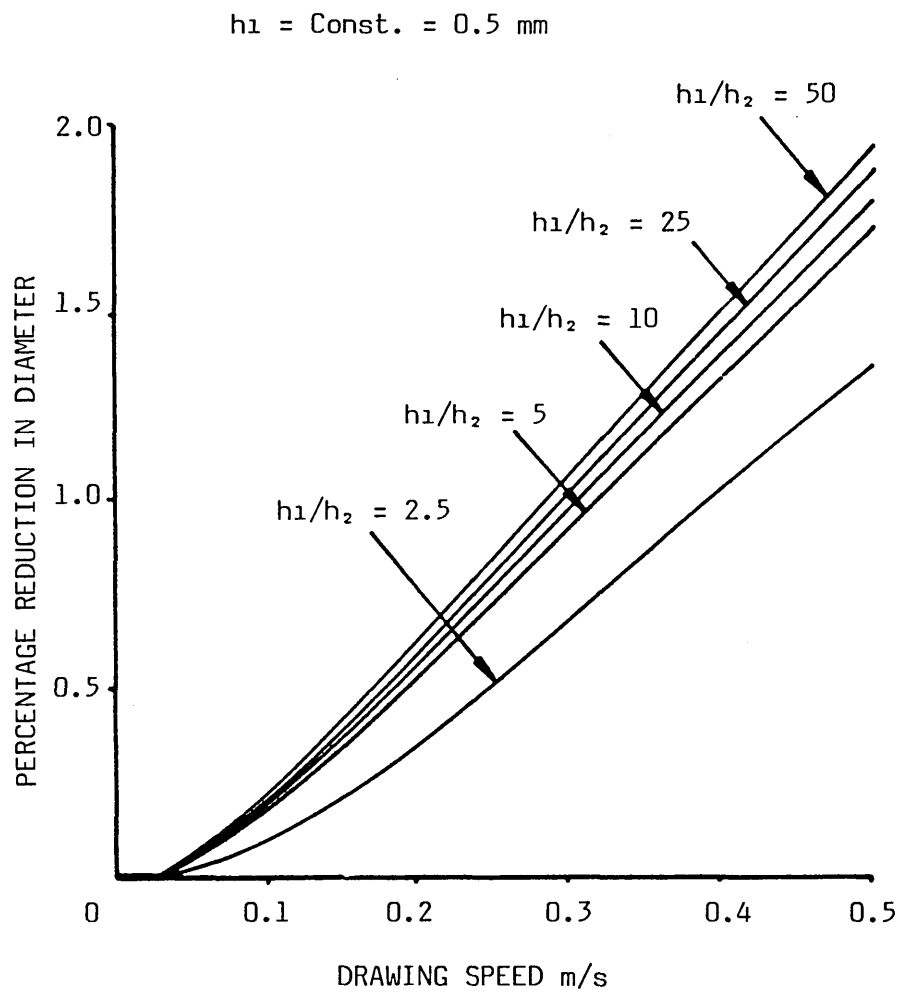


FIG 146(a) - THEORETICAL EFFECT OF GAP RATIO ON PERCENTAGE REDUCTION IN DIAMETER FOR COPPER TUBE

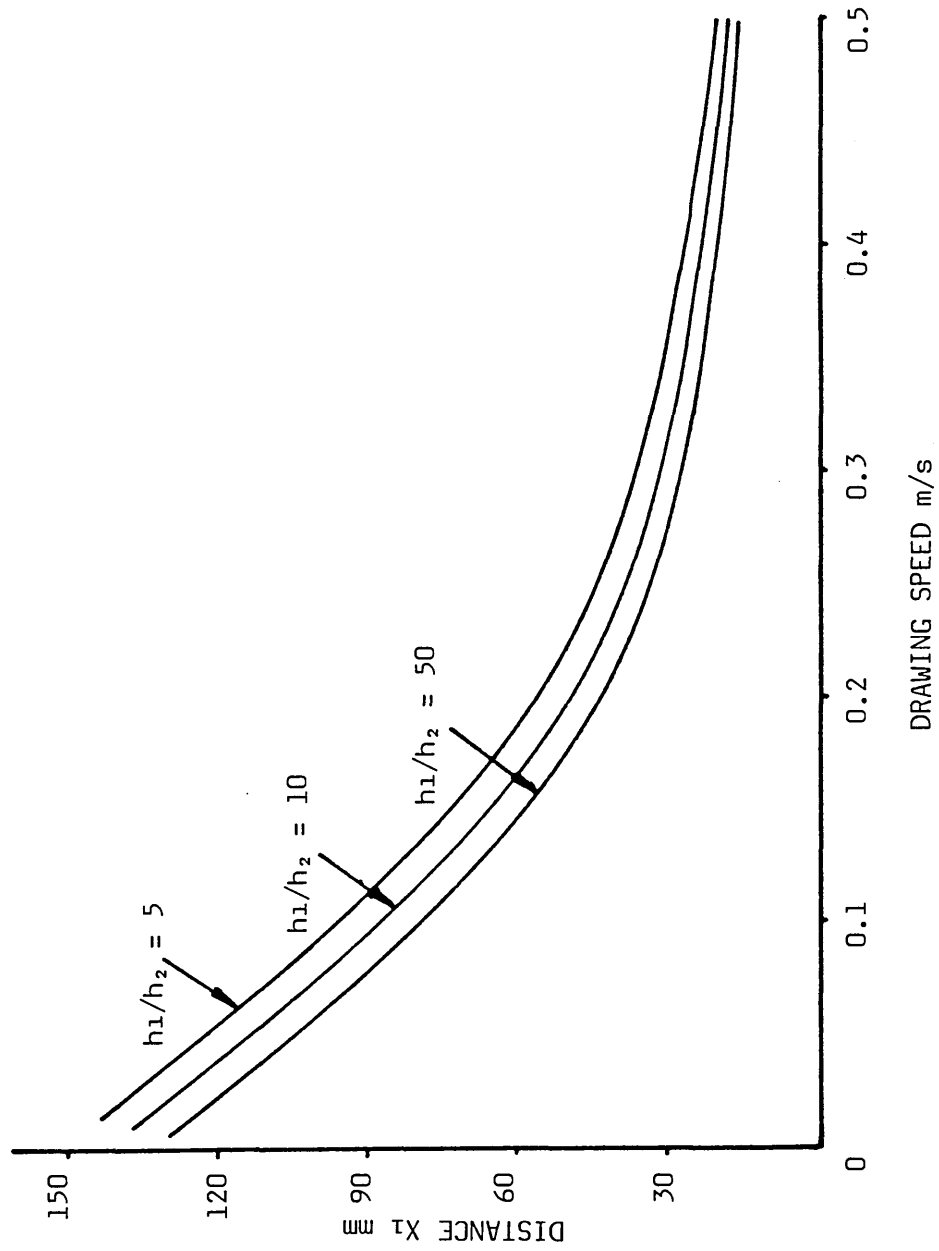


FIG 146(b) - THEORETICAL EFFECT OF GAP RATIO ON YIELDING POSITION OF COPPER TUBE

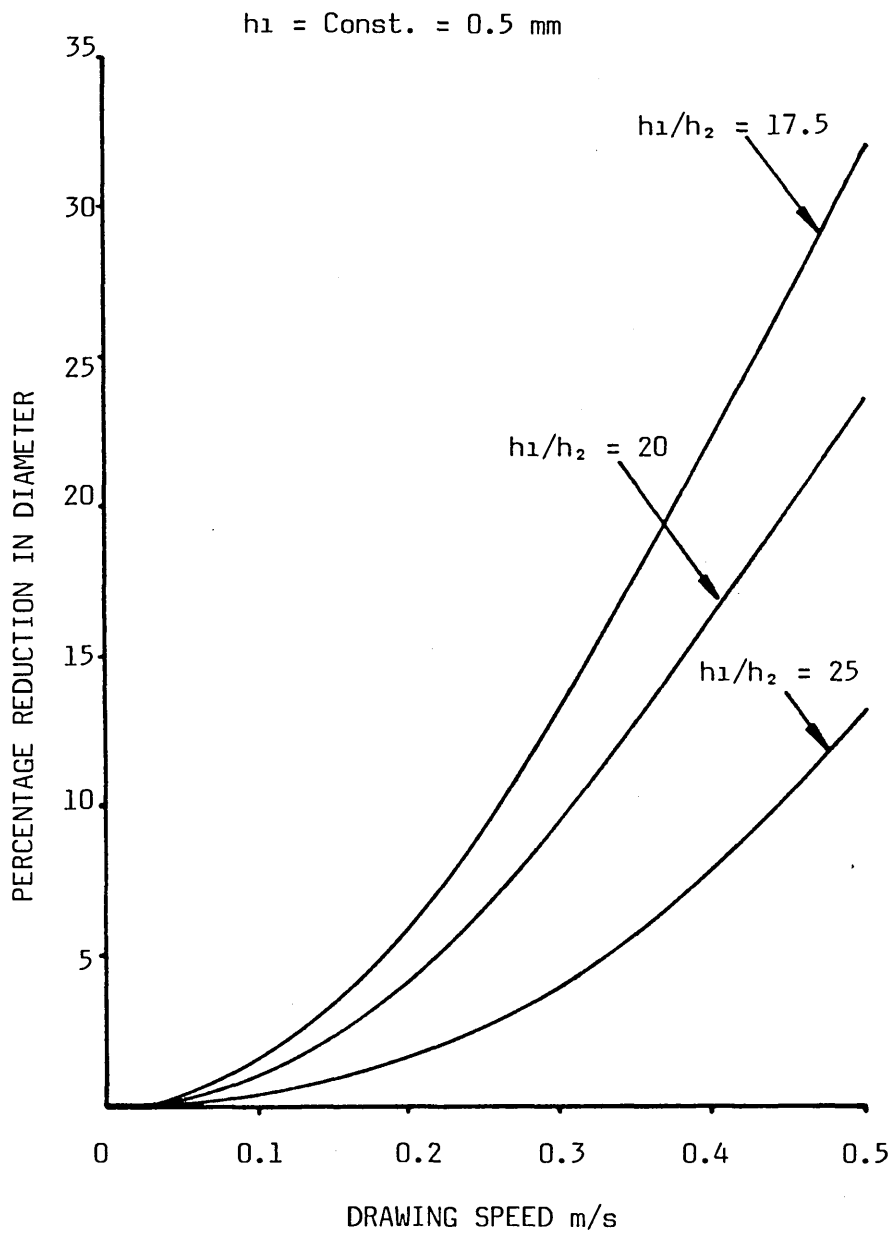


FIG 147 - THEORETICAL EFFECT OF GAP RATIO ON PERCENTAGE REDUCTION IN DIAMETER FOR ALUMINIUM TUBE

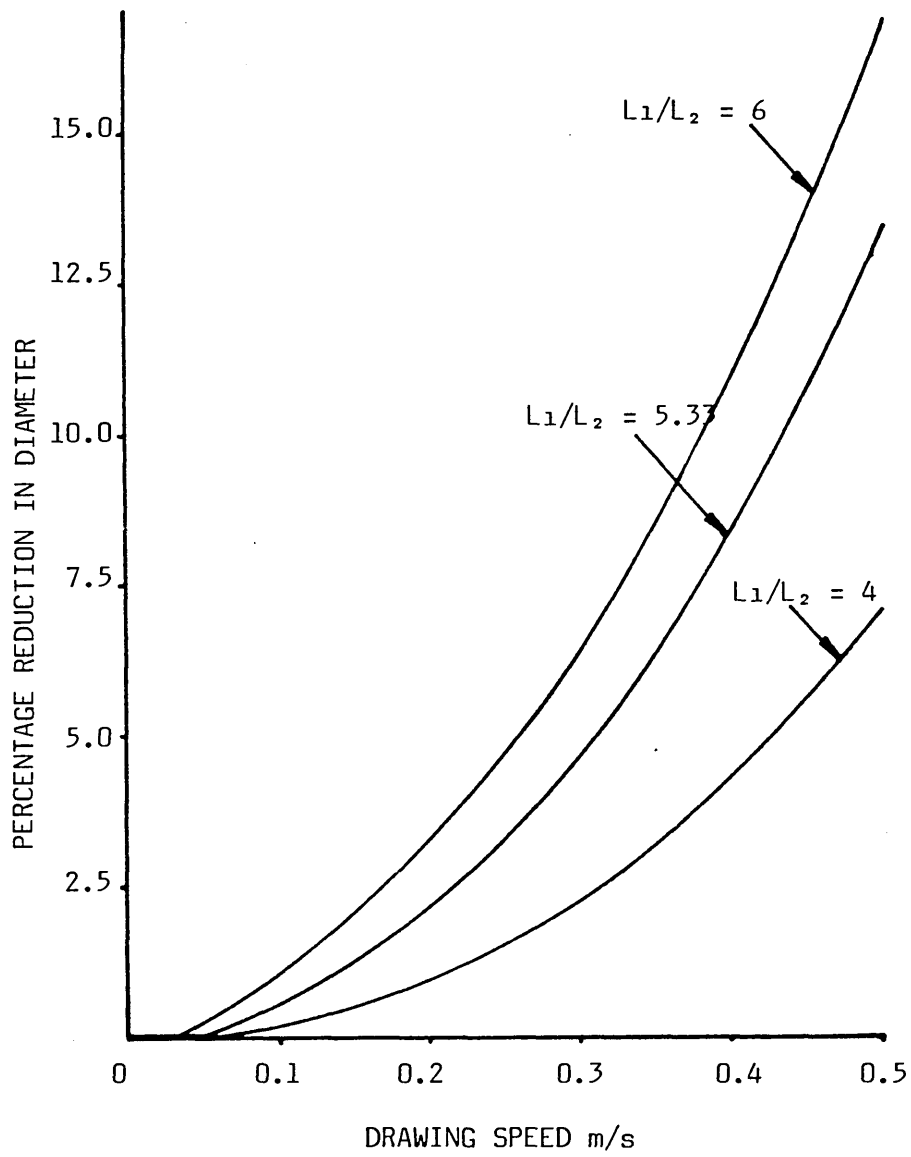


FIG 148(a) - THEORETICAL EFFECT OF LENGTH RATIO ON PERCENTAGE REDUCTION IN DIAMETER FOR ALUMINIUM TUBE

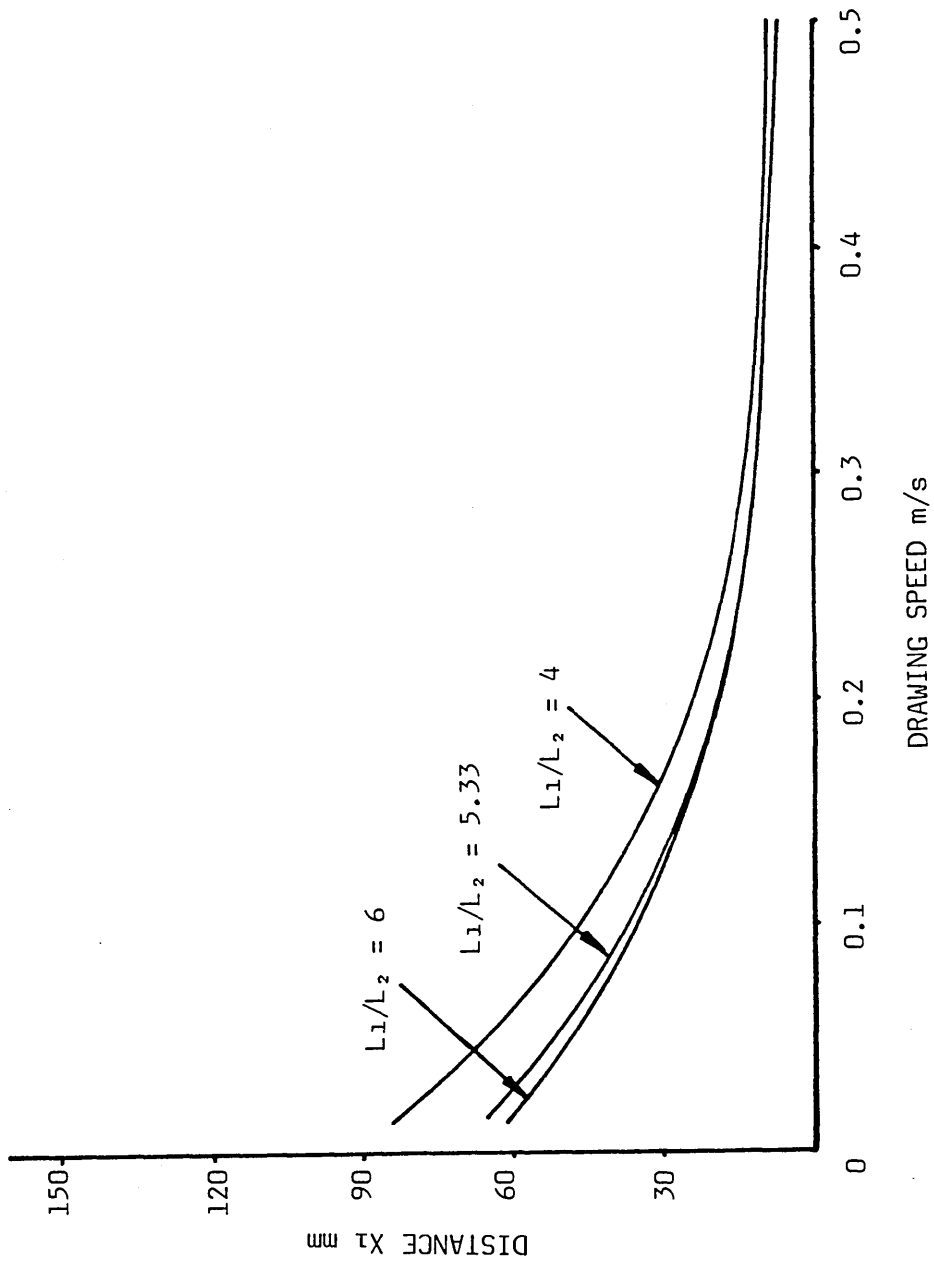


FIG 148(b) - THEORETICAL EFFECT OF LENGTH RATIO ON YIELDING POSITION OF ALUMINIUM TUBE

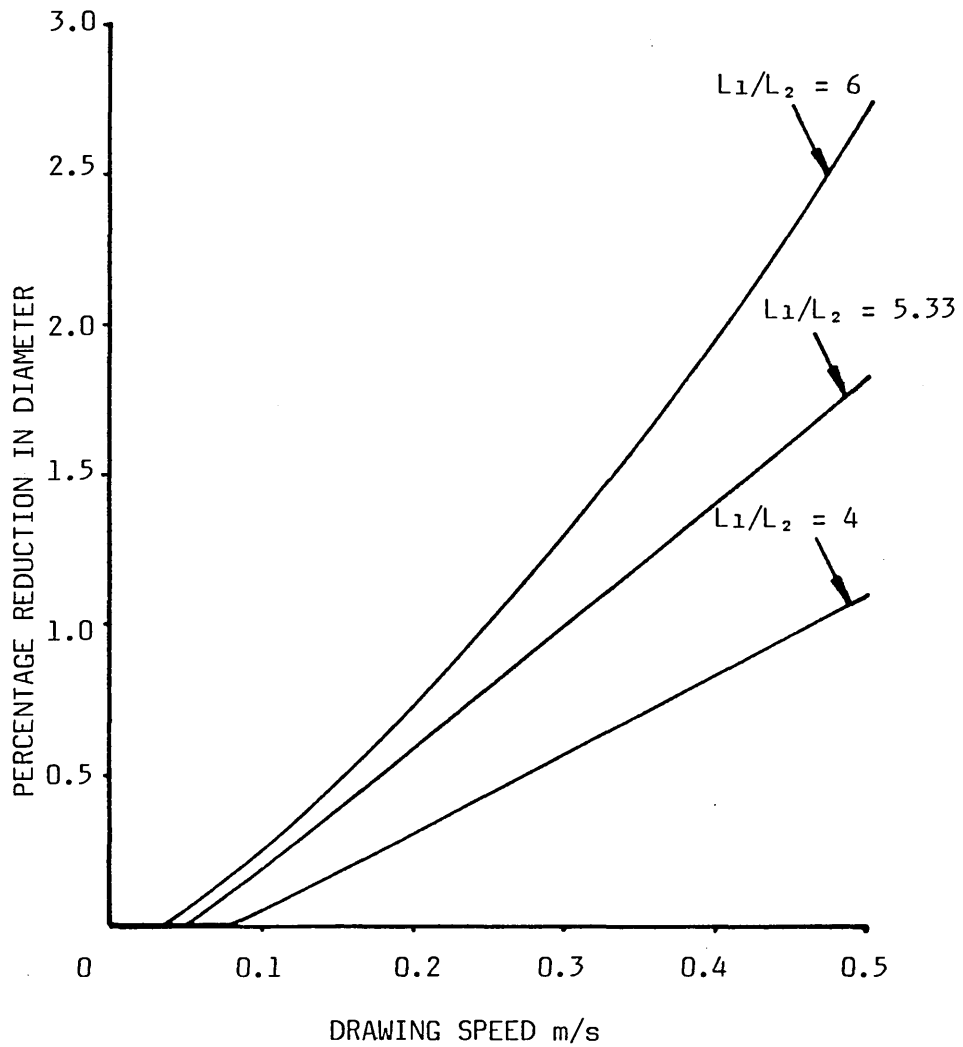


FIG 149(a) - THEORETICAL EFFECT OF LENGTH RATIO ON PERCENTAGE REDUCTION IN DIAMETER FOR COPPER TUBE

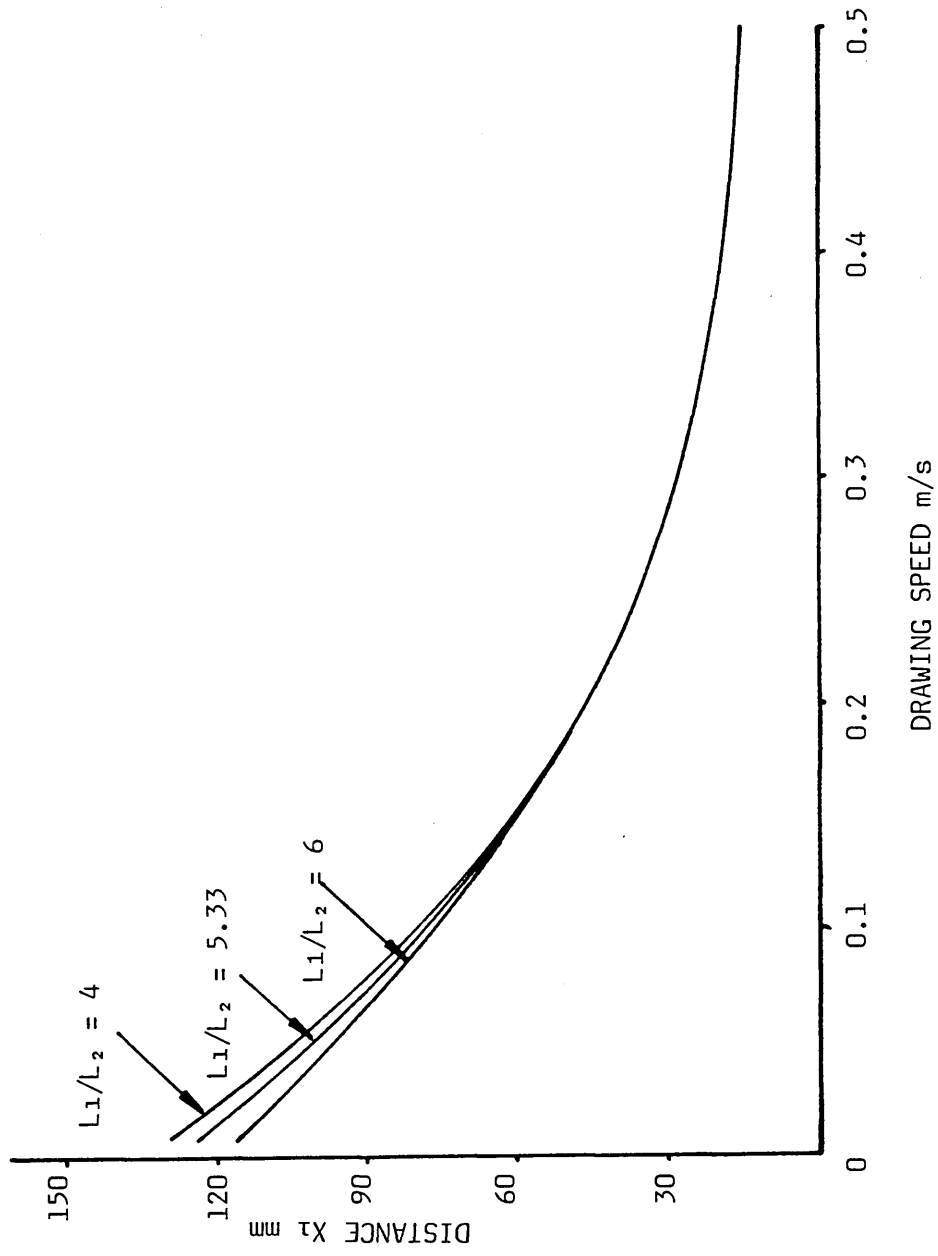


FIG 149(b) - THEORETICAL EFFECT OF LENGTH RATIO ON YIELDING POSITION OF COPPER TUBE

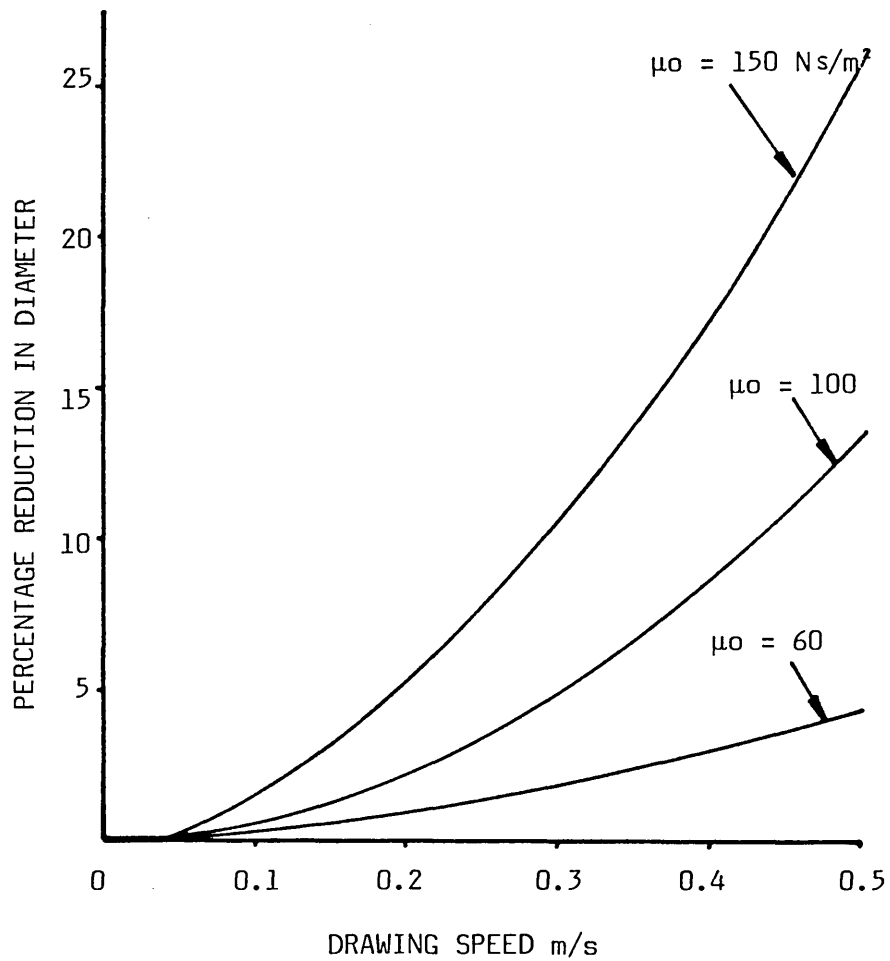


FIG 150(a) - THEORETICAL EFFECT OF VISCOSITY ON PERCENTAGE REDUCTION IN DIAMETER FOR ALUMINIUM TUBE

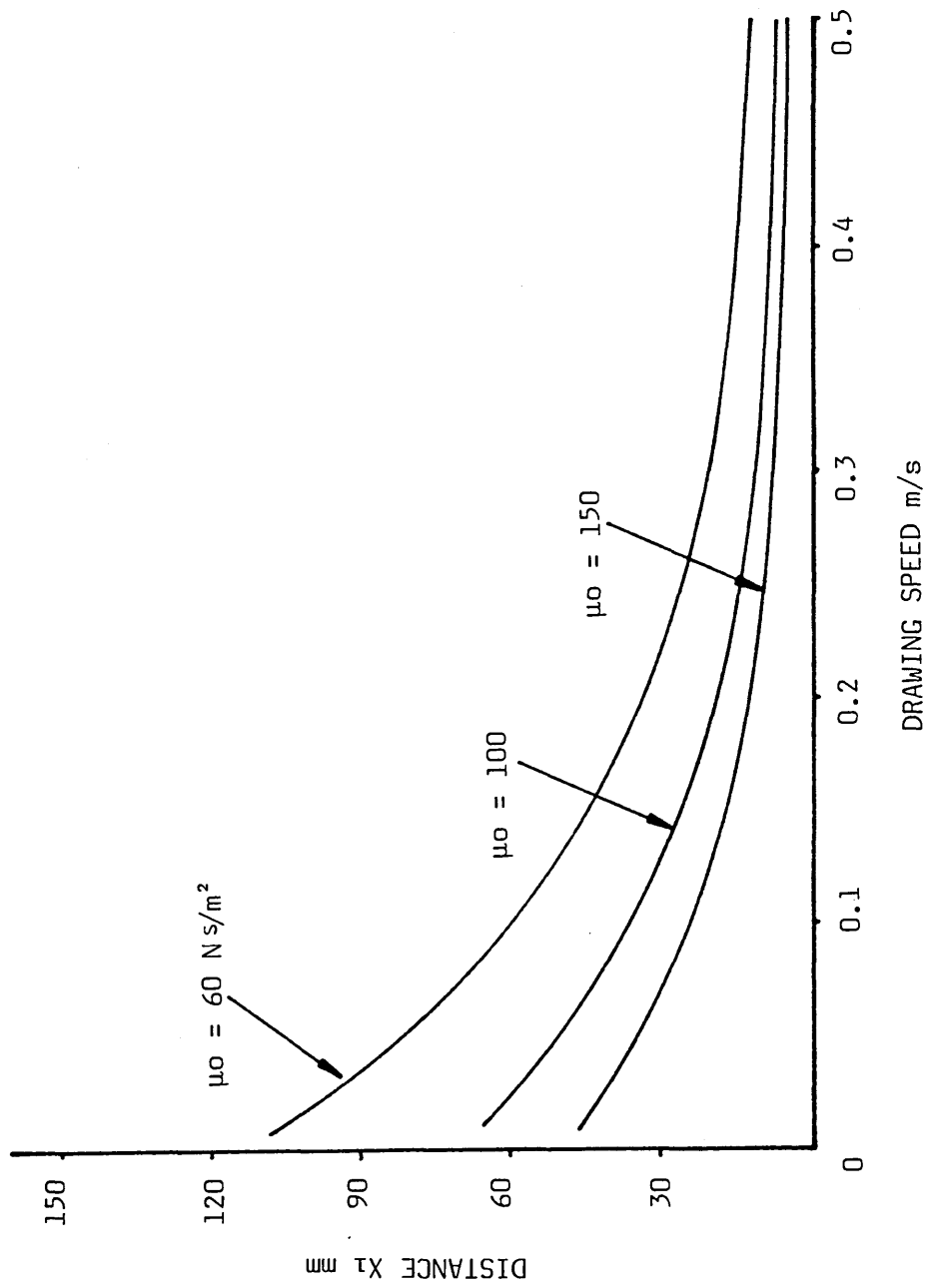


FIG 150(b) - THEORETICAL EFFECT OF VISCOSITY ON YIELDING POSITION OF ALUMINIUM TUBE

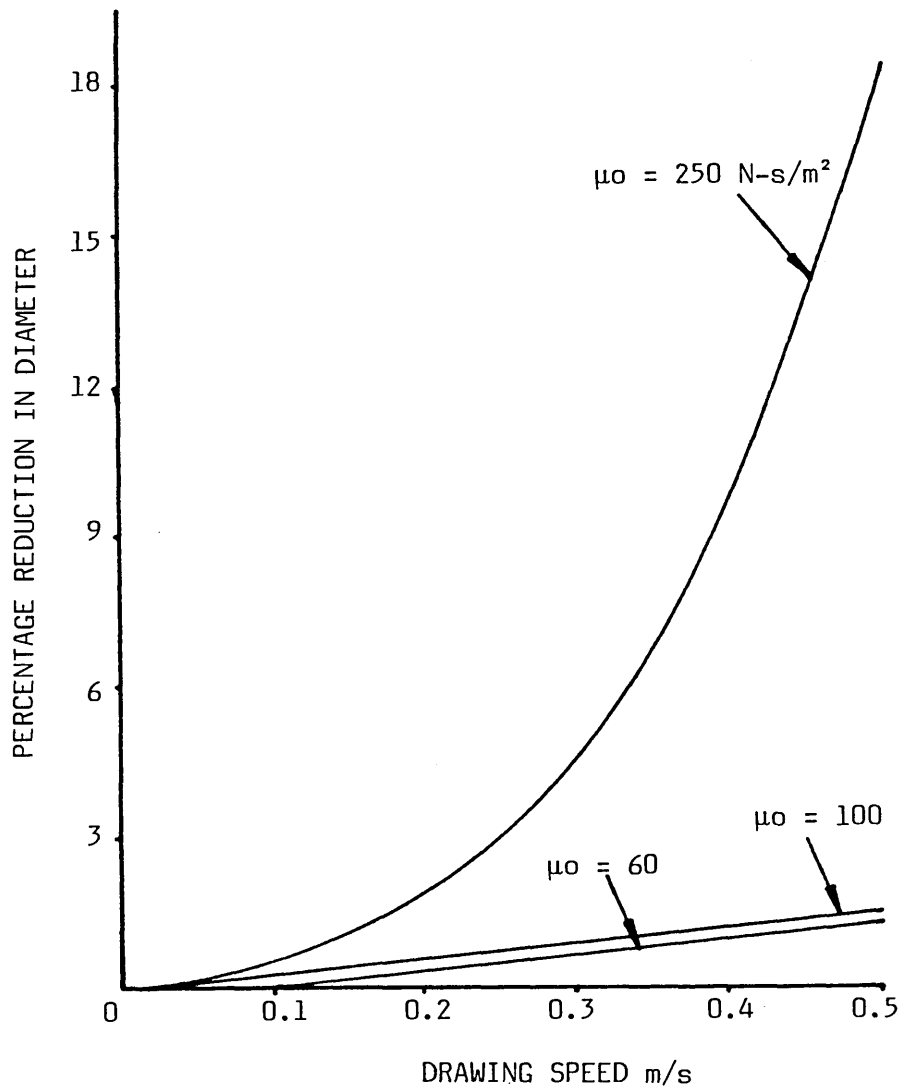


FIG 151(a) - THEORETICAL EFFECT OF VISCOSITY ON PERCENTAGE REDUCTION IN DIAMETER FOR COPPER TUBE

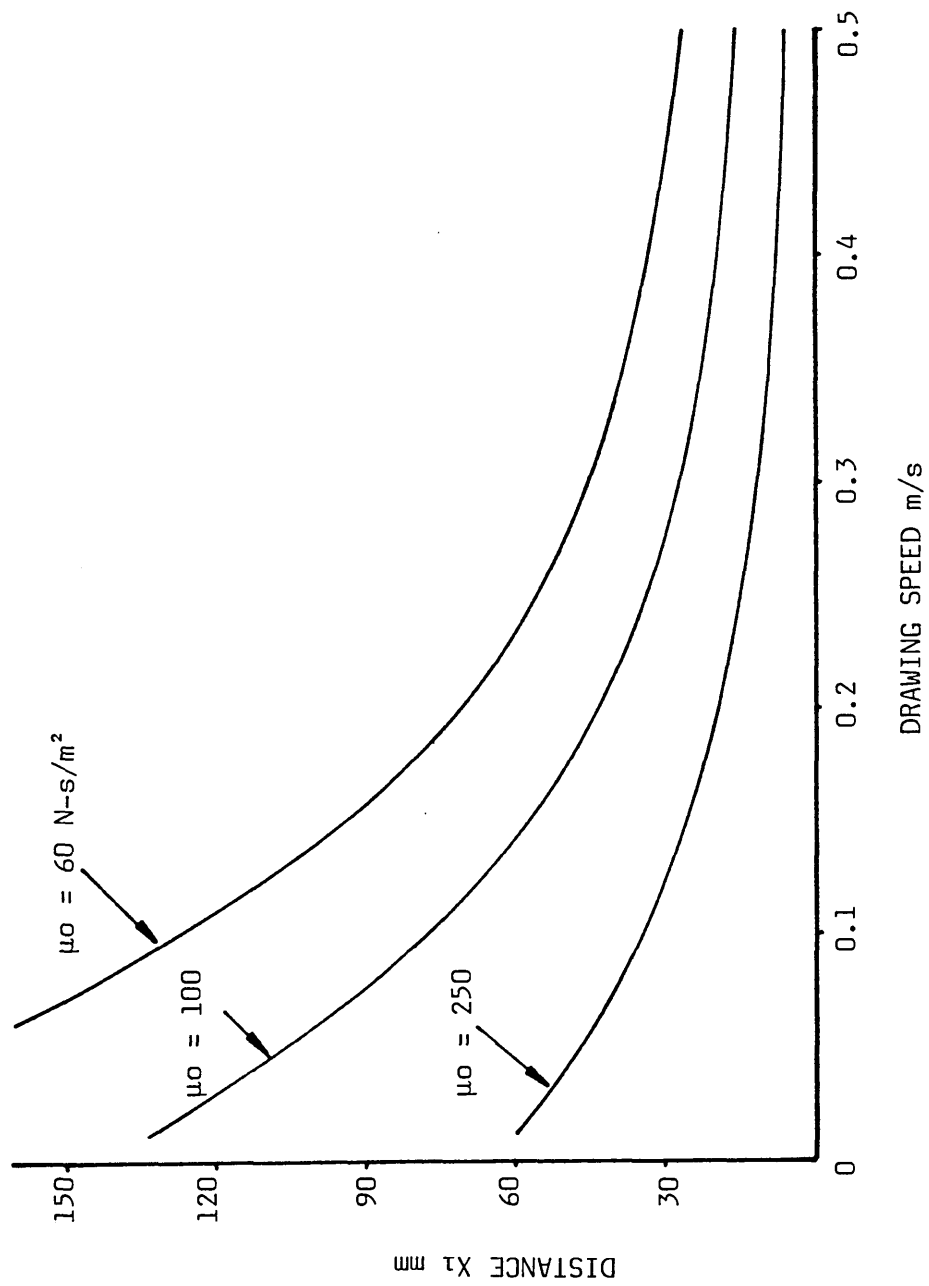


FIG 151(b) - THEORETICAL EFFECT OF VISCOSITY ON YIELDING POSITION OF COPPER TUBE

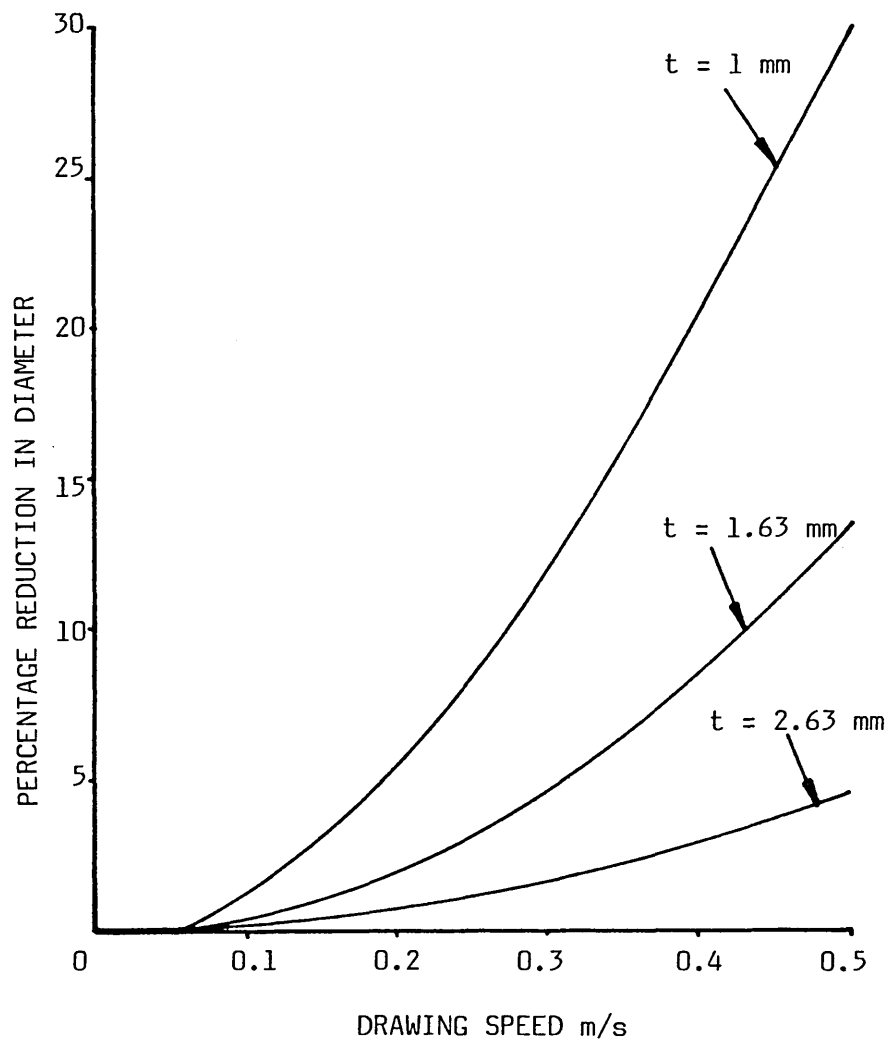


FIG 152 - THEORETICAL EFFECT OF TUBE-WALL THICKNESS ON PERCENTAGE REDUCTION IN DIAMETER FOR ALUMINIUM TUBE

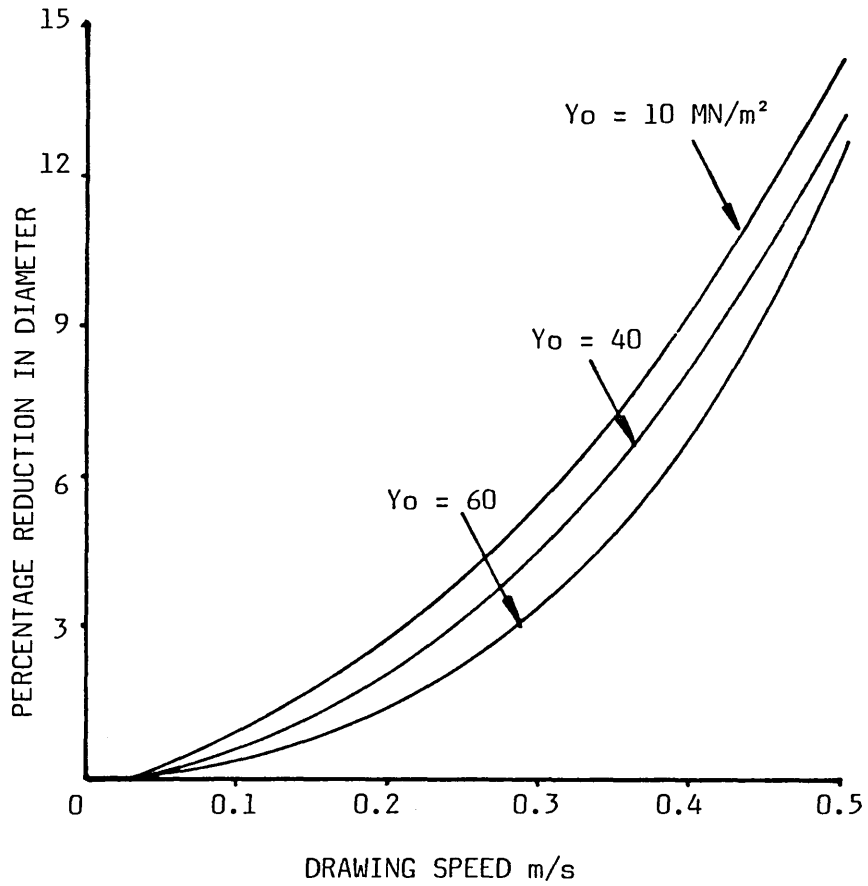


FIG 153(a) - THEORETICAL EFFECT OF INITIAL YIELD STRESS ON PERCENTAGE REDUCTION IN DIAMETER FOR ALUMINIUM TUBE

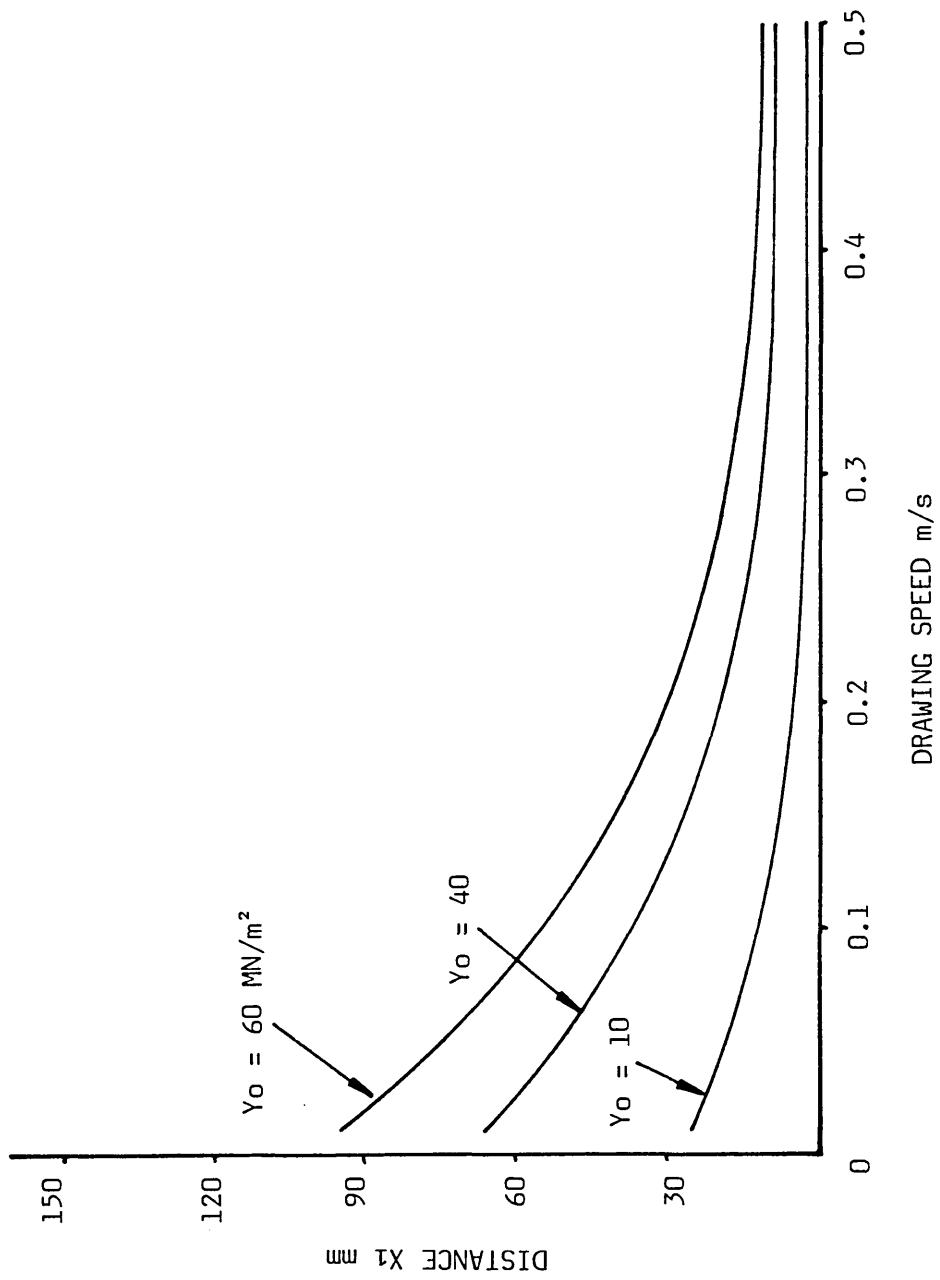


FIG 153(b) - THEORETICAL EFFECT OF INITIAL YIELD STRESS ON YIELDING POSITION OF ALUMINIUM TUBE

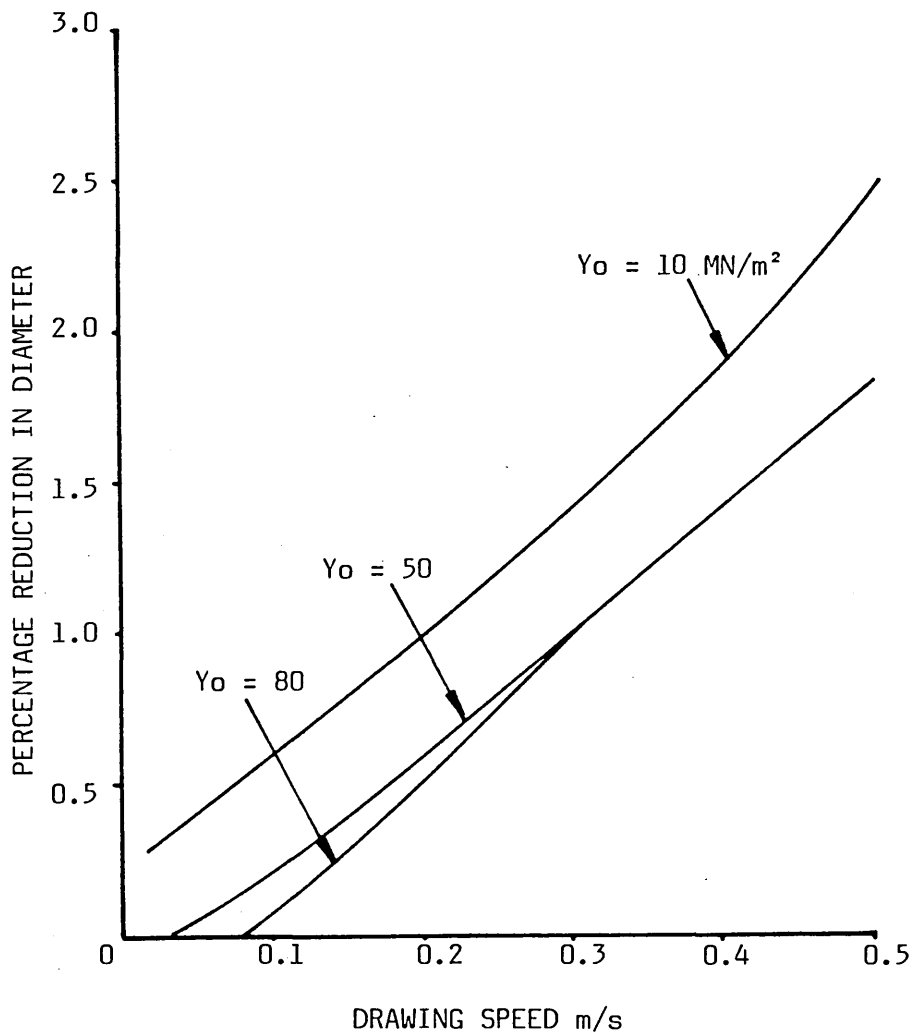


FIG 154(a) - THEORETICAL EFFECT OF INITIAL YIELD STRESS ON PERCENTAGE REDUCTION IN DIAMETER FOR COPPER TUBE

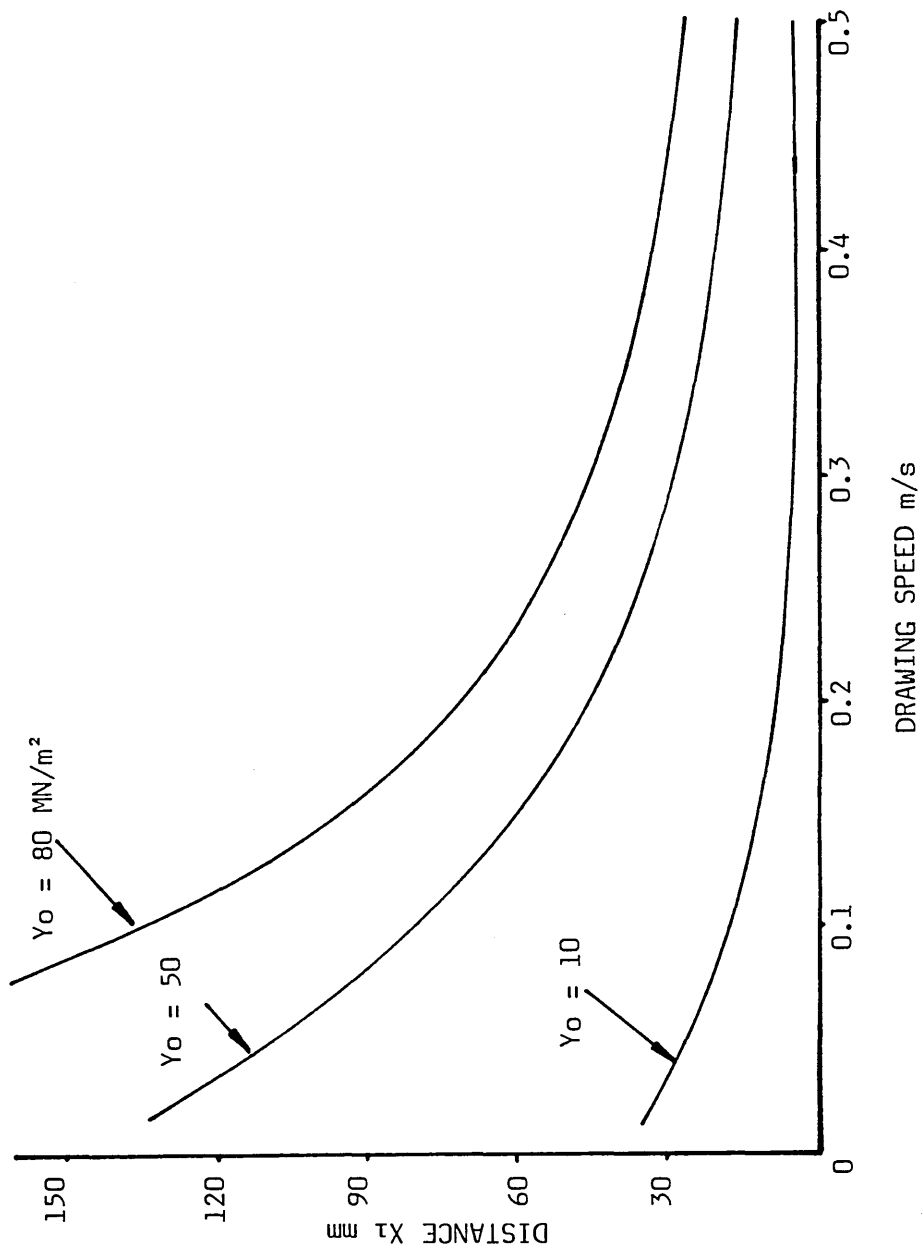


FIG 154(b) - THEORETICAL EFFECT OF INITIAL YIELD STRESS ON YIELDING POSITION OF COPPER TUBE

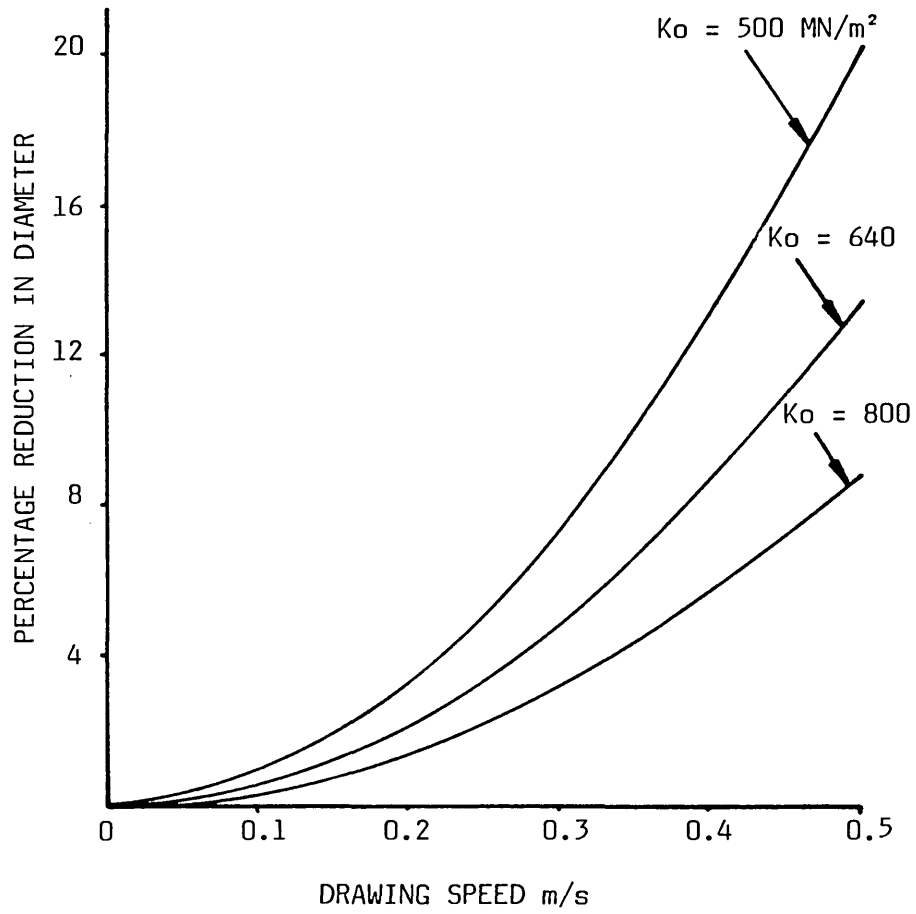
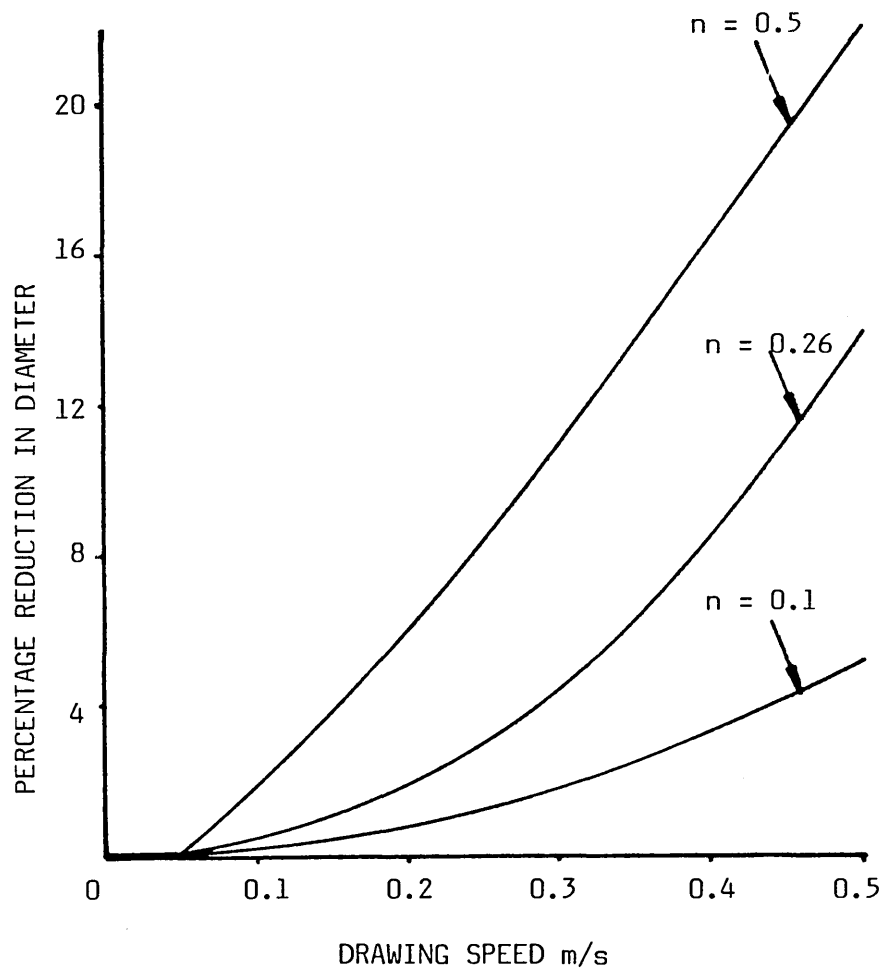


FIG 155 - THEORETICAL EFFECT OF STRAIN HARDENING CONSTANT ON PERCENTAGE REDUCTION IN DIAMETER FOR ALUMINIUM TUBE



**FIG 156 - THEORETICAL EFFECT OF STRAIN HARDENING INDEX ON
PERCENTAGE REDUCTION IN DIAMETER FOR ALUMINIUM TUBE**

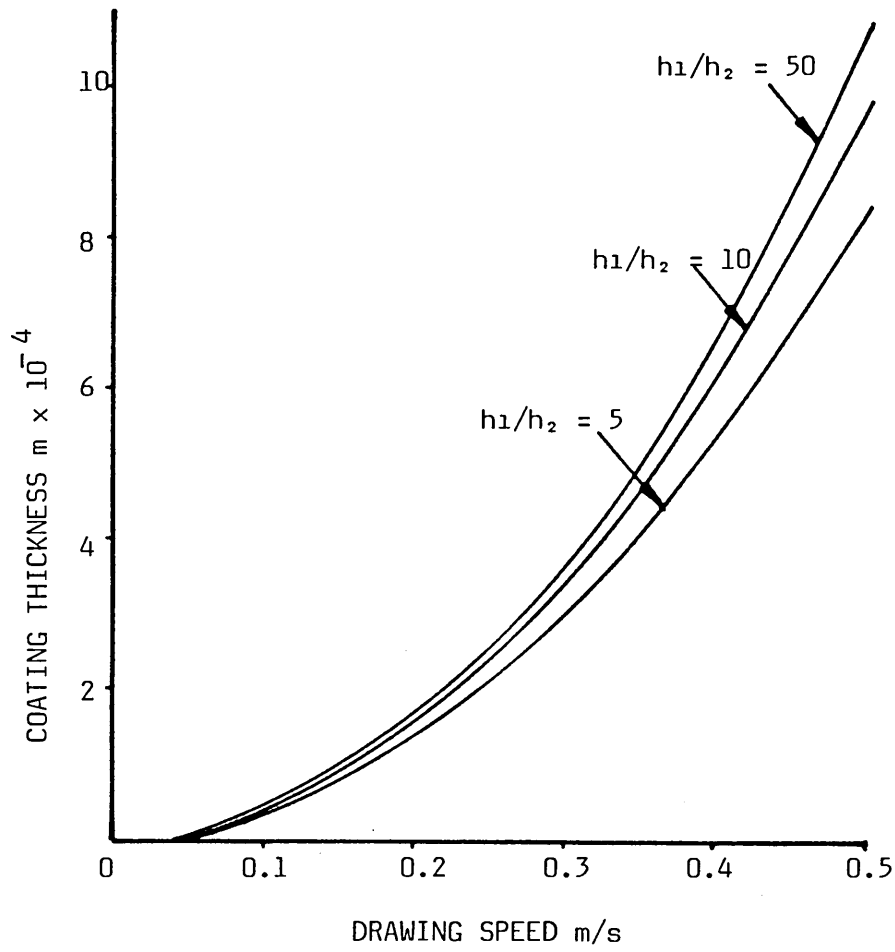


FIG 157 - THEORETICAL EFFECT OF GAP RATIO ON COATING THICKNESS FOR ALUMINIUM TUBE

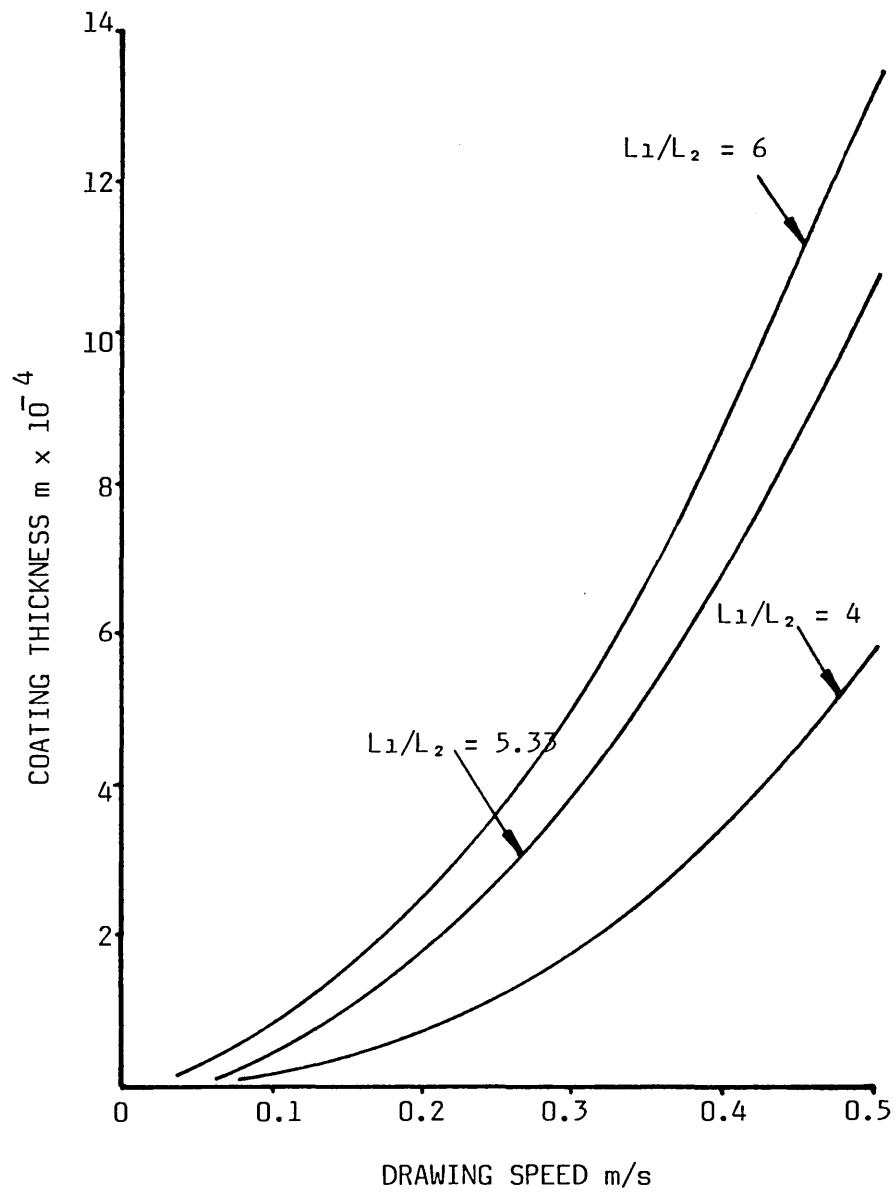


FIG 158 - THEORETICAL EFFECT OF LENGTH RATIO ON COATING THICKNESS FOR ALUMINIUM TUBE

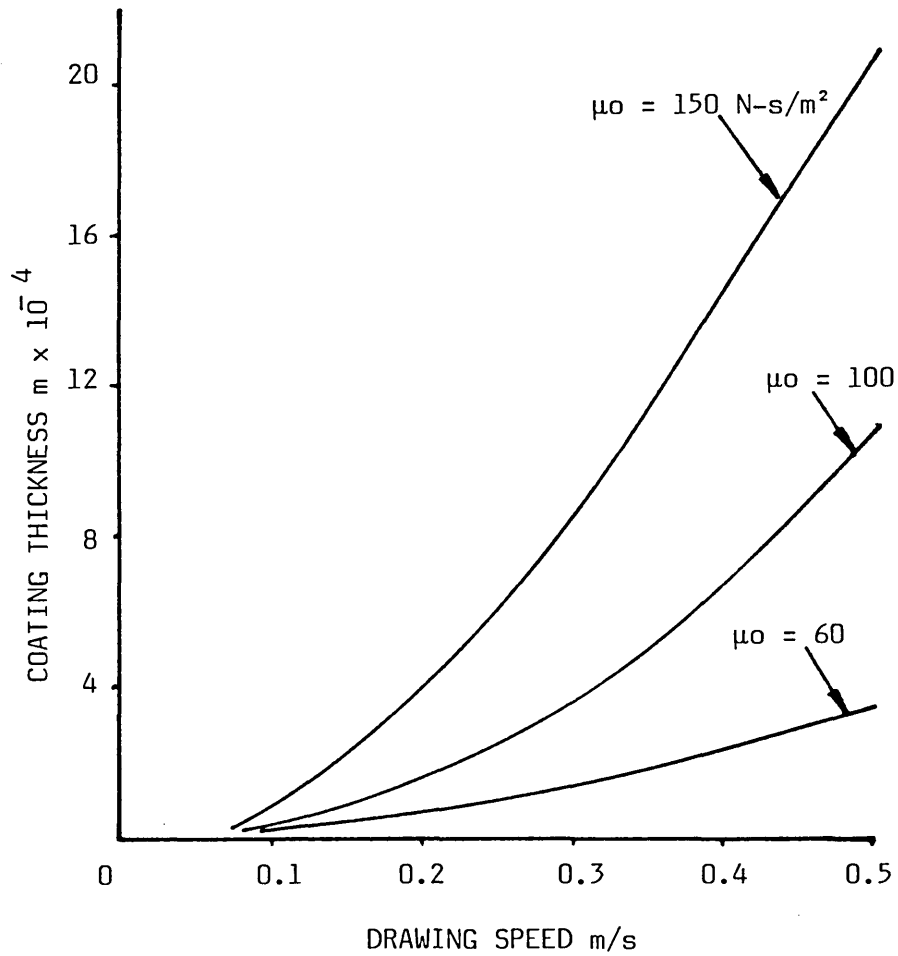


FIG 159 - THEORETICAL EFFECT OF VISCOSITY ON COATING THICKNESS FOR ALUMINIUM TUBE

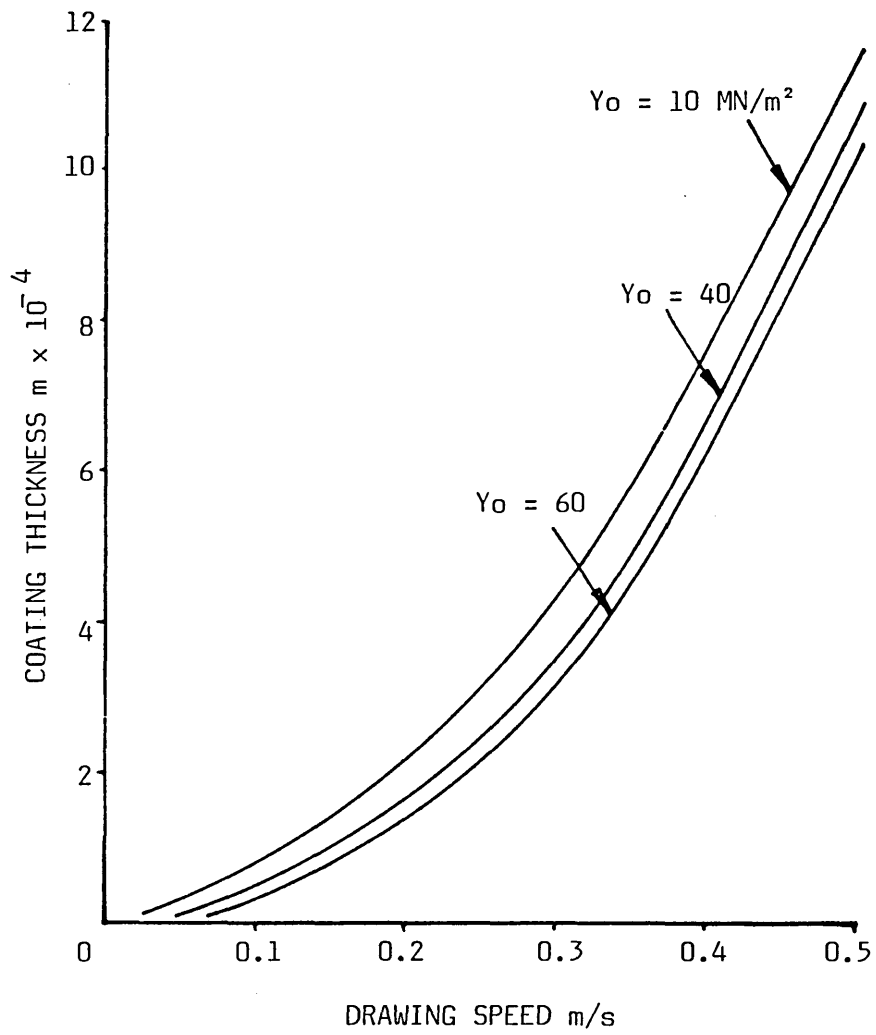


FIG 160 - THEORETICAL EFFECT OF INITIAL YIELD STRESS ON COATING THICKNESS FOR ALUMINIUM TUBE

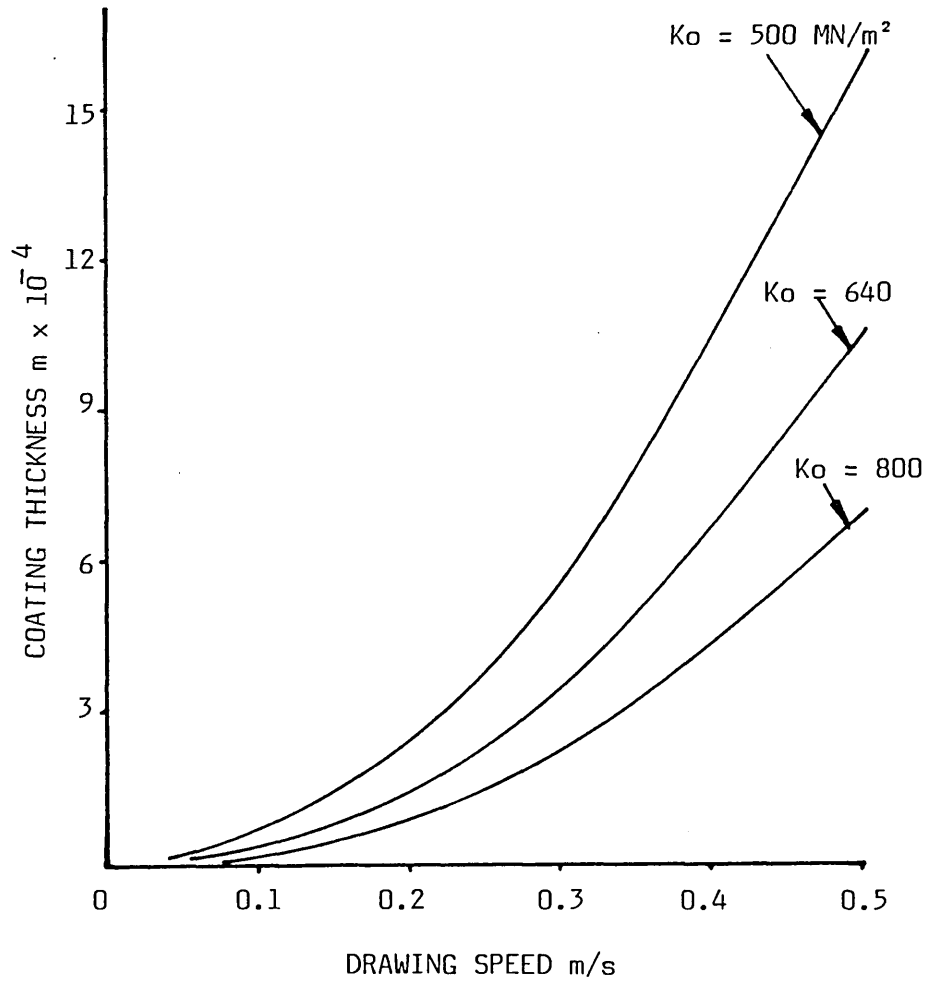


FIG 161 - THEORETICAL EFFECT OF STRAIN HARDENING CONSTANT ON COATING THICKNESS FOR ALUMINIUM TUBE

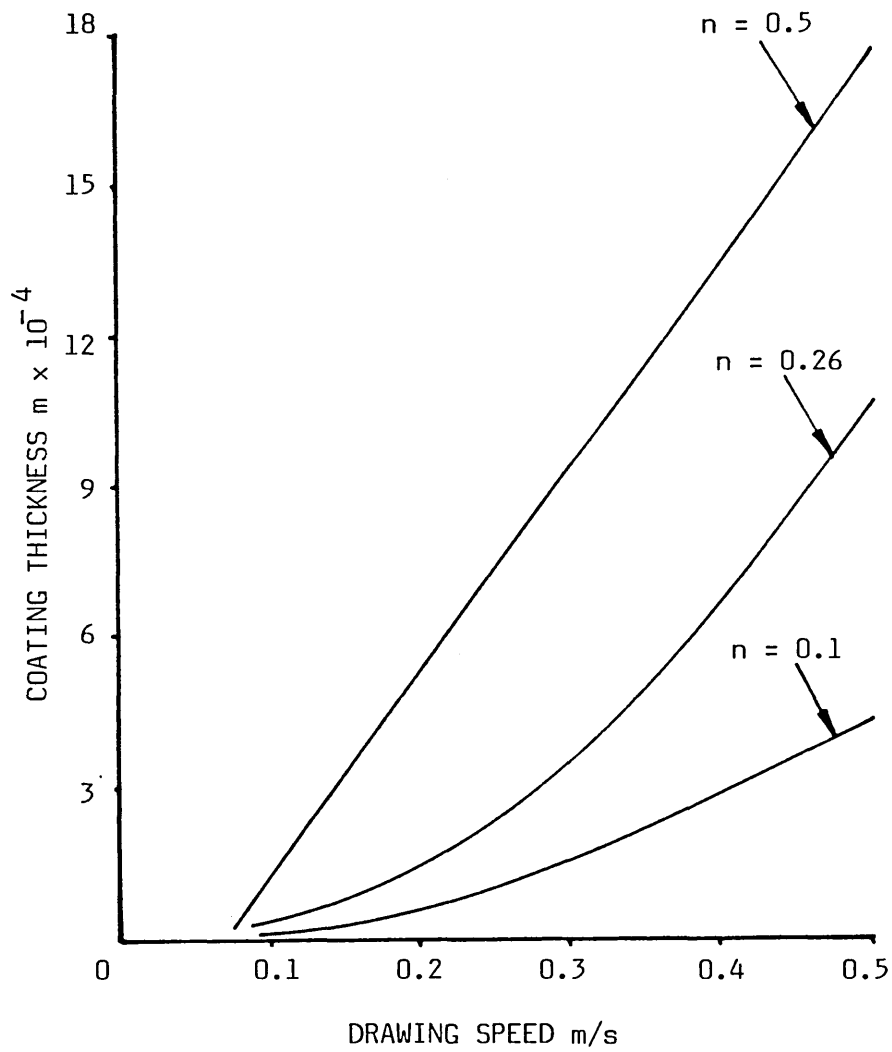


FIG 162 - THEORETICAL EFFECT OF STRAIN HARDENING INDEX ON COATING THICKNESS FOR ALUMINIUM TUBE

5.3.3 Numerical Solution

This analysis produced results which are in better agreement with the experimental results in comparison with those predicted on the basis of assumed linear and curved deformation profiles.

The theoretical percentage reduction in diameter was calculated using equation (5.4C). Figs (163a) and (b) show the effect of gap ratio on percentage reduction in diameter and yielding position of the copper tubes. This figure indicates that the reduction in diameter increases with the drawing speed at a greater rate and reaches a magnitude of about 17 per cent corresponding to a drawing speed of 1.0 m/s and a gap ratio of 50. As the gap ratio is decreased, plastic deformation commences further away from the entry side of the unit and lower percentage reduction in diameter is predicted for a given drawing speed.

The effect of gap ratio on percentage reduction in diameter and yielding position of the aluminium tubes with drawing speed is demonstrated in Figs (164a) and (b). This figure indicates that for higher value of h_1/h_2 plastic deformation commences further away from the step, for a given drawing speed and greater percentage reduction in diameter should be obtained. A maximum reduction in diameter was predicted (about 28%) for the gap ratio of 50 at 1.0 m/s.

Fig (165) shows the variations in percentage reduction in diameter with the drawing speed for copper tubes for different values of L_1/L_2 . This figure suggests that for higher values of L_1/L_2 greater percentage reduction in diameter should be obtained at higher drawing speeds. With a length ratio of 6, the reduction in diameter of about 20 per cent should be obtained for the drawing speed of 1 m/s.

The effect of viscosity on the percentage reduction in diameter and yielding position of the copper tubes is shown in Fig (166a) and (b) respectively. It is evident from this figure that higher viscosity should initiate deformation further away from the step of the die-less reduction unit and should cause greater percentage reduction diameter. With a viscosity of 130 Ns/m^2 , the reduction in diameter of about 25 per cent should be obtained for the drawing speed of 1.0 m/s .

Figs (167a) and (b) show the effect of viscosity on percentage reduction in diameter and yielding position of the aluminium tubes. The general trends of the results were found to be the same as those in Fig (166). The amount of reduction in the aluminium tube was predicted to be higher in a comparison with that in the copper tube with the same viscosity (130 Ns/m^2).

The effect of the initial yield stress, Y_0 , of the tube material on the percentage reduction in diameter and yielding position x_1 of the copper tubes is shown in Figs (168a) and (b) respectively. Calculations were carried out with different values of initial yield stress ' Y_0 ' varying from 30 to 70 MN/m^2 . This figure shows that for lower values of Y_0 relatively greater permanent deformation could be obtained.

Figs (169a) and (b) show the effect of the initial yield stress on percentage reduction in diameter and yielding position of the aluminium tube. Calculations were carried out for this tube material with different values of Y_0 varying from 22 to 60 MN/m^2 . This figure shows similar trends as in Fig (168) for copper tubes.

The effect of strain hardening constant on percentage reduction in diameter for copper tubes with drawing speed is demonstrated in

Fig (170). This figure indicates that lower values of K_0 cause greater percentage reduction in diameter of the tube. With a strain hardening factor of 500 MN/m^2 , the percentage reduction in diameter predicted was about 28 per cent for the drawing speed of 1.0 m/s .

Fig (171) shows the effect of strain hardening index 'n' on the percentage reduction in diameter for copper tubes with drawing speed. This figure suggests that with a strain hardening index 'n' of 0.6, the reduction in diameter of about 19 per cent should be obtained for the drawing speed of 1.0 m/s .

The effects of changes in the wall-thickness on the percentage reduction in diameter and yielding position x , of the copper tube is demonstrated in Figs (172a) and (b). The wall-thickness of the copper tube was varied from 2.00 to 2.50mm. For a drawing speed of 1.0 m/s , this figure shows that permanent reduction in diameter of about 24 per cent could be obtained in a tube of 2.00mm wall-thickness, but for higher value of tube wall-thickness (2.50mm) only 16 per cent reduction in diameter may take place at the same drawing speed, ie 1.0 m/s .

Figs (173a) and (b) show the effect of changing the diameter on the percentage reduction in diameter and yielding position of the copper tube. This figure indicates that for higher values of D_1 relatively greater permanent deformation should be obtained, but the percentage reduction in diameter decreases for lower values of D_1 .

Fig (174) shows the effect of strain rate sensitivity index, T , of the tube material on the percentage reduction in diameter for copper tube. This figure shows that lower values of 'T' cause greater percentage reduction in diameter at higher drawing speed.

The effect of strain rate sensitivity constant, N , on percentage reduction in diameter with drawing speed for copper tube is demonstrated in Fig (175). This figure suggests that with a strain rate sensitivity constant ' N ' value of 125×10^3 , the reduction in diameter of about 17 per cent should be obtained for the drawing speed of 1.0 m/s.

The coating thickness was calculated by using equation (5.18C). Fig (176) shows the effect of gap ratio on coating thickness for copper tubes. This figure shows that for higher values of gap ratio relatively greater coating thickness should be obtained.

The effect of length ratio on coating thickness for copper tubes is demonstrated in Fig (177). This figure suggests that as the length ratio is increased, the coating thickness is also increased. The maximum coating thickness obtained for a length ratio of 6 at 1 m/s.

Fig (178) shows the effect of viscosity on the coating thickness for copper tubes with drawing speed. This figure suggests that higher viscosity should cause greater coating thickness.

Fig (179) shows the effect of the initial yield stress, Y_0 , on the coating thickness for copper tube. The trends of the results obtained are similar to those of the percentage reduction in diameter (see Fig (168a)). This figure suggests that lower values of Y_0 , cause greater coating thickness.

The effect of tube wall-thickness on the coating thickness for copper tube is shown in Fig (180). This figure indicates that higher coating thickness should be obtained at lower values of tube wall-thickness and higher values of ' t ', caused smaller coating thickness.

Theoretically calculated deformation profiles for copper tube at different drawing speeds are shown in Fig (181). This figure shows that the theoretically predicted deformation profiles have close similarity with those observed experimentally (shown in Fig (111)).

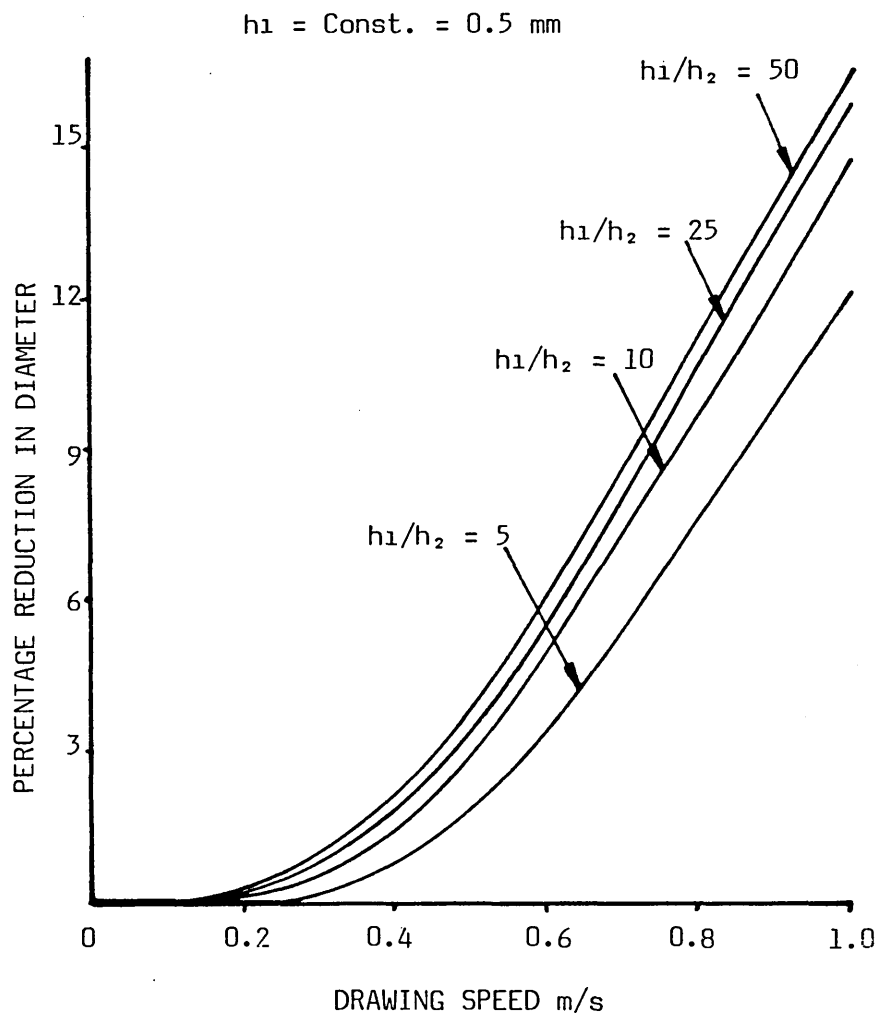


FIG 163(a) - THEORETICAL EFFECT OF GAP RATIO ON PERCENTAGE REDUCTION IN DIAMETER FOR COPPER TUBE

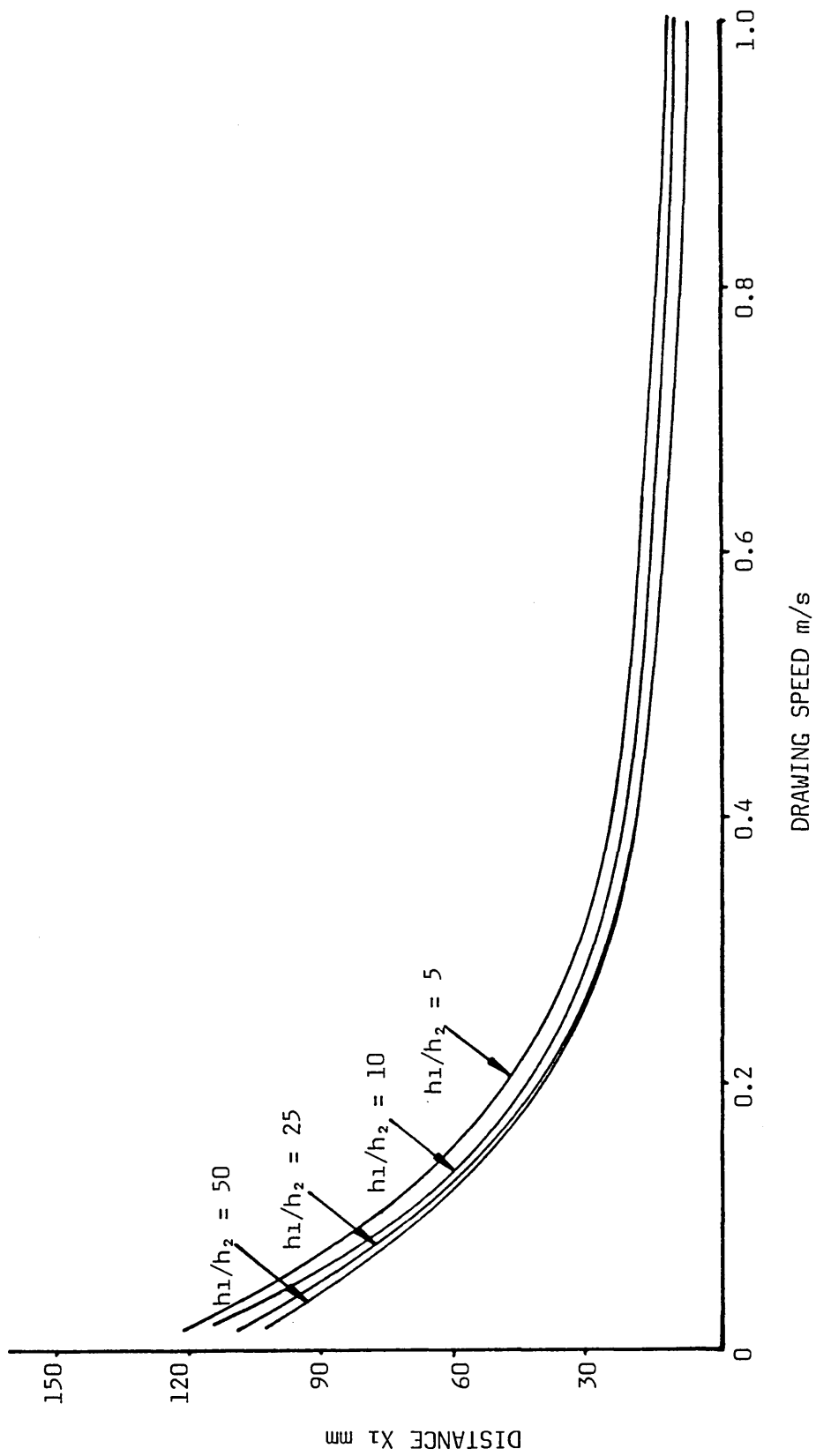


FIG 163(b) - THEORETICAL EFFECT OF GAP RATIO ON YIELDING POSITION OF COPPER TUBE

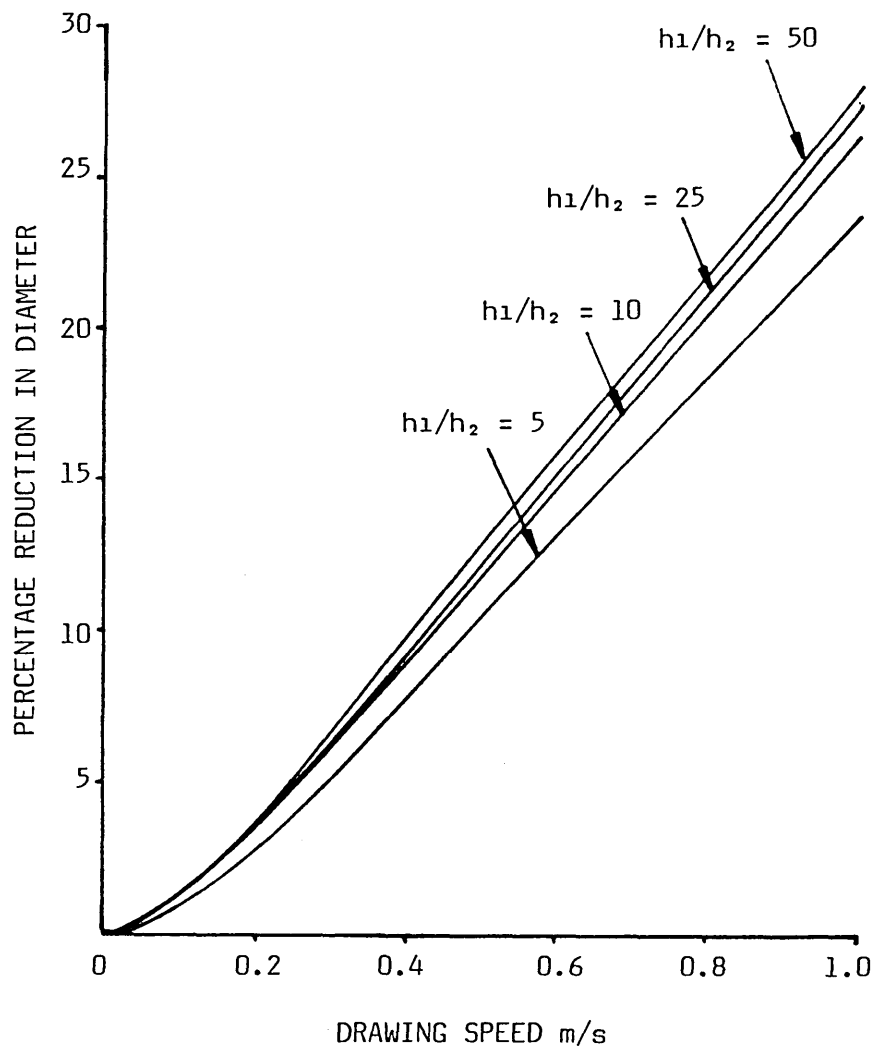


FIG 164(a) - THEORETICAL EFFECT OF GAP RATIO ON PERCENTAGE REDUCTION IN DIAMETER FOR ALUMINIUM TUBE

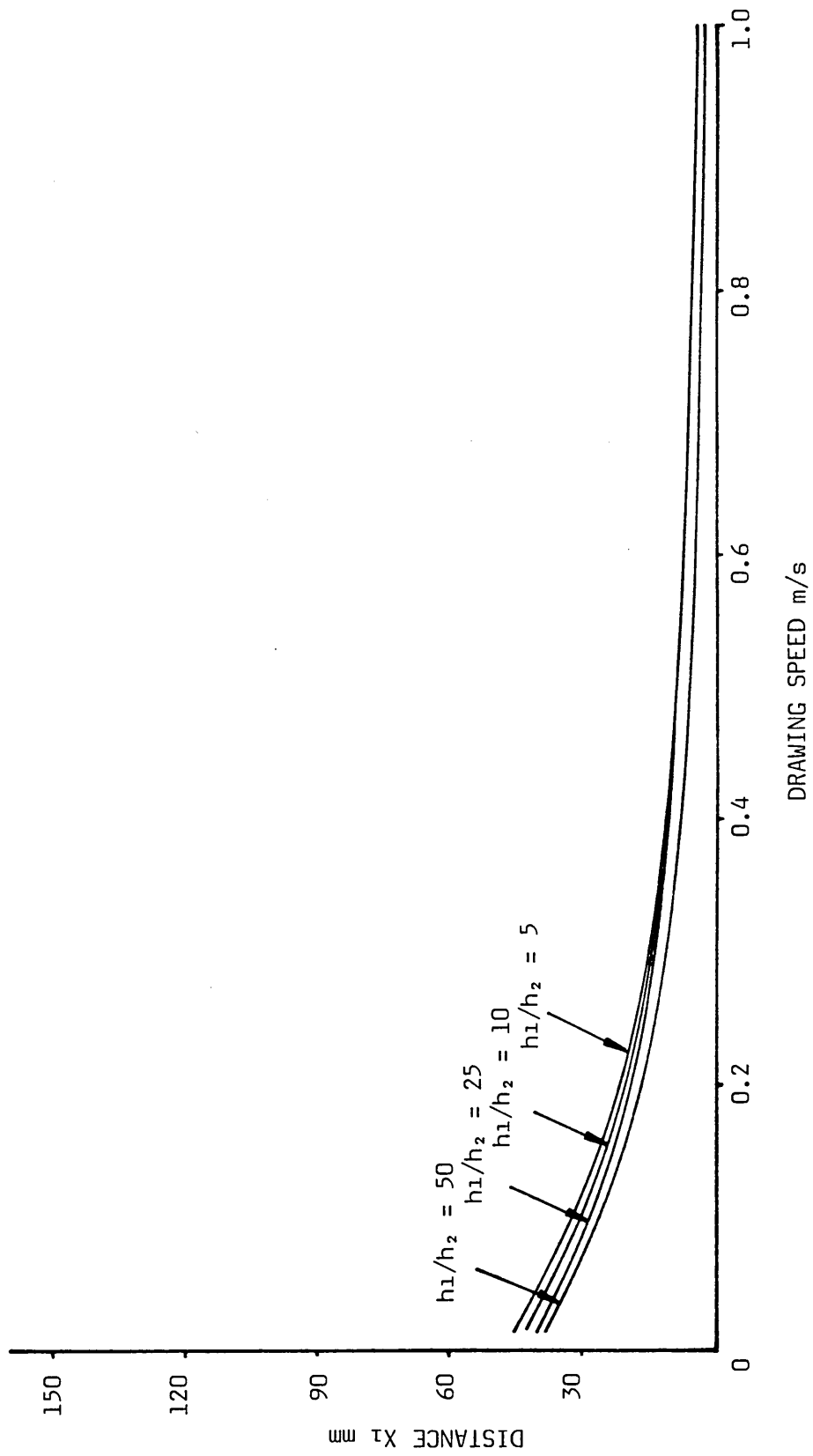


FIG 164(b) - THEORETICAL EFFECT OF GAP RATIO ON YIELDING POSITION OF THE ALUMINIUM TUBE

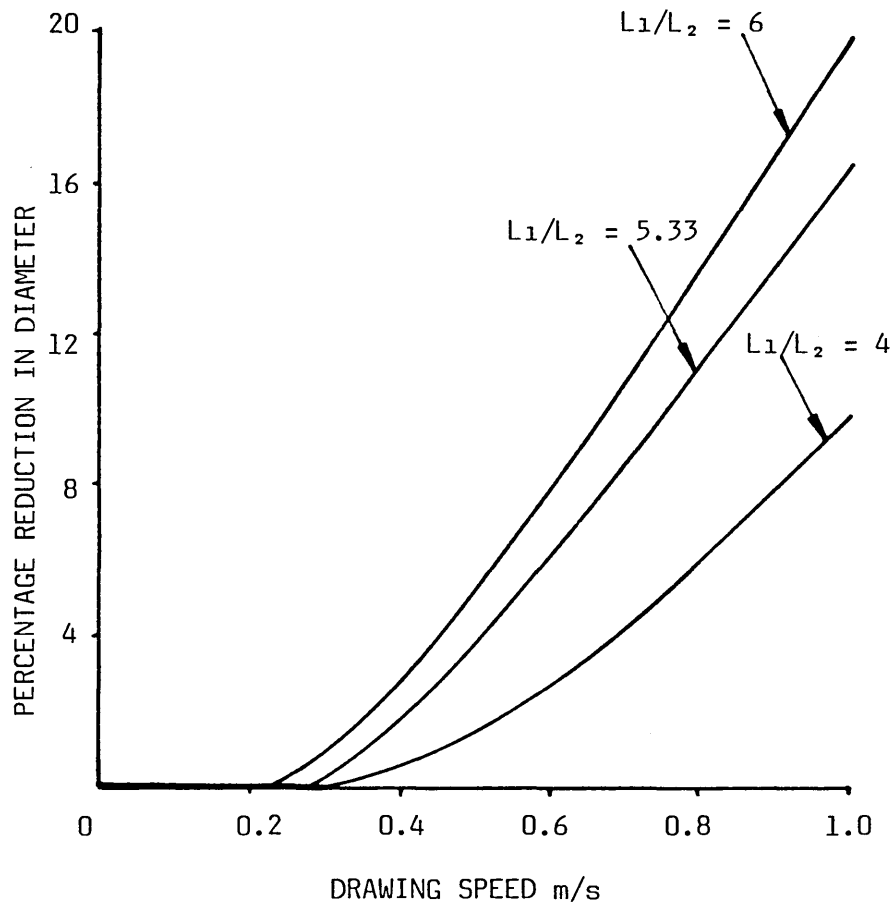


FIG 165 - THEORETICAL EFFECT OF LENGTH RATIO ON PERCENTAGE REDUCTION IN DIAMETER FOR COPPER TUBE

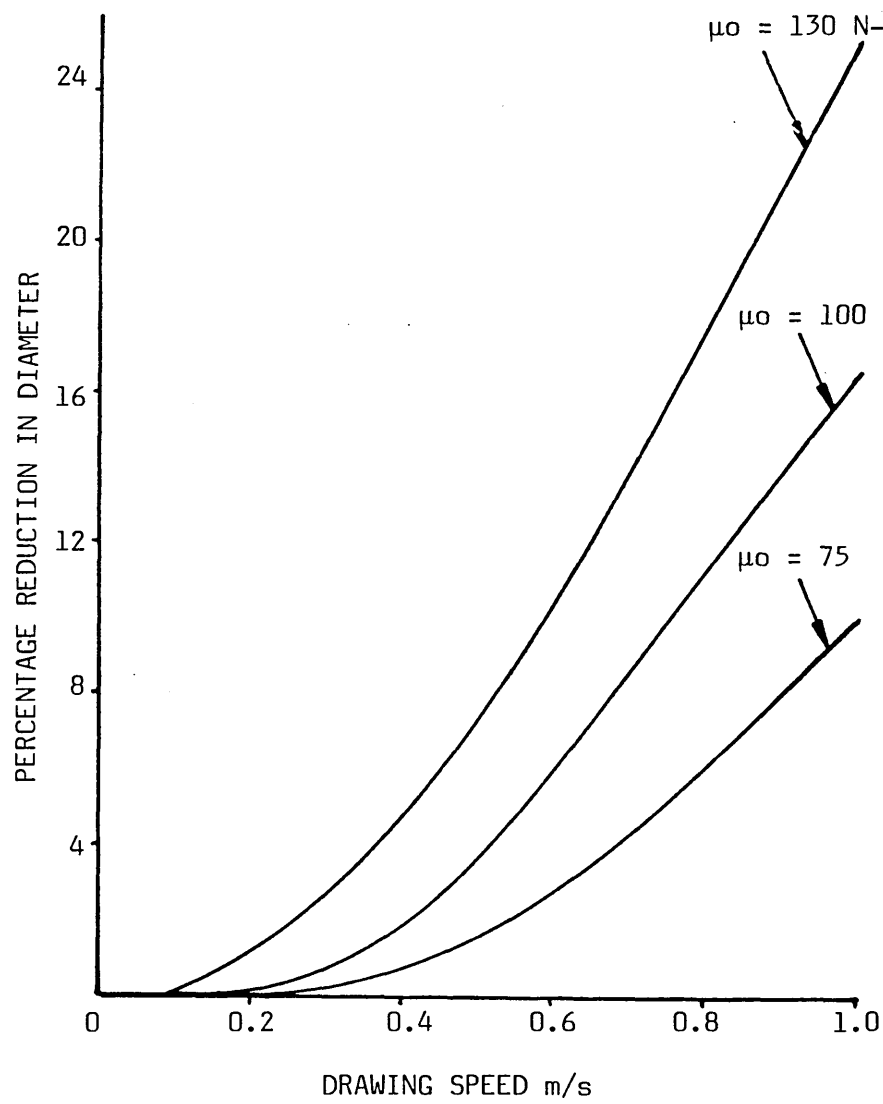


FIG 166(a) - THEORETICAL EFFECT OF VISCOSITY ON PERCENTAGE REDUCTION IN DIAMETER FOR COPPER TUBE

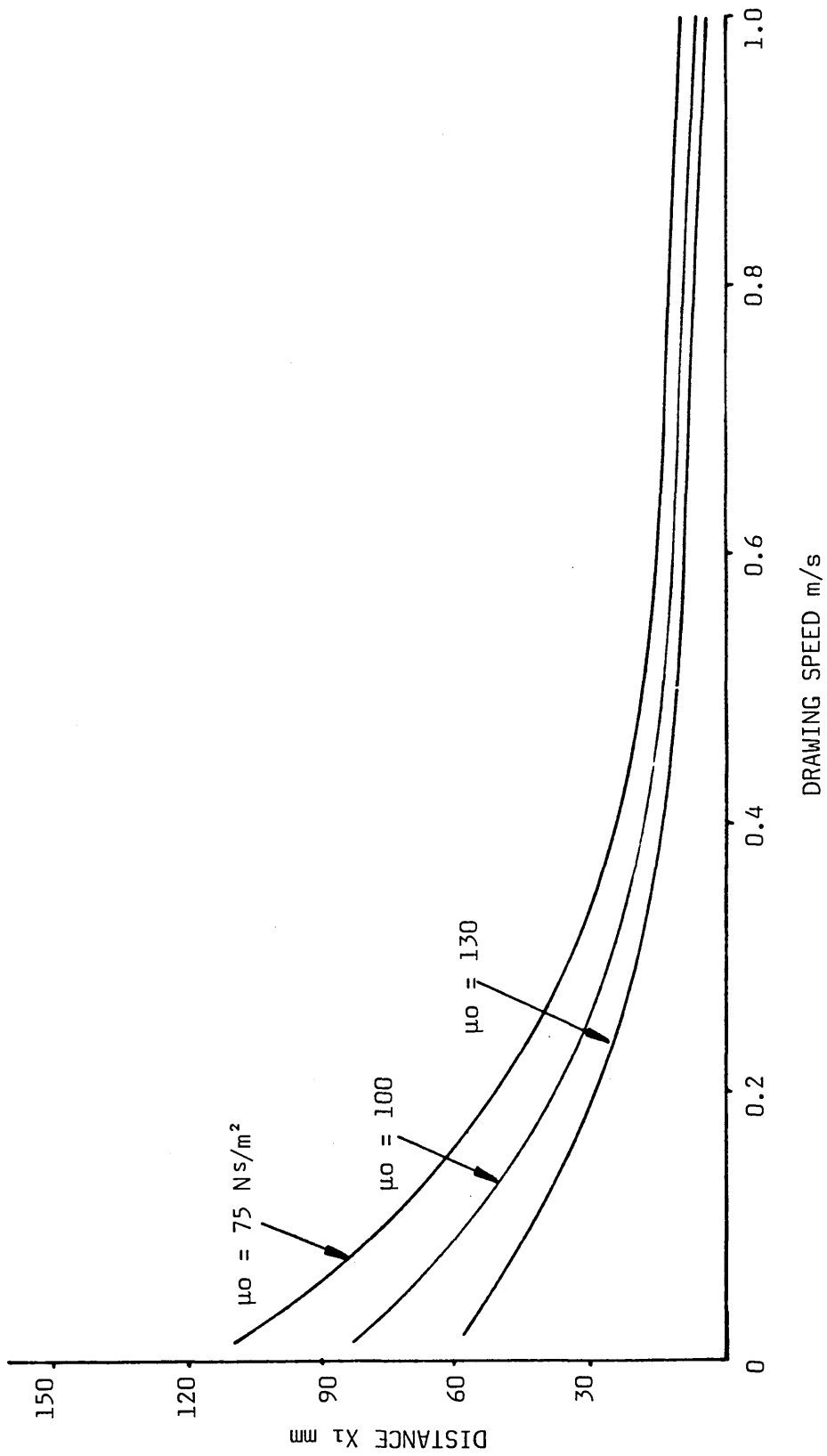


FIG 166(b) - THEORETICAL EFFECT OF VISCOSITY ON YIELDING POSITION OF COPPER TUBE

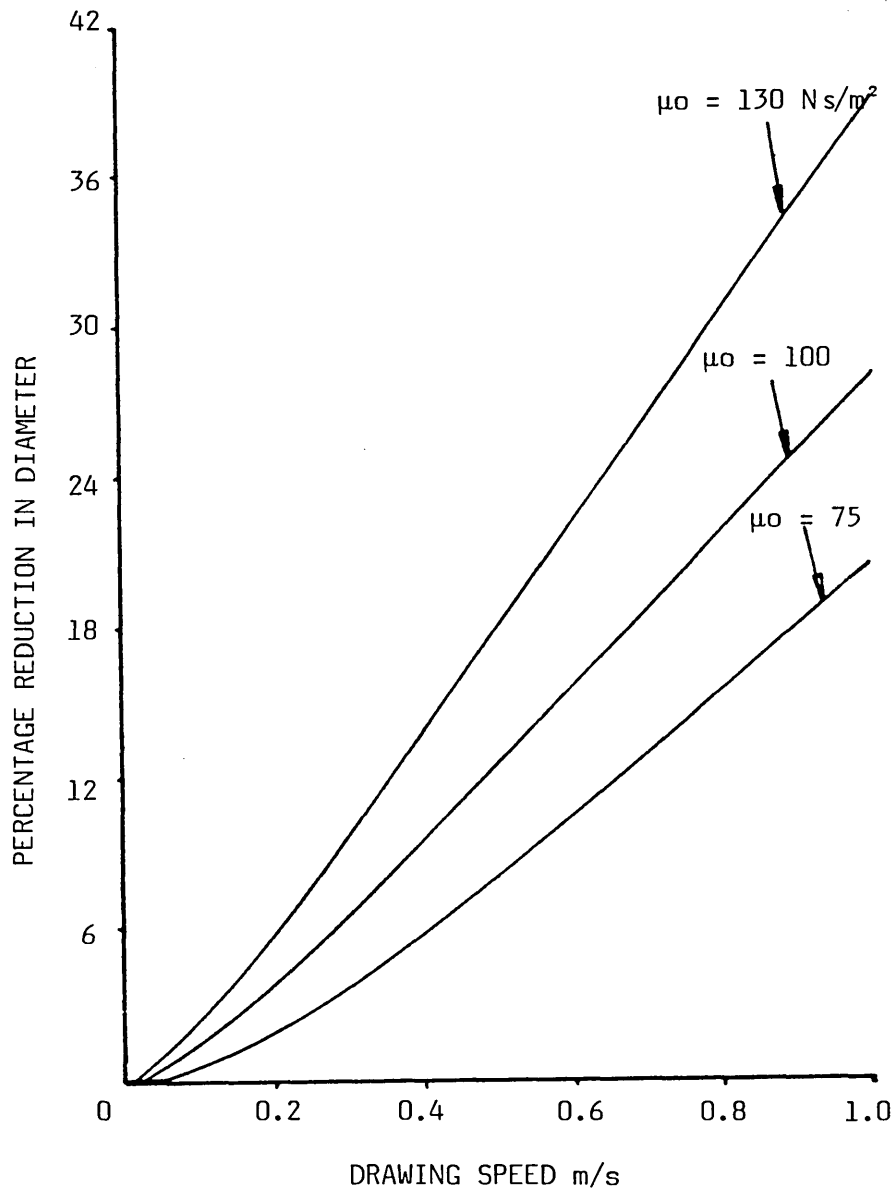


FIG 167(a) - THEORETICAL EFFECT OF VISCOSITY ON PERCENTAGE REDUCTION IN DIAMETER FOR ALUMINIUM TUBE

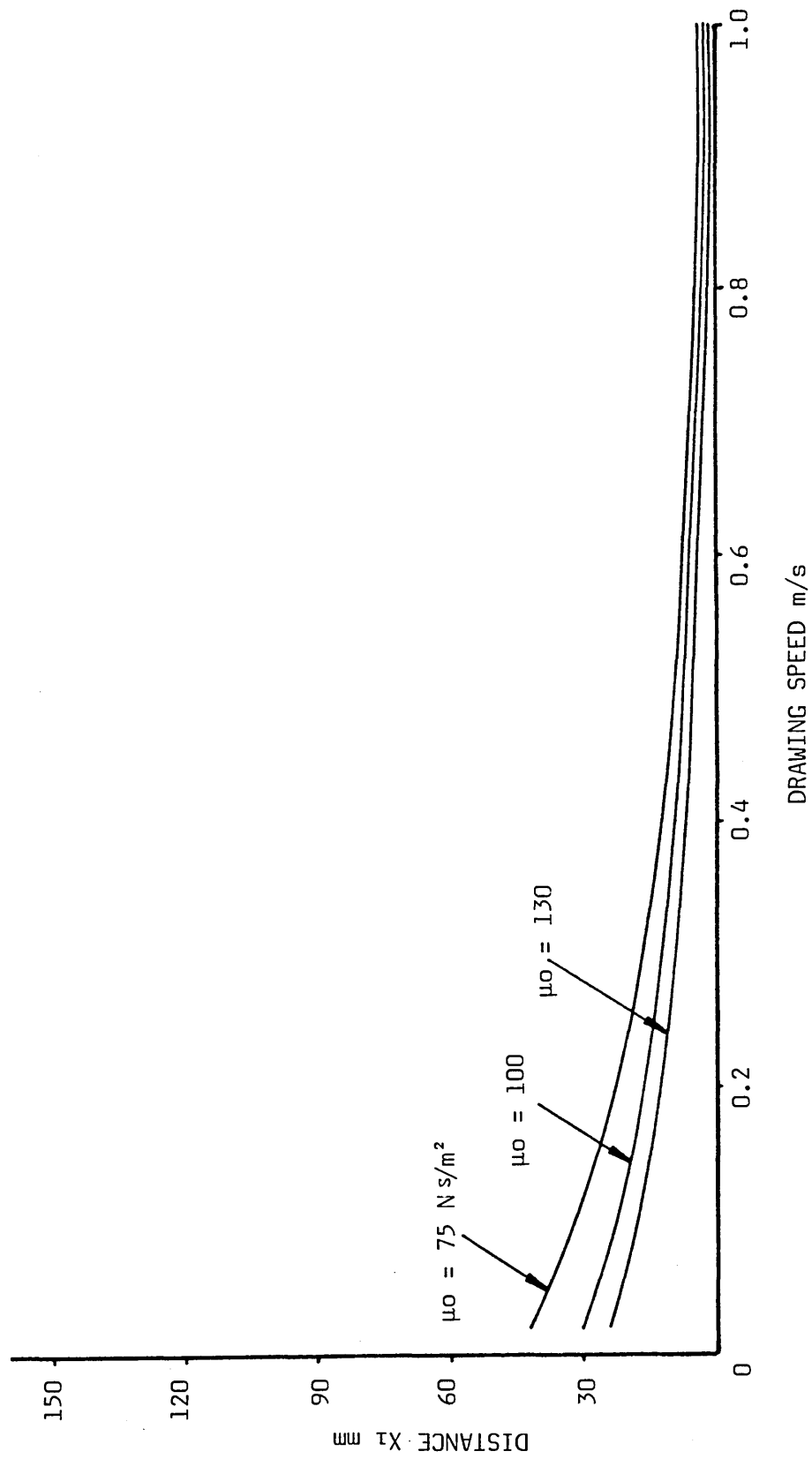


FIG 167(b) - THEORETICAL EFFECT OF VISCOSITY ON YIELDING POSITION OF ALUMINIUM TUBE

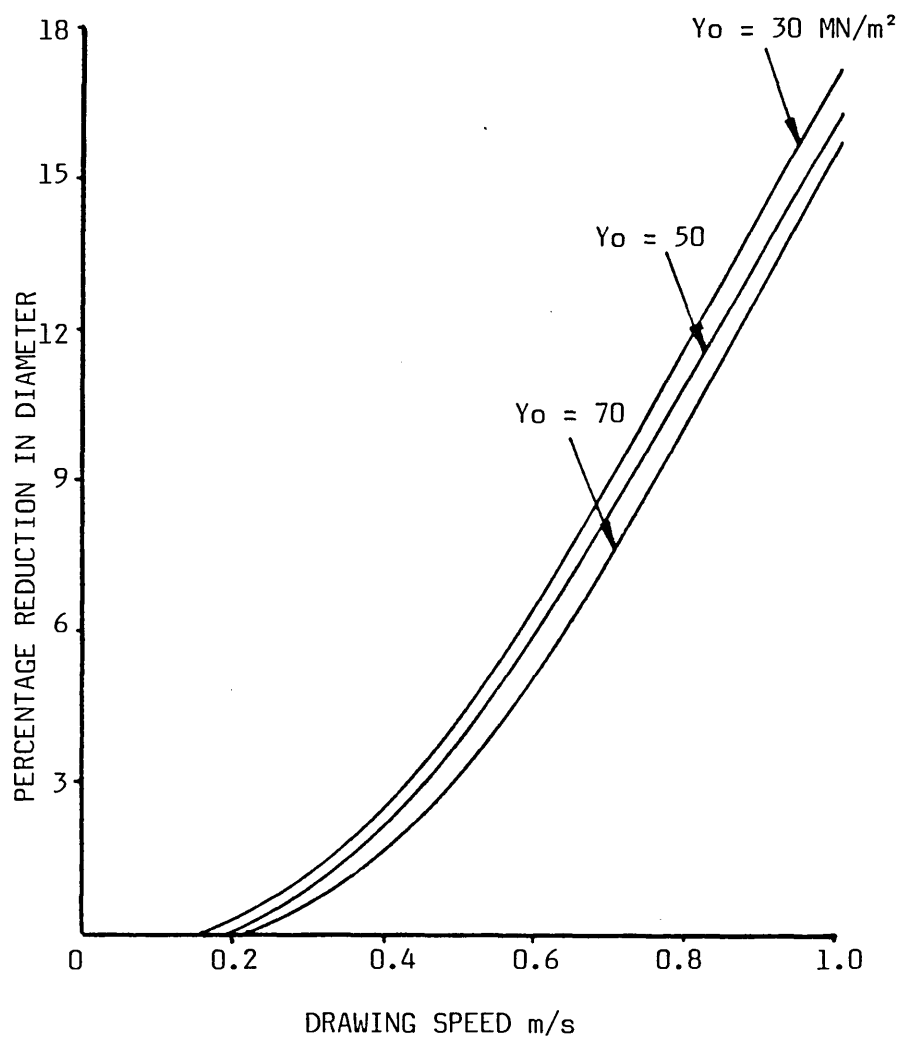


FIG 168(a) - THEORETICAL EFFECT OF INITIAL YIELD STRESS ON PERCENTAGE REDUCTION IN DIAMETER FOR COPPER TUBE

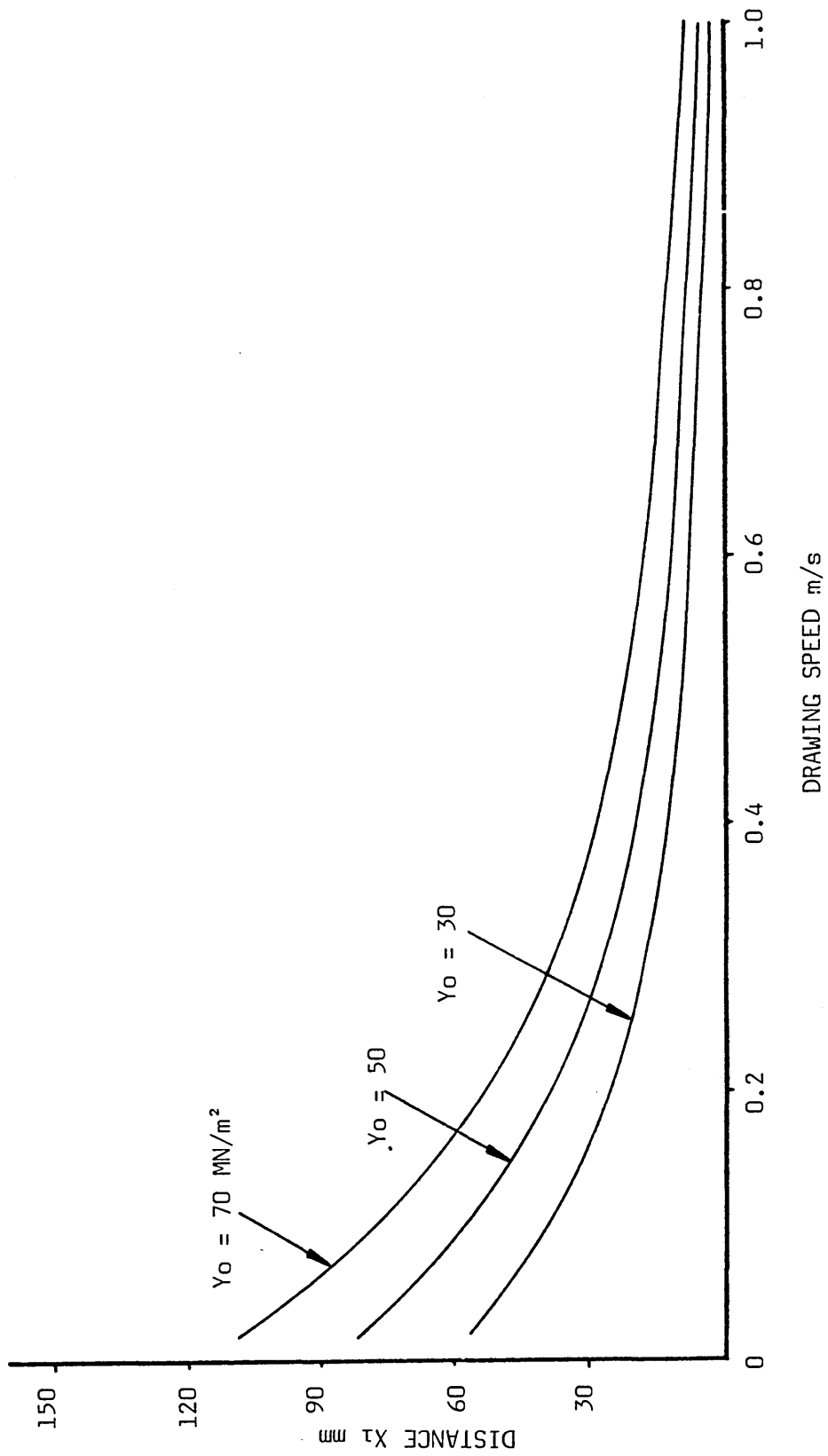
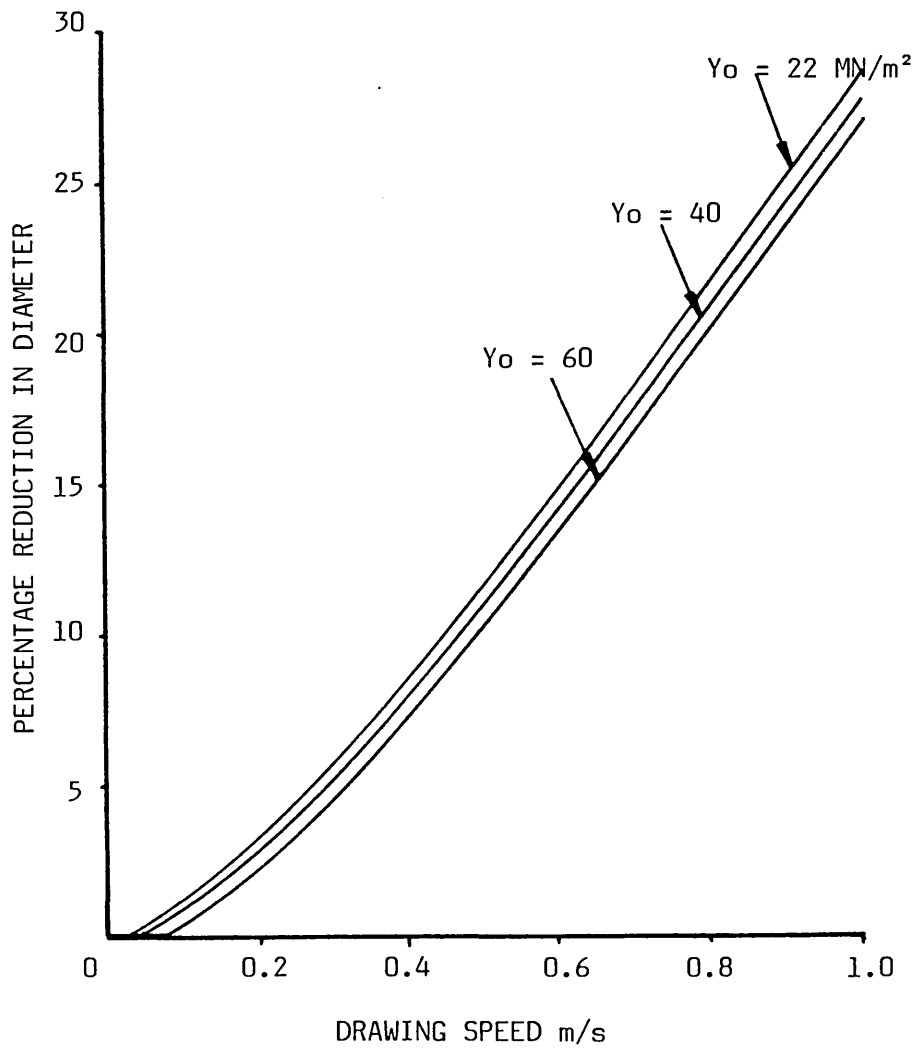


FIG 168(b) - THEORETICAL EFFECT OF INITIAL YIELD STRESS ON YIELDING PORTION OF COPPER TUBE



**FIG 169(a) - THEORETICAL EFFECT OF INITIAL YIELD STRESS ON
PERCENTAGE REDUCTION IN DIAMETER FOR ALUMINIUM TUBE**

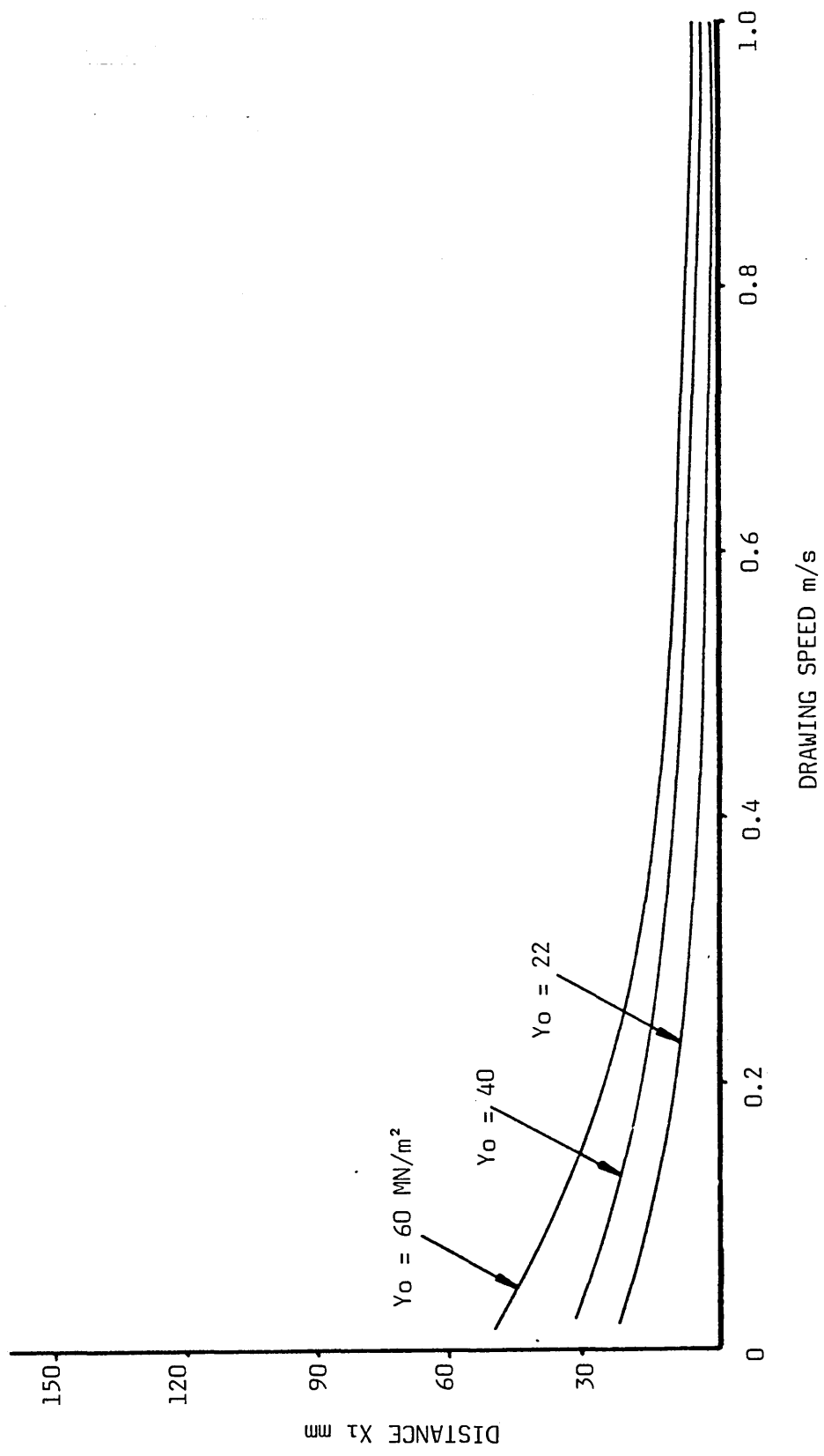


FIG 169(b) - THEORETICAL EFFECT OF INITIAL YIELD STRESS ON YIELDING POSITION OF ALUMINIUM TUBE

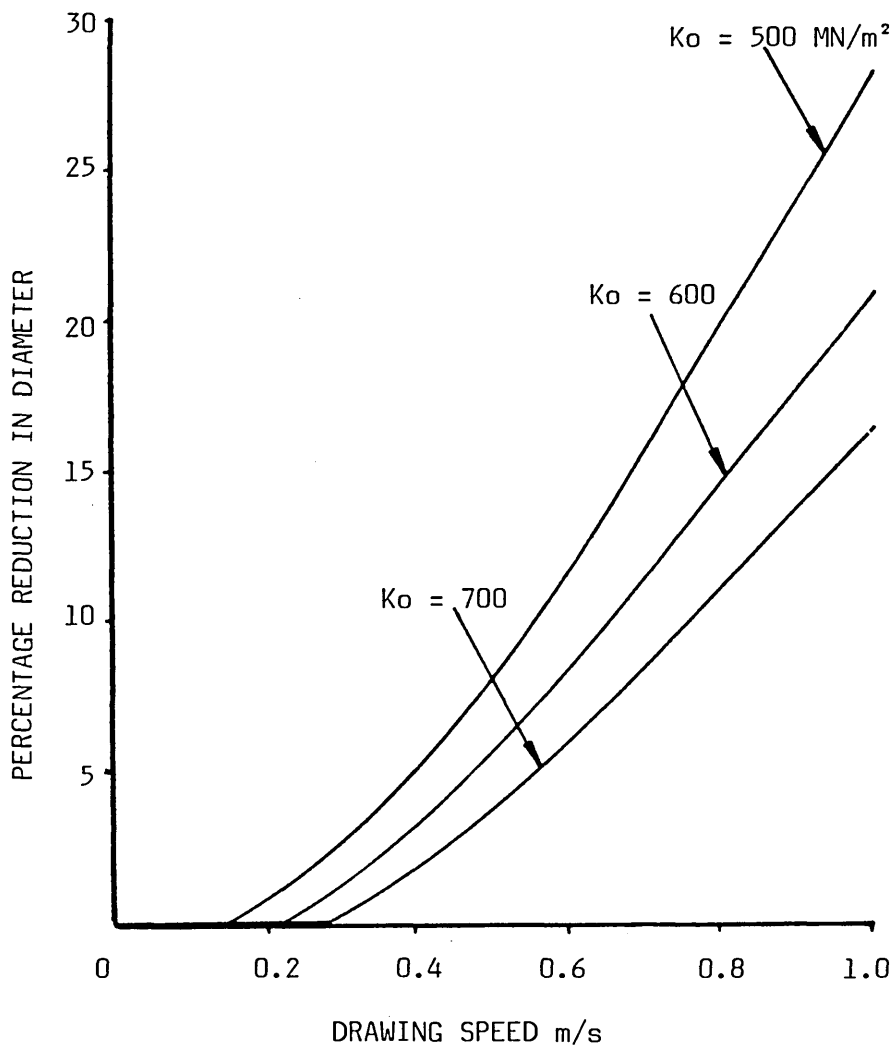


FIG 170 - THEORETICAL EFFECT OF STRAIN HARDENING CONSTANT ON PERCENTAGE REDUCTION IN DIAMETER FOR COPPER TUBE

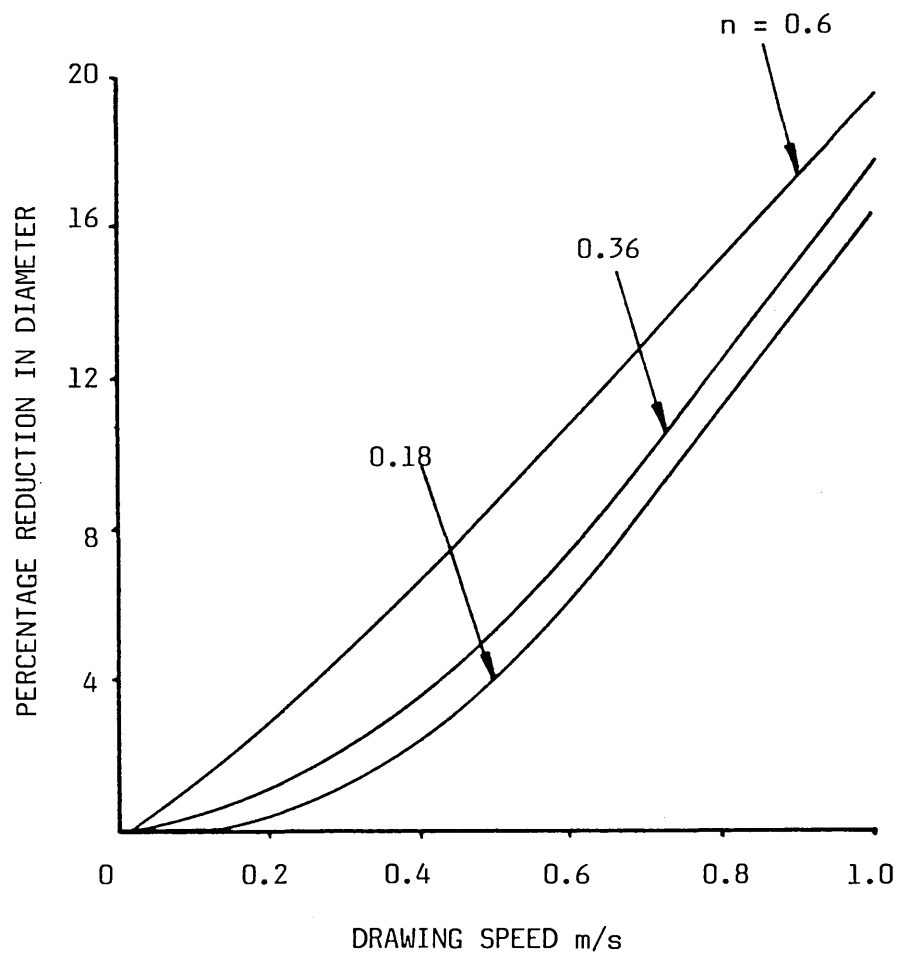
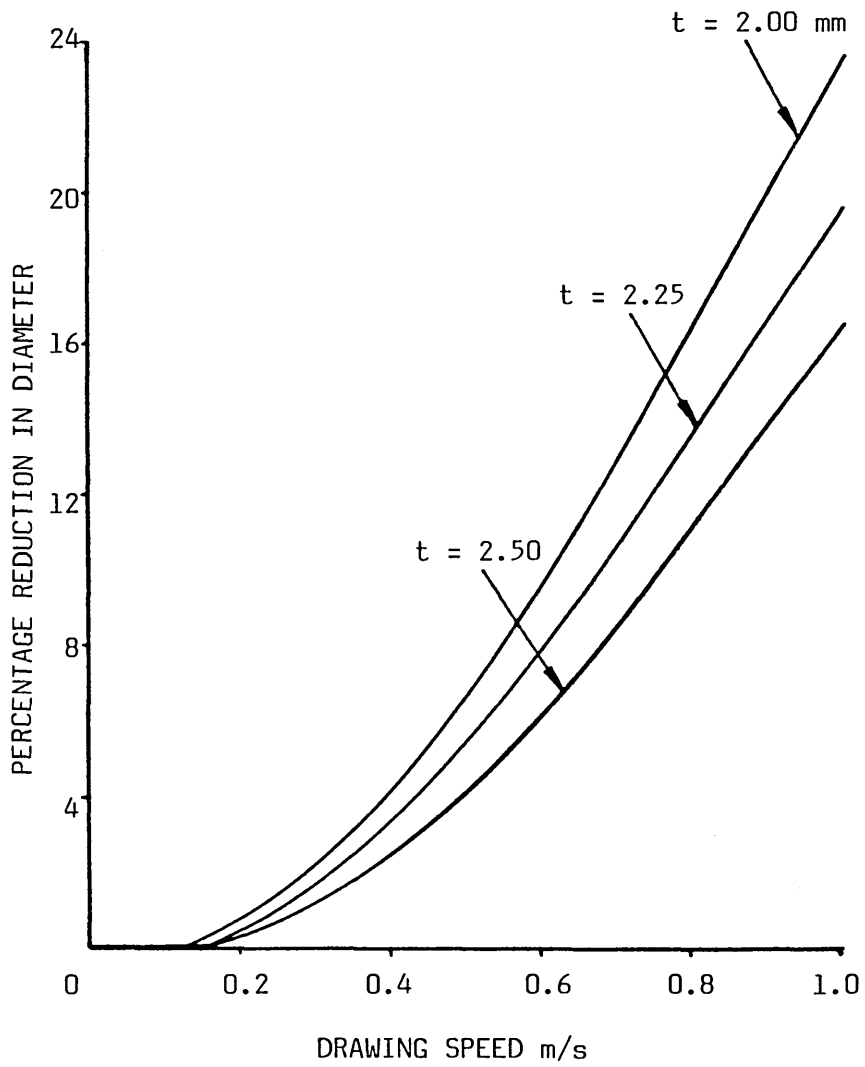


FIG 171 - THEORETICAL EFFECT OF STRAIN HARDENING INDEX ON PERCENTAGE REDUCTION IN DIAMETER FOR COPPER TUBE



**FIG 172(a) - THEORETICAL EFFECT OF TUBE WALL-THICKNESS ON
PERCENTAGE REDUCTION IN DIAMETER FOR COPPER TUBE**

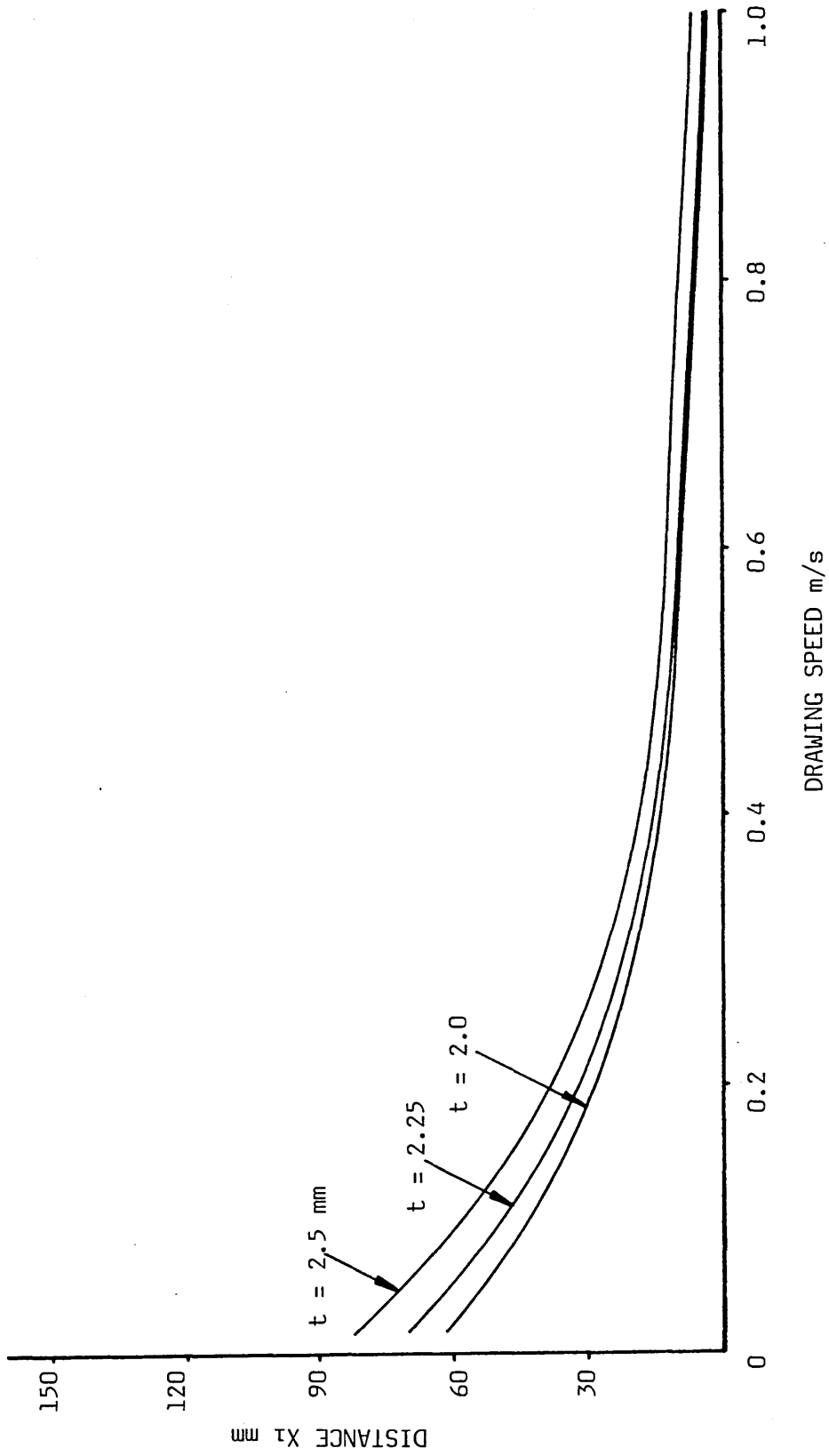


FIG 172(b) - THEORETICAL EFFECT OF TUBE WALL-THICKNESS ON YIELDING POSITION OF COPPER TUBE

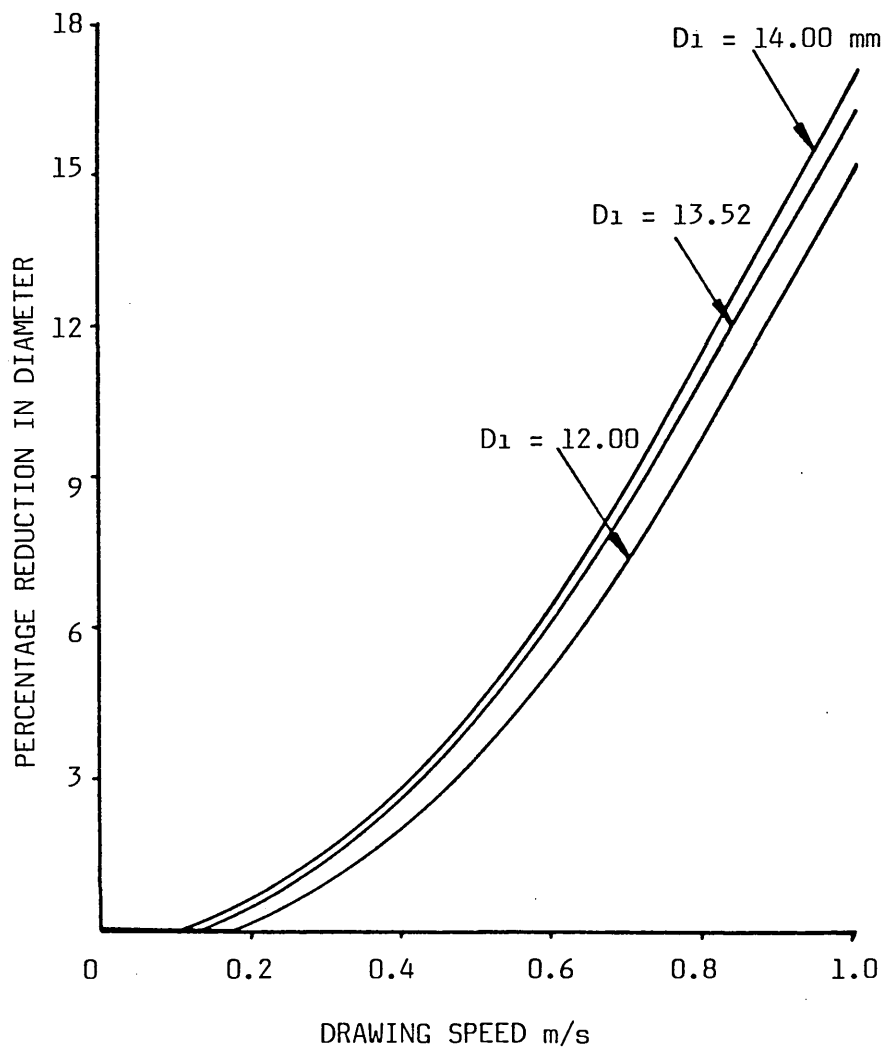


FIG 173(a) - THEORETICAL EFFECT OF TUBE DIAMETER ON PERCENTAGE REDUCTION IN DIAMETER FOR COPPER TUBE

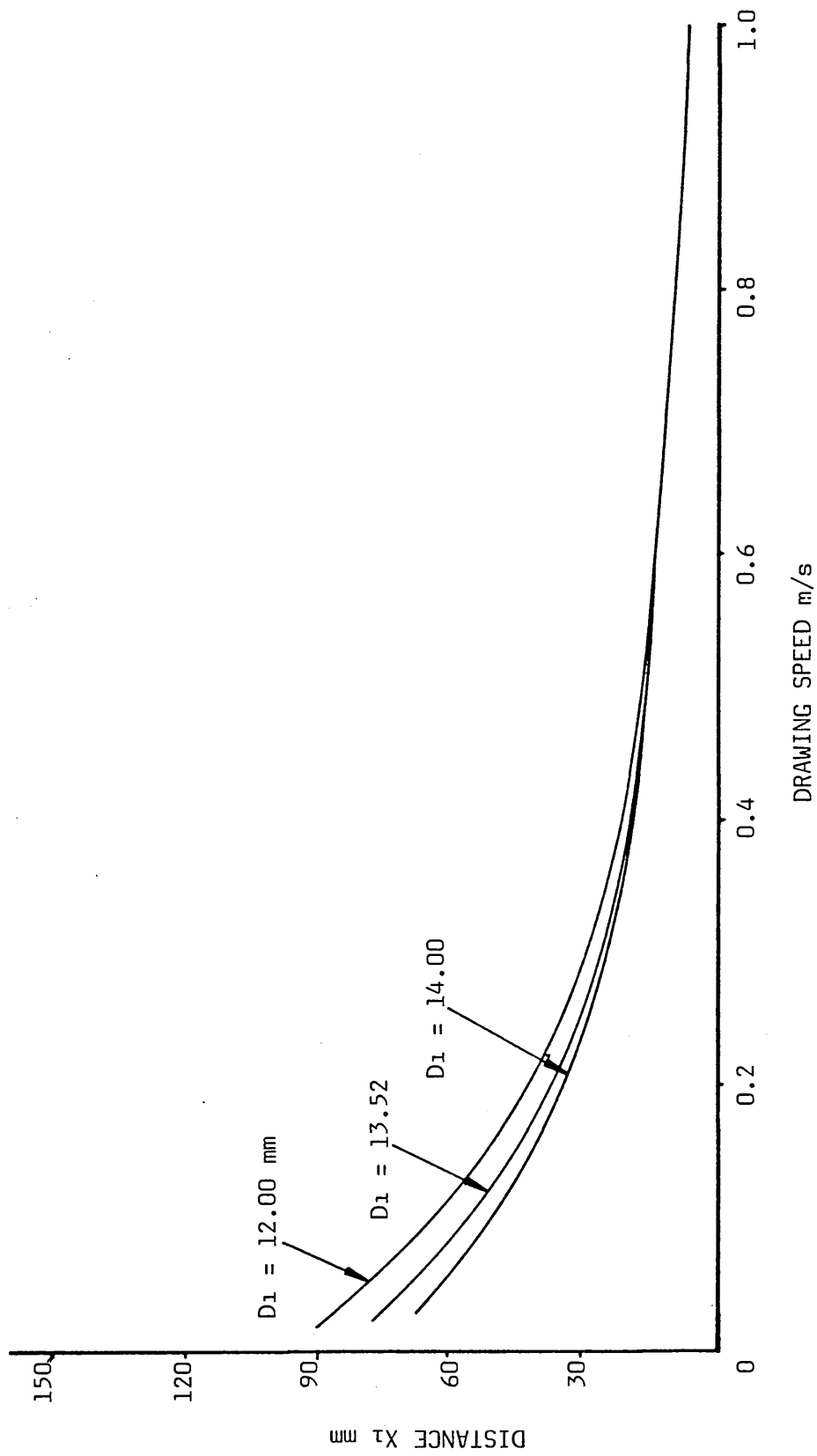


FIG 173(b) - THEORETICAL EFFECT OF TUBE DIAMETER ON YIELDING POSITION OF COPPER TUBE

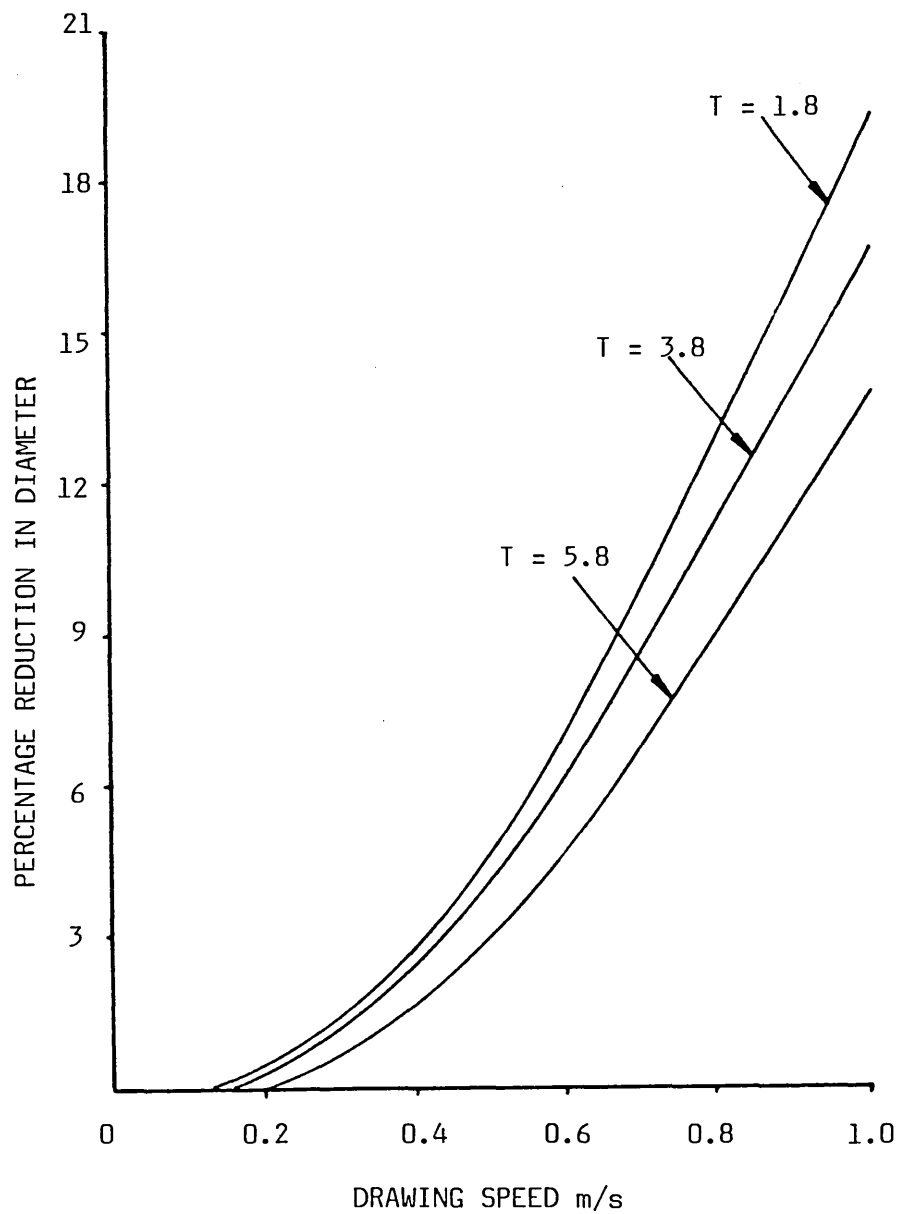


FIG 174 - THEORETICAL EFFECT OF STRAIN RATE SENSITIVITY INDEX ON PERCENTAGE REDUCTION IN DIAMETER FOR COPPER TUBE

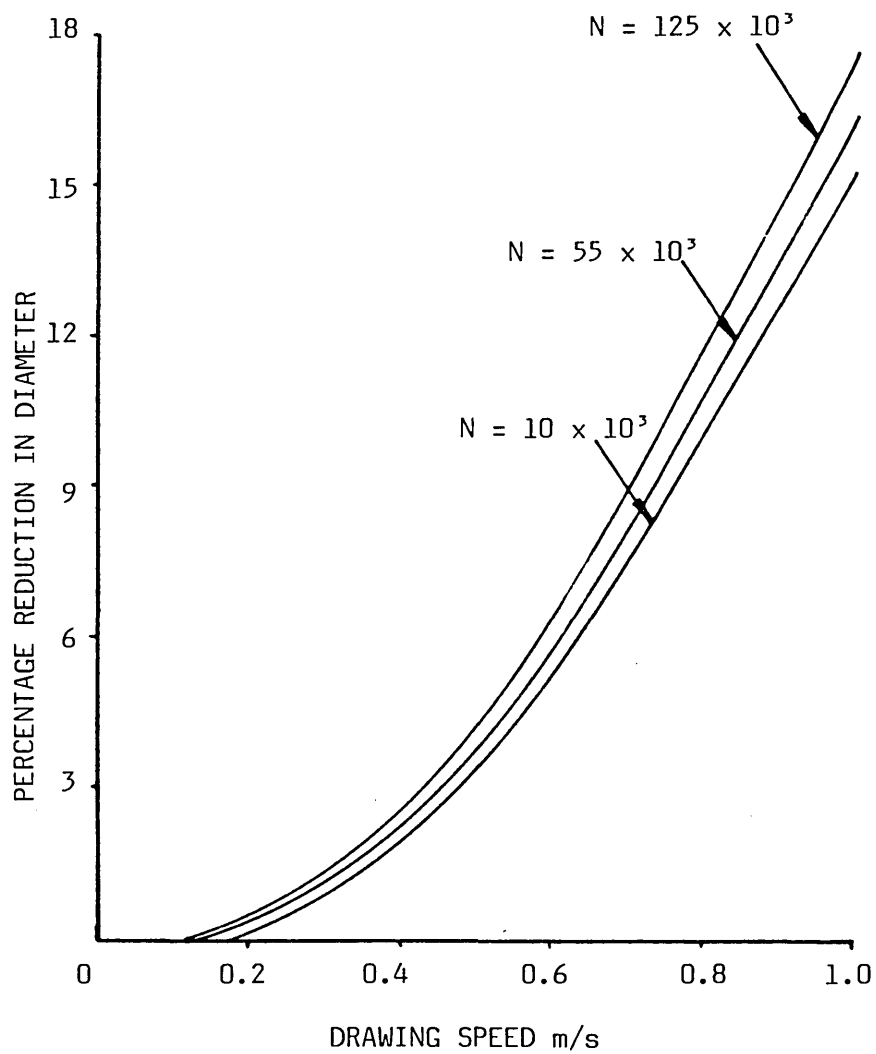


FIG 175 - THEORETICAL EFFECT OF STRAIN RATE SENSITIVITY CONSTANT ON PERCENTAGE REDUCTION IN DIAMETER FOR COPPER TUBE

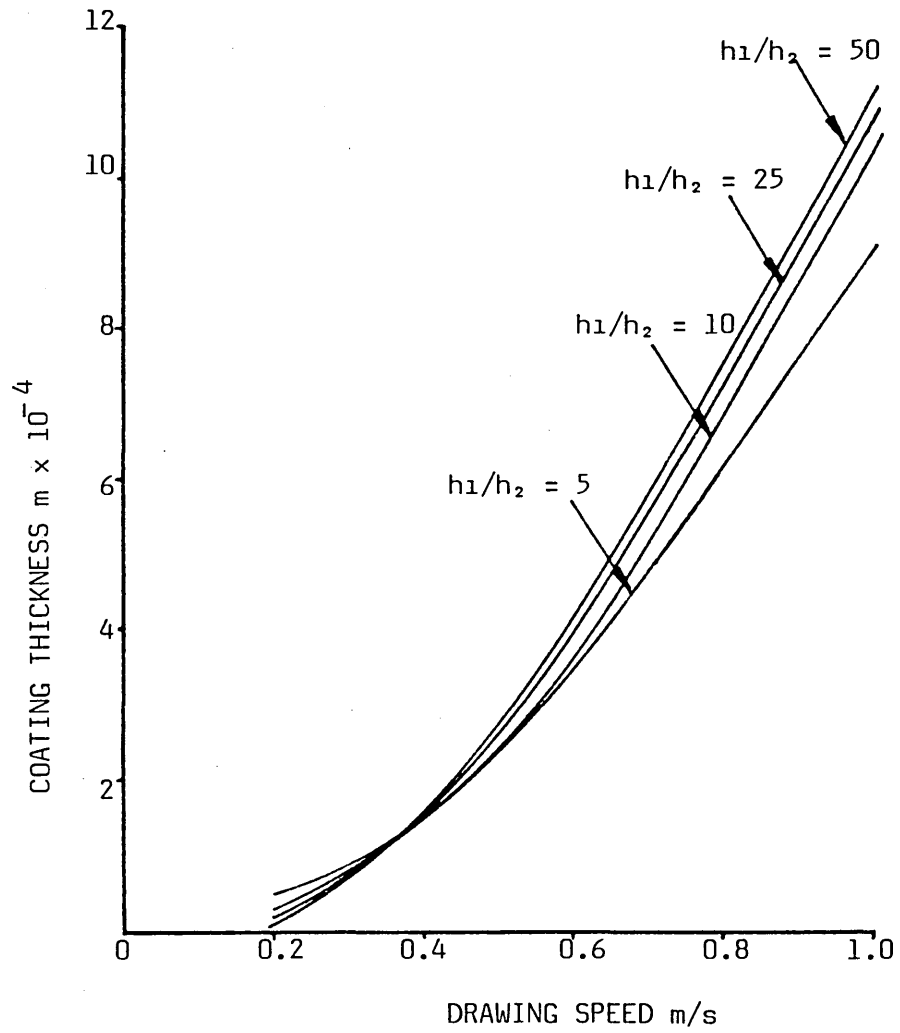


FIG 176 - THEORETICAL EFFECT OF GAP RATIO ON COATING THICKNESS FOR COPPER TUBE

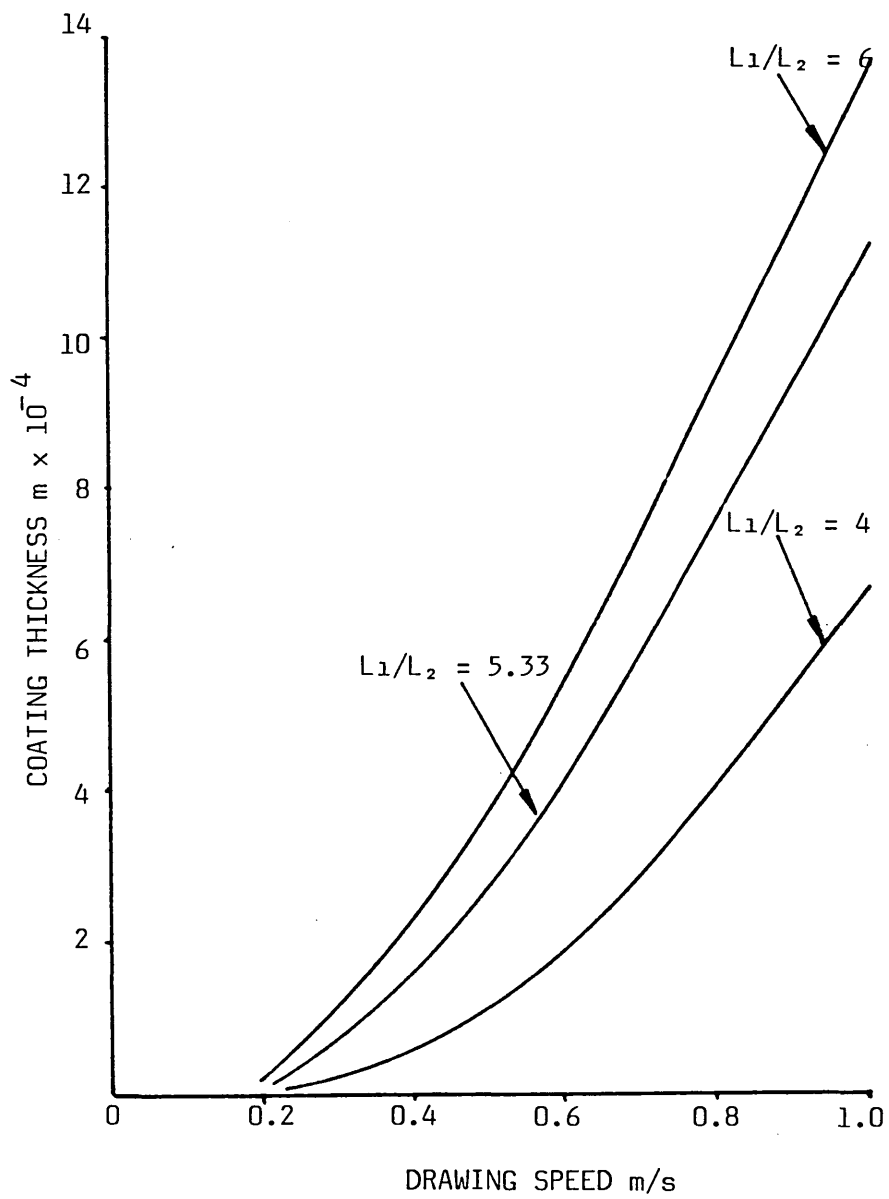


FIG 177 - THEORETICAL EFFECT OF LENGTH RATIO ON COATING THICKNESS FOR COPPER TUBE

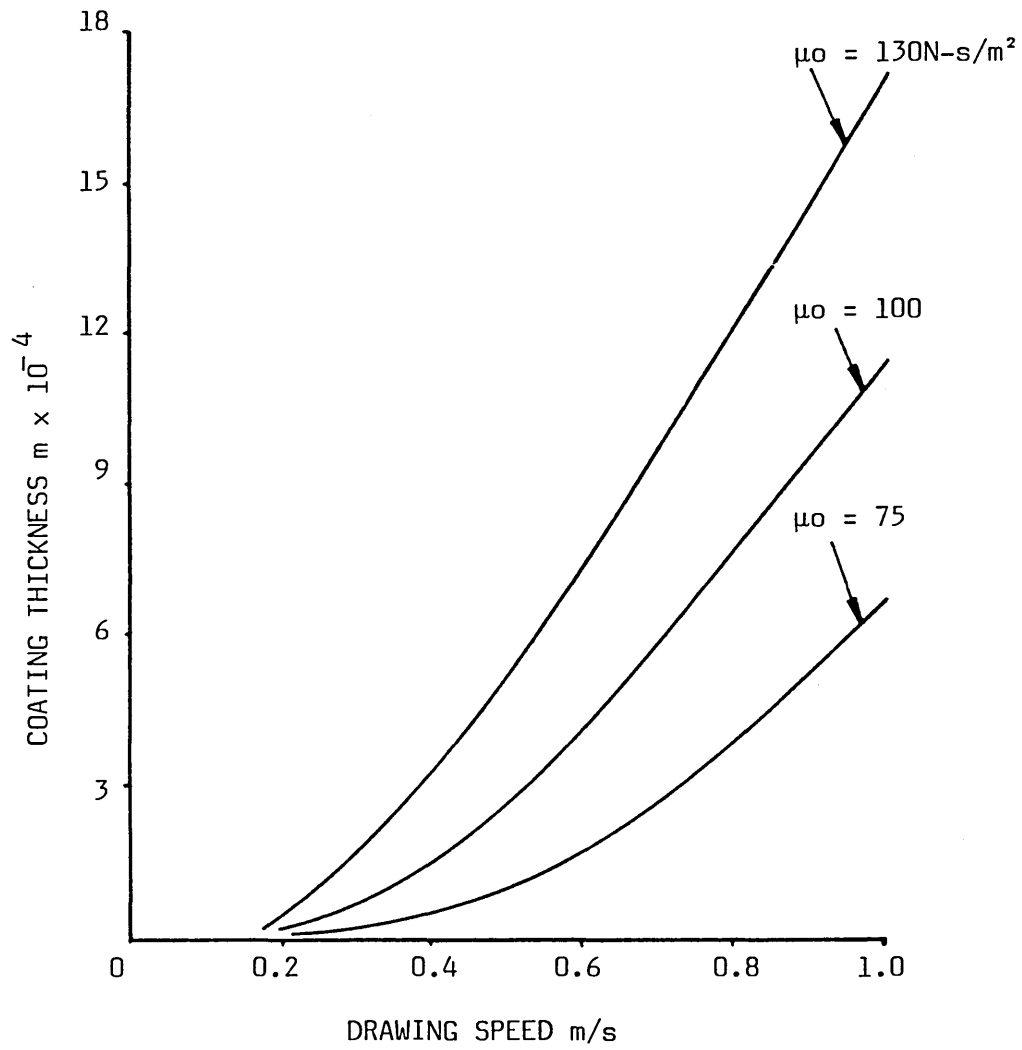


FIG 178 - THEORETICAL EFFECT OF VISCOSITY ON COATING THICKNESS FOR COPPER TUBE

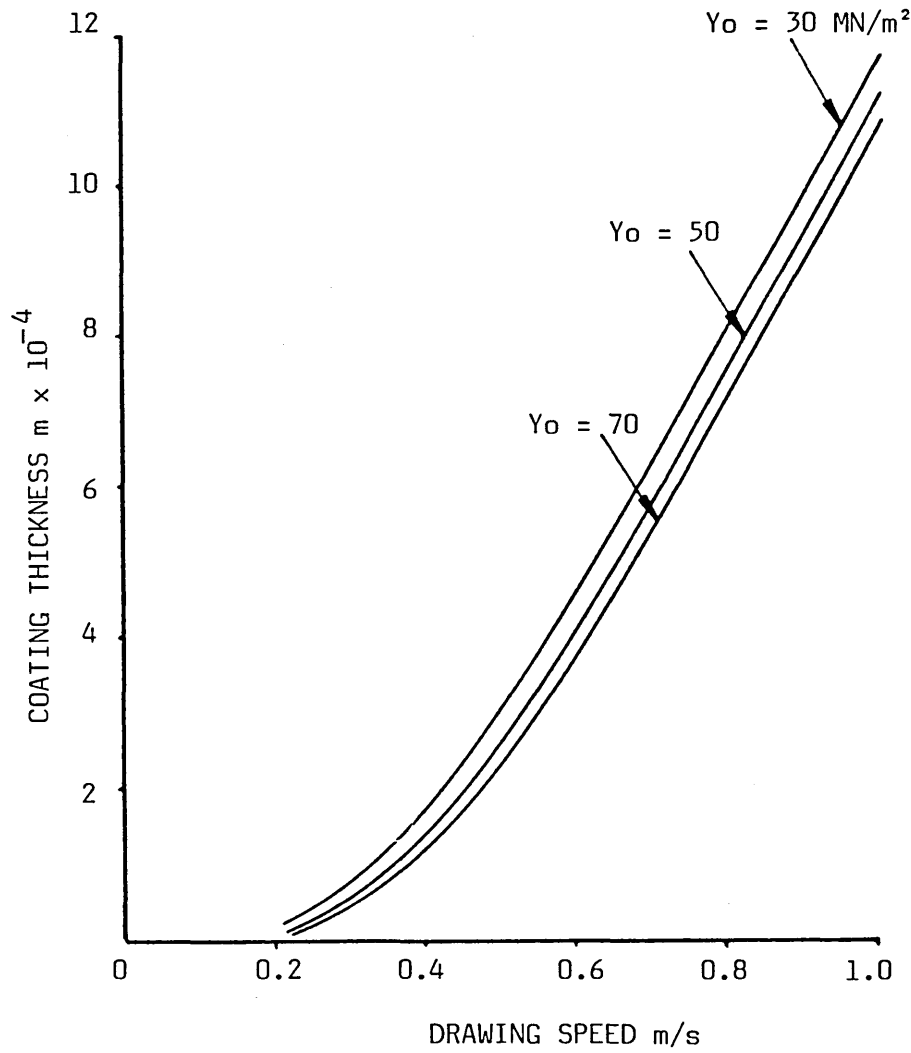


FIG 179 - THEORETICAL EFFECT OF INITIAL YIELD STRESS ON COATING THICKNESS FOR COPPER TUBE

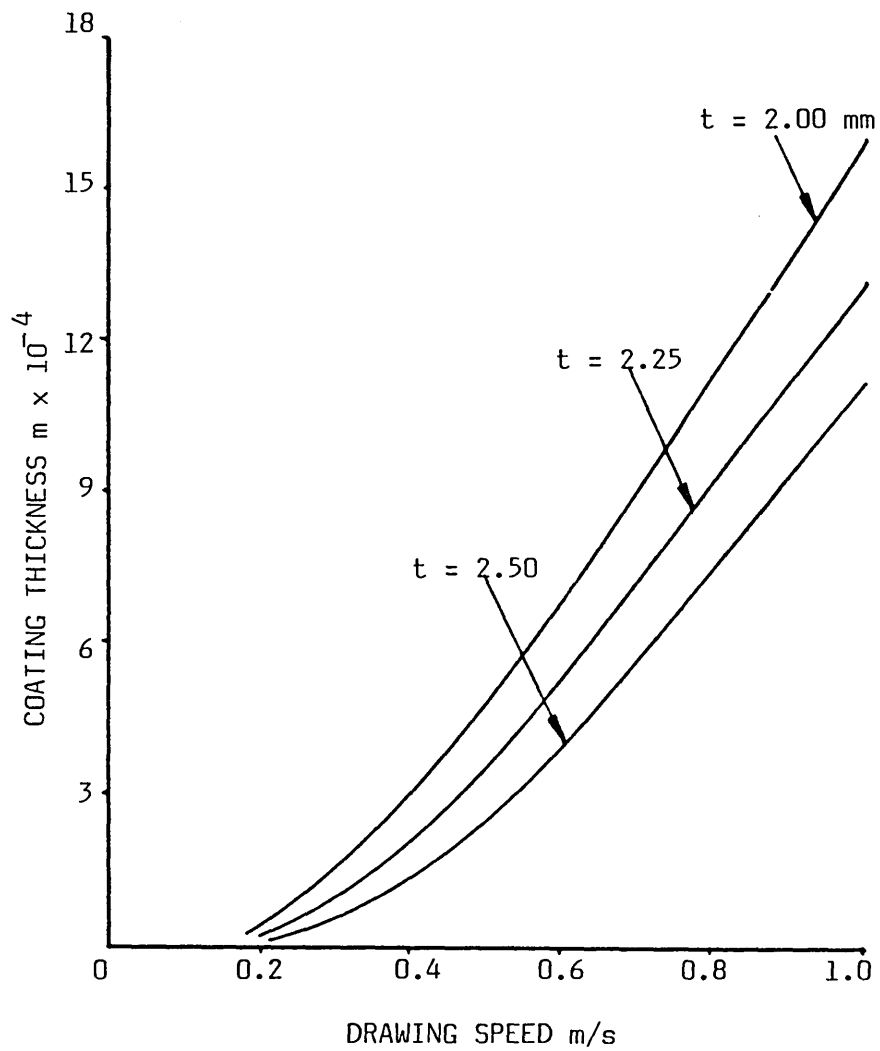


FIG 180 - THEORETICAL EFFECT OF TUBE WALL-THICKNESS ON COATING THICKNESS FOR COPPER TUBE

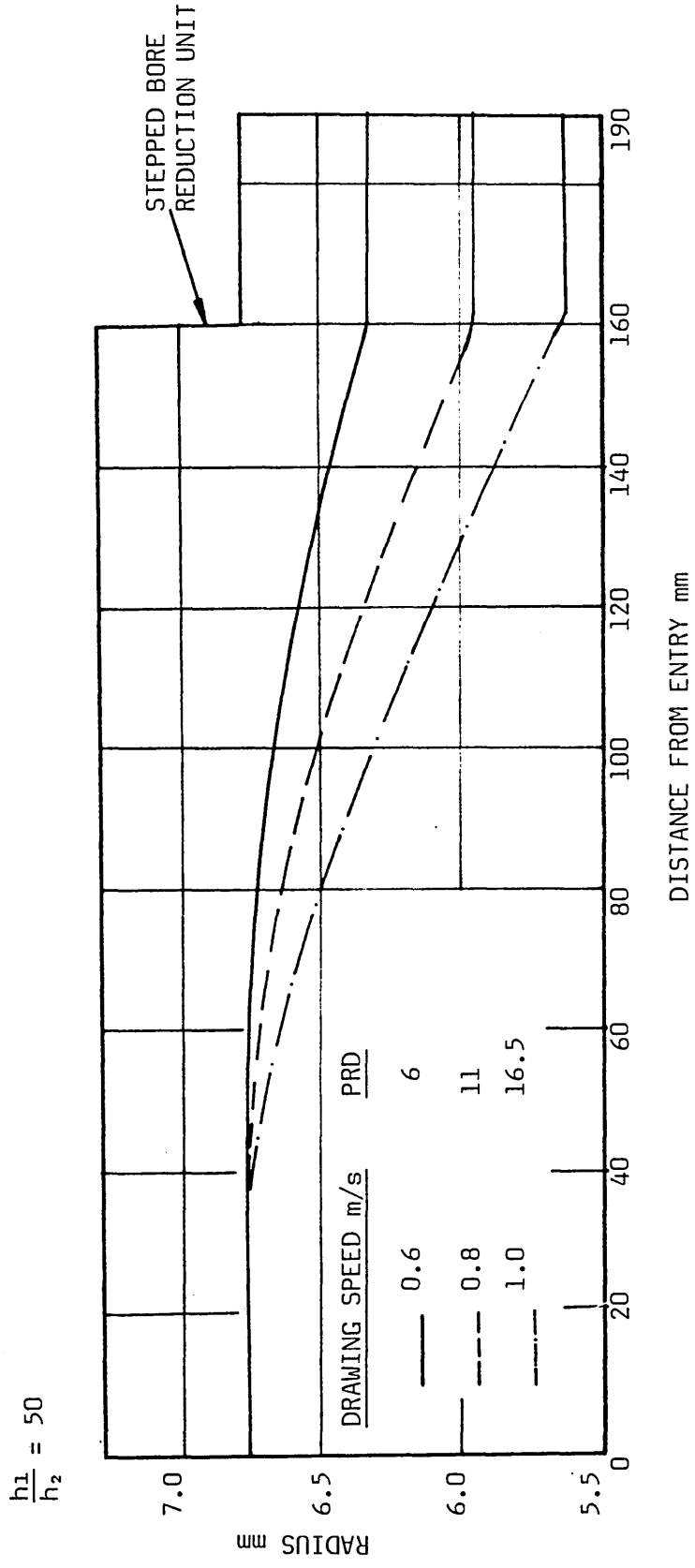


FIG 181 - THEORETICAL DEFORMATION PROFILES FOR COPPER TUBE

6.1 Introduction

The mathematical model developed in Chapter 5 was based on the assumptions that the fluidic pressure medium possesses Newtonian characteristics. The resulting theoretical results based on this model when compared with those observed experimentally shows that the agreement is not good at higher drawing speeds. One of the reasons could be the fact that the polymer melt used in the experimental work does not behave like a Newtonian fluid. It was thus thought that a better agreement may be achieved if the mathematical model is formulated on the basis of non-Newtonian characteristics of the pressure medium. This Chapter outlines details of such a model developed by the author for tube sinking. Polymer melt as a lubricant in wire drawing was introduced by Symmons and Thompson⁹ in conjunction with a pressure tube and a reduction die. They assumed that the polymer melt could be treated as a Newtonian fluid, using the concept of apparent viscosity. They also introduced critical and sub-critical flow of polymer melt in their analysis. Hashmi et al¹³ published a paper giving non-Newtonian analysis of wire drawing process for polymer melt lubrication incorporating the effect of pressure and shear rate on the viscosity of the polymer melt. They also included strain hardening and strain rate sensitivity of the deforming metal together with the critical and sub-critical flow of polymer into the analysis. All the above analyses refer to systems where a conventional die is used whose minimum bore size is always smaller than the incoming wire diameter. More recently Parvinmehr³⁸ has introduced a non-Newtonian plasto-hydrodynamic analysis of the wire drawing using a stepped bore die-less reduction unit in which polymer melt was used as the pressure medium. In the present analysis the geometrical

configuration is different from the conventional tube sinking process. In this system no reduction die is used and the minimum bore size of the stepped bore reduction unit is greater than the diameter of the undeformed tube. A non-Newtonian plasto-hydrodynamic analysis of the tube sinking process is presented for a stepped bore reduction unit in which polymer melt is used as the pressure medium. The effects of shear rate and pressure on the viscosity of the polymer together with the shear stress are included in the analysis. Also the strain hardening and strain rate sensitivity of the tube material are incorporated in the analysis.

6.2 Analysis

The following analysis is based on the geometrical configuration shown in Fig 131. In order to formulate the analysis the following assumptions were made:

- (a) Flow of the polymer melt is laminar.
- (b) The process is isothermal.
- (c) Flow of the polymer melt is purely axial.
- (d) The thickness of the polymer melt layer is small compared to the dimensions of the stepped bore reduction unit. Analysis of the stepped bore reduction unit is presented into two parts;
 - (i) Analysis before deformation.
 - (ii) After deformation.
- (i) Analysis before deformation

As the thickness of the polymer melt layer contained in the DRU is small compared with the dimensions of the DRU, the analysis of flow is carried out in rectangular rather than cylindrical co-ordinates.

An empirical equation relating shear stress and shear rate of polymer melt can be expressed as

$$\tau + k\tau^3 = \mu \frac{du}{dy} \quad (1)$$

This relationship was proposed first by Rabinowitsch³⁹ and later used by Hung and Muster⁴⁰ to determine the non-Newtonian flow in infinite length step-shaped bearings and also used by Rotem and Shinnar⁴¹ and Swamy et al⁸ to investigate flow of non-Newtonian fluid. Again the flow of polymer melt in the stepped bore reduction unit is divided into two sections;

(i) entry part of the unit before the step.

(ii) after the step.

In the first part of the unit in Fig 131(a) the relationship between the pressure and shear stress gradient in between the outer surface of the tube and the inner surface of the DRU may be expressed as:

$$\left(\frac{dP}{dx}\right)_1 = \left(\frac{d\tau_1}{dy}\right)_1 \quad (2)$$

Integrating the above equation with respect to y gives;

$$\tau_1 = \left(\frac{dP}{dx_1}\right) y + c_1$$

At the surface of the tube $y = 0$, hence $c_1 = \tau_{c1}$

Therefore,

$$\tau_1 = P'_1 y + \tau_{c1} \quad (3)$$

where $\left(\frac{dP}{dx_1}\right) = P'_1$ and τ_{c1} is the shear stress on the tube at $y = 0$.

Substituting equation (3) into (1) we get

$$P'_1 y + \tau_{c1} + k(P'_1 y + \tau_{c1})^3 = \mu \left(\frac{du}{dy_1}\right)$$

or

$$P'_1 Y + \tau_{c1} + k(P'_1{}^3 Y^3 + \tau_{c1}{}^3 + 3P'_1{}^2 Y^2 \tau_{c1} + 3P'_1 Y \tau_{c1}{}^2) = \mu \left(\frac{du}{dy} \right)$$

integrating above equation with respect of y and noting that, μ and P'_1 remain constant at value of y at a given value of x , we have

$$\mu u_1 = \frac{P'_1 Y^2}{2} + \tau_{c1} Y + k \left(\frac{1}{4} P'_1{}^3 Y^4 + \tau_{c1}{}^3 Y + P'_1{}^2 Y^3 \tau_{c1} + \frac{3}{2} P'_1 Y^2 \tau_{c1}{}^2 \right) + c_2 \quad (4)$$

Two boundary conditions may be considered, at speeds at which slip does not occur. For condition of no-slip,

(i) At $y = 0$ (at the surface of the tube), $u_1 = v'$

and

(ii) at $y = h_1$ (at the inner surface of the unit), $u_1 = 0$

where u_1 is the velocity of the pressure medium at any point $0 \ll y \ll h_1$ and v' is the velocity of the tube before deformation occurs.

Applying boundary condition (i) in equation (4) we get,

$c_2 = \mu v'$ which after substitution gives,

$$\mu u_1 = \frac{P'_1 Y^2}{2} + \tau_{c1} Y + k \left(\frac{1}{4} P'_1{}^3 Y^4 + \tau_{c1}{}^3 Y + P'_1{}^2 Y^3 \tau_{c1} + \frac{3}{2} \tau_{c1}{}^2 P'_1 Y^2 \right) + \mu v' \quad (5)$$

Applying boundary condition (ii) in equation (5) we get,

$$0 = \frac{P'_1 h_1^2}{2} + \tau_{c1} h_1 + k \left(\frac{1}{4} P'_1{}^3 h_1^4 + \tau_{c1}{}^3 h_1 + P'_1{}^2 h_1^3 \tau_{c1} + \frac{3}{2} \tau_{c1}{}^2 P'_1 h_1^2 \right) + \mu v'$$

which after rearrangement and dividing by kh_1 can be written as,

$$\tau_{c1}{}^3 + \tau_{c1}{}^2 \left(\frac{3}{2} P'_1 h_1 \right) + \tau_{c1} \left(\frac{1}{k} + P'_1{}^2 h_1^2 \right) + \left(\frac{\mu v'}{kh_1} + \frac{P'_1 h_1}{2k} + \frac{1}{4} P'_1{}^3 h_1^3 \right) = 0 \quad (6)$$

Now, let

$$J_1 = \frac{3}{2} P'_1 h_1, \quad M_1 = \frac{1}{k} + P'_1{}^2 h_1^2$$

and

$$N_1 = \frac{\mu v'}{k h_1} + \frac{P_1' h_1}{2k} + \frac{1}{4} P_1'^3 h_1^3$$

so that,

$$\tau_{c1}^3 + J_1 \tau_{c1}^2 + M_1 \tau_{c1} + N_1 = 0 \quad (7)$$

Also, let

$$\tau_{c1} = \phi_1 - \frac{J_1}{3} \quad (8)$$

Substituting for τ_{c1} from equation (8) into (7) we get,

$$\left(\phi_1 - \frac{J_1}{3}\right)^3 + J_1 \left(\phi_1 - \frac{J_1}{3}\right)^2 + M_1 \left(\phi_1 - \frac{J_1}{3}\right) + N_1 = 0$$

which, after substitution for J_1 , M_1 and N_1 from above and simplification becomes,

$$\phi_1^3 + \phi_1 \left(\frac{1}{k} + \frac{1}{4} P_1'^2 h_1^2\right) + \frac{\mu v'}{k h_1} = 0$$

which may be written as

$$\phi_1^3 + A_1 \phi_1 + B_1 = 0 \quad (9)$$

where

$$A_1 = \frac{1}{k} + \frac{1}{4} P_1'^2 h_1^2$$

and

$$B_1 = \frac{\mu v'}{k h_1}$$

Equation (9) is a cubic equation which can be solved by applying Cardan's⁴² formula as outlined in Appendix 2.

$$\therefore \phi_1 = \left[-q + (q^2 + p^3)^{\frac{1}{2}} \right]^{\frac{1}{3}} + \left[-q - (q^2 + p^3)^{\frac{1}{2}} \right]^{\frac{1}{3}}$$

Substituting the values of ϕ_1 , A_1 , B_1 and J_1 in above equation becomes;

$$\tau_{c1} = \left[-\frac{\mu v'}{2kh_1} + \left\{ \frac{\mu^2 v'^2}{4k^2 h_1^2} + \frac{1}{27} \left(\frac{1}{k} + \frac{1}{4} P_1' 2h_1^2 \right)^3 \right\}^{\frac{1}{2}} \right]^{\frac{2}{3}} + \left[-\frac{\mu v'}{2kh_1} - \left\{ \frac{\mu^2 v'^2}{4k^2 h_1^2} + \frac{1}{27} \left(\frac{1}{k} + \frac{1}{4} P_1' 2h_1^2 \right)^3 \right\}^{\frac{1}{2}} \right]^{\frac{1}{3}} - \frac{1}{2} P_1' h_1 \quad (10)$$

Equation (10) gives the shear stress on the tube before deformation for known value of P_1' . The flow of the liquid polymer in axial direction within the gap before the step may be given by;

$$Q = \int_0^{h_1} u_1 dy$$

which upon substitution for u_1 from equation (5) and integrating, gives;

$$Q = \frac{P_1' h_1^3}{6\mu} + \frac{h_1^2 \tau_{c1}}{2\mu} + \frac{k}{\mu} \left(\frac{1}{20} P_1'^3 h_1^5 + \frac{1}{2} h_1^2 \tau_{c1}^3 + \frac{1}{4} P_1'^2 h_1^4 \tau_{c1} + \frac{1}{2} P_1' h_1^3 \tau_{c1}^2 \right) + v h_1 \quad (11)$$

The continuity equation for the flow of the liquid polymer can be written as,

$$\frac{d}{dx} Q_{x1} + \frac{d}{dy} Q_{y1} + \frac{d}{dz} Q_{z1} = 0$$

Since under laminar flow condition

$$\frac{d}{dy} Q_{y1} = \frac{d}{dz} Q_{z1} = 0$$

hence

$$\frac{d}{dx} (Q_1) = 0$$

substituting for τ_{c1} from equation (10) into (11) and differentiating it can be shown that,

$$\left(\frac{d^2 P}{dx^2} \right)_1 = 0,$$

hence

$$\left(\frac{dP}{dx} \right)_1 = P_1' = \text{constant} = \frac{P_m}{L_1}$$

where,

P_m is the pressure at the step and

L_1 is the length of the first section of the unit.

At this stage P_m is still undetermined but for continuity of flow we have,

mass flow rate in = mass flow rate out

or $Q_1 = Q_2$

The expression of Q_2 for the second part of the unit after the step may be obtained in the following manner. The steady state flow in the second part of the unit gives the relation between the pressure and shear stress gradient as

$$\left(\frac{dP}{dx}\right)_2 = - \left(\frac{d\tau_2}{dy}\right)_2$$

Integrating the above equation with respect to y gives

$$\tau_2 = - \left(\frac{dP}{dx}\right)_2 y + c_3$$

Once again at the surface of the tube,

where $y = 0$, $\tau_2 = \tau_{c2}$.

Hence c_3 the constant for integration is equal to τ_{c2} .

Therefore,

$$\tau_2 = - P'_2 y + \tau_{c2} \quad (12)$$

where,

$$\left(\frac{dP}{dx}\right)_2 = P'_2$$

Combining equations (12) and (1) we have,

$$- P'_2 y + \tau_{c2} + k(- P'_2{}^3 y^3 + \tau_{c2}{}^3 + 3P'_2{}^2 y^2 \tau_{c2} - 3\tau_{c2}{}^2 P'_2 y) = \mu \left(\frac{du}{dy}\right)_2$$

which upon integration with respect to y gives,

$$u_2 = \frac{-P'_2 y^2}{2\mu} + \frac{\tau_{c2} y}{\mu} + \frac{k}{\mu} \left(-\frac{1}{4} P'_2{}^3 y^4 + \tau_{c2}{}^3 y + P'_2{}^2 y^3 \tau_{c2} - \frac{3}{2} P'_2 y^2 \tau_{c2}{}^2 + c_4\right)$$

(13)

Again we have the boundary conditions that,

$$\text{at (i) } y = 0 \quad u_2 = v'$$

and

$$\text{at (ii) } y = h_2 \quad u_2 = 0$$

where,

u_2 is the velocity of the pressure medium at any point

$0 \leq y \leq h_2$ and v' is the velocity of the tube.

Applying the boundary condition (i) into equation (13) we get

$$c_4 = \mu v'_2$$

so that,

$$\mu u_2 = -\frac{P'_2 y^2}{2} + \tau c_2 y + k\left(-\frac{1}{4}P'_2{}^3 y^4 + \tau c_2{}^3 y + P'_2{}^2 y^3 \tau c_2 - \frac{3}{2}P'_2 y^2 \tau c_2{}^2\right) + v'_2 \mu \quad (14)$$

Applying the boundary condition (ii) into equation (14) we obtain

$$0 = -\frac{P'_2 h_2^2}{2} + \tau c_2 h_2 + k\left(-\frac{1}{4}P'_2{}^3 h_2^4 + \tau c_2{}^3 h_2 + P'_2{}^2 h_2^3 \tau c_2 - \frac{3}{2}P'_2 h_2^2 \tau c_2{}^2\right) + v'_2 \mu.$$

Now, rearranging the above equation and dividing by kh_2 we

get,

$$\tau c_2^3 + \tau c_2^2\left(-\frac{3}{2}P'_2 h_2\right) + \tau c_2\left(\frac{1}{k} + P'_2{}^2 h_2^2\right) + \left(\frac{\mu v'}{kh_2} - \frac{P'_2 h_2}{2k} - \frac{P'_2{}^3 h_2^3}{4}\right) = 0$$

Let

$$J_2 = -\frac{3}{2}P'_2 h_2$$

$$M_2 = \frac{1}{k} + P'_2{}^2 h_2^2$$

and

$$N_2 = \frac{\mu v'}{kh_2} - \frac{1}{4}P'_2{}^3 h_2^3 - \frac{P'_2 h_2}{2k}$$

Hence,

$$\tau c_2^3 + J_2 \tau c_2^2 + M_2 \tau c_2 + N_2 = 0 \quad (15)$$

$$\text{Let } \tau c_2 = \phi_2 - \frac{J_2}{3} \quad (16)$$

Substituting for τc_2 from equation (16) into (15) and simplifying we get

$$\phi_2^3 + A_2 \phi_2 + B_2 = 0 \quad (17)$$

where,

$$A_2 = \frac{1}{k} + \frac{1}{4} P_2' h_2^2$$

and

$$B_2 = \frac{\mu v'}{k h_2}$$

Again equation (17) has two imaginary roots and one real roots, the real roots being, (see Appendix)

$$\phi_2 = \left[-\frac{B_2}{2} + \left(\frac{B_2^2}{4} + \frac{A_2^3}{27} \right)^{\frac{1}{2}} \right]^{\frac{1}{3}} + \left[-\frac{B_2}{2} - \left(\frac{B_2^2}{4} + \frac{A_2^3}{27} \right)^{\frac{1}{2}} \right]^{\frac{1}{3}}$$

Substituting for A_2 and B_2 into above equation and combining with equation (16) we have

$$\tau c_2 = \left[-\frac{\mu v'}{2k h_2} + \left\{ \frac{\mu^2 v'^2}{4k^2 h_2^2} + \frac{1}{27} \left(\frac{1}{k} + \frac{1}{4} P_2' h_2^2 \right)^3 \right\}^{\frac{1}{2}} \right]^{\frac{1}{3}} + \left[-\frac{\mu v'}{2k h_2} - \left\{ \frac{\mu^2 v'^2}{4k^2 h_2^2} + \frac{1}{27} \left(\frac{1}{k} + \frac{1}{4} P_2' h_2^2 \right)^3 \right\}^{\frac{1}{2}} \right]^{\frac{1}{3}} + \frac{1}{2} P_2' h_2 \quad (18)$$

Equation (18) gives shear stress on the tube in the second part of the unit for known value of P_2' . The flow of the liquid polymer in axial direction within the gap after the step may be given by

$$Q_2 = \int_0^{h_2} u_2 dy$$

which upon substitution for u_2 from equation (14) and integrating becomes

$$Q_2 = -\frac{P_2' h_2^3}{6\mu} + \frac{\tau c_2 h_2^2}{2\mu} + \frac{K}{\mu} \left(-\frac{1}{20} P_2'^3 h_2^5 + \frac{1}{2} h_2^2 \tau c_2^3 + \frac{1}{4} P_2'^2 h_2^4 \tau c_2 - \frac{1}{2} P_2' h_2^3 \tau c_2^2 \right) + v h_2 \quad (19)$$

Again for laminar flow we have

$$\frac{d}{dx} (Q_2) = 0$$

Combining equations (18) into (19) and differentiating it can be shown as before, that

$$\left(\frac{d^2P}{dx^2}\right)_2 = 0$$

hence,

$$\left(\frac{dP}{dx}\right)_2 = P'_2 = \text{constant} = -\frac{P_m}{L_2}$$

where,

P_m is the pressure at the step and L_2 is the length of the unit after the step. It is shown that the pressure profile in the second part of the unit is also linear. We know that if pressure increases, the viscosity of polymers also increases and for better model this effect should be included in the analysis. A generalized equation relating viscosity and pressure may be of the form (See Fig 20)

$$\mu = \mu_0 + \frac{a + bP_m^2}{\dot{\gamma}}$$

where a and b are constants, μ_0 is the initial viscosity of the polymer melt, P_m is the pressure at the step and $\dot{\gamma}$ is the apparent shear rate and is assumed to be

$$\dot{\gamma} = \frac{v'}{h_1}$$

By putting the value of $\dot{\gamma}$ into the above equation, we get

$$\mu = \mu_0 + \frac{h_1}{v'}(a + bP_m^2) \quad (20)$$

In equation (20) only the parameter P_m is unknown for finding the viscosity of the polymer. Numerical values of P_m and hence P'_1 and P'_2 may be substituted into equation (10), (11), (18), (19) and (20) which may then be solved

simultaneously, using an iteration technique, until the continuity equation of flow $Q_1 = Q_2$ is satisfied. Therefore, pressure in the unit, viscosity of the polymer melt and the shear stresses on the tube can be determined.

Criterion for Plastic Deformation

Considering the axial force equilibrium of an element of the tube, within the die-less reduction unit before any deformation commences (see Fig 131(b)) we have,

$$d\sigma_x \times 2\pi r t - 2\pi r \cdot dx \cdot \tau_{c1} = 0$$

so that

$$d\sigma_x = \frac{\tau_{c1} dx}{t}$$

Integrating of the above equation gives,

$$\sigma_x = \frac{\tau_{c1} x}{t} + c_5$$

at $x = 0$, $\sigma_x = 0$, hence $c_5 = 0$ and

$$\sigma_x = \frac{\tau_{c1} x}{t} \tag{21}$$

The radial force equilibrium gives

$$P \cdot r d\theta \cdot dx = 2\sigma_\theta \cdot t \cdot dx \cdot \sin \frac{d\theta}{2}$$

which for small angle, $d\theta$, becomes

$$\sigma_\theta = \frac{Pr}{t}$$

where σ_θ is the hoop stress and P is the pressure and

$$\sigma_x < P < \sigma_\theta.$$

For plastic deformation to commence the yield criterion according to Tresca gives

$$\sigma_1 - \sigma_3 = y_0$$

where y_0 is the yield stress of the tube material.

But $\sigma_1 = \sigma_x$ and $\sigma_3 = -\sigma_\theta$, so that

$$\sigma_x + \sigma_\theta = y_0 \quad (22)$$

Let x_1 be the distance from the entry to the step where plastic deformation commences, so that $\sigma_{x_1} = \frac{\tau_c x_1}{t}$

$$\text{and } \sigma_\theta = \frac{Pr}{t} = \frac{Pm x_1 r_1}{L_1 t}$$

$$\text{since } P = \frac{Pm x_1}{L_1}$$

Equation (22) thus becomes

$$\frac{\tau_c x_1}{t} + \frac{Pm x_1 r_1}{L_1 t} = y_0$$

so that,

$$x_1 = y_0 / \left(\frac{\tau_c}{t} + \frac{Pm r_1}{L_1 t} \right) \quad (23)$$

Once yielding occurs, plastic deformation will continue as long as the yield criterion

$$\sigma_{x_1} + \sigma_{\theta_1} = y = y_0 + k\epsilon^n$$

is satisfied for a strain hardening material of the tube.

(ii) After Deformation

Consider the zone of the stepped bore reduction unit where deformation of the tube takes place. Let us assume that between any two points distance ' dx ' apart on the deforming tube, the deformation takes place linearly at an angle α .

Considering a small section of the deforming tube, (shown in Fig 134(b)), the equilibrium of forces acting normal to the surface we have,

$$P \left(r d\theta \frac{dr}{\sin \alpha} \right) - \sigma_\theta \left(t \frac{dr}{\sin \alpha} \right) d\theta \cos \alpha = 0$$

After simplification becomes,

$$Pr = \sigma_\theta t \cos \alpha$$

$$\text{or } P = \sigma_\theta \frac{t}{r} \cos \alpha \quad (24)$$

Hence P is very small in comparison to σ_θ when $\frac{t}{r}$ is small. The stresses in this deformation process are therefore such that $\sigma_\theta > P > \sigma_x$.

Equilibrium of forces in the x -direction gives;

$$(\sigma_x + d\sigma_x)(r + dr)\Delta\theta(t + dt) - \sigma_x r t \Delta\theta + \sigma_\theta \left(t \frac{dr}{\sin \alpha}\right) \Delta\theta \sin \alpha + \tau_c \left(r \Delta\theta \frac{dr}{\sin \alpha}\right) = 0$$

which after simplification, neglecting second-order smaller quantities and dividing by dr becomes,

$$\frac{d}{dr} (\sigma_x r t) + \sigma_\theta t + \tau_c \frac{r}{\sin \alpha} = 0$$

Let the wall-thickness of the tube remain unaltered during the deformation, so that the above equation becomes;

$$\frac{d}{dr} (\sigma_x r) + \sigma_\theta + \tau_c \frac{r}{t \sin \alpha} = 0$$

after differentiating above equation gives;

$$r \frac{d\sigma_x}{dr} + \sigma_x + \sigma_\theta + \tau_c \frac{r}{t \sin \alpha} = 0 \quad (25)$$

Substituting for $(\sigma_x + \sigma_\theta)$ in equation (25) we get

$$r \frac{d\sigma_x}{dr} + \tau_c \frac{r}{t \sin \alpha} = 0$$

or

$$d\sigma_x = -\tau_c \frac{dr}{r} - \tau_c \frac{dr}{t \sin \alpha} \quad (26)$$

This is the governing equation which enables prediction of the axial stress in the tube within the deformation zone.

Let

$$\frac{dr}{dx} = \tan \alpha = B$$

which in finite difference form can be expressed as,

$$\frac{r_{i-1} - r_i}{\Delta x} = \frac{r_{i-1} - r_i}{x_i - x_{i-1}} = \tan \alpha = B$$

so that

$$r_i = r_{i-1} - B\Delta x \quad (27)$$

The variation of gap in between the outer surface of the tube and inner surface of the DRU in the deformation zone can similarly be written as,

$$dh = dr = Bdx$$

which in finite difference form becomes

$$h_i = h_{i-1} + \Delta x B \quad (28)$$

where B is the slope of the deformation line along distance 'dx'.

The variation of speed of the tube in the deformation zone may be determined from the continuity of flow of metal through the small element (as shown in Fig 134(b))

Thus,

$$(r + dr)\Delta\theta(t + dt)(v + dv) = r\Delta\theta tv$$

which after simplification and neglecting second-order smaller quantities becomes,

$$\frac{dr}{r} + \frac{dv}{v} + \frac{dr}{r} \frac{dv}{v} = 0$$

hence,

$$\frac{dv}{v} = - \frac{dr}{r + dr}$$

Rewriting the above equation in finite difference form and rearranging we have

$$v_i = \frac{v_{i-1}}{1 - \frac{(r_{i-1} - r_i)}{r_{i-1}}} \quad (29)$$

Rewriting equation (26) in finite difference form and rearranging we have,

$$\sigma_{xi} = \frac{(r_{i-1} - r_i)}{r_i} \gamma_i + \frac{\tau_{ci}}{t} \sqrt{(r_{i-1} - r_i)^2 + (x_i - x_{i-1})^2} + \sigma_{xi-1} \quad (30)$$

Equation (30) is a function of shear stress and it must be determined independently.

The expression for the shear stress on the surface of the deformed tube may be given by equation (10) by simply re-writing in finite difference notations

$$\begin{aligned} \tau_{ci} = & \left[-\frac{\mu v_i}{2kh_i} + \left\{ \frac{\mu^2 v_i^2}{4k^2 h_i^2} + \frac{1}{27} \left(\frac{1}{k} + \frac{1}{4} P_i^2 h_i^2 \right)^3 \right\}^{\frac{1}{2}} \right]^{\frac{1}{3}} + \left[-\frac{\mu v_i}{2kh_i} \right. \\ & \left. - \left\{ \frac{\mu^2 v_i^2}{4k^2 h_i^2} + \frac{1}{27} \left(\frac{1}{k} + \frac{1}{4} P_i^2 h_i^2 \right)^3 \right\}^{\frac{1}{2}} \right]^{\frac{1}{3}} - \frac{1}{2} P_i h_i \end{aligned} \quad (31)$$

Again, equation (31) is a function of pressure gradient and it must be determined separately. Flow of the polymer melt in the deformation zone may be expressed in finite difference notation as,

$$\begin{aligned} Q_1 = & \frac{P_i h_i^3}{6\mu} + \frac{\tau_{ci} h_i^2}{2\mu} + \frac{k}{\mu} \left(\frac{1}{20} P_i^3 h_i^5 + \frac{1}{2} h_i^2 \tau_{ci}^3 + \frac{1}{4} P_i^2 h_i^4 \tau_{ci} + \right. \\ & \left. \frac{1}{2} P_i h_i^3 \tau_{ci}^2 \right) + v_i h_i. \end{aligned}$$

The continuity equation for the flow of the liquid polymer gives $Q_1 = Q_2$. Rearranging the above equation leads to,

$$\begin{aligned} \left(\frac{kh_i^5}{20\mu} \right) P_i^3 + \left(\frac{kh_i^4 \tau_{ci}}{4\mu} \right) P_i^2 + \left(\frac{h_i^3}{6\mu} + \frac{kh_i^3 \tau_{ci}^2}{2\mu} \right) P_i + \left(v_i h_i + \right. \\ \left. \frac{h_i^2 \tau_{ci}}{2\mu} + \frac{kh_i^2 \tau_{ci}^3}{2\mu} - Q_1 \right) = 0 \end{aligned} \quad (32)$$

Equations (31) and (32) may be solved simultaneously in order to determine P_i and τ_{ci} by iterating P_i at point "i" in the deformation zone, until the equation (32) is satisfied. Once P_i is so obtained then the pressure in the deformation is simply expressed as

$$P_i = \left(\frac{dP}{dx} \right)_i = \frac{P_i - P_{i-1}}{\Delta x}$$

$$\text{or } P_i = P_i \Delta x + P_{i-1} \quad (33)$$

where P_i is the pressure at any point within the deformation zone.

The hoop stress in the deformation zone is given by equation (24), which after rewriting in finite difference form leads to;

$$\sigma_{\theta i} = \frac{P_i r_i \sqrt{(x_i - x_{i-1})^2 + (r_{i-1} - r_i)^2}}{t(x_i - x_{i-1})} \quad (34)$$

where σ_{θ} is the hoop stress in the deformation zone.

The stress-strain relationship of the tube material has been shown in Figs 28 and 29 to take the form,

$$y = y_0 + k_0 \epsilon^n$$

$$\text{where } \epsilon = \ln\left(\frac{r_1}{r}\right)$$

$$\text{therefore } y = y_0 + k_0 \left(\ln \frac{r_1}{r}\right)^n$$

The above equation in finite difference notation becomes,

$$y_i = y_0 + k_0 \left(\ln \frac{r_1}{r_i}\right)^n \quad (35)$$

The strain rate sensitivity of the tube material may also be taken into account in the analysis. The mean strain rate of the material over a small distance "dx" may be expressed as;

$$\bar{\epsilon} = \left(-2 \frac{dr}{r}\right) \frac{1}{dt}$$

or

$$\bar{\epsilon}_{mi} = \frac{1}{x_i - x_{i-1}} \int_{r_{i-1}}^{r_i} \bar{\epsilon} dx$$

where $x = x_{i-1}$ at $r = r_{i-1}$

and $x = x_i$ at $r = r_i$

By substituting $\bar{\epsilon}$ in above equation gives;

$$\bar{\epsilon}_{mi} = \frac{1}{\Delta x} \int_{r_{i-1}}^{r_i} -2 \frac{dr}{r} \frac{dx}{dt}$$

where $x_i - x_{i-1} = \Delta x$

but $\frac{dx}{dt} = v_i$

Therefore,

$$\bar{\epsilon}_{mi} = -\frac{2v_i}{\Delta x} \int_{r_{i-1}}^{r_i} \frac{dr}{r}$$

Integration gives;

$$\bar{\epsilon}_{mi} = \frac{2v_i}{\Delta x} \ln \left(\frac{r_i - 1}{r_i} \right) \quad (36)$$

A flow rule of the form;

$$s = \frac{y_d}{y_s} = 1 + \left(\frac{\bar{\epsilon}_m}{N} \right)^T$$

where y_d = dynamic yield stress of the material

and y_s = static yield stress of the material

has been proposed by Hashmi⁴³ and Ting.⁴⁴ In finite difference notation the above equation takes the form;

$$s_i = 1 + \left(\frac{\bar{\epsilon}_{mi}}{N} \right)^T$$

where T and N are material constant.

Combining the above equation with equation (35) gives,

$$y_i = s_i \left(y_0 + k_0 \left(\ln \frac{r_1}{r_i} \right)^n \right) \quad (37)$$

Equation (37) represents the yield stress of the tube, incorporating strain hardening and strain rate sensitivity of the material. Substituting for y into equation (30) we have

$$\sigma_{x_i} = \left(\frac{r_{i-1} - r_i}{r_i} \right) s_i \left(y_0 + k_0 \left(\ln \frac{r_1}{r_i} \right)^n \right) + \frac{t c_i}{t} \sqrt{(r_{i-1} - r_i)^2 + \sqrt{(x_i - x_{i-1})^2 + \sigma_{x_{i-1}}}} \quad (38)$$

At any point within the deformation zone, the Tresca theory of yielding gives;

$$\sigma_x + \sigma_\theta = y \quad (\text{as before})$$

Representing this equation in finite difference form we obtain;

$$\sigma_{x_i} + \sigma_{\theta_i} = y_i \quad (39)$$

Solution Procedure

At any point "i" in the deformation zone, r_i and h_i may be calculated from equation (27) and (28) respectively for an arbitrary value of "B" and a step size of Δx . r_i may be substituted into equation (29) which gives v_i . Also by substituting v_i and h_i into equation (31) and (32) which gives τ_{ci} and P'_i simultaneously by iterating for P'_i until equation (32) is satisfied. Hence substituting P'_i into equation (33) gives P_i . $\sigma_{\theta i}$ can be calculated from equation (34) by substituting for P_i and r_i . Then τ_{ci} , r_i and s_i may be substituted into equation (38) to evaluate σ_{xi} . Substituting values of r_i , h_i and v_i into equations (36) and (37), the yield stress y_i may be calculated. Other variables in the above equations are the known physical parameters.

Having calculated σ_{xi} , $\sigma_{\theta i}$ and y_i values of "B" may be iterated. Unit equation (39) is satisfied at any point in the deformation zone. This procedure may be repeated in suitable steps of Δx from the position of yield of the tube inside the stepped bore reduction unit where $i = 1$ at $x = x_1$ and up to the step. This procedure may be repeated at each speed increments. Therefore at the step, when equation (39) is satisfied, the drawing speed, final tube diameter and the final gap are given by;

$$\text{drawing speed } v_d = v_i$$

$$\text{final tube diameter } D_2 = D_i \text{ or } 2r_2 = 2r_i$$

$$\text{final gap } h_3 = h_i - h_1 + h_2$$

respectively.

Condition of Slip

It is known that polymers have a critical shear stress at which slip occurs. It is assumed that slip takes place at the tube-polymer interface only and not at the unit wall-polymer interface. Boundary conditions for slip are;

when,

$$\text{at (i) } y = h_1 \quad u_1 = 0$$

and

$$\text{at (ii) } y = 0 \quad u_1 = v_s$$

Therefore equation (11) becomes;

$$Q_s = \frac{P_1 h_1^3}{6\mu} + \frac{h_1^2 \tau_{ca}}{2\mu} + \frac{k}{\mu} \left(\frac{1}{20} P_1^3 h_1^5 + \frac{1}{2} h_1^2 \tau_{ca}^3 + \frac{1}{4} P_1^2 h_1^4 \tau_{ca} + \frac{1}{2} P_1 h_1^3 \tau_{ca}^2 a \right) + v_s h_1 \quad (40)$$

where Q_s is the mass flow rate of molten polymer when slip occurs and v_s is the velocity at which slip occurs.

v_s may be determined from no-slip conditions when τ_{ca} has reached the critical value. In references (15 to 19), the critical shear stress is shown to have values between 0.1 to 1.0 mN/m² for different polymer melts. When polypropylene and polystyrene polymers were being extruded at 200°C and 230°C, evidence of slip were observed at about 0.25×10^6 N/m² and 0.15×10^6 N/m² respectively. Critical shear stress for polyethylene polymer was shown by Westover³⁴ to take place at about 0.7×10^6 N/m² and also critical shear stress for Rigidex was 0.5×10^6 N/m² shown by Westover³⁷ and Cogswell.³⁶ Therefore an average critical shear stress of 0.4×10^6 N/m² is assumed for the slip in the analysis.

Equation (40) shows that when slip occurs, flow of polymer remains constant and subsequently pressure and shear

stress will also remain constant. Hence as drawing speed increases after slip, the reduction in diameter of the tube should progressively reduce. Equations governing the deformation zone are those derived previously, therefore they are only listed here,

$$r_i = r_{i-1} - B\Delta x \quad (41)$$

$$h_i = h_{i-1} + B\Delta x \quad (42)$$

$$v_i = \frac{v_{i-1}}{1 - \frac{(r_{i-1} - r_i)}{r_{i-1}}} \quad (43)$$

$$\sigma_{\theta i} = \frac{P_i r_i \sqrt{(x_i - x_{i-1}) + (r_{i-1} - r_i)}}{t(x_i - x_{i-1})} \quad (44)$$

$$\bar{\epsilon}_{mi} = \frac{2v_i}{\Delta x} \ln \left(\frac{r_{i-1}}{r_i} \right) \quad (45)$$

$$s_i = 1 + \left(\frac{\bar{\epsilon}_{mi}}{N} \right)^{\frac{1}{T}} \quad (46)$$

$$y_i = s_i \left(y_0 + k_0 \left(\ln \frac{r_1}{r_i} \right)^n \right) \quad (47)$$

$$\sigma_{x_i} = \frac{(r_{i-1} - r_i)}{r_i} s_i \left(y_0 + k_0 \left(\ln \frac{r_1}{r_i} \right)^n \right) + \frac{\tau_{ca}}{t} \sqrt{(r_{i-1} - r_i)^2 + \sqrt{(x_i - x_{i-1})} + \sigma_{x_{i-1}}} \quad (48)$$

Solution procedure is the same as before. The only exception is that P_i remains constant for every speed increment after the slip. For a suitable step of Δx and an arbitrary value of B , r_i , h_i , and v_i may be calculated from equations (41), (42) and (43) respectively.

Substituting r_i in equation (44) we get $\sigma_{\theta i}$. Substituting r_i and v_i into equation (45) gives $\bar{\epsilon}_{mi}$ and equation (46) gives s_i . Substituting s_i and r_i into equations (47) and (48), y_i and σ_{xi} may be calculated. Having calculated y_{mi} , $\sigma_{\theta i}$ and σ_{xi} , numerical values of 'B' may be iterated in above equations until equation $\sigma_{xi} + \sigma_{\theta i} = y_i$ is satisfied. This procedure may be repeated at Δx intervals in the deformation zone from $i = x_1$ up to the step where $i = L_1 - x_1$.

A computer programme was written to solve the relevant equations.

6.3 Results from the Analysis

Theoretical results were calculated on the basis of equations derived in the theoretical analysis section. The data below are the known parameters which were used to solve the equations and were varied to show their effect on the performance of the unit. The results predicted based on this analysis were found to be in closer agreement with those obtained experimentally than those predicted using Newtonian analysis.

(i) Dimensions of the die-less reduction unit;

Total length of the die-less reduction unit = 190 mm

Position of step from inlet, $L_1 = 160$ mm

Position of step from outlet, $L_2 = 30$ mm

Inlet gap, $h_1 = 0.5$ mm, Outlet gap, $h_2 = 0.01$ mm

$h_1/h_2 = 50$

$L_1/L_2 = 5.33$

(ii) Data for polymer;

$\mu_0 = 100$ Ns/m²

$K = 5.6 \times 10^{-11}$ m⁴/N²

$a = 12 \times 10^4$ N/m²

$b = 4 \times 10^{-11}$ m²/N

$\tau_{ca} = 4 \times 10^5$ N/m²

(iii) Data for copper tube;

$D_1 = 13.52$ mm

$t = 2.50$ mm

$Y_0 = 50$ MN/m²

$K_0 = 700$ MN/m²

$n = 0.18$

$T = 3.8$

$N = 55 \times 10^3$

In order to predict the theoretical results presented in this section the non-Newtonian viscosity parameter of the polymer was adjusted using a division factor. The use of this factor caused not only the trend but also the magnitudes of the results to be in close agreement with those observed experimentally. Different factors were used ranging from 1.5 to 5 but finally it was found that 3 is the most appropriate value. The justification of using the division factor is the fact that during the deformation process temperature rises due to high shear rate and plastic work which in turn causes the viscosity to change. The exact magnitude of this change is difficult to ascertain and hence the division factor was obtained by trial and error.

6.3.1 Percentage Reduction in Diameter

Figs (182) and (183) show the effect of gap ratios on percentage reduction in diameter. In order to predict these results h_1 was kept constant whilst h_2 was changed. As the gap ratio was increased the percentage reduction in diameter also increased. However, as the drawing speed was increased the effect became gradually negligible. The results in Fig (183) suggest that for lower values of h_1/h_2 greater percentage reduction in diameter should be obtained at lower drawing speeds. These results were obtained by changing h_1 whilst keeping h_2 constant.

Fig (184) shows the variation in percentage reduction in diameter with the drawing speed for different values of L_1/L_2 . This figure suggests that for higher values of L_1/L_2 greater percentage reduction in diameter should be obtained at lower drawing speeds and also that the critical shear stress occurred at these speeds.

Fig (185) shows the theoretical effect of changing the initial viscosity of the pressure medium on the percentage reduction in diameter. This figure indicates that an increase in the viscosity caused the percentage reduction in diameter to increase, especially, at lower drawing speeds.

The effect of initial yield stress of the tube material on percentage reduction in diameter is shown in Fig 186. These results were calculated with different values of Y_0 varying from 30 to 80 MN/m². This figure suggests that for lower values of Y_0 , relatively greater permanent deformation should be obtained at a given drawing speed.

Fig (187) shows the effect of the strain hardening constant, K_0 , on percentage reduction in diameter. This figure shows similar trend as in above figure.

Fig (188) shows the effect of the strain hardening index, n , on the percentage reduction in diameter. This figure indicates that with the strain hardening index, $n = 0.38$, a reduction in diameter of about 10 per cent should be obtained for the drawing speed of 0.1 m/s and that for lower values of ' n ' smaller reduction in diameter is predicted at the same drawing speed of 0.1 m/s.

The effects of changes in the wall-thickness of the tube on percentage reduction in diameter is demonstrated in Fig (189). The wall-thickness of the tube was changed from 2.00 to 2.50 mm. For a drawing speed of 0.1 m/s, it is evident that permanent reduction in diameter of about 9.5 per cent should be obtained in a tube of 2.00 mm wall-thickness, but only 5 per cent reduction in diameter may take place for a higher value of tube wall-thickness (2.50 mm) at the same drawing speed of 0.1 m/s.

Fig (190) shows the effect of changing the diameter of the tube on the percentage reduction in diameter. This figure suggests that for higher values of D_1 relatively greater permanent deformation could be obtained at lower drawing speeds.

The theoretical effect of changing shear stress constant, K , is shown in Fig (191) where the percentage reduction in diameter is shown to increase as ' K ' is reduced. Also as a result of increase in the shear stress constant, the critical shear stress was predicted to occur at lower drawing speeds.

The effects of other variables were also examined theoretically in order to investigate their influence on the percentage reduction in diameter. Increasing the values of the viscosity constant, coefficient of pressure and the critical shear stress, higher percentage reduction in diameter should be obtained at lower drawing speeds. In order that the effect of strain rate sensitivity constant, N , and strain rate sensitivity index, T , on percentage reduction in diameter could be studied, results were calculated and it was found that as the magnitude of ' N ' was increased the percentage reduction in diameter was also increased and reduction in ' T ' causes smaller percentage reduction in diameter in the tube.

6.3.2 Coating Thickness

Results of the coating thickness exhibited similar trends as those of the percentage reduction in diameter. Fig (192) shows the effect of the gap ratio on the coating thickness. This figure shows that for higher value of gap ratio relatively greater coating thickness would be obtained.

Fig (193) shows the effect of length ratio on coating thickness. To introduce different length ratios, L_2 was kept constant. These results show that as the length ratio was increased, the coating thickness also increased. The maximum coating thickness was obtained for a length ratio of 5.50 at 0.1 m/s.

Fig (194) shows the effect of initial yield stress on the coating thickness. The trend of the results predicted are similar to that of the percentage reduction in diameter (see Fig 186). This figure suggests that lower values of Y_0 cause greater coating thickness at lower drawing speeds.

The effect of the tube wall-thickness on the coating thickness is shown in Fig (195). This figure indicates that higher coating thickness should be obtained for lower values of tube wall-thickness.

Fig (196) shows the effect of the tube diameter on the coating thickness. The trends of the results obtained are similar to those of the percentage reduction in diameter (see Fig 190). This figure suggests that higher values of D_1 , cause greater coating thickness.

6.3.3 Yielding Position of the Tube

The positions at which the tube was predicted to yield plastically seemed to be generally constant except at lower drawing speeds where x_1 increases slightly as the drawing speed is reduced.

Fig (197) shows the theoretical effect of the gap ratio on the yielding position of the tube. This figure shows that for a higher value of h_1/h_2 plastic deformation commences further away from the step and greater percentage reduction in diameter should be obtained.

Fig (198) shows the effect of the length ratio on the position of yield of the tube. As the length ratio was increased, the

undeformed length of the tube (x_1) was decreased. For drawing speeds in excess of 0.2 m/s, a constant value of $x_1 = 15$ mm was predicted for all length ratios.

Fig (199) shows the effect of the initial yield stress on the yielding position of the tube. As the initial yield stress was reduced, the distance x_1 also reduced, thus increasing the deformation zone.

6.3.4 Pressure

Fig (200) shows the theoretical pressure distributions for different gap ratios but at same drawing speed of 0.3 m/s. This figure indicates that higher values of h_1/h_2 , cause higher pressure. The maximum pressure readings were predicted at the step for both gap ratios.

Figs (201) and (202) show the effects of initial yield stress and tube wall-thickness respectively on pressure distributions for same gap ratio and drawing speed. Again in all cases the theoretical pressure was predicted to be the maximum at the step. The maximum pressure was predicted to vary between 150-172 MN/m².

Fig (203) shows the effect of the tube diameter on the pressure distributions for constant gap ratio and drawing speed. This figure suggests that for higher values of D_1 relatively lower pressure was predicted.

6.3.5 Drawing Stress

The theoretical predicted effect of the gap ratio on the drawing stress is shown in Fig (204). This figure shows that the drawing stress was maximum when the reduction in diameter was maximum, ie at drawing speed of about 0.1 m/s. The maximum drawing stress (about 36 MN/m²) was predicted for the gap ratio of 50. Drawing stresses for all the gap ratios decreased as the drawing speed was

increased. At speeds in excess of 0.2 m/s approximately constant drawing stresses were predicted.

The effect of the length ratio on the drawing stress is shown in Fig (205). These results show similar trend as shown in Fig (204), lower drawing speeds producing higher drawing stresses.

Fig (206) shows the effect of the tube diameter on the drawing stress. This figure suggests that for higher values of D_1 relatively higher drawing stress would be developed at lower drawing speeds. The diameter of the tube was varied from 14.50 to 12.00 mm and it is evident that at the drawing speed of 0.1 m/s, the drawing stress of about 41 MN/m² was predicted for a tube of 14.50 mm diameter and about 28 MN/m² for a tube of 12.00 mm diameter.

Fig (207) shows the effect of the strain hardening index on drawing stress. These results show similar trends as shown in Fig (206). For higher values of 'n' higher drawing stress would be developed.

6.3.6 Deformation Profile

Theoretically calculated deformation profiles at different drawing speeds are shown in Fig (208). This figure shows that the theoretically predicted deformation profiles have close similarity with those observed experimentally (shown in Fig 111).

6.4 Discussion on the Theoretical and Experimental Results

A new technique of die-less tube sinking has been developed, in which a polymer melt is used in order to generate hydrodynamic pressure within a tubular unit. An extensive experimental and theoretical programme of study was undertaken to investigate the performance of the die-less reduction unit which produced a considerable amount of data. This section aims to highlight the results obtained experimentally and theoretically and provide comparison of typical results.

6.4.1 Test Procedure and Experimental Results

In this study a number of interesting observations were made while carrying out the experimental tests. In the experimental programme, parameters such as gap and length ratio of the die-less reduction unit, polymer type, melt temperature, tube material, the diameter and wall-thickness of the tube and the drawing speed were varied in order to investigate their effect on the performance of the die-less reduction unit.

The results of the percentage reduction in diameter versus drawing speed using WVG23, KM61, Rigidex and polystyrene polymers as the pressure medium are shown in Figs 31 to 38 respectively. All these figures show that at higher gap ratio, the reduction in the diameter of the tube obtained is higher with lower drawing speeds. The result of decreasing the inlet gap was to reduce the deformation of the tube. This may be explained in terms of the pressure generated due to the geometry of the die-less reduction unit, ie as the inlet gap decreases, the polymer flow rate also decreases in the unit which in turn is thought to be responsible for lower pressure. An increase in the inlet gap may cause back flow of the polymer melt which would also reduce pressure and

therefore reduce the percentage reduction in the diameter. An increase in the exit gap may also reduce the deformation of the tube. The reason for this is that as the exit gap increases, the flow of the polymer becomes less restricted hence lower pressures are generated which leads to smaller reduction in diameter. An optimum gap ratio is thus present for which a balance is struck between these effects.

The drawing speed was found to be the dominant factor to affect the performance of the die-less reduction unit. This is due to the effect of the shear rate on the viscosity of the polymer which leads to the condition of slip in the polymer at higher drawing speeds. Two types of the flow of polymer are thought to occur as the drawing speed is increased. These are sub-critical and critical flow which are observed more in the case of WVG23 polymer. It is possible that at low speeds the stick-slip phenomenon of the polymer melt along the surface of the tube produced a discontinuity in pressure generation. As the speed was increased, a critical shear stress value was surpassed which then caused slip to be continuous, producing a constant pressure (irrespective of speed) and hence the performance of the die-less reduction unit was reduced.

Figs 39 to 42 show the effect of the length ratio on the percentage reduction in diameter. The trend of the results were found to be similar to those of gap ratio. At higher length ratio, the reduction in the tube diameter obtained was higher. This was due to the fact that increasing the length ratio resulted in higher pressures in the die-less reduction unit.

Fig 43 shows the effect of viscosity on the percentage reduction in diameter using WVG23 polymer as a pressure medium at different

melt temperatures. The effect of increasing the melt temperature was to reduce the viscosity of the polymer and hence to reduce the pressures generated which caused less deformation in the tube.

The results of the percentage reduction in diameter using KM61 polymer at different melt temperatures (Figs 44 and 48) indicate that, unlike the WVG23 polymer, the initial flow of the polymer and slip are both dependent upon the speed. After commencement of the flow of the polymer, the percentage reduction in diameter for copper tube decreased as the drawing speed was increased. The transition of the flow of the polymer was only observed for copper tube which occurred at about 0.2 m/s. At speeds less than 0.2 m/s the reduction of the tube was found to be random. The reason for the random reduction in the diameter of copper tube, prior to initial flow of the polymer is thought to be the excessive axial stress due to back pull of the polymer. At the melt temperature of 200°C, aluminium tube was found to be squeezed and folded along the length. The reason for this phenomenon is higher pressures generated in the unit which caused buckling instability and hence folding.

Shark-skin is another defect associated with the flow of the polymer melt which appears on the polymer extrudates at shear stresses below the critical value. This was confirmed while KM61 and polystyrene polymers were being extruded through an extrusion rheometer (see Figs 11 and 13). It is also shown that the formation of the shark-skin takes place outside the extrusion die.¹⁵ It is doubted that the condition in an extrusion rheometer can be considered to be similar to that in this particular case since polymer melt was subjected to pressures much higher than those applied in an extrusion rheometer.

The drawing load was monitored from the load indicator shown in Plate 2 which is presented in this section in terms of the drawing stress. The drawing stress followed the same trends as the percentage reduction in diameter, ie at low speeds the drawing stresses were found to be higher which decreased as the speed was increased. This again provides evidence of slip in the unit. Immediately after engaging the dog with the chain, the sudden increase in the drawing stress was noted which was maintained for about one second before full drawing stress was established. The time taken for the development of the flow of the polymer in the die-less reduction unit is thought to be responsible for the delay in reaching the full drawing stress.

The decrease in the gap ratio of the die-less reduction unit, when WVG23 polymer was used, increased the drawing stress at slower drawing speeds as shown in Fig 51. The extra amount of polymer flow in the unit is thought to be responsible for the increase in the drawing stress. The effect of increasing the melt temperature was to reduce the viscosity of the polymer which caused less deformation in the tube and hence lower drawing stresses were measured (see Figs 63 to 70).

Three pressure transducers were mounted on the die-less reduction unit and for each speed increment the trace of the pressure at each location was recorded on the U.V. paper. The schematic diagram of the arrangement for pressure measurement is shown in Fig 23. Figs 71 to 102 show the measured pressures for different tube materials and polymers used for the tests. The effect of increasing the melt temperature was to reduce the viscosity of the polymer and hence to reduce the generated pressures which caused less deformation in the tube.

The result of the pressure with WVG23 polymer at 180°C is shown in Fig 72. For drawing speeds in excess of about 0.2 m/s the pressure readings were found to be approximately independent of speed at positions 1 and 2 whilst at position 3 (step) the measured pressure decreased with the drawing speed. The reason for the sudden decrease in pressure was probably the transition from no-slip to slip in the polymer melt, ie at low drawing speeds (below 0.3 m/s) slip did not occur and high pressure was developed. As the speed was increased, a transition from no-slip to slip occurred and the polymer melt was unable to develop such higher pressures since the velocity gradient became discontinuous. A critical speed was reached at approximately 0.3 m/s when slip was total around the tube. For increasing the speed, therefore, no further change in the pressure occurred.

Fig 73 gives the pressures generated for copper tube with KM61 polymer at melt temperature of 200°C. Pressures at positions 1 and 2 fell sharply with drawing speed. This trend may be explained by the fact that at the melt temperature of 200°C KM61 polymer just about melts and very high viscosity of the melt provides greater resistance to flow through the die-less reduction unit. At higher drawing speeds there is more chance of slip occurring and hence reduction in pressure.

The effect of the higher pressures on the polymer melt may also be a contributing factor. It has been reported that at very high pressures (above 140 mN/m²) polymer melts tended to recrystallise.³⁵ It is possible that recrystallisation was occurring in the parts of the die-less reduction unit, giving rise to pressure (and velocity) discontinuities. The effect of the discontinuities could be to initiate the squeezing, folding

and buckling of the tube in the die-less reduction unit.

It was also noted that the pressure behaviour of WVG23 and Rigidex polymers are similar, ie at lower drawing speeds minimum pressures were noted at all positions. The pressure behaviour of KM61 and polystyrene polymers was noted to be opposite to those of WVG23 and Rigidex polymers. When these polymers were used as pressure medium maximum pressures were recorded at lower drawing speeds. The magnitude of pressure at all positions decreased as the drawing speed was increased.

The trends of the results of coating thickness were found to be similar to those of percentage reduction in diameter. Figs 103 to 110 show coating thickness obtained when copper and aluminium tubes were drawn using WVG23, KM61, Rigidex and polystyrene polymers at different melt temperatures. These results showed that coating thickness decreased as the drawing speed was increased. An increase in the polymer temperature reduced the viscosity of the polymer which caused less deformation in the tube and hence reduced coating thickness was obtained at all speeds. Crampton¹¹ showed that using WVG23 polymer as a lubricant in conventional wire drawing, reduced coating thickness was obtained as the drawing speed was increased. He also suggested that the reduction in the thickness of the polymer coating was the consequence of slip in the melt.

The results of the coating thickness with KM61 polymer at different melt temperatures is shown in Fig 104. At the melt temperature of 200°C flow of this polymer commenced at about 0.2 m/s and below this speed thin coating thickness was obtained. The reason for the thin coating thickness was the very high viscosity of the polymer melt which tend to resist to flow through the die-less reduction unit.

The deformation profiles measured experimentally showed that the formation of the effective deformation profile was dependent upon the drawing speed which varied for different tube materials (see Figs 111 and 112). In conventional tube drawing process, the deformation of the tube takes the shape of the reduction die, therefore the roundness of the final diameter is decided by the roundness of the reduction die. A qualitative test, therefore, was conducted to examine the products obtained using the die-less method. Roundness test was undertaken to check the circularity of the drawn tubes and the results showed that the amount of error measured in the tubes, in the case of WVG 23, KM61, Rigidex and polystyrene polymers were similar to those observed on tubes drawn by the conventional method (see Figs 113 to 130). This seems to suggest that the applied stresses on the tube (hoop stress and axial stress) were fairly uniform for all four polymers.

6.4.2 Discussion on the Analyses and the Theoretical Results

Four different analytical models have been developed which enabled percentage reduction in diameter, drawing stress, pressure, hoop stress, coating thickness, position of yield of the tube inside the die-less reduction unit, stress in the tube and the deformation profile of the tube. The following assumptions were made in order to simplify the analyses.

- (a) The flow of the fluid pressure medium in the die-less reduction unit is laminar - this seems to be a reasonable assumption since the drawing speeds of the tube are low, viscosity of the pressure medium is high and the gaps are small.

- (b) The flow of the fluid pressure medium is axial - once flow through the die-less reduction unit has commenced, little or no back flow is expected. This assumption allowed one dimensional flow to be considered.
- (c) The thickness of the fluid layer is small compared to the dimensions of the die-less reduction unit - this assumption enabled the analysis to be conducted in rectangular rather than cylindrical co-ordinates.
- (d) The pressure in the fluid medium is uniform in the thickness direction - this assumption simplified calculation of the pressure in the die-less reduction unit and allowed the viscosity constants to be evaluated.
- (e) The process is isothermal - this assumption may introduce some error in the results since it is known that the temperature of the tube increases during the drawing process.

In addition to the above, the following assumptions were also made:

The non-Newtonian equation commonly used to predict the behaviour of the polymer melt, as proposed by Rabinowitsch, takes the form;

$$\tau + K\tau^3 = \mu \frac{du}{dy}$$

This equation was used in the analysis to predict the pressure and the shear stress in the pressure medium and this assumption is accurate within the no-slip range. The non-Newtonian factor "K" and the initial viscosity " μ " were both determined experimentally by curve fitting (see Chapter 2). The above equation represents the effect of the shear stress on the viscosity only. It is known that the pressure increases the viscosity of the polymer melt. To incorporate this effect in the analysis, the

data provided by Westover³⁷ for the Alkathene polymer was used. Westover's results show the combined effects of shear stress and pressure on polyethylene and indicate that pressure modifies the initial viscosity of the polymer as represented by Fig 20. Using Figure 20, a generalised equation was derived to predict the viscosity of the pressure medium at known pressures and shear rates which is shown to take the form;

$$\mu = \mu_0 + \frac{(a + b P m^2)}{\dot{\gamma}}$$

where a and b are constants. $\dot{\gamma}$ is the apparent shear rate in the first part of the unit and is assumed to be $\frac{v'}{h_1}$. The accuracy of Westover's results is not known and unfortunately the polymer used for his experiments was not WVG23 polymer, therefore small errors may be involved in the determination of the constants a and b.

Slip in the polymer is believed to occur and the experimental results justified this. The magnitude of the critical shear stress have been estimated to be between 0.1 to 1.0 MN/m² (15-19). When polypropylene and polystyrene polymers were being extruded at 200°C and 230°C, evidence of slip was observed at shear stress of about 0.25 MN/m² and 0.153 MN/m² respectively. Critical shear stress for polyethylene polymer was shown by Westover to be about 0.7 MN/m² and also critical shear stress for Rigidex was shown by Westover and Cogswell to be 0.5 MN/m². Therefore an average critical shear stress of 0.4 MN/m² is assumed for the slip in the analysis. It must be remembered that the pressures and shear stresses applied on the polymer melt were much greater than those created in an extrusion rheometer, therefore the critical shear stress chosen for the condition of slip was only an approximation. In order to calculate the flow of the

pressure medium after slip, a pressure ratio between no-slip and slip of polymer should be known which was not easily determinable. Therefore it was assumed that the pressure medium could not accommodate further increase in pressure at the onset of slip and that the flow of the pressure medium remained constant for any further increase in the drawing speed. The presence of slip is justified since the experimental results show that the reduction in diameter and the coat thickness reduced as the drawing speed was increased. The above assumptions permitted the results to be obtained easily after slip was predicted in the die-less reduction unit.

The analysis of the die-less reduction unit was carried out in two parts, (i) before deformation, the flow of the pressure medium which enabled the pressure in the unit, the shear stress on the tube and the position of yield of the tube in the unit to be calculated, and (ii) the deformation zone, which allowed the axial stress, hoop stress and the deformation profile of the tube to be determined.

The results of the percentage reduction in diameter showed that,

- (a) In the case of Newtonian analysis, the percentage reduction in diameter increased with the drawing speed. But in the case of non-Newtonian analysis results showed the opposite trend ie the percentage reduction in diameter decreased as the drawing speed was increased.
- (b) When slip occurred, the percentage reduction in diameter reduced as the drawing speed was increased even further.

Various trends became apparent as the input parameters were altered;

- (i) An increase in the gap ratio increased the percentage reduction in diameter. Increasing the length ratio

initial viscosity and pressure coefficient of viscosity also had the same effect.

- (ii) An increase in the initial yield stress reduced the percentage reduction in diameter and had little effect on the critical drawing speed. A similar effect was also observed when the strain hardening constant, tube wall-thickness and the strain rate sensitivity index were increased.
- (iii) An increase in the non-Newtonian factor 'K', decreased the percentage reduction in diameter.
- (iv) Increasing the original diameter of the tube, strain rate sensitivity constant and strain hardening index increased the percentage reduction in diameter.

The observations and results outlined above are important in many ways. The predicted deformation of the tube seemed to be very sensitive to changes in the inlet gap of the die-less reduction unit whilst the exit gap was kept constant. The results are shown in Figs 147 and 183. With the gap ratio of 49, the slip was predicted at very slow drawing speeds and higher percentage reductions in diameter were obtained. When the exit gap of the die-less reduction unit (h_2) was changed, keeping the inlet gap (h_1) constant, it was noted that the effect on percentage reduction in diameter was comparatively less than when the gap h_1 was changed (see Figs 135, 145, 146, 163, 164 and 182). For very small gaps, only reduced polymer flow rates can occur, the percentage reduction in diameter is therefore low. For larger inlet gaps, back flow could occur which would reduce the pressure and therefore reduce the percentage reduction in diameter. An optimum gap is suggested when a balance is struck between these

two effects. The length ratio had similar effect on the reduction in diameter. This was again due to higher pressures predicted in the unit. The increase in the initial viscosity increased the percentage reduction in diameter. The increase in the initial yield stress of the tube reduced the percentage reduction in diameter. A similar effect was observed for the increase in the strain hardening constant ' K_0 ' and tube wall-thickness.

The critical drawing speed was found to be effected slightly by changing the above parameters (Y_0 , K_0 and t). These parameters simply increased the flow stress of the tube which reduced the amount of deformation. The increase in the strain hardening index ' n ' however, increased the percentage reduction in diameter. As the index ' n ' was increased the stress-strain curves became more parabolic (softer tube material), hence lesser stresses were needed for the flow of the material at higher strains.

The increase in the tube diameter increased the percentage reduction in diameter. The percentage reduction in diameter was increased because the ratio of the changes in the diameter to the original diameter was reduced and very high hoop stress and axial stress on the tube were predicted, this also increased the deformation zone. The effect of the strain rate sensitivity constant on the percentage reduction in diameter was that, if it was increased, the predicted percentage reduction in diameter was also increased. This parameter influences the mean strain rate and hence the dynamic yield stress of the tube material (see equation 36 in Chapter 6). Another interesting result was that a decrease in the non-Newtonian factor ' K ' caused an increase in

the percentage reduction in diameter (see Fig 191).

The trends of the theoretical results obtained for the coating thickness were found to be similar to those of the percentage reduction in diameter as shown in Figs 157 to 162, 176 to 180 and 192 to 196.

Prediction of the yielding position of the tube in the die-less reduction unit produced another set of interesting results. In the case of Newtonian analysis, the yielding position of the tube was seen to depend on the drawing speed, ie higher drawing speeds moved yielding position nearer to the entry side of the unit. On the other hand, in the case of non-Newtonian analysis the yielding position seemed to be generally constant except at very low drawing speeds at which ' x_1 ' increased slightly as the drawing speed was reduced (see Figs 197 to 199). The following observations were made from the results.

- (a) The increase in the gap ratio reduced the undeformed length of the tube in the die-less reduction unit. The length ratio, initial viscosity, tube diameter and viscosity constants had similar effect.
- (b) The increase in the non-Newtonian factor 'K', increased the undeformed part of the tube. So did the increase in the initial yield stress.

A close inspection of the equations predicting x_1 would suggest that an increase in the initial yield stress simply would increase the undeformed length x_1 . Similarly any parameter which predicted higher hoop and axial stress in the die-less reduction unit, reduced the undeformed length of the tube.

Theoretical pressure distribution is shown in Fig 200 which indicates that smaller values of h_1/h_2 caused lower pressures.

This may be explained in terms of the pressure generated due to the geometry of the die-less reduction unit, ie as the exit gap increases, the flow of the polymer is therefore less restricted hence lower pressures are generated. Increasing the initial yield stress and tube wall-thickness causes higher pressures to be predicted (see Figs 201 and 202). This trend may be explained by the fact that the amount of deformation was reduced because the hoop stress on the tube was predicted to reduce according to equation 24 in Chapter 6. Note that before deformation occurs the pressure is predicted to be linear. After deformation commences, the pressure distribution is no longer expected to be linear.

Results of the drawing stress with different parameters are shown in Figs 204 to 207. These figures confirmed that the drawing stress was maximum when the reduction in diameter was maximum.

6.4.3 Comparison Between the Experimental and Theoretical Results

In the previous two sections the experimental and theoretical results were discussed and in some cases discrepancies were apparent. In this section, it is aimed to point out these discrepancies and discuss the possible causes of their occurrence. Fig 209 shows typical experimental results of the percentage reduction in diameter for the copper tube and theoretical results obtained using various theoretical models under similar conditions. It is clear that the predictions from all three models based on Newtonian characteristics differ from the experimental results both in magnitude and trend, especially at speeds less than about 0.4 m/s. The predicted result from the non-Newtonian analysis, however is reasonably close to the experimental results, both in magnitude and trend. At speeds in

excess of about 0.4 m/s even this model predicts results which differ significantly from the experimental ones. The main reason for the discrepancies between the experimental results and those predicted using theoretical models based on Newtonian characteristics, is the fact that the pressure medium used did not behave anything like a Newtonian fluid. Thus, whilst these models are quite useful in understanding the mechanics of the process, they are unsatisfactory for predicting results when the fluid demonstrates non-Newtonian characteristics.

The discrepancy which is still present between the theory and the experiment even with non-Newtonian approach is possibly due to the difficulties in ascertaining the viscosity and shear rate relationship of the pressure medium and also the fact that the analysis do not take account of any variation from the assumed iso-thermal and laminar flow conditions during the process.

The effects of other variables were also examined theoretically in order to investigate their influence on the predicted results. It is thought that errors could have arisen from the viscosity constants 'a' and 'b'. A large change in 'a' was found necessary for a reasonable change in the theoretical results and the overall trends remained more or less the same as before. Increase in the pressure coefficient of viscosity 'b' increased the overall results and predicted slip at slower drawing speeds. It is believed that μ_0 , K, N and T were reasonably accurate.

Parameters representing the flow stress of the tube material (Y_0 , K_0 and n) were determined experimentally and it is also believed that they contained very little error. Variations in these parameters also did not reduce the amount of discrepancy existing between the experimental and the theoretical results.

The trends of the results for the coating thickness were found to be very similar to those of the percentage reduction in diameter, therefore the above discussion is also applicable for the coating thickness.

Fig 210 shows the experimental and the theoretical drawing stress at different drawing speeds. A reasonably close correlation was observed between the theoretical (non-Newtonian) and the experimental results at lower drawing speeds. Once again, the Newtonian solution (numerical) showed a totally different trend compared to the other results. The results from the models based on assumed linear and curved deformation profiles were no better and hence are not shown in this figure.

Figs 211 and 212 show the experimental and the theoretical pressure distributions at two different drawing speeds. At the drawing speed of 0.3 m/s, good agreement was observed between the non-Newtonian and the experimental results. The Newtonian analysis appeared to under estimate the pressure, although the trend is accurately predicted (see Fig 211). At the drawing speed of 0.5 m/s (Fig 212) very good agreement appeared to exist between the experimental and the theoretical results.

Comparison between the measured and the predicted deformation profiles of the copper tube are shown in Figs 213 and 214. The measured deformation profile showed that yielding occurred nearer to the step and that the deformation took place in a much steeper manner, producing 5% reduction in diameter at the drawing speed of 0.3 m/s. The two theoretically calculated deformation profiles at different drawing speeds but for the same percentage reduction in diameter have very good correlation, but differ from the experimentally observed profiles (see Fig 213). At the slower drawing speed (0.1 m/s) the theoretically predicted

deformation profile have close similarity with that observed experimentally (see Fig 214), the percentage reductions in diameter, however, were not the same.

$h_1 = \text{Const} = 0.5$

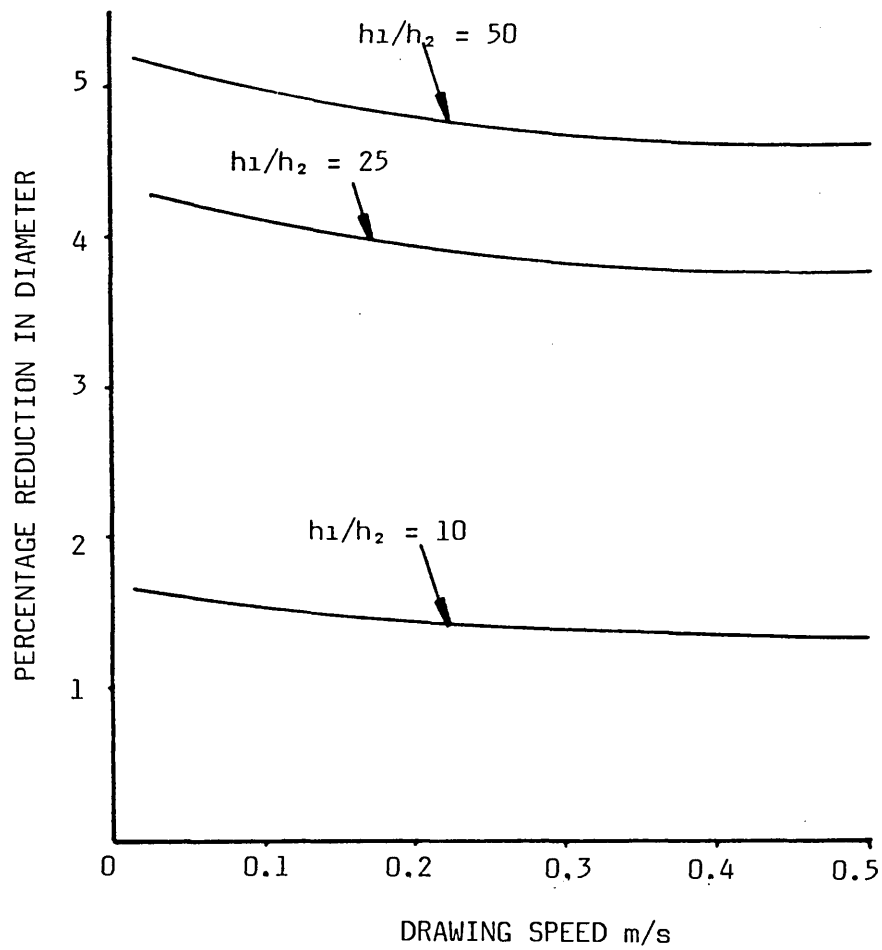


FIG 182 - THEORETICAL EFFECT OF GAP RATIO ON PERCENTAGE REDUCTION IN DIAMETER

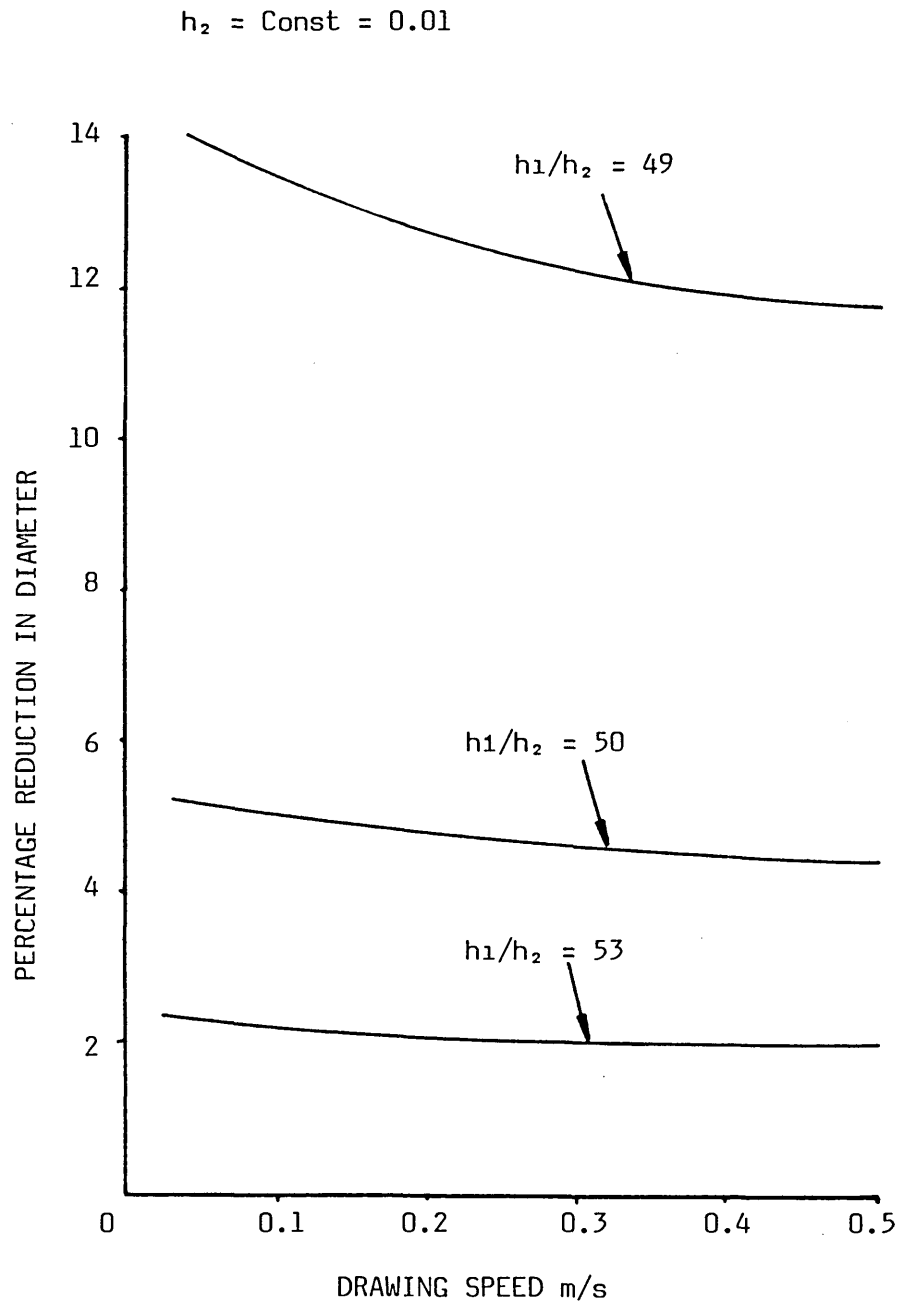


FIG 183 - THEORETICAL EFFECT OF GAP RATIO ON PERCENTAGE REDUCTION IN DIAMETER

$$h_1/h_2 = 50$$

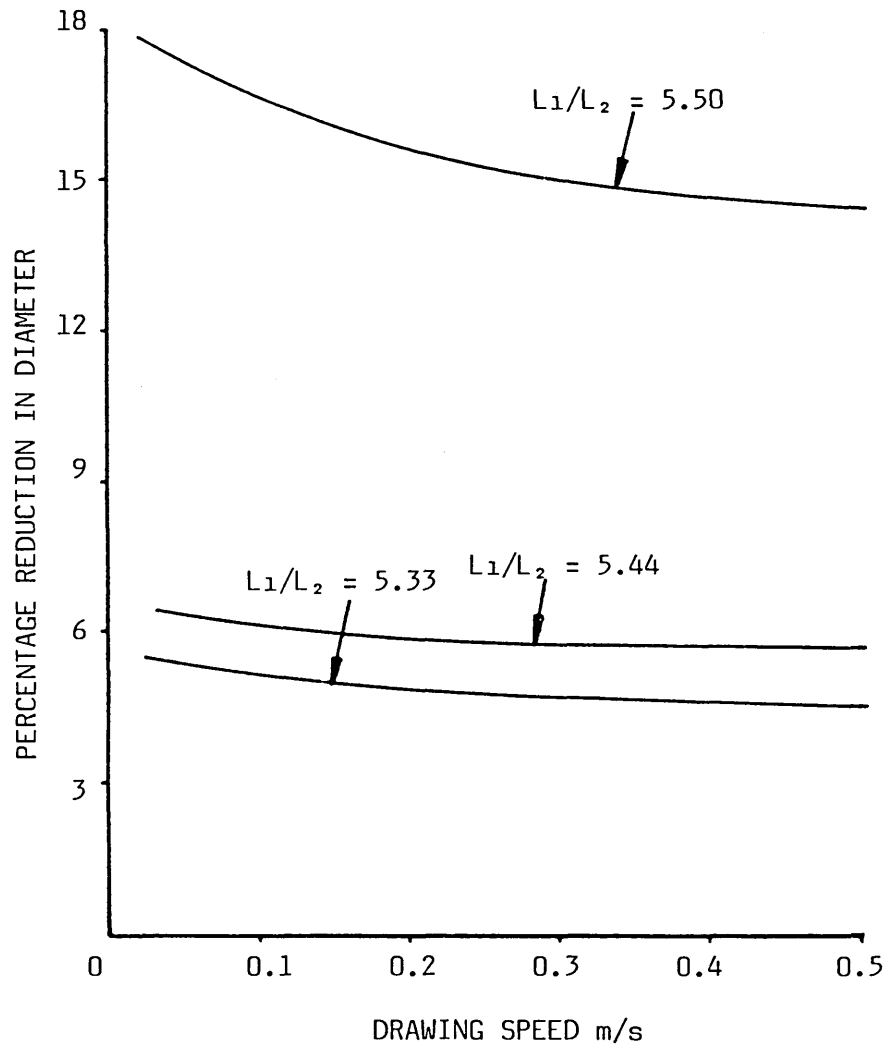


FIG 184 - THEORETICAL EFFECT OF LENGTH RATIO ON PERCENTAGE REDUCTION IN DIAMETER ($L_2 = \text{Const} = 30 \text{ mm}$)

$$h_1/h_2 = 50$$

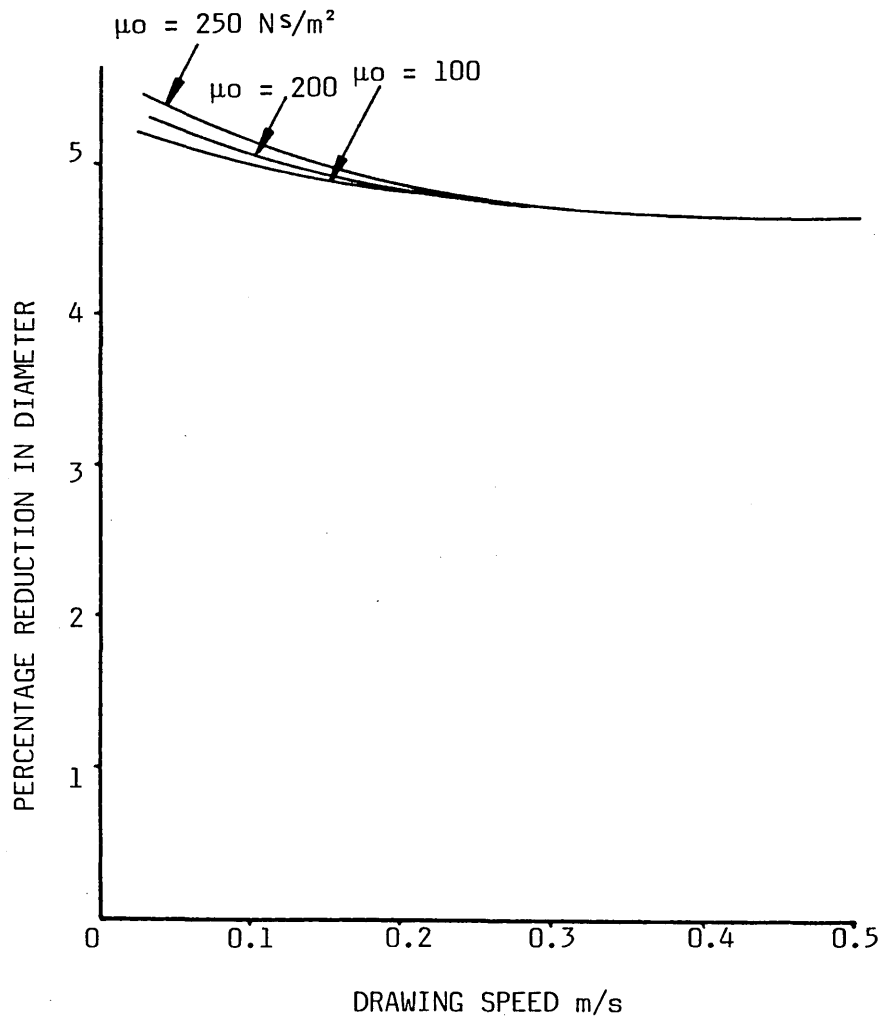
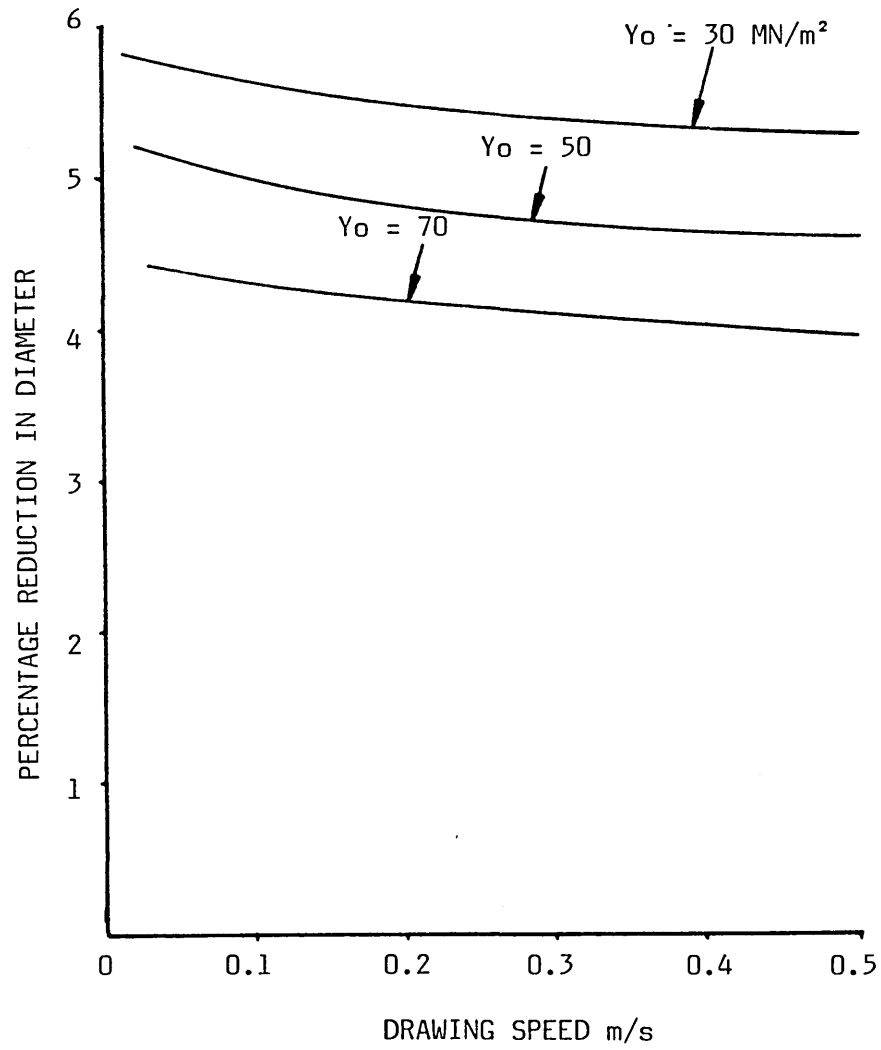


FIG 185 - THEORETICAL EFFECT OF INITIAL VISCOSITY ON PERCENTAGE REDUCTION IN DIAMETER

$$h_1/h_2 = 50$$



**FIG 186 - THEORETICAL EFFECT OF INITIAL YIELD STRESS ON
PERCENTAGE REDUCTION IN DIAMETER**

$$h_1/h_2 = 50$$

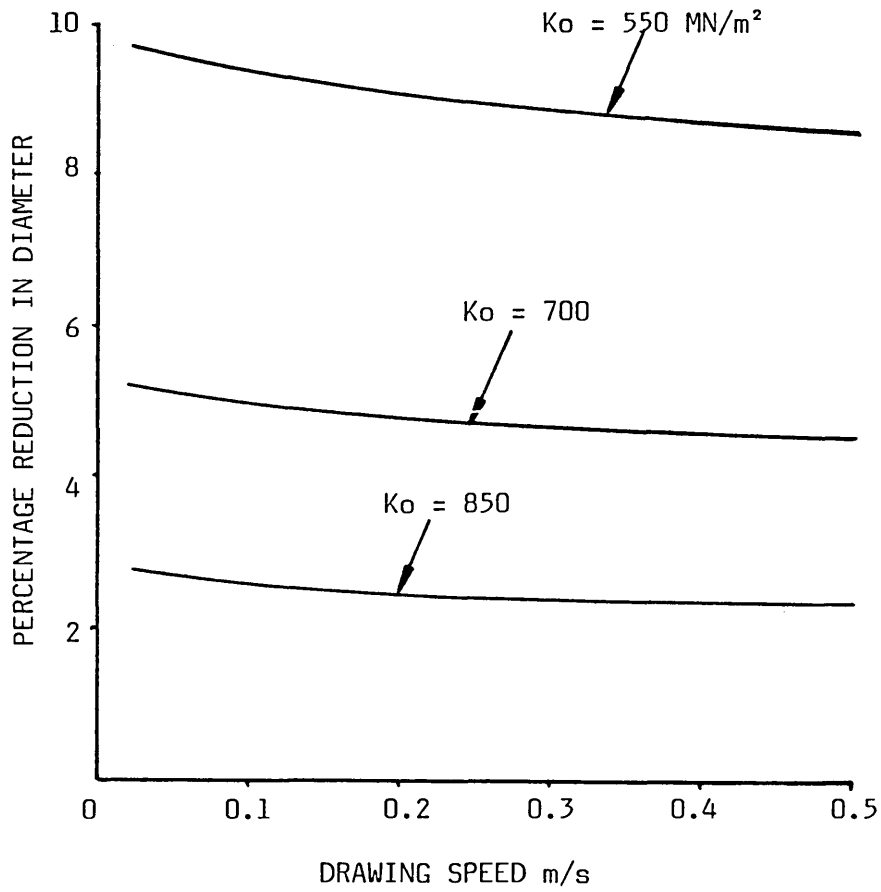


FIG 187 - THEORETICAL EFFECT OF STRAIN HARDENING CONSTANT ON PERCENTAGE REDUCTION IN DIAMETER

$$\frac{h_1}{h_2} = 50$$

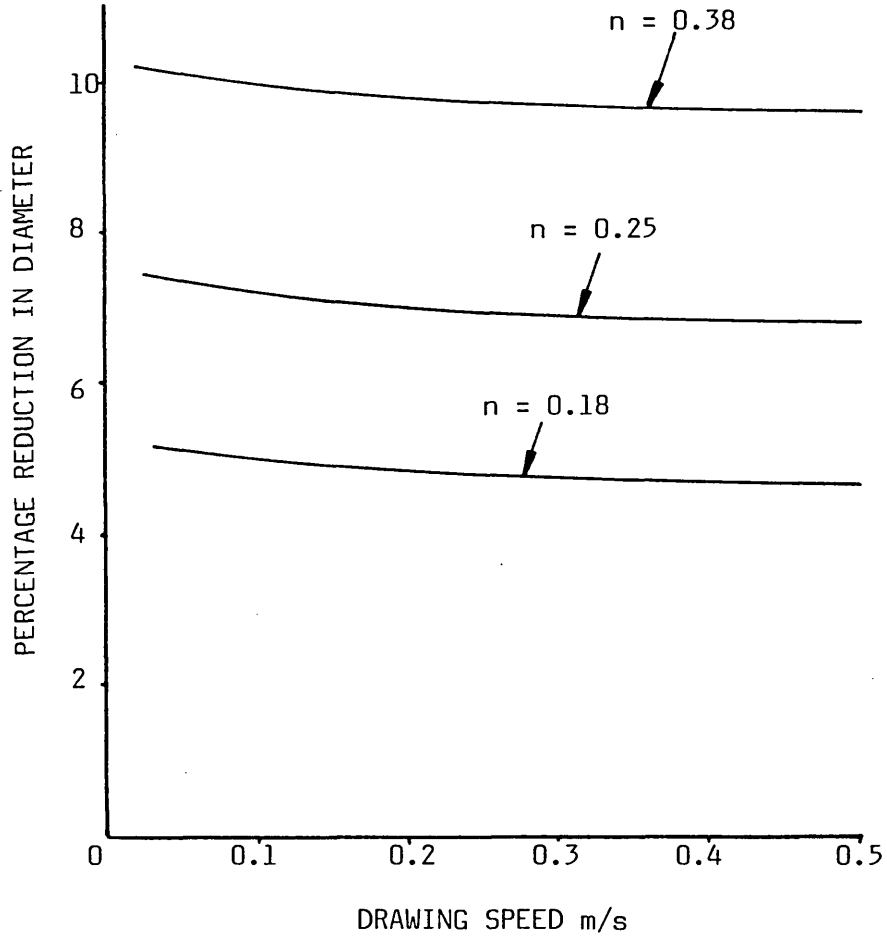


FIG 188 - THEORETICAL EFFECT OF STRAIN HARDENING INDEX ON PERCENTAGE REDUCTION IN DIAMETER

$$\frac{h_1}{h_2} = 50$$

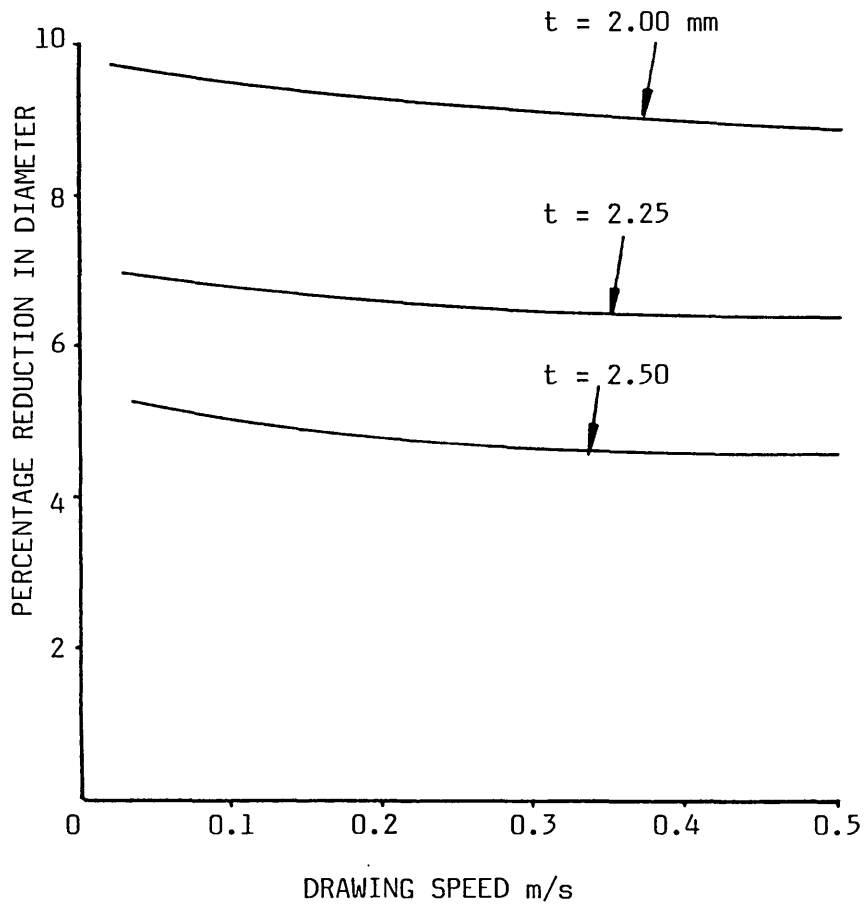


FIG 189 - THEORETICAL EFFECT OF TUBE WALL-THICKNESS ON PERCENTAGE REDUCTION IN DIAMETER

$$\frac{h_1}{h_2} = 50$$

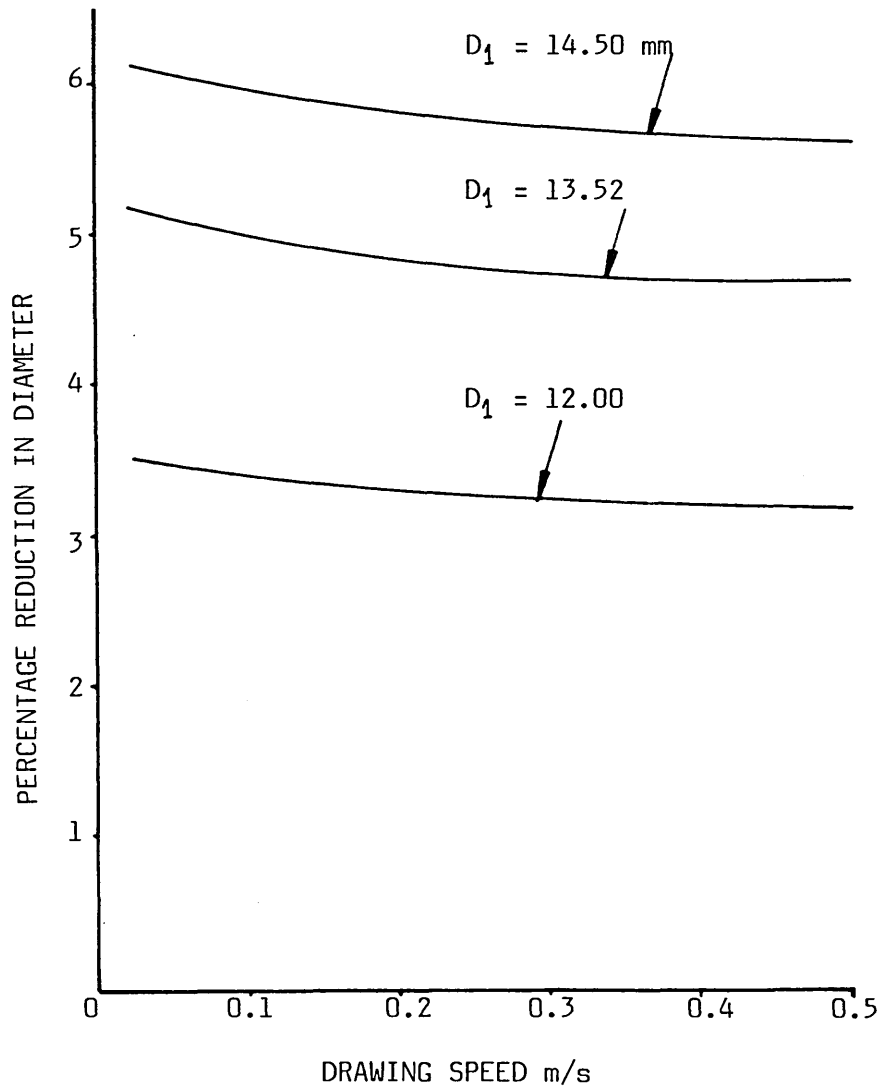


FIG 190 - THEORETICAL EFFECT OF TUBE DIAMETER ON PERCENTAGE REDUCTION IN DIAMETER

$$\frac{h_1}{h_2} = 50$$

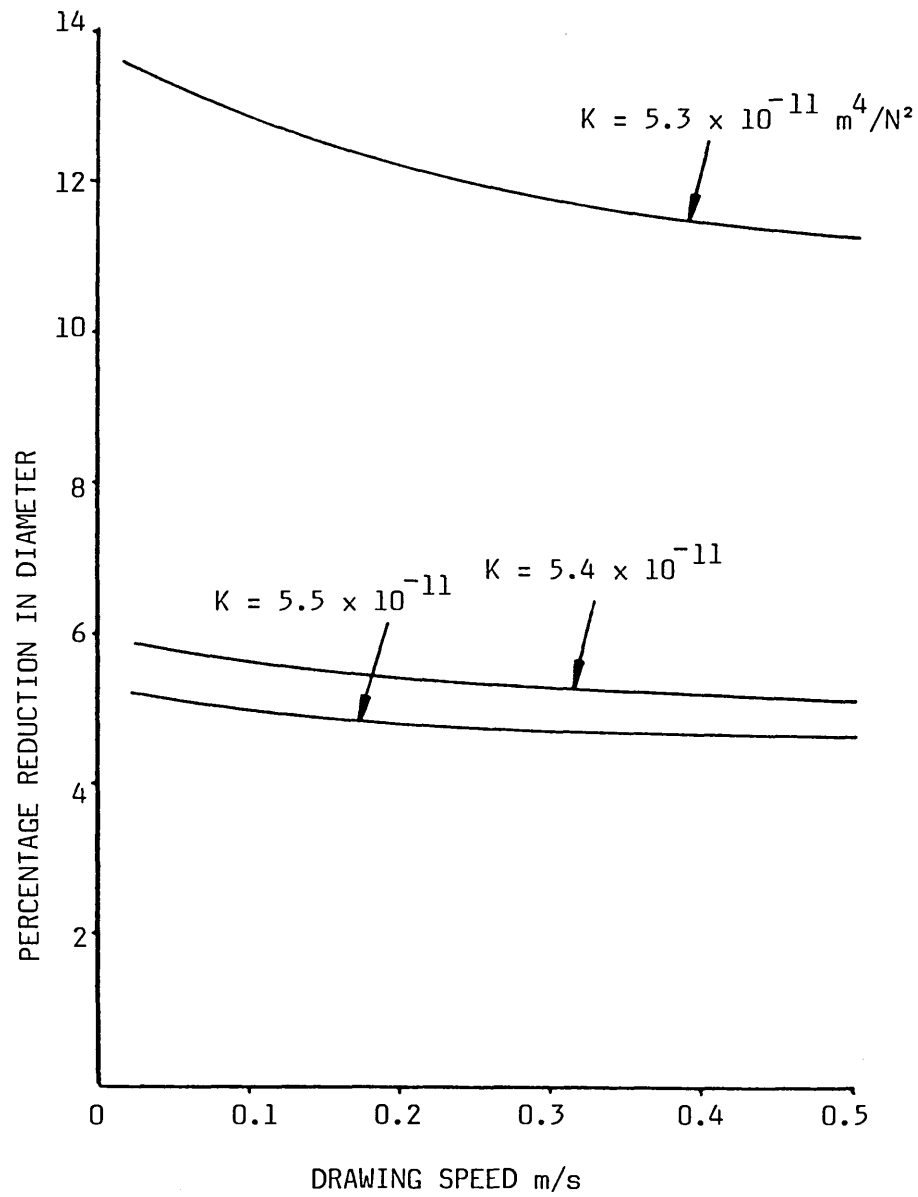


FIG 191 - THEORETICAL EFFECT OF SHEAR STRESS CONST. ON
PERCENTAGE REDUCTION IN DIAMETER

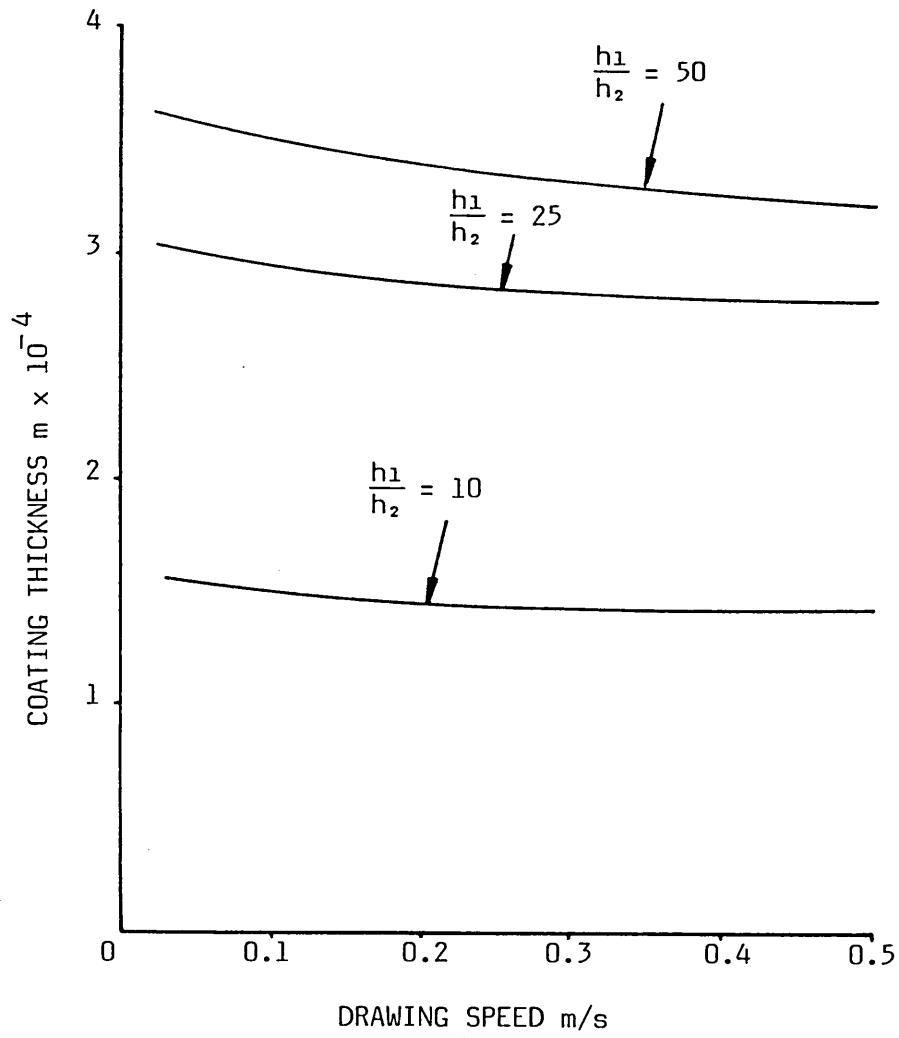


FIG 192 - THEORETICAL EFFECT OF GAP RATIO ON COATING THICKNESS

$$\frac{h_1}{h_2} = 50$$

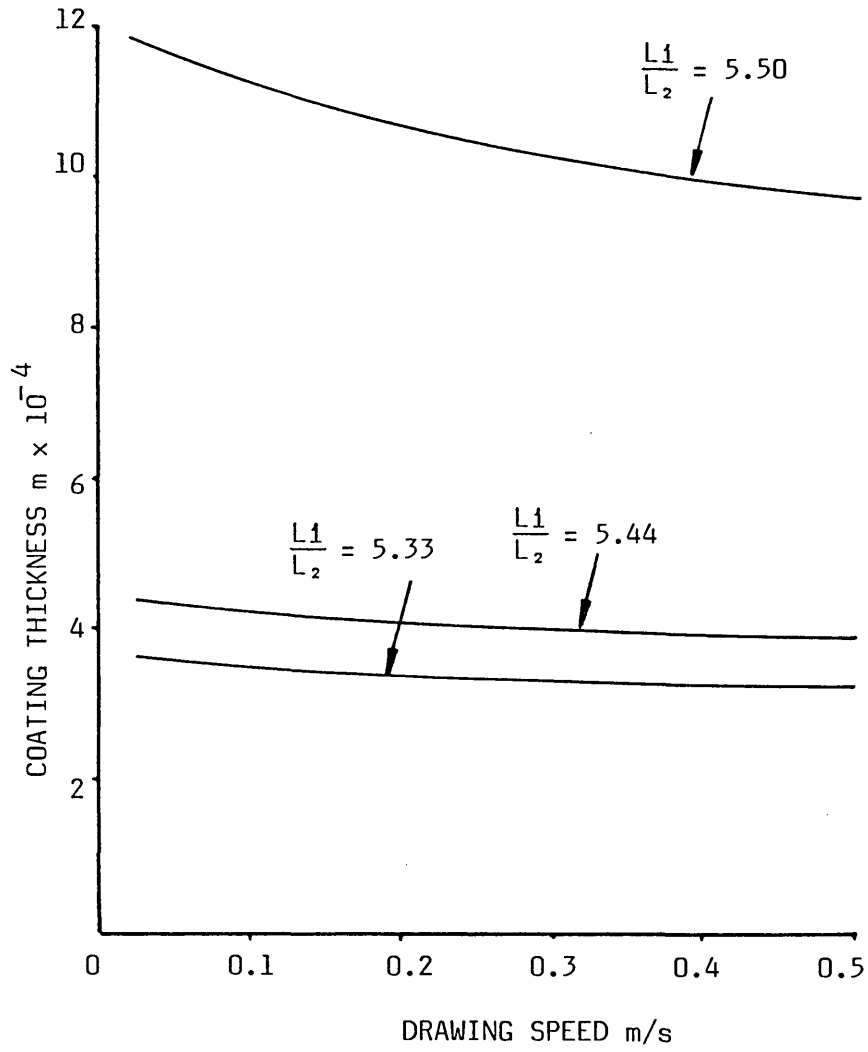


FIG 193 - THEORETICAL EFFECT OF LENGTH RATIO ON COATING THICKNESS

$$\frac{h_1}{h_2} = 50$$

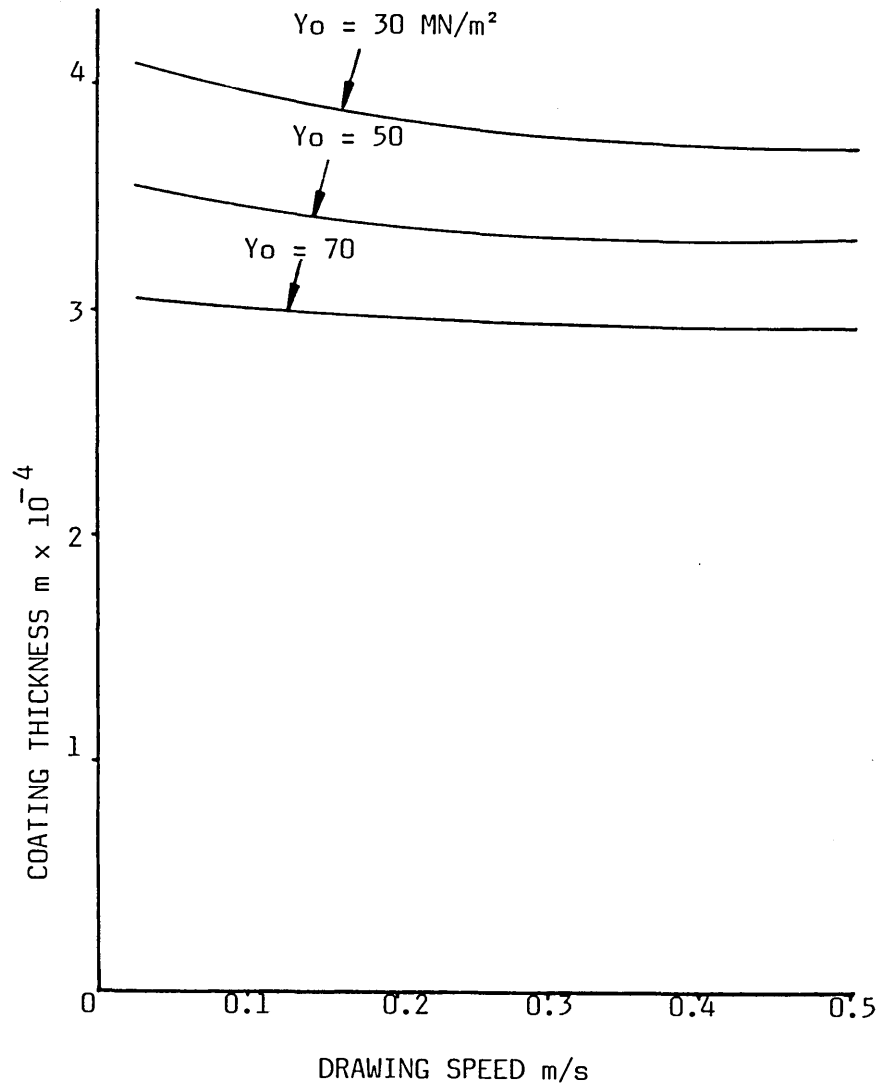


FIG 194 - THEORETICAL EFFECT OF INITIAL YIELD STRESS ON COATING THICKNESS

$$\frac{h_1}{h_2} = 50$$

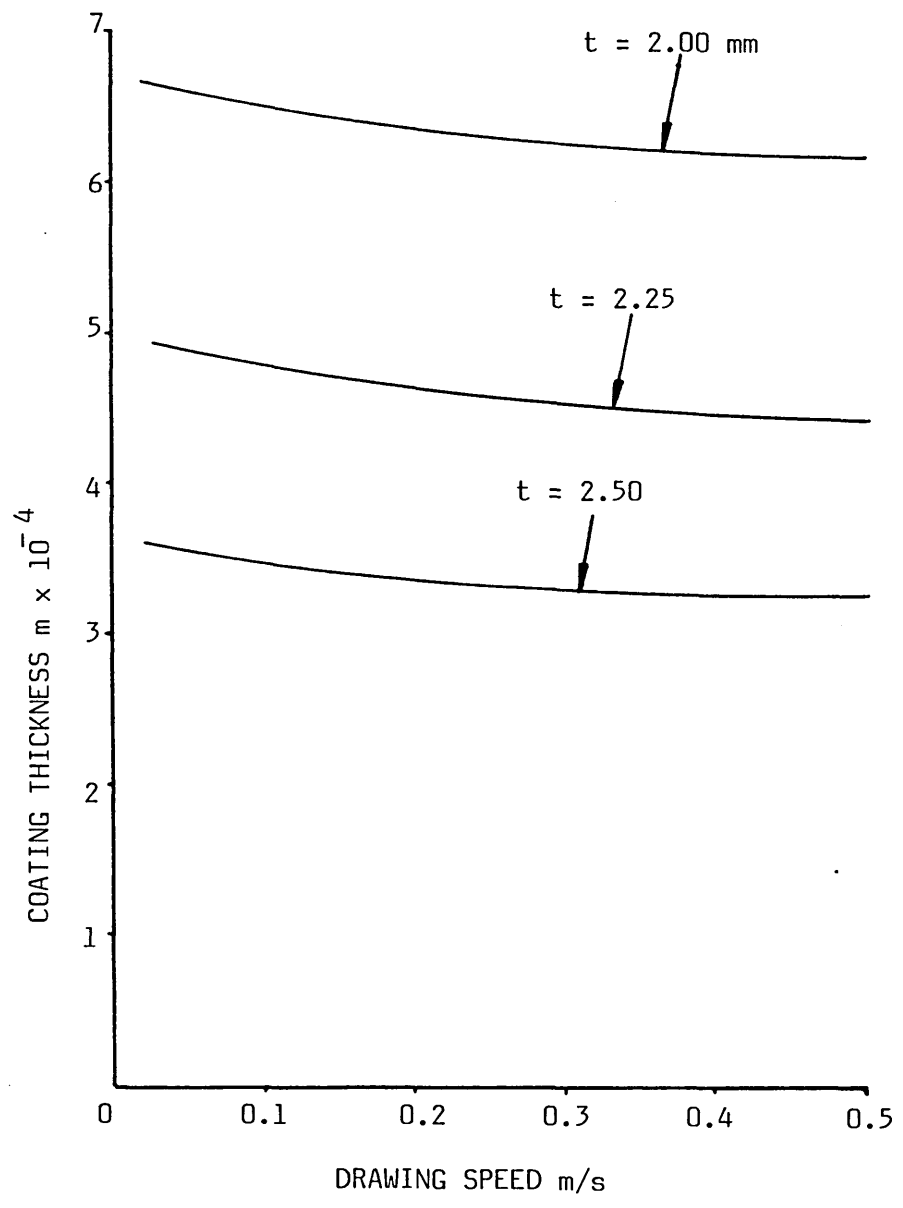


FIG 195 - THEORETICAL EFFECT OF TUBE WALL-THICKNESS ON COATING THICKNESS

$$\frac{h_1}{h_2} = 50$$

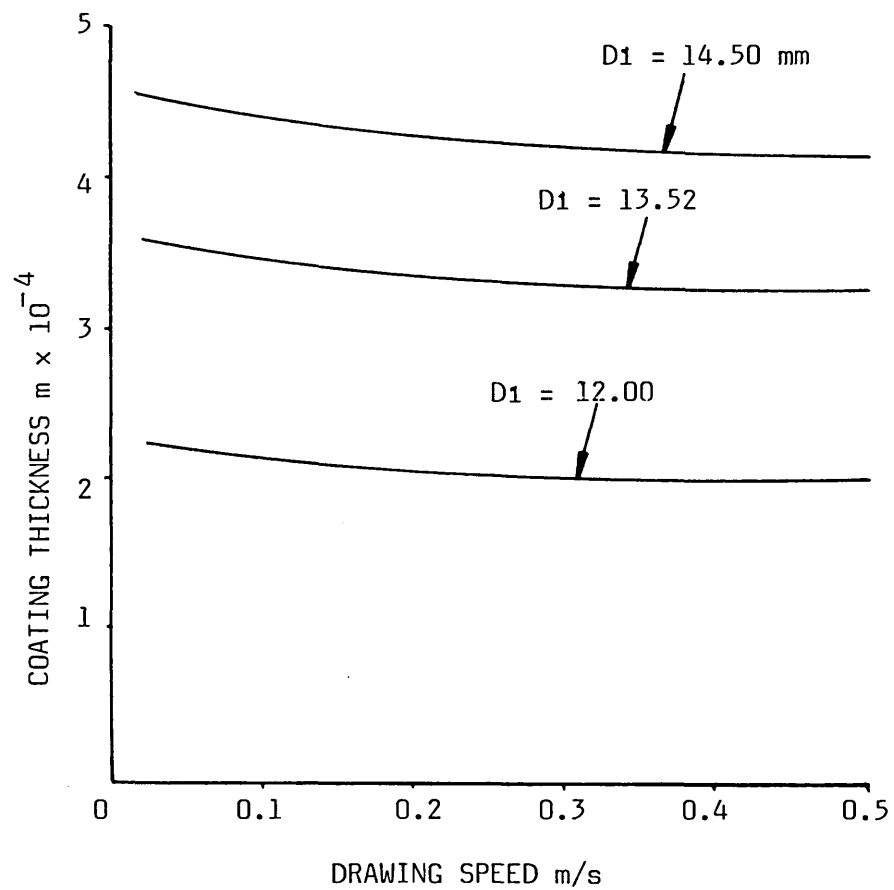


FIG 196 - THEORETICAL EFFECT OF TUBE DIAMETER ON COATING THICKNESS

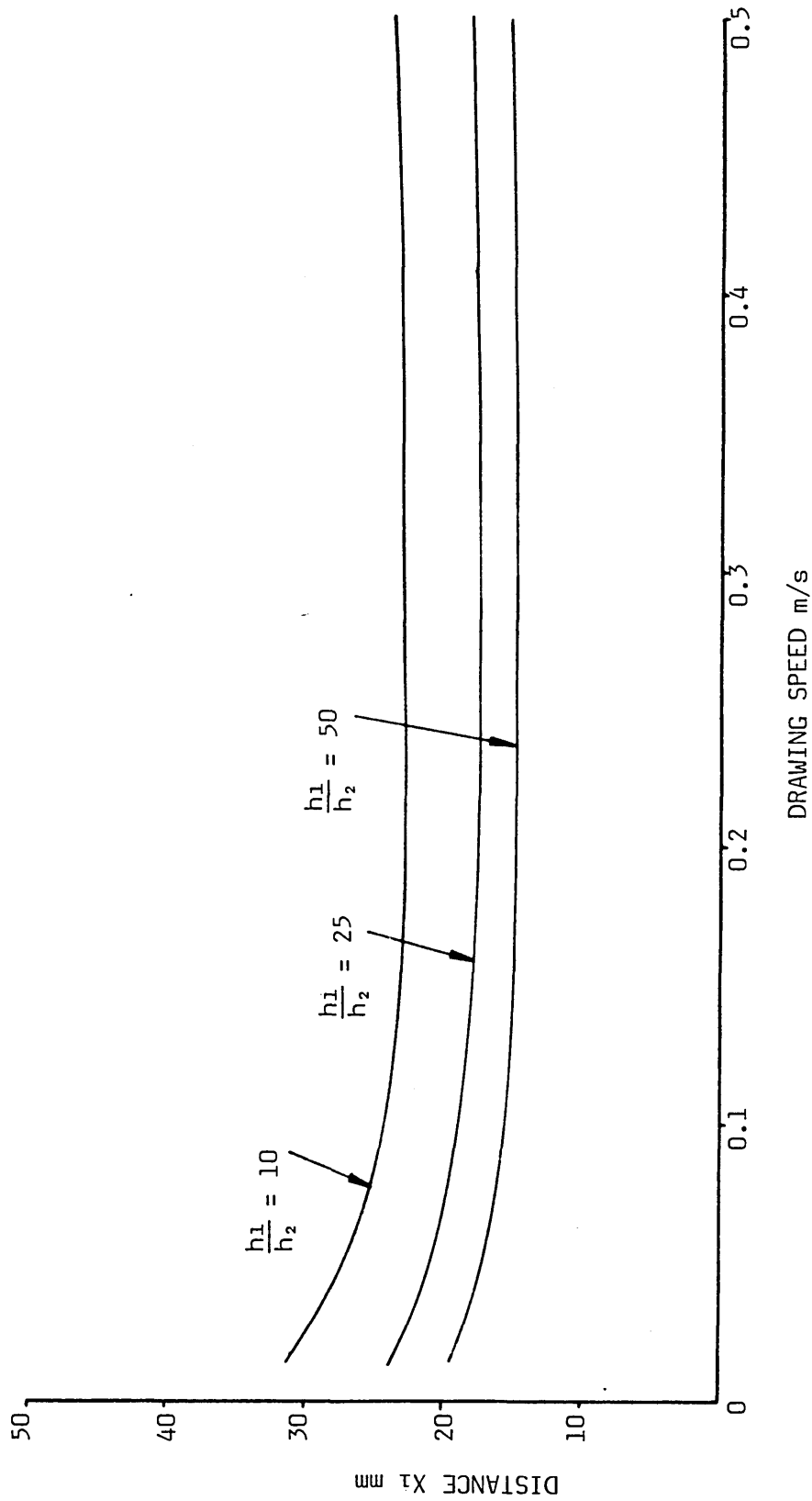


FIG 197 - THEORETICAL EFFECT OF GAP RATIO ON YIELDING POSITION OF TUBE

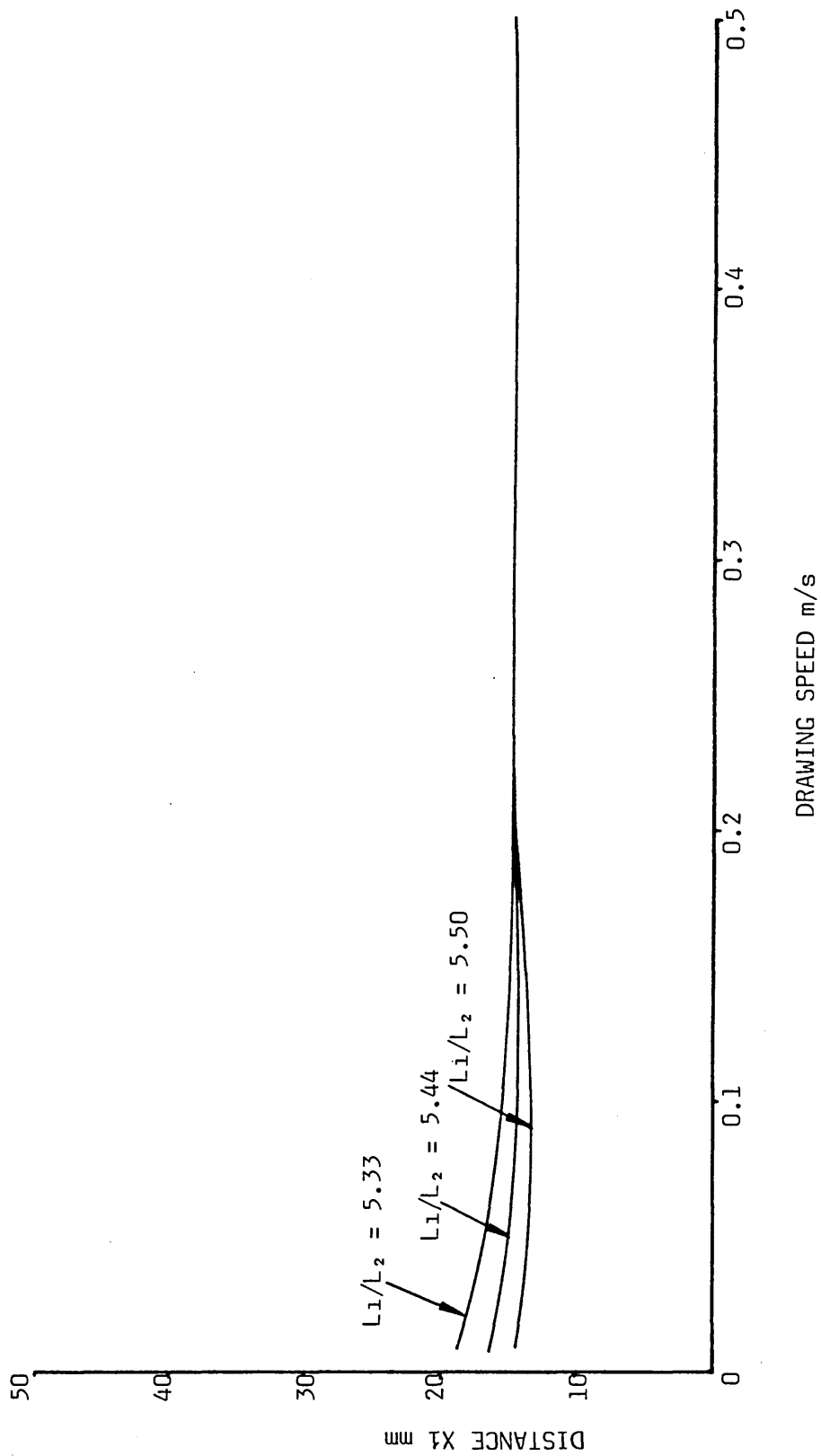


FIG 198 - THEORETICAL EFFECT OF LENGTH RATIO ON YIELDING POSITION OF TUBE

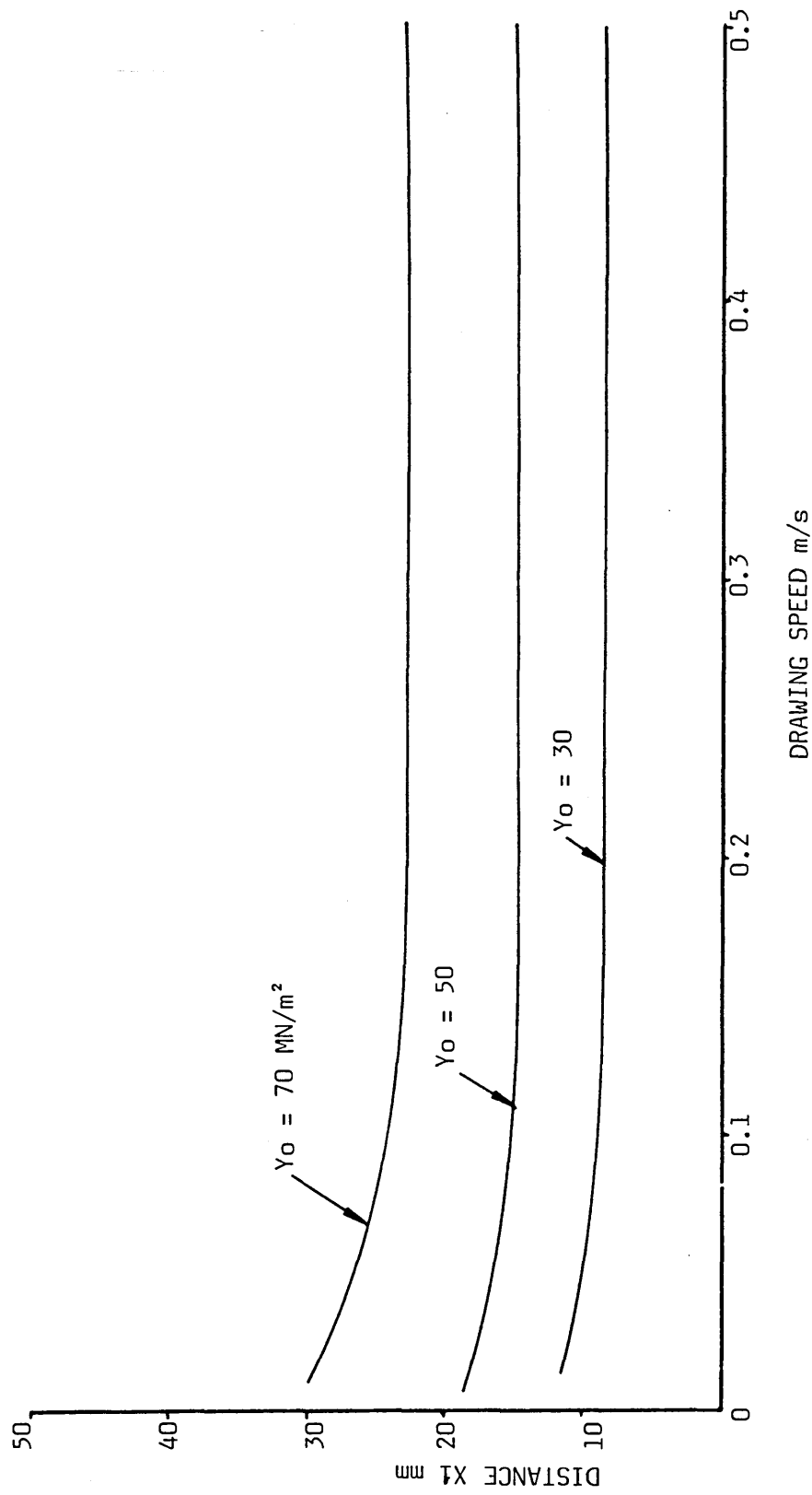


FIG 199 - THEORETICAL EFFECT OF INITIAL YIELD STRESS ON YIELDING POSITION OF TUBE

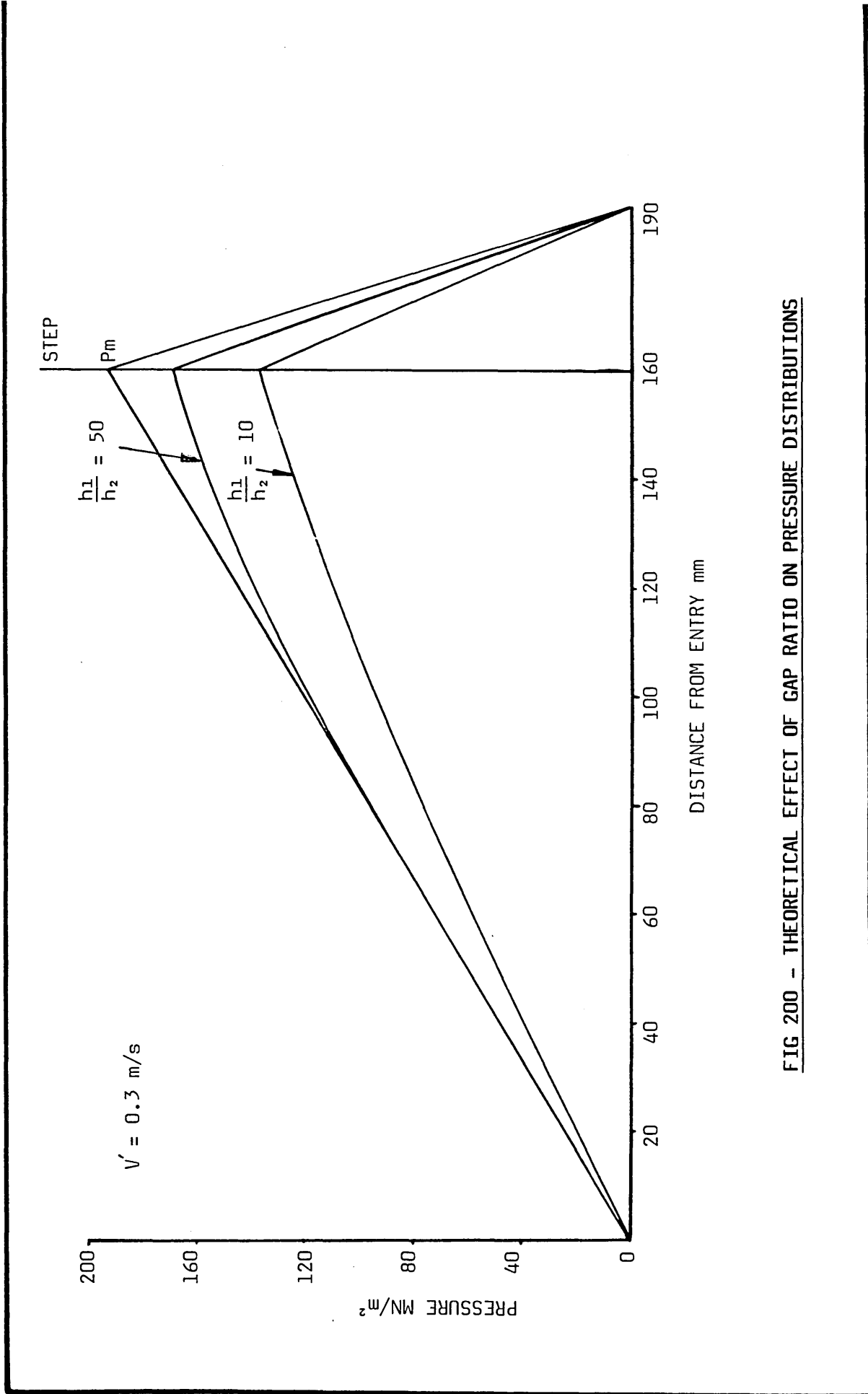


FIG 200 - THEORETICAL EFFECT OF GAP RATIO ON PRESSURE DISTRIBUTIONS

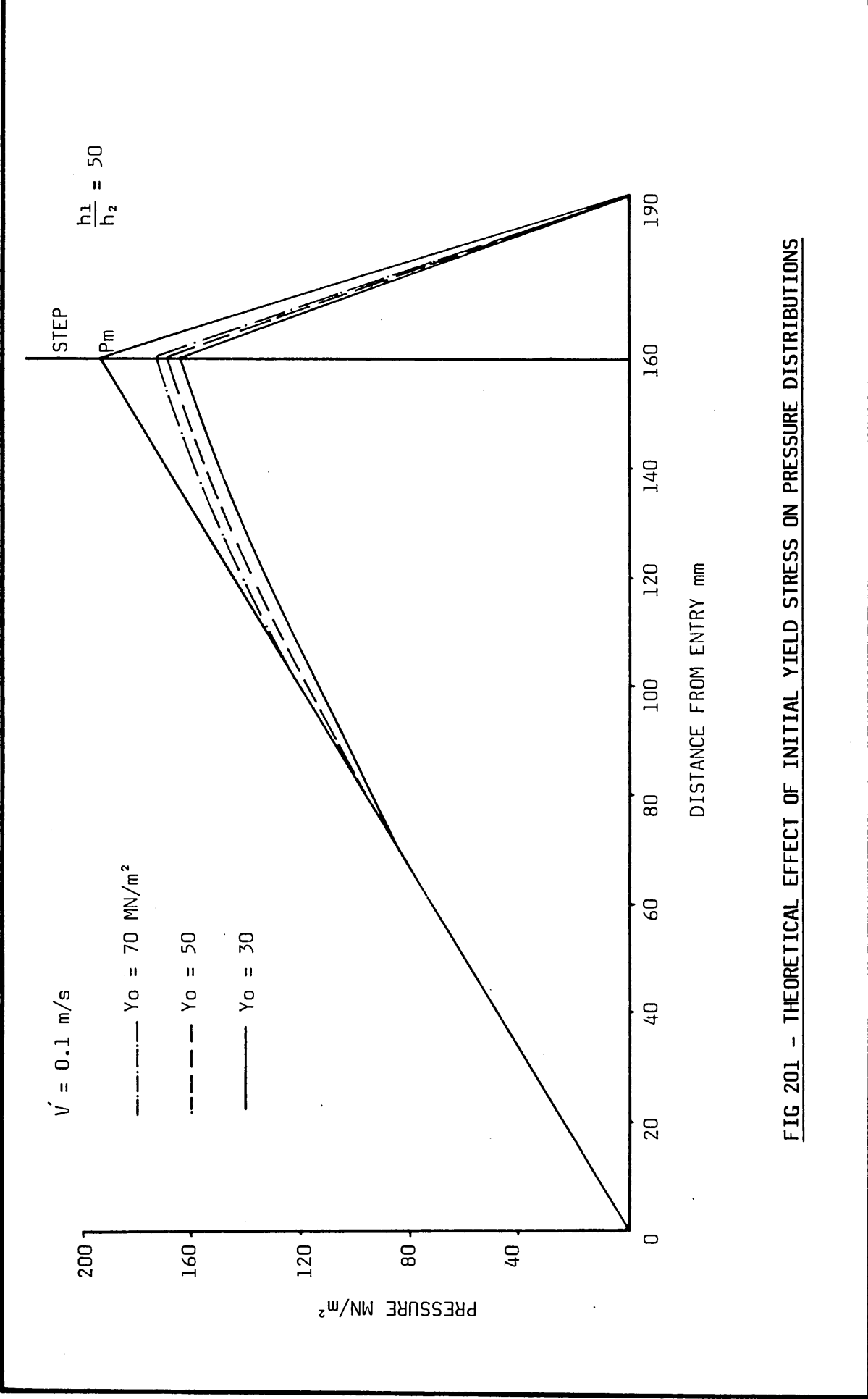


FIG 201 - THEORETICAL EFFECT OF INITIAL YIELD STRESS ON PRESSURE DISTRIBUTIONS

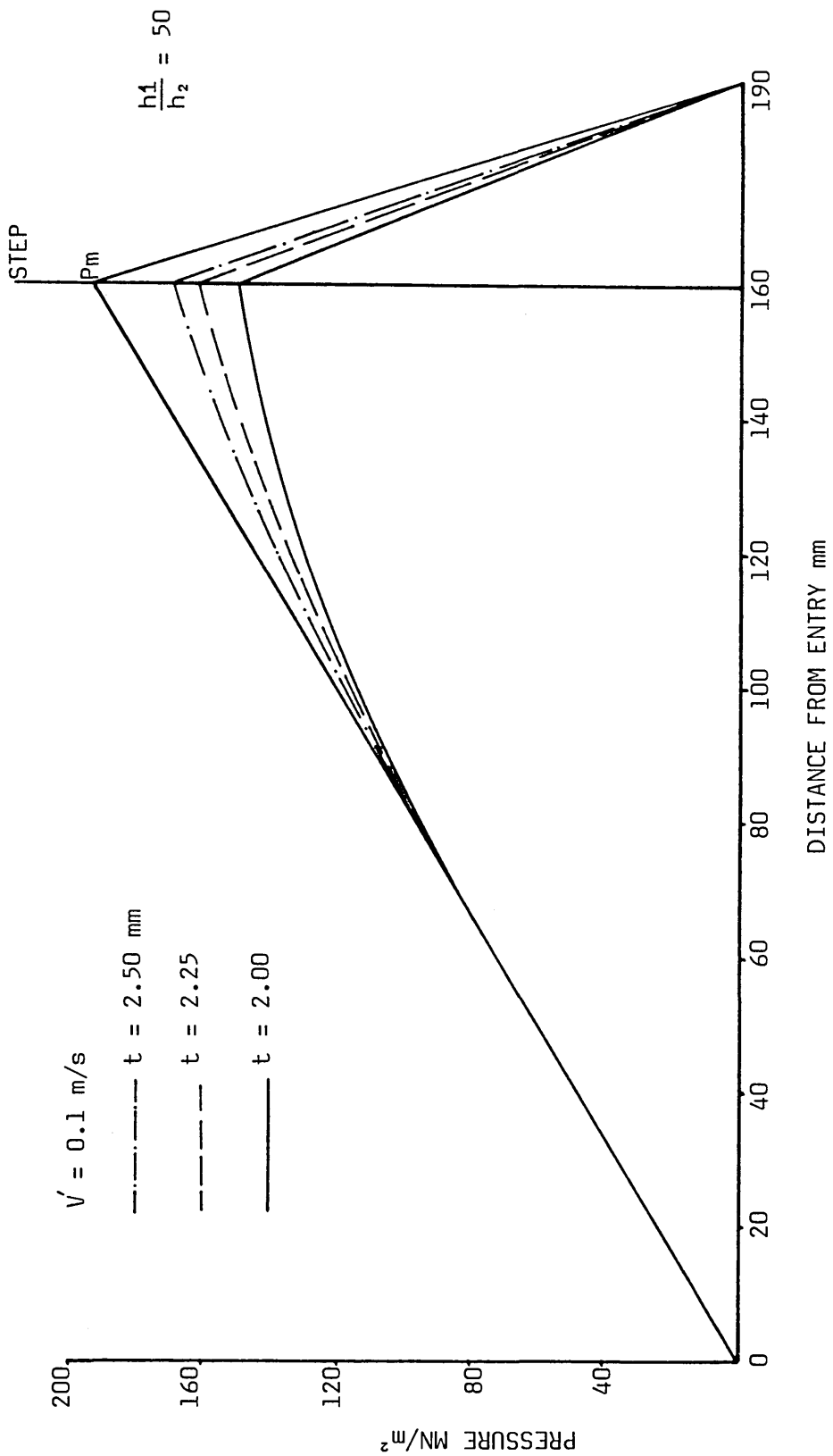


FIG 202 - THEORETICAL EFFECT OF TUBE WALL-THICKNESS ON PRESSURE DISTRIBUTIONS

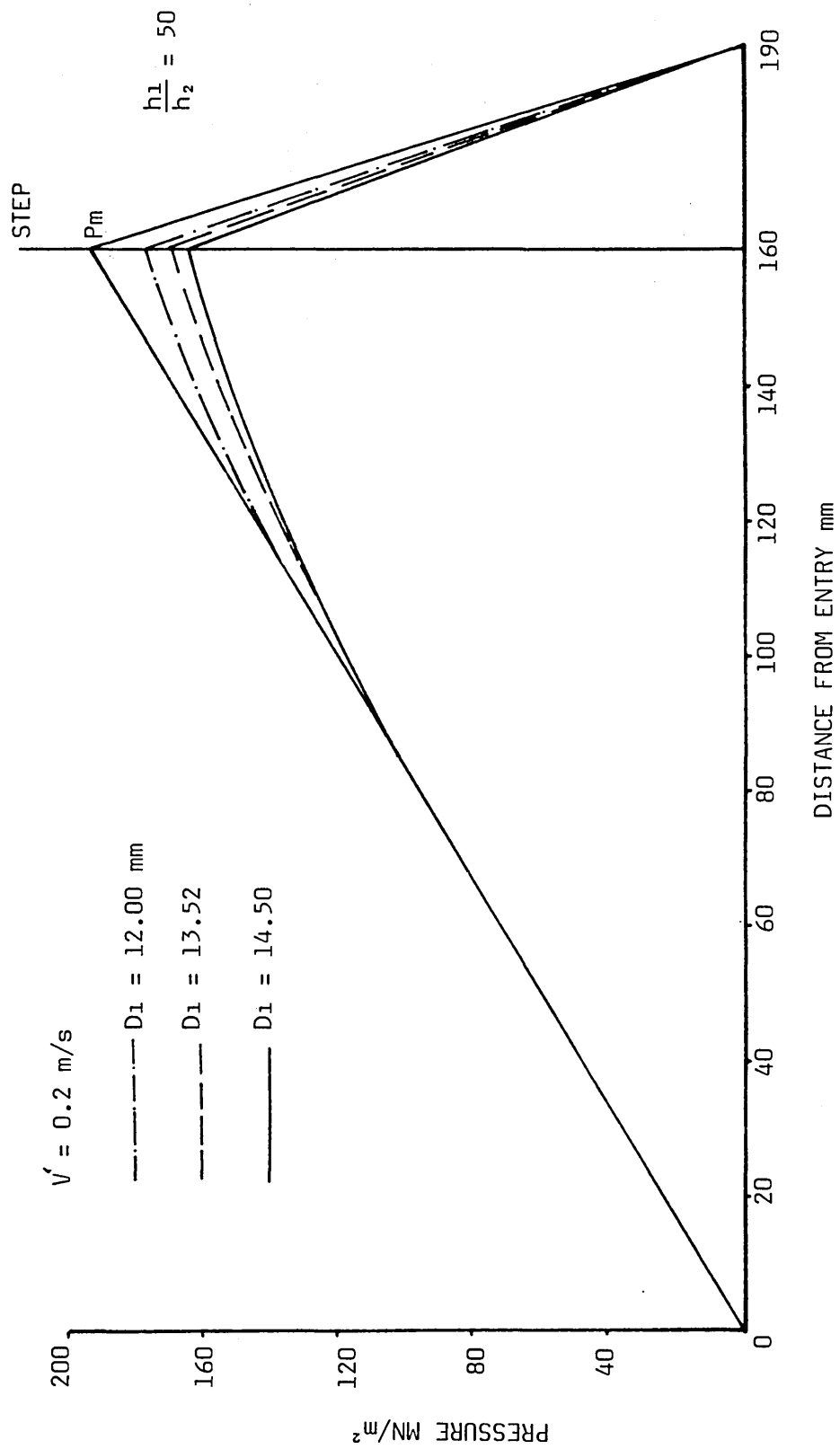


FIG 203 - THEORETICAL EFFECT OF TUBE DIAMETER ON PRESSURE DISTRIBUTIONS

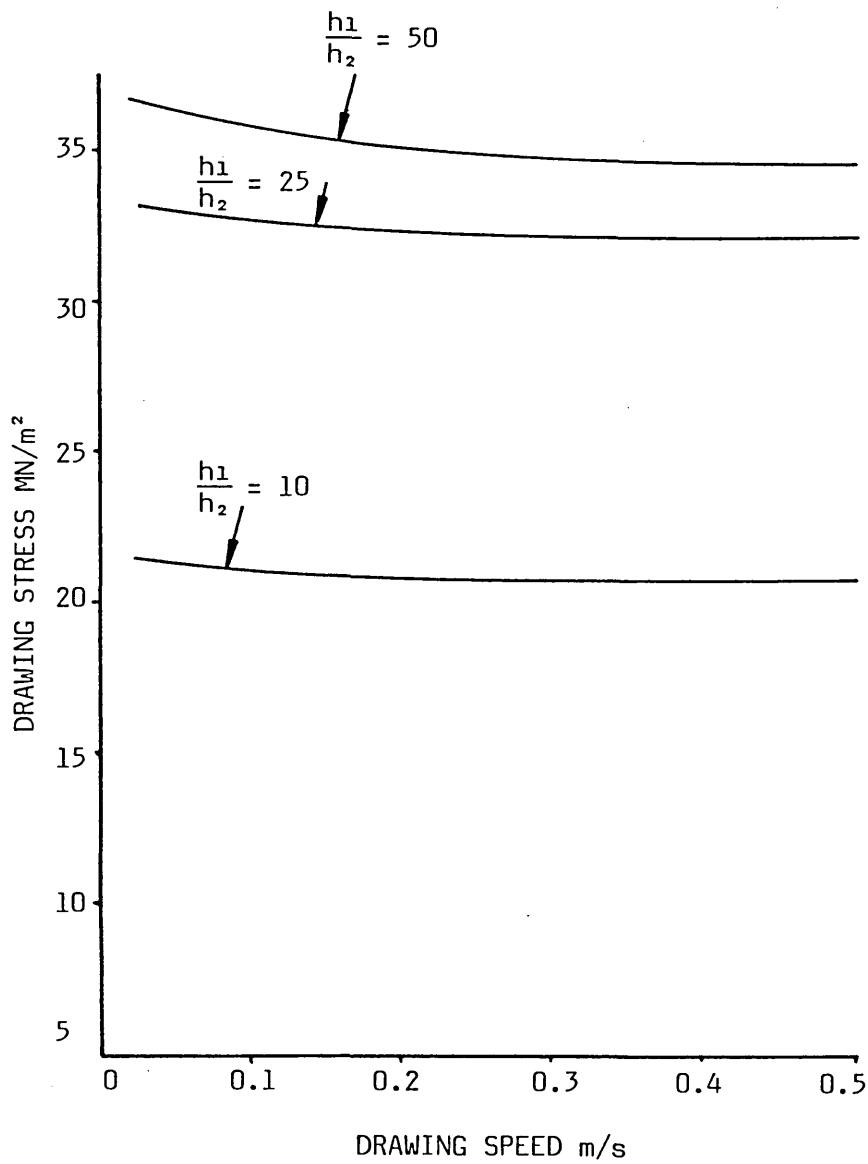


FIG 204 - THEORETICAL EFFECT OF GAP RATIO ON DRAWING STRESS

$$\frac{h_1}{h_2} = 50$$

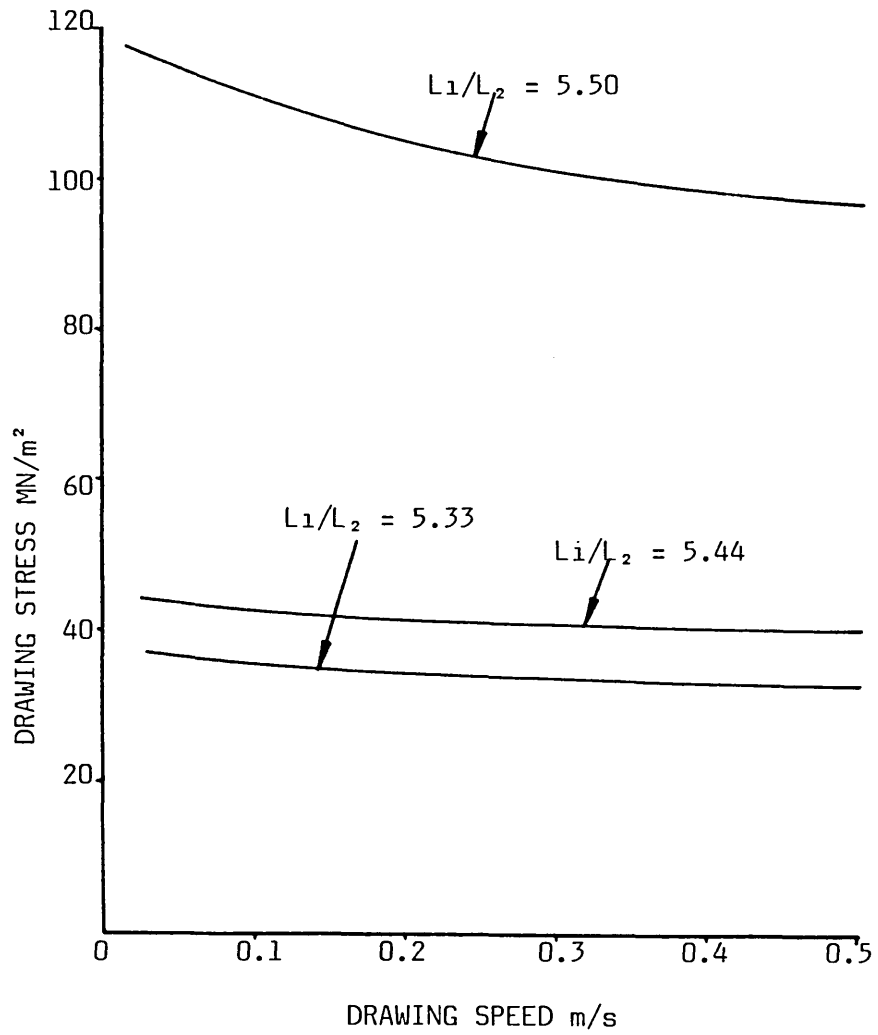


FIG 205 - THEORETICAL EFFECT OF LENGTH RATIO ON DRAWING STRESS

$$\frac{h_1}{h_2} = 50$$

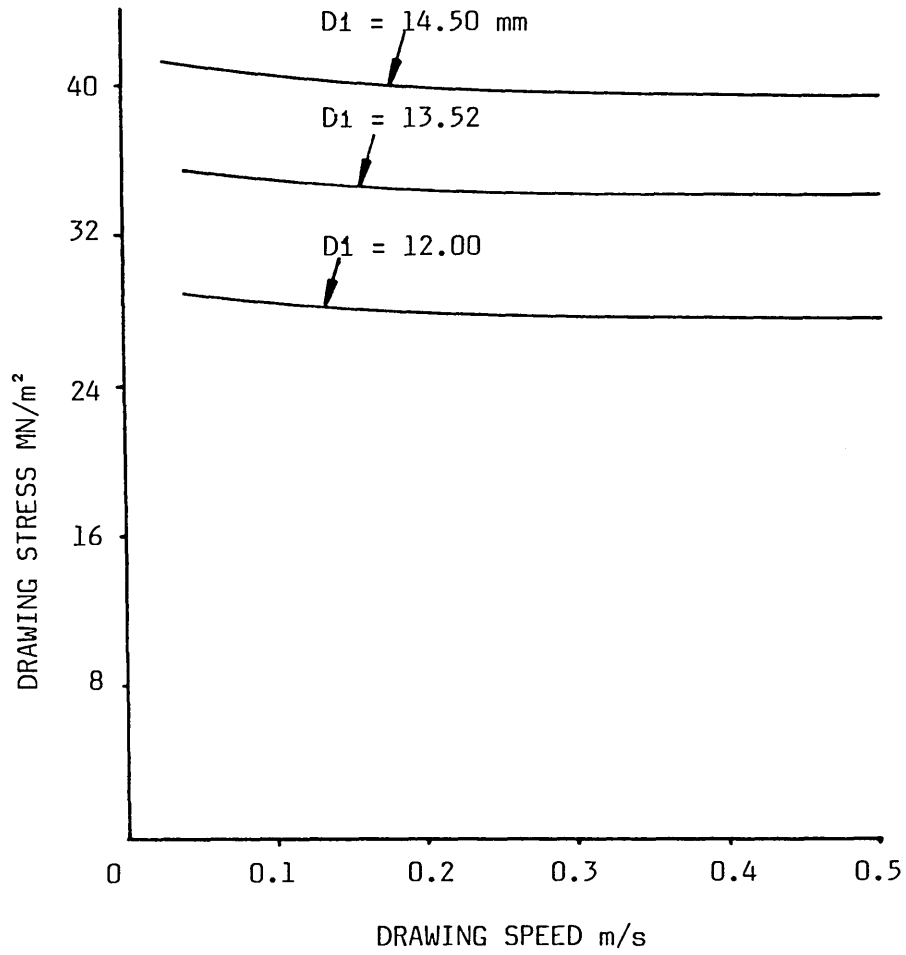


FIG 206 - THEORETICAL EFFECT OF TUBE DIAMETER ON DRAWING STRESS

$$\frac{h_1}{h_2} = 50$$

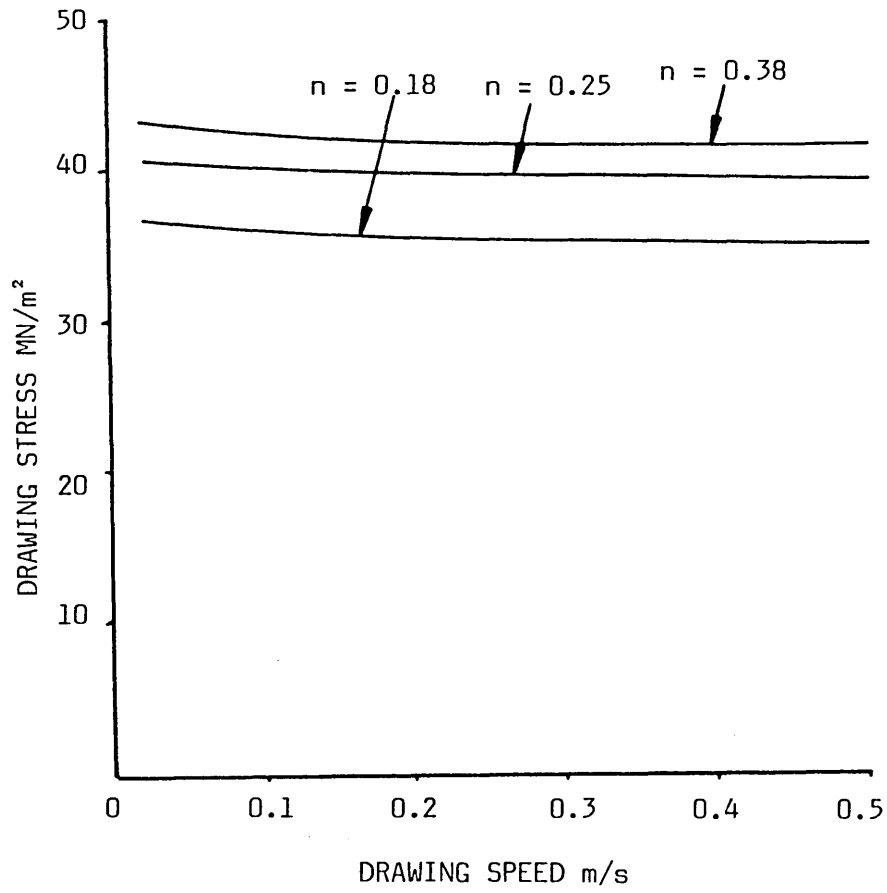


FIG 207 - THEORETICAL EFFECT OF STRAIN HARDENING INDEX ON DRAWING STRESS

$$\frac{h_1}{h_2} = 50$$

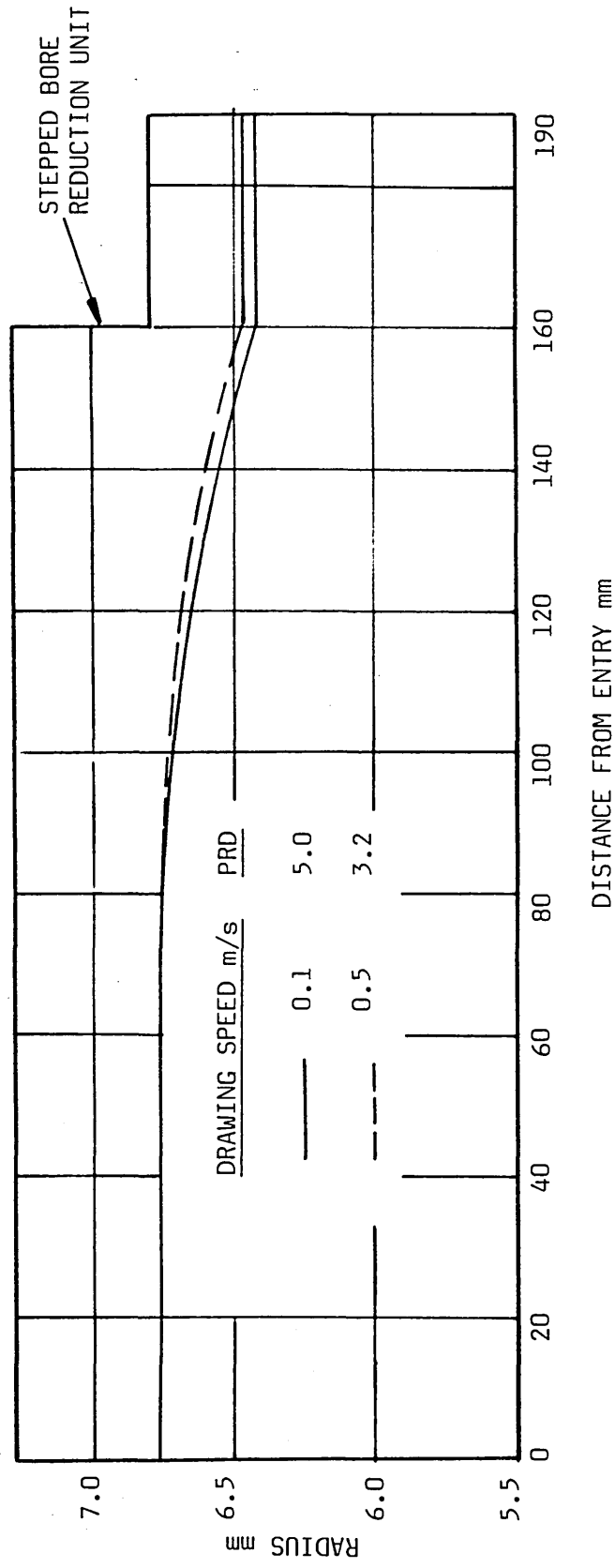


FIG 208 - THEORETICAL DEFORMATION PROFILES

- EXPERIMENT
- NON-NEWTONIAN ANALYSIS
- - - - - NEWTONIAN (NUMERICAL SOLUTION)
- x - x - CURVED DEFORMATION PROFILE ANALYSIS
- · - · - LINEAR DEFORMATION PROFILE ANALYSIS

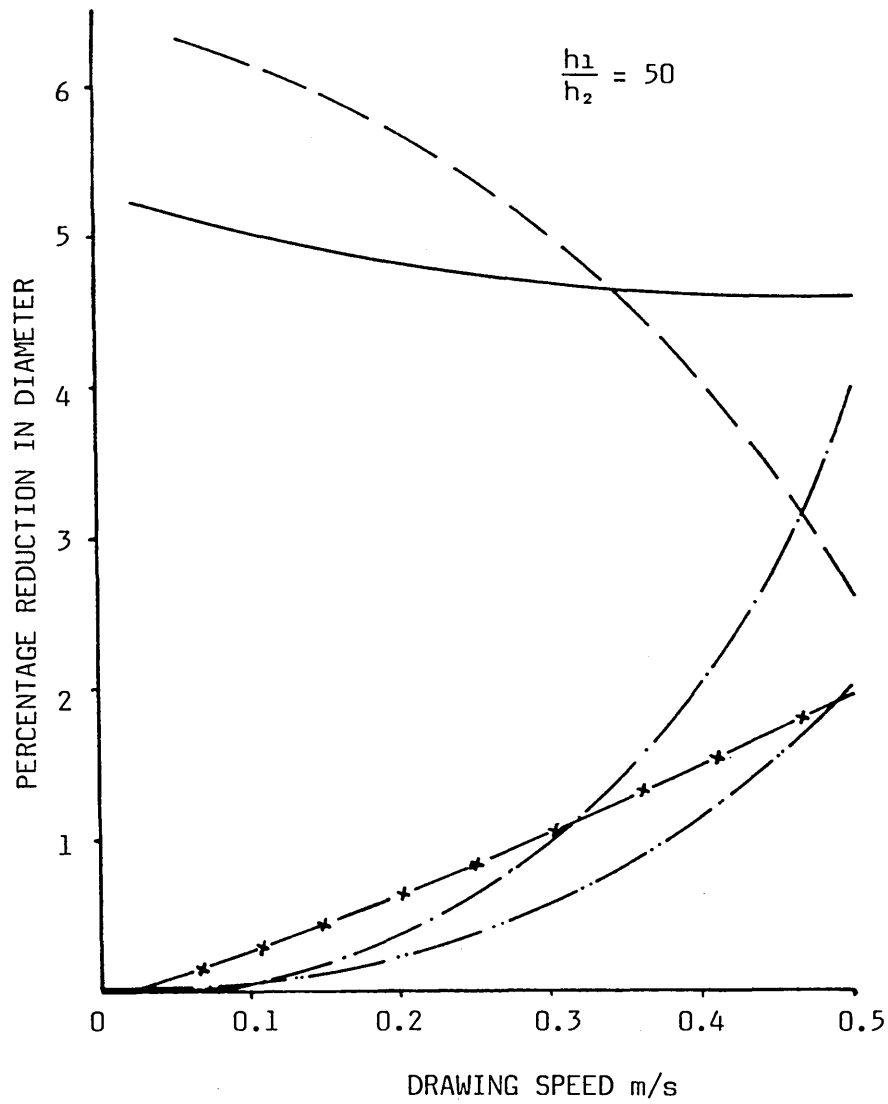


FIG 209 - COMPARISON BETWEEN EXPERIMENTAL AND THEORETICAL PERCENTAGE REDUCTION IN DIAMETER FOR COPPER TUBE

$$\frac{h_1}{h_2} = 50$$

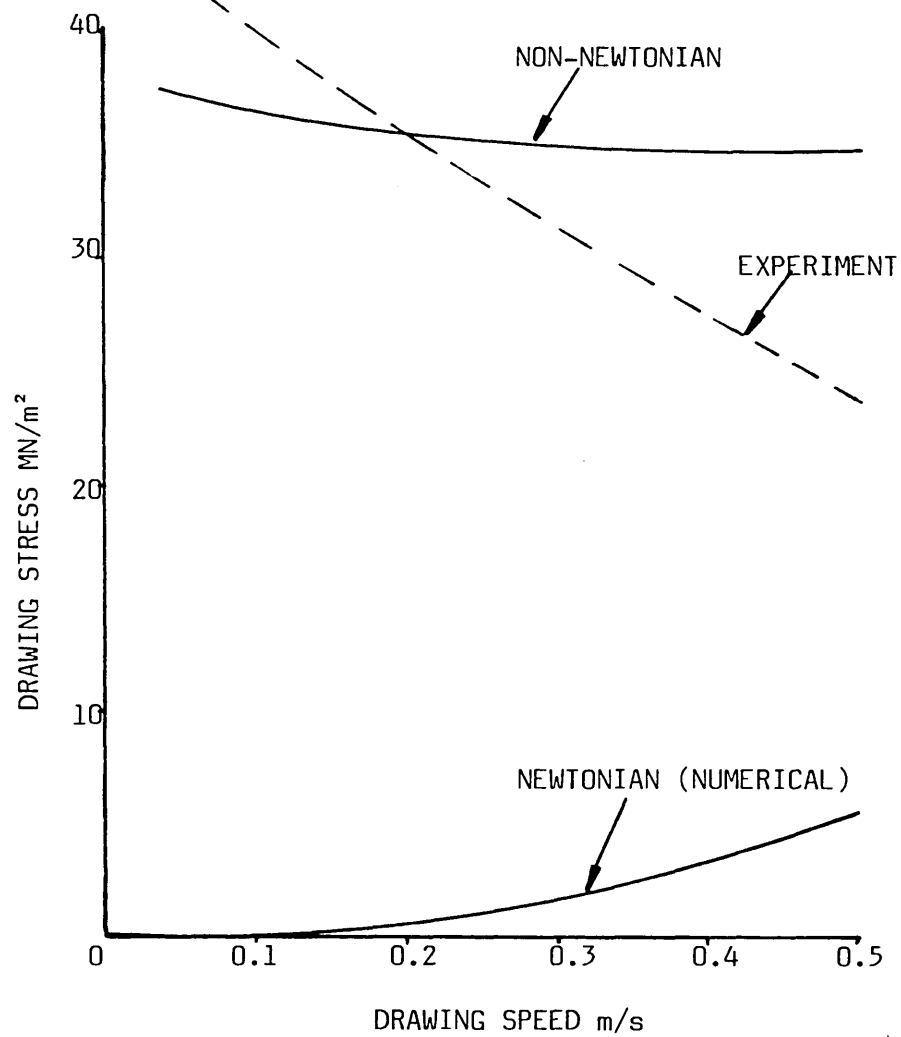


FIG 210 - COMPARISON BETWEEN EXPERIMENTAL AND THEORETICAL DRAWING STRESS FOR COPPER TUBE

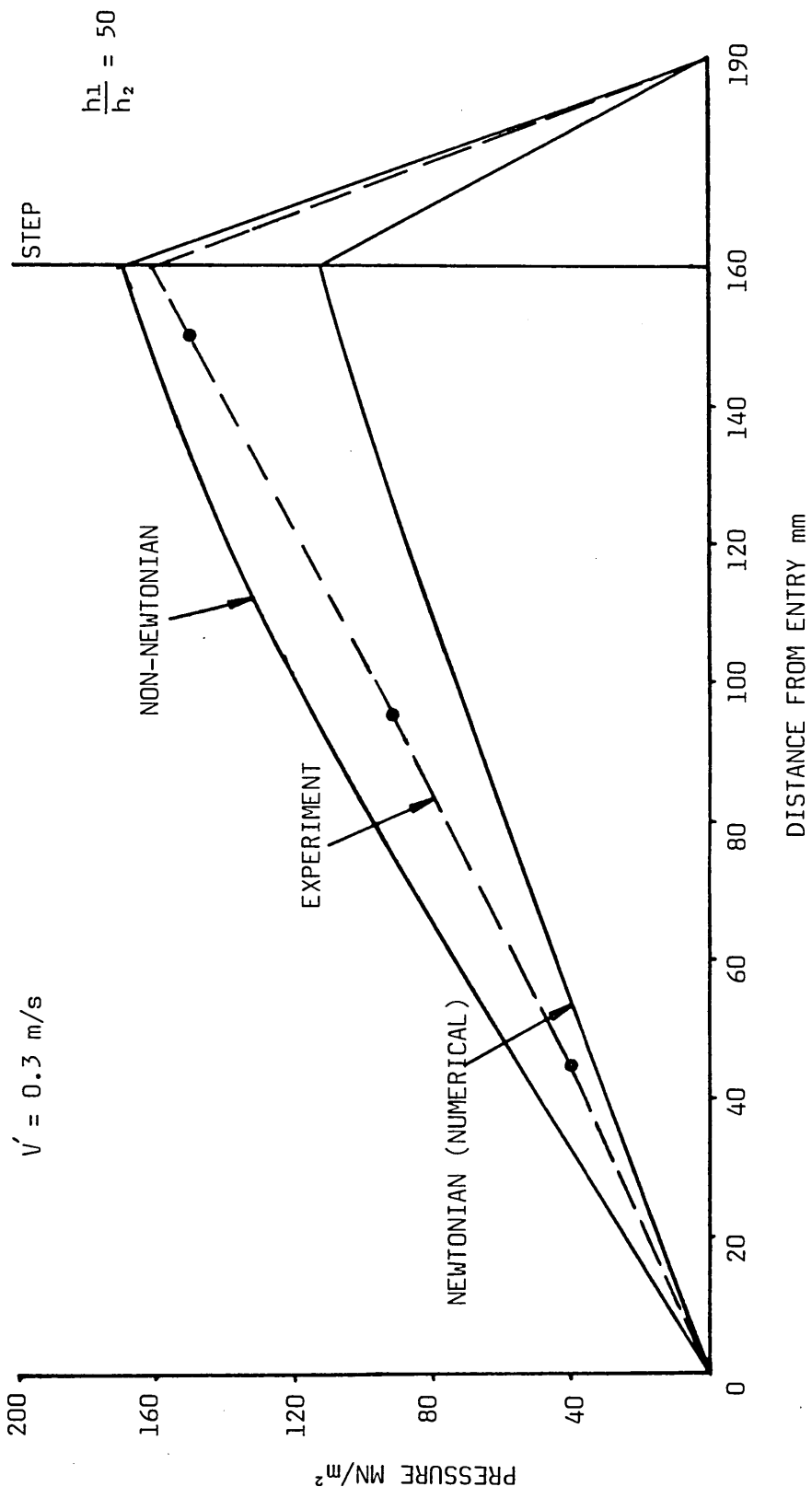


FIG 211 - COMPARISON BETWEEN EXPERIMENTAL AND THEORETICAL PRESSURE DISTRIBUTIONS FOR COPPER TUBE

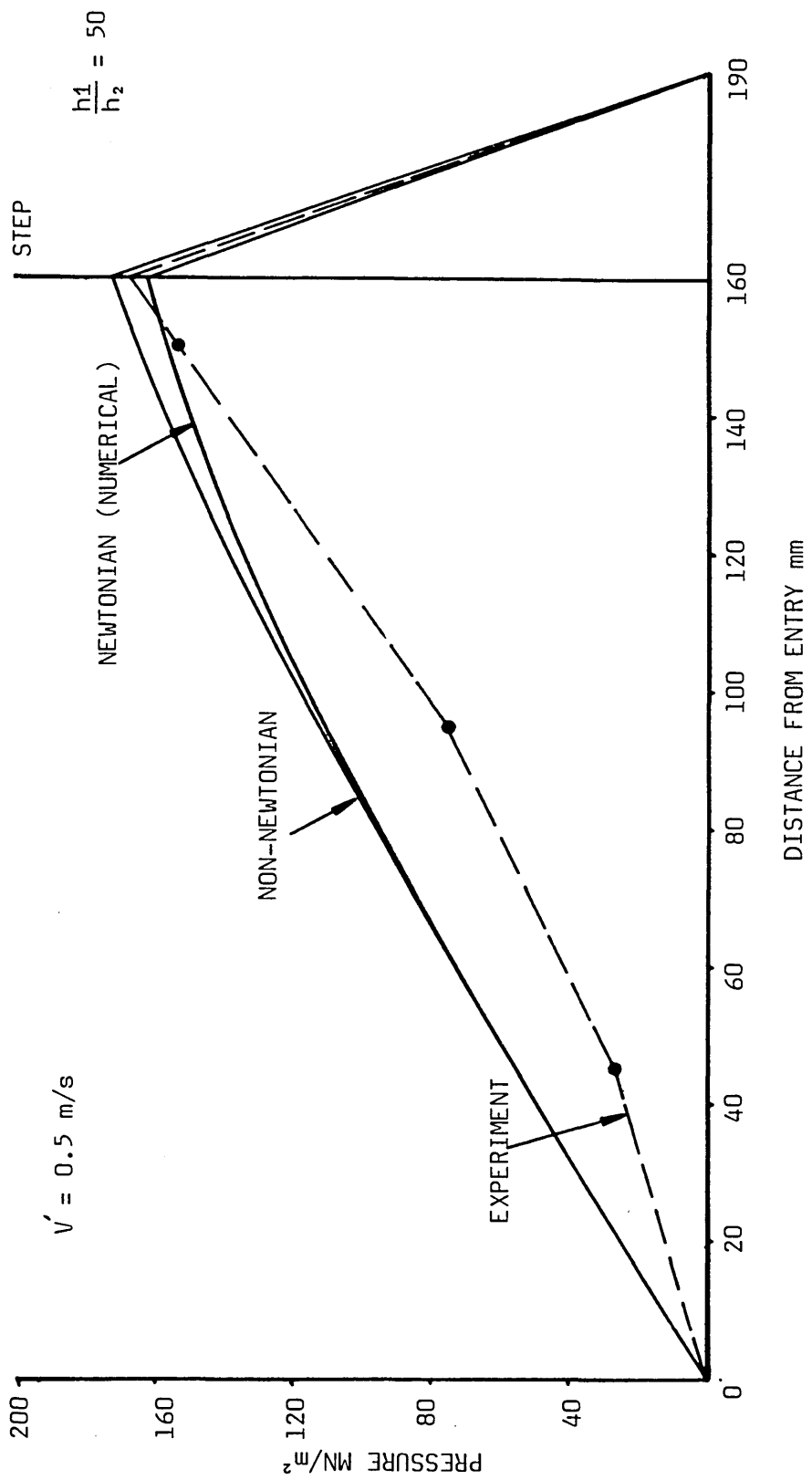


FIG 212 - COMPARISON BETWEEN EXPERIMENTAL AND THEORETICAL PRESSURE DISTRIBUTIONS FOR COPPER TUBE

$$\frac{h_1}{h_2} = 50$$

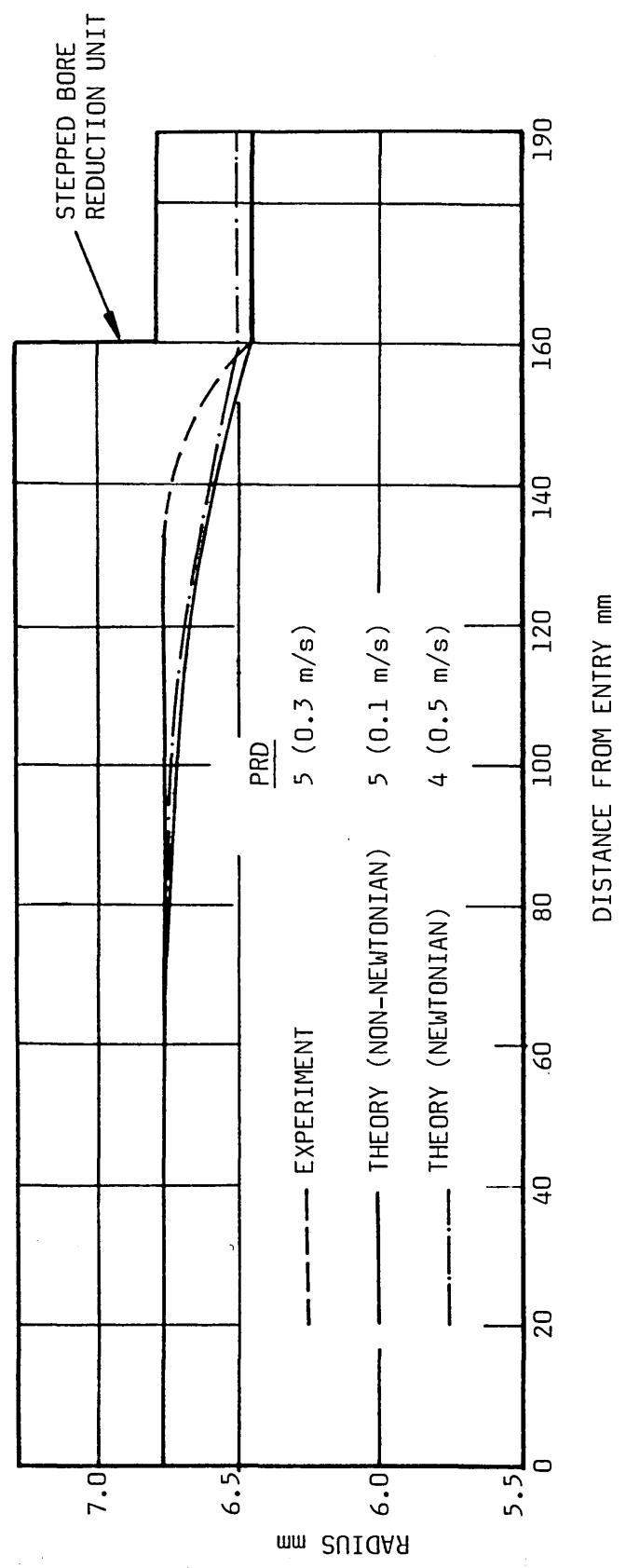


FIG 213 - COMPARISON BETWEEN EXPERIMENTAL AND THEORETICAL DEFORMATION PROFILES FOR COPPER TUBE

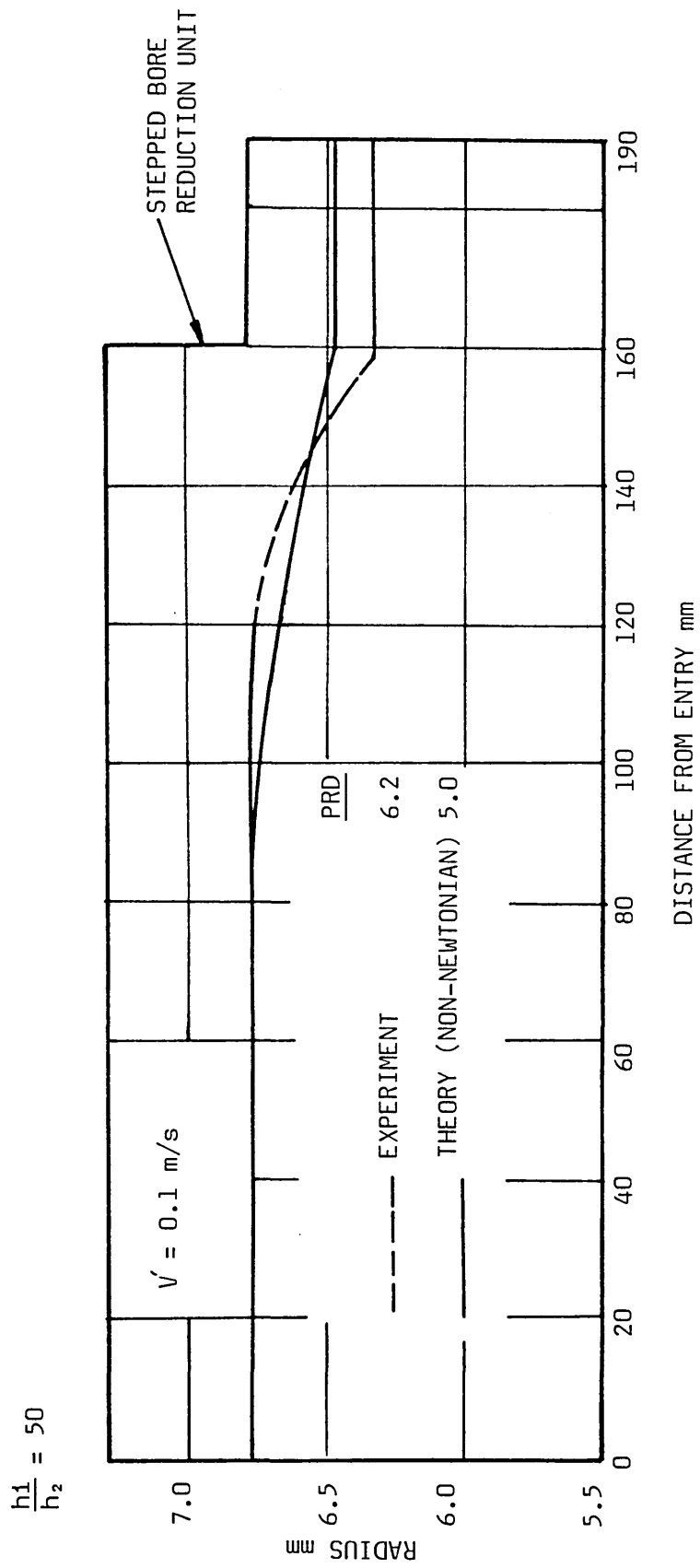


FIG 214 - COMPARISON BETWEEN EXPERIMENTAL AND THEORETICAL DEFORMATION PROFILES FOR COPPER TUBE

CHAPTER 7 : CONCLUSIONS AND SUGGESTIONS FOR FUTURE WORK

7.1 Conclusions

A new technique for tube sinking has been developed in which the conventional reduction die is replaced by a die-less reduction unit. The deformation is induced as a result of hydrodynamic pressures generated in the unit due to the motion of the tube and viscosity of the pressure medium. The dimensions of the die-less reduction unit are such that the smallest bore size is greater than the nominal tube diameter, thus metal to metal contact and hence wear, will no longer be a problem. As no conventional reduction die is used, the need for a reduced diameter leading end is also eliminated.

Experimental work has been carried out on copper and aluminium tubes to investigate the performance of the new system using four different types of polymers as the pressure medium. These are polyethylene (Alkathene WVG23), high density polyethylene (Rigidex), polypropylene (KM61) and polystyrene polymers. Initial research on the new system showed certain limitations as follows:

- (i) When a thin wall tube was drawn at slower drawing speeds and using polymer melt at lower temperatures, onset of circumferential buckling occurred resulting in folded tube.* This buckling disappeared at higher drawing speeds, producing smaller reduction in diameter.
- (ii) In the case of thick wall tube, higher reduction in diameter may only be obtained at very slow drawing speeds and the performance of the unit at higher speeds

* This also occurs in conventional sinking process.

decreased. This could be due to the effect of a phenomenon referred to as the slip condition, where at a certain speed, the value of the shear stress acting on the tube reaches a maximum and remains constant, irrespective of the increase in speed.

The quality of the tubes drawn by the die-less method was found to be comparable to those drawn using the conventional reduction dies.

In this study four different analytical models have been developed to investigate the performance of the die-less reduction unit and to optimise the process.

Although the first three models, based on Newtonian fluid characteristics, provided a greater insight into the mechanics of the process, but predicted percentage reduction in diameter differ from the experimental results significantly both in magnitude and trend. The fourth model, based on non-Newtonian fluid characteristics predicted results which show reasonable agreement with those observed experimentally, both in magnitude and trend.

7.2 Suggestions for Future Work

The new technique of tube sinking developed in this study showed some limitations and practical difficulties. In the case of thin wall tube buckling occurred resulting in longitudinally folded tube at lower drawing speeds and temperatures. The other main limitation observed was the fact that lower reductions in diameter were obtained at higher drawing speeds when polymer melt was used as the pressure medium. Furthermore, the theoretically predicted results showed considerable discrepancy even when the fluid characteristics are assumed to be non-Newtonian. Clearly

some further work could be done both experimentally and theoretically to enhance the understanding of the process.

1- Experimentally

It must be noted that the performance of the system was dependent on the type of the pressure medium and the geometry of the die-less reduction unit. The performance of the unit was partially improved at higher drawing speeds by employing a higher viscosity polymer melt as a pressure medium. Further experimental investigations using other viscous pressure mediums and the geometry of the die-less reduction unit should be carried out to establish the viability of the process.

It is known that the polymer melts are shear thinning fluids (discussed in Chapter 2). However in Reference 20, it is reported that certain polymer solutions are shear thickening fluids (dilatant). It is thought that if a dilatant pressure medium could be used the problem of slip may be solved hence improved performance of the die-less reduction unit at higher drawing speeds should be achievable. The buckling, folding and squeezing effect on the thin walled tube require further investigations. Attempt should be made to draw the tube using solid mandrel and die-less unit for reducing the wall thickness.

2- Theoretically

In the present study, the process was assumed to be isothermal. In reality, however, some temperature change occurs during the process due to mechanical work, heat conduction etc. It is well known that the viscosity of the pressure medium is sensitive to temperature change,

hence incorporation of a relationship giving the change in viscosity due to variation in temperature should improve the theoretical results.

The rheology of the pressure medium should be better understood in terms of the effect of pressure and temperature on its viscosity and slip characteristics. This in turn should improve the ability of the theoretical models to predict results which are in better agreement with those observed experimentally. Finally, a thorough technological and economic viability of the process should be undertaken in order to establish its merits in comparison with the existing techniques.

CHAPTER 8 : REFERENCES

- 1 Swift, H W "Stresses and Strains in Tube Drawing", Phil, Mag. Ser. 7, 11, Pg. 883-902 (1949).
- 2 Chung, S Y "Theory of Hollow Sinking of Thin-Walled Tubes", Metallurgia, May 1951, Pg. 215-218.
- 3 Kragell, Skill, I V and Shchedrove, V S "Development of the Science of Friction", Izel - Vo An SSSR, 1956.
- 4 Milliken, M P "Pressurized Die for Wire Drawings", Wire and Wire-Products, 1955, 30 (5).
- 5 Christopherson, D G and Naylor, H "Promotion of Fluid Lubrication in Wire Drawings", Instn. Mech. Engrs. 169, Pg. 643-653 (1955).
- 6 Wistreich, J G "Lubrication in Wire Drawing", Wear, Pg. 505-511, March (1957).
- 7 Kalmogorov, V L and Selishchev, K P "Cold Drawing Tubes with Improved Lubrication", Stall in English, Pg. 830-831, 9 (1962).
- 8 Swamy, S T N, Prabhu, B S and Rao, B V A "Calculated Load Capacity of Non-Newtonian Lubricants in Finite Width Bearings", Wear, Pg. 277-285, (1975).
- 9 Symmons, G R, Stevens and Thompson. "Hydrodynamic Lubrication and Coating of Wire Using a Polymer Melt During the Drawing Operation", Wire Industry, Pg. 469-483, (1978).
- 10 Stevens, A J "A Plasto-Hydrodynamic Investigation of the Lubrication and Coating of Wire using a Polymer Melt During Drawing", M.Phil Thesis, Sheffield City Polytechnic, (1979).
- 11 Crampton, R. "Hydrodynamic Lubrication and Coating of Wire Using a Polymer Melt During Drawing Process", Ph.D Thesis, Sheffield City Polytechnic, 1980.
- 12 Crampton, R, Symmons, G R and Hashmi, M S J, "A Non-Newtonian Plasto-Hydrodynamic Analysis of the Lubrication and Coating of Wire Using a Polymer Melt During Drawing", Int. Symposium, Metal Working Lubrication, San Francisco, USA, Pg. 107, August (1980).
- 13 Hashmi, M S J, Crampton and Symmons, "Effects of Strain Hardening and Strain Rate Sensitivity of the Wire Material During Drawing Under Non-Newtonian Plasto-Hydrodynamic Lubrication Conditions", Int. J. Mach. Tool Des. Res., Pg. 71-86, (1981).
- 14 Hashmi, M S J, Symmons and Parvinmehr, H. "A Novel Technique of Wire Drawing", Inst. Mech. Engrs., Vol 24, No 1, (1982).

- 15 Benbow, J J and Lamb, P. "SPE Trans.", Jan. (1963).
- 16 Tordella, J P "Trans. Soc. Rheol.", 1, 203 (1957).
- 17 Tordella, J P "J. Appl. Phys.", 27, 454 (1956).
- 18 Pearson, J R A "Plastics Polymer", 37, 285 (1969).
- 19 Brydson, J A "Flow Properties of Polymer Melts", Published by Van Nostrand Reinhold, New York (1970).
- 20 Lenk, R S "Plastics Rheology", Interscience, New York (1968).
- 21 Crawford, R J "Plastics Engineering", Published by Pergamon Press (1981).
- 22 Abbas, K B and Porter, R S "J. Appl. Polymer Sci.", 20, 1289 (1976).
- 23 Nason, K H "J. Appl. Phys.", 16, 338 (1945).
- 24 Dillon, R E and Spencer, R S "J. Colloid Sci.", 4, 241, (1949).
- 25 Severs, E T "Ph.D Thesis", Univ. of Delaware, New York (1950).
- 26 Tordella, J P "SPE Journal", 13, No 8, 36, Aug (1957).
- 27 Clegg, P L "Trans. Plastics Inst.", 26, 151 (1958).
- 28 Dienes, G J "Journal Appl. Phys.", 24, 779 (1953).
- 29 Carley, J F "J. Modern Plastics", Dec (1961).
- 30 Macedo, P B and Litovitz, T A "J. Chem. Phys.", 42, 245 (1965).
- 31 Nielsen, L E "Polymer Rheology", New York (1977).
- 32 Sanchez, I C "J. Appl. Phys.", 45, 4204 (1974).
- 33 Cohen, M and Turnbull, D "J. Chem. Phys.", 31, 1164, (1959).
- 34 Westover, R F "Polymer Eng. Sci.", 6, 83 (1966).
- 35 Maxwell, B and Jung, A "J. Modern Plastics", 35, 174, Nov (1957).
- 36 Cogswell, F N "Plastics and Polymers", Feb (1973).
- 37 Westover, R F "SPE Technical Papers", 6, 801 (1960).
- 38 Parvinmehr, H. "Optimisation of Plasto-hydrodynamic System of Wire Drawing Using Polymer Melts", Ph.D Thesis, Sheffield City Polytechnic, 1983.
- 39 Rabinowitsch, B. "Uber Die Viskostat Und Elastizitat Von Solen", Z. Phys. Chem. (1929), A145, Pg. 141.

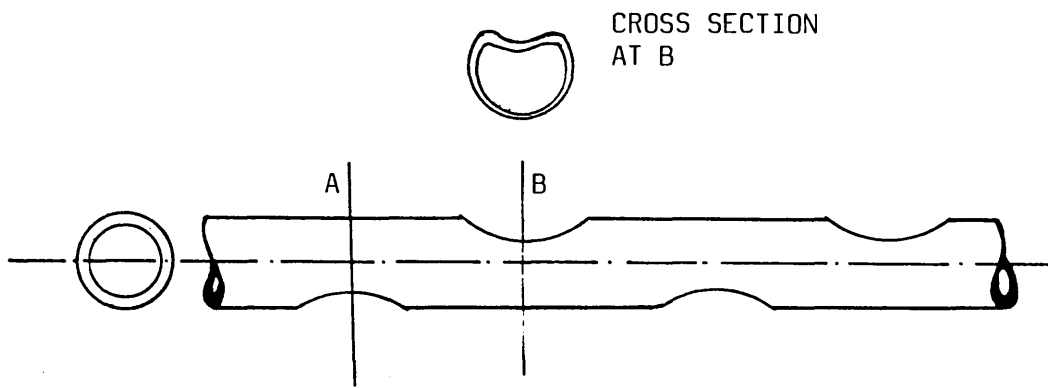
- 40 Hung, D and Muster, D. "Non-Newtonian Flow in Infinite Length Step Shaped Bearings", Naval Research Report, No 17, University of Houston, 1-14, 1969.
- 41 Rotem, Z and Shinnar, R. "Non-Newtonian Flow between Parallel Boundaries in Linear Movement", Chem. Eng. Sci. (1961), Vol 15, Pg. 130.
- 42 Rekterys, K. "Survey of Applicable Mathematics", Illiffe Publications, Pg. 77-79, (1969).
- 43 Hashmi, M S J. "Strain Rate Sensitivity of Commercially Pure Copper at Room Temperature and Strain Rate of Up To 10^6 per second", Sheffield City Polytechnic Technical Report No SCP/MPE/R10, Oct 1978.
- 44 Ting, T C T. "The Plastic Deformation of a Cantilever Beam with Strain Rate Sensitivity Under Impulsive Loading", TR 70, Brown University, Contract Nonr - 562 (10) July 1961.

APPENDIX 1

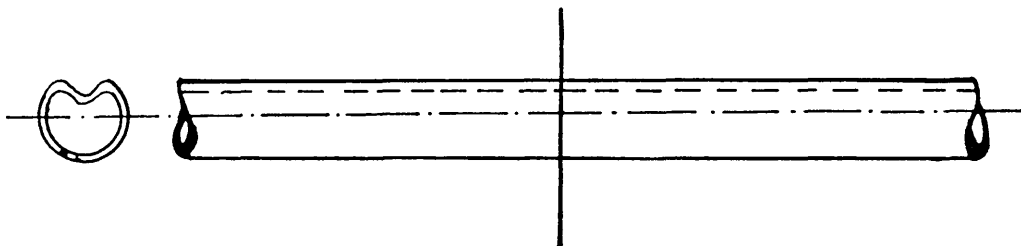
Experimental Results Obtained Using Thin Wall Copper Tubes

When 15 mm O.D and 0.7 mm wall-thickness tubes were drawn through the die-less reduction unit at lower temperatures and speeds, two different types of defects were observed on the products. The first type showed a regular pattern of dimples occurring alternately on diametrically opposite sides of the tubes. This type of defect is shown in the photograph in Figs 30(a) and also in A1(a). The tube appeared to have failed in localised buckling mode under very high plasto-hydrodynamic radial pressure. The frequency of these dimples along the length of the drawn tube changed with the magnitude of the drawing speed and also with the melt temperature.

The second type of defect appeared as a continuous depression or fold along the entire length of the drawn tube. This type of defect is shown in the photograph in Figs 30(b) and also in A1(b) and occurred at very low drawing speeds when a high viscosity polymer melt was used as the pressure medium. The reason for this phenomenon is higher pressures generated in the die-less reduction unit which caused buckling instability and hence folding. It has been reported that at very high pressures (above 140 MN/m²) polymer melts tend to recrystallise.³⁵ It is possible that recrystallisation was occurring in the parts of the die-less reduction unit, giving rise to pressure (and velocity) discontinuities. The effect of the discontinuities could be to initiate the folding and buckling of the tube in the die-less reduction unit.



(a)



(b)

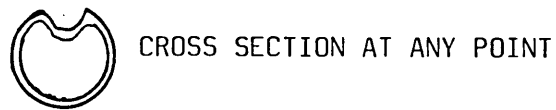


FIG A1 - (a) ALTERNATE DIMPLE TYPE AND (b) CONTINUOUS FOLDING TYPE DEFECTS

APPENDIX 2 - SOLUTION OF THE CUBIC EQUATION

In Chapter 6, Equation (9) is a cubic equation which can be solved by applying Carden's formula. This equation however, is shown to have two imaginary roots and one real root.

The cubic equation is of the form,

$$\phi_1^3 + 3P\phi_1 + 2q = 0 \quad (A_2 - 1)$$

Where $3P = A_1$, so that $P = \frac{A_1}{3}$

and

$$2q = B_1 \text{ such that } q = \frac{B_1}{2}$$

The discriminant of the equation $(A_2 - 1)$ is the number

$$J_1 = -P^3 - q^2$$

Substituting the value of P and q in the above equation gives;

$$J_1 = -\frac{A_1^3}{27} - \frac{B_1^2}{4}$$

According to Carden's formula the real root of equation $(A_2 - 1)$ is

$$\phi_1 = U_1 + V_1$$

Where,

$$U_1 = [-q + (q^2 + P^3)^{\frac{1}{2}}]^{\frac{1}{3}} \text{ and } V_1 = [-q - (q^2 + P^3)^{\frac{1}{2}}]^{\frac{1}{3}}$$

A3.1 - Assumed Linear Deformation Profile

```

100 PRINT "THIS PROGRAMME CALCULATES THEORETICAL."
110 PRINT "PERCENTAGE REDUCTION IN DIA. OF CAPPAR"
120 PRINT "TUBE WITH STEPPED CORE REDUCTION UNIT"
125 PRINT "USING POLYMER MELT AS A PRESSURE MEDIUM"
130 PRINT "***** LINEAR PROFILE *****"
140 F=F+1
150 VEL=F/10
160 VIS=100
170 H1=5E-04
180 H2=1E-05
190 L1=160E-03
200 L2=30E-03
210 R1=676E-05
220 T=250E-02
230 Y0=5E07
235 K0=7E08
237 N=0.15
240 PM=6*VIS*VEL*(H1-H2)/((H1**3)/L1+(H2**3)/L2)
250 TC1=-VIS*VEL/H1-PM*H1/(2*L1)
270 X1=Y0/((PM*R1)/(T*L1)+(TC1/T))
280 GX1=(TC1*X1)/T
290 P1=(PM*X1)/L1
300 PRINT'VEL='; VEL, 'PM='; PM, 'TC1='; TC1,
      & 'X1='; X1,
330 X=L1-X1
340 INC=0.001
350 B=B+INC
360 H=H1+B*X
370 R=R1-B*X
375 Y=Y0+K0*LOG(R1/R)**N
380 PS=6*VIS*VEL*(H1)/(2*B*(H**2))-1/(B*H)+1/(2*H1*B))&
      & -PM/L1*(H1**3)/(2*B*(H**2))-H1/(2*B)-X1
390 TC=-H*0.5*((6*VIS*VEL*B*X)/(H**3)+(H1**3)*PM/L1)&
      & (H**3))- (VIS*VEL/H)
400 GX=Y0*LOG(R1/R)+(K0/(N+1))*(LOG(R1/R)**(N+1))+&
      & GX1+(TC*B*X)*(1+B**2)**0.5/(T*B)
410 GTH=(PS*R*(1+B**2)**0.5)/T
420 YM=GX+GTH
425 RES=YM-Y
430 IF ABS(RES)<=1E-05 THEN GOTO 490
440 IF RES>0 THEN GOTO 350
460 IF RES<0 THEN GOTO 470
470 B=B-INC
475 INC=INC/10 : GOTO 350
490 PRINT'B='; B, 'X='; X, 'H='; H,
      & 'R='; R, 'GTH='; GTH, 'PS='; PS,
500 H3=H2+(B*X)
510 TC2=(H3*PS)/(2*L2)-(VIS*VEL)/H3
520 GX2=(TC2*L2)/T
530 G2=GX+GX2
540 PRED=100*(B*X)/R1
545 IF PRED<0 THEN PRED=0
550 PRINT'H3='; H3, 'G2='; G2, 'PRED='; PRED,
555 PRINT'-----'
560 IF F>=5 THEN GOTO 590
570 GOTO 140
580 END

```

A3.2 - Assumed Curved Deformation Profile

```

100 PRINT "THIS PROGRAMME CALCULATES THEORETICAL"
110 PRINT "PERCENTAGE REDUCTION IN DIA. OF COPPER"
120 PRINT "TUBE WITH STEPPED BORE REDUCTION UNIT"
130 PRINT "USING POLYMER MELT AS A PRESSURE MEDIUM"
135 PRINT "***** CURVED PROFILE *****"
140 T=0.1
150 VEL=F/10
160 VIS=100
170 H1=5E-04
180 H2=1E-03
190 L1=140E-03
200 L2=30E-03
210 R1=674E-05
215 G1=1353E-05
220 T=250E-05
230 Y0=5E07
235 K0=7E09
237 N=0.19
240 PM=6+VIS*VEL*(H1-H2)/((H1**3)/L1+(H2**3)/L2)
250 TC1=-VIS*VEL/H1-PM/H1/(2*L1)
260 G1=(VEL*H1)/2-(H1**3)*(PM)/(1.7*VIS*L1)
270 X1=Y0/((PM*R1)/(T*L1)+(TC1/T))
280 GX1=(TC1*X1)/T
290 P1=(PM*X1)/L1
295 PRINT'-----'
300 PRINT'VEL='; VEL , 'PM='; PM , 'TC1='; &
    & TC1 , 'X1='; X1,
330 X=L1-X1
340 INC=0.001
350 B=B+INC
360 H=H1+B*(X**2)
370 R=R1-B*(X**2)
373 A=SOR(H1/B)
374 C=((A**2)+(X**2))**2
375 YH=Y0+K0*LOG(R1/R)**N
380 PS=6*VIS*VEL*(ATN(X/A)/(B*(A**3)*(C**2))+((X**3)A
    & -(A**2)*X)/(B*(A**2)*(C**2)*C))+PM/L1*(X1+(3/B*A)&
    & *ATN(X/A)+(5*(A**2))+((3*(A**2)*(X**3))/(B*C))
390 TC=-VIS*VEL*((A**2)+4*(X**2))/(B*C)-(PM*H1*&
    & (A**4))/(3*L1*C)
400 GX=GX1+Y0*LOG(R1/R)+(K0/(N+1))*((LOG(R1/R))&
    & **((N+1))-(SOR(B)*TC*SOR(R1-R))/(B*T))
410 GTH=(PS*R)/(T*(1-4*B*R1+4*B*R)**0.5)
420 RES=GX+GTH-YH
430 IF ABS(RES) <=1E-05 THEN GOTO 490
440 IF RES>0 THEN GOTO 350
460 IF RES<0 THEN GOTO 470
470 B=B+INC
475 INC=INC/10
480 GOTO 350
490 PRINT'B='; B , 'X='; X , 'H='; H , 'R='; R , &
    & 'GX='; GX , 'GTH='; GTH , 'PS='; PS
500 H3=H2+B*(X**2)
510 TC2=(H3*PS)/(2*L2)-(VIS*VEL)/H3
520 GX2=(TC2*L2)/T
530 GD=GX+GX2
540 PRED=100*(2*B*(X**2))/D1
545 IF PRED<0 THEN PRED=0
550 PRINT'H3='; H3 , 'GD='; GD , 'PRED='; PRED
560 IF F>=5 THEN GOTO 380
570 GOTO 140

```

A3.3 - Numerical Solution

```

10 DIM P(500),S(500),YM(500),X(500),Y(500)
20 DIM R(500),H(500),RS(500),V(500)
30 PRINT"THIS PROGRAMME CALCULATES THEORETICAL",A
  & "PERCENTAGE REDUCTION IN DIA. OF COPPER TUBE",A
  & "WITH STEPPED BORE REDUCTION UNIT USING POLYMER",A
  & "MELT AS A PRESSURE MEDIUM"
35 PRINT"***** NUMERICAL SOLUTION (NEWTONIAN) *****"
40 L1=140E-03 : L2=30E-03
45 H1=5E-04 : H2=1E-05
50 R1=676E-03 : T=230E-05
60 Y0=5E07 : K0=7E08 : NH=18E-02
70 TM=3.E : NC=3.5E04
80 VIS=100
87 F=0.0
90 F=F+1
100 VEL=F/10
110 PM=4*VIS*VEL*(H1-H2)/((H1**3)/L1+(H2**3)/L2)
120 TC1=-VIS*VEL/H1-PM*H1/(2*L1)
130 Q1=-((H1**3)*PM)/(12*VIS*L1)+(0.5*VEL*H1)
140 X1=Y0/((PM*R1)/(T*L1)+(ABS(TC1)/T))
150 GX1=(ABS(TC1)*X1)/T
160 PRINT"VEL="; VEL ; "PM="; PM ; "TC1="; TC1 ;&
  & "X1="; X1 ; "GX1="; GX1
410 IF X1>L1 THEN GOTO 90
420 TEM=INT(X1*1000)+1
430 Z=L1*1000-TEM
440 P(1)=(PM*X1)/L1
450 Y(1)=Y0
460 S(1)=(ABS(TC1)*X1)/T
470 HS(1)=(P(1)*R1)/T
480 YM(1)=S(1)+HS(1)
490 R(1)=R1
500 H(1)=L1
510 V(1)=VEL
520 X(1)=X1
530 DX=0.001
550 FOR I1=1 TO Z
560 J=I1+1
580 INC=1E-03
600 B=0.0
620 B=B+INC
640 X(J)=X(J-1)+DX
650 R(J)=R(J-1)-(B*DX)
660 H(J)=H(J-1)+(B*DX)
670 V(J)=V(J-1)/(1-((R(J-1)-R(J))/R(J-1)))
680 DP=(12*VIS)/(H(J)**3)*((V(J)*(H(J))/2)-Q1)
660 P(J)=DP*DX+P(J-1)
670 HS(J)=(P(J)*R(J)*(SQRT((DX**2)+((R(J-1)-R(J))*&
  & **2))))/(T*DX)
680 SRS=0.0
900 MER=2*V(J)*(LOG(R(J-1)/R(J)))/DX
910 SRS=(MER/NC)**(1/TM)
920 Y(J)=(1+SRS)*(Y0+(K0*((LOG(R(1)/R(J)))*NH)))
930 S(J)=(Y(J)*(R(J-1)-R(J))/R(J)+(ABS(TC1)*&
  & *(SQRT(((R(J-1)-R(J))**2)+(DX**2)))/T)+S(J-1)
940 YM(J)=S(J)+HS(J)
950 RES1=YM(J)-Y(J)
960 IF ABS(RES1)<=5E05 THEN GOTO 1040
980 IF RES1<0 THEN GOTO 1000
990 INC=INC

```

```

995 GOTO 620
1000 B=B+INC
1010 INC=INC/E
1020 GOTO 670
1040 PRINT'F='; F(J) , 'HS='; HS(J) , 'S='; S(J) ,&
    & 'YM='; YM(J) , 'Y='; Y(J) , 'X='; X(J) ,&
    & 'H='; H(J) , 'R='; R(J)
1050 PRED=(1-(R(J)/(R1)))*100
1060 H3=H(J)-H1+HE
1065 SD=S(J)+(L2/T)*((H3*(F(J))/2*L2)-(VIS*(U(J))/H3))
1070 PRINT'PRED='; PRED , 'UD='; U(J) , 'H3='; H3 ,&
    & 'E='; E , 'SD='; SD
1071 PRINT'-----'
1073 NEXT I:
1075 IF F>=5 THEN GOTO 1080
1077 GOTO 90
1080 END

```

```

10 DIM P(500),S(500),YM(500),X(500),Y(500)
20 DIM R(500),H(500),HS(500),V(500)
30 PRINT"THIS PROGRAMME CALCULATES THEORETICAL",&
  & "PERCENTAGE REDUCTION IN DIA. OF COPPER TUBE",&
  & "WITH STEPPED BORE REDUCTION UNIT USING POLYMER",&
  & "MELT AS A PRESSURE MEDIUM"
35 PRINT"***** NON-NEWTONIAN SOLUTION *****"
40 L1=160E-03 : L2=30E-03
45 H1=5E-04 : H2=1E-05
50 R1=676E-05 : TW=250E-05
60 Y0=5E07 : K0=7E08 : NM=0.15
70 TM=3.9 : NC=5.5E04
80 QVIS=100 : PC=5.6E-11
82 TCA=4E05
85 AP=1.2E05 : BP=4.0E-11
87 F=0.0
90 F=F+1
100 VEL=F/10
110 SRT=VEL/H1
120 INC1=1E08
130 REM1=1E-09
140 TC1=0.0
150 P1=0.0
160 P1=P1+INC1
180 VIE=(QVIS+(((P1**2)*(BP))+AP)/3.0))/SRT
190 DP1=P1/L1
200 PEE1=(4+(PC*(DP1**2)*(H1**2)))/(12*PC)
210 QUE1=(VIS*VEL)/(2*PC*H1)
213 Z11=-QUE1+(SOR((PEE1**3)+(QUE1**2)))
215 Z22=QUE1+(SOR((PEE1**3)+(QUE1**2)))
220 PHY1=(Z11**0.3333)-(Z22**0.3333)
230 TC1=PHY1-(DP1*H1*0.5)
235 X1=Y0/((P1*R1)/(TW*L1)+(ABS(TC1)/TW))
240 Q1=((DP1*(H1**3))/(6*VIS))+((TC1*(H1**2)/(2*VIS))+((VEL*H1)&
  & +(PC/VIS)*((DP1**3)*(H1**5)/20)+((TC1**3)*(H1**2)*0.5)&
  & ((DP1**2)*(H1**4)*TC1*0.25)+(0.5*(TC1**2)*DP1*(H1**3)))
250 DP2=P1/L2
260 PEE2=(4+(PC*(DP2**2)*(H2**2)))/(12*PC)
270 QUE2=(VIS*VEL)/(2*PC*H2)
273 Z33=-QUE2+(SOR((PEE2**3)+(QUE2**2)))
275 Z44=QUE2+(SOR((PEE2**3)+(QUE2**2)))
280 PHY2=(Z33**0.3333)-(Z44**0.3333)
290 TC2=PHY2+(DP2*H2*0.5)
300 Q2=-((DP2*(H2**3))/(6*VIS))+((TC2*(H2**2)/(2*VIS))+((VEL*H2)&
  & +(PC/VIS)*(-(DP2**3)*(H2**5)/20)+((TC2**3)*(H2**2)*0.5)&
  & ((DP2**2)*(H2**4)*TC2*0.25)-(0.5*(TC2**2)*DP2*(H2**3)))
310 RES1=Q1-Q2
320 IF ABS(RES1)<=REM1 THEN GOTO 400
340 IF RES1 <0 THEN GOTO 360
350 IF RES1 >0 THEN GOTO 160
360 P1=P1-INC1
370 INC1=INC1/10
380 GOTO 160
400 PRINT"VEL="; VEL , "PM="; P1 , "TC1="; TC1 ,&
  & "VIS="; VIS , "X1="; X1
410 IF X1>L1 THEN GOTO 90
420 TEM=(INT(X1*1000)+1)
430 W=L1*1000-TEM
440 P(1)=(P1*X1)/L1
450 Y(1)=Y0

```

```

460 S(1)=(ABS(TC1)*X1)/TW
470 HS(1)=(P(1)*R1)/TW
480 YM(1)=S(1)+HS(1)
490 R(1)=R1
500 H(1)=H1
510 V(1)=VEL
520 X(1)=X1
530 DX=0.001
540 FOR A=1 TO W
550 J A+1
560 INC2=1E-03
570 REM2=5E05
600 B=0.0
620 R=R+INC2
640 X(J)=X(J-1)+DX
650 R(J)=R(J-1)-(B*DX)
660 H(J)=H(J-1)+(B*DX)
670 V(J)=V(J-1)/(1-((R(J-1)-R(J))/R(J-1)))
680 DP=0.0
690 REM3=1E-09
700 INC3=5E08
720 HP=DP+INC3
740 PEE3=(4+(PC*(DP**2)+(H(J)**2)))/(12*PC)
750 QUE3=(VIS*V(J))/(2*PC*H(J))
755 ZEE3=QUE3*(SOR((PEE3**3)+(QUE3**2)))
755 Z66=QUE3*(SOR((PEE3**3)+(QUE3**2)))
760 PHY3=(ZEE3**0.3333)-(Z66**0.3333)
770 TC=PHY3-(DP*H(J)*0.3)
780 RES2=((DP*(H(J)**3))/(6*VIS))+(TC*(H(J)**2)/(2*VIS))+(V(J)*H(J))&
& +(PC/VIS)*(((DP**3)*(H(J)**5)/20)+((TC**3)*(H(J)**2)/2)+((DP**2)*&
& *(H(J)**4)*TC/4)+((TC**2)*DP*(H(J)**3)/2))-R1
790 IF ABS(RES2)<=REM3 THEN GOTO 840
810 IF RES2 < 0 THEN GOTO 830
820 IF RES2 > 0 THEN GOTO 720
830 DP=DP+INC3
840 INC3=INC3/10
850 GOTO 720
860 P(J)=DP*DX+P(J-1)
870 HS(J)=(P(J)*R(J)*(SOR(((X(J)-X(J-1))**2)+((R(J-1)-R(J))**2))))
/((TW*(X(J)-X(J-1))))
890 SRS=0.0
900 MER=2*V(J)*(LOG(R(J-1)/R(J)))/DX
910 SRS=(MER/NC)**(1/TN)
920 Y(J)=(1+SRS)*(Y0+(K0*((LOG(R(1)/R(J)))**NH)))
930 S(J)=(Y(J)*(R(J-1)-R(J))/R(J)+(ABS(TC)*(SOR(((R(J-1)-R(J))**2)
+((X(J)-X(J-1))**2)))/TW))/S(J-1)
933 IF S(J) < Y(J) THEN GOTO 940
935 PRINT "FRACTURE OCCURS IN TUBE AT THIS SPEED"
937 GOTO 90
940 YM(J)=S(J)+HS(J)
950 RES3=YM(J)-Y(J)
955 IF (ABS(TC1)>TCA) THEN GOTO 1090
960 IF ABS(RES3)<=REM2 THEN GOTO 1040
980 IF RES3 < 0 THEN GOTO 1000
990 IF RES3>0 THEN GOTO 620
1000 B=B+INC2
1010 INC2=INC2/10
1020 GOTO 620
1040 PRINT "P="; P(J) , "HS="; HS(J) , "S="; S(J)&
& , "YM="; YM(J) , "Y="; Y(J) , "X="; X(J)&
& , "H="; H(J) , "R="; R(J)

```

```

1070 PRED=(1-((2*R(J))/(2*R1)))*100
1080 H3=H(J)-H1+H2
1085 SD=S(J)+(TC2*LE/TW)
1070 PRINT"PREDE="; PRED, "VE="; V(J), "H3="; H3&
& "SD="; SD
1071 PRINT"-----"
1073 NEXT A
1075 IF F>5 THEN GOTO 1420
1077 GOTO 90
1090 PRINT"*****CONDITION OF CLIP IS DETECTED*****"
1130 FOR A=1 TO W
1135 J1=A+1
1140 INCA=LE-03
1150 RTMA=BE05
1160 B4=0.0
1170 B4=B4+INCA
1175 X(J1)=X(J1-1)+DX
1180 R(J1)=R(J1-1)-(B4+DX)
1190 H(J1)=H(J1-1)+(B4+DX)
1200 U(J1)=U(J1-1)/(1-((R(J1-1)-R(J1))/R(J1-1)))
1205 P(J1)=BP+DX+P(J1-1)
1210 FC(J1)=(P(J1)*R(J1))/(GOR(((X(J1)-X(J1-1))*2)+((R(J1-1)-R(J1))*2)))
& /(TW*(X(J1)-X(J1-1)))
1215 SR5=0.0
1220 MER=2*U(J1)*(LOG(R(J1-1)/R(J1)))/DX
1230 SR5=(4MER/HC)**(1/TM)
1240 Y(J1)=(1+SR5)*(Y0+(FC*(LOG(R(1)/R(J1))*WNH)))
1250 S(J1)=(Y(J1)*(R(J1-1)-R(J1))/R(J1)+(ABS(TC1)*(GOR(((R(J1-1)-R(J1))*2)
& **2)+((X(J1)-X(J1-1))*2)))/TW)+S(J1-1)
1255 IF S(J1) < Y(J1) THEN GOTO 1260
1255 PRINT"FRACTURE OCCURE IN TUBE AT THIS SPEED"
1257 GOTO 1411
1260 Y(J1)=S(J1)+HE(J1)
1270 REB4=YM(J1)-Y(J1)
1280 IF ABS(REB4)<REMA THEN GOTO 1270
1290 IF REB4<0 THEN GOTO 1300
1310 IF REB4>0 THEN GOTO 1170
1320 B4=B4-INCA
1330 INCA=INCA/10
1340 GOTO 1170
1370 PRINT"VEL="; VEL, "P="; P(J1), "H3="; H3(J1),
& "S="; S(J1), "YM="; YM(J1), "Y="; Y(J1),
& "X="; X(J1), "H="; H(J1), "R="; R(J1), "UD="
& V(J1),
1380 H3=H(J1)-H1+H2
1390 PRED=(1-((2*R(J1))/(2*R1)))*100
1395 SD=S(J1)+(TC2*LE/TW)
1400 PRINT"PREDE="; PRED, "H3="; H3, "SD="; SD
1405 PRINT"-----"
1410 NEXT A
1411 F=F+1
1412 VEL=F/10
1413 U(1)=VEL
1414 IF F>5 THEN GOTO 1420
1418 GOTO 1130
1420 END

```

DIE-LESS TUBE SINKING: A PLASTO-HYDRODYNAMIC ANALYSIS BASED ON NEWTONIAN FLUID CHARACTERISTICS

M I Panwhar, R Crampton and M S J Hashmi
Sheffield City Polytechnic, Sheffield, England

ABSTRACT

In conventional tube sinking process the tube is pulled through a tungsten-carbide reduction die principally to reduce the outer diameter with very little change in the wall-thickness. During the sinking process lubrication is used to reduce the drawing load, die wear and hence improve the machine life and the surface finish of the product, but still there is die wear due to metal to metal contact.

In this paper a new technique of tube sinking has been studied in which the tube is pulled through a die-less reduction unit having stepped parallel bores filled with polymer melts, the smallest bore diameter being greater than the initial nominal tube diameter.

Since the smallest bore size of such a device is dimensionally greater than the nominal tube diameter, thus metal to metal contact and hence wear, would no longer be a problem. As no conventional reduction die is used, the need for a swaged down diameter leading end is also eliminated. The polymer melt, in addition to acting as a plasto-hydrodynamic pressure medium, is found to form a coating on the drawn tube. This coating is thought to be useful in protecting the tube against corrosion during storage. After drawing the diameter of the tube is found to be fairly constant over the entire drawn length and there is no sign of any ovality or out of circularity in the cross-section.

Introduction

Tube sinking (or Hollow-sinking) is a well known process for reducing the diameter of the tube. In conventional tube sinking process, a tube is pulled through a tungsten-carbide reduction die and the material deforms plastically whilst passing through the die. In this case the die acts primarily to reduce the tube diameter to a specific size with an acceptable surface finish. A standard industrial die is usually designed to have tapered profile of angles between 20 and 40 degrees, and possible reduction in area at each die varies from about 10 to 50%. In conventional tube sinking practice lubrication is used to reduce the drawing load and die wear and hence improve the machine life and surface finish of the product, but still there is die wear due to metal to metal contact.

In 1955, Christopherson and Naylor¹ presented a paper which showed a method of reducing friction in wire drawing by hydrodynamic lubrication. It had been assumed that friction in conventional wire drawing was of a boundary nature and that a change of mode to hydrodynamic lubrication should greatly reduce friction, and all the experiments were limited to wire drawing.

In 1961, the first tests were conducted on tube sinking under condition of hydrodynamic lubrication.² On the basis of the experience of wire drawing under hydrodynamic conditions, the equipment was employed for tube drawing

with soda soap powder as a lubricant. The aim of the above work was to reduce the drawing load, die wear and to improve the surface finish. Nevertheless, the problem of die wear was still present due to metal to metal contact. A recent programme of research has been undertaken at the Sheffield City Polytechnic with a view to introducing alternative lubricating systems in wire drawing which would have very different characteristics from those currently in use. It has been shown that a pressure tube based on the work of reference (1) improved some of the operating characteristics when polymer melt was used as the lubricant (3-5). On the basis of the experimental evidence it is apparent that the deformation of the wire commences within the tube itself before reaching the reduction die, which effectively acted only as a seal. Under these conditions the die geometry becomes of secondary importance and deformation actually takes place as if an effective die of continuously changing die angle is being used.

Furthermore, experimental work carried out by Hashmi et al⁶ showed that reduction of the wire diameter should be possible using a polymer melt in conjunction with a stepped bore tubular unit only, thus eliminating the need for a conventional reduction die, the least diameter of the stepped bore reduction unit being greater than the nominal wire diameter.

A new technique of tube sinking is being developed based on the works reported in reference (3-6) in relation to wire drawing. This new technique would be useful in a number of ways in solving the problems associated with the conventional tube sinking process, eg die wear and the need for a swaged down leading end for easy insertion through the reduction die. With these aims experimental programmes were undertaken using a stepped bore die-less reduction unit (DRU) (a schematic diagram is shown in Fig.1). The gap between the die-less reduction unit and the tube was filled with polymer melt and the pulling action of the tube through the viscous fluid generates hydrodynamic pressure and gives rise to drag force. The combined effect of these pressure and drag force may be sufficient to cause plastic yielding and to subsequently deform the tube permanently. The results of the initial research on tube sinking, led to the suggestion that under certain conditions, it may be possible to eliminate the conventional reduction die and yet generate enough pressure within the DRU to deform the tube. Since the smallest bore size of such a device is dimensionally greater than the nominal tube diameter, thus metal to metal contact and hence wear would no longer be a problem. As no conventional reduction die is used, the need for a reduced diameter leading end is also eliminated. The polymer melt, in addition to acting as the pressure medium also forms a coating on the drawn tube. This coating is thought to be useful in protecting the tube against damage during handling and storage. In this paper we shall present the results of experimental work carried out on copper tubes using the stepped bore die-less reduction unit. A theoretical model has been formulated and the results predicted based on this model are also presented.

ANALYSIS

Symmons et al⁶ presented a theoretical model for die-less wire drawing based on Newtonian characteristics of the pressure medium and compared the predicted results with those observed for copper, mild steel and aluminium wires. In this section we shall develop a theoretical model for die-less tube sinking also based on Newtonian fluid characteristics of the pressure medium.

The following analysis is based on the geometrical configuration, shown in Fig. 2(a), during tube sinking using a die-less reduction unit (DRU) filled with liquid, the pressure medium. In order to analyse the deformation process, the following assumptions were made:

- a) The fluid pressure medium has Newtonian characteristics.
- b) The flow of the fluid pressure medium is laminar and axial.
- c) The thickness of the fluid layer is small compared to the bore size of the DRU.
- d) The pressure in the fluid is uniform in the thickness direction at any point along the length of the DRU.
- e) The deformation within the DRU takes place in a linear profile.

Analysis before deformation commences

From the geometrical configuration shown in Fig. 2(a) the gap between the DRU and the tube deformation is given by

$$\begin{aligned} h &= h_1 \text{ for } x \leq L_1 \\ \text{and } h &= h_2 \text{ for } L_1 < x \leq (L_1 + L_2) \end{aligned} \quad (1)$$

For Newtonian fluid the pressure gradient is given by

$$\left(\frac{\partial P}{\partial x}\right)_1 = \frac{\partial \tau}{\partial y} \quad (2)$$

and the shear stress is expressed as

$$\tau = \mu \frac{\partial u}{\partial y} \quad (3)$$

where μ is the fluid viscosity and u is the fluid velocity at a distance y from the surface of the tube.

Differentiating equation (3) with respect to y and substituting in equation (2) we obtain

$$\frac{\partial^2 u}{\partial y^2} = \frac{1}{\mu} \left(\frac{\partial P}{\partial x}\right)_1 \quad \text{or} \quad \frac{\partial^2 u}{\partial y^2} = \frac{1}{\mu} P'_1 \quad (4)$$

where $P'_1 = \left(\frac{\partial P}{\partial x}\right)_1$

Integrating and noting that $\frac{\partial P}{\partial x}$ is assumed to be constant with y .

$$\frac{\partial u}{\partial y} = \frac{1}{\mu} P'_1 y + C_1 \quad (5)$$

integrating again, it becomes

$$u = \frac{P'_1 y^2}{2\mu} + C_1 y + C_2 \quad (6)$$

where C_1 and C_2 are constant.

Applying the boundary conditions that at the surface of the tube where $y = 0$; $u = V$ and at the inner surface of the unit where $y = h_1$; $u = 0$ we have $C_2 = V$ and

$$C_1 = -\frac{P_1' h_1}{2\mu} - \frac{V}{h_1}$$

Substituting the value of C_1 and C_2 in equation (6) we get

$$u = \frac{P_1'}{\mu} (y^2 - yh_1) + V(1 - \frac{y}{h_1}) \quad (7)$$

The flow of the liquid medium in axial direction within the gap before the step may be given by:-

$$Q_1 = \int_0^{h_1} u dy \text{ which upon substitution for } u \text{ from equation (7) and integrating gives,}$$

$$Q_1 = -\frac{h_1^3}{12\mu} \left(\frac{\partial P}{\partial x}\right)_1 + \frac{Vh_1}{2} \quad (8)$$

The maximum pressure (P_m) for the case when no deformation takes place within the length L_1 can be obtained from the continuity of flow. Thus, mass flow rate in, $Q_1 =$ mass flow rate out, Q_2 .

The expression for Q_2 after the step can be derived in the same manner as above. Hence,

$$Q_2 = \frac{h_2^3}{12\mu} \left(\frac{\partial P}{\partial x}\right)_2 + \frac{Vh_2}{2} \quad (9)$$

Equating the expressions for Q_1 and Q_2 and noting that

$$\left(\frac{\partial P}{\partial x}\right)_1 = \frac{P_m}{L_1} \text{ and } \left(\frac{\partial P}{\partial x}\right)_2 = \frac{-P_m}{L_2} \text{ we have,}$$

$$P_m = \frac{6\mu V(h_1 - h_2)}{\left(\frac{h_1^3}{L_1} + \frac{h_2^3}{L_2}\right)} \quad (10)$$

The expression for the Shear Stress on the tube surface when no deformation takes place may be obtained as follows.

Differentiating equation (7) with respect to y we have

$$\frac{\partial u}{\partial y} = \frac{1}{2\mu} P_1' (2y - h_1) - \frac{V}{h_1} \quad (11)$$

which after combining with equation (3) gives the shear stress at any depth in the fluid for $0 < y < h_1$. Thus,

$$\tau_1 = \frac{1}{2} P_1' (2y - h_1) - \frac{\mu V}{h_1} \quad (12)$$

At the surface of the tube, $y = 0$

hence,

$$\tau_1 = -\left(\frac{h_1}{2} P_1' + \frac{\mu V}{h_1}\right) \quad (13)$$

But $P'_1 = \left(\frac{\partial P}{\partial x}\right)_1 = \frac{P_m}{L_1}$ is constant and hence the shear stress before deformation τ_1 is given by

$$\tau_1 = -\left(\frac{h_1}{2} \frac{P_m}{L_1} + \frac{\mu V}{h_1}\right) \quad (14)$$

The axial stress on the tube at any point distance x_1 from the entry when no deformation occurs, can be obtained by considering the shear force acting on the surface of the tube. Thus

$$\sigma_{x_1} = \frac{\tau_1 x_1}{t}$$

Substituting τ_1 from equation (14), we get

$$\sigma_{x_1} = -\frac{x_1}{t} \left(\frac{h_1}{2} \frac{P_m}{L_1} + \frac{\mu V}{h_1}\right) \quad (15)$$

where t is the constant wall-thickness of the tube.

Onset of Plastic Deformation

Considering the radial force equilibrium of an element of the tube subjected to external pressure, p , and axial stress, σ_x , it can easily be shown that the hoop stress, σ_θ , is given by $\sigma_\theta = pr/t$ where t is the wall-thickness and r is the outer radius. If the element under consideration is at a distance x_1 from the entry to the unit, then

$$p = P_m x_1 / L_1 \text{ so that } \sigma_\theta = P_m x_1 r / L_1 t.$$

Hence $\sigma_x \leq P \leq \sigma_\theta$.

Plastic yielding will thus occur only when an appropriate yield criterion is satisfied. According to the Tresca yield criterion the onset of plastic deformation should occur when the condition $\sigma_x + \sigma_\theta = Y_0$ is met where Y_0 is the yield stress of the tube material. Thus,

$$\frac{x_1}{t} \left(\frac{h_1 P_m}{2L_1} + \frac{\mu V}{h_1}\right) + \frac{P_m x_1 r}{L_1 t} = Y_0$$

which upon rearrangement gives,

$$x_1 = \frac{Y_0 t}{\left(\frac{h_1 P_m}{2L_1} + \frac{P_m r}{L_1 t} + \frac{\mu V}{h_1}\right)} \quad (16)$$

where x_1 denotes the position within the unit where plastic deformation of the tube commences.

Analysis after the onset of plastic deformation

Once plastic deformation commences the yield criterion must be satisfied in order to continue the deformation process. For a strain hardening material this means the condition

$$\sigma_x + \sigma_\theta = Y = Y_0 + K_0 \epsilon^n$$

must be met where K_0 and n are the material constants and $\epsilon = \ln\left(\frac{r_1}{r}\right)$.

Pressure in the deformation zone

The continuity equation for the flow of the liquid polymer can be written as

$$\frac{\partial}{\partial x}(Q_x) + \frac{\partial}{\partial y}(Q_y) + \frac{\partial}{\partial z}(Q_z) = 0$$

Since $\frac{\partial}{\partial y}(Q_y) = \frac{\partial}{\partial z}(Q_z) = 0$, therefore $\frac{\partial}{\partial x}(Q_x) = 0$.

Thus, from equation (8) we get

$$\begin{aligned} & \frac{\partial}{\partial x} \left\{ -\frac{1}{12\mu} \left(\frac{\partial P}{\partial x} \right) h^3 + \frac{Vh}{2} \right\} = 0 \\ \text{or} \quad & \frac{\partial}{\partial x} \left(h^3 \frac{\partial P}{\partial x} \right) = \frac{\partial}{\partial x} (6\mu v h) \end{aligned} \quad (17)$$

where $h = h_1 + bx$ the gap thickness in the deformation zone, b , is the slope of the profile and x is measured from the point where plastic deformation commences.

Now, for a given velocity V and viscosity μ , equation (17) becomes

$$\frac{\partial}{\partial x} \left(h^3 \frac{\partial P}{\partial x} \right) = 6\mu v \frac{\partial h}{\partial x}$$

$$\text{but} \quad \frac{\partial h}{\partial x} = b$$

$$\text{hence} \quad \frac{\partial}{\partial x} \left(h^3 \frac{\partial P}{\partial x} \right) = 6\mu v b$$

which upon integration becomes

$$h^3 \left(\frac{\partial P}{\partial x} \right) = 6\mu v b x + C_3 \quad (18)$$

where C_3 is the constant of integration.

Applying the boundary condition that $\frac{\partial P}{\partial x} = \frac{P_m}{L_1}$ at $x = 0$ the constant C_3 is given by

$$C_3 = h_1^3 \frac{P_m}{L_1}$$

where P_m is the maximum pressure at the step under no deformation condition. By putting the value of h , equation (17) then becomes

$$\frac{\partial P}{\partial x} = 6\mu v \frac{bx}{(h_1 + bx)^3} + \frac{P_m}{L_1} \frac{h_1^3}{(h_1 + bx)^3} \quad (19)$$

Integrating equation (19), we obtain

$$P = 6\mu v \left\{ -\frac{1}{b(h_1 + bx)} + \frac{h_1}{2b(h_1 + bx)^2} - \left(\frac{P_m}{L_1} \right) \frac{h_1^3}{2b(h_1 + bx)} \right\} + C_4 \quad (20)$$

Applying the boundary condition that at $x = 0$, the pressure,

$P = P_m x_1 / L_1$. Thus

$$P = \left(\frac{P_m x_1}{L_1} \right)$$

$$\frac{P_m x_1}{L_1} = 6\mu v \left(-\frac{1}{2bh_1} \right) - \frac{P_m \left(\frac{h_1}{2b} \right)}{L_1} + C_4$$

so that $C_4 = \frac{P_m x_1}{L_1} + \frac{3\mu v}{bh_1} + \frac{P_m h_1}{L_1 2b}$.

Substituting for C_4 equation (20) becomes

$$P = \frac{6\mu v}{b} \left[\frac{h_1}{2(h_1 + bx)^2} - \frac{1}{(h_1 + bx)} + \frac{1}{2h_1} \right] - \frac{P_m}{L_1} \left(\frac{h_1^3}{2b(h_1 + bx)^2} - \frac{h_1}{2b} - x_1 \right) \quad (21)$$

Equation (21) gives the pressure distribution for $x_1 \leq x \leq (L_1 - x_1)$ within the DRU.

The expression for the shear stress on the surface of the deformed tube may be given by equation (14) by simply replacing τ_c for τ_1 , h for h_1 and $\frac{\partial P}{\partial x}$ from equation (19). Thus,

$$\tau_c = -\frac{1}{2}(h_1 + bx) \left\{ 6\mu v \frac{bx}{(h_1 + bx)^3} + \frac{P_m}{L_1} \frac{h_1^3}{(h_1 + bx)^3} \right\} - \frac{\mu v}{h_1 + bx} \quad (22)$$

Hoop Stress in the deformation zone

Referring to Fig. 2(b) Let us consider the stresses acting on a small element of the wall, bounded by meridian planes inclined at angle $\Delta\theta$ and resolve the forces perpendicular to the element.

Thus,

$$P(r \Delta\theta \frac{dr}{\sin\alpha}) - \sigma_\theta (t \frac{dr}{\sin\alpha}) \Delta\theta \cos\alpha = 0$$

which upon simplification and rearrangement becomes,

$$\sigma_\theta = \frac{Pr}{t \cos\alpha} \quad (23)$$

where $\cos\alpha = \frac{1}{\sqrt{1 + b^2}}$

Hence P is very small in comparison to σ_θ when $\frac{t}{r}$ is small. The stresses in this deformation process are therefore such that $\sigma_\alpha > P > \sigma_\theta$.

Substituting for P from equation (21) into equation (23) we get

$$\sigma_\theta = \frac{r(1 + b^2)^2}{t} \left[\frac{6\mu v}{b} \left[\frac{h_1}{2(h_1 + bx)^2} - \frac{1}{(h_1 + bx)} + \frac{1}{2h_1} \right] - \frac{P_m}{L_1} \left(\frac{h_1^3}{2b(h_1 + bx)^2} - \frac{h_1}{2b} - x_1 \right) \right] \quad (24)$$

Axial Stress in the deformation zone

Resolving forces parallel to the effective deformation profile it can be easily shown that

$$\frac{d}{dr} (\sigma_x r) + \sigma_\theta + \tau_c \frac{r}{t \sin \alpha} = 0 \quad (25)$$

so that $r \frac{d\sigma_x}{dr} + \sigma_x + \sigma_\theta + \tau_c \frac{r}{t \sin \alpha} = 0$ (26)

According to the Tresca yield criterion

$$\sigma_1 - \sigma_3 = Y$$

but $\sigma_1 = \sigma_x$ and $\sigma_3 = -\sigma_\theta$

Therefore, the yield criterion becomes,

$$\sigma_x + \sigma_\theta = Y \quad (27)$$

Substituting for $(\sigma_x + \sigma_\theta)$ in equation (26) we obtain

$$d\sigma_x = -Y \frac{dr}{r} - \tau_c \frac{dr}{t \sin \alpha} \quad (28)$$

Substituting for $Y = Y_0 + K_0 \varepsilon^n$ into equation (28) we obtain,

$$d\sigma_x = -Y_0 \frac{dr}{r} - K_0 \left(\ln \frac{r_1}{r}\right)^n \frac{dr}{r} - \frac{\tau_c}{t \sin \alpha} dr \quad (29)$$

Integration of equation (29) gives,

$$\sigma_x = -Y_0 \ln r + \frac{K_0}{n+1} \left(\ln \frac{r_1}{r}\right)^{n+1} - \frac{\tau_c r}{t \sin \alpha} + C_5 \quad (30)$$

where C_5 is the constant of integration.

Applying boundary conditions that when $r = r_1$ at $x = x_1$, $\sigma_x = \sigma_{x_1}$, the axial stress at the point of yielding, equation (30) gives,

$$C_5 = \sigma_{x_1} + Y_0 \ln r_1 + \frac{\tau_c r_1}{t \sin \alpha}$$

Back-substitution for C_5 in equation (30) gives,

$$\sigma_x = Y_0 \ln \left(\frac{r_1}{r}\right) + \frac{K_0}{n+1} \left(\ln \frac{r_1}{r}\right)^{n+1} + \frac{\tau_c}{t \sin \alpha} (r_1 - r) + \sigma_{x_1}$$

By substituting the expression for σ_x from equation (15), x_1 from (16) and τ_c from (22), the axial stress in the x_1 deformation zone is obtained as,

$$\begin{aligned} \sigma_x = Y_0 \ln \left(\frac{r_1}{r}\right) + \frac{K_0}{n+1} \left(\ln \frac{r_1}{r}\right)^{n+1} + \frac{(1+b^2)^{\frac{1}{2}} (r_1 - r)}{bt} \left(-3\mu v \frac{bx}{(h_1+bx)^2} - \right. \\ \left. \frac{P_m}{L_1} \frac{h_1^3}{2(h_1+bx)^2} - \frac{\mu v}{h_1+bx}\right) + \frac{Y_0}{\left(\frac{\tau_1}{t} + \frac{P_m r_1}{t L_1}\right)} \left(-\frac{h_1}{2t} \frac{P_m}{L_1} - \frac{\mu v}{t h_1}\right) \end{aligned} \quad (31)$$

where, $r = r_1 - bx$, τ_1 is given by equations (14) and P_m by equation (10).

Since, the deformation profile within the DRU is assumed to be linear as shown in Fig.2(a), $r = r_1 - bx$ where b is the slope given by $\tan\alpha$ and r_1 is the radius of the tube before deformation.

Substituting for σ_x , σ_θ , P in equation (31) it can be seen that only the parameter 'b' is unknown.

For a given drawing speed the value of 'b' may be determined using iteration technique to satisfy this equation. Once the value of 'b' is established the deformation profile is obtained and the reduction in diameter at any point for $x_1 < x < L_1$ is given by $\Delta D = (D_1 - 2bx)$.

The total percentage reduction in diameter is then given by

$$\text{PRD} = 100 \times \{2b(L_1 - x_1)\}/D_1 \quad (32)$$

where D_1 is the undeformed diameter of the tube. The drawing stress ' σ_d ' at the exit end of the DRU is then given by,

$$\sigma_d = \sigma_s + \sigma_{x_2} \quad (33)$$

where, σ_s is the axial stress at the step and σ_{x_2} is given by

$$\sigma_{x_2} = \frac{\tau_{c_2} L_2}{t} \quad (34)$$

The shear stress in the small bore section of the unit may be expressed as

$$\tau_{c_2} = \frac{h_2 P_m}{2L_2} - \frac{\mu v}{h_2} \quad (35)$$

and the film thickness of the pressure medium can be written as

$$h_3 = h_2 + b(L_1 - x_1). \quad (36)$$

Experimental Work

Experimental work was carried out with copper tubes of 13.52 mm O.D. and 2.5 mm wall thickness. For these tests a low density polyethylene (Alkathene WVG23) polymer melt was used as the pressure medium at temperatures varying from 130°C to 180°C and the tubes were drawn at speeds varying from 0.1 to 0.5 m/sec. All these tests have been carried out on a chain driven draw bench. The schematic diagram of the draw bench is shown in Fig.3. A variable speed driven system with speed range of 0.1 to 1.0 m/sec was used to draw the tube.

The stepped bore die-less reduction unit (DRU) is bolted to the hinged die plate which rests against a load cell during drawing. The melt chamber and the DRU are held together with four socket cap screws.

The melt chamber is filled with polymer through a hopper (usually in granulated form) and is allowed to "soak" until steady state temperature has been reached. Heater bands are used to melt the polymer and keep the molten polymer at the desired temperature by means of the temperature regulators. The tube is then pushed through the melt chamber and the die-less reduction unit, and clamped into the dog-jaw clamping device.

The drawing speed is adjusted before the test run by setting the speed regulator. The motor is then started and the dog jaws device is engaged with the chain which disengages when it reaches the emergency ramp. During the drawing procedure the drawing load is noted from the load indicator.

Results and Discussion

When copper tubes were drawn through the die-less reduction unit (DRU) the diameter of the drawn tube was found to be fairly constant over the entire length and the ovality or out of circularity in the cross-section, as shown in Fig (4), was found to be negligibly small.

Experimental results indicate that the percentage reduction in diameter of the tube depends on the gap and length ratios of the dieless reduction unit and also on the viscosity of the fluid pressure medium and the drawing speed. In Figs. (5)-(7), the variation in experimentally observed percentage reduction in diameter and drawing load is shown against the drawing speed. The curves in Fig. (5) correspond to gap ratios of 50, 40 and 25 for a constant length ratio of 5.33. It is evident that both the reduction in diameter and drawing load decrease with drawing speed for all gap ratios. The percentage reduction in diameter is maximum at about 0.1 ms^{-1} and for drawing speeds in excess of about 0.7 ms^{-1} no reduction in diameter is observed.

The effect of length ratio on the extent of reduction in diameter and drawing load can be seen in Fig. 6(a) and 6(b) respectively. The results show similar trends as seen in Fig. 5; higher speeds producing relatively smaller reductions in diameter and correspondingly lower drawing loads. The pressure medium used in order to obtain the results presented in Figs 5 and 6 is WVG23 polymer melt at 130°C .

The effect of using pressure mediums of different viscosity is demonstrated in Fig. 7, which shows the variation in the reduction in diameter and the drawing load with drawing speed. It is evident that the higher the viscosity of the pressure medium, the greater is the reduction in diameter and drawing load for a given drawing speed and die-less reduction unit.

Theoretical results were calculated on the basis of equations derived in the theoretical analysis section. In order to calculate theoretical results, the following standard values of the parameters were used;

Total length of the stepped bore die-less reduction unit
(DRU) = 190 mm
Step position from inlet, $L_1 = 160 \text{ mm}$
Step position from outlet, $L_2 = 30 \text{ mm}$
Initial gap, $h_1 = 0.5 \text{ mm}$, final gap, $h_2 = 0.01 \text{ mm}$
Original diameter of the copper tube, $D_1 = 13.52 \text{ mm}$
Wall thickness of copper tube, $t = 2.5 \text{ mm}$
Initial yield stress of the tube material, $Y_0 = 50 \text{ MNm}^{-2}$
Strain hardening constant of the tube material, $K_0 = 700 \text{ MNm}^{-2}$
Strain hardening index of the tube material, $n = 0.18$
Viscosity of the polymer melt = 100 Nsm^{-2}

The theoretical percentage reduction in diameter (PRD) was calculated using equation (32). The reduction in diameter for different drawing speeds was plotted as shown in Fig. 8 which indicates that the reduction in diameter

increases with drawing speed and reaches a magnitude of about 8% corresponding to a drawing speed of 1 ms^{-1} . No deformation is predicted for drawing speeds of less than about 0.35 ms^{-1} . This trend is in total contrast with that observed from experimental results in which the maximum reduction in diameter was found at a drawing speed of about 0.1 ms^{-1} , and for speeds greater than 0.1 ms^{-1} , the reduction in diameter decreased. Experimentally, no deformation was evident at speeds in excess of about 0.7 ms^{-1} (see Fig. 5). The main reason for this anomolous result is possibly the fact that the polymer melt used in the experiments does not possess the characteristics of a Newtonian fluid. Some form of non-Newtonian fluid characteristics may, when incorporated in the analysis produce theoretical results in closer agreement with those obtained from experiments. Such an analysis, to be reported elsewhere in the near future, does not provide a closed form of solution and the use of numerical analysis has to be made. The present closed form analysis is considered very effective in understanding the mechanics of the process and hence useful as a first step towards more complicated solutions.

The variation in the distance, x , where deformation commences, with drawing speed for different gap ratios, calculated theoretically, can be seen in Fig. 8(b). The theoretically calculated drawing loads for drawing speeds of up to 1 ms^{-1} are shown in Fig. 9. These results tie up with the theoretically calculated reduction in diameter as shown in Fig. 8(a) and hence do not agree with those measured experimentally for very much the same reasons stated earlier. As shown in Fig. 5(b), the maximum experimental drawing load occurs at a drawing speed of about 0.1 ms^{-1} after which it decreases with increased drawing speeds. The theoretically calculated drawing load increases with the drawing speed. The effect of viscosity of the pressure medium on the obtainable reduction in diameter with drawing speed is shown in Fig. 10(a). This figure suggests that higher viscosity should cause greater reduction in diameter. With a viscosity value of 130 Nsm^{-2} , the reduction in diameter of about 11% should be obtained for the drawing speed of 1 ms^{-1} . However, if the viscosity is reduced to 100 Nsm^{-2} , a reduction in diameter of about 8% is predicted for the same drawing speed. In order that the effect of the wall thickness of the tube on the extent of permanent deformation may be studied, reduction in diameter with drawing speed was calculated theoretically for three different wall thicknesses and the results are shown in Fig. 10(b). In calculating these results, the viscosity parameter for the pressure medium was kept constant. It is evident that for smaller wall thicknesses, greater reduction in diameter is predicted for a given drawing speed and pressure medium. For a tube of wall thickness 1.5 mm, the reduction in diameter of about 15% is predicted at a drawing speed of 1 ms^{-1} , but only 5% reduction in diameter may be obtained for a tube of wall thickness of 3.5 mm at the same drawing speed of 1 ms^{-1} .

Fig. 11(a) shows the effect of initial yield stress, Y_0 , of the tube material on the reduction in diameter obtainable with drawing speeds of up to 1 ms^{-1} . The theoretical results were calculated with different values of Y_0 varying from 10 to 80 MNm^{-2} . This figure shows that for lower values of Y_0 , relatively greater permanent deformation could be obtained at a given drawing speed. The effect of the diameter of the tube on the deformation is demonstrated in Fig. 11(b) which shows the theoretically calculated variation in the reduction in diameter obtainable with drawing speed. The diameter of the tube was varied from 14.5 to 12 mm :

and it is evident that for a drawing speed of 1 ms^{-1} , permanent reduction in diameter of about 8.5% may take place in a tube of 14.5 mm diameter and about 7% in a tube of 12 mm diameter. By way of explaining this phenomenon, it should be noted that the polymer melt does not behave like a Newtonian fluid and its viscosity decreases with increasing shear rate and hence the drawing speeds. From the above experimental results, it is also evident that it should be possible to carry out tube sinking using the die-less reduction unit where no metal to metal contact takes place. It should also be noted that there is no necessity for reducing the leading end of the tube since the undeformed tube diameter is smaller than the smallest bore size of the die-less reduction unit.

References

- 1 Christopherson, D.G. and Naylor, H. "Promotion of fluid lubrication in wire drawing". Instn. Mech. Engrs. 1955, 169, pp 643-653.
- 2 Kalmogarov, V.L. and Selishchev, K.P. "Cold drawing tubes with improved lubrication". Stall in English, 1962 (9) pp 830-831.
- 3 Symmons, G.R., Stevens and Thompson, "Hydrodynamic lubrication and coating of wire using a polymer melt during the drawing operation", Wire Industry, 1978, pp 469-483.
- 4 Crampton, R. Symmons and Hashmi, "A non-Newtonian plasto hydrodynamic analysis of the lubrication and coating of wire using a polymer melt during drawing", Int. Symposium, Metal working lubrication, San Francisco, USA, August 1980, pp 107.
- 5 Hashmi, M.S.J. Crampton and Symmons, "Effects of Strain hardening and strain rate sensitivity of the wire material during drawing under non-Newtonian plasto-hydrodynamic lubrication conditions", Int. J. Mech. Tool Des. Res., 1981, 21, pp 71-86.
- 6 Hashmi, M.S.J. Symmons and Parvinmehr, H. "A novel technique of wire drawing", Inst. Mech. Engrs, 1982, Vol 24, No 1.

Notation

r	Radius of the tube within the deformed zone.
r_1	Initial tube radius.
r_2	Final tube radius.
b	Factor determining theoretical profile.
h	Gap between the tube and DRU during the deformation.
h_1	Gap between the undeformed tube and inlet bore of DRU.
h_2	Gap between the undeformed tube and outlet bore of DRU.
h_3	Gap between the deformed tube and outlet bore of DRU.
K_0	Material constant.
L_1	Length of the DRU before the Step.
L_2	Length of the DRU after the Step.
n	Material constant.
P	Pressure.
P_1	Maximum pressure if deformation occurs.
P_m	Maximum pressure if no deformation occurs.
Q	Flow of lubrication.
t	Constant wall-thickness of the tube.
τ_c	Shear stress along tube surface.
τ	Shear stress before the deformation.
σ	Axial stress in the tube
σ_θ	Hoop stress in the tube.
μ_0	Polymer viscosity
U	Velocity of the lubrication.
V	Drawing speed.
x	Position of the yielding of the tube.
X	Distance from X_1 when deformation occurs.
X_1	Length of the undeformed tube in the DRU.
Y	Flow stress of the tube material.

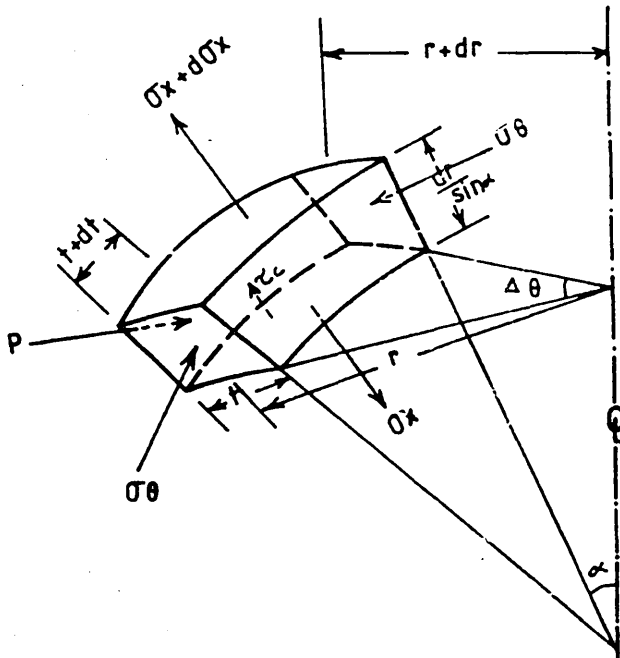
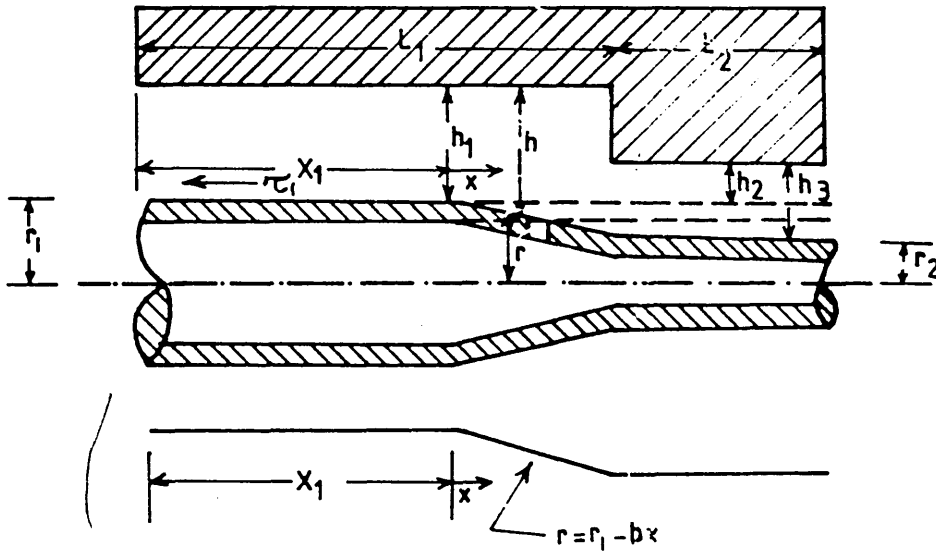
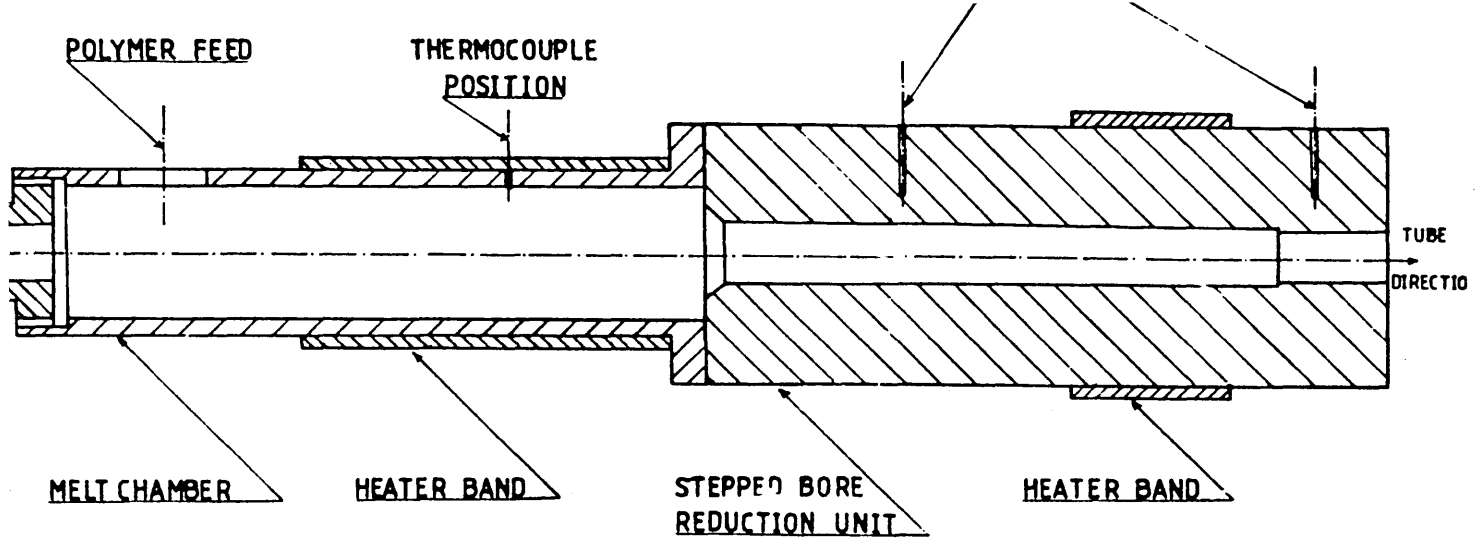


Fig.1

Stepped bore reduction unit assembly

Fig.2(a)

Theoretically assumed deformation mode within the DRU

Fig.2(b)

Stresses acting on a small element of the tube

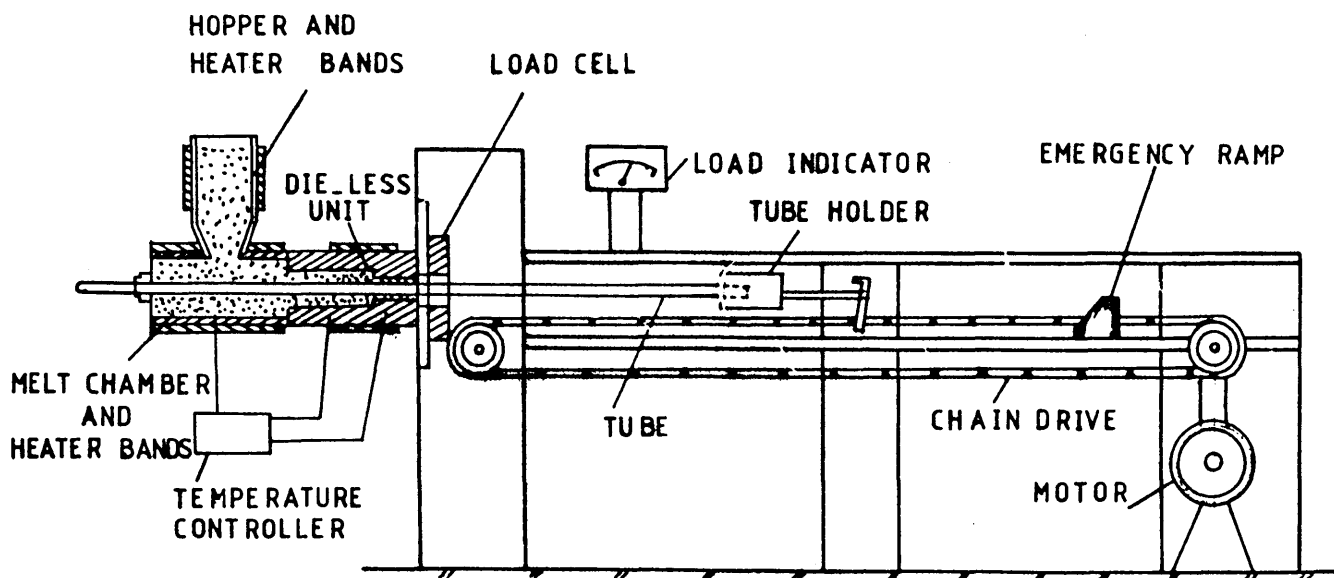


Fig.3 Die-less tube sinking drawing bench

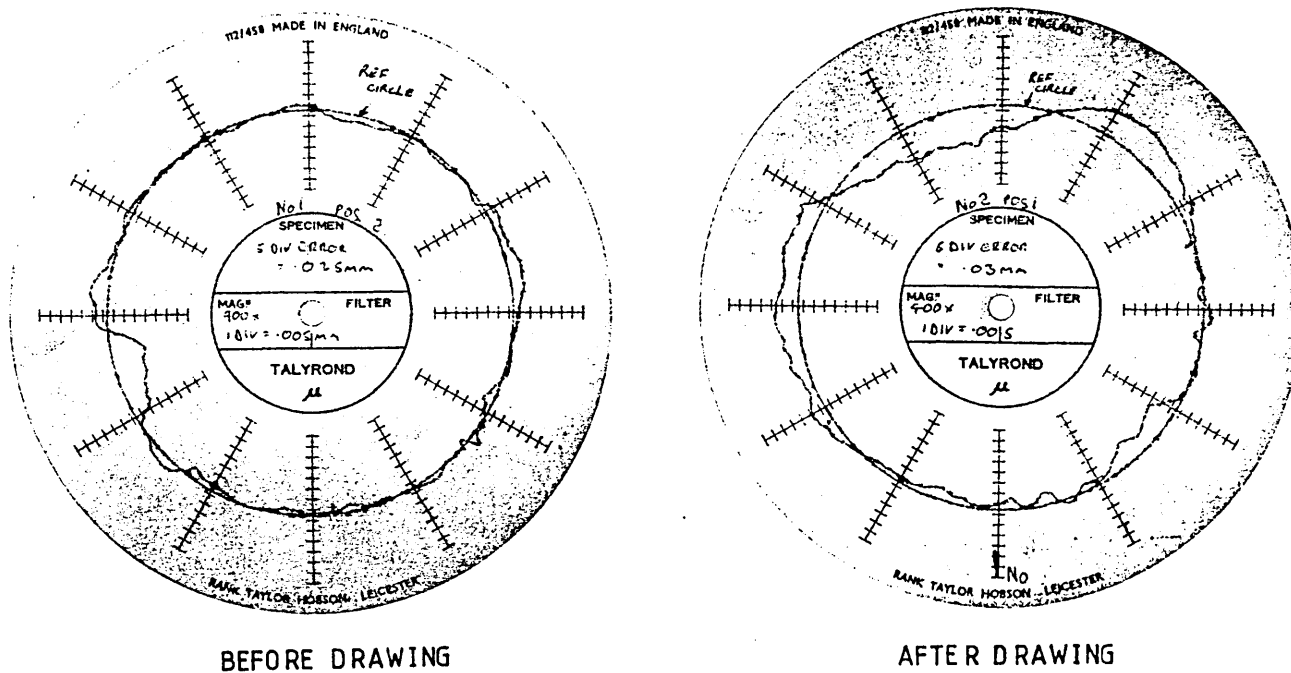


Fig.4 Roundness test at drawing speed of 0.1 m/s, reduction in dia 7% with WG 23 at 130°C

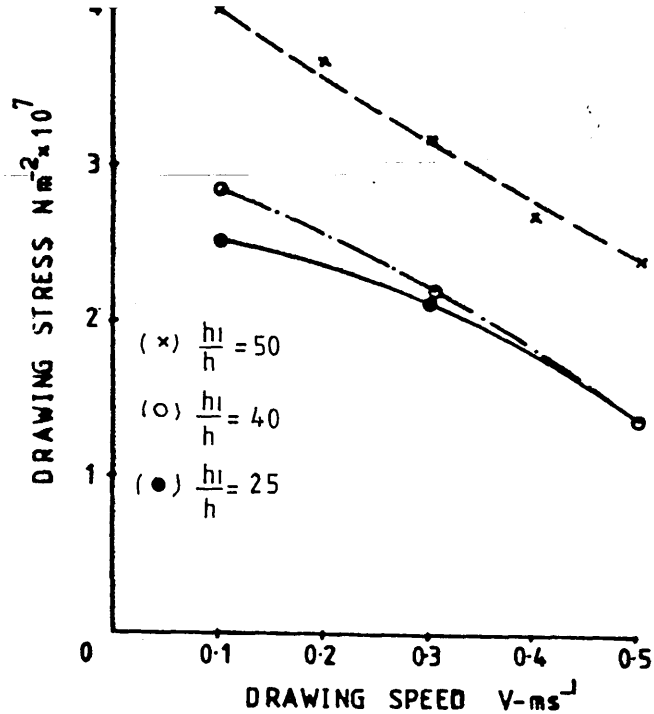
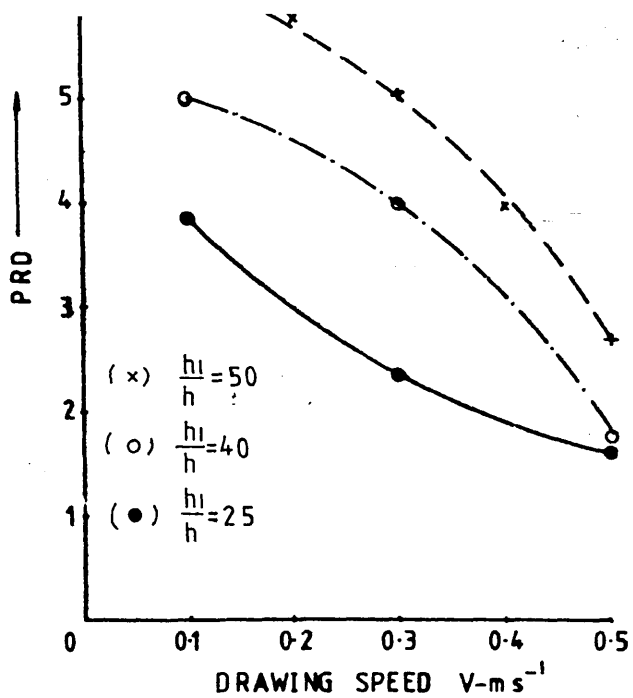


Fig.5(a) Experimental effect of gap ratio on percentage reduction in diameter

Fig.5(b) Experimental effect of gap ratio on drawing stress

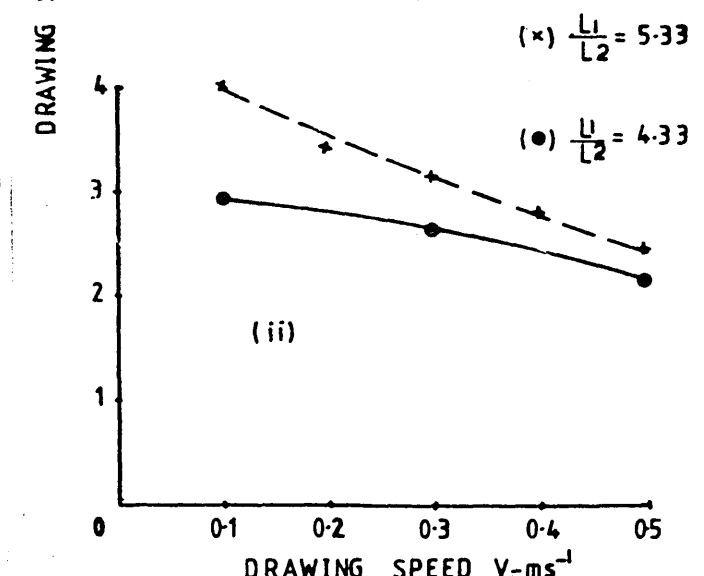
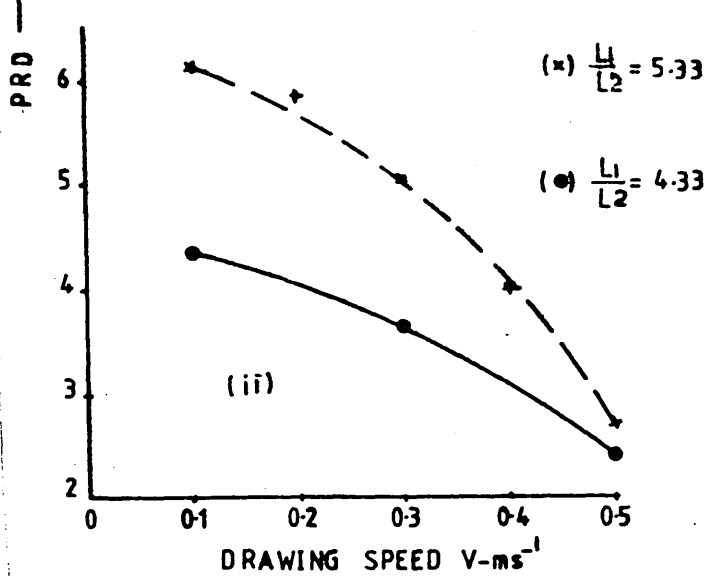
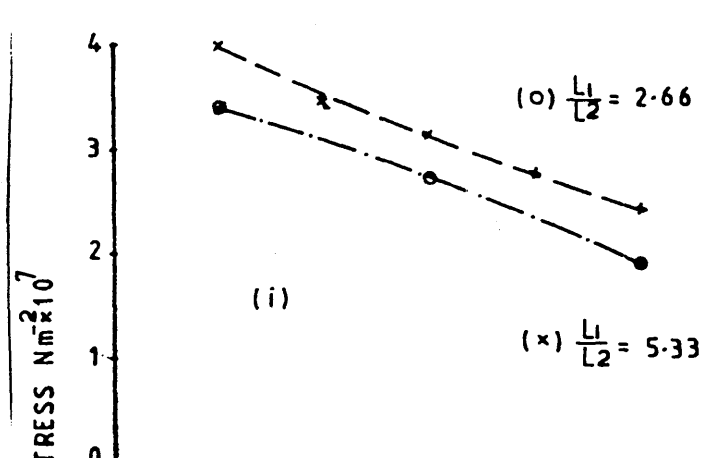
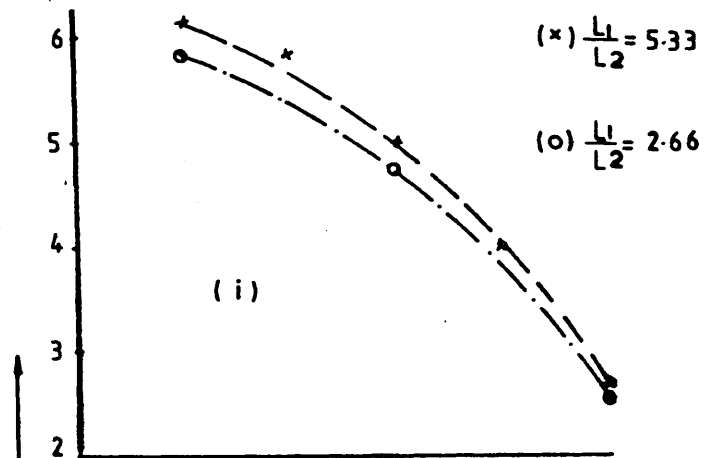


Fig.6(a) Experimental effect of length ratio on percentage reduction in diameter (i) $L_1 = \text{const.}$ (ii) $L_2 = \text{const.}$

Fig.6(b) Experimental effect of length ratio on drawing stress (i) $L_1 = \text{const.}$ (ii) $L_2 = \text{const.}$

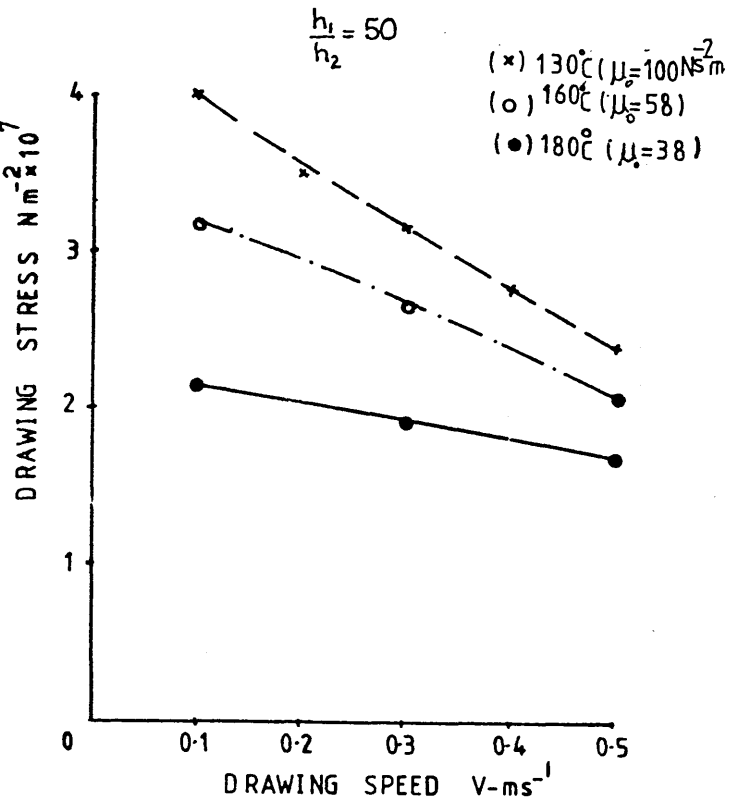
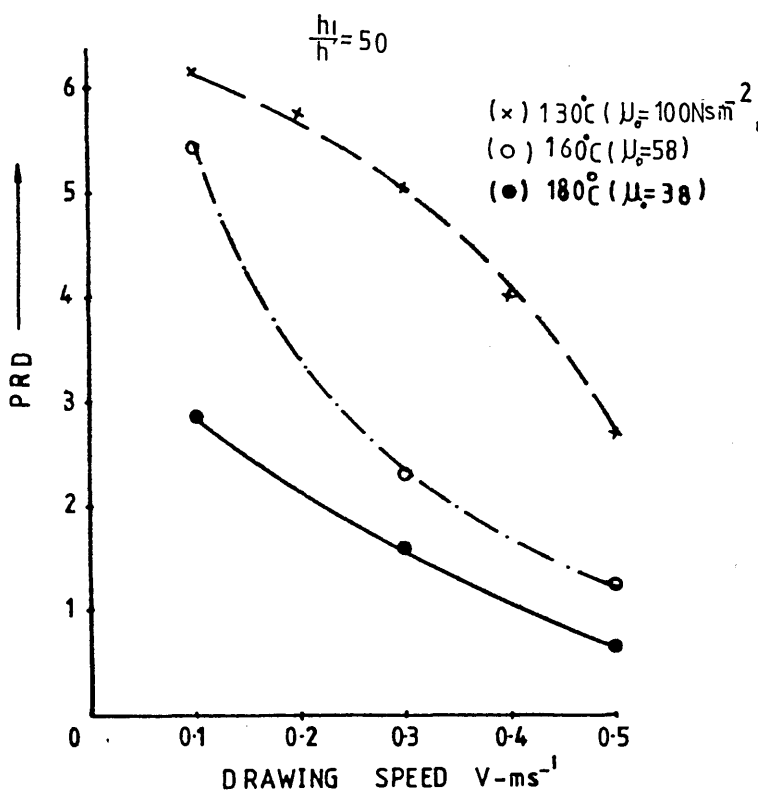


Fig.7(a) Experimental effect of viscosity on percentage reduction in diameter (using WVG 23)
 Fig.7(b) Experimental effect of viscosity on drawing stress (using WVG 23)

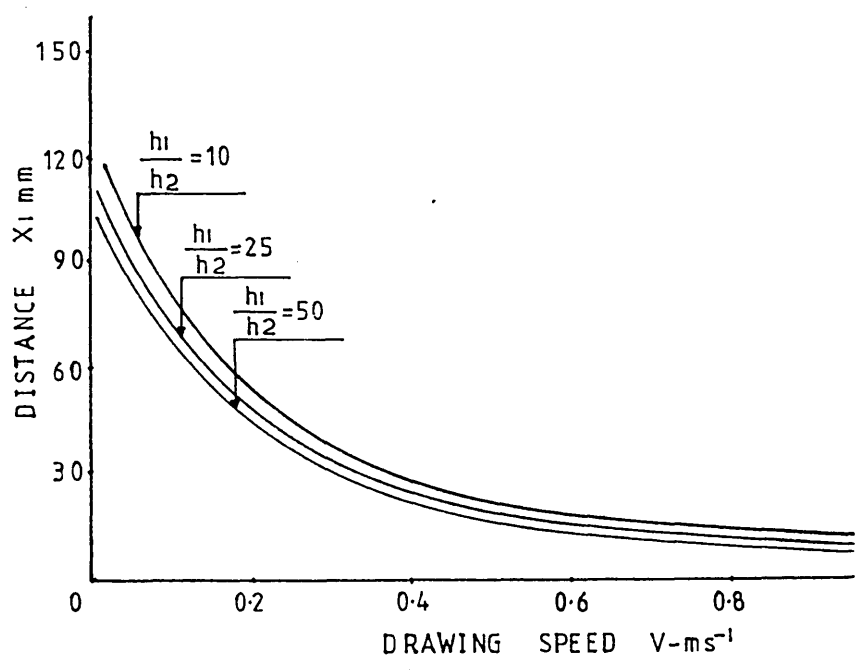
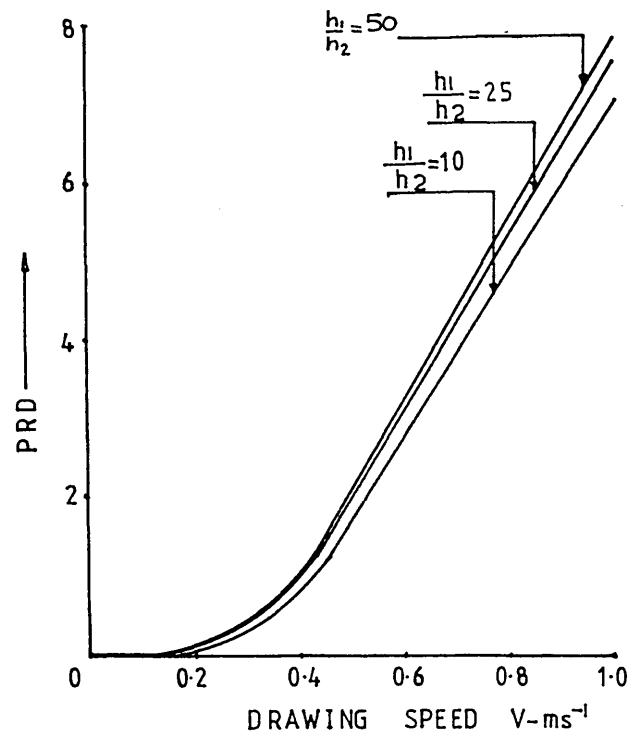


Fig.8(a) Theoretical effect of gap ratio on percentage reduction in diameter
 Fig.8(b) Theoretical effect of gap ratio on yielding position of tube

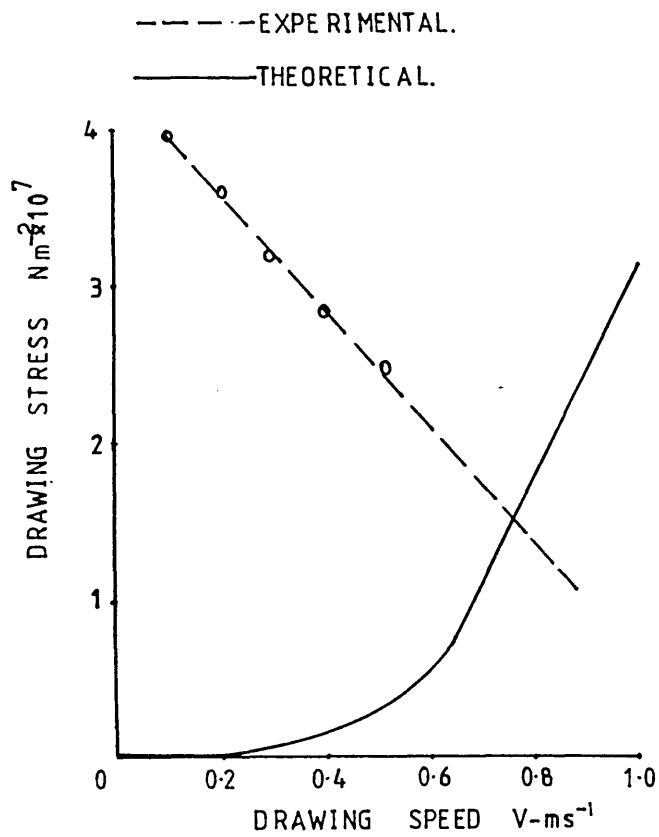


Fig.9 Comparison between experimental and theoretical drawing stress

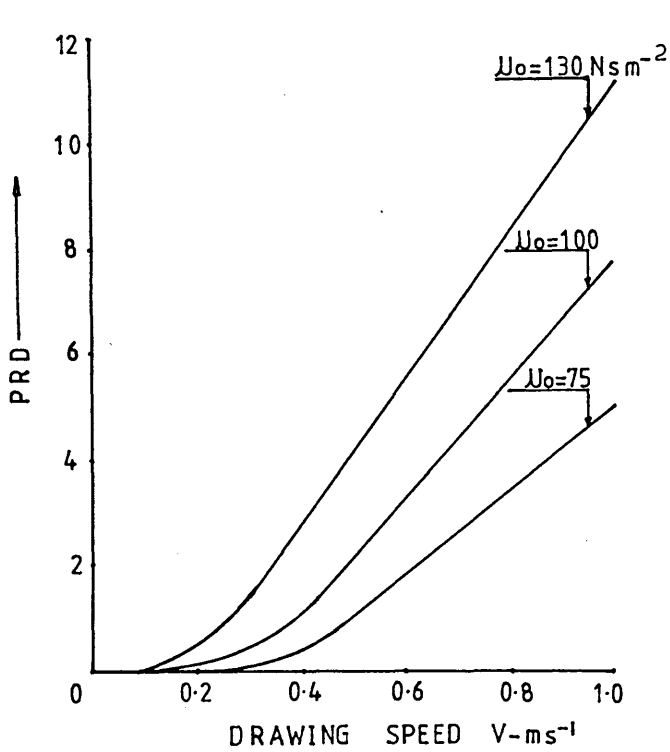


Fig.10(a) Theoretical effect of viscosity on percentage reduction in diameter

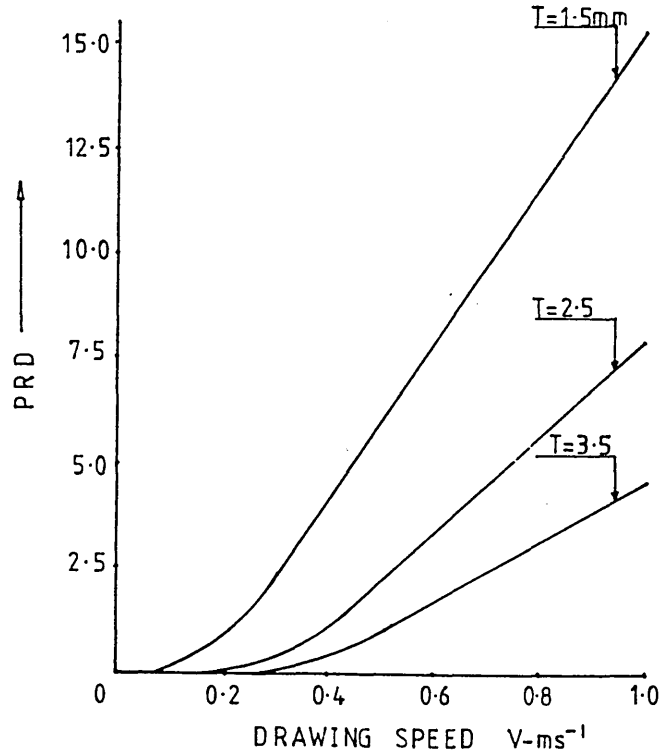


Fig.10(b) Theoretical effect of tube wall-thickness on percentage reduction in diameter

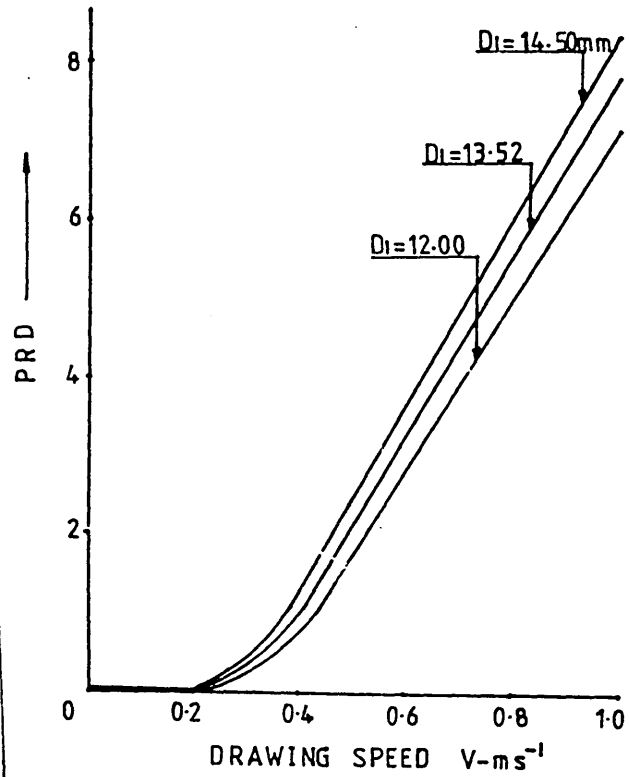
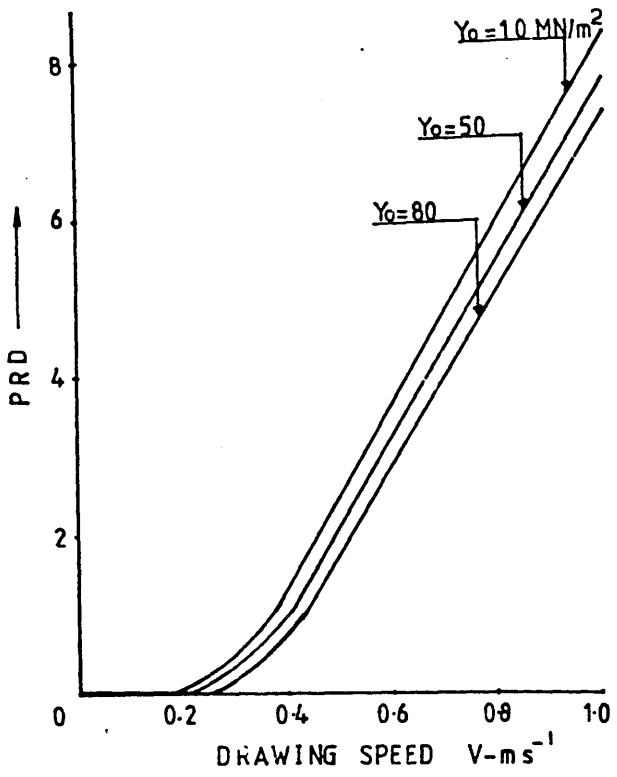


Fig.11(a) Theoretical effect of initial yield stress on percentage reduction in diameter

Fig.11(b) Theoretical effect of tube diameter on percentage reduction in diameter